IMPACTS OF LAND USE/ LAND COVER CHANGES ON MICRO-CLIMATE AND OPTIMUM ADAPTATION MEASURES

Ph.D. Thesis

SURENDRA PRATAP SINGH
(Id. No.: 2012RCE9011)

DEPARTMENT OF CIVIL ENGINEERING
MALAVIYA NATIONAL INSTITUTE OF TECHNOLOGY
JAIPUR

March, 2018

Impacts of Land Use/ Land Cover Changes on Micro-climate and Optimum Adaptation Measures

Submitted in

fulfillment of the requirements for the degree of

Doctor of Philosophy

by

Surendra Pratap Singh
(Id. No.: 2012RCE9011)

Under the Supervision of

Dr. Mahesh Kumar Jat

Department of Civil Engineering
Malaviya National Institute of Technology Jaipur
Jaipur, India

March, 2018

This thesis is dedicated to my parents and beloved wife
for their endless love, support and encouragement.

CERTIFICATE

This is to certify that the thesis entitled **"Impacts of Land Use/ Land Cover Changes on Micro-climate and Optimum Adaptation Measures"** is being submitted by **Mr. Surendra Pratap Singh (ID. NO: 2012RCE9011)** to the Malaviya National Institute of Technology Jaipur for the award of the degree of **Doctor of Philosophy** is a bonafide record of original research work carried out by him. He has worked under my guidance and supervision and has fulfilled the requirement for the submission of this thesis, which has reached the requisite standards.

The thesis embodies the original work done by him and has not been carried out earlier to the best of my knowledge and belief.

Place: Jaipur

Date :

Dr. Mahesh Kumar Jat
(Associate Professor)
Department of Civil Engineering
M.N.I.T Jaipur, India

DECLARATION

I Surendra Pratap Singh, declare that this Ph.D. thesis entitled **"Impacts of Land Use/ Land Cover Changes on Micro-climate and Optimum Adaptation Measures"** and the work presented in it, are my own. I further declare that:

- This work has been done while in candidature for Ph.D. degree at MNIT Jaipur.
- Where I have consulted the published work of others, the same has been clearly attributed.
- Where I have quoted from the work of others, the source has been given, with the exception of such quotations; this thesis is entirely my own work.
- I have acknowledged all main sources of help.

Place: Jaipur

Date :

Mr. Surendra Pratap Singh
2012RCE9011
Department of Civil Engineering
M.N.I.T Jaipur, India

ABSTRACT

Urbanization changes natural surfaces into synthetic surfaces and introduces anthropogenic heat into urban climate. These changes modify the micro-climate as well as changes radiative, thermal, moisture and aerodynamics properties of the urban areas. It is well established that climate is changing and its adverse effects seem to be more pronounced, if assessed at local and regional scale as compared to global scale. At the global scale, its effects are generalized due to loss of regional and local details of the climate. The Surface Energy Balance (SEB), which gives an idea of the heat generated and contained by an area, could help in understanding the overall climate dynamics of an area. Urban and semi urban areas experience intense LULC changes due to increase in population, industrialization, aspiration of better living, unplanned development, loss of vegetation and increase in impervious surfaces. Such a large scale LULC transformation will lead to changes in land, atmospheric energy and water transfer processes due to alterations in albedo and emissivity of the LULC classes. The effect of LULC changes and their relative contribution in changing the climate needs to be studied to reduce its adverse impact through suitable mitigation and adaptations. Variety of methods and models are available to investigate the effects of LULC changes on climate ranging from statistical methods, regional and global climate models, OMR based methods, LST based methods and surface energy balance modelling based approaches. Surface energy and water balance based distributed models have been used in recent past to investigate effects of direct and indirect LULC change mechanisms on climate. Also, for understanding the link between urbanization and micro-climate it is vital for urban environment sustainability to determine effective design strategies, e.g. altering the LULC like increasing vegetation and enhancing irrigation regime, using more reflective paved surfaces and materials in order to improve the urban climate. The knowledge of how to purposefully manipulate the SEB by changing urban land cover is crucial to urban climate adaptation. Therefore, energy balance based approach has been found to be promising in investigating the impacts of LULC changes on changing the micro-climate of an area.

Therefore, present study has been carried out to assess the climate change in terms of trends in mean and extreme events of selected meteorological parameters at different temporal resolutions i.e., daily, month, seasonal and annual for two areas of Delhi using the statistical techniques. For future climate projection in terms of representative meteorological

parameters i.e., temperature and rainfall, CanESM2 GCM model outputs corrosponding to the CMIP5 experiment has been downscaled using SDSM for three different RCP scenarios (i.e., RCP2.6, RCP4.5 and RCP8.5) for Delhi. Further, the effects of LULC changes on micro-climate in terms of changes in surface energy balance components and surface temperature have been studied using modelling of surface energy balance through SUEWS model. Also, efforts have been made to investigate the potential of different adaptation measures in terms of purposeful LULC alterations for favourably changing the SEB of an area, to contain the adverse effects of possible climate change.

Over the years (1973 to 2014) significant urbanization has been observed in both the selected study areas i.e., Palam and Safdarjung in Delhi. The results of Sen's slope, percentage change in mean & extreme average rainfall, temperature (annual/seasonal), and shift detection of trends revealed significant changes in micro-climate at both meteorological stations over the years (1969 to 2012). The downscaling results of three RCP scenarios are also indicating a significant increase in temperature in future over the selected study area in different scenarios and thus, indicating possible climate change in future also.

The SUEWS model has been conceptualized for the study areas and found to be successful in simulating the SEB. The model sensitivity to selected constants/coefficients has been analysed to determine the most significant parameters that could affect the performance of the SUEWS model. The results revealed that inverse relationship exists between albedo & emissivity with net all-wave radiation. The SEB fluxes have been found to be most sensitive to albedo and emissivity. Also, model results are found to be sensitive to the drainage parameter significantly. The SUEWS model calibration has been achieved by determining values of important input parameters at which simulated SEB components are closest to the reference SEB fluxes for the year 1999. Model results are validated by comparing simulated SEB fluxes and reference hourly SEB flux values at different temporal scales and also by comparing seasonal day time and night time values of fluxes. The model validation was found to be satisfactory.

The influence of LULC characteristics on micro-climate has been investigated in terms of changes in SEB fluxes for three scenarios: Scenario-A (actual conditions), Scenario-B (considering changes in LULC in different years and constant meteorology of base year) and Scenario-C (constant LULC and meteorology of the respective years). Also, extreme values of day time and night time fluxes and surface temperature have been determined.

Scenario-B has shown significant changes in fluxes and surface temperature extreme values as compared to other two scenarios. Comparing the results of three scenarios, Scenario-B results are indicating the relative contribution of urbanization in changing micro-climate in terms of adverse change in surface energy fluxes and surface temperature. Loss of vegetation and reduction in green areas, as a result of urbanization have contributed to increase in day and night time surface temperature. The relationship between LULC changes and surface energy fluxes have been established in terms of empirical relationship. Relationship equations have been developed using linear and non-linear regression techniques. The significant relationship has been found between annual day time as well as night time values of net all-wave radiation and storage heat flux for both areas.

Potential of different adaptation measures related to purposeful alterations in LULC classes in changing the surface temperature and SEB fluxes have been determined quantitatively by simulating the SEB corresponding to those adaptations. The relative influence of each proposed adaptation measure has been identified. Possible adaptation by partial conversion of barren/open land with areas with vegetation/grass and covering of roof tops with vegetation/grass have been found to be most effective adaptation measures in limiting the adverse changes in surface energy fluxes and surface temperature. A reduction of 0.17 to 0.21^{o}C in annual average maximum hourly surface temperature has been found from the optimum case of adaptation.

The study has been found to be successful in determining the relative contributions of LULC changes on micro-climate of an area. Also study is successful in demonstrating quantitatively that suitable adaptation measures related to LULC alterations are effective in limiting the adverse effects of climate change due to urbanization.

Keywords: Urbanization, Trend Analysis, Climate Change, LULC, SUEWS Model

ACKNOWLEDGMENTS

First of all, I would like to thank the Almighty for giving me strength and courage throughout the research work. This dissertation is an outcome of several years of research and would not have been possible without the help, cooperation and support of many people.

It is a great pleasure and privilege to convey my deepest gratefulness and immense admiration to my supervisor Dr. Mahesh Kumar Jat for his constant guidance, invaluable inspiration, encouragement, and continuous supports in taking the challenge of this research idea and give this thesis a final shape. His extensive knowledge, patience, motivation, and team building qualities are remarkable that provided me a very comfortable and healthy research environment. In my tough time, he was always there for me to encourage and support. I feel privileged to work with such a great personality and even could not have imagined having a better advisor and mentor for my Ph.D. journey.

Besides my supervisor, I would like to thank the rest of my thesis committee: Prof. Gunwant Sharma (HOD), Dr. Urmila Brighu, Dr. Sumit Khandelwal and Dr. Sanjay Bhatter for their insightful comments and encouragement, but also for the hard question which incented me to widen my research from various perspectives.

My sincere thanks also go to Dr. Santosh Pingle for supporting and sharing his expertise and always responding in detail to all my queries at any point of time which helped me a lot in my Ph.D.

I am grateful to Prof. Yaragatti, Director, MNIT Jaipur for providing an excellent research environment in the institute by strengthening the necessary facilities. I extend my deep thank to the people at Dean Academic Affairs' office, for their immense cooperation in academic activities.

I would like to acknowledge the Ministry of Human Resource and Development (MHRD), India for providing financial assistantship.

I am particularly grateful to my lovely juniors;

Ms. Shuchi Mala, her support and help are really appreciable. In my tough time, she always motivated and helped me in finding the solutions to the very complex problems without which it would have been very difficult for me to successfully complete my Ph.D. Ms. Ankita Saxena, her moral support and help during my thesis work. Ms. Arjita Saxena, her expertise and timely help are really grateful without which this study would never be perfectly accomplished. A special thanks to my friends, Jeripottu Gopala Rao, Nitish

Dhaulakhandi, Devendra Singh, Pravin Kumar Navin, Kuldeep and Deepak Prajapat for supporting me and being there for me whenever I was in need.

It's my pleasure to acknowledge the staff of Department of Civil engineering, MNIT Jaipur, especially Mr. Rajesh Saxena, Mr. Ramji Lal Ji, Rajender Jangid and Babu Ram for their constant support throughout my Ph.D.

I cannot express my heartiest gratitude in just a few words for my beloved wife Dr. Swagatika Jena who helped me in writing this thesis day and night, and for her constant encouragement and support throughout. Without her precious support in every front of my life, I would have never been able to complete my thesis.

At the end of my thesis I would like to thank all those people who contributed in many ways to the success of this study and made it an unforgettable experience for me. This thesis is the end of my journey in obtaining my Ph.D. This thesis has been kept on track and been seen through to completion with the support and encouragement of numerous people including my well-wishers, my family, friends and colleagues.

TABLE OF CONTENT

LIST OF FIGURES

LIST OF TABLES

ABBREVIATIONS USED

ASTER	Advanced Spaceborne Thermal Emission and Reflection Radiometer
AR5	Fifth Assessment Report
B	Built-up Fraction
CDD	Cooling Degree Days
CanESM2	Canadian Earth System Model 2
CMIP5	Coupled Model Inter-Comparison Project 5
CORINE	Coordination of Information on Environment
CCL	Commission for Climatology
CLIVAR	Climate Variability and Predictability
CCDC	Continuous Change Detection and Classification
CBL	Convective Boundary Layer
CTTC	Cluster Thermal Time Constant
ETCCDMI	Expert Team on Climate Change Detection, Monitoring and Indices
ETM+	Enhanced Thematic Mapper Plus
ERDAS	Earth Resources Data Analysis System
ESRI	Environmental Systems Research Institute
GCM	Global Circulation Model
GIS	Geographic Information System
ha	Hectare
hr	Hour
HDD	Heating Degree Days
IMD	India Meteorological Department
IPCC	Intergovernmental Panel on Climate Change
IMD	India Meteorological Department
ISBA	Interactions Between Soil Biosphere and Atmosphere
IDW	Inverse Distance Weighted
km	Kilometers
km^2	Kilometers square
LISS	Linear Imaging Self Scanner Sensor
LULCC	Land Use Land Cover Change

LULC	Land Use Land Cover
LUCY	Large Scale Urban Consumption of Energy
LAI	Leaf Area Index
LUMPS	Local-Scale Urban Meteorological Parameterization Scheme
LST	Land Surface Temperature
Max	Maximum
Min	Minimum
MMK test	Modified Mann-Kendall Test
MK test	Mann-Kendall Test
MLC	Maximum Likelihood Classifier
mm	Milimeters
MDV	Multidecadal Variability
MODIS	Moderate Resolution Imaging Spectro radiometer
NRSC	National Remote Sensing Centre
NARP	Net All-Wave Radiation Parameterization
NCAR	National Center for Atmospheric Research
NCEP	National Centers for Environmental Prediction
NDVI	Normalized Difference Vegetation Index
NOAA	National Oceanic and Atmospheric Administration
OMR	Observation Minus Reanalysis
OHM	Object Hysteresis Model
PMW	Pettit-Mann-Whiteney
Q*	Net All-Wave Radiation
QH	Sensible Heat Flux
QE	Latent Heat Flux
QS	Storage Heat Flux
RMSE	Root Mean Square Error
RCM	Regional Climate Model
RCP	Representative Concentration Pathways
RVRC	Road, Vegetation, Roof and Canyon
SEB	Surface Energy Balance
SDSM	Statistical Downscaling Model
SUEWS	Surface Urban Energy Water Scheme

SQ-MK test	Sequential Mann-Kendall test
SSE	Sum of Squared Errors
SNHT	Standard Normal Homogeneity Test
TEB	Town Energy Balance
Tsurf	Surface Temperature
Temp	Temperature
TM	Thematic Mapper
UTM	Universal Transverse Mercator (World Geodetic System 84)
Ud	User Defined
V	Vegetation Fraction
WRF	Weather Research and Forecasting
Wm^{-2}	Watt Per Meters Square
WMO	World Meteorological Organization
WCRP	World Climate Research Programmer
%	Percentage
^{o}C	Degree Celsius

CHAPTER 1

INTRODUCTION

1.1 GENERAL

Climate change is widely discussed and important issue for everyone throughout the world. "Climate change refers to a change in the state of the climate that can be identified (e.g. using statistical tests) by changes in the mean and/or the variability of its properties, and that persists for an extended period, typically decades or longer (IPCC, 2007). It refers to any change in climate over time, whether due to natural variability or as a result of human activity." As per the United Nations Framework Convention on Climate Change (UNFCCC), "Climate change refers to a change of climate that is attributed directly or indirectly to human activity that alters the composition of the global atmosphere in addition to natural climate variability observed over comparable time periods".

Recent studies and observations continue to indicate changing climate in terms of trends in representative meteorological parameters and these are consistent with warming driven by increase in atmospheric greenhouse gas concentrations. In 2015, the global average temperature was 0.77 ± 0.1°C above the 1961-90 average. The year 2016 was recorded as warmest year dating back to 1850 (Met Office, 2017). Although, climate change is occurring over a period of time, but its adverse effects appear in the form of changes in temperature (increase in day and night time), erratic variation in precipitation pattern (magnitude and distribution), extreme weather conditions (increase in extreme events), hydrological disasters (floods, droughts and storms), rise in sea water level, change in other hydrological phenomenon (runoff distribution, evaporation and evapotranspiration), adverse health effects (Dengue outbreaks, Malaria etc.), reduction in agricultural yields, stress on water resources, increase in heat waves etc. (Easterling et al., 2000; Prentice et al., 2001; Rogers et al., 2002; Perkins et al., 2012). There have been heat waves in Europe, India, Pakistan, and around the Persian Gulf in year 2015, which lead to a lot of casualties.

It is well established from many studies (Pingale et al., 2014, 2015) that effects of climate change are location specific. Climate change seems to be more pronounced, if assessed at local and regional scale as compared to global scale. At global scale its effects are generalised due to loss of regional and local details of the climate that are influenced by spatial and anthropogenic heterogeneities. A flood in Mumbai in year 2005 is the

example of localized effects of climate change. Climate change may be limited to a specific region, or may occur across the whole world because of several forcing agents/factors. They are categorized into two parts: external factors and internal factors. The examples of external factors are Milankovitch variations (Astronomical theory of climate variation) and solar activities (Hays et al., 1976; Ferraro et al., 2003) whereas internal factors are human induced changes like LULC changes, greenhouse gases (especially CO2), burning of fossil fuels, aerosols & clouds (Solid sulphate particles), anthropogenic changes (energy consumption, transport pollution and artificial heat sources like air conditioners) and natural activities (Volcanic eruptions and others) (Hansen, 2005). As per the IPCC (IPCC, 2001; 2007; 2014) cumulative impact of climate change forcing activities may result in increase in average air temperature by 4 oC by the year 2100.

In recent past, climate change have been assumed to be mainly due to increase in concentration of greenhouse gases (IPCC, 2001; 2007; Trenberth, 2007; Pachauri and Meyer, 2014) due to natural and anthropogenic factors; especially CO2 resulting from human activities. Recent research shown that LULC changes are one of the significant factors influencing climate adversely i.e., temperature trends in addition to greenhouse gases (Bonan, 1997; Gallo et al., 1999; Chase et al., 2000; Roy and Sparks, 2000; Feddema, 2005; Sidek et al., 2006; Christy et al., 2006; Mahmood et al., 2010; Pachauri and Meyer, 2014; Pingale et al., 2014, 2015; Cinar, 2015; IPCC Working Group III, 2015). In year 2014, IPCC concluded in its 5th assessment report (Pachauri and Meyer, 2014) that human emission and other activities have caused more than 50% of the observed increase in global temperature during 1951 to 2010. It has also been concluded that human influences (which also include LULC changes) on climate has contributed to observed changes in frequency and intensity of daily temperature extremes throughout the world, since middle of the 20th century. The number and intensity of climatic extremes are very sensitive to changes in the average conditions and adversely influencing the society. In many cases, human influence can be seen to have affected their severity or frequency (Pingale et al., 2014, 2015; Cinar, 2015; IPCC Working Group III, 2015). The relative differences in probability of extreme events can be assessed by comparing climate simulations all around world by only considering natural influences caused by human induced changes. The effects or problems of climate change in the urban areas are more dominant than rural areas (Stathopoulou and Cartalis, 2007; Huang et al., 2009; Pingale et al., 2014, 2015; Wang and McBean, 2014) because of more people under risk. Therefore, study of urban climate and impact of LULC changes on micro-climate of urban areas is important and vital.

1.2 URBANIZATION AND CLIMATE CHANGE

Urbanization plays an important role in human induced climate change at the regional scale through altered land-atmosphere interactions over urban areas. These changes will never come to an end due to ever increasing population and aspiration for better living. A strong linkage exists between urban growth and climate change (Lankao et al., 2008). Assessing the impacts of urbanization and land use change on surface temperature is a challenging task. Urban and semi urban areas experience intense LULC changes due to population growth, unplanned development, loss of vegetation and increase in impervious surfaces (Sharma and Tomar, 2010). Urbanization i.e., conversion of pervious and vegetative areas to impervious areas will lead to decrease in albedo and emissivity with consequent change in surface energy balance. The decrease in surfaces of high albedo & emissivity will leads to more storage heat flux, less latent heat, more sensible heat flux means change in surface energy balance causing increase in surface and atmospheric temperature, which will affect the thermal comfort of population in urban areas. The thermal discomfort of urban population will somehow lead to more energy consumption for cooling, which may further increase in pollution and greenhouse gases originating from power generation systems.

Several studies have attempted to assess the effect of urbanization and industrialisation on temperature trends (De and Rao, 2004a; Gadgil and Dhorde, 2005; Dash and Hunt, 2007; Dhorde and Gadgil, 2009; Sajjad et al., 2009; Tigga, Anuja, 2011) in different parts of the world. Temperature in urban areas has been found to be more by 2 to 5oC as compared to rural areas (Ackerman, 1985). Some studies have tried to establish a link between some of the intense man-made activities of urban industrial areas & temperature trends and found that increased density of population, LULC changes, reduction in the fraction of vegetative areas, exclusive use of fossil fuel combination, emission of waste heat from industries, automobiles & construction activities (roads, buildings, reservoirs, etc.), excessive use of air conditioning, changing level of aerosols, etc. responsible for such urban-rural contrast in temperature trends (Thapliyal and Kulshrestha, 1991; Goodridge, 1992; Fujibe, 1995; Bounoua et al., 2004; Oleson et al., 2008; Yilmaz et al., 2009).

Urbanization transforms natural landscape to artificial landscape and therefore alters radiative, thermal, roughness and moisture properties of the surface and the atmosphere above (Huang et al., 2006). Some of the urban locations are becoming increasingly vulnerable to natural hazards related to weather and climate (De and Rao,

2004b). With increase in urbanization this problem further magnifies, as more pervious areas would become impervious, which leads to decrease in vegetation and increase in temperature creating threats to the urban climate. Therefore, the study of urban climate is attracting significant attention in present days (Souch and Grimmond, 2006). Through various studies, it is well established that change in LULC can significantly influence meteorological characteristics like minimum & maximum temperature trends (Gallo et al., 1999; Hale et al., 2006, 2008; Cinar, 2015; Morris et al., 2015, 2016; Arrowsmith and Mandla, 2017). The impacts of historical LULC changes (such as deforestation, urbanization, and increasing or decreasing crop land) on surface temperature changes have been extensively studied and reported (Fu, 2003; Chung et al., 2004; De and Rao, 2004a; Roy and Balling, 2004; Gadgil and Dhorde, 2005; Dash and Hunt, 2007; Sajjad et al., 2009; Dhorde and Gadgil, 2009; Pongratz et al., 2010; Anuja, 2011; Yoshida et al., 2012, 2014; Noblet-Ducoudré et al., 2012; Cinar, 2015).

1.3 OPTIMUM ADAPTATION MEASURES

Interactions between LULC change and regional climate variations have been found to be complicated, yet at the same time very important for environmental adaptation and management (Pielke, 2005; Oleson et al., 2008; Rindfuss et al., 2008). LULC changes due to urbanization affect local surface energy balance by changing the amount of solar energy reflected, the magnitude & duration over which absorbed energy is released as heat, and the amount of energy that is diverted to non-heating fluxes through evaporation consequently impact local climate adversely. To control these adverse effects of LULC changes, various measures have been proposed. Since, mitigation of LULC changes is not possible, there is a need for effective adaptation measures to minimize them. Today, adaptation measures are very critical because increasing demands of people for better facilities is causing and will cause continuous change in LULC. One of the most widely used adaptation measure reported is increase in vegetation in urban areas which reduces both urban air and land surface temperature (Kurn et al., 1994; Weng and Yang, 2004; McPherson et al., 2011; Gillner et al., 2015; Larsen, 2015).

Other measure include wetting streets and roofs, open water bodies and fountains, high albedo pavement instead of asphalt, constructing optimal shading in buildings, compact building and trees, warning systems, monitoring and inspection. Such changes in land surfaces will affects the local surface energy balance. Till now, qualitative methods have been proposed to minimize these adverse effects but these methods are incapable to

determine how much change is required to minimize a specified quantity of heat flux components. Therefore, quantitative methods for adaptation are required to overcome this limitation (Grawe and Ã, 2007; Baltas, 2009; Lindley and Levermore, 2014; Klemm and Lenzholzer, 2015). Therefore, understanding the link between urbanization and micro-climate is vital for sustainability urban environmental and to determine effective design strategies, e.g. altering the LULC like increasing vegetation and enhancing irrigation regime, using more reflective paved surfaces and materials in order to improve urban climate. The knowledge of how to purposefully manipulate the SEB by changing urban land cover is crucial to urban climate adaptation.

Therefore, to understand the climate change considering effects of LULC at the regional and local scale is very important to plan and implement the suitable mitigation or adaptation measures. Understanding of relative contribution of LULC in climate change using appropriate techniques/approach is also very important to plan and implement corrective measures like adaptation.

1.4 STATEMENT OF THE PROBLEM

Several methods have been developed to understand and assess the climate change such as statistical methods (trend analysis), simulation models (GCMs and RCMs), downscaling global climate projections (statistical and dynamical downscaling), surface energy balance based methods, water balance and terrestrial carbon balance based approaches. Spatial resolutions of GCMs are usually quite coarser because of their significant complexity and need to provide multi-century integrations. This results in the loss of regional and local details of the climate that are influenced by spatial heterogeneities missing from these models. Therefore, GCM simulations of local climate on spatial scales smaller than grid cells are often poor, especially when the area has a complex topography (Schubert, 1998; Timbal and McAveney, 2001; Liu et al., 2011; Li et al., 2013; Zhang et al., 2014, 2017; Halder et al., 2016). Several studies have shown significant climate impacts of LULC change through sensitivity experiments (Bonan, 1997, 1999; Gordon et al., 2005; Pielke, 2005; Findell et al., 2009; Kumar et al., 2010; Avila et al., 2012; Kharol et al., 2013). However, such studies are based on using GCM output with different LULC forcing in different future scenarios which have very high level of uncertainties and may not be suitable in determining relative contribution of LULC changes in changing the climate (Pitman et al., 2009; Noblet-Ducoudré et al., 2012; Deng et al., 2013; Mimura et al., 2014). In many regions, GCMs may significantly underestimate or overestimate current

temperature and precipitation. Further, most of these models do not consider the impact of LULC change explicitly while simulating the climate. So far, not much work has been done on identifying a regional radiative forcing and its response in GCM models. It is not very clear how to decide which method should be adopted to diagnose a regional forcing and its response for the observational record. Regional forcing can lead to a global climate response and the global forcing can be associated with the regional climate response. Impact of urbanization and LULC changes on climatic variables have been studied through comparative study of climatic trends for urban and rural meteorological stations also (Karl et al., 1988a; Easterling et al., 1997; Hansen et al., 2013; Pingale et al., 2014, 2015; Peng et al., 2016) and satellite imagery (Gallo et al., 1999; Peterson et al., 1999).

In recent studies, remote sensing data and geo-spatial techniques have been used to investigate the relationship between LULC change and land surface temperature using different analysis methods and found positive correlation between surface temperature and impervious surfaces (Carlson and Arthur, 2000; Chen et al., 2006; Xiao and Weng, 2007; Cinar, 2015). In few studies, the negative correlation has also been found between land surface temperature and vegetation index (NDVI) and cooling effect observed from vegetative areas (Lin et al., 2009; Weng, 2009; Araya and Cabral, 2010; Dong et al., 2013). In few studies, the positive correlations were found between air temperature trends (decadal) and LULC decadal changes derived from satellite data using statistical techniques like regression analysis (Cinar, 2015).

In few studies, efforts have been made to develop statistical models/functions to co-relate LULC change and local temperature response. Such statistical models mimics the response of a complex climate change model to a given forcing change (Murphy et al., 2007; Hanasaki et al., 2008; Iizumi et al., 2009; Yoshida et al., 2014). Through studies of urban heat islands also impacts of LULC impacts on temperature have been discussed (Karl et al., 1988b; IPCC, 2001; Peterson and Schwing, 2003; IPCC, 2007; Martin L. et al., 2007; Rogan et al., 2013; Morabito et al., 2016; Peng et al., 2016). Looking at the importance of this issue National Research Council in USA has recommended to include LULC for climate change research (Jacob et. al., 2005).

In last few decades, many authors have used Observed Minus Re-analysis (OMR) approach to estimate impact of LULC changes by commuting difference between the trends of surface temperature observations and reanalysis datasets (Kalnay and Cai, 2003; Zhou et al., 2004; Frauenfeld et al., 2005; Lim et al., 2005; Kalnay et al., 2006; Pielke et al., 2007; Lim, 2008; Nunez et al., 2008; Mahmood et al., 2010; Wang et al., 2014; Feng et al.,

2016). It is found in previous OMR approach based studies that warming is associated with urbanization (Karl et al., 1988a; Arnfield, 2003; Zhou et al., 2004; Hale et al., 2006, 2008; Mahmood et al., 2010; Huang et al., 2013; Qian, 2014; Wang et al., 2014). Most of these studies are qualitative in nature where LULC changes were related statistically with change in representative meteorological characteristics.

LULC changes affect surface climate as a result of change in surface energy, water balance components and carbon with in the atmosphere, ecosystem and soil (Kalnay and Cai, 2003). These urban climate effects are due to the differences in the budgets of heat, mass, and momentum between the city and its pre-existing landscape (Oke and Cleugh,1987). This transition will have an impact on the surface energy balance through the alteration of surface properties affecting net all-wave radiation and heat storage, and consequently affects local climate. It has been noted that land surface and atmospheric alteration by urbanization leads to the development of distinct urban climates (Landsberg, 1981; Oke and Cleugh, 1987; Middel et al., 2012; Cinar, 2015). Surface energy and water balance based distributed methods have been used in recent past to investigate effects of direct and indirect LULC change on climate (Copeland and Pielke, 1996; Betts, 2001; Pielke et al., 2002; Sr et al., 2003; Feddema, 2005; Järvi et al., 2011; Middel et al., 2012; Kleczek et al., 2014; Liu et al., 2014). To understand how urban morphology influences local climate (energy and water exchanges), it is necessary to undertake detailed investigations of local meteorology including water and energy balances in conjunction with an understanding of urban surfaces i.e., land use/land cover. A variety of models and methods have been developed for computing the surface energy fluxes through using energy and water balance approaches (Holtslag and Van Ulden, 1983; Grimmond and Oke, 1995, 1999; Best, 1998; Crawford and Bluestein, 2000; Järvi et al., 2011; Middel et al., 2012). The limitation of these models and methods is that they consider lumped effect of LULC or few others only consider one or more fluxes. In few studies, complete energy balance have been undertaken at suburban residential sites (Grimmond and Oke, 1995, 1999; Middel et al., 2012; Sanchez-Lorenzo et al., 2015). However, how LULC changes are affecting surface energy balance components with respect to climate change has not been discussed well.

In weather forecast models, the fluxes are generally parameterized in terms of variables predicted by the model. A number of studies were carried out over cites but there is still lack of knowledge about exchange process and partitioning of energy. Nevertheless, our understanding of the energy and moisture flux transfer and their role in

mesoscale/regional climate models and associated biophysical processes involved in the generation of urban climates is limited. Direct observations of energy and mass exchanges in urban areas have been collected only in a limited number of cities, with a small range of surface morphologies and climates (Budyko, 1972; Oke, 1988; Grimmond and Oke, 1991; Heisler et al., 1994; Christen and Vogt, 2004).

As discussed above, several methods have been explored to determine and understand the effects of LULC changes on climate change. The limitations of the existing methods are; data limitation in statistical methods, coarse resolution problem in GCM models, non-inclusion of LULC changes explicitly, forcibly downscaling of average data of global scale to the regional scale and the absence of quantitative relationship between LULC changes and climate. Current land surface and atmospheric models are suitable to determine few impacts of land cover change (predefined vegetation cover). However, uncertainties exist in representing vegetation dynamics (gradual transition) and this issue needs to be addressed. There are few models which consider LULC changes and their effects on climate but still there is a need to evaluate how efficiently these models represent the true complexity of the land surface. For modelling applications, it is important to classify land use at appropriate scale. The developed models do not use land use classifications directly and in place of land use classification these models use fundamental physical parameters such as heat capacity, roughness lengths, and canopy resistance. Thus, available models are inefficient in considering LULC changes over the period and their effects on climate at local and regional-scale have not been investigated efficiently.

Fundamental work is required to develop robust relationships between the LULC and key surface energy balance (fluxes) components. This information is important for decision and policy makers operating at a range of spatial scales (properties, blocks, neighbourhoods, cities) relating to the provision of water or imposing water restrictions, mitigating or responding to extreme conditions for human comfort, air pollution prediction and exposure alerts. Therefore, to understand the effect of LULC changes on climate at different scales and to quantify their relative contribution in changing climate in terms of important climatic parameter like temperature, estimation of surface energy components (Fluxes) corresponding to different LULC changes is the need of the hour.

With increase in developmental demands over the period LULC changes have taken place and this is to be continued in near future to meet the development demands of ever increasing population (Suribabu et al., 2012; Shamir et al., 2015). Therefore, after quantification of relative impact of LULC changes on climate at different scale, suitable

mitigation or adaptation measures needs to be identified and implemented to reduce the adverse impacts of such a climate change (Musakwa and Niekerk, 2013; Solecki et al., 2015). It is necessary to use mitigation and adaptation together to deal with the effects of climate change. Such adaptation measures are required more in urban area where climate change impacts are more pronounced and more population is under risk of adverse consequences. To reduce surface temperature in urban areas, some adaptive measures can be taken such as shading of ground and buildings, covering of ground by vegetation, changing colour of blacktop roads, covering roof tops with grass, partial covering of parking lots and paved areas with pervious material and vegetation. Due to the limited resources no individual can adopt optimum adaption measures to maintain surface energy balance at equilibrium state to restrict increase in surface/air temperature. Investigators have suggested several methods to minimize the effects of climate change in qualitative manner (Grundström and Pleijel, 2014; Skelhorn et al., 2014; Klemm et al., 2015) but no one have suggested to establish quantitative relationships between effects of climate change and their radiative forces, which is necessary to evaluate the effectiveness of mitigation or adaptation measures. Therefore, some relationships between effects of climate change in term of change in surface energy balance with respect to change in radiative forcing in a quantitative manner is necessary to adopt optimum mitigation and adaptation measures to minimize the climate change effects.

Therefore, present study is aimed to understand the effects of LULC changes on micro-climate in terms of changes in surface energy balance components (fluxes) & surface temperature through modelling of surface energy balance. Surface Urban Energy and Water Balance Scheme (SUEWS) model (Grimmond et al., 1986; Grimmond and Oke, 1991; Järvi et al., 2011; Ward et al., 2016) has been used to model the surface energy balance of the selected study areas (Palam and Safdarjung areas in Delhi, India) to investigate the impacts of LULC on micro-climate representative surface energy fluxes. Further, efforts have been made to investigate the potential of different adaptation to contain the adverse changes in surface energy fluxes and temperature due to change in LULC.

1.5 RESEARCH QUESTIONS

Therefore, present study is proposed to address following research questions.

- Whether climate is changing in urban areas and its effects are more pronounced at local scale?

- Is LULC change is (a type of anthropogenic radiative climate change forcing) contributing to the change in climate in general and micro-climate particularly?
- How change in LULC will alter the surface energy fluxes and what is their relationship?
- How much is the relative contribution of LULC change in alteration of micro-climate of an urban area in terms of change in surface energy balance fluxes and surface temperature?
- What are the possible adaptation measures which can be explored in urban areas to contain adverse changes in surface energy fluxes on account of change in LULC?
- How much effective are the different selected adaptation measures in limiting the adverse changes in surface energy fluxes?

1.6 RESEARCH OBJECTIVES

Present study is aimed to understand the effects of LULC changes on climate and to identify optimum adaptation measures in controlling adverse impacts of climate change in terms of indicative meteorological parameters like temperature through surface energy balance modelling. Specific objectives of the study are -

i) Assessment of climate change at different temporal scales using appropriate methodology and meteorological data.
ii) Identification of impact of LULC changes on climate in terms of indicative meteorological parameters or phenomenon.
iii) Assessment of relative impact of LULC on climate through indicative meteorological parameter or phenomenon.
iv) Identification of various adaptation measures to deal with adverse climate change effects due to LULC specifically in urban and semi urban areas.
v) Determination of optimum adaptation measures and their relative impact on climate change indicative meteorological parameters or phenomenon.

1.7 ORGANISATION OF THESIS

This thesis has been arranged in nine chapters as described below:

Chapter one provides background for the research and the objectives which are carried out in this research work.

Chapter two presents the literature review related to assessment of climate change at different temporal scales and on extreme events in changing climate in urban areas. The

reviews on changes in LULC and its impacts on climate in urban areas has also been presented. This chapter also covers the definition of climate change and surface enegy balance modelling to simulate LULC changes in changing climate, times series analysis, downscaling of climatic variables to the local scale. Further, possible adaptation measures are also discussed related to LULC changes in reducing the adverse impacts of climate change in urban areas.

Chapter three describes the study area and used database information. The general characteristics of study area have been described in detail. Types of data required for this study are also presented in this chapter.

Chapter four presents preparation of LULC maps and extraction LULC information required for the conceptualisation of SUEWS model.

Chapter five presents methodology adopted for the assessment of climate change. Chapter also presents details of the surface energy balance modelling and methodology followed to determine the relative contribution of LULC in changing the micro-climate of urban areas in terms of change in SEB constituents. Further, chapter presents methodology used to investigate the potential of different adaptation measures in favorably altering the SEB fluxes.

Chapter six presents the results of assessment of climate change at different temporal scales i.e., annual, seasonal, monthly mean and extreme events in the Delhi region using the statistical analysis techniques. Further, results of the future climate projection carried out through downscaling of GCM outputs using SDSM model under three RCP scenarios (i.e. RCP 2.6, RCP4.5 and RCP 8.5).

Chapter seven presents the results and discussion of the generalised modelling framework of surface energy balance for quantification of the change in heat fluxes changes due to change in LULC over the years. Chapter presents results of the SEB modelling carried out for three different Scenarios formulated to investigate the relative impacts of LULC changes in changing the SEB of the selected study areas. Further, Chapter presents development of empirical equation to establish quantitative relationship between SEB constituents and LULC fractions.

Chapter eight presents the results of SEB simulations carried out to determine the potential of different adaptation measures in terms of purposeful alteration in LULC to favourably change the SEB fluxes.

Chapter nine comprises the summary, important conclusions drawn from the study and future scope of the work.

CHAPTER 2

REVIEW OF LITERATURE

2.1 INTRODUCTION

Present study is aimed to understand the effects of land use land cover (LULC) changes on climate in terms of long-term changes in representative meteorological characteristics and change in surface energy balance of an area, which indicate possible change in climate. Detailed literature review has been done to understand the present state of the knowledge of the selected research area and to define the research problem for the present work. Literature review helps in understanding the different aspects of the selected research topic like climate change and its assessment methods, LULC and its impact on micro-climate of an area specifically urban, assessment of the relative impact of LULC changes on micro-climate of urban areas and possible adaptation measures related to LULC changes in reducing the adverse impacts of climate change in urban areas.

To have an ease in understanding, literature review has been classified into following categories; (1) climate change assessment (ii) urbanization (LULC changes) and its impact on climate (iii) adaptation measures. Present state of the knowledge related to these topics and contributions made by various researchers have been discussed below in detail and research issues have been identified.

2.2 CLIMATE CHANGE ASSESSMENT

2.2.1 Climate Change Assessment using Trend Analysis

Climate change and its adverse effects are considered as important issues and lot of emphasis have been given to assess climate change using variety of techniques and models. It is well established that climate is changing and a variety of factors and forces which include pollution, anthropogenic activities and natural phenomenon are responsible. LULC changes are also one of the important human induced climate change forcing. Different methods and techniques used in recent past for assessment and monitoring of climate change which includes time series analysis of historical climatic data, surface energy balance approach, land surface temperature (LST) based methods, climate simulation models, Regional Climate Model (RCMs), machine learning based methods and regression analysis based methods.

In recent past, various trend analysis techniques are used to assess the climate variability in terms of changing trends in climatic time series (Basistha et al., 2007, 2008; Ezber et al., 2007; Kampata et al., 2008; Motiee and McBean, 2009; Sahoo and Smith, 2009; Patra et al., 2012 ; Pingale et al., 2013, 2014, 2015). In the present section, recent developments in the area of climate change assessment using time series analysis has been discussed through representative case studies and research articles. Available trend analysis techniques i.e., Mann-Kendall (MK) test, Modified Mann-Kendall (MKK) test, Pettitt-Mann-Whitney (PMW) test, Sen's slope estimator are summarized and discussed with few case studies.

Parthasarathy and Dhar (1974) analyzed secular variations in regional rainfall trend in India over a period of 1901-1960. The study found a positive trend in yearly rainfall in Indian Western Peninsula through central parts of India. In addition, increasing rainfall trend was observed in some sub-divisions like Punjab, Himachal Pradesh, and Assam, although, only in south Assam rainfall trend was found negative.

Roy et al. (1987) studied the trends of regional variations and periodicities of annual rainfall in Bangladesh for 32 years between 1947 and 1979 at 30 meteorological stations. The study revealed that most of the stations follow a normal trend for yearly rainfall. In addition, both the trends positive and negative were found for annual rainfall.

Oron et al. (2002) studied the climatic trends for Thar region (India-Pakistan-Afghanistan) to assess the climate change. Study results revealed that average precipitation has decreased by 5 to 25% due to climate change in the region. In addition, annual average increase in temperature have been found to be 1.5 to 2.25 ^{o}C in winter and from 2 to 2.5^{o}C in summer. The study revealed changes in precipitation and temperature in some parts of arid and semi-arid regions. The models and empirical considerations suggested that frequency, intensity, and area of tropical disturbances may increase.

Gadgil and Dhorde (2005) have studied temporal variation in temperature over Pune city of India, during the period 1901–2000. The long-term change in temperature has been evaluated by MK rank statistics and linear trend analysis technique. The analysis revealed a significant decrease in mean annual and mean maximum temperature. This decrease in temperature was more pronounced during the winter season, the study results revealed that a significant cooling trend in mean annual temperature exist, which is more predominant during the winter season. Summer season have also showed significant cooling trend due to a decrease in maximum temperature. The result indicated a significant decrease in winter temperature by 0.01^{o}C.

Arora et al. (2005) have detected the increasing trends in temperature at annual and seasonal temporal scale using the MK test at global and regional scales. It was observed that annual mean temperature, mean maximum temperature and mean minimum temperature have increased at the rate of 0.42, 0.92 and 0.09 ^{o}C (100 years)-1, respectively. On a regional basis, stations of southern and western India show a rising trend of 1.06 ^{o}C and 0.36 ^{o}C (100 years)-1, respectively, while stations of the north Indian plains show a falling trend of 0.38 ^{o}C (100 years)-1. The seasonal mean temperature had increased by 0.94 ^{o}C (100 years)-1 for the post-monsoon season and by 1.1^{o}C (100 years)-1 for the winter season. The results proved that climate is changing.

Basistha et al. (2007) studied spatial trends of rainfall over Indian sub-divisions over a period of (1872-2005) using time series analysis techniques i.e., MMK test. The results indicate decreasing trends of rainfall over north India excluding Punjab, Haryana, West Rajasthan, Saurashtra and increasing trends in the South India excluding Kerala and Madhya Maharashtra. Further, MMK test and PMW test were used to detect the shift in rainfall pattern from the year 1901 to 1980. The increasing trend of rainfall was found up to the year 1964 and decreasing trend during 1965-1980 years. It was concluded in the study that more research is required to assess the spatial patterns of trends of other climatic variables minimum, average and maximum temperature, relative humidity, wind speed, ET, number of rainy/wet days and their inter-relationship including trends of annual and seasonal climatic parameters.

Ezber et al. (2007) used statistical and numerical modelling technique to determine the trends in temperature for Istanbul to find the effect of urbanization on climate. The MK test was used to determine the significant temperature trends and the years in which changes were started. The effect of urbanization on climate was studied using the mesoscale atmospheric model. Both the statistical and atmospheric models have found significant warming in the atmosphere over urbanized area. The MK test found a significant positive trend in average monthly minimum temperature over urban and rural areas. The seasonal analysis shows that the effect of urbanization was more pronounced in the summer season.

Gowda and Manjuantha (2008) studied the climatic trends over local region of Devangere district for a period of 32 years using statistical analysis techniques. The climatic parameters i.e. rainfall, relative humidity, maximum temperature, minimum temperature, sunshine hour and wind speed were analyzed to assess the climate change. The statistical analysis showed that such a small data set may not represent the correct

picture of the climate change and requires long-term data. Similar studies were also carried out at local region of Roorkee (Yadav et al., 2014).

Pal and Al-Tabbaa (2009) have investigated the long-term trends and variations of the monthly maximum and minimum temperatures and their seasonal fluctuations for various climatological regions of India. The magnitude of the trends and their statistical significance were determined by parametric ordinary least square regression techniques. The results showed that the monthly maximum temperature increased, though unevenly, over the last century. Minimum temperature changes were more variable than maximum temperature changes, both temporally and spatially, with results of lesser significance. Study indicates climate variability for India over the last century.

Krishna Kumar et al. (2009) studied the temporal variations of rainfall at different temporal scales i.e., monthly, seasonal, and annually over Kerala, India during 1871 to 2015 using Man-Kendall rank statistics and linear trend. Results indicates significant decrease in southwest monsoon rainfall while increase in post-monsoon season. No significant trends were found for winter and monsoon seasons. Significant decreasing trends were reported for June and July months while increasing trends were observed for January to April months.

Schaefer (2007) presented temperature time series analysis results for the Japan and found out that climate of Japan is changing. A comparison between temperature time series of Japan was compared with global trends. Statistical methods like Gaussian binominal low-pass filter, trend analysis (linear regression model) including the trend-to-noise-ratio have been used for the trend analysis. Results revealed that annual mean temperature has increased from 0.35 to 2.95 ^{o}C in last 100 years. Also, seasonally increasing trends were observed for winter and summer seasons.

Sahoo and Smith (2009) have analysed the trends in several hydro-climatic variables in the rapidly urbanizing semi-arid San Antonio River Basin. The Mann-Kendall non-parametric test was used to detect change and significance of trend was determined using permutation method. Annual and seasonal trends in precipitation were determined and its impact on regional steam flows was also determined. A greater number of significant trends were observed in all hydro-climatic variables during all seasons and significant positive trends of precipitation were found in the winter season. Effect of urbanization was clearly visible in the results, in urbanized areas base flow to the streams have reduced significantly.

Goenster et al. (2015) have reported significant increasing trends in annual rainfall in most of the districts of Chhattisgarh. The MK, MMK (nonparametric) and Spearman's rho test (parametric) were used for trend detection. The study revealed that the northern parts of the district have shown the highest annual rainfall variability, and the eastern and southwestern parts have declined variability.

Mohsin and Gough (2010) have studied the long-term trends (31-162 years) of temperature change for Greater Toronto Area (GTA) in Canada. The study investigated annual and seasonal time series for a number of urban, suburban, and rural weather stations. Non-parametric statistical techniques such as, MK test and Theil-Sen slope estimation were used primarily for the assessment of significance and detection of trends. In addition, sequential Mann test was used to detect any abrupt change in climate. Statistically significant trends for annual mean and minimum temperatures were noticed for almost all stations. It was concluded in the study that urbanization has contributed an increase of annual mean temperature during the past three decades.

Kumar et al. (2010) have studied monthly, seasonal and annual trends of rainfall for 30 sub-divisions in India using monthly data series of 135 years (1871–2005). Half of the sub-divisions showed increasing trend in annual rainfall, but for only three (Haryana, Punjab and Coastal Karnataka), this trend was statistically significant and for the whole India, no significant trend was detected for annual, seasonal, or monthly rainfall.

Kumar and Jain, (2010);Kumar et al. (2010) performed time series analysis for rainfall/rainy days at annual and seasonal temporal scales for three stations of Kashmir for two common periods from 1903 to 1982 i.e. 80 years and from 1962-2002 i.e. 41 years. Different statistical techniques were used for the trend analysis. The decreasing trend in winter rainfall was found to be statistically significant (95% confidence) at respective stations. No significant trends were observed at seasonal and annual scales.

Li et al. (2011) analyzed the impacts of human-induced land use and climate changes on hydrological processes. The MK test was used to identify the long-term monotonic trends in precipitation and temperature for the period of (1980–2005). The results suggest no significant change in annual precipitation and a significant increase in annual temperature, particularly in February, April, July, and September. Hydrological simulations have shown that the influence of climate change on hydrological processes was stronger than those of LULC change.

Subash et al. (2011) have analyzed observed trends in extreme rainfall indices during monsoon months as well as seasonally at four stations located in different agro-

ecological zones of Bihar, namely Samastipur (zone-I), Madhepura (zone-II), Sabour (zone-IIIA) and Patna (zone-IIIB). The MK test was used to determine the vulnerability of extreme rainfall indices on productivity using simple correlations. All the sites showed an increasing trend in number of days with a rainfall of 10.0 cm or more (very heavy precipitation event) during monsoon season. Results showed a significant increasing trend of 0.4 and 0.6 cm day/decade, respectively during monsoon and annually.

Pal and Al-Tabbaa (2011) have assessed seasonal precipitation trends in India using parametric and non-parametric statistical techniques for the period of 1954–2003. It was shown that there were decreasing trends in the spring and monsoon rainfall and increasing trends in the autumn and winter rainfalls.

Tabari et al. (2011) performed the trend analysis of rainfall and temperature for west, south and southwest Iran for the period of 1966–2005. Climatic trends were determined from the slope of regression lines and statistical significance was determined using Mann-Kendall, Mann-Whitney rank statistics test. The main aim of this study was to investigate trends in maximum and minimum air temperatures in the annual, seasonal and monthly time-scales for 19 synoptic stations during period 1966–2005. Results concluded that the majority of the trends in the annual, seasonal and monthly Tmax and Tmin time series are increasing during the last decades. On average, the magnitudes of the significant positive trends in annual Tmean, Tmax and Tmin were (+) 0.412, (+) 0.452 and (+) 0.493 ^{o}C per decade, respectively.

Naidu et al. (2011) determined the variability of summer monsoon over India using the sub-divisional rainfall record for the period (1871–2012). It was observed that the rainfall activity over India during the last three decades had decreased. It was found that the summer monsoon rainfall had decreased during the recent three decades of the global warming era.

Patra et al. (2012) have detected the rainfall trends in the twentieth century using the parametric and nonparametric statistical trend analysis tests for temporal variation in monthly, seasonal and annual rainfall was studied for the Orissa state using the data from 1871 to 2006. The analysis revealed a long-term insignificant declining trend in annual as well as monsoon rainfall, although increasing trend in post-monsoon season in winter and summer seasons showed an increasing trend.

Duncan et al. (2012) analysed the temporal trends during year 1951 to 2007 in annual Indian summer monsoon (ISM) precipitation, frequency of severe drought and onset dates of ISM using quarter degree daily gridded data of precipitation and Mann-

Kendall test. A greater extent of the country experienced significant trends ($p<0.05$) of increasing inter-annual variation rather than simply increasing or decreasing trends in annual precipitation and onset date of the summer monsoon.

Jhajharia et al. (2012) have investigated the trends in rainfall, number of rainy days and daily maximum rainfall using the Mann-Kendall non-parametric test at twenty-four locations of for Assam, India. The trends were statistically confirmed by both the parametric and non-parametric methods and the magnitudes of significant trends were obtained through the linear regression test. The results presented normal trends either increasing or decreasing.

Jain and Kumar (2012) have studied the trends of rainfall and temperature for India at river basin scale. Decreasing trends were observed for annual rainfall in 15 basins and significant decreasing trends in one basin. Increasing trends were found in 6 basins with significant trend in one. Increasing trends were observed for most of the locations. Mixed i.e., increasing/decreasing trends were observed for annual minimum temperatures in different basins.

Duhan et al. (2013) studied the spatial and temporal variability of precipitation at 45 districts of the Madhya Pradesh, India over a period of 102 years (1901–2002) on the annual and seasonal basis. Mann–Kendall test and Sen's slope estimator were used to detect monotonic trends and magnitude of change over time on the annual and seasonal basis. The results showed a shift in rainfall pattern due to increase and decrease in annual precipitation.

Jain et al. (2013) reviewed all the studies relating to trends in rainfall, rainy days and temperature all over India. Sen's non-parametric estimator of the slope was used to estimate the magnitude of the trend. The statistical significance of this test has been assessed by the Mann–Kendall test. It was concluded that there were differences in the results of the various studies of trend analysis, and there was no clear picture available for rainfall trend. Similarly, trends in temperature, the mean maximum temperature series showed a rising trend at most of the stations.

Sonali and Kumar (2013) studied the trends of annual, monthly and seasonal temperatures (Tmax, Tmin) for India for three-time periods 1901–2003, 1948–2003 and 1970–2003. Time series of extreme temperature of India at different spatial scale i.e., whole country, homogeneous regions viz. western Himalaya, northwest, northeast, north central, east coast, west coast and interior peninsula were analyzed and trends are

determined. Sequential MK test was used. Results indicates definite trend in minimum temperature at all spatial and temporal scale in last three decades.

Gocic and Trajkovic (2013) analysed annual and seasonal trends of seven meteorological variables for twelve weather stations in Serbia during 1980–2010. Gocic, used non-parametric Mann-Kendall and Sen's methods to determine whether there was a positive or negative trend in weather data with their statistical significance. In this study, the increasing trends were indicated in both annual and seasonal minimum and maximum air temperatures series. The relative humidity decreased significantly in summer and autumn, although the vapor pressure had a significant increasing trend in spring, summer, and autumn. Besides, no significant trends were detected in summer and winter precipitation series.

Pingale et al. (2014) have studied the extreme annual daily rainfall and temperature trends at different spatial and temporal scales for all the 33 urban centers of the arid and semi-arid state of Rajasthan. Mann–Kendall test and Sen's slope estimator statistical trend analysis techniques, were used to examine trends during 1971–2005 at the 90% significance level. Both positive and negative trends in mean and extreme events of rainfall and temperature were observed for different urban centers. The spatial variations of the trends in mean (seasonal and annual temporal scale) and extreme annual daily rainfall and temperature were also determined using the inverse-distance-weighted (IDW) interpolation technique. The results of IDW interpolation were found to be helpful in identifying trends and variability in mean and extreme rainfall and temperature in space and time.

Zarenistanak et al. (2014) presented results of trend analysis and change points detected for precipitation and temperature (mean, maximum, and minimum) at annual and seasonal temporal scales for a duration of 57 years (1950-2007). Statistical tests including Pettitt's test, Sequential Mann-Kendall test (SQ-MK test) and Mann-Kendall rank test (MK-test) were used for the analysis. The results obtained for precipitation series indicated that most stations showed insignificant trends in annual and seasonal scale however, significant trends were observed during the winter season. Results indicated significant increasing trend for summer and spring seasons. The results of change point detection indicated that most of the positive significant mutation points in TM, TMAX and TMIN began in the 1990s.

Pingale et al. (2015) assessed the effect of climate change at different spatial and temporal scale i.e., regional and local through time series analysis of temperature and

precipitation at different temporal scales in 35 years using statistical trend analysis techniques like MK, MK–PW, MMK test and Pettitt–Mann–Whitney (PMW). Analysis was carried out for the Rajasthan State, Ajmer district and Ajmer city scale. Study indicates significant warming trends in annual and seasonal average temperature, when assessed at a fine spatial resolution (Ajmer city) as compared to a coarser spatial resolution (Ajmer District and Rajasthan State resolutions). Increasing trend was observed in minimum, mean and maximum temperature at all spatial scales; however, trends were more pronounced at a finer spatial resolution (Ajmer city). Results indicates contribution of LULC change and several other local anthropogenic activities in changing climate.

Singh and Kumar (2015) studied temporal variation in temperature over Junagadh (Saurashtra Region) of Gujarat, India, during the period of 1980-2011. The long-term change in temperature had been evaluated by Mann-Kendall rank statistics and linear trends. Authors studied the temperature parameters and observed cooling trends not significant at any level but indicated a significant slight decrease in winter temperature at 0.01^{o}C. This suggested that the last decade had witnessed a phenomenal epoch in temperature series, leading to a decreasing trend from non-significant to significant.

Singh et al. (2015) studied the daily extreme temperature indices over Sutlej Basin, N-W Himalayan Region of India over a period of 1970 – 2005. Fourteen extreme indices for temperature as specified by the World Meteorological Organization (WMO), Commission for Climatology (CCL)/Climate Variability and Predictability (CLIVAR) Expert Team on Climate Change Detection, Monitoring and Indices (ETCCDMI) were derived using RClimDex software. Linear regression method was used to determine trends in annual and monthly extreme indices of temperature. Study indicates rise in diurnal temperature range for the basin as a whole.

Taxak et al. (2014) analyzed the gridded rainfall data to study long-term spatial and temporal trends on annual and seasonal scales in Wainganga river basin located in Central India during 1901–2012. After testing the presence of autocorrelation, Mann-Kendall (Modified Mann-Kendall) test was applied to non-auto correlated (auto correlated) series to detect the trends in rainfall data. Results of grid points show a significant decreasing trend in monsoon rainfall and non-significant in pre-monsoon and winter rainfall over the last 112 years.

Pingale et al. (2016) studied the trends and variations in climatic variables i.e., rainfall, wet day frequency, surface temperature, cloud cover, and reference and potential evapotranspiration at seasonal and annual temporal scales for Ajmer district in Rajasthan

state of India using parametric and nonparametric statistical techniques i.e., the MK and MMK tests over a period of 100 years. Results indicated no significant trends in seasonal and annual rainfall, however, noticeable trends were observed in day frequency, surface temperature, cloud cover, and reference and potential evapotranspiration during non-monsoon season.

Bera (2017) analyzed and reported the results of rainfall trends for Ganga Basin of India during a period of 1901 – 2000. Statistical trend analysis techniques like Mann-Kendall test and Sens slope was used using rainfall data of 236 districts. Study indicates decreasing trends of precipitation at different temporal scales i.e., seasonal and annual in most of the districts.

It can be concluded from the above-mentioned studies that statistical trend analysis techniques are suitable method of climate change assessment including climate variability for an area in term of trend in representative climatic variables mainly, temperature and rainfall. For the Delhi area, where climate is very dynamic due to dynamic LULC characteristics and anthropogenic activities, climatic trends at different temporal resolutions have not been reported in the literature. Therefore, parametric and nonparametric statistical trend analysis techniques/tests i.e., MK, MK–PW, MMK test and PMW are used in the present study to assess climate change in term of the trends in climatic characteristics of Palam and Safdarjung areas of Delhi.

2.2.2 Future Climate Simulations

In the last few decades, climate models were very essential and regional climate effects were determined by using general circulation models (GCMs) (Hansen et al., 1983; Gregory and Mitchell, 1995; Woodward et al., 1995; Cox et al., 1998; Heaney et al., 1999; Martilli et al., 2002; Pauleit et al., 2005 ; Zhang et al., 2010). While these models evaluate the effects of climate change at the global scale and therefore they cannot effectively simulate the climate change at regional and local scale. Recently, regional atmospheric models have been developed to overcome some of the limitations of GCMs (Deng et al., 2010; Georg et al., 1994; Liu and Deng 2011b ; Liu et al., 2013). The reason behind the use of regional climate model (RCM) over GCMs is the higher resolution of RCM as compared to GCMs. So GCMs cannot be used to describe the complex terrain and land surface characteristics (Gao et al., 2003; Wang et al., 2003 ;Trusilova et al., 2008). Some of the medium resolution regional climate models being used in recent past are WRE, RegCM2, RegCM3, RAMS, RIEMS, RegCM-NCC, and IPCR-RegCM (Grimmond and

Oke, 2002; Kalnay and Cai, 2003; Liu et al., 2010; Liu and Deng, 2011a; Cheng et al., 2012; Deng et al., 2013; Tian et al., 2013; Deng et al., 2014; Gao et al., 2013; Li et al., 2013; Scheiter et al., 2013 ; Wang et al., 2014a). To study the climate change related to LULC change the most important parameter is scale because the global average of LULC is negligible because of offsetting the regional signals (Lin et al., 2013). Land cover change affects the regional climate as well as the global climate. So, it is important to study climate change at both the scales (global scale & regional scale). Several investigations have been performed to explore the regional impacts of land cover on climate using a variety of approaches ranging from statistical to regional simulation models (Gao and Yu, 1998; Gao et al., 2003; Zhang et al., 2007 ; Cui and Shi, 2012).

2.2.2.1 Climate models

Climate models are mathematical representations of the climate system, expressed as computer codes and run on powerful computers. There are different kinds of climate models that range from simple energy balance models to complex earth system models (Pall et al., 2011).

In order to estimate the impacts of anthropogenic emissions on climate, a mathematical model called a Global Circulation Model (GCM) has to be constructed for the complete climate system, which must include the atmosphere, oceans, land and cryosphere. GCM model is a mathematical description of the earth's climate system, firstly, it has broken down into layers (both above and below sea level) and then each grid is broken down into boxes or 'cells'. GCMs are the only credible tools currently available for simulating the response of global climate systems. It is standard practice to use observed data in the form of daily or monthly time series representing the current baseline period and to apply changes derived from GCM information to these observed data (Baede et al., 2000).

2.2.2.2 Global climate projections through CMIP5

The World Climate Research Programme (WCRP) develops global climate projections through its Coupled Model Inter-comparison Project (CMIP) roughly every 5 to 7 years. These projections have informed Intergovernmental Panel on Climate Change Assessment Reports. Such activities have primarily been served by CMIP phase 3 (CMIP3) results since 2007. During 2012-2013, WCRP released global climate projections from CMIP phase 5 (CMIP5); Both phases featured developing climate

projections using a new generation of global climate models representing recent advancements in climate science. Also, for CMIP5, the projections are based on using an updated set of global greenhouse gas emissions scenario (Brekke et al., 2013).

Experiments are necessary in order to support a systematic evaluation of climate models and their simulated future climate. Since, a large group of modelling centers around the world runs this suite of simulations aims to test each model's ability to simulate the observed climate through this will assess confidence in climate model performance as a whole. Generally, phases five of the Coupled Model Inter-comparison Project (CMIP5), which coordinated and archived climate model simulations based on shared model inputs by modelling groups from around the world. The CMIP5 data set includes projections using the Representative Concentration Pathways (RCPs). Each RCP includes the concentration pathways and corresponding emissions and land use pathways, which are used as input to climate model for developing GCM projections, have near term up to 2035 and long term covers up to 2100 and an extended one up to 2300.

2.2.2.3 The representative concentration pathways (RCPs)

The RCPs are the latest climate change scenarios. The RCPs are used in the 5th IPCC assessment report (AR5) (Table 2.1). The implications of climate change for the environment and society will depend not only on the response of the Earth system to changes in irradiative forcing but also on how humankind responds to changes in technology, economy, lifestyle and policy. The main reasons for developing the new RCP scenarios were as a result of SRES scenarios that do not consider climate policy. Latest developments in climate models require detailed information of emissions by source type, and to allow consistent usage of scenarios through the collaboration of various disciplines. The new scenarios are thus intended to connect work on climate change, impacts and adaptation and mitigation (IPCC, 2013). Unlike SRES, RCPs start with pathways of radioactive forcing (the change in the balance between incoming and outgoing radiation to the atmosphere caused primarily by changes in atmospheric composition), not with detailed socioeconomic narratives or scenarios (Van Vuuren et al., 2011).The RCPs were selected from scenarios published in the literature to span a wide range of those factors that determine future climate change (radioactive forcing of greenhouse gasses and land use change). Four RCPs pathways named according to radioactive forcing levels of 8.5, 6, 4.5 and 2.6 Wm^{-2} by the end of 2100 (Table 2.1).

Table 2.1: Types of representative concentration pathways (Source: (Moss et al., 2010))

Name	Radioactive forcing	Concentration (ppm)	Pathways	Provided by
RCP 8.5	>8.5 Wm^{-2}	1,370CO2-equiv. In 2100	Rising	MESSAGE
RCP 6.0	6 Wm^{-2}	~850CO2-equiv.	Stabilizing without overshoot	AIM
RCP 4.5	4.5 Wm^{-2}	~650CO2-equiv. (at stabilization after 2100)	Stabilizing without overshoot	GCAM
RCP 2.6	Peak at 3 Wm^{-2}	Peak at ~490CO2-equiv. Before 2100 and then declines	Peak and decline	IMAGE

Note: MESSAGE: Model for Energy Supply Strategy Alternatives and their General Environmental Impact, International Institute for Applied Systems Analysis, Austria; AIM: Asia-Pacific Integrated Model, National Institute for Environmental Studies, Japan; GCAM: Global Change Assessment Model, Pacific Northwest National Laboratory, USA (previously referred to as MiniCAM); IMAGE: Integrated Model to Assess the Global Environment, Netherlands Environmental Assessment Agency, The Netherlands.

2.2.2.4 Downscaling techniques

The resolution of the GCMs is too coarse (100–200 km grid) size for simulation of hydrological processes. This is where, Regional Climate Downscaling (RCD) has an important role to play by providing projections with much greater detail and more accurate representation of localized extreme events[1].

Global climate models (GCMs) are coarse in resolution and are unable to resolve significant sub-grid scale features such as, topography, clouds and land use (Grotch and MacCracken, 1991). Climate downscaling techniques are used to bridge the spatial and temporal resolution gaps between what climate modelers are currently able to provide and what impact assessors require (Wilby and Dawson, 2007). There is a significant gap between the large spatial resolution GCMs and regional and local watershed processes. This scale mismatch causes a considerable problem for the assessment of climate change impact using hydrological models. Hence, significant attention should be given to the development of downscaling methodologies for obtaining high-resolution climate or climate change information from relatively coarse-resolution GCMs. This will help for

[1] http://www.cordex.org/community/domain-east-asia-cordex.html

better prediction of climate change consequences at hydrological scale (Bekele, 2009). There are two main approaches available for the downscaling of large spatial resolution GCM outputs to a finer spatial resolution- Dynamical and Statistical downscaling.

Dynamical downscaling seeks to couple large-scale climate dynamics and local climate features. It does so by utilizing higher resolution regional climate models (RCMs) that respond to the output of GCMs. The GCM output is provided as boundary conditions, which are the values at the edges of the spatial domain of the RCM. Horizontal resolution for most RCMs is in the order of tens of kilometers which could capture important orographic and physical geography details to the simulations. In terms of temporal resolution, RCMs are usually most skillful at monthly or coarser time scales (Rindfuss et al., 2008).

Statistical downscaling consists of modelling the relationship between GCM output and observations to produce results that are used as inputs to sector models or for direct use in decision making. The general principle is to form empirical relationships between predictors and historically observed values, then apply the empirical relationship to future projections. Statistical models are simpler in nature, significantly easier to construct and manage, and require much less computational time than dynamical downscaling (Khadka and Pathak, 2016).

Statistical Downscaling Model (SDSM) is a hybrid of multiple linear regression and stochastic downscaling model developed by (Harpham and Wilby, 2005; Wilby and Dawson 2007).It is a freely available decision support tool for assessing local climate change impact using a robust statistical downscaling technique. In SDSM downscaling, a multiple linear regression model is developed between a selected large-scale predictor variables and local scale predictands such as, temperature and precipitation. The parameters of the regression equation are estimated using an ordinary Least Squares algorithm. Precipitation is modeled as a conditional process in which the local precipitation amount is correlated with the occurrence of wet days. As the distribution of precipitation is skewed, a fourth root transformation is applied to the original series to convert it to the normal distribution, and then used in the regression analysis. Minimum and maximum temperatures are modeled as unconditional process, where a direct link is assumed between the large scale predictors and local scale predictand.

SDSM which is designed to downscale climate information from coarse-resolution of GCMs to local or site level is applied here to downscale the precipitation, maximum and minimum temperatures for the study area. SDSM uses linear regression

techniques between predictor and predictand to produce multiple realizations (ensembles) of synthetic daily weather sequences. The predictor variables provide daily information about large scale atmosphere condition, while the predictand described the condition at the site level. It is appropriate to use this software when the impact assessments are required at small-scale or regional level, provided that quality observational data and large scale daily GCMs climate variables are available. Additionally, the mode can also produces a range of statistical parameter such as, variances, frequencies of extremes and spell lengths for the downscaled climatic parameters (Wilby and Dawson, 2007). SDSM software is published in different version at various times, among them the latest version is adopted for this particular study (i.e. version 4.2.2 SDSM software coded in Visual Basic 6.0 and Version 5.1.1) (Wilby and Dawson, 2007).

The representative studies are discussed in the following section:

Cui et al. (2006) applied a general atmospheric circulation model (ECHAM5) to investigate the impacts of land use changes on the Tibetan Plateau (TP) on local and global climate. The control simulation with current land cover reasonably represented the large-scale circulation and state of the atmosphere over the Tibetan Plateau and the surrounding region. Modifying the land cover to a hypothetical non-anthropogenically-influenced vegetation cover shows significant modifications to the local and remote climate. The study also indicated that human-induced land use changes on the Tibetan Plateau have had a significant impact on local to regional, and to some extent global climate.

Alpert et al. (2008) analyzed regional climate modelling performed at the International Centre for Theoretical Physics, Trieste, Italy, are analyzed for the E. Mediterranean region. It is found that the average temperature over the Mediterranean area has increased by 1.5–4 ^{o}C in the last 100 years.

Hertig and Jacobeit (2008) for the assessment of Mediterranean temperature under anthropogenic influential climatic conditions canonical correlation models was established for the period 1948–98. The study assessed temperature rise varies depending on regions and season, but overall substantial temperature changes of partly more than 4 ^{o}C by the end of this century have to be predicted under enhanced urbanization conditions.

Stine et al. (2009) observed decreasing trend in amplitude of the annual cycle of surface temperature and a shift in earlier seasons. However, few of the global climate models presented in the IPCC Fourth Assessment Report can replicate these trends. In present study, annual cycle of global mean surface temperature was studied to analyse trends in the phase (timing of seasons) and the amplitude of that cycle, over the period of

1954-2007. The study revealed that land surface temperatures show trends predominantly towards earlier seasons over the past 54 years (1.7) days earlier on average.

McCarthy et al. (2010) integrated the urban land surface scheme to a GCM to quantify the impact of large-scale and local drivers of climate change on the urban environment. In addition, study demonstrated that these effects should not be treated independently when making projections of urban climate change. Warming and extreme heat events due to urbanization and increased energy consumption are simulated to be as large as the impact of doubled CO2 in some regions, and climate change increases the disparity in extreme hot nights between rural and urban areas. Climate change results in a greater increase of hot nights for cities than neighboring rural areas, increasing the thermal stress and vulnerability to heat waves of urban citizens in a warmer climate compared to their rural counterparts.

Christidis et al. (2011) studied the anthropogenic influence on maximum daytime temperatures at global and regional scales. Formal detection and attribution studies of daily temperature extremes have previously detected anthropogenic influence on the recently increased severity of extremely warm nights and, less robustly, decreased the severity of extremely cold days and nights. The authors also detect anthropogenic influence on extreme temperatures at the regional scale with changes in the warmest nights detected in almost all regions.

Xiao et al. (2012) studied the effects of anthropogenic climate change and it revealed that the magnitude and frequency of intense precipitation events are expected to increase in next few decades for the mid-western United States. The goal of this study was to study statistically downscaled and debiased precipitation projections derived from 14 General circulation models and to assess the projected precipitation changes for the mid–21st century in a way that is relevant to water-resource decision making.

Dimri et al. (2013) studied the possible regional climate change over South Asia with a focus on India as simulated by three very high-resolution regional climate models (RCMs). All models show a clear signal of gradually wide-spread warming throughout the 21st century. The ensemble mean warming over India is 1.5 ^{o}C at the end of 2050, whereas it is 3.9 ^{o}C at the end of the century with respect to 1970–1999.

Yoshida et al. (2014) developed statistical models (called impact functions) that mimicked the responses of summer mean, maximum, and minimum surface temperatures to given LULC changes simulated with a regional climate model (RCM). Moreover, the impact functions were analyzed which indicated that land use change induced changes in

summer mean temperature potentially range from −0.4 (when the forest was converted to paddy) to +1.3 ºC (when the forest was converted to building lots). The study revealed that, on an area mean basis, the cooling achieved through land-use management was limited in its ability to offset climate change-induced warming in future decades.

Argüeso et al. (2014) projected the impact of future urban expansion on local near-surface temperature for Sydney (Australia) using a future climate scenario (A2). A comparison between areas with projected land use changes and their surroundings was conducted to evaluate how urbanization and global warming will act together and to ascertain their combined effects on local climate. Results indicated that the changes were mostly due to increased heat capacity of urban structures and reduced evaporation in the city environment.

Mahmood and Babel (2014) predicted future changes in extreme temperature events using the statistical downscaling model (SDSM). In the 21st century, climate change is considered to be one of the greatest environmental threats to the world, and the changes in climate extremes are estimated to have greater negative impacts on human society and the natural environment than the changes in mean climate. Results concluded like that the intensity and frequency of warm temperature extremes are likely to be higher and the intensity and frequency of cold temperature extremes to be lower in the future.

Kumar et al. (2014) did an assessment of land use change impacts that can be applied to common all-forcings experiments and does not require single-forcing LULC change experiment. The proposed methodology was based on comparing climate change impacts between two neighbouring regions in which one region has experienced land use change and the other had not. In the 8.5 Wm-2 representative concentration pathways RCP8.5 21st-century climate simulations, all 14 CMIP5 climate models showed more summer warming in historical land use change regions than in the surrounding regions. These uncertainties could be due to the differences in regional climate characteristics, changes in land-atmosphere interaction in the 21st century, and methodological biases.

Qian et al. (2015) investigated upon simulated impacts of land cover change on summer climate in the Tibetan Plateau by using the GCM data. Results showed that land-cover change from vegetated land to bare ground decreases the radiation absorbed by the surface and it resulted in a weaker surface thermal effects, which lead to lower atmospheric temperature, as well as weaker vertical ascending motion, low-layer cyclonic, upper level anticyclonic, and summer monsoon circulation. Richter, (2016) investigated upon urban climate change-related effects on extreme heat events in

Germany using a model that focuses on interactions between land use and surface temperatures and on specific air conditions in cities. The model enables urban surface temperature differences to be projected with regard to different assumptions of (future or planned) LULC and its specific characteristics. The results revealed a range of outcomes, from an enlargement of vulnerable areas to the near eradication of climate change-related heat effects in several areas.

Zeng (1991) analyzed the impacts of urbanization on future climate in China. The Weather Research and Forecasting model were used to downscale future projections using RCP 4.5 simulations from the Community Earth System Model. Results for 2050 showed decreased latent and increased sensible heat fluxes over the urban area, therefore, leading to higher surface temperatures and less humidity. Future climate projections revealed that urbanization produces strong warming effects, up to 1.9 ^{o}C at regional and local/urban scales. Due to these significant impacts, this study suggested that urbanization should be included in model projections to provide a more realistic and complete depiction of future climate. Human-induced land cover changes exert significant impacts on climate at regional and global scales by modifying the energy, water, and momentum exchanges between the land surface and atmosphere.

Zarenistanak et al. (2015) assessed the trends and projections of temperature, precipitation during December, January, February, March, and April months was estimated. Trends in these parameters were tested by linear regression and significance was determined by t-test. MK test was also employed to check the results of linear regression for change detection used Sequential MK test in the series. The investigation of temperature trends revealed a significant increase during February and April. Temperature projections showed that temperature may increase between 1.12 to 7.87 ^{o}C by 2100 and in precipitation series indicated that majority of the stations recorded insignificant trends during the twentieth century.

2.3 URBANIZATION (LULC CHANGES) AND ITS IMPACT ON CLIMATE

2.3.1 Impacts of LULC Changes on Climate

The main causative factors of climate change are Greenhouse gases, aerosols, human induced anthropogenic changes and natural phenomenon. Urbanization is one of the anthropogenic activities that affects the land-atmosphere relationships through change in interaction between land surface and incoming solar radiations. It is well established that

LULC changes due to urbanization affect local climate adversely (Oke and Cleugh, 1987; Zeng, 1991; Weng and Yang, 2004; Feddema, 2005; Christy et al., 2006; Mallick and Bharath, 2008; Calzadilla et al., 2013; Mohan and Kandya, 2015). Increase in population, industrialization, aspiration of better living and livelihood promotes rampant urbanization and with time, it is going to be increased. Urbanization, population and economic growth are strongly interlinked and have adverse effects on natural environment which are also responsible for various direct and indirect effects on other climatic variables.

Urban growth induces replacement of natural land covers with the impervious urban materials, the modifications of the biophysical environment and the alterations of the land surface energy processes indicates change in surface energy balance leading to change in climate which may leads to many adverse impacts like urban heat island, extreme heat stresses, heat waves, floods, droughts and rise in sea level (Zeng, 1991; Lo and Quattrochi, 2003; Pielke, 2005; Solomon and IPCC, 2007; Wang et al., 2012; Calzadilla et al., 2013; Howe and Leiserowitz, 2013; Mimura et al., 2014; Ren and Zhou, 2014; Mohan and Kandya, 2015). Strong association between increasing urbanization and climate change at regional at local scale has been reported by many authors (Solomon et al., 2007; Lankao et al., 2008; Mimura et al., 2014; Morris et al., 2015, 2016). Such adverse effects are more pronounced in urban areas at local scale, which leads to increase in urban population vulnerability to future global environment change (Grimmond, 2007).

Research work reported related to LULC changes and their impact on climate has been discussed below in the form of representative case studies and research articles.

Kalnay and Cai, (2003) assessed the impact of urbanization on surface temperature by comparing observed surface temperature in cities with those in surrounding rural areas. The study revealed that there is a huge effect of LULC change on surface temperature. The study revealed that surface temperature was much higher i.e. almost twice in the case of taking all LULC classes effect into consideration as compared to the effect of urban only.

Davis et al. (2004) have studied the impacts of climate change and seasonal climate-human mortality relationships in different US cities. The climate-mortality seasonality patterns were examined for spatial and temporal (decadal-scale) variability. Authors have concluded that mortality in future could be reduced with a winter dominant warming but increase with pronounced summer warming.

Sailor and Lu (2004) have studied the periodic and seasonal anthropogenic heating profiles for selected urban areas. A generalized approach for estimating season specific

diurnal profiles of anthropogenic heating for cities was presented. Authors have reported that anthropogenic heating values at urban core, which is 5-10 times the magnitude of the city-scale is proportional with daytime population density at urban core which is of 5-10 times of the city-scale value.

International Peatland Society (2008) have studied the sensitivity of near-surface temperature and precipitation to the historical LULC changes. Study results were compared with observed precipitation, minimum and maximum temperature. Also, the sensitivity of temperature to precipitation and LULC change was studied at large scale.

Giorgi and Lionello (2008) investigated climate change trends at global and regional scale and the study was a part of international collaborative projects. The pronounced warming was found maximum in the summer season. The study revealed that inter-annual variability was mostly increased especially in summer, along with the mean warming that would cause extremely high-temperature events.

Fischer and Schär (2009) predicted future changes in daily summer temperature variability driving processes and role for temperature extremes. Anthropogenic effects may result in more frequent extreme summer temperature which are due to the increase in mean warming and changes in temperature variability, which is a sign of climate change.

Christidis et al. (2010) found that advancements in climate change fingerprinting methodologies are promising in determining the effect of human influences on regional-scale trends of climate. The results indicate cooling which has not been consistent with what would be expected under global warming. Study results revealed positive role of anthropogenic forcing in changing climate at sub-continental scale. The authors have suggested additional simulations of climate change under anthropogenic conditions and natural forcing conditions.

Gibbs (2015) have studied the impacts of climate change and adaptation at the city scale. The study showed a strong variation in climate change impacts with location and site conditions. The study reported that quantification and valuation of large future risks of climate change can be a key step to raising awareness.

Manwell et al. (2002) acclaimed in a report that natural and human systems are increasingly affected by climate change. Authors have also presented the facts and variables of climate change. They have further emphasized that anthropogenic activities are also responsible for climate change confirming the similar scientific evidences produced in IPCC third, fourth and fifth assessment reports.

Huang et al. (2015a) have studied the inter-relationship between LULC change and climate variations over Loess Plateau in China. Their analysis indicates larger contribution ratio (based on comparison of standard deviation of each contributing factor-induced climate changes and that of total) from climate variation than from LULC change i.e., 0.95 from climate variation and 0.35 from LULC change) for variations in temperature. They have found that spatial variation of LULC change impacts on precipitation implied that human activities might have larger impacts on precipitation in the regions arid north than in its humid south. Using both leaf area index (LAI) and areal coverage of each of the major land types, LULC change attribution analysis suggested that LULC change observed in the 2000's resulted primarily from human activities rather than climate variations (0.99 contribution ratio from human activities vs. 0.26 from climate variation).

Cinar (2015) has studied the relationship between LULC change and temporal climatic anomalies in term of mean minimum and maximum monthly air temperature. Author has used CORINE (Coordination of Information on Environment) index to determine LULC diversity for an urban fringe. Further, classified LULC change values for three decades were related with decadal air temperature anomalies. Simple linear regression model in Minitab-17 software was used to determine the correlation between decadal air temperature anomalies based on annual climatic mean data (1940–2013) and LULC change. Authors have found that minimum air temperature has increased with increase in urban fabric. Author has obtained a high positive correlation coefficient for urban fabric land use and mean monthly air temperature anomalies per decade.

2.3.2 Assessment of Impacts of LULC Changes on Climate

As discussed above and reported extensively that LULC changes are one of the anthropogenic activities affecting climate adversely. LULC changes due to urbanization affect local surface energy balance by changing the amount of solar energy reflected, the magnitude and duration over which absorbed energy is released as heat, and the amount of energy that is diverted to non-heating fluxes through evaporation consequently impact local climate adversely. Natural surfaces are replaced with material with higher heat capacity and thermal conductivity and different radiative characteristics (lower surface albedo and emissivity). Also surface energy balance further influenced by increase in surface area and roughness of urban form, size, shape and density of buildings, roads, distribution of green spaces, anthropogenic heat and air pollution (Stone and Norman,

2006; Hart and Sailor, 2009; Middel et al., 2012). Significant reduction in vegetation due to urbanization leads to change in surface energy fluxes, heat, moisture and momentum. So, modifying the vegetation cover can change the lower boundary conditions of the atmosphere and hence, affects the climate (Pielke et al., 2002; Arnfield, 2003; Thuiller et al., 2005; Yin and Liebscher, 2006; Pessacg and Solman, 2012; Steinschneider et al., 2012; Huang et al., 2015a; Lejeune et al., 2015). Looking at the importance of this issue National Research Council in USA has recommended to include LULC (Jacob et al., 2005) for climate change research.

Assessing the impacts of urbanization and LULC changes on climate is a challenging task. Several studies have attempted to assess the effect of urbanization and industrialization on climatic parameters like temperature trends (De and Rao, 2004; Gadgil and Dhorde, 2005; Dash and Hunt, 2007; Ezber et al., 2007; Dhorde and Gadgil, 2009; Sajjad et al., 2009; McCarthy et al., 2010; Anuja;, 2011; Brovkin et al., 2012; Kueppers and Snyder, 2012; Yoshida et al., 2014; Cinar, 2015). However, such local influences often are only crudely included in climate modelling exercises, if at all. A better understanding of local land conversion dynamics can serve to inform inputs for climate models and increase the role for land use planning in climate management policy.

Several methods have been developed to understand and assess the climate change such as, statistical methods (trend analysis), simulation models (GCMs and RCMs), downscaling global climate projections (dynamical downscaling and statistical downscaling), land surface temperature based methods, observed minus reanalysis (OMR) approach, sensitivity experiments; surface energy balance based methods, water balance based approaches and terrestrial carbon balance based approaches. Surface energy and water balance based distributed methods have been used in recent past to investigate effects of direct and indirect LULC change mechanisms on climate (Copeland et al., 1996; Betts, 2001; Eastman et al., 2001; Pielke et al., 2002; Feddema, 2005; Järvi et al., 2011, 2014).

Further, quantitative estimation of change in surface energy fluxes corresponding to change in LULC fractions over an area provides a quantitative basis to evaluate the relative contribution of LULC changes in altering the climate. Also, surface energy balance based methods provides an analytical basis to deal with such a complex phenomenon along with considering the local conditions.

Therefore, surface energy balanced approaches are seems to be promising and used in the present research. Present state of the knowledge about some of the important

methods and techniques used in recent past for assessment of LULC change effects on climate has been discussed in the present section through representative studies published in recent past.

2.3.2.1 Surface energy balance based approaches

Klysik (1996) analyzed the potential of vegetation as an urban climate control variable in the subtropical city of Gaborone, Botswana. An inventory of heat fluxes from different types of the neighborhood was made for the 214 km^2 of Lodz. Mean annual heat flux over the 80 km^2 urbanized area was found to be 28.5 Wm^{-2}, ranging from 12 Wm^{-2} in July to 54 Wm^{-2} in January. New areas of blocks of flats (about 30 km^2) have a mean annual flux of 35 Wm^{-2} (73 Wm^{-2} in winters, and 14 Wm^{-2} in summer). Values of anthropogenic heat flux calculated in the central districts of the city, where, there are industrial factories and residential dwellings, have a mean annual flux of 40 Wm^{-2}, 71 Wm^{-2} in January and 18 Wm^{-2} in July). The large anthropogenic heat emissions are important contributors to the city's climate in winter.

Arnfield and Grimmond (1998) studied the storage heat flux of an urban canyon and the resulting Object Hysteresis Model (OHM) parameters with a numerical model of a dry urban canyon energy budget. Model was found to be satisfactory. Numerical experiments revealed significant effects on the OHM parameters due to change in the ratio of building height to separation distance and building wall thermal properties. Air temperature and the timing of the wind speed curve also have minor significance.

Ja (1999) presented the results of an experimental study where a series of energy balance measurements were carried out in a suburban natural vegetated area in the south of the Mexico City. Authors have concluded that net radiation was mainly dissipated by sensible and latent heat fluxes. The Bowen ratio was found to be 1.92 and 0.04 during the dry and wet season, respectively.

Grimmond and Oke (1999) studied the relationship between sensible heat and storage heat fluxes for seven different cities of North USA. In all cases, measured storage heat flux was determined as the energy balance residual from direct observations of net all-wave radiation, sensible and latent heat fluxes conducted using the radiometer and eddy correlation techniques. Results indicated that storage heat flux was a significant component of the surface energy balance at all sites and it was found to be highest at downtown and light industrial sites. At all locations, Hysteresis behavior, of varying degrees, was observed. A simple objective hysteresis model (OHM), which calculates

storage heat flux as a function of net all-wave radiation and the surface properties of the site was found to be satisfactory for most cases.

Oke et al. (1999) presented the energy balance of central Mexico City during the dry season. The first measurements of the energy balance fluxes of a dry, densely built-up, central city site were presented. The most important finding of this study was that during daytime, evaporation is very small (< 4% of net radiation), and therefore sensible heat uses dominant (Bowen ratio > 8), the uptake of heat by the buildings and substrate was so large (58%) that convective heating of the atmosphere was reduced to a smaller role than expected (38%).

Pearlmutter et al. (1999) analyzed microclimatic parameters of compact urban canyons in an arid zone. Analysis of microclimatic parameters and overall energy balance suggested that in summer, overheating within the canyon was sensed primarily as a night-time phenomenon and that during hours of substantial heat stress in a desert climate, the compact Canyon is, a potential "cool island", mainly due to internal solar shading. In winter, a compact geometry was found to provide relatively warm conditions, with the key factor being protection from strong winds during cold night hours.

Masson (2000) presented an urban surface scheme for atmospheric mesoscale models. A generalization of local canyon geometry was defined instead of the usual bare soil formulation currently used to represent cities in atmospheric models. Finally, a comparison with a vegetation scheme showed that the suburban environment can be represented with a bare soil moisture formulation for large temporal or spatial averages (typical of global climatic studies), but that a surface scheme dedicated to the urban surface was necessary, when smaller scales were considered for town meteorological forecasts, mesoscale or local studies.

Cleugh and Grimmond (2001) studied regional scale surface energy exchanges and convective boundary layer (CBL) growth in a heterogeneous urban-rural landscape. This study explored the use of an integral CBL method to inter-regionally averaged fluxes in a landscape that has at least three major sources of heterogeneity irrigated, non-irrigated rural land use and a large urban area (Sacramento region, California). The study revealed that the integral CBL budget method provides adequate estimates of regionally-averaged surface heat fluxes in a landscape that was characterized by surface types with distinctly different surface energy budgets.

Nagar et al. (2002) estimated radiative fluxes of short wave, long wave radiations as well as non-radiative fluxes such as, sensible heat flux and the surface soil heat flux

during daytime and for the dry convective period in May 1997 over a bare soil at a tropical station. The results were compared with real-time data and surface temperature assessed by Fourier's law for heat conduction and found to be in good agreement with the observed values with 5% RMSE error.

Su and Su (2002) proposed surface energy balance System for the estimation of atmospheric turbulent fluxes and evaporative fraction using satellite earth observation data, in combination with meteorological information at proper scales. Results proved that methods are capable of estimating turbulent heat fluxes and an evaporative fraction at various scales with acceptable accuracy. The uncertainties in the estimated heat fluxes are comparable to in-situ measurement uncertainties.

Grimmond and Oke (2002) presented a linked set of simple equations i.e., local-scale urban meteorological parameterization scheme (LUMPS), designed to calculate heat fluxes for the urban environment. The LUMPS requires only standard meteorological observations and basic knowledge of surface cover. LUMPS works based on net all-wave radiation and heat storage from the urban areas was calculated using objective hysteresis model (OHM) after parameterized from net all-wave radiation and surface cover information. Turbulent sensible and latent heat fluxes were calculated from the partitioning of available energy using Bruin and Holtslag. A new approach to calculate Bruin and Holtslag parameters was also presented. The scheme was expected to have broad utility in models used to calculate air pollution dispersion and the mixing depths of urban areas or to provide surface forcing for mesoscale models of urban regions.

Arnfield (2003) analyzed two decades of urban climate research published in the International Journal of Climatology through a review of turbulence, exchanges of energy and water, and the urban heat island. It was concluded in the review that conceptual advances made in microclimatology and boundary layer climatology in general since 1980. The role of scale, heterogeneity, dynamic source areas for turbulent fluxes and the complexity introduced by the roughness sublayers over rigid roughness elements of cities were described. The state of knowledge about urban heat islands around 1980 was described and work since then was assessed in terms of similarities to and contrasts with that situation. Finally, the main advances were summarized and recommendations for urban climate work in the future were made.

Offerle and Grimmond (2003) evaluated a simple scheme for estimating the net all-wave radiation using annual datasets in three urban settings (Chicago, Illinois; Los Angeles, California; and Lodz, Poland). Results were compared with the results of a

regression model based on incoming solar radiation and with an urban canopy-layer model incorporating a canyon geometry radiation scheme that requires a larger set of meteorological and surface property inputs. This net all-wave radiation parameterization (NARP) scheme found to be sensitive to albedo and the effects of clouds on incoming longwave radiation. It was observed that results of the NARP and the complex canopy scheme are similar while considering observations of down welling longwave radiations.

Lemonsu et al. (2004) proposed the Town Energy Balance (TEB) model, which uses local scale energy and water exchanges between urban surfaces and the atmosphere by considering urban area as a series of urban canyons, coupled to the interactions between soil, biosphere, and atmosphere (ISBA) scheme. Model was implemented for Marseille, France. Model results were compared with the field measurements. Model results were found to be good when parameterized with wall, road and roof surface temperature. Results indicated that overall TEB scheme is robust and consistent with previous studies.

Bourbia and Awbi, (2004) studied the interaction between urban canyon geometry and incident solar radiation in Algeria. In the study effect of building height and street width on the shading of the street surfaces and ground for different orientations were examined to determine the extent up to which these parameters affect temperature in the street. It was aimed to explore the extent to which these parameters affect the temperature in the street. Study revealed that there is a good correlation between street geometry, sky view factor and surface temperatures.

Souch and Grimmond (2006) presented a detailed review about advancements in methods and technologies of urban climate data collection, instrumentation, computational models, sensor placement, etc. for understanding the urban environment. Available challenges in the area of urban climatology were also discussed. One of the critical gas highlighted was how best to archive the urban climate data.

Offerle et al. (2006) investigated temporal variations in heat fluxes over a central European city centre in Poland. Ab. Ghani et al., (2010) have investigated temporal changes in energy balance partitioning over different seasons and conditions were determined along with investigating the role of heat storage and anthropogenic fluxes in the energy balance. Partitioning of the energy fluxes were found to be consistent in at monthly and seasonal temporal scales in two years. Latent heat flux is found to be significant portion of the total turbulent fluxes.

Das and Padmanabhamurty (2008) measured the surface energy balance components in suburban vegetated area of the southern Delhi. Measurements were carried out continuously for several days of winters (January, February, November, and December) and summers (April, May, June) of year 1998 and 1999. Authors find net radiation in the range of 108 Wm-2 in winters of 1998 to 423.43 Wm-2 in summers of 1999. Sensible and latent heat were found to be 63% and 16% of the net radiation during summers of 1998. Around 34% of the net radiations was transformed into soil heat flux in both summers as well as in winters of 1998 and 1999. Turbulent heat fluxes shown erratic behavior due to local conditions

Lin et al. (2009) simulated trends in urban climate to explore the impacts of land-use vegetation change (LUC) by utilizing Australian Bureau of Meteorology Research Centre (BMRC) model in China. Model revealed moderate but statistically significant local impacts by LULC changes, with significantly different surface temperature responses in winters and summers due to two regimes dominating surface energy balance in the region. This is largely due to the fact that fundamental processes affected by land use cover, including changes in surface albedo and roughness length.

Lamptey et al. (2005) investigated the effect of urban landscape at global and regional scale using surface energy budgeting, which was done using empirical equations and remote sensing data. Study concluded that urban land cover has least impact on sensible and latent heat fluxes as compared to other land cover type at global scale, however, effect of urban landscape at regional scale were significant.

Das and Padmanabhamurty (2009a) computed the surface energy and water balance components for the land- atmospheric boundary layer over Delhi for two year i.e., 1997-98 and 1998-99. Authors have measured the net radiation and storage heat flux from the field and estimated sensible heat, and latent heat fluxes using bulk-aerodynamic method. Thorn Thwaite's model was used for water balance estimation. Study concluded that there is a persistent energy imbalance in both the seasons for urban/dry as well as rural/moist areas. Urban areas have +ve energy balance whereas in rural/moist areas energy imbalance was negative.

Das and Padmanabhamurty (2009b) studied the incoming shortwave, albedo, incoming longwave, outgoing longwave and net radiations for five representative sites of the Delhi for winter and summer seasons of year 1998 and 1999. The study finds that the incoming shortwave radiations are higher in rural areas as compared to urban areas.

Incoming longwave radiations were found to be more in urban areas. Albedo was found to be less in urban areas where as net radiations were higher in urban areas.

CSB et al. (2010) performed a thorough comparison of 33 models urban climate models to understand the complexity required to model energy and water exchanges. There was evidence that some classes of models perform better for individual fluxes but no model performs best or worst for all surface energy fluxes. In general, the simpler models perform as well as the more complex models based on all statistical measures. Generally, the schemes have the best overall capability to model net all wave radiation and least capability to model latent heat flux.

Järvi et al. (2011) presented an urban energy and water balance model (SUEWS) based on relatively a small number of commonly available meteorological parameters and LULC information. Model results were compared with the field measurements and it was found that model reproduces the diurnal cycle of the turbulent fluxes but underestimates the latent heat flux and overestimates the sensible heat flux during day time. Model has been found to be successful in estimating the surface energy balance with a root mean square error for net all-wave radiation, turbulent sensible and latent heat fluxes as 25-47 Wm-2, 30-64 Wm-2 and 20-56 Wm-2, respectively. The model has the potential to be used for multiple applications; for example, to predict effects of regulation on urban water use, landscaping, and planning scenarios, or to assess climate mitigation strategies.

Ping et al., (2012) presented results of a local-scale above-canopy study of intra-urban land cover mixes in two cities to analyze the relative effects of surface morphology and local climate on the surface energy balance. Study was conducted for urban areas in Phoenix, Arizona and Portland, Oregon, cities with distinct climate. Local Scale Urban Meteorological Parameterization Scheme (LUMPS) was used to analyze the relative contributions of local weather extremes and land cover variations on urban energy balance. Partitioning of energy balance into its components like sensible, latent and ground storage heat fluxes was studied for a dry summer month and two extreme weather scenarios. Results revealed that LUMP is sensitive to incoming solar radiations and daytime Bowen ratio vary inversely with vegetation fraction between and within cities all weather scenarios. Impervious surface cover was found to be positively correlated to the available energy that is partitioned into sensible heat. Results suggest that land cover manipulation could offset influences of weather extremes on ET in Portland to a certain degree but not in Phoenix.

Kharol et al. (2013) studied the long-term effects of LULC changes in Rajasthan state of India on land-atmosphere fluxes, in precipitation and aerosol loading. Multispectral satellite data, Aerosol index records and MERRA re-analysis dataset was used in the study. MERRA 2D dataset was used to obtain some parameters (latent heat, sensible heat, specific humidity) related to land-atmosphere fluxes. The study indicated that the natural aerosol trends and variability in precipitation is much more influenced by the general monsoonal circulation (i.e. meteorological dynamics and intensity of the monsoon) and partly can be associated with local phenomena, such as, LULC changes and modifications in land-atmosphere fluxes.

Deng et al. (2013) presented a review of the advances in the research on the influences of LULC on regional climate, including how LULC changes influence the regional climate, simulations models and their applications. Authors have concluded that effects of LULC impacts on regional climate are documented well. Regional climate models were used extensively at higher resolution to determine change in climatic characteristics due to local forcing. Authors concluded that there is still great uncertainty in the simulations of effects of the LULC changes on regional climate because of multiscale dynamics and interactions between multiple weather systems and large variation in the influence of the land use changes in different regions on the climate system. Authors emphasized the need of correct representation of LULC information in the models, needs of study land surface processes and field observations for model parameterization. Authors concluded that regional climate models are not considering urbanization processes and LULC complexities. Authors concluded that there is still need to investigate the effects of future changes in LULC on climate.

Das et al. (2014) presented a simple parameterization for some radiative fluxes and pollution parameters at Atmospheric Boundary layer in Delhi. The surface energy balance fluxes data sets obtained during the experimental field campaigns were related with the pollutant concentrations and LULC parameters through regression analysis. Moderate to high correlation was found between radiation gradient and pollution gradient.

Kleczek et al. (2014) estimated the change in heat fluxes with respect to projected land transformations over next 40 years across China using Weather Research and Forecasting (WRF) model. Impacts of four future scenarios of the LULC i.e., reclamation, overgrazing, afforestation, and urbanization were investigated in term of change in energy balance fluxes. Study results revealed that with increase in urbanization will lead to increase in sensible heat flux in tune of 40 Wm-2.

Liu et al. (2014) investigated the effects of LULC on land surface energy balance and climate from 1990 to 2005 using a Simple Biosphere Model (SiB2). The spatial patterns of the components of surface energy balance i.e., net radiation, latent heat, sensible heat, and albedo and climate (i.e., canopy temperature, diurnal temperature range), as well as the roles of land cover type in variations of energy balance and climate, were investigated. The results showed that there was a change in trends in net radiation, latent heat, sensible heat, and albedo due to change in the LULC process.

Sanchez-Lorenzo et al. (2015) studied the changes in surface energy balance fluxes due to forest fires using remote sensing images and surface energy balance modelling for Mediterranean forest of Spain. A two source energy balance approach was applied on Landsat data to estimate surface fluxes. Study concluded that effects of change in vegetation structure and surface variables like temperature, albedo are responsible for change in surface energy fluxes.

2.3.2.2 Observed minus re-analysis (OMR) approach

Kalnay et al. (2006) estimated the impact of land use changes for West Coast of USA using observation minus reanalysis (OMR) method by computing differences between the trends of the surface temperature observations and the NCEP-NCAR reanalysis surface temperatures. These differences not only include urbanization effects but also changes in agricultural practices, such as, irrigation and deforestation, as well as other near-surface forcing related to industrialization, e.g. aerosols. Authors have verified OMR trends of surface impacts on mean temperature with results derived from satellite observations of night light to discriminate between rural and urban stations, with regions of large positive and negative trends, in contrast with the urban corrections based on population density, which are uniformly positive and much smaller.

Mahmood et al. (2010) have investigated the sensitivity of surface temperature trends to LULC change over conterminous United States using observation minus reanalysis (OMR) approach. OMR trends were estimated over a period of 1979-2003 using US Historical Climate Network (USHCN) and the NCEP-NCAR North American Regional Reanalysis (NARR) data sets. They found that NARR capture the climate variability at different temporal scales and it often gives larger warming trends than adjusted observations. Study concluded that OMR trends are sensitive to land cover types. They have investigated the decadal OMR trends as a function of land type obtained from Advanced Very High Resolution Radiometer (AVHHR) and land cover data sets from

year 1992 – 2001. It has been found that LULC change leads to more warming then the cooling. They have concluded that OMR approach robust method in detecting non-climatic changes at station level and providing a quantitative estimate of additional warming trends associated with LULC changes. Further, authors have suggested incorporation of LULC changes in addition to greenhouse gases-driven radiative forcing in long-term climate model simulations. Authors have used ArcGIS for interpolation of observed data from different stations and OMR obtained for different stations, to convert point data into areal data into gridded format. Further, OMR grid points that belongs to each LULC type were selected and exported for each type for establishing sensitivity of LULC with temperature. Authors have found out that all areas that have experienced urbanization are associated with positive (increasing) OMR trends with values ranging from 0.103 (conversion from agriculture to urban) to 0.066 ^{o}C (conversion from forest to urban). This trend is also supported by Lim et al., (2005) and Lim, (2008). Results are consistent with findings from studies such as, Kuckla et al., (1986); Arnfield, (2003); Zhou et al., (2004) and Hale et al., (2006, 2008) which find warming often associated with urbanization.

Yang et al. (2011) investigated the effect of rapid urbanization on temperature change Monthly mean surface air temperature data from 463 meteorological stations, including those from the 1981–2007 ordinary and national basic reference surface stations in east China and from the National Centers for Environmental Prediction and National Center for Atmospheric Research (NCEP/NCAR) Reanalysis, are used to investigate the effect of rapid urbanization on temperature change.

Nayak and Mandal, (2012) studied the regional temperature trends over western India and contribution of LULC changes using 37 years of data (1973 –2009). LULC contribution to warming or cooling was estimated based on differences in observations and re-analysis datasets. Results indicated that LULC changes have contributed to warming in the region by 0.06 ^{o}C per decade. Change in temperature regime is mainly due to reduction in vegetation.

Yang et al. (2013) studied the impact of urbanization and human activities on temperature trends over China using observed data of 274 stations and National Centers for Environmental Prediction (NCEP)–National Center for Atmospheric Research (NCAR) re-analysis temperature dataset from 1979 to 2010. Observation minus reanalysis (OMR) method was used to determine the urban influences. Results concluded that urbanization and human activities have contributed in warming in the region.

Wang et al. (2014b) presented the OMR trends for eastern China during 1979-1998 and 1989-2008. MOR trends were found to be inconsistent for the region experiencing rapid urbanization. Secular trend and multi-decadal variability (MDV) was determined from the temperature observations using Empirical Mode Decomposition and further compared with corresponding reanalysis dataset. Results indicated that MDV in the reanalysis dataset is weaker as compared to observed data.

Wang et al. (2014b) investigated the effects of LULC changes on climate for Jiangxi Province of China using OMR method and observed rainfall and temperature data. Results indicated contribution of LULC in warming of the areas. OMR trends for temperature were found to be sensitive to the vegetation.

Qian (2014) studied the impacts of LULC changes on surface solar radiation in eastern China during 1979–2008 in term of change in diurnal temperature range and observation minus reanalysis approach. Results indicate reduction in solar radiations during 1979-2008. Results indicate warming in maximum and minimum temperature in eastern China. Impact of LULC changes indicated cooling in maximum temperature and warming in minimum temperature.

2.3.2.3 Land surface temperature method (LST)

Weng, (2014) has discussed the environmental issues in China at local scale using the integration of remote sensing and GIS technologies for detecting urban growth and assessing its impacts on surface temperature. An analytical procedure was developed based on a spectral mixing model in Indianapolis, United States. The environmental changes were observed on local surface temperature due to increase in impervious surfaces, changes in vegetation cover and inter-relation of these parameters. These parameters were derived with an unconstrained least square method. The correlation analyses were performed between the land surface temperature (LST) with impervious surface and vegetation cover. It was found an inverse relationship between these parameters.

Stathopoulou and Cartalis (2007) utilized Landsat 7 ETM+ thermal band data to identify the hottest surface within the urban settings and correlated with urban surface characteristics in major cities of Greece. The Corine land cover (CLC) database was also used to define links between surface emissivity, land surface temperature, and urban surface characteristics.

Raj and Fleming (2008) have estimated the surface temperature using the Landsat ETM+ satellite imagery for a part of Baspa basin, northwest Himalaya, India. The Top of atmospheric radiance was extracted from the digital (DN) values and then surface radiance was estimated from Top of atmospheric using reference channel emissivity method. The good correlation was found between the surface temperatures from surface radiance and the observed surface temperature. The emissivity of the study area was assumed constant (0.97, the emissivity of glacier ice). The surface temperature was estimated without assessing the climate change due to LULC change.

Kant et al. (2009) study analyses land surface temperature (LST) estimation using temporal ASTER (Advanced Spaceborne Thermal Emission and Reflection Radiometer) datasets (day time and night time) over National Capital Territory Delhi using the surface emissivity information at the pixel level. It was observed that fallow land, waste land/ bare soil, commercial/industrial and high dense built-up area have high surface temperature values during the daytime, compared to those over water bodies, agricultural cropland, and dense vegetation. During night time high surface temperature values were found over high dense built-up, water bodies, industrial and low dense built-up than over fallow land, dense vegetation and agricultural cropland.

Yang et al. (2013) studied the impacts of urbanization on surface air temperature series by utilizing the satellite data for year 1970s 1980s and 2000s to determine whether or not the station entered the city. The strongest effect of urbanization on annual Tmean, Tmax, and Tmin trends occurred at urban stations, with corresponding contributions of 35.824, 14.286, and 45.161 % of the total warming, respectively. The study also suggests that urban expansion has important impacts on the evaluation of regional climate change.

Rogan et al., (2013) investigated the linkages between urban tree cover loss events related to invasive species eradication and urban heat trends. In this study, variation in Land surface temperature (LST) was examined using Landsat-5 Thematic Mapper (TM) thermal imagery. It was found that the areas with an increase in exposed impervious surface produced greater temperature increases than areas of tree loss, future tree replanting efforts may focus on locations that reduce exposed impervious surfaces.

Polydoros and Cartalis (2015) did an assessment of the impact of urban expansion on the thermal environment in Athens for the period 1994–2010. Studied through the estimation of land surface temperature (LST) using Landsat satellite data. This was an important finding regarding urban climate as a temporal modification of the LST pattern

in the peri-urban areas of Athens over the years, may potentially impact energy exchange, local circulation patterns, thermal comfort as well as energy consumption for cooling.

Chakraborty et al. (2015) used Landsat and MODIS data to retrieve biophysical parameters for estimating land surface temperature (LST) and heat fluxes diurnally in summer and winter seasons of year 2000 and 2010 for Delhi and understanding the effects on anthropogenic flux. Results indicates that with increase in industrialization (4.92 to 11.87%) and settlement (5.66 to 11.74%) have affected the land surface temperature and heat fluxes including anthropogenic heat flux. Study found that Landsat derived LST is more accurate as compared to LST derived from MODIS.

Peng et al. (2016) conducted a case study to illustrate LULC change and its impact on land surface temperature (LST) variations in urban and semi-urban and also found out the land transformation effects. The LULC classification and change detection were accomplished by using the Continuous Change Detection and Classification (CCDC) algorithm. Results showed that the overall LULC classification and change detection accuracies were 89% and 92%, respectively. The high-intensity urban land had the largest mean LST value of 294.9 K and yearly amplitude of 17.4 K. A comparison of the trend component between urban and non-urban land covers showed a difference of 1.8 K per decade. Temporal thermal signatures were created to characterize and quantify the impact of urban LULC changes.

Morabito et al. (2016) evaluated the impact of built-up surfaces on land surface temperatures in Italian urban areas by using MODIS remote sensing data. The effect of annual and seasonal land surface temperature (LST) modifications resulting from increased urban built-up coverage, was analyzed throughout the whole year, and specifically in two different periods (cool/cold and warm/hot periods). The relationships between the dependent (mean daily, daytime and night-time LST values) and independent (built-up surfaces) variables were investigated through linear regression analyses. Statistically significant linear relationships (0.001) between built-up surfaces and spatial LST variations were observed in all the cities.

2.3.3 Regional Climate Model (RCMs)

Montavez et al. (2000) had formulated a model for the urban canyon meteorological conditions of weak winds at night time. Thermal radiation, conductivity, and convection were simulated by means of the Monte Carlo method. These were the main physical processes of energy transfer that gave rise to the characteristic temperature distribution.

The predictions of the model under more realistic conditions accurately reproduce the observational results. A strong temperature gradient across streets, with the canyon corners up to 4 ^{o}C warmer than the canyon center, was found for the deepest canyons.

Sarma et al. (2001) suggested that human activities in terms of LULC changes might be responsible for local climatic alterations. The decreasing trend in daytime and increase in night-time temperature and increased rainfall during the past three decades in the Godavari deltaic region were the result of a large-scale increase in vegetation cover as well as wetlands in the form of shrimp/fish ponds. Analysis of the climatic data of years from 1970-1998 for different stations indicated that the daytime temperature has decreased by 0.2 to 0.7 ^{o}C while the night time temperature has increased by 0.5 to 0.6 ^{O}C during the past three decades.

Harman (2003) investigated about the surface morphology in determining the surface energy balance of an urban area and the subsequent impacts on the planetary boundary layer. An analytical approach was used to investigate the exchange of diffuse radiation in a street canyon. Results revealed that in urban area temperature was more due to multiple reflections of radiation were found to play an important role.

Zhou et al. (2004) customized a multi-scale numerical modelling system to simulate the urban environment. Different type of urban surfaces was considered along with roughness was replaced with building drag factor. Also, effects of building distribution, azimuth, screening of shortwave radiation and the influence of anthropogenic heating was also considered in the customized model. Results were in close agreement with the observed data and it was concluded that model could be used to simulate the urban meteorological environment.

Chen et al. (2006) have discussed the effect of LULC change (1990-2000) on the land surface temperature (LST) for Zhujiang Delta in China. Remote sensing data was used to extract the LULC information and thermal band was used to determine land surface temperature. They demonstrated that remote sensing and GIS technologies can be used for determining the LST. Study concluded that urbanization in Zhujiang Delta caused increase in LST by 4.56 ^{o}C.

Yoshida et al. (2012) have evaluated the impact of historical land-use changes (LUCs) from 1987 to 2006 on surface warming rates and rice yield on the island of Shikoku, Japan. Authors have performed two types of numerical simulations i.e., with historical LUCs and with fixed land uses using regional atmospheric model (JMA-NHM) and a large-area rice-growth model (PRYSBI). It was found that LUCs from paddy field

to buildings and road caused warming rates in and around paddy field were five times those in and around other land uses. Rice yield was also found to reduce by 0.27% in 2006 as compared to year 1987. Authors have performed two types of simulations using the JMA-NHM non-hydrostatic regional atmospheric model (Saito et al., 2007) and the PRYSBI rice growth model (Iizumi et al., 2009). In the first simulation, land uses in the JMA-NHM model were changed year by year for 1987 to 2006 on the basis of their recorded values (hereafter, the "historical run"). In the second simulation, land uses in the model were fixed at the 1987 values throughout the study period (hereafter, the "fixed run"). In both simulations, authors have used the daily weather data simulated by the JMA-NHM model as inputs for the PRYSBI model to simulate rice yields. Land use for the JMA-NHM 5-km grid was expressed as a set of five land surface parameters: surface albedo (a), evaporative efficiency (b), roughness length (zo), heat capacity (cr), and thermal conductivity (l).

Ha and Yun (2011) studied regional climatic change in terms of minimum summers temperature for Seoul. Effects of water vapour and temperature on total number of days was determined using long term historical data. For this, total number of days were defined as days when the daily minimum temperature is greater than 25 ^{o}C. Long-term records showed a gradually increasing trend of 13 days/100-years, which results from the changes in the sensible heat and Tmean. This study can contribute to improving scientific understanding of observed changes in extreme climate conditions.

Li et al. (2013) conducted a simulation study on the regional temperature variation induced by future deforestation in European Russia boreal forest region based on future LULC change and the Weather Research and Forecasting (WRF) model. The results indicated that the model has good ability to simulate the temperature change and land cover change conversion from boreal forests to croplands (boreal deforestation) over a large period of time. The study revealed that regional annual temperature would decrease by 0.58 ^{o}C in the future 100 years, resulting in cooling effects to some extent and making the near-surface temperature decrease in most seasons except the spring.

Jiang et al. (2014) investigated the regional climatic response to irrigation especially on heat fluxes and near-surface temperature in the future in northern China. Weather Research and Forecasting model was used to compare results of three land cover scenarios i.e. the control scenario (CON), the irrigation scenario (IRR), and the irrigated cropland expansion scenario (ICE). Simulation model results suggested that the conversion to irrigated agriculture at the contemporary scale leads to an increase in annual

mean latent heat fluxes of 12.10 Wm−2, a decrease in annual mean sensible heat fluxes of 8.85 Wm−2, and a decrease in annual mean temperature of 1.3 ^{o}C this change impacts on the total heat flux in the study area.

Wang et al. (2014a;b) conducted a study for assessment of the regional scale impact of LULC change on climate. To obtain reliable climate trends, the standard normal homogeneity test (SNHT) was applied to surface air temperature and precipitation data for a period of 1951–1999. The study suggested that LULC integrating regional topography should be considered as a force in regional climate modelling.

Yoshida et al. (2014) studied the responses of summer mean, maximum and minimum surface temperatures to given LULC changes through statistical analysis which is named as impact function. These impact functions were derived by relating the RCM simulated sensitivity of temperature to changes of 5 land-surface parameters (surface albedo, evaporative efficiency, roughness length, heat capacity, and thermal conductivity). Authors determined the impact function in term of relative importance of a specific land-surface parameter for the local temperature like greater sensitivity of daily mean temperature to evaporation efficiency. Impacts functions were compared with RCM simulations to assess how well estimated results are matched with historical LUC-induced RCM warming simulations in the area between 1987 and 2006. Efforts have been made to estimate the potential warming range for different LULC scenarios. Cubic spline function was selected to fit in the generated data to mimic the gradual increase or decrease in value of the temperature variables associated with the change in value of land surface parameter.

Xu et al. (2015) investigated the diurnal and seasonal climatic response to LULC changes in Asia through two numerical experiments with potential and current vegetation cover using the fully coupled Community Earth System Model. Authors showed that LULC changes leads to a reduced diurnal temperature range due to the enhanced (reduced) diurnal cycle of the ground heat flux. Daily minimum surface air temperature exhibits a clear seasonality over India as it increases most in the pre-monsoon season and least during the summer monsoon season. The study stated that bio-geophysical mechanisms are responsible for the region-specific LULC change induced diurnal and seasonal response.

Lejeune et al. (2015) have studied the impact of future deforestation of Amazon forest on climate i.e., increase in temperature. Authors have used a regional climate model at 50 km spatial resolution over South American Continent to simulate the effect of

Amazon forest deforestation on climate and temperature regime. Change in climate i.e., temperature has been studied corresponding to different Amazon deforestation scenarios. Authors have performed four ERA interim-driven simulations with prescribed land cover maps corresponding to present day vegetation, two deforestation scenarios for twenty first century, and a totally deforested Amazon case. In response to projected land cover changes for 2100, authors have found out an annual mean surface temperature increase of 0.5 ^{o}C over the Amazonian region and an annual mean decrease in rainfall of 0.17 mm/day compared to present-day conditions. These estimates found to reach 0.8 ^{o}C and 0.22 mm/day in the total-deforestation case. Their results suggest that the bio-geo-physical effects of deforestation alone are unlikely to lead to a tipping point in the evolution of the regional climate under present day climate conditions. However, the conducted synthesis of the literature reveals that this behavior may be model dependent, and the greenhouse gas induced climate forcing and biogeochemical feedbacks should also be taken into account to fully assess the future climate of this region.

Zhang, (2015) presented a review about natural and human induced changes in summer climate over the East Asian monsoon region in the last half century and a significant warming trend occurred in summer and rainfall in summer over eastern China exhibited a change in spatial distribution at the decadal time scale, in response to the decadal shifts. Author expected the reason behind the roles of anthropogenic factors, such as, greenhouse gases, aerosols, and LULC changes.

Heo et al. (2015) evaluated the climate change due to human induced activities from 1970 – 2009 with respect to temperature and precipitation. It was found that for 0.9 ^{o}C increase in temperature there was 10.9% decrease in precipitation. The temperature exhibited a lower increasing trend and precipitation showed a similar decreasing trend as compared to previous studies. The dominant LULC trend was grass and forest conversion into bush/shrub and developed land and cropland into barren and grassland. These modifications indicated that changes in temperature and precipitation in the study area might be linked to changes in land cover, although, human involvement was recognized as the major LULC change contributor for the short term.

Fan et al. (2015) studied the impacts on the temperature and precipitation due to significant changes in vegetation coverage during 2001–2009. A new attribution method was developed and applied to observed data for investigating the interrelationships between climate variation and LULC change. Regional climate attribution analysis indicated a larger contribution ratio (based on a comparison of standard deviations of each

contributing factor-induced climate changes and that of total change) from climate variation than from LULC change (0.95 from climate variation vs. 0.35 from LULC change) for variations in temperature. Impacts on precipitation indicated more spatial variations than those on temperature. LULC change attribution analysis suggested that LULC change observed in year 2000 resulted primarily from human activities rather than climate variations (0.99 contribution ratio from human activities vs. 0.26 from climate variation).

Stone and Hansen (2016) studied the rapid systematic assessment for detection and attribution of regional anthropogenic climate change. Use of the method on 116 regional assessments of recent temperature and precipitation changes indicated that existing rules for detectability of climate change are ignoring the sources of uncertainty, most predominantly the importance of adequate observational monitoring.

Huang et al. (2015b) investigated the changes in land use, climate and the environment in China during 1980–2012. Statistical and spatial analysis revealed that urbanization (92.7%) has taken place at the loss of farm land. The significant increase in scattering radiance and earth's albedo caused by the urbanization leads to (Pearson correlation coefficient (r) between urban land and scattering radiance = 0.86, $p<0.0001$; r between farmland and scattering radiance = −0.92, $p < 0.0001$) warming in the regional. The study also revealed that LULC change and human activities may be the primary reason for the rising temperature.

Deng et al. (2015) analysed the impacts of LULC changes on surface energy and water balance in the Heihe river basin of China during 2000-10. A series of indicators of energy and water balance were simulated using WRF model. Model simulations revealed that conversion from grass land to barren land have significant effect on energy balance.

As discussed above it is well established that climate is changing and LULC changes also have significant effect in changing the climate. Effects of climate change were discussed extensively in the literature (Oke and Cleugh, 1987; Weng and Yang, 2004; Feddema, 2005; Christy et al., 2006; Javed Mallick and B.D.Bharath, 2008; Chang et al., 2010; Calzadilla et al., 2013; Liu et al., 2014; Ren and Zhou, 2014; Mohan and Kandya, 2015). There are various methods and approaches used in recent past for the assessment of LULC change impacts on climate including statistical methods (trend analysis), simulation models (GCMs and RCMs), downscaling global climate projections (dynamical downscaling and statistical downscaling), land surface temperature based methods, observed minus re-analysis (OMR) approach, sensitivity experiments; surface

energy balance based methods, water balance based approaches and terrestrial carbon balance based approaches.

Spatial resolutions of GCMs are usually quite coarser because of their significant complexity and need to provide multi-century integrations. This results in the loss of regional and local details of the climate that are influenced by spatial heterogeneities missing from these models. Therefore, GCM simulations of local climate on spatial scales smaller than grid cells are often poor, especially when the area has a complex topography (Schubert, 1998; Timbal and McAveney, 2001; McBean and Motiee, 2006; Liu and Deng, 2011b; Li et al., 2013, 2017; Wang et al., 2014a; Halder et al., 2016).

Several studies have shown significant climate impacts of LU change through sensitivity experiments (e.g. (Bonan, 1997, 1999; Gordon et al., 2005; Pielke, 2005; Li and Molders, 2008; Findell et al., 2009; Kumar et al., 2010; Avila et al., 2012; Kharol et al., 2013)). However, such studies are based on using GCM output with different LULC forcing in different future scenarios which have very high level of uncertainties and may not be suitable in determining relative contribution of LULC changes in changing the climate (Pitman et al., 2009; Noblet-Ducoudré et al., 2012; Deng et al., 2013; Mimura et al., 2014).

Impact of urbanization and LULC changes on climatic variables were studied through comparative study of climatic trends for urban and rural meteorological stations (Karl et al., 1988; Easterling, D. R., Horton B., Jones Ph. D., Peterson Th. C., Karl Th. R., Parker D. E., Salinger M. J., Razuvayev V., Plummer N., 1997; Pingale et al., 2014, 2015) and satellite imagery (Gallo and Owen, 1999; Peterson et al., 1999; Hansen et al., 2013; Peng et al., 2016).In recent studies, remote sensing data and geo-spatial techniques have been used to investigate the relationship between LULC change and land surface temperature using different analysis methods and found positive correlation between surface temperature and impervious surfaces (Carlson and Arthur, 2000; Chen et al., 2006; C et al., 2010; Cinar, 2015).

In few studies, the negative correlation has also been found between land surface temperature and vegetation index (NDVI) and cooling effect observed from vegetative areas (Lin et al., 2009; Weng, 2009; Araya and Cabral, 2010; Dong et al., 2013).

In few studies, the positive correlations were found between air temperature trends (decadal) and LULC decadal changes derived from satellite data using statistical techniques like regression analysis (Wang et al., 2014a; Cinar, 2015). In few studies, efforts have been made to develop statistical models/functions (statistical emulation) to

co-relate LULC change and local temperature response. Such statistical model mimics the response of a complex climate change model to a given forcing change (Good and Hardin, 2006; Murphy et al., 2007; Hanasaki et al., 2008; Iizumi et al., 2009; Yoshida et al., 2014; Huang et al., 2015c). Through studies of urban heat islands also impacts of LULC impacts on temperature have been discussed (Kuckla et al., 1986; IPCC TAR, 2001; Peterson and Schwing, 2003; Parry Martin L. et al., 2007; B, 2008; Rogan et al., 2013; Morabito et al., 2016; Peng et al., 2016). Looking at the importance of this issue National Research Council in USA has recommended to include LULC (Jacob et al., 2005) for climate change research.

In last few decades, many authors have used observed minus re-analysis (OMR) approach to estimate impact of LULC changes by commuting difference between the trends of surface temperature observations and reanalysis datasets (Kalnay and Cai, 2003; Zhou et al., 2004; Frauenfeld et al., 2005; Lim et al., 2005; Kalnay et al., 2006; Pielke et al., 2007; Lim, 2008; Nunez et al., 2008; Fall et al., 2010; Wang et al., 2014a; Feng et al., 2016). It is found in previous OMR approach based studies that warming is associated with urbanization (Kuckla et al., 1986; Arnfield, 2003; Zhou et al., 2004; Hale et al., 2006, 2008; Fall et al., 2010; Feng et al., 2016). Most of these studies are qualitative in nature where, LULC changes were related statistically with change in representative meteorological characteristics.

LULC changes affect surface climate as a result of change in surface energy, water balance components and carbon with in the atmosphere, ecosystem and soil (Kalnay and Cai, 2003; Järvi et al., 2011). Surface energy and water balance based distributed methods have been used in recent past to investigate effects of direct and indirect LULC change mechanisms on climate.

A variety of models and methods have been developed for computing the surface energy fluxes through using energy and water balance approaches (Holtslag and Van Ulden, 1983; Grimmond and Oke, 1995, 1999; Copeland et al., 1996; Betts, 2001; Pielke et al., 2002; Feddema, 2005; Offerle et al., 2006; Das and Padmanabhamurty, 2008; CSB et al., 2010; Järvi et al., 2011; Middel et al., 2012; Deng et al., 2013; Kleczek et al., 2014; Liu et al., 2014; Sanchez-Lorenzo et al., 2015). The limitation of these models and methods is that they consider lumped effect of LULC or few other only consider one or more fluxes. In few studies, complete energy balance have been undertaken at suburban residential sites (Grimmond and Oke, 1995, 1999; Järvi et al., 2011; Middel et al., 2012).

However, how LULC changes are affecting surface energy balance components with respect to climate change has not been discussed well.

2.4 CLIMATE CHANGE AND ITS OPTIMUM ADAPTATION MEASURES

Recent studies and observations continue to demonstrate changing climate and that may be the reason of many extreme climatic events impacting on people, infrastructure, and natural systems like increased heatwaves in many parts of Europe and Asia including India, extreme rainfall events and flooding in many part of world, severe Cyclones in many parts etc. As discussed above climate change is happening due to gaseous pollution and different natural and human induced anthropogenic activities including LULC changes (Bonan, 1997; Gallo and Owen, 1999; Chase et al., 2000; Baidya Roy and Avissar, 2002; Feddema, 2005; Christy et al., 2006; Fall et al., 2010; Pingale et al., 2014, 2015; Cinar, 2015). Development, urbanization and LULC change are inevitable due to ever increasing population and demand for enhancement of living standards. Also, adverse effects of climate change are more pronounced at local scale and in urban areas, where large population is under increased risk.

Therefore, appropriate mitigation and adaptation measures should be designed and implemented to minimize the adverse effects of climate change. The standard mitigation and adaptation measures are curb on greenhouse gases, forced land use planning, provisions to protect infrastructure and ecosystems, regulations related to land use, early response and recovery. Mitigation of climate change is very difficult and a very long term process.

Appropriate adaptation measures are another approach to deal with climate change and becoming popular. So, only available option is to implement different type of adaptation measures including measures related to purposeful transformations of LULC. In the urban areas, LULC related adaptation measures includes reduction in the surface temperature by shading of ground and building surfaces, increase in vegetation, covering roof tops with grass, and use of more reflective construction materials. Through, such LULC transformations turbulent and convective heat transport can be decreased and adverse impacts of climate change can be reduced (Spronken-Smith and Oke, 1999; Saaroni, 2003; Streiling and Matzarakis, 2003; Ali-Toudert et al., 2005; Potchter et al., 2006; Ali-Toudert and Mayer, 2007; Gill et al., 2007; Lin and Matzarakis, 2008; Shashua-Bar et al., 2009, 2012; Georgi and Dimitriou, 2010; Thorsson et al., 2011; Oliveira, S.,

Andrade, H., and Vaz, 2011; Sun and Chen, 2012; Cohen et al., 2012; Handmer et al., 2012; Charalampopoulos et al., 2013).

The above discussion illustrates that dealing climate change with adaptation measures plays a very important role especially in urban and semi-urban areas where a large percentage of the population reside and prone to adverse effects of climate change. Several adaptation measures have been reported in the literature which can be adopted to minimize the effects of climate change in a qualitative manner. Understanding the link between urbanization and microclimate is imperative for urban environmental planning to determine effective design strategies, e.g. altering the paved areas, open land, vegetation and irrigation regime, in order to improve urban climate.

The knowledge of how to purposefully manipulate the SEB by changing urban LULC is crucial to urban climate adaptation. Knowledge of the relative impact of adaptation measures in controlling climate change in term of indicative meteorological parameters like, surface energy balance or temperature is still lacking, which is necessary to plan and implement the optimum adaptation measures.

Literature review covering various aspect of different ideas and techniques adopted by the researchers to minimize the adverse impacts of heat fluxes especially in urban areas details of this methodology adopted by the researchers subsequently given below.

Spronken-Smith and Oke (1998) studied the thermal regime of urban parks in two cities with different summer climates. Differences between the temperature of vegetated urban parks and that of their surrounding built environment were reported. In the study area, parks are typically 1-2 ^{o}C, but in ideal conditions can be almost 5 ^{o}C cooler than their surroundings. But irrigated green-space can be 5-7 ^{o}C cooler. Park type, especially the extent of irrigation and the presence of trees are important. During day time, trees may play an important role in establishing a cool park effect, perhaps through a combination of shade and evaporative cooling. At night, it appears that the surface geometry and moisture status of the park are important controls on surface cooling. Open parks (with higher sky view factors) that have dry soils (and hence lower thermal admittance) cool the most.

Upmanis et al. (1998) studied the influence of green areas on nocturnal temperatures in a high latitude city (Goteborg, Sweden). The maximum temperature difference found between a park and a built-up area was 5.9 ^{o}C (summer), and the extension of the cool park climate into the built-up area was over 1100 m from the park

border. The green area cooled at a faster rate than the built-up area, although there were large variations within each area. At the rural station, located at an open site, the cooling was less than at the open part of the green area. Differences in sky obstruction between the sites explained some of the variations in cooling and temperature. However, the relationship between the urban park temperature difference and sky view factor was not statistically significant.

Scherer et al. (1999) presented the climate maps to enable planning authorities taking care of the urban climate and its interrelations with urban structures. Climate maps containing the results of the analysis and evaluation of the urban climate were estimated by the involved planners to be a valuable tool meeting their practical requirements for urban planning and adaption measures need.

Lazar and Podesser (1999) analyzed the climate of Graz and its significance for urban planning in the tributary valleys east of Graz (Austria). The results of the study, above all the map of city climates, are based on the latter a map of planning tips serve as an important basis for urban planning and have already been used for the setting up of a LULC and development plan. The conclusion is that from climatological results in urban planning is unique within Austria and is now also being practiced in other cities of the province of Styria.

Planning et al. (2000) investigated if, how and when knowledge about the climate is used in the urban planning process. The research strategy was developed in an interdisciplinary research group involving climatologists and planners. Case studies involving different interview techniques and historical data were carried out by different actors involved in urban planning at the municipality level in three cities in Sweden. The study showed that urban planners were interested in climatic aspects but the use of climatic information was unsystematic and the results confirmed that climatology has a low impact on the planning process. It is important that urban climatologists meet the planner's demand-driven needs by providing them with good arguments, suitable methods, and tools.

Dhakal and Hanaki (2002) had analyzed the implications of anthropogenic heat discharges into the urban thermal environment of Tokyo. The improvements in the urban thermal environment via the various measures were analyzed for two types of scenarios, namely, scenarios related to the management of heat discharge sources and urban surface modifications. The maximum improvement in average temperature for daytime was found to be 0.47 ^{o}C (at noon) as a result of greening the areas around the buildings of Tokyo.

Similarly, the maximum improvement in average temperature for the evening was found to be 0.11 ºC by discharging all heat to the ground.

Shashua-Bar and Hoffman (2003) investigated on geometry and orientation aspects in passive cooling of canyon streets with trees. Recently, studies based on the street cluster thermal time constant (CTTC) model have been carried out by the authors with a view to assessing the thermal effects of alternative architectural designs of the flanking buildings and inner courtyards. The effect of green spaces especially that of shade trees which play a significant role in solar radiation penetration, has not yet been considered. The present study suggested that how much effects can climate change cause due to the presence of shade trees. It directly influences the air temperature, moisture and wind flow within the streets as well as the urban surrounding area and has been the topic in several urban climatology studies.

Jonsson (2004) analyzed the influence of vegetation on the urban climate in the subtropical city Gaborone, Temperature records from an urban and a rural station were analyzed for the period 1985-96. In present study an attempt has been made to explain the possible seasonal change in vegetation, NOAA satellite normalized difference vegetation index imagery. Evapotranspiration lowers the temperature, which was detected by high humidity in areas of lush vegetation. This becomes apparent at midday, when densely vegetated areas were up to 2 ºC cooler than rural sites. There was an apparently opposed effect of rural and urban vegetation, whereby the former is hindering the temperature from falling and the latter is cooling the environment through evapotranspiration. This can be explained by the overwhelming amounts of imported water in the city promoting evaporative cooling.

Shashua-Bar and Hoffman (2004) have presented a quantitative analysis for predicting the air temperature variations within urban clusters with trees. The clusters considered were streets and attached courtyards which together constitute a major part of the residential areas. In this study, the cooling effect of trees was quantified, using the analytical "Green CTTC model" developed recently by the authors. The empirical and analytical approaches provide corroborative estimates and conclusions. The results indicated that the combined simulated cooling effect of the above three factors was about 4.5 K, at midday in summer (July-August) in the Mediterranean coastal region of Israel, a cooling which is about 50% of the air temperature rise from sunrise to noon hours.

Saitoh and Yamada (2004) conducted an experiment to demonstrate the subscale thermal plume over constructions in the urban surface layer. A new subscale modelling

for the urban surface layer was proposed. The feasibility of the proposed model was discussed by comparing the two-dimensional numerical simulation results. The numerical simulation showed a significant temperature increase of more than 5 ^{o}C in the region over the urban structures. Information and results collected from this research could be used for future practical applications in planning, redevelopment, and restructuring urban cities.

Hageback et al. (2005) examined the change and variability in climate, land use and farmer's perception, adaptation and response to change in Danang watershed in the Chinese Loess Plateau. Their first focus was to look at how climate data recorded at meteorological stations recently have evolved, and how farmers perceived these changes. Further, observed how the farmers respond and adapt to climate variability and what the resulting impact on land use. This adaptation makes them less vulnerable to climate variability. It was found that government policies and reforms had a stronger influence on LULC than climate variability. Small-scale farmers should, therefore, be considered as adaptive to changing situations, planned and non-consciously planned.

Cavan et al. (2006) have developed a good practice adaptation action plans to help coordinate the delivery of adaptation strategies within the project partner's areas. The preparation of these adaptation action plans was informed by an assessment tool, which highlights climate change vulnerabilities and risks in urban areas. The approach was based on the findings of the Adaptation Strategies for Climate change in the Urban Environment (ASCCUE) project, which implements a risk framework, focusing on the three elements; hazard, vulnerability, and exposure. The project aims to facilitate the much-needed exchange of knowledge and experience as well as the actual transfer of good practice on climate change adaptation strategies to local and regional authorities.

Ahmed et al. (2013) studied about LULC dynamics and their impacts on land surface temperature (LST) in fast-growing mega-cities like Dhaka, Bangladesh. Landsat satellite images of 1989, 1999, and 2009 of Dhaka Metropolitan (DMP) area were used for analysis. The findings of this study possess a major challenge for urban planners working in similar contexts. However, the technique presented in this study would help urban planners to quantify the impacts of different scenarios (e.g., vegetation loss to accommodate urban growth) on LST and consequently to devise appropriate policy measures.

Viegas et al. (2013) studied on urban land planning and role of a master plan in influencing local temperatures. Land use planning (LUP) was central for managing issues

related to climatic variation in urban environments. However, Master Plans (MPs) usually do not include climatic aspects, and few studies have addressed climate change at the urban scale, especially in developing countries. This study proposed a framework with ten categories for assessment of climatic variation in urban LUP. Each category comprises attributes that describe a complex of relationships in influencing local temperature variations. So it can be concluded that the master plan does not offer answers to all the imbalances related to land use, and therefore gives insufficient support to tackle the issue of rising temperatures.

Halder et al. (2015) investigated the impact of LULC change on Indian summer monsoon daily rainfall and temperature during 1951–2005 using a regional climate model. Mean and extreme near-surface daily temperature during the monsoon season have also increased by a maximum of 1–1.5 ^{o}C. Simulation by a high-resolution regional climate model (RegCM4) with prescribed vegetation cover of 1950 and 2005 demonstrated the changes in moderate rainfall events and temperature caused by LULC change. The results also showed that LULC alone causes warming in the extremes of daily mean and maximum temperatures by a maximum of 1–1.2 ^{o}C, that is comparable with the observed increasing trend in the extremes. The study showed the necessity for inclusion of projected anthropogenic changes in (LULC change) in future climate change scenarios for developing better adaptation and mitigation strategies.

Cinar (2015) evaluated the climatic response of urban landscape conversion and examined the relationship between LULC change and land surface temperature (LST) data collected using advanced remote sensing (RS) techniques instead of atmospheric temperature. The findings revealed an important relationship between monthly mean air temperature and land changes over recent decades, which resulted in an increase in urban fabric land use, deforestation land cover changes and conversion of permanent crop fields to artificial greenhouses for earlier vegetable production; the R- square values for these regressions were 97.7%, 88.5%, and 90.6% respectively. The results should be used to support better urban landscape plans and architectural designs to improve human thermal comfort for sustainable urban living and green spaces should be examined carefully in urban planning and design for climate adaptation.

2.5 CONCLUDING REMARKS

Different aspects of the climate change assessment, effects of LULC changes on climate, different methods/models for assessment of LULC change impacts on climate and various

type of adaptation measures and their effectiveness in controlling the adverse impacts of climate in urban areas have been studied and discussed. Following conclusions have been drawn from the literature review.

1. Climate change effects are more pronounced at regional and local scale as compared to global scale.
2. LULC change is one of the important forcing agents of climate change in addition to the Greenhouse gases (i.e. CO_2).
3. LULC change and its effects on climate is more significant for urban and semi-urban areas.
4. Understanding of LULC change and its effects on climate is in its early stage. No quantitative relationships are reported so far, which reveal the LULC change effects of climate change.
5. To understand climate change and its effects on climate various methods and models have been developed by the researchers, which primarily consider greenhouse gases as forcing agents at a global scale. However, all these methods are still having considerable uncertainties in the results and have issues related to some rigid boundaries regarding the data, specific results and time consuming for calculating results. In the case of models used for climate change assessment, resolution problem and mixed land use remains a challenge.
6. Climate change cannot be mitigated quickly and major emphasis is to be given for appropriate adaptation measures to deal with adverse effects of climate change.
7. Understanding the link between urbanization and microclimate is imperative for urban environmental planning to determine effective design strategies, e.g. altering the paved areas, open land, vegetation and irrigation regime, in order to improve urban climate. The knowledge of how to purposefully manipulate the SEB by changing urban LULC is crucial to urban climate adaptation.
8. Most of the researchers define the relationship between forcing agent and its effect on climate in qualitative terms but failed to develop in quantitative terms. So, there is a need to develop a quantitative relationship among forcing agents and adaptation measures to find out optimum adaptation measures before their actual implementation.

9. Advanced technologies and remote sensing and GIS can be used for such studies to limit the uncertainties due to spatial and temporal variations of climate change forcing agents.

CHAPTER 3

STUDY AREA AND DATA USED

3.1 INTRODUCTION

Present study is aimed to investigate the effect of LULC change on micro-climate of an area in term of resulting change in surface energy balance which can be assumed to be proportional to change in local climate. LULC changes are taking place more in urban areas as compared to rural areas owing to large scale conversion of pervious and vegetative areas in to impervious surfaces and built-up areas to satisfying the development needs to ever-increasing and aspiring population. Also, it is evident from historical climatic data that climate of urban areas is changing more as compared to rural areas, due to gaseous pollution and increased anthropogenic activities including LULC changes. Large number of people are residing in urban areas and are under higher risk of adverse impacts of change in climate.

An attempt has been made to select such areas for the present investigation where, lot of LULC changes have taken place in recent past. Another criterion based on which selection of study area was based, is availability of climatic data at required resolution. Therefore, two areas surrounding to two meteorological stations i.e., Palam and Safdarjung in Delhi, Capital of India, have been selected as study areas. In recent past, significant LULC changes have been observed in both areas. LULC have been found to be more in Palam area as compared to Safdarjung area. Palam area has witnessed lot of development in last two decades including a big international airport, where lot of pervious land has been converted into paved areas, runway and other type of impervious cover. Another reason of selection of these two areas for present research is availability of meteorological data for both the locations. Meteorological data including radiation information is available at hourly time step for both the stations. Extent of two study areas, surrounding to both the India Meteorological Department (IMD) stations have been finalized in term of square areas inscribing a circle of 5 km radius, assuming that there is no significant variation in meteorological characteristics within 5 km radius (McVeigh, 1983). Location of the study areas have been presented in Figure 3.1 and salient features are discussed in subsequent sections.

3.2 SALIENT FEATURES OF THE STUDY AREA

3.2.1 Location

Both the areas selected for the present investigation are part of Delhi, Capital city of India. Delhi is situated in the north Indian great plain. Palam and Safdarjung Meteorological stations are at the center of selected study areas, respectively. Safdarjung area is located at 28.58° N Latitude, 77.20° E Longitude, whereas Palam is located at 28.57° N Latitude, 77.12° E Longitude. Location of the study areas has been shown in Figure 3.1.

Palam is a major suburb and residential area in South West Delhi. The Indira Gandhi International Airport, formerly known as Palam Airport, the main airport of National Capital Region is situated here. Palam is situated 20 km southwest to the New Delhi city center. It is surrounded by Dwarka, Janakpuri and Delhi Cantt. Palam comes in the Dwarka Sub-division of South West Delhi District. Safdarjung area consists of mainly two localities in South Delhi namely, Safdarjung Enclave and Safdarjung Development Area (SDA). There are several districts (called, colonies) in Delhi, located south to the Tomb of Safdarjung, second, Nawab of Awadh, and an important administrator in the Mughal Imperial courts in Delhi, under Muhammad Shah in the 18th century.

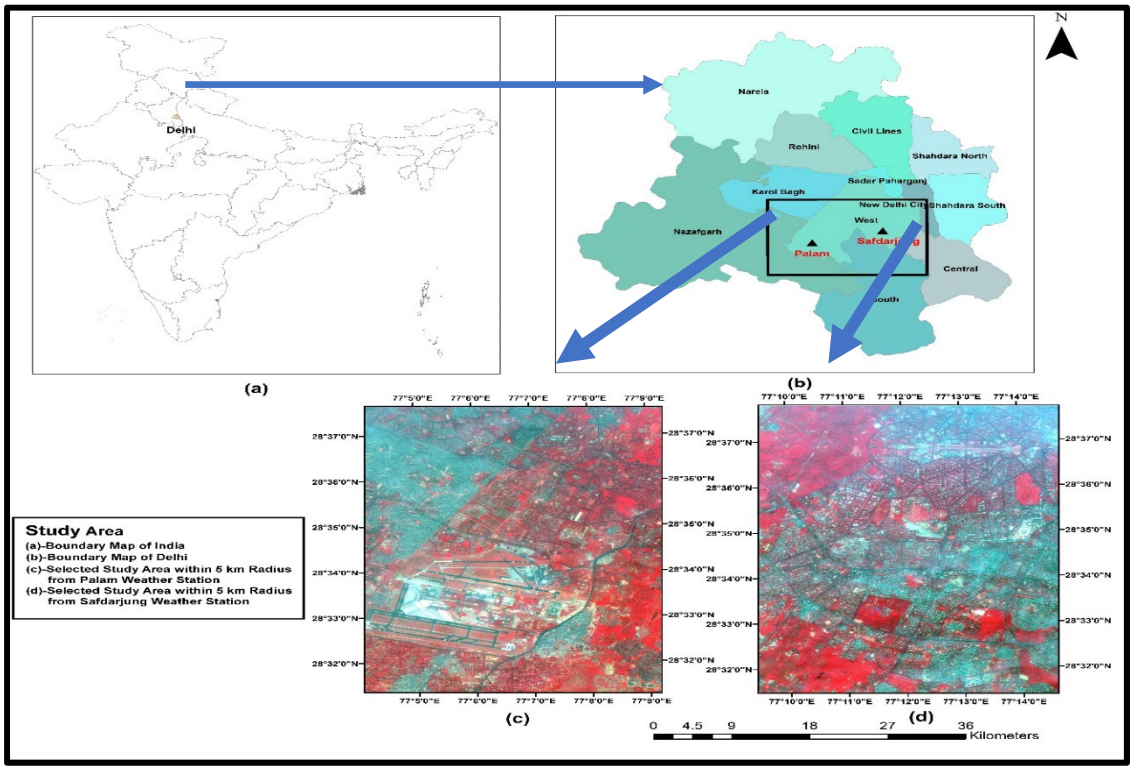

Figure 3.1 : Map for the two study areas (Palam and Safdarjung)

3.2.2 Land Use / Land Cover

Both areas are urbanized having predominant LULC class is built-up. Main LULC classes available in the study area are i.e. settlement, road & paved surface, barren land, forest, trees, grass and water. Both areas have urbanized in last 30-40 years with increase in population and migration of people from different parts of country. Significant area has converted into impervious cover over the period to satisfy development needs of people. Built-up area has increased significantly in last five decades. In Palam area, built-up which include settlement, paved and road land use class have increased from 1546.20 ha in year 1973 to 7747.70 ha in 2014. Similarly, in Safdarjung area, built-up has increased from 2910.90 ha in year 1973 to 8499 ha in year 2014. Details about the LULC and its changes have been discussed in detail in Chapter 4. Built-up area in both areas has increased at the expense of open land, water bodies and vegetative areas like shrubs and forest. Relative peak changes in percentage (%) of bare soil and forest area shows decreasing trend in both areas. Such a large-scale conversion of pervious areas into impervious surface have significant effects on surface energy balance of the area which may lead to adverse effects on micro-climate.

3.2.3 Physiography and Soil

Physically, the natural capital territory of Delhi can be divided into 3 segments - the Yamuna flood plain, the Ridge and the Plain. The ridge constitutes the most dominating physiographic features of this territory. It originates from the Aravali hills of Rajasthan and entering the union territory from the south extends in a north-eastern direction. It encircles the city on the North West and west. The point near Bhatti has a height of 1045 ft. Tughlaquabad fort is located on one of the highest spurs of the ridge.

Because of the human migrant influx, the city is dominated by a mixture of human settlements, govt. offices, and residential and commercial complexes with some vegetated areas. Same character of the city is also available in both the selected areas. The ridge constitutes the most dominating physiographic features of this territory. The green area includes forest area, area under district parks, city parks, community parks, neighborhood parks and the open area covered under plantation in the residential as well as the large complexes (FSI, 2013).

Four major geomorphic land forms have been identified in the soils of Delhi. Soil of Delhi have been grouped into 15 soil series (Chibbar, 1985). About 15% of this area is

affected by salinity or alkalinity and about 64% of the total area is irrigated. Soils of Delhi are generally low in available nitrogen, low to medium in phosphorus, medium to high in potassium, adequate in calcium, magnesium and Sulphur. In most of area at both study areas soil has been found to be sandy loam and sandy clay loam. The soil type on Delhi ridge has been reported as sandy loam to loam (Chibbar, 1985).

3.2.4 Meteorological Condition

Climate in Palam and Safdarjung can be classified as humid subtropical. Temperatures in these areas usually range from 5 to 40 °C, with the lowest and highest temperatures ever recorded being −2.2 and 48.4 °C, respectively (Rahman and Kumar, 2011). The average annual temperature recorded in Delhi is 31.5°C based on the records over the period of 70 years as reported by the IMD. The cold season begins at the end of November, and extends to the late February. The mean relative humidity in the areas has been found around 66%. Winters are usually cold and night temperatures often fall to 2.0°C during the period between December and February. Predominant wind direction is generally W-NW but during monsoon E-SE, with a range of average speed varying from 2.5 to 3 ms^{-1}. Average annual rainfall of in these area is 625 mm, of which 95% occurs during the monsoon season (July to September).

3.3 ENVIRONMENTAL CONDITION

Rapid development process and ever-increasing population pressure have posed enormous challenges in maintaining environmental sustainability in Delhi. The city suffers from air pollution caused by transportation, road dust, industries and pollutant emissions. Noise pollution comes mainly from industries, transportation, aircraft etc. Water pollution and lack of adequate solid waste treatment facilities have caused serious damage to the river on whose bank's Delhi grew, the Yamuna, several steps have been taken in the recent past to improve the environmental condition which includes massive focus on afforestation, universal use of CNG by commercial vehicles, ban on plastic use, better management of solid waste, treatment of waste water and improvement of sewage system etc. Conversion of water bodies into constructional land is the visible impact of urbanization in Delhi. Depletion of ground water due to excessive withdrawal for industrial and domestic use to fulfill the growing demand, posing an additional environmental problem (Sharma and Dikshit, 2016).

3.4 DATA USED

In the present research, LULC changes and its impact on micro-climate has been investigated. Work includes assessment of climate change, determination of LULC changes over selected duration, and surface energy balance modelling to ascertain changes in surface energy balance components due to change in LULC. Variety of data and information have been used in the present work which includes historical data of LULC, long term meteorological information, topographical information, water uses data and LULC surface energy interaction coefficients (Table 3.1).

Table 3.1 : Detailed information of satellite images used

Sr. No.	Satellite	Sensor	Year	Spatial Resolution (m)	No. of Spectral Bands
1	LANDSAT 1-4	MSS multi-spectral	1973	60 m	4 bands(1,2,3,4)
2	LANDSAT 1-4	MSS multi-spectral	1977	60 m	4 bands(1,2,3,4)
3	LANDSAT 4-5	TM multi-spectral	1986	30 m	6 bands(1,2,3,4,5,7)
4	LANDSAT 4-5	TM multi-spectral	1991	30 m	6 bands(1,2,3,4,5,7)
5	LANDSAT 4-5	TM multi-spectral	1998	30 m	6 bands(1,2,3,4,5,7)
6	LANDSAT 4-5	TM multi-spectral	1999	30 m	6 bands(1,2,3,4,5,7)
7	LANDSAT 7	ETM+ multi-spectral	2002	30 m	6 bands(1,2,3,4,5,7)
		Panchromatic ETM+		15 m	1 band (8)
8	LANDSAT 7	ETM+ multi-spectral	2006	30 m	6 bands (1,2,3,4,5,7)
		Panchromatic ETM+		15 m	1 band (8)
9	LANDSAT 4-5	TM multi-spectral	2009	30 m	6 bands (1,2,3,4,5,7)
10	RESOURCE SAT -2	LISS-4	2011	5.8 m	3 bands (B2, B3, B4)
11	LANDSAT-8	Operational Land Imager (OLI)	2013	30 m	8 bands (1,2,3,4,5,6,7,9)
		Panchromatic		15 m	1 band (8)
12	LANDSAT-8	Operational Land Imager (OLI)	2014	30 m	8 bands (1,2,3,4,5,6,7,9)
		Panchromatic		15 m	1 band (8)

Another important information used in the study is historical LULC information. LULC information for 12 different years have been extracted from remote sensing images of respective years (Table 3.1). Multi-spectral remote sensing data for 12 years (1973,

1977, 1986, 1991, 1998, 1999, 2002, 2006, 2009, 2011, 2013 and 2014) captured from different satellites and sensors have been used. For some years, satellite data was procured from National Remote Sensing Centre (NRSC) Hyderabad and other year's satellite data was obtained from NASA archives. Details of the satellite used in the study for extraction of LULC information have been presented in Table 3.1

In present work, 46 years (1969–2014) of hourly meteorological data which includes, wind speed, relative humidity, air temperature (Max, Min), air pressure, rainfall and incoming solar radiation have been used for both the areas. Meteorological data for both the stations i.e., Palam and Safdarjung have been procured from the India Meteorological Department (IMD) Pune.

Some other important data/ information required for the modelling of surface energy balance are land surface and energy interaction characteristics like, albedo, emissivity, roughness coefficient, drainage coefficient, storage capacity and leaf area index etc. for different LULC surfaces. Such data have been obtained from literature. Data used for the surface energy balance modelling and parameterization of SUEWS model has been presented in Table 7.1.

CHAPTER 4

GIS DATABASE PREPARATION

4.1 INTRODUCTION

Present study is aimed to investigate the impacts of land use/ land cover (LULC) changes on micro-climate in term of changes in representative surface energy balance components. Change in surface energy balance components have been simulated corresponding to different LULC changes through surface energy balance modelling using SUEWS Model. For parameterization of SUEWS model, variety of data/information is required which include meteorological characteristics, surface reflectance information, radiation data and most important is temporal LULC information. Different type of data used in the study have been discussed in the Chapter 3. A suitable GIS database has been created for the geo-spatial information required for the present study including LULC maps. In the present study LULC information has been extracted from the classified multi-spectral remote sensing images. Processing of remote sensing images using different tools, techniques/softwares and creation of GIS database used in the present study have been discussed in this Chapter.

4.2 SOFTWARE USED

Temporal LULC information is a very important part of any GIS database. In the present study multi-spectral remote sensing images of different years have been analysed digitally to extract LULC and converted into thematic LULC maps using GIS. Standard image processing techniques like pre-processing, rectification, enhancement and classification are used to analyze the images through ERDAS Imagine software (Leica Geosystems). Further, GIS database has been created for LULC information using Arc Info software (ESRI Inc.). The salient details of the softwares used have been presented.

Table 4.1 : Details of the software used for the geographic database creation

S. No.	Software	Version	Developed by
1.	ArcGIS	10.1	Environmental systems research Institute (ESRI), Redlands California, USA
2.	ERDAS Imagine	9.2	Earth Resources Data Analysis System (ERDAS), Atlanta, Georgia, USA

4.2.1 ArcInfo GIS

ArcInfo software has been used in the present study to integrate the different geo-spatial data/information required for the study and for creation of GIS database. ArcInfo is the full-featured Geographical Information System (GIS) in the AcrGIS Desktop product line developed by the ERSI Inc. (Inc and Inc, 2004; Esri, 2008). ArcInfo includes various sub modules such as, ArcScene, ArcGlobe, ArcMap, ArcCatalog, ArcToolbox etc. ArcInfo is a vector based software and also have raster data handling capabilities. ArcInfo has three main modules i.e., ArcMap. ArcCatalog, ArcTool Box. ArcCatalog is used to create, manage and explore the spatial data files on local disk. ArcMap is used to perform operations on spatial data in the form of vector or raster. ArcToolbox consists various operational tools like, analysis tools, spatial analysis tools, statistical analysis tools, mathematical tools, data management tools, 3D analyst tools etc. used to perform on raster or vector data. Details about ArcInfo can be found at official website of Esri.[1]

4.2.2 ERDAS Imagine

ERDAS Imagine is a broad collection of software tools developed by Leica Geosystems (USA) for digital image processing of images. ERDAS Imagine Software comprises various important modules of image processing techniques ranging from simple mapping to advanced features extraction techniques like, techniques for radiometric correction, image rectification, image enhancement, data merging, data sub-setting, image classification, interpolation, geostatistical analysis, stereo data processing, raster data processing and many more. Basic capability of GIS are also available in ERDAS Imagine. Details about ERDAS Imagine can be found at Leica Geosystems official website.[2]

4.3 IMAGE ANALYSIS AND EXTRACTION OF LULC

LULC information can be extracted by performing a set of operations over remotely sensed satellite data through ERDAS Imagine software. The preliminary task of image analysis is to perform radiometric corrections over satellite images to remove/ reduce noise from the data. After noise removal, geometric corrections are required for satellite data which is known as image rectification or geo-referencing. Multi-spectral satellite

[1] http://www.esri.com/
[2] http://www.leica-geosystems.in/en/Image-Processing-Partner-Software_86148.htm

data are stacked to combine all bands information into single image to prepare False Colour Composite (FCC). The satellite data obtained from various sources may not be of appropriate extent required for present study so, we perform subletting/ masking to extract correct extent of study area. Subsequently, spatial and spectral profiles are prepared to have an idea about separable LULC classes from the images. Such an analysis helps in identifying the number of LULC classes and gives an idea about range of reflectance values and their separability for different LULC classes, which further helps in the training of classification algorithm. Further, training samples corresponding to different targeted LULC classes have been selected through AOI tools to train the supervised classification algorithm. Group of pixels selected for training are called signatures. Subsequently, signatures were examined to judge their quality and appropriateness through histogram analysis and refined. Further, signature separability was examined through contingency matrices. Transformed diversion Index has been used to determine the optimum band combination corresponding to maximum separability among targeted LULC classes. After refinement of signatures, images have been classified using Maximum Likelihood Classifier.

Present study uses twelve satellite images of the different years (1973, 1977, 1986, 1991, 1998, 1999, 2002, 2006, 2009, 2011, 2013, and 2014). The salient details have been presented in Chapter 3, Table 3.1. Moreover, Analysis of satellite imagery has been discussed in detail in subsequent sections. Methodology used to process the satellite images of different years to extract the LULC information has been explained in Figure 4.1. Detailed process followed for the image analysis has been discussed below.

4.3.1 Study of Satellite Data

The satellite data was georeferenced and projected through UTM WGS 84 projection system. The data were converted into desired extent of the study area. Further images have been examined visually and by drawing spectral and spatial profiles to have an idea about separable LULC classes. Spectral profiles are helpful in ascertaining the range of reflectance values in different spectral bands for different LULC classes and also separability of targeted LULC classes in different spectral bands. Such an analysis helped in identifying the eight possible LULC classes which can be extracted from the satellite images.

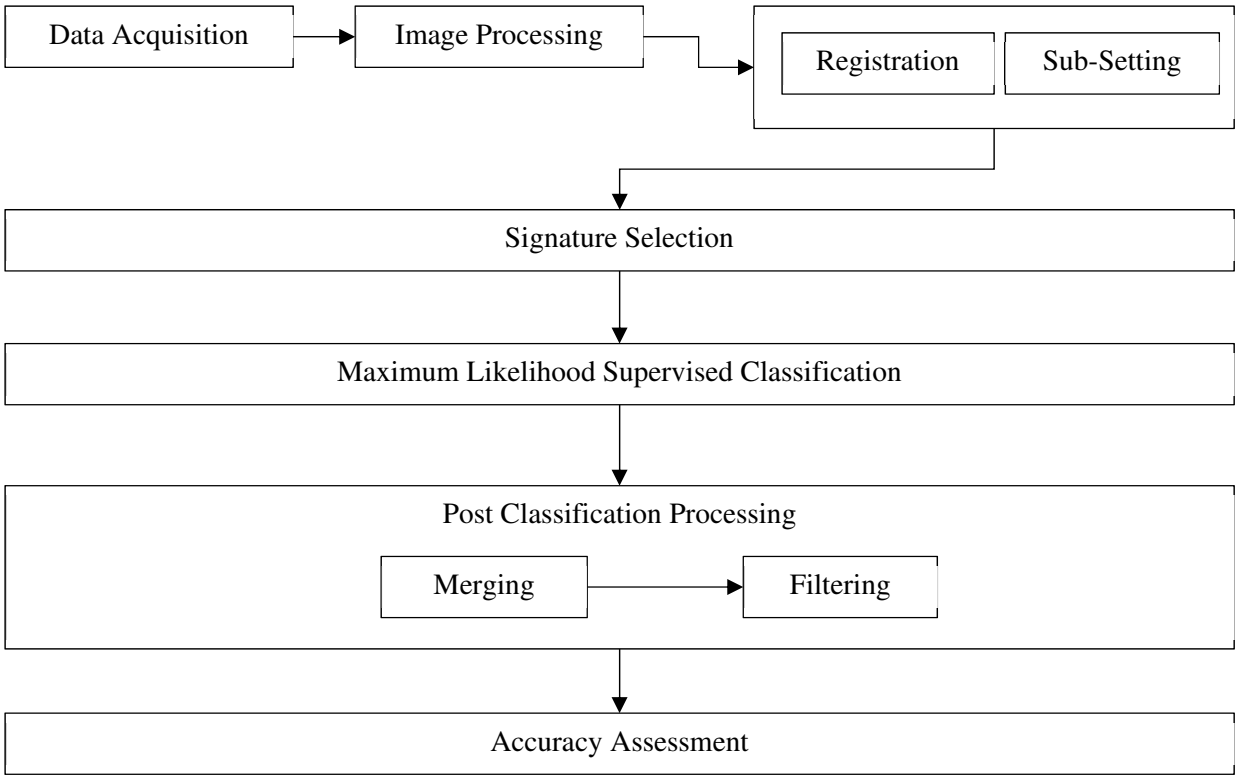

Figure 4.1 : Methodology for extraction of LULC information.

The satellite data was georeferenced and projected through UTM WGS 84 projection system. The data were converted into desired extent of the study area. Further, images have been examined visually and by drawing spectral and spatial profiles to have an idea about separable LULC classes. Spectral profiles are helpful in ascertaining the range of reflectance values in different spectral bands for different LULC classes and also separability of targeted LULC classes in different spectral bands. Such an analysis helped in identifying the eight possible LULC classes which can be extracted from the satellite images.

(i) **Settlement:** This is one of the important land use information used in the present study for surface energy and water balances calculation. All type of constructions used for human habitation as well as working infrastructure such as, buildings, industries, houses, concrete paved etc. comes under built-up category. However, we have classified these into separate classes as given below. Housing construction, buildings and industries have been classified as settlement and we have separated the paved and roads classes as discussed below. The settlement class is identifiable on the classified imagery by its magenta color.

(ii) **Paved:** A hard surface area generally used for footpaths has been considered as paved class. It is made up of paving material that's why somewhat similar

reflectance has been observed as of settlement land use class. Sometimes, it is covered with a perforated hard surface so reflectance is very high and looks white in FCC. Paved is identifiable in classified images by white color.

(iii) **Water Bodies:** Natural and man-made water bodies have been classified as water body class which includes rivers, lakes, ponds etc. Water can absorb much sunlight but negligible reflectance is there so, it looks black in satellite imagery. Waterbody class has been signified with dark blue color.

(iv) **Forest:** Area with the dense vegetative has been considered as forest in present study. It includes forest areas as well as areas with thick vegetation in residential areas or along the roads. In FCC, it appears dark red in color due to its FCC. However, we have signified forest as dark green in classified imagery.

(v) **Sparse Vegetation:** The thin vegetative areas has been classified as sparse vegetation. It has smooth red texture in FCC of satellite images. Though, it has been assigned chartreuse green color in classified output.

(vi) **Trees:** Trees can be recognized as dull red color in FCC of satellite images. This can be identified near roadside areas, recreational areas and nearby residential colonies. Trees are classified as light green color.

(vii) **Open Land:** The vacant land or land not in use and barren land have been classified as open land. It may have peculiar texture in FCC of satellite imagery like light green, yellow, dusky yellow, brown and many more. Although, it is orange in color in classified images.

(viii) **Roads:** Roads can be identified as long impervious strip in a satellite image. Its texture is much similar to paved areas for concrete roads. It can be identified as violet color in classified imagery.

4.3.2 Training of Classification Algorithm

After analyzing and processing of satellite data, image classification was performed. There are various classification algorithms which can be broadly classified into two categories i.e. Supervised and Unsupervised classification. Unsupervised classification algorithm does not require any external supervision or training. On the other hand, supervised classification method requires training of classification algorithm and thus user have control over classification process. In the present study, supervised classification method has been used for classification of satellite images. Supervised classification requires training of algorithm. Based on the prior knowledge and study of

the images, suitable cluster of pixels have been selected from respective FCC, as training samples for different LULC classes, through AOI tools in ERDAS Imagine. Such collected pixels are called signatures and process is called signature selection. Signatures have been selected for eight LULC classes (as discussed above). Minimum number of pixels selected for each LULC class was more than n* 10 numbers, where n is the number of LULC classes. It is recommended to select samples/signatures ten times of the total number of classes to get better training data.

After selection of training pixels, signatures have been examined to ascertain their correctness through histograms of individual signatures. Histogram of signatures should be uni-model and have bell shaped, range of pixel values should be small. First, histograms were plotted for all the signatures in single as well as multiple bands to check whether all the signatures maintain the bell shaped curve which signifies that signatures selected for a particular class lies in the range of same pixel value and are not misclassified. Typical histograms for selected signatures for a particular year have been presented in Figure 4.2. Signatures are refined and improved by removing wrong pixels and addition of new pixels into signatures to the satisfaction level. After plotting histograms, we again checked signature separability using contingency matrices. The contingency matrices revealed misclassification among training pixels. Further, signatures were refined based on the feedback from the contingency matrices. After refinement, it was evident from Table 4.3 that few pixels have misclassified due to overlapping of reflectance, however, misclassification after refinement is negligible. So, these signatures were finalized for the classification of satellite imagery. Contingency in percent for different years for the study area have been presented in Table 4.2(a) to Table 4.2(d).

4.3.3 Supervised Classification

After finalization of signatures, Maximum Likelihood Classifier (MLC) was used in ERDAS Imagine for classification of satellite images of different years. The MLC classifier is one of the well-known parametric method used for supervised classification. It computes the weighted distance or likelihood D for unknown pixel X belong to one of the known LULC classes Mc can be defined using Bayesian equation.

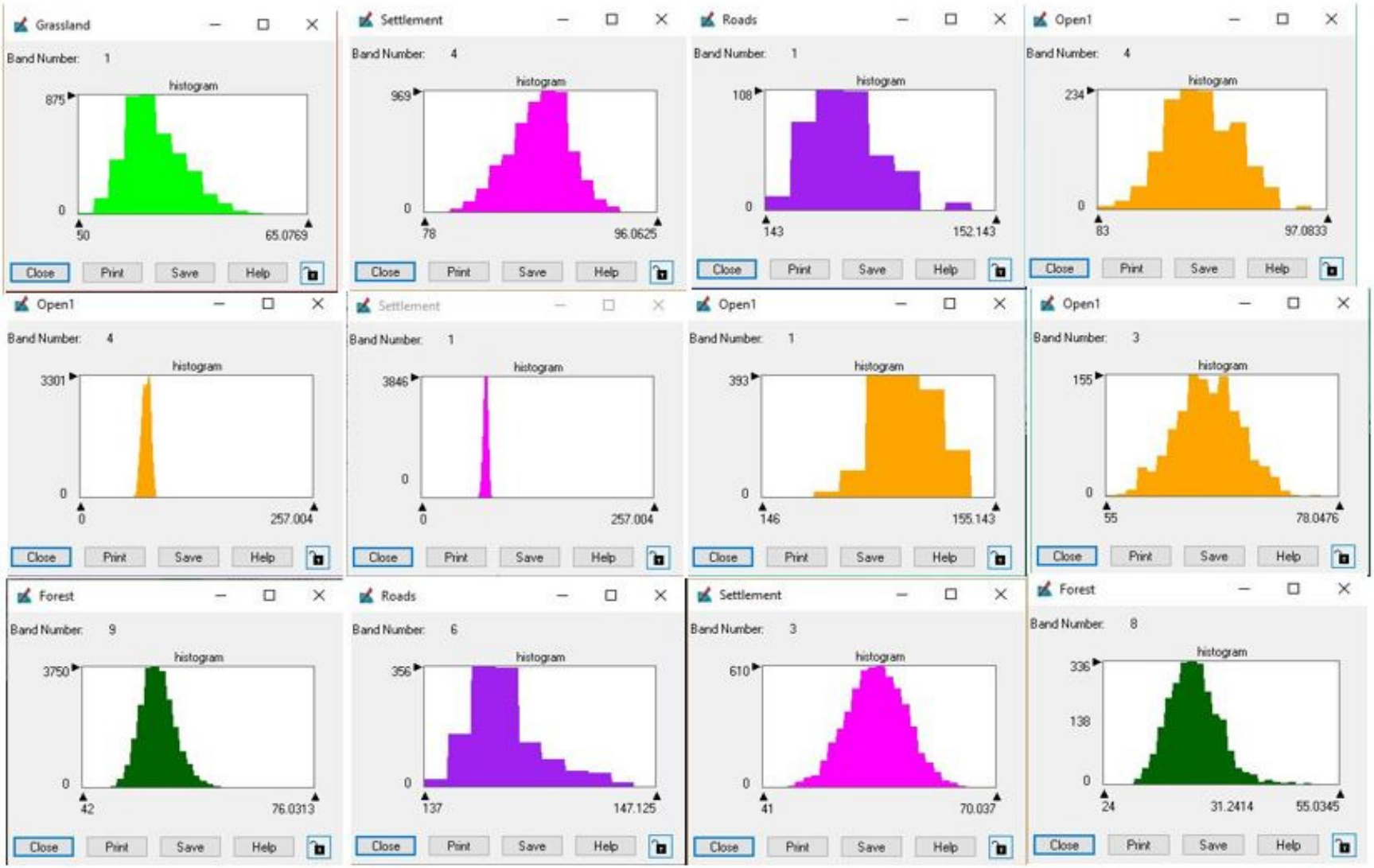

Figure 4.2 : Typical histograms for signatures

Table 4.2 (a): Signature evaluation using contingency matrices (1)

Contingency Matrix of Year 1973 (in %)								
Classified Data	Forest	Grassland	Settlement	Roads	Paved	Waterbody	Trees	Open
Forest	97.37	22.08	0.00	0.06	0.00	6.93	0.00	0.00
Sparse vegetation	1.63	77.23	0.02	0.00	0.00	0.00	1.14	1.14
Settlement	0.01	0.05	98.78	0.12	0.20	0.00	0.00	0.00
Roads	0.97	0.29	0.63	98.96	0.00	93.07	0.28	0.51
Paved	0.00	0.18	0.56	0.37	99.11	0.00	0.00	1.75
Waterbody	0.00	0.00	0.00	0.00	0.00	0.00	0.00	0.00
Trees	0.00	0.03	0.00	0.24	0.00	0.00	98.58	0.02
Open	0.01	0.14	0.01	0.24	0.69	0.00	0.00	97.57
Contingency Matrix of Year 1977 (in %)								
Classified Data	Forest	Grassland	Settlement	Roads	Paved	Waterbody	Trees	Open
Forest	94.51	13.55	0.00	0.00	0.00	0.00	5.35	0.07
Sparse vegetation	3.26	79.17	0.00	0.00	0.00	0.00	9.33	0.04
Settlement	0.00	0.00	98.54	1.65	0.00	0.00	0.00	0.00
Roads	0.00	0.00	1.35	94.72	0.00	0.00	0.00	0.85
Paved	0.00	0.00	0.00	0.00	99.78	0.00	0.00	2.71
Waterbody	0.00	0.00	0.00	0.00	0.00	100	0.00	0.00
Trees	1.69	7.28	0.00	0.00	0.00	0.00	84.80	2.00
Open	0.54	0.00	0.11	3.63	0.22	0.00	0.52	94.34
Contingency Matrix of Year 1986 (in %)								
Classified Data	Forest	Grassland	Settlement	Roads	Paved	Waterbody	Trees	Open
Forest	98.03	0.06	0.10	0.00	0.00	0.58	2.97	0.00
Sparse vegetation	0.00	98.75	0.00	0.00	0.00	0.00	2.97	0.00
Settlement	0.00	0.00	98.71	0.61	0.00	0.00	0.00	0.03
Roads	0.10	0.00	1.11	99.39	0.00	1.16	0.00	0.23
Paved	0.00	0.00	0.00	0.00	100.00	0.00	0.00	0.00
Waterbody	0.73	0.00	0.00	0.00	0.00	98.26	0.00	0.00
Trees	1.14	0.69	0.02	0.00	0.00	0.00	93.89	0.00
Open	1.14	0.50	0.06	0.00	0.00	0.06	0.17	99.74

Table 4.2 (b): Signature evaluation using contingency matrices (2)

Contingency Matrix of Year 1991 (in %)								
Classified Data	Forest	Grassland	Settlement	Roads	Paved	Waterbody	Trees	Open
Forest	96.12	0.11	0.00	1.75	0.00	0.00	0.00	0.00
Sparse vegetation	0.17	98.59	0.00	0.00	0.00	0.00	0.00	0.00
Settlement	0.00	0.00	98.36	1.55	0.00	0.00	0.11	0.00
Roads	3.63	0.00	1.19	96.70	0.00	0.00	0.11	0.00
Paved	0.00	0.00	0.39	0.00	100	0.00	0.00	0.67
Waterbody	0.00	0.00	0.00	0.00	0.00	100	0.00	0.00
Trees	0.08	1.30	0.06	0.00	0.00	0.00	98.63	3.21
Open	0.00	0.00	0.00	0.00	0.00	0.00	1.14	96.12
Contingency Matrix of Year 1999 (in %)								
Classified Data	Forest	Grassland	Settlement	Roads	Paved	Waterbody	Trees	Open
Forest	94.51	13.55	0.00	0.00	0.00	0.00	5.35	0.07
Sparse vegetation	3.26	79.17	0.00	0.00	0.00	0.00	9.33	0.04
Settlement	0.00	0.00	98.54	1.65	0.00	0.00	0.00	0.00
Roads	0.00	0.00	1.35	94.72	0.00	0.00	0.00	0.85
Paved	0.00	0.00	0.00	0.00	99.78	0.00	0.00	2.71
Waterbody	0.00	0.00	0.00	0.00	0.00	100	0.00	0.00
Trees	1.69	7.28	0.00	0.00	0.00	0.00	84.80	2.00
Open	0.54	0.00	0.11	3.63	0.22	0.00	0.52	94.34
Contingency Matrix of Year 2002 (in %)								
Classified Data	Forest	Grassland	Settlement	Roads	Paved	Waterbody	Trees	Open
Forest	92.52	4.57	0.00	0.10	0.00	0.00	1.57	0.01
Sparse vegetation	3.25	91.47	0.00	0.10	0.00	0.00	3.13	0.00
Settlement	0.09	0.00	98.60	0.30	0.10	0.00	0.00	0.31
Roads	0.78	0.13	0.63	96.23	0.00	0.00	1.88	0.22
Paved	0.00	0.00	0.19	0.00	95.27	0.00	0.00	11.00
Waterbody	0.00	0.00	0.00	0.20	0.00	100	0.00	0.00
Trees	3.04	3.53	0.28	2.88	0.00	0.00	92.48	7.22
Open	0.32	0.29	0.29	0.20	4.63	0.00	0.94	81.24

Table 4.2 (c): Signature evaluation using contingency matrices (3)

Contingency Matrix of Year 2006 (in %)								
Classified Data	Forest	Grassland	Settlement	Roads	Paved	Waterbody	Trees	Open
Forest	98.03	0.06	0.10	0.00	0.00	0.58	2.97	0.00
Sparse vegetation	0.00	98.75	0.00	0.00	0.00	0.00	2.97	0.00
Settlement	0.00	0.00	98.71	0.61	0.00	0.00	0.00	0.03
Roads	0.10	0.00	1.11	99.39	0.00	1.16	0.00	0.23
Paved	0.00	0.00	0.00	0.00	100.00	0.00	0.00	0.00
Waterbody	0.73	0.00	0.00	0.00	0.00	98.26	0.00	0.00
Trees	1.14	0.69	0.02	0.00	0.00	0.00	93.89	0.00
Open	1.14	0.50	0.06	0.00	0.00	0.06	0.17	99.74
Contingency Matrix of Year 2011 (in %)								
Classified Data	Forest	Grassland	Settlement	Roads	Paved	Waterbody	Trees	Open
Forest	90.84	8.34	0.01	1.34	0.00	0.00	0.06	0.12
Sparse vegetation	4.79	90.83	0.00	0.01	0.00	0.00	0.26	0.14
Settlement	0.00	0.00	91.70	2.11	0.91	0.00	0.03	0.44
Roads	0.57	0.01	1.31	82.26	0.00	0.00	0.00	0.01
Paved	0.00	0.00	0.43	0.00	96.52	0.00	0.00	2.02
Waterbody	0.00	0.00	0.05	2.29	0.00	100	0.00	0.00
Trees	2.78	0.76	0.07	0.00	0.00	0.00	92.66	8.50
Open	0.93	0.07	0.33	0.12	2.57	0.00	5.52	88.76
Contingency Matrix of Year 2013 (in %)								
Classified Data	Forest	Grassland	Settlement	Roads	Paved	Waterbody	Trees	Open
Forest	96.12	0.11	0.00	1.75	0.00	0.00	0.00	0.00
Sparse vegetation	0.17	98.59	0.00	0.00	0.00	0.00	0.00	0.00
Settlement	0.00	0.00	98.36	1.55	0.00	0.00	0.11	0.00
Roads	3.63	0.00	1.19	96.70	0.00	0.00	0.11	0.00
Paved	0.00	0.00	0.39	0.00	100	0.00	0.00	0.67
Waterbody	0.00	0.00	0.00	0.00	0.00	100	0.00	0.00
Trees	0.08	1.30	0.06	0.00	0.00	0.00	98.63	3.21
Open	0.00	0.00	0.00	0.00	0.00	0.00	1.14	96.12

Table 4.2 (d): Signature evaluation using contingency matrices (4)

Contingency Matrix of Year 2014 (in %)								
Classified Data	Forest	Grassland	Settlement	Roads	Paved	Waterbody	Trees	Open
Forest	97.37	22.08	0.00	0.06	0.00	6.93	0.00	0.00
Grassland	1.63	77.23	0.02	0.00	0.00	0.00	1.14	1.14
Settlement	0.01	0.05	98.78	0.12	0.20	0.00	0.00	0.00
Roads	0.97	0.29	0.63	98.96	0.00	93.07	0.28	0.51
Paved	0.00	0.18	0.56	0.37	99.11	0.00	0.00	1.75
Waterbody	0.00	0.00	0.00	0.00	0.00	0.00	0.00	0.00
Trees	0.00	0.03	0.00	0.24	0.00	0.00	98.58	0.02
Open	0.01	0.14	0.01	0.24	0.69	0.00	0.00	97.57

$$D = \ln(ac) - [0.5\ln(|covc|)] - [0.5(X - Mc)T(covc - 1)(X - Mc)]\ldots \quad 4.1$$

On the basis of highest probability of an unknown pixel to belong to a class, it is assigned to that class. The MLC classifier has the capability of accounting variance/co-variance for a class distribution and normally distributed data. Moreover, it can perform better than any other parametric classifier. Though, for non-normally distributed data results may be unsatisfactory (Otukei and Blaschke, 2010).

4.3.4 Accuracy Assessment

Accuracy assessment is an important process to ascertain the correctness of the classified images. In accuracy assessment, LULC classes of selected locations in classified output are checked for their correct LULC class on ground through ground truthing or by comparing with actual LULC class on a reference geographical data, which is assumed to be accurate. There are various methods to assess accuracy of classified images (Congalton and Green, 1999; Foody, 2002). In the present study, referenced data collected from high resolution satellite data and other available maps have been used for the accuracy assessment. A set of 100 sample pixels, distributed over the classified output were selected as test pixels using stratified random sampling to check the accuracy of classified maps. It was ensured during selection of sample data that each class has more than 10 test pixels. Accuracy assessment has been done in ERDAS Imagine and Kappa statistics & accuracy percentage were calculated for each classified output (Table 4.3). Accuracy percentage shows the ratio of correctly classified pixels out of total pixels of a sample data and kappa statistics are the agreement between the classification map and referenced

map. Average accuracy assessment details for different years have been presented in Table 4.3.The accuracy percentage for year 1973, 1977 and 1986 are found fair enough (more than 70%). Accuracy for these year is not very good due to the coarser resolution of satellite data. At that time only satellite images available were from LANDSAT program having spatial resolution of 80 m. Classification accuracy for other years have been found to be satisfactory i.e., >80%. Classification accuracy for the image of year 1991 has been found to be 80 %, for year 1998 and 1999 accuracy is 81.25 %. For year 2002 image classification accuracy has been found to be 87.5 % and for year 2006 accuracy is 86.25 %. Average classification accuracy of 83.75 % has been obtained for year 2009, 85 % accuracy for year 2011, 81.25 % for 2013 and 86.25 % for year 2014. Classification has been found to be satisfactory and acceptable for medium resolution satellite imagery (Table 4.3).

Table 4.3: Detailed results of accuracy assessment and kappa coefficient for derived LULC for different years

Sr.No.	Years	Classification accuracy (%)	Overall Kappa coefficient statistics
1	1973	72.50	0.65
2	1977	78.75	0.73
3	1986	78.75	0.74
4	1991	80.00	0.74
5	1998	81.25	0.75
6	1999	81.25	0.76
7	2002	87.50	0.84
8	2006	86.25	0.82
9	2009	83.75	0.78
10	2011	85.00	0.79
11	2013	81.25	0.73
12	2014	86.25	0.80

It has been seen in classified imagery that trees in roadside areas are not correctly identified by the classifier. Settlement and roads are classified in a better way, however, it showed some misclassification at some places due to similar texture of roads and settlement. Sparse vegetation and forest are correctly classified in most of the images, however, trees are misclassified in other vegetation classes (i.e. sparse vegetation and

forest) due to similar reflectance values. Also, at some places concrete paved areas are misclassified with the settlement class due to similar reflectance value.

4.3.5 Preparation of Land Use/ Land Cover Maps

Land use and land cover are two distinct terms but often used interchangeably. Land cover is the naturally available cover over the earth surface e.g. forest, ocean, rivers, Iceland, mountains etc. On the other side, land use are the man-made or artificial utilization of natural land cover such as, residential colony, roads, agriculture, artificial lakes, ponds etc.(Comber et al. 2005). In the present work, land use / land cover information corresponding to the 12 years i.e., (1973, 1977, 1986, 1991, 1998, 1999, 2002, 2006, 2009, 2011, 2013 and 2014) have been obtained from the classified satellite images as discussed earlier. Eight land use land cover classes have been identified and these are presented in Figure 4.3, 4.4, 4.4, 4.5 & 4.6 given below. Urban settlement and vegetation in form of forest, sparse vegetation and trees have been found as the main LULC classes in the study area. We studied LULC outputs for two areas selected as study area i.e. Palam and Safdarjung are discussed below.

Palam-The area under settlement has increased significantly from 1027.3 ha to 5873.8 ha from year 1973 to 2014. The dense vegetation cover has vastly reduced from 2946.5 ha to 221.1 ha from year 1973 to 2014, this may be due to the rampant urbanization in Palam area. Recreational things like park has been increased from 202.4 ha to 985.4 over the years which shows development of Palam area. Also, water bodies have almost been dried up and converted into other LULC class over the years. If we see the open land in Palam area it was only left with 1176.5 ha in year 2014 from 4744.8 ha in year 1973 which is an indication of huge growth in this area (Table 4.4). The increased urbanization and reduced vegetation are the causes of increased surface temperature which has also been verified in present study.

The fractional area of LULC classes has been calculated for conceptualization of SUWES model and are presented given in Table 4.5.

Safdarjung-The settlement area of Safdarjung region has speedily increased from 2449.1 ha in year 1973 to 7113 ha in year 2014 which is more as compared to Palam region (discussed in above section). Water bodies has been greatly reduced to 9.72 ha in year 2014 from 79.25 ha in year 1973. The dense vegetation cover also has significantly reduced from 4142.48 ha in 1973 to 1099.0 ha in year 2014. However, due to the attention and a positive drive of development authorities in Safdarjung area, vegetation cover now

has started being protected and plants are planted in many public spots. It is clear from the Table 4.6 that after a continuous degradation of vegetative area up to year 2013 (923 ha) it grown to 1099.0 ha in year 2014. The open land has also utilized much for conversion into other LULC classes (mainly Settlement class). We were left with only 214.0 ha open land in Safdarjung area in year 2014 from 3122.29 ha in year 1973 (Table 4.6).

In addition, SUEWS model for surface energy modelling requires LULC fractions for the parameterization. Some LULC classes have been grouped and renamed based on similar reflectance characteristics while parameterizing the SUEWS like Settlement, Roads + Paved, Bare soil, Forest, Deciduous Trees (Dec Trees in table), Park and Water. The LULC class fractions were determined by dividing the class area from total area for every class. These areal fractions were utilized for the parameterization of SUEWS model. The areal fraction for settlement class has continuously been increased i.e. 0.08 in year 1973 to 0.52 in 2014 in Palam region. Also, it shows a continuous increase in settlement in Safdarjung as well. Other LULC class fractions can be found in Table 4.5 & 4.7. The fractional area of LULC classes has been calculated for conceptualization of SUWES model and are presented given in Table 4.7.

Table 4.4: Detailed information about land use /land cover changes in different years for Palam area in ha

Classes	1973	1977	1986	1991	1998	1999	2002	2006	2009	2011	2013	2014
Settlement	1027.3	1393.5	2851.2	3321.0	3598.2	3608.5	3626.9	4377.0	5229.4	5430.0	5693.0	5873.8
Roads + Paved	518.9	873.7	980.0	1110.3	1198.2	1234.0	1261.4	1330.6	1598.0	1632.6	1667.4	1873.9
Open	4744.8	3633.7	3278.5	3078.5	2869.0	2843.0	3058.1	2964.8	2225.0	1789.7	1491.2	1176.5
Forest	2946.5	2546.9	1572.0	1140.0	998.4	987.1	234.5	180.6	440.9	576.7	409.0	221.1
Deciduous (Trees)	2085.5	2784.4	2528.2	2428.2	2469.2	2358.4	2384.3	1527.2	1638.1	1680.4	1891.7	1261.1
Sparse vegetation	202.4	246.3	280.3	320.3	366.1	355.1	816.1	1004.4	318.8	364.4	302.2	985.4
Water	34.8	29.6	17.3	11.3	7.8	8.0	10.5	7.5	6.8	0.9	2.2	0.0

Table 4.5: LULC information in fraction for Palam area

Land Cover	1973	1977	1986	1991	1998	1999	2002	2006	2009	2011	2013	2014
Buildings	0.0889	0.121	0.248	0.291	0.3127	0.3167	0.3184	0.3842	0.4565	0.473	0.4969	0.52
Roads + Paved	0.0449	0.076	0.085	0.097	0.1041	0.1083	0.1107	0.1168	0.1395	0.142	0.1455	0.16
Bare soil	0.4104	0.316	0.285	0.270	0.2493	0.2495	0.2684	0.2602	0.1942	0.156	0.1302	0.10
Forest	0.2549	0.221	0.136	0.100	0.0868	0.0866	0.0205	0.0158	0.0385	0.050	0.0357	0.02
Deciduous (Trees)	0.1804	0.242	0.220	0.213	0.2146	0.2069	0.2093	0.1341	0.1429	0.146	0.1651	0.11
Sparse vegetation	0.0175	0.021	0.024	0.028	0.0318	0.0311	0.0716	0.0882	0.0278	0.032	0.0264	0.09
Water	0.003	0.003	0.002	0.001	0.0007	0.0007	0.0009	0.0007	0.0006	0.0001	0.0002	0.00

Table 4.6: Detailed information about land use /land cover changes in different years for Safdarjung area in ha

Land use Classes	1973	1977	1986	1991	1998	1999	2002	2006	2009	2011	2013	2014
Settlement	2449.1	2788.29	2910.3	3145	3198.96	3205.96	4522	4769	5083	6834	6930	7113
Roads + Paved	661.822	761.559	768	778.0	788.47	810.47	1017	1110.5	1116.05	1152.37	1329.0	1386.0
Open	3122.29	2951.07	2256.9	1548.4	1359.96	1347.96	303	165	431	111.65	209	214.0
Forest	4142.48	3576.82	3297.4	2437.0	1611.1	1607	1640	1676	1011.69	802	923	1099.0
Deciduous (Trees)	1016.94	1395.77	1545	2476.7	3126.5	3113	3009	2880	2959	1535.87	1047	1262.0
Sparse vegetation	303.781	188.117	887.3	1029	1335	1339	925	815	883.62	967	1005	360
Water	79.25	60.75	58.1	35.5	24.1	23.53	11.36	11.45	8.19	13.74	10.26	9.72

Table 4.7: LULC information in fraction for Safdarjung

Land use	1973	1977	1986	1991	1998	1999	2002	2006	2009	2011	2013	2014
Buildings	0.208	0.238	0.247	0.275	0.2795	0.28	0.3957	0.4174	0.442	0.598	0.6052	0.6216
Roads + paved	0.056	0.065	0.066	0.068	0.069	0.071	0.089	0.0969	0.0970	0.101	0.116	0.1211
Bare soil	0.265	0.252	0.193	0.135	0.1188	0.1180	0.0265	0.0146	0.038	0.01	0.0182	0.0187
Forest	0.352	0.305	0.281	0.213	0.1408	0.14	0.1435	0.1468	0.088	0.07	0.0806	0.096
Deciduous (Trees)	0.086	0.119	0.132	0.216	0.2732	0.272	0.2633	0.252	0.258	0.135	0.0914	0.1103
Sparse vegetation	0.026	0.016	0.076	0.09	0.1166	0.117	0.081	0.0713	0.076	0.085	0.0877	0.0315
Water	0.007	0.005	0.005	0.003	0.0021	0.002	0.001	0.001	0.001	0.001	0.0009	0.0008

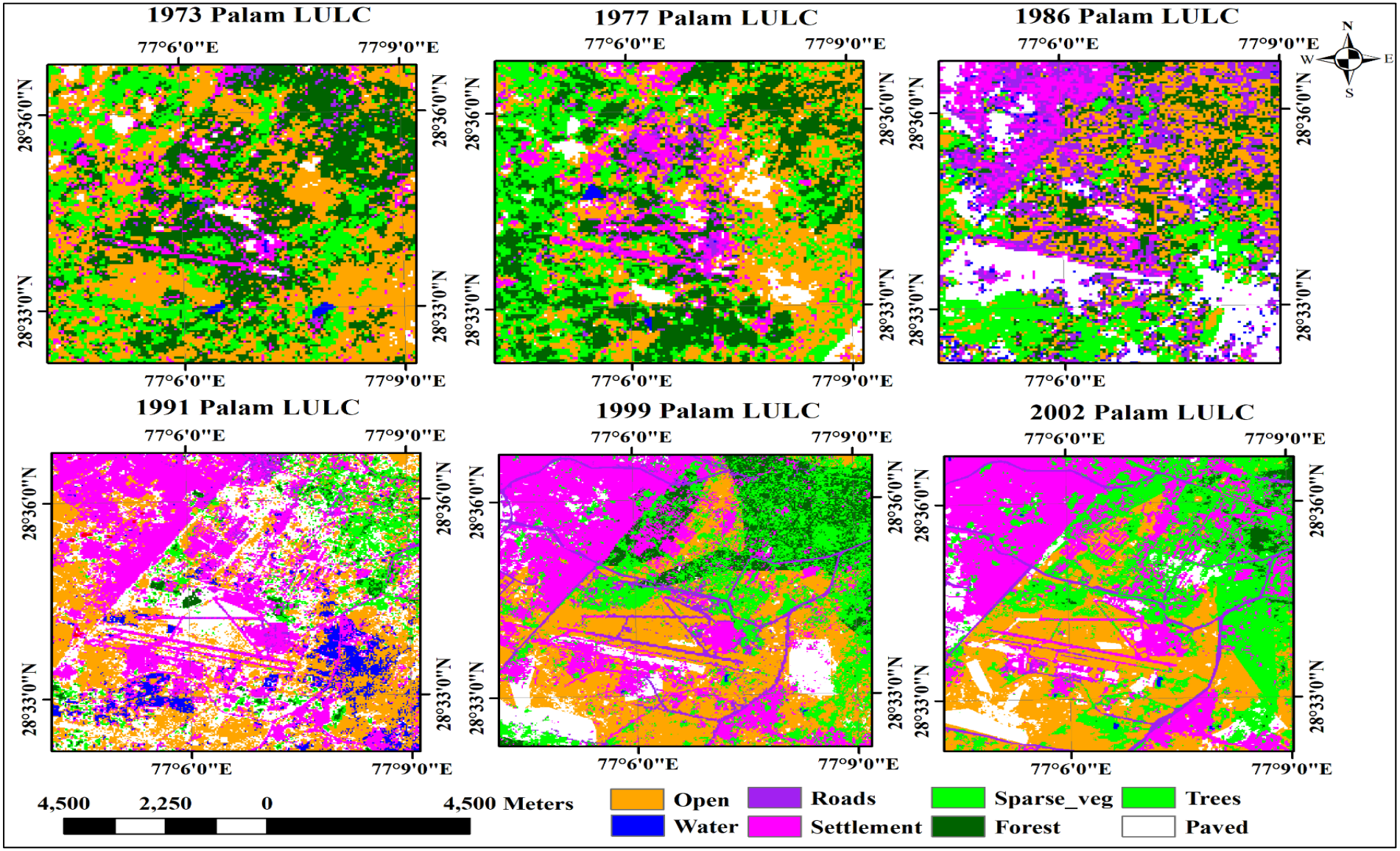

Figure 4.3 : Classified images for Palam area for the year 1973, 1977, 1986, 1991, 1999 and 2002

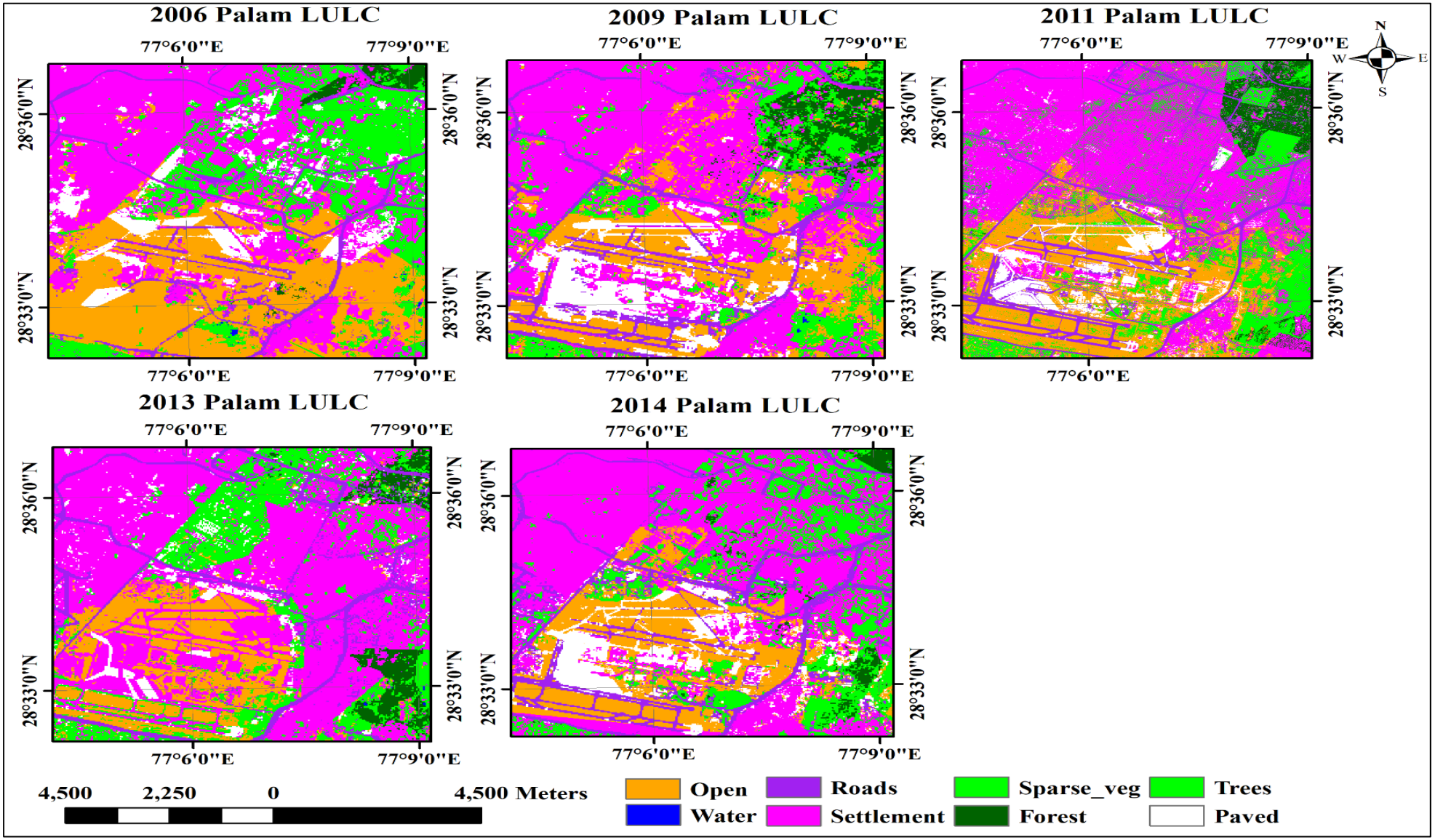

Figure 4.4 : Classified images for Palam area for the year 2006, 2009, 2011, 2013 and 2014

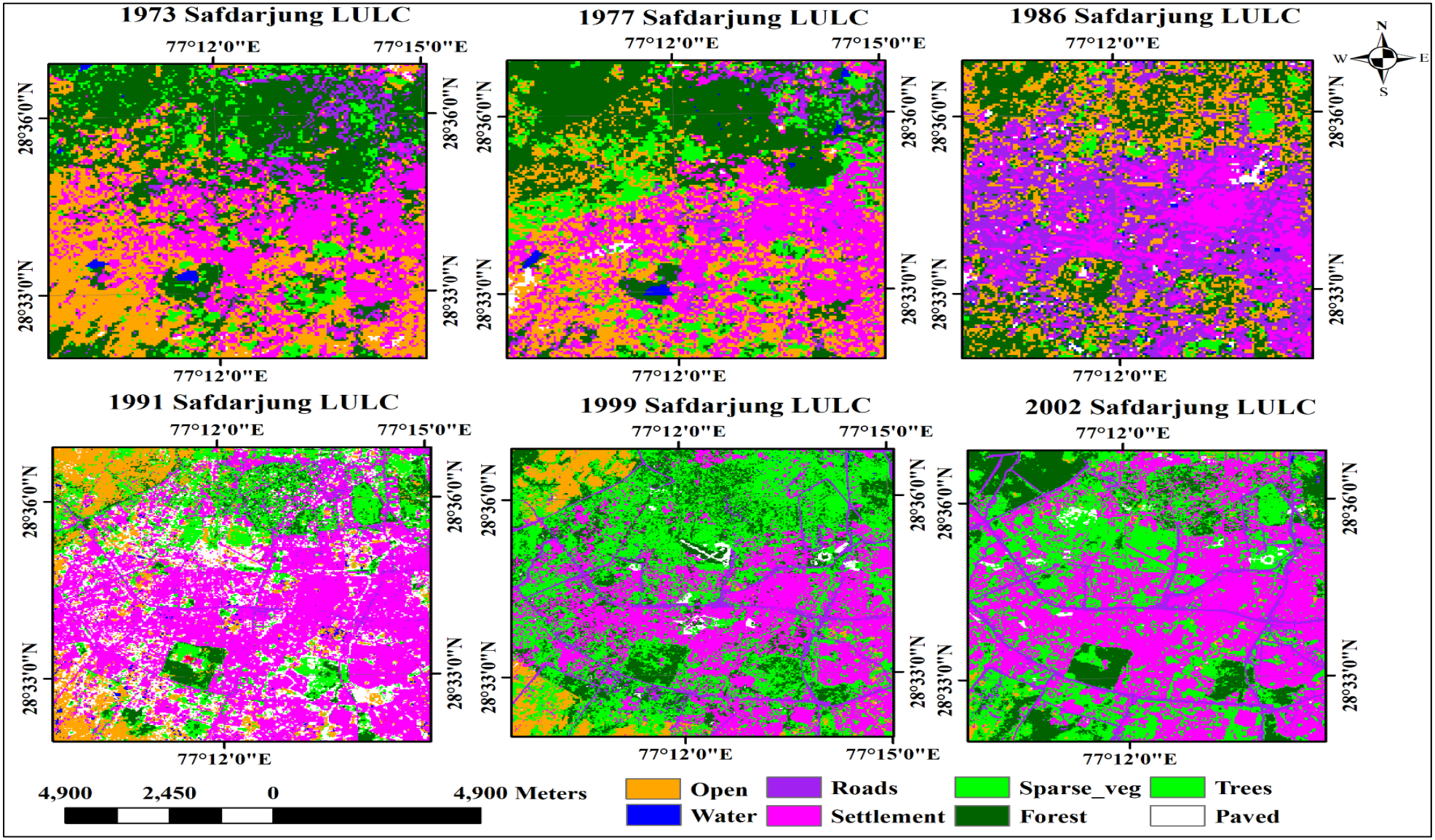

Figure 4.5 : Classified images for Safdarjung area for the year 1973, 1977, 1986, 1991, 1999 and 2002

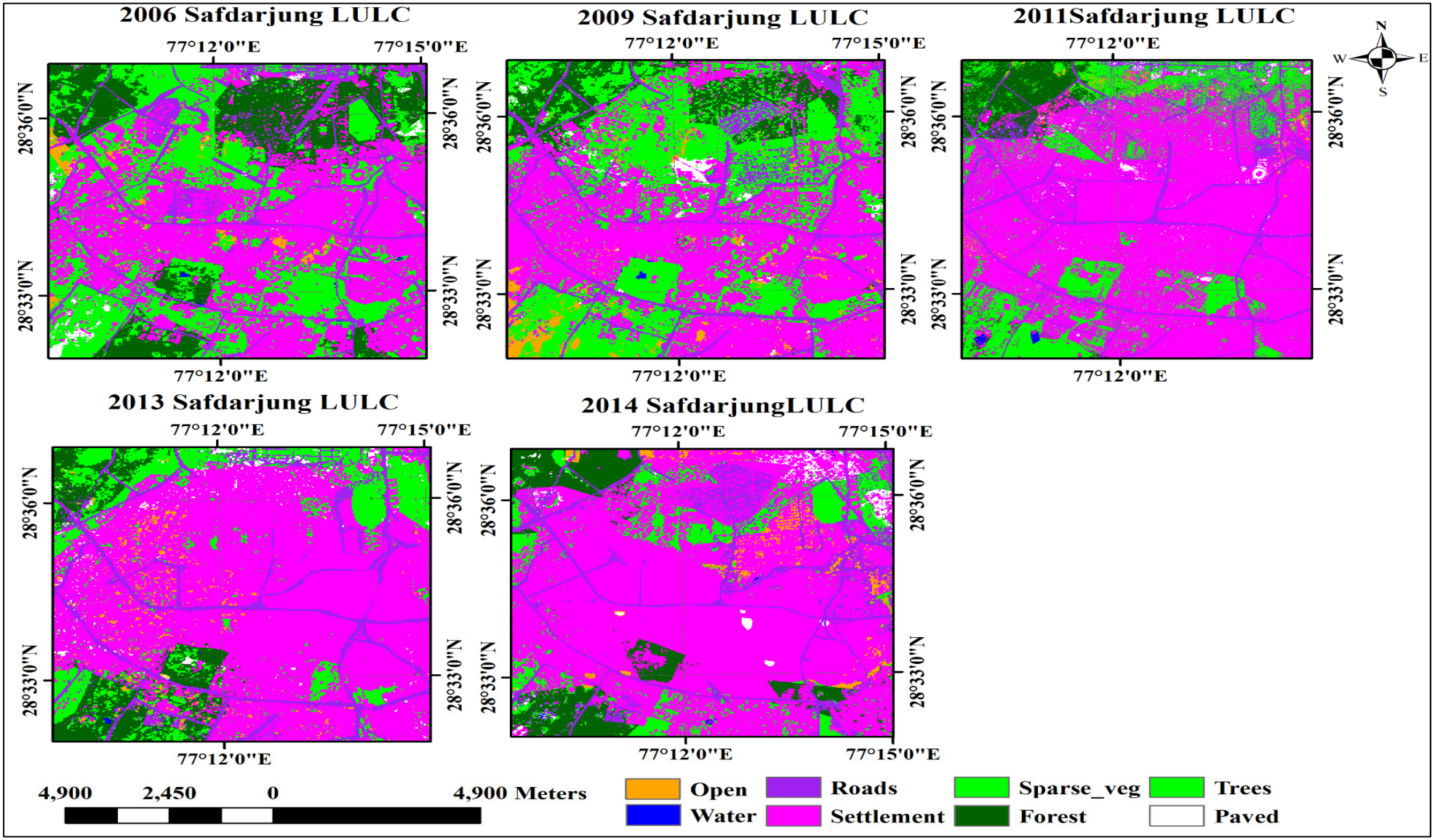

Figure 4.6 : Classified images for Safdarjung area for the year 2006, 2009, 2011, 2013 and 2014

CHAPTER 5

METHODOLOGY

5.1 INTRODUCTION

This chapter deals with research methodology that has been adopted to accomplish objectives of the present study including the mathematical formulations. Time series analysis of 44 years climatic data has been performed for the assessment of climate change, which is the first objective of the present work. The methods involved in this analysis are parametric and non-parametric statistical methods such as Mann-Kendall test, Modified Mann-Kendall test, Sen's slope estimator and Pettitt–Mann–Whitney shift detection test. Climate change assessment has been performed by determining trend in representative meteorological parameters (discussed in Chapter 3) over a period, as mentioned above, as well as, predicting the future climate using statistical downscaling of General Circulation Model (climate models) outputs. Methodology adopted for the climate change assessment has been presented in subsequent sections of this Chapter below. The second generation Canadian Earth System Model (CanESM2, a GCM model) data generated under Coupled Model Inter-comparison Project 5 (CMIP5) for three different representative concentration pathways (RCP2.6, RCP4.5 and RCP8.5) has been downscaled statistically to predict future climate for the selected study areas (area surrounding to Palam and Safdarjung meteorological stations in Delhi). The results of climate change assessment are presented in Chapter 6. As discussed in Chapter 2, major factors causing climate change are gaseous pollutants and anthropogenic activities like LULC changes. According to IPCC (IPCC, 2007 and IPCC, 2014), LULC change activities are one of the important factors affecting climate over the years and further emphasised study of impacts of LULC changes on climate. LULC change is predominant in urban centers as compared to rural areas. Urban areas have high population density and therefore, more people are at risk of adverse effects of LULC change on micro-climate (Mohan and Kandya 2015). Therefore, main objective of the present work is the study of impacts of LULC changes on micro-climate through quantification of changes in surface energy balance. To extract LULC change information, image classification of multi-spectral remote sensing images has been performed and GIS database is prepared as discussed in Chapter 4. In the present study, an attempt has been made to study possible effect of LULC changes on micro-climate in terms of change in surface energy components which indicate possible changes in micro-climate over the years. SUEWS (Surface Urban Energy and Water Balance Scheme) model (Mitchell et. al.,

2008; Järvi et al., 2011) has been used to model the surface energy balance of the study area for different LULC scenarios. Further changes in surface energy components due to change in LULC are also determined for different years in different scenarios. The methodology adopted for conceptualization of SUEWS model, sensitivity analysis and validation process have been discussed in the following sections. After determining the influence of LULC change on surface energy fluxes, quantitative relationship between LULC fractions and surface energy fluxes have been established by using regression technique. These equations can be used to quantify surface energy fluxes using LULC characteristics for any area. Thus, it would be helpful in developing adaptation measures so that adverse impact of LULC change on micro-climate could be minimized. Detailed results of the surface energy balance modelling are discussed in Chapter 7. It is well established that LULC change in urban areas is a continuous process to meet the development demands of the increasing population. To contain the adverse effects of LULC on micro-climate, potential of different land use transformation based adaptation measures have been investigated and their effectiveness is determined. The results of the adaptation measures, their potential and effect on surface energy balance are discussed in Chapter 8. The flowchart of complete methodology followed to achieve different research objectives has been shown in Figure 5.1. The detailed discussion of methodology used for each objective has been presented in the following sections.

5.2 ASSESSMENT OF CLIMATE CHANGE BY USING TIME SERIES ANALYSIS

To perform an assessment of climate change, happened in recent past, time series analysis has been performed. Parametric and non-parametric statistical techniques have been used to determine trends in climate at different temporal scales over the years in terms of trends in representative meteorological parameters i.e., rainfall and temperature for Palam and Safdarjung area of Delhi. The trend analysis has been carried for temperature & rainfall (mean, minimum and maximum) at different temporal scales like month, seasonal and annual using meteorological hourly measured data of 44 years (1969-2012). Hourly data has been used and converted into data corresponding to different temporal scales. Also, the analysis is carried out at one more temporal scales i.e., monsoon (June, July, August, and September) and non-monsoon (January, February, March, April, May, October, November and December).

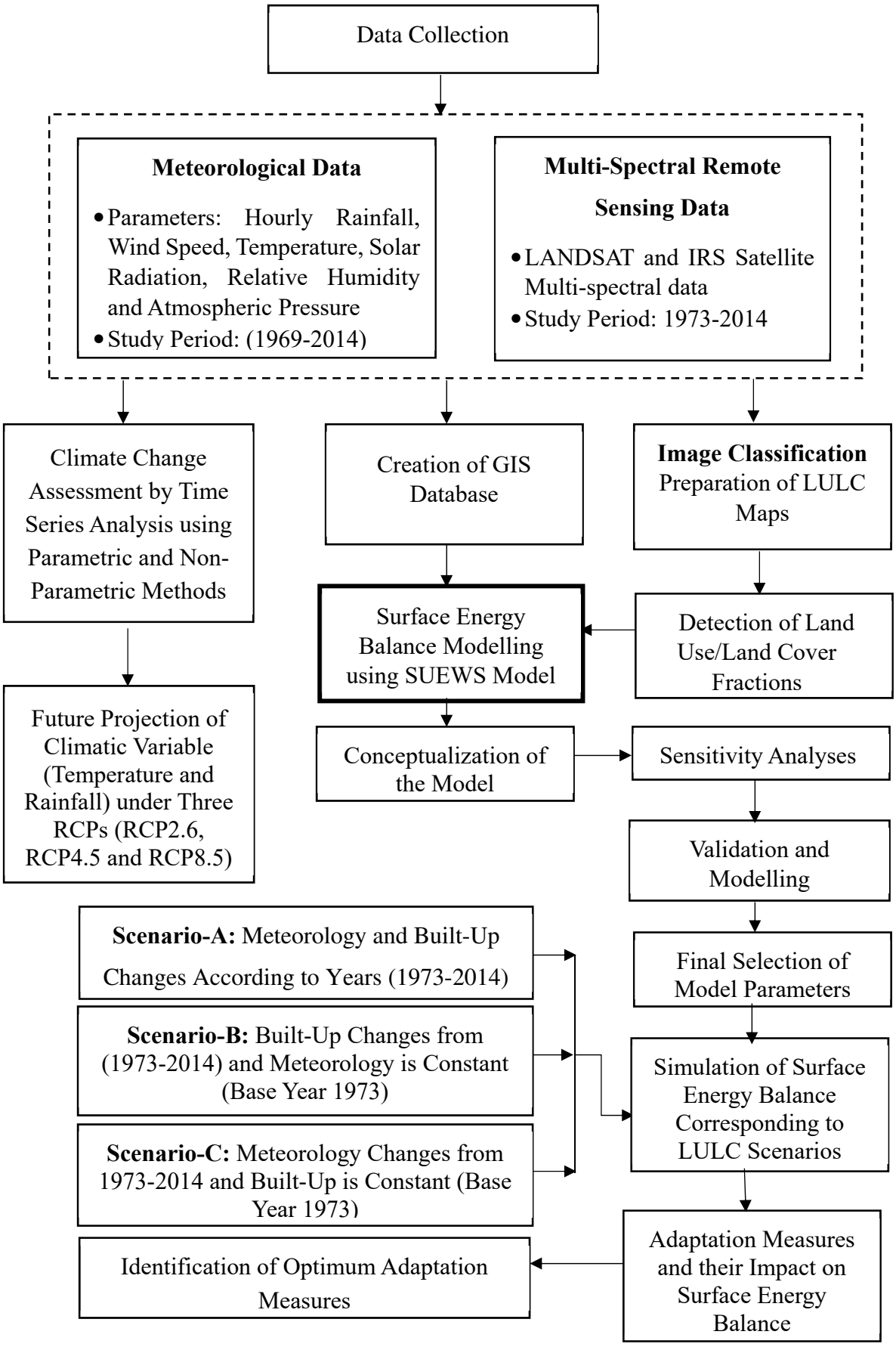

Figure 5.1 : Overall methodology of the research work

The parametric and non-parametric methods used for the analysis are Mann-Kendall (MK test), Modified Mann-Kendall (MMK test), Sen's slope estimator and Pettitt–Mann–Whitney shift detection test. Mann-Kendall test has been used to determine existence and direction of trend in the meteorological data. Meteorological data such as, rainfall data may be auto-correlated and therefore, for the analysis of auto-correlated data, Modified Mann-Kendall test has been used. After identifying trend and its direction in meteorological data, Sen's slope estimator method has been used to determine the magnitude of the existing trend in the data. Further, shift detection test has been used to determine the year from which trend has been shifted. Also, the percentage change in each climatic parameter over the years have been determined. The conceptual framework adopted in this study is shown in Figure 5.2.

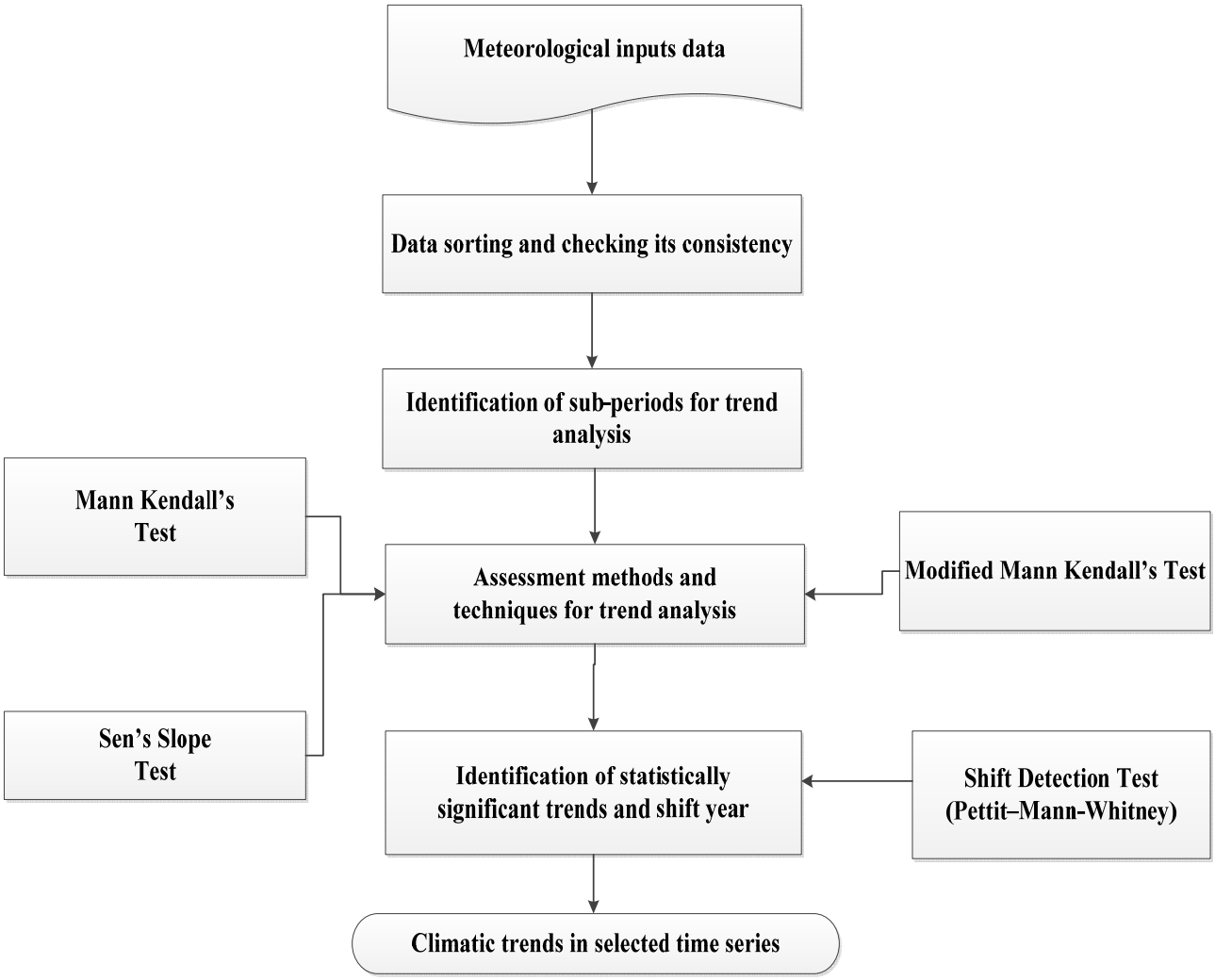

Figure 5.2 : Methodology of time series analysis used for climate change assessment

5.2.1 Normalisation and Autocorrelation Analysis of Time Series

To determine the outliers present in the time series data, normalization has been performed and the equation 5.1 has been used to normalize climatic data (Rai et al., 2010).

$$X_t = (x_t - \bar{x})/\sigma \tag{5.1}$$

where, X_t is the normalized anomaly of the series, x_t is the observed time series, and $\bar{x}$ is the long-term mean and σ is standard deviation of annual/seasonal temperature rainfall time series. The autocorrelation test has been performed to determine the randomness and periodicity in the time series of temperature and rainfall data at all considered temporal resolutions (Modarres and Silva, 2007). MK test has been applied to the actual time series, if lag-1 serial coefficients are not statistically significant (Karpouzos et al., 2010). The MMK test was applied to statistically significant time series after removing the effect of serial correlation. The serial correlation coefficients of normalized climatic series have been computed for different lags, where, k is the maximum lag (i.e. k = n/3); n is the length of the series.

The autocorrelation coefficient of discrete time series for lag-k has been estimated from:

$$r_k = \frac{\sum_{k=1}^{n-k}(X_t - \bar{X}_t)(X_{t+k} - \bar{X}_{t+k})}{\left[\sum_{k=1}^{n-k}(X_t - \bar{X}_t)^2 (X_{t+k} - \bar{X}_{t+k})^2\right]^{0.5}} \tag{5.2}$$

where, r_k is the lag-k serial correlation coefficient. The hypothesis of serial independence is then tested by the lag-1 autocorrelation coefficient as $H0: r1 = 0$ against $H1: |r1| \geq 0$ using the test of significance of serial correlation following (Yevjevich, 1971; Rai et al., 2010):

$$(r_k)_{t_g} = \frac{-1 \pm t_g (n-k-)^{0.5}}{n-k} \tag{5.3}$$

where, $(r_k)_{t_g}$ is the normally distributed value of r_k , t_g is the normally distributed statistic at 'g' level of significance. The value of t_g are 1.645, 1.965 and 2.326 at significance level 0.10, 0.05 and 0.01, respectively. If $|r_k| \geq (r_k)_{t_g}$, the null hypothesis about serial independence is rejected at significance level α (here, 0.05). For non-normal series, MK test is appropriate choice for trend analysis (Mann, 1945). Therefore, MK test was used wherever the autocorrelation is non-significant at 5% level of significance.

5.2.2 Mann-Kendall Test

To detect trends in given time series data, MK test has been used, which is a non-parametric test for detecting trends (Mann, 1945). The non-linear trend and the turning point distribution has been derived from Kendall test statistics (Griffin, 1975). The MK method searches for a trend in given time series without specifying whether the trend is linear or nonlinear. According to various studies, this method has been considered to be an excellent tool for trend detection and used to assess the trends in hydro-climatic time series such as, temperature, rainfall, water quality, stream flow, temperature and precipitation (Basistha et al., 2009; Rai et al., 2010; Patra et al., 2012; Nalley et al., 2013; Pingale et al., 2015). The MK test can be applied to a time series x_i ranked from $i = 1, 2 \ldots n-1$ and x_j ranked from $j = i+1, 2 \ldots n$ such that:

$$\operatorname{sgn}(x_j - x_i) = \begin{cases} 1 & if\ (x_j - x_i) > 0 \\ 0 & if\ (x_j - x_i) = 0 \\ -1 & if\ (x_j - x_i) < 0 \end{cases} \tag{5.4}$$

The Kendall test statistic (S) is given as:

$$S = \sum_{k=1}^{n-1} \operatorname{sgn}(x_j - x_k) \tag{5.5}$$

where, $\operatorname{sgn}(x_j - x_k)$ is the signum function. The test statistic (S) has been assumed to be asymptotically normal, with $E(S) = 0$ for sample size $n \geq 8$ and variance as below:

$$V(S) = \frac{[n(n-1)(2n+5) - \sum_t t(t-1)(2t+5)]}{18} \tag{5.6}$$

where, t_i is number of ties up to sample i. The standardized MK test statistics (Z_{mk}) is estimated as follows:

$$Z_{mk} = \begin{cases} \dfrac{S-1}{\sqrt{V(S)}} & if\ S > 0 \\ 0 & if\ S = 0 \\ \dfrac{S+1}{\sqrt{V(S)}} & if\ S < 0 \end{cases} \tag{5.7}$$

The standardized MK test statistics (Z_{mk}) follows the standard normal distribution with mean of zero and variance of one. If $\pm Z_{mk} \leq Z_{\alpha/2}$ (here, $\alpha = 0.05$), then null hypothesis for no trend was accepted in a two-sided test for trend and the null hypothesis for no trend were

rejected, if $\pm Z_{mk} \geq Z_{\alpha/2}$. Failing to reject $H0$ i.e. null hypothesis does not mean that there is no trend. Rather, it is a statement that the evidence available is not sufficient to conclude that there is a trend (Helsel & Hirsch, 2002, Pingle et. al., 2014). A positive value of Z_{mk} indicates an 'upward trend' and negative value indicates 'downward trend'. The significance levels (p-values) for each trend test are obtained from (Coulibaly et al., 2005):

$$p = 0.5 - \phi(|Z_{mk}|) \tag{5.8}$$

where, $\phi(\,)$ represents cumulative distribution function (CDF) of standard normal variate. At a significance level of 0.05, if $p \leq 0.05$, then existing trend was considered to be statistically significant.

5.2.3 Modified Mann-Kendall Test

First of all pre-whitening was carried out for the serially auto-correlated time series. Pre-whitening of the time series involves computation of correlation and removing it, if serial correlation is significant at 0.05 significance level. The Pre-whitening of time series has been achieved as below-

$$X_t^{'} = (x_{k+1} - r \times x_k) \tag{5.8a}$$

where, x_k = original time series with autocorrelation for time interval *k*; $X_t^{'}$= pre-whitened time series; and $r1$ = the lag-1 autocorrelation coefficient. This pre-whitened series is then subjected to MK test for detecting the trend.

The MK test with pre-whitening of time series was used to detect a trend in a time series in presence of auto-correlation (Cunderlik and Burn, 2004). However, pre-whitening reduces the detection rate of a significant trend in the MK test (Yue and Hashino, 2003). Therefore, MMK test was employed for trend detection of an auto-correlated temperature and rainfall series (Hamed & Rao, 1998; Rao & Sivakumar, 2003, Pingle et. al., 2013, 2014). Only significant values of ρ_k have been used to calculate the variance correction factor n/n_s^* , as the variance of *S* is underestimated when the data are positively auto-correlated:

$$n/n_s^* = 1 + \frac{2}{n(n-1)(n-2)} \times \sum_{i=1}^{n-1} (n-i)(n-i-1)(n-i-2)\rho_s(i) \tag{5.9}$$

where, n is the actual number of observations, n_s^* is considered as an 'effective' number of observations to account for autocorrelation in time series, and $\rho_s(i)$ is the

autocorrelation function of the ranks of the observations which is given as below (Charles Griffin, 1975):

$$\rho_s(i) = \sin^{-1}\left(\frac{\rho(i)}{2}\right) \tag{5.10}$$

where, $\rho(i)$ is parent auto-correlation function of observation rank. The corrected variance is then computed as mentioned below:

$$V^*(S) = V(S) \times n/n_s^* \tag{5.11}$$

where, $V(S)$ is obtained from equation (5.6). Further, the remaining process of trend analysis is same as discussed in the MK test section by incorporating corrected variance in equation 5.7. A significance level of 5% was used for autocorrelation of the rank $\rho_s(i)$, which produce the best overall empirical significance level. The advantages of using corrected variance is that it does not require either normalize data or their autocorrelation function (Rai et al., 2010).

5.2.4 Sen's Estimator of Slope and Percentage Change over a Period

If a linear trend is available in a time series, then the true trend slope can be determined by using a simple non-parametric procedure given by (Theil, 1950; Sen, 1968). The Slope of the trend is determined using following equation:

$$Q_i = Median\left(\frac{x_j - x_k}{j - k}\right) \forall k \leq j \tag{5.12}$$

where, x_j and x_k are data values at times *j* and *k (j > k),* respectively. The median of N values of Q_i is Sen's slope estimator. If N is odd, then Sen's estimator is computed by $Q_{med} = Q_{(N+1)}/2$ and if N is even, then Sen's estimator is computed by $Q_{med} = \left[Q_N/2 + Q_{(N+2)}/2\right]/2$. Finally, Q_{med} is tested using a two-sided test at $100\,(1-\alpha)\,\%$ confidence interval and, the true slope may be determined from the non-parametric test.

The percentage change ($\%$) was estimated assuming the linear trend in which magnitude by Theil and Sen's median slope, and mean are used (Basistha et al., 2009; Pingale et al., 2015). The $\%$ changes over a period were expressed as follows:

$$\%\, change = \left(\frac{MedianSlope \times lengthof\ period}{mean}\right) \tag{5.13}$$

5.2.5 Pettitt–Mann–Whitney Shift Detection Test

The PMW shift detection test was used for estimation of shift in the temperature and rainfall time series (Pettitt, 1979). This test was performed using the evaluation version of XLSTAT (version 2015.1) software. This test can be briefly described below using PMW statistics (Kiely et al., 1998; Basistha et al., 2009). Let T be the length of the time series and τ be the year of the most likely change point. Considering the time series as two samples represented by $X_1 \ldots X_\tau$ and $X_{\tau+1} \ldots X_T$, the index V_τ is defined as:

$$V_\tau = \sum_{j=1}^{T} \mathrm{sgn}(X_\tau - X_j) \quad \text{for any } \tau \tag{5.14}$$

Let an index U_τ be defined as:

$$U_\tau = \sum_{i=1}^{\tau} \sum_{j=1}^{T} \mathrm{sgn}(X_i - X_j) \tag{5.15}$$

A plot of U_τ against τ for a time series with no change point would result in a continually increasing value of $|U_\tau|$. However, if there is a change point (even a local change point), then $|U_\tau|$ would increase up to the change point and then begin to decrease. The most significant change point τ can be identified as the point where the value of $|U_\tau|$ is maximum as given below:

$$K_T = \max_{1 \le \tau \le T} |U_\tau| \tag{5.16}$$

The probability of a change point being at a year where, $|U_\tau|$ is the maximum, as approximated by:

$$p = 1 - \exp\left[\frac{-6K_T^2}{T^3 + T^2}\right] \tag{5.17}$$

Further for $1 \le \tau \le T$, the series

$$\hat{U}(\tau) = |U_\tau| \tag{5.18}$$

is introduced and defined as presented below:

$$p(\tau) = 1 - \exp\left[\frac{-6\hat{U}(\tau)^2}{T^3 + T^2}\right] \tag{5.19}$$

In this way, series consisting of probabilities of change point at each year are obtained for shift detection in time series of annual and seasonal temperature and rainfall over a period for different temporal resolutions.

The above described methods have been used to perform time series analysis for assessment of possible climate change in Delhi in term of trends in climatic time series of temperature and rainfall and the results have been presented in chapter 6.

5.3 FUTURE PREDICTION OF CLIMATIC VARIABLES

Global Circulation Models (GCMs) or Global Climate Models are important tools used to produce a virtual estimate of future climate, but the information they provide remains relatively coarse in resolution. The two type of downscaling models such as Statistical (Wilby et al., 2002) and Dynamical Downscaling (Hessami et al., 2008) are widely used to downscale the coarse resolution predicted climate to regional and local scale. In statistical downscaling, statistical relationships are established between large-scale (the predictors) and local scale (the predictand) climate using multiple linear regression techniques. These relationships are developed using observed weather data at meteorological stations. Assuming that these relationships remain valid in the future, they can be used to obtain downscaled local climate information from the GCM predictors. Dynamical downscaling requires running high-resolution climate models on a regional sub-domain, using observational data or lower-resolution climate model output as a boundary condition. These models use physical principles to reproduce local climates, but are computationally intensive and require lot of data which may not be available. Therefore, in the present study statistical downscaling method and Statistical Downscaling Model (SDSM) has been used (Wilby et al., 1998, 2002). Various countries have proposed GCM[1] models like BCC-CSM1.1 (Beijing Climate Centre, China Meteorological Administration), CFSv2-2011(Center for Ocean-Land-Atmosphere Studies and National Centers for Environmental Prediction), NICAM.09 (Non-hydrostatic Icosahedral Atmospheric Model Group), GISS-E2-H, GISS-E2-H-CC GISS-E2-R and GISS-E2-R-CC (NASA Goddard Institute for Space Studies) and CanESM2 (Canadian Centre for Climate Modelling and Analysis (CCCma) of Environment Canada) GCM model (Khan et al., 2006). In the present study, CanESM2 GCM has been used to predict future climate for the Delhi. CanESM2 is the second generation of Earth System Model. Climate scenarios from the

[1] http://cmip-pcmdi.llnl.gov/cmip5/availability.html

Coupled Model Inter-comparison Project Phase 5 (CMIP5) (Taylor et al., 2012) has been used as the input to GCM. Similar scenarios have been used in the latest Intergovernmental Panel on Climate Change (IPCC) Assessment Report 5 (AR5). It is usually not appropriate to directly use outputs from GCMs for investigating environmental impacts of climate change at regional scale. GCMs have been widely used in the study of climate change, and lots of work has been done in simulating the influences of LULC change on the global temperature and precipitation at a coarser scale. However, it is difficult to simulate the regional climate at small scales precisely with GCMs. (Mimura et al., 2014). IPCC in its fifth assessment report (AR5) has adopted Representative Concentration Pathways (RCPs) which are four greenhouse gas concentration (not emissions) trajectories, to simulate the future climate.

These pathways are used for climate modelling and research. They describe three possible climate futures, all of which are considered possible depending on how much greenhouse gases are emitted in the years to come (Weyant et al., 2009). The four RCPs such as, RCP2.6, RCP4.5, RCP6 and RCP8.5 have been proposed after a possible range of radiative forcing values in the year 2100 relative to pre-industrial values (+2.6, +4.5, +6.0 and +8.5 W/m^2, respectively). Three representative concentration pathways RCPs (RCP2.6, RCP4.5 and RCP8.5) have been considered in the present study to predict future climate using CanESM2 GCM and the results are discussed in Chapter 6. The calibration of a model is a process used in downscaling models based on multiple linear regression equations, given daily weather data (the predictand) and coarse scale atmospheric (predictor) variables. The parameters of the regression model are written to a standard format file with the extension *.PAR, along with meta–data recording details of the calibration period, model type, predictors used, etc. Calibration process has been carried out by the regression relationship between coarse scale predictor variables of GCM with local scale predictand variable. There are 26 predictor variables available from GCM and among them only a few variables have a significant relationship with the predictand variable.

A combination of the correlation matrix, partial correlation and p-value at a significant level of 0.05 has been considered. The selected predictor variables for temperature and precipitation are downscaled for two sites of Delhi. For assessing the reliability of the calibrated model, the simulated results are validated by comparing it with the observed data for 37 years period from 1969 to 2005. General statistics of the compared data i.e., downscaled and observed are extracted in general like statistics mean, maximum, minimum, maximum range, minimum range and extreme events at different temporal

scales. Detailed results of downscaling are discussed in Chapter 6 and flow chart of methodology followed for downscaling has been presented in Figure 5.3.

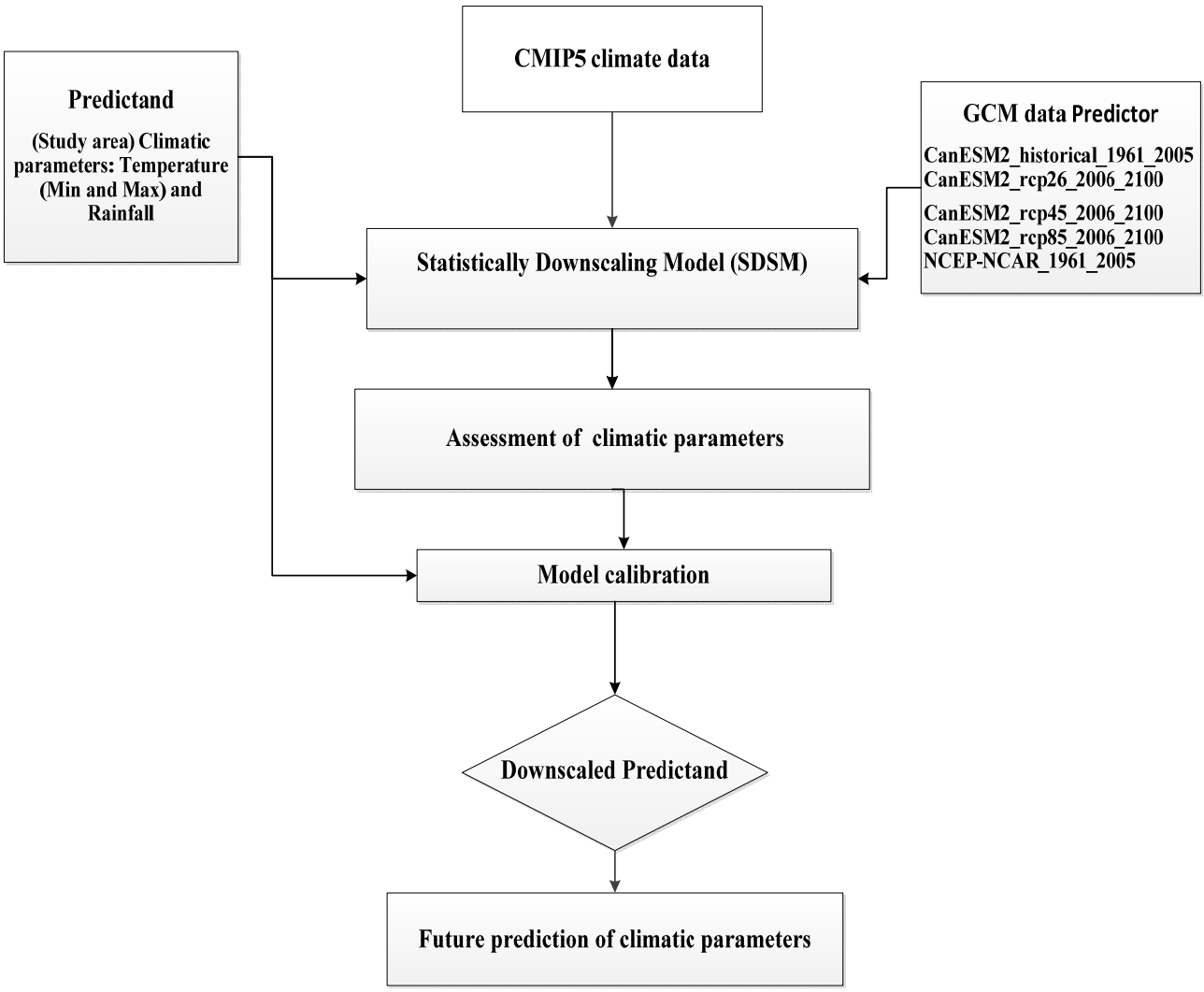

Figure 5.3 : Methodology of statistical downscaling used for future prediction of climatic variable

5.4 SURFACE ENERGY BALANCE MODELLING

Surface energy balance can be defined as the heat generated within and stored by a system, including all the exchanges of energy and radiative heat fluxes. For urban areas, the surface energy balance is applied to a control volume extending from the ground to the top of the urban surface. Each surface energy balance term is influenced by the urban environment and thus contributing to urban heat. Due to rapid and continuous urbanization, natural surfaces are changed into artificial surfaces and introduces anthropogenic heat generation in the urban areas. These actions change the micro and mesoscale climate (Landsberg,

1981; A. Oke, Keller, & Adams, 1978; IPCC, 2014). Surface energy balance has been used to quantify the realistic influence of urbanization on climate (Krpo, Clappier, & Muller, 2006; Lemonsu & Grimmond, 2004; Masson & Grimmond, 2002; Jarvi et al., 2011) but also investigated the impact of strategies to minimize the adverse effect of urban heat (Hamdi, Schayes, & R. Hamdi, 2008; Tubiello & Rosenzweig, 2008; Yu & Hien, 2006; Middle et al., 2012). Surface energy balance is an integration of various fluxes such as, total heat flux, storage heat flux, sensible heat flux and latent heat flux.

Net all-wave radiation is the contribution of all other heat fluxes i.e. (storage heat flux, sensible heat flux, latent heat flux). So, the net all-wave radiation behaviors depend on these heat fluxes, storage heat flux is basically absorbed heat flux during day time by the different land cover and radiate in night time and contributes in total heat fluxes. Another two heat fluxes are interchangeable to each other sensible heat flux and latent heat flux. Solar insolation and albedo are the primary determinants of the surface energy balance. The roughness of the surface is important as it impacts the determination of the rate of convective heating/cooling of the surface (sensible heat flux). The moisture availability determines the potential for evaporative cooling of the surface (latent heat flux) and also influences surface albedo. In addition to these, surface characteristics, substrate thermal properties (thermal conductivity and capacitance) can play a significant role in the storage of heat during the day and the release of heat at night. While the primitive surface characterization implemented in most mesoscale meteorological models is limiting for all regional modelling applications, it is particularly problematic for simulations of the urban climate.

5.4.1 Surface Energy Balance Equation

The mathematically surface energy balance can be expressed as in equation 5.20 (Järvi et al., 2011).

$$Q^* + Q_F = Q_E + Q_H + \Delta Q_S \qquad [Wm^{-2}] \tag{5.20}$$

where, Q* is the net all-wave radiation, Q_F is the anthropogenic heat flux, Q_H is the turbulent sensible heat flux, Q_E is the turbulent latent heat flux and ΔQ_S is the net storage heat flux. Each component of surface energy balance is discussed in the following subsections.

5.4.1.1 Daily anthropogenic heat flux (Q_F)

Estimation of the heat flux generated by anthropogenic activities in the urban area classified by source such as, buildings, transportation and other human activities is called anthropogenic heat flux and is expressed by equation 5.21 (Järvi et al., 2011). In this study, Large Scale Urban Consumption of Energy (LUCY) model has been used to calculate anthropogenic heat flux while modelling surface energy balance. The results of this model have been used as one of the inputs in SUEWS model. Although two simple anthropogenic heat flux models have been used in SUEWS (Järvi et al., 2011) model, but to improve the performance, LUCY model has been suggested by (Järvi et al., 2014b). LUCY model calculates all the components (traffic, metabolism and building energy) of anthropogenic heat fluxes for any city or region around the world at a spatial resolution of 2.5 x 2.5 arc-minutes. The model has been developed in collaboration with UMET@KCL at King's College London. The model includes a database of different working patterns and public holidays – vehicle use and energy consumption in each country (Boberski and Allen, 2014). The databases can be edited to include specific diurnal and seasonal vehicle and energy consumption patterns including local holidays and flows of people within a city. In the present study, temperature, population and traffic gridded data have been used for the estimating the anthropogenic heat flux.

$$\mathrm{QF\,p}_{(\mathrm{wd.we})} = \mathrm{a}_{0\,(\mathrm{wd.we})} + \mathrm{a}_{1(\mathrm{wd.we})}\mathrm{CDD} + \mathrm{a}_{2(\mathrm{wd.we})}\mathrm{HDD} \quad (5.21)$$

In equation 5.21, $\mathrm{a}_{0(\mathrm{wd.we})}$ is the base value of Q_F which is the integrated heat flux per p from all sources relative to a base human comfort temperature 18.2°C (Sailor and Vasireddy, 2006) for weekdays (wd) and weekends (we). The relation for a study area between (cooling degree days) CDD ($\mathrm{a}_{1(\mathrm{wd.we})}$) and (heating degree days) HDD ($\mathrm{a}_{2(\mathrm{wd.we})}$) needs to be specified. The daily Q_F is partitioned using user-definable diurnal profiles for *we* and *wd*. The daily anthropogenic heat flux (Wm^{-2}) per population density (p, units: capita ha^{-1}) is calculated for two temporal scale such as, weekdays (*wd*) and weekends (*we*).

5.4.1.2 Turbulent sensible heat flux ($\mathrm{Q_H}$)

The mathematical formulation of sensible heat flux is presented below in equation 5.22

$$\mathrm{Q_H} = \frac{(1-\alpha)+\left(\frac{\gamma}{s}\right)}{1+\left(\frac{\gamma}{s}\right)}(\mathrm{Q^*} - \Delta\mathrm{Q_S}) - \beta \quad (5.22)$$

where, *s* is the slope of the saturation vapor pressure versus temperature curve, γ is the psychrometric ‘‘constant,’’ α and β are empirical parameters. These parameters are based on a simplification of the Penman-Monteith approach, which takes into account the Priestley-Taylor coefficient *PT* for extensive wet surfaces but extends it to include non-saturated areas. To evaluate the turbulent Sensible Heat Flux, the two parameters α and β must be specified.

5.4.1.3 Turbulent latent heat flux(Q_E)

Evaporation from each surface is calculated with the Penman–Monteith equation (Penman, 1948; Monteith, 1965) which was modified for urban areas (Grimmond et al., 1991), as given in equation 5.23.

$$Q_E = \frac{s(Q^* + Q_F - \Delta Q_S) + c_p \rho V / r_a}{s + \gamma(1 + r_s / r_a)} \tag{5.23}$$

This is applicable to dry surfaces. When the surface is completely wet the surface resistance r_s is set to zero. To link the two surface stages (dry and wet), r_s is replaced with a redefined surface resistance (r_{ss}) (Shuttleworth, 1978) and expressed in equation 5.24.

$$r_{ss} = \left[\frac{W}{r_b\left(\frac{s}{\gamma}+1\right)} + \frac{(1-W)}{r_s + r_b\left(\frac{s}{\gamma}+1\right)}\right]^{-1} - r_b\left(\frac{s}{\gamma} + 1\right) \tag{5.24}$$

where, *W* is a function of the amount of water on the canopy of the individual surface (C_i) relative to the canopy surface water storage capacity (S_i) and expressed in equation 5.25.

$$W = 1 \qquad C_i \geq S_i \tag{5.25}$$

$$W = (K-1) / (K - S_i/C_i) \qquad C_i < S_i$$

K relates to the aerodynamic (r_a) and surface (r_s) resistances and expressed in equation 5.26.

$$K = \frac{r_s / r_a / (r_a - r_b)}{r_s + r_b\left(\frac{s}{\gamma}+1\right)} \tag{5.26}$$

Where, r_b is the boundary layer resistance (Shuttleworth, 1983) and r_b is considered as presented in equation 5.27.

$$r_b = 1.1 u_*^{-1} + 5.6 u_*^{1/3} \tag{5.27}$$

Q_E depends on the surface wetness state and therefore, it is calculated with 5 min time step. Sensible heat flux is calculated as a residual from the hourly available energy minus the hourly latent heat flux.

5.4.1.4 Aerodynamic resistance (r_a)

The aerodynamic resistance is calculated using the logarithmic wind profile for each hour using equation 5.28.

$$R_a = \frac{[\ln(\frac{z_m - z_d}{z_{0m}}) - \varphi_m][\ln(\frac{z_m - z_d}{z_{0v}}) - \varphi_v}{k^2 u} \quad (5.28)$$

where, z_m is the height at which horizontal wind speed u is measured, z_d is the zero plane displacement height, z_{0m} is the roughness length for momentum, z_{0v} is the roughness length for heat and water vapour, k is the Von Karman constant (0.4). φ_m and φ_v are the stability functions for momentum and water vapour. The stability function for unstable conditions for momentum (Holtslag and Van Ulden, 1983) is:

$$\varphi_m = 2\ln(\frac{1+X}{2}) + \ln(\frac{1+X^2}{2}) - tan^{-1}(X) + \frac{\pi}{2} \quad (5.29)$$

where, $X = (1 - 15.2\xi)^{0.25}$ (Högstrom, 1988) and $\xi = (z_m - z_d)/L$ for heat and water vapour (Van Ulden & Holtslag, 1985).

$$\varphi_v = 2\ln(\frac{1+Y^2}{2}) \quad (5.30)$$

where, $Y = 0.95((1 - 15.2\xi)^{0.5})$ (Högstrom, 1988). The function for a stable condition for momentum (Holtslag and Van Ulden, 1983) is:

$$\varphi_m = -17(1 - \exp(-0.29\xi)) \quad (5.31)$$

and for heat and water vapour (Högstrom, 1988) are expressed in equation 5.32 and 5.33.

$$\varphi_v = -4.5\,\xi \quad (5.32)$$

$$z_{0v} = z_{0m}\exp(2.0 - a\frac{z_{0m}u}{v}) \quad (5.33)$$

where, a is an empirical constant depending on the surface cover, v is the molecular viscosity of air which can be adopted as $1.46 \cdot 10^{-5} m^2$. For n vegetated urban surfaces, Kanda (2006) proposed $a = 1.29$. (CSB et al., 2010):

$$a = 1.2 - 0.9 f_v^{0.29} \quad (5.34)$$

where, 'a' depends on the fraction of vegetation cover (f_v).

Surface resistance (r_s) can be calculated from equation 5.35.

$$r_s^{-1} = g_s = G_1 \sum_{i=3}^{6} \left(f_i g_{imax} \frac{LAI_{d,i}}{L_{m,i}} \right) g(K\downarrow)\, g(\Delta q) g(T) g(\Delta\theta) \quad (5.35)$$

This allows g_s to respond by vegetation type (i) to $LAI_{d,i}$ relative to its maximum ($L_{m,i}$) for its fraction of cover (f_i), maximum conductance values (g_{imax}), and environmental variables of incoming shortwave radiation ($K\downarrow$,Wm^{-2}):

$$g(K\downarrow) = \frac{K\downarrow/(G_2 + K\downarrow)}{K\downarrow_m/(G_2 + K\downarrow_m)} \quad (5.36)$$

Specific humidity deficit ($\Delta q, g\ kg^{-1}$) is expressed in equation 5.37.

$$g(\Delta q) = \begin{cases} 1 - G_3 \Delta q, \Delta q < G_4 \\ 1 - G_3 G_4, \Delta q \geq G_4 \end{cases} \quad (5.37)$$

Temperature is expressed as T (°C) and g(T) can be obtained from equation 5.38.

$$g(T) = \frac{(T - T_L)(T_H - T)^{T_c}}{(G_5 - T_L)(T_H - G_5)^{T_c}} \quad (5.38)$$

where, Tc = $(T_H - G_5)$/ ($(G_5 - T_L)$, and soil moisture deficit ($\Delta\theta$, mm) as presented in equation 5.39.

$$g(\Delta\theta) = 1\text{-}\exp\{G_6(\Delta\theta - \left(\frac{s_1}{G_6}\right) + s_2)\} \quad (5.39)$$

where, s_1 and s_2 are parameters related to the maximum $\Delta\theta$. To obtain the parameters G_1–G_6 observations of Q_H and Q_E are used to determine 'measured' values of r_s from:

$$\mathrm{r_s} = \left(\frac{\mathrm{s}\beta}{\gamma} - 1\right)\mathrm{r_a} + \frac{\mathrm{c_p}\rho\mathrm{V}}{\gamma \mathrm{Q_E}} \quad (5.40)$$

5.4.1.5 Storage heat flux ($\mathrm{Q_s}$)

Storage heat flux ($\mathrm{Q_s}$) includes the conduction of heat into or out of the surface media comprising the volume (e.g. walls, roofs, trees, ground, etc.), and changes in the sensible and latent heat content of the air volume itself. A similar approach is taken to the storage heat flux in forested canopies (Oliphant et al., 2004). If all other terms of the surface energy balance are independently evaluated, $\mathrm{Q_s}$ can be found as the residual $\mathrm{Q_s}$ and calculated using the Objective Hysteresis Model (Arnfield and Grimmond, 1998; Grimmond and Oke, 2002) which is able to capture the characteristic magnitude and diurnal hysteresis of the storage heat flux in cities (Offerle et al., 2003, 2006). Storage heat flux can be calculated using equation 5.41.

$$\mathrm{Q_s} = \mathrm{Q^*} + \mathrm{Q_F} - \mathrm{Q_H} - \mathrm{Q_E} \quad (5.41)$$

where, $\mathrm{Q^*}$ is the net all-wave radiation flux; $\mathrm{Q_F}$ the anthropogenic heat flux and $\mathrm{Q_H}$, $\mathrm{Q_E}$ are turbulent sensible and latent heat flux respectively (Grimmond et al., 1991). Heat storage values determined by residual $\mathrm{Q_s}$ will be used here to provide test data but such data are not routinely available. There is a need to develop a simple way to obtain the heat storage in urban systems. One approach is to examine heat flow into materials such as grass, concrete or other urban materials and use these as a surrogate for urban behavior. Kerschgens & Hacker, (1985) have used measurements of the substrate heat fluxes from grassed & paved sites and combine them into an urban system estimate by weighting the results according to the fraction of green and impervious cover in the upwind region.

$$\mathrm{Q_s} = \sum_{\mathrm{i}=1}^{\mathrm{n}} \alpha_\mathrm{i}(\mathrm{a_i Q^*} + \mathrm{b_i}) \quad (5.42)$$

where, α_i is the fraction of the urban area covered by the i^{th} surface (Oke & Cleugh, 1987). The general performance of this objective linear model was satisfactory especially used for a periods of a day or more.

5.4.2 Surface Energy Balance Models

Surface energy balance modelling requires integration of above models and equations at suitable spatial and temporal resolution. In recent past, many surface energy balance models have been developed having different capabilities and require different level of input parameters.

Some of the popular models reported in the literature are Building Effect Parameterization (BEP02) (Martilli et al., 2002), Canyon Air Temperature (CAT) Erell and Williamson (2006), Community Land Model – Urban (CLMU) (Oleson et al., 2008), Environmental Meteorology Model (ENVImet) ((Bruse and Fleer, 1998) and Green Cluster Thermal Time Constant Model (GCTTC) (Shashua-Bar and Hoffman, 2002, 2004). Urbanized version of DMI-HIRLAM Model (HIRLAM-U) ((‘ISBA scheme performance in high resolution modelling for low winds conditions’, 2006; Zilitinkevich et al., 2006; Baklanov et al., 2008), Local-scale Urban Meteorological Parameterization Scheme (LUMPS) (Grimmond and Oke, 2002; Offerle et al., 2003), Penn State/NCAR Mesoscale Model (MM5u) (Dandou et al., 2005), Multi-layer Urban Canopy Model (MUCM) (Kondo and Liu, 1998; Kondo et al., 2005), Microscale Urban Climate Model (MUKLIMO) (Sievers, 1995), Noah Land Surface Model/ Single-layer Urban Canopy Model (NSLUCM) (Kusaka et al., 2001; Chen, 2007), Soil Model for Sub-Meso Scale Urbanized Version (SM2U) (Dupont and Mestayer, 2006), Met Office Urban Surface Exchange Scheme (MOUSES) (Harman et al., 2004a, b), Slab Urban Energy Balance Model (SUEB) (Fortuniak et al., 2004; Fortuniak and Offerle, 2005), Simple Urban Energy Balance Model for Meso-Scale Simulation (SUMM) (Kanda, 2006), Simple Urban Neighborhood Boundary Energy Exchange Model (SUNBEEM) (Arnfield, 2000), Urban Canopy Layer Model (UCLM) (Mills, 1997), Surface Urban Energy and Water Balance Scheme (SUEWS) (Järvi et al., 2011, 2014b). A detailed comparison of the popular surface energy balance models has been given in Table 5.1.

These models were developed for different related applications where, one or more components of the surface energy balance can be estimated. Different models have different capabilities, input data requirement and suitable for different spatial and temporal scales.

Table 5.1 : Comparison of SEB models on the basis of the model output parameters (Grimmond et al. 2010)

Model	Model name	Reference	Time Step	Q*	Q_H	Q_E	Q_S	T_s	LULC Fractions	Albedo (α)
BEP02	Building Effect Parameterization	Martilli et al. (2002)	Ud	YES	YES	NO	YES	YES	NO	NO
BEP05	Building Effect Parameterization	Hamdi (2005); Hamdi and Schayes (2007)	Ud	YES	YES	NO	YES	YES	V	NO
CAT	Canyon Air Temperature	Erell and Williamson (2006)	1h	NO	YES	YES	NO	NO	NO	YES
CLMU	Community Land Model – Urban	Oleson et al. (2008a, b)	1200-3600s	YES	YES	YES	YES	YES	RVRC	NO
ENVImet	Environmental Meteorology Model	Bruse and Fleer (1998)	Typ.2-10s	YES	YES	YES	YES	YES	OPTIONAL	NO
GCTTC	Green Cluster Thermal Time Constant model	Shashua-Bar and Hoffman (2002,2004)	24h	YES	YES	YES	YES	YES	RVRC	YES
HIRLAM-U	Urbanised version of DMI-HIRLAM model	Baklanov et al. (2006, 2008); Mahura et al. (2006); Zilitinkevich et al. (2006)	Ud.typ.300s	NO	NO	NO	NO	NO	RVRC	YES
LUMPS	Local-scale Urban Meteorological Parameterization Scheme	Grimmond and Oke (2002); Offerle et al. (2003)	1 hr	YES	NO	NO	NO	NO	RVRC	YES
MM5u	Penn State/NCAR Mesoscale Model, where urban modifications have been incorporated	Dandou et al. (2005)	Ud	NO	NO	NO	NO	NO	RVRC	YES
MOSES1T	Met. Office Surface Exchange Scheme 1 Tile	Best (2005); Essery et al. (2003)	Ud	NO	NO	NO	NO	NO	RVRC	YES
MOSES2T	Met. Office Surface Exchange Scheme 2 Tile	Best et al. (2006); Essery et al. (2003)	Ud	YES	YES	YES	YES	YES	RVRC	YES
MUCM	Multi-layer Urban Canopy Model	Kondo et al. (2005); Kondo and Liu (1998)	10-120s	YES	YES	YES	YES	YES	RVRC	YES
MUKLIMO	Microscale Urban Climate Model	Sievers (1995)	Ud. typ. 3h	NO	NO	NO	NO	NO	RV	NO

Model	Model name	Reference	Time Step	Q*	Q_H	Q_E	Q_S	T_s	LULC Fractions	Albedo (α)
NSLUCM	Noah land surface model/Single-layer Urban Canopy Model	Kusaka et al. (2001); Chen et al. (2004)	Us (0 -60 min)	YES	YES	YES	YES	YES	RVRC	NO
SM2U	Soil Model for Sub-Meso Scale Urbanized Version	Dupont and Mestayer (2006); Dupont et al. (2006)	Ud. typ 300s	YES	YES	YES	YES	YES	RVRC	NO
MOUSES∗	Met Office Urban Surface Exchange Scheme	Harman et al. (2004a, b)	Ud	YES	YES	YES	YES	YES	RVRC	NO
SUEB∗	Slab Urban Energy Balance Model	Fortuniak et al. (2004, 2005)	1 s	NO	NO	NO	NO	NO	NO	YES
SUMM∗	Simple Urban Energy Balance Model for Meso-Scale Simulation	Kanda et al. (2005a, b)	Ud	YES	YES	YES	YES	YES	RVRC	NO
SUNBEEM	Simple Urban Neighbourhood Boundary Energy Exchange Model	Arnfield (2000)	Ud	YES	YES	YES	YES	YES	NO	NO
TEB∗	Town Energy Balance	Masson (2000); Masson et al. (2002); Lemonsu et al. (2004)	60-900s typ.300s	YES	YES	YES	YES	NO	RVRC	NO
TEB07∗	Town Energy Balance 07	Hamdi and Masson (2008)	Ud	YES	YES	YES	YES	NO	RV	NO
TUF2D/ TUF3D∗	Temperatures of Urban Facets in 2D	Krayenhoff and Voogt (2007)	Variable(type.10-100)	YES	YES	NO	YES	YES	NO	NO
UCLM∗	Urban Canopy Layer Model	Mills (1997)	1 hr	YES	YES	YES	YES	YES	NO	YES
VUCM∗	Vegetated Urban Canopy Model	Lee and Park (2008)	Ud	YES	YES	YES	YES	YES	RVRC	NO
SUEWS	Surface Urban Energy and Water Balance Scheme	L. Järvi 2014 (Manual)	hourly	YES	YES	YES	YES	YES	RVRC	YES

Note : Ud – user defined; RVRC – road, vegetation, roof and canyon

Different models have been compared considering simulation time step, the capability to simulate different surface energy balance components, the inclusion of LULC and Albedo.

5.4.2.1 Selection of surface energy balance model

According to literature survey, various models have been proposed to calculate energy fluxes for any study area. The comparison of various existing models has been shown in the Table 5.1. In the present study, after comparing various models, SUEWS model has been selected due to the following advantages:

1. There are various models capable to perform better for individual fluxes but no model performs best or worst for all fluxes. Simple as well as complex models are based on statistical methods and are able to determine net all-wave radiation and least capability to model latent heat flux (Grimmond et al., 2010). However, SUEWS model is capable to perform better than existing models for all fluxes including latent heat flux.
2. Few existing models have been developed for urban runoff and they do not consider complete urban water balance (Bertheir et al., 2004) whereas, in SUEWS model urban water balance scheme has been taken into account.
3. On comparing the number of input parameters required by existing models to simulate energy fluxes, SUEWS model requires relatively less number of input parameters because various sub-models have been integrated in it, which are designed to minimize the number of input variables required.
4. SUEWS model takes both the surface and soil below, into account whereas other models mostly work with surface characteristics.
5. According to best of our knowledge, SUEWS model is one of the best model to simulate energy fluxes at neighborhood or local scale. Also, this model provides results at hourly basis and these results are aggregated into daily, monthly and annual time period.

After carefully study of all the models and available data for the selected study area, Surface Urban Energy and Water Balance Scheme (SUEWS) has been chosen for the present study to simulate surface energy balance.

5.4.3 Surface Urban Energy and Water Balance Scheme (SUEWS)

SUEWS model has been designed to simulate energy and water balance terms at a neighborhood scale (≥1 km^2) and requires site specific meteorological data and a detailed

description of the surface. Surface urban energy and water balance scheme (SUEWS) Version 2014b (8 October 2014) has been used for the generation of heat fluxes for selected two study area i.e., Palam and Safdarjung in Delhi. SUEWS (Järvi et al., 2011) is able to simulate the urban radiation, energy and water balances using commonly measured meteorological variables and information about the surface cover. SUEWS utilizes an evaporation interception approach similar to that used in forests to model evaporation from urban surfaces. The model uses seven surface types such as, paved, buildings, coniferous trees, deciduous trees, irrigated grass, non-irrigated grass and water. The surface state for each surface type at each time step is calculated from the running water balance of the canopy, where, the evaporation is calculated from the Penman-Monteith equation. The soil moisture below each surface (excluding the water) is also taken into account. Horizontal movements above and below ground level are permitted. The time step used in SUEWS is 60 minutes. The model provides the radiation, energy balance components, surface and soil wetness and drainage of each surface, surface & soil runoff and surface temperature.

5.4.3.1 Sub models of SUEWS

SUEWS model is a combination of various sub-models and these are discussed below:

- NARP (Net All-wave Radiation Parameterization) radiation scheme (Offerle et al., 2003; CSB et al., 2010).
- Storage heat flux which is calculated with OHM (objective hysteresis model) (Grimmond et al., 1991; Grimmond and Oke, 1999; Masson et al., 2002).
- LUMPS (Local-scale Urban Meteorological Parameterisation Scheme) (Grimmond and Oke, 2002) does the initial turbulent sensible and latent heat fluxes calculation for stability.
- Two simple anthropogenic heat flux models (Järvi et al., 2011).
- A simple urban water use model (Grimmond et al., 1991).

5.4.3.2 Basic inputs parameters required to conceptualize SUEWS model

The SUEWS model is based on GIS grid information specifying the fractional land cover type, fractional tree, grass coverage and the meteorological parameters like radiation, temperature, precipitation etc., for the study area. According to Järvi et al., (2011), each input parameter has been examined and prepared carefully for the study area. These input values could be determined either by the values pertaining to the study area itself or based on recommended values for the model as discussed in various relevant research articles.

Important individual values and reasoning behind choosing each input value have been discussed in Chapter 7. The various input parameters and equations used in SUEWS model are discussed below:

5.4.3.2.1 Albedo

Albedo is defined as the fraction of shortwave radiation reflected from the study area back into space. Surface Albedo ($\propto_0$) has been calculated using equation 5.43.

$$\propto_0 (\varphi) = \alpha + (1 - \alpha)\exp[-0.1\varphi - \frac{(1-\alpha)}{2}] \quad (5.43)$$

where, α is albedo at a maximum solar elevation and φ is elevation angle in degrees (U.S. Environmental Protection Agency, 1999).

5.4.3.2.2 Emissivity

Emissivity is the measure of an object's ability to emit energy in the form of radiation. Emitted energy is proportional to the temperature of the object. Emissivity can have a value from 0 (shiny mirror) to 1.0 (blackbody). Net radiation and emissivity are related as -

$$R_n = (1 - A)K \downarrow + L \downarrow - \varepsilon\, \sigma {T_0}^4 \quad (5.44)$$

where, R_n is net radiation balanced by sensible, latent, and conduction heat fluxes, $K \downarrow$ is incoming short wave radiation. (Wm^{-2}), $L \downarrow$ is incoming long wave radiation (Wm^{-2}), A is albedo, T_0 is surface temperature (Kelvin), ε is emissivity and σ is Stefan-Boltzmann constant. The temperature is calculated in degrees Celsius using equation 5.45.

$$L \uparrow = \varepsilon\, \sigma(T_s + 273.15)^4 \quad (5.45)$$

where, $(T_s + 273.15)$ is absolute temperature in Kelvin (K) and $\sigma = 5.67 \times 10^{-8}$ W m^{-2} K^{-4} is the Stefan-Boltzmann constant. The emissivity (ε) of an object generally ranges from 0.95 to 1.0. A blackbody has an emissivity equal to one. Most natural surfaces are 'grey bodies', with emissivity less than one.

5.4.3.2.3 Drainage equation

Determination of the drainage rate for urban areas is complex and not easily available. This term does not correlate directly with urban runoff. It has to be predicted as that loss from the storage layer which is no longer available for evaporation and which may enter into a drainage system or infiltrate into the soil. The drainage function describes the rate at which water drains from the moisture store. It is set proportional to the current water status of this store. Rutter, Kershaw, Robins, & Morton, (1971) proposed the drainage as -

$$D = D_0 \exp\{b(C-S)\} \quad (5.46)$$

D_0 = Drainage rate when C=S or C< S (No drainage)

where, *b* is empirical coefficient and *S* is the amount of water the canopy stores / retains after the rainfall and through fall cease. C< S (No Drainage) is the assumption proposed by the researcher for the forest areas and the rate of drainage from the flat roofs can be assumed to be the same as the paved surface of 1% slope. In this study, it was not possible to directly test the performance of any individual drainage equation.

5.4.3.2.4 Storage capacity

The values of the surface storage capacity, like the drainage functions, were adopted from the literature for the areas with similar surface environment. The capacity for the surface type is assumed to be constant through time for all types except, deciduous vegetation, where, the allowance is made for the changes between winter and summer. This is done by the addition to the winter storage capacity (S_{dw}) of an increment ($S_d st$):

$$S_d st = (S_{ds} - S_{dw}) / (te - tb) \quad (5.47)$$

Where, S_{ds} is summer deciduous storage capacity (mm), t_e is Julian day on which the transition ends and t_b is Julian day on which the transition ends.

5.4.3.2.5 Conduction parameter

After the inputs of energy, the most important factor governing the rate of evaporation is the efficiency of removal of water vapor from the surface for a given wind speed and vapours pressure. The rate of removal of water vapor depends on the atmospheric turbulence created by the wind blowing over the surface roughness elements. The integrated transfer coefficient for water vapour between the evaporating surface and some reference height in the free atmosphere is termed as the aerodynamic resistance (r_a) or its reciprocal that is aerodynamic conductance $(g_{a)}$. It can be estimated using the following equations -

$$r_a = (1/g_a) = \{\ln [(Z-d)/Z_0]\}^2 / K^2 u) \quad (5.48)$$

where, *Z* is wind speed measurement height (m), *d* is displacement length (m), Z_0 is momentum roughness length (m), *k* is Von Karman's constant and *u* is horizontal wind speed (m/s^{-1}). The general form of these models (expressed as a conductance (g_s) is (g_s)= P_1 L g (variables), where, P_1 is maximum value of the surface conductance (ms^{-1}), *L* is Leaf area index (LAI) and *g* is (variables) functions of the environmental variables, which have values between zero and unity.

5.4.3.3 Impact of LULC on climate change using SUEWS model

Surface Urban Energy and Water Balance Scheme (SUEWS) model has been used in the present study to perform surface energy balance modelling to investigate the change in

surface energy fluxes i.e., net all-wave radiation, storage heat flux, sensible heat flux and latent heat flux) as a result of change in LULC for 12 different years on hourly temporal scale for two area Palam and Safdarjung of Delhi region. In the present study, input data has been prepared in the required format and then conceptualized for the study area. Model coefficients have been decided based on the literature survey related to meteorologically and spatially significant areas. Primary input data used are hourly meteorological parameters and LULC information. Multispectral satellite data obtained for different years have been processed and classified by supervised classification method to LULC maps for different years (1973, 1977, 1986, 1991, 1998, 1999, 2002, 2006, 2009, 2011, 2013, and 2014). Details of data used for the present study are discussed in Chapter 3. The details of preparation of LULC maps and GIS database creation has been presented in Chapter 4.

First of all, model input parameters have been extracted from the GIS database and converted into the suitable format of the SUEWS. SUEWS model was conceptualized for the two study areas by supplying the required parameters at suitable temporal and spatial resolution. The model was tested for initial datasets to determine model functionality. Subsequently, the model was run iteratively for a range of different selected important parameters to carry out the sensitivity analysis. Further, the model was validated by comparing model outputs and observed data of heat fluxes for different locations of Delhi. Finally, model parameters have been selected corresponding to best fit model results while comparing observed data for two years 1998 and 1999. Further, three scenarios (A, B, and C) were conceptualized to investigate the effect of LULC changes on surface energy balance components for 12 different years. The details about the values of input parameters used and surface energy balance results using SUEWS model for the study area have been presented in Chapter 7. The methodology followed for surface energy balance modelling has been presented in Figure 5.4.

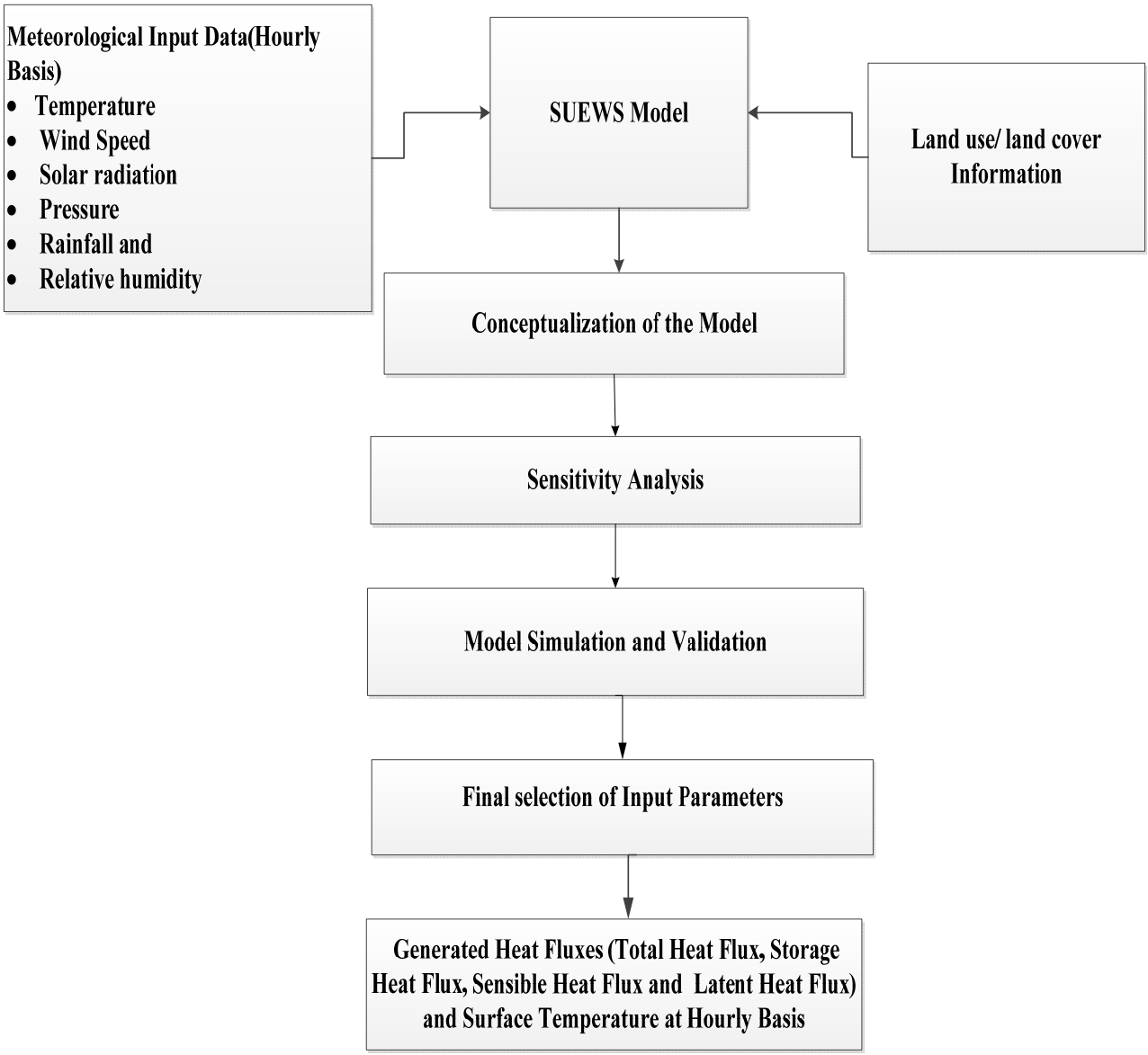

Figure 5.4 : Surface energy balance approach used in SUEWS model

5.5 SENSITIVITY ANALYSIS OF SUEWS MODEL

SUEWS sensitivity analysis is performed to check the model sensitivity with respect to different important model coefficients and parameters. Sensitivity analysis is the process of varying model input parameters over a reasonable range (range of uncertainty in values of model parameters) and observing the relative change in model response from the original inputs values. Sensitivity analysis has been performed by altering the values of selected inputs parameters up to ±40%. Sensitivity analysis has been carried out for the selected study areas using the input data of the year 1999 and 1998 for two season summer and winter. Sensitivity analysis performed for selected inputs parameters are albedo, emissivity,

drainage, maximum conductance, conductance parameters, storage capacity minimum, and storage capacity maximum.

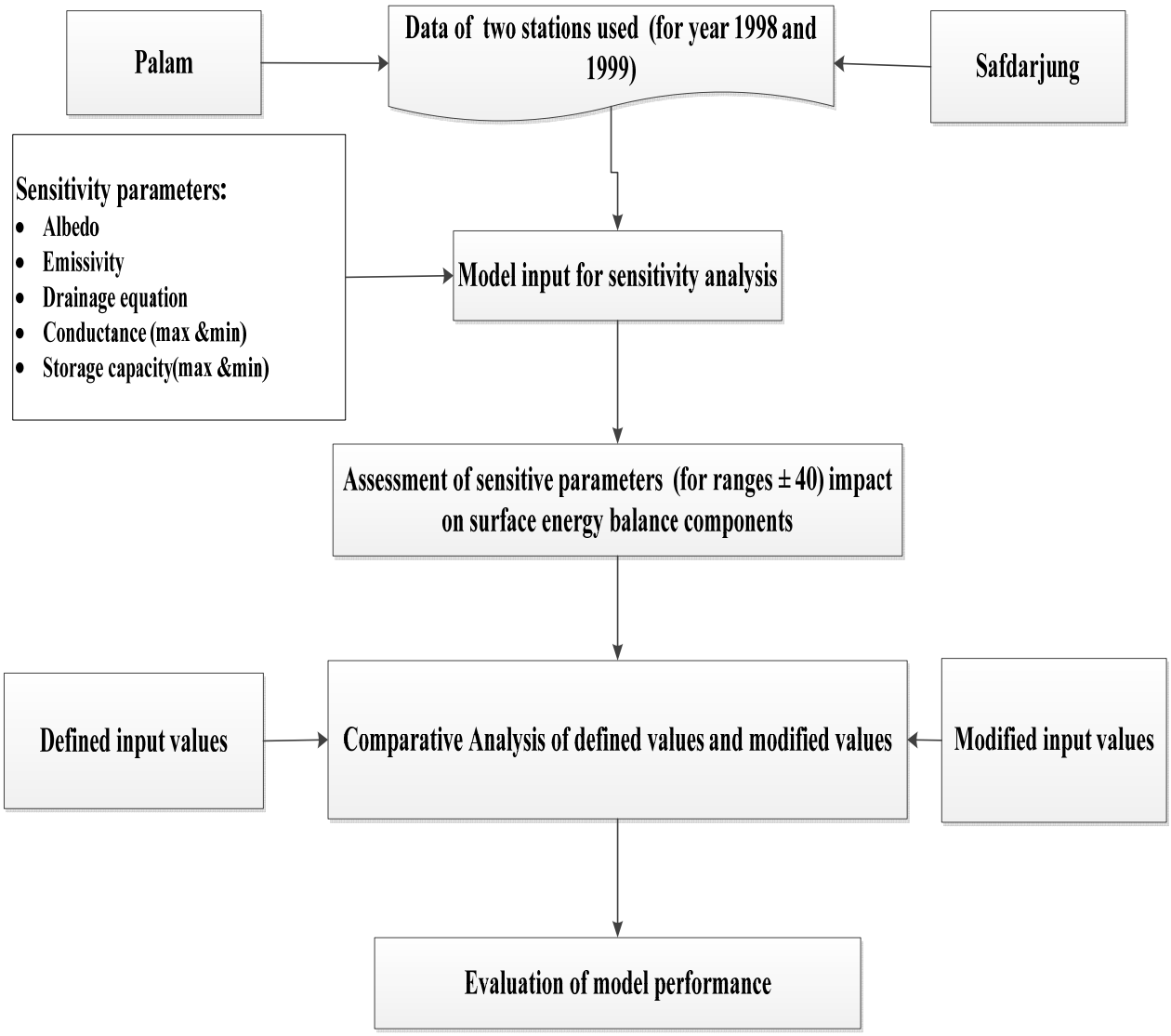

Figure 5.5 : Methodology of sensitivity analysis used for SUEWS Model

The model has been run for a number of times iteratively for a range of selected model parameters, in such a way that at a time only one parameter values are changed iteratively for a given range, keeping values of other parameters constant. Model responses to such a range of parameter are recorded to determine the relative change in model response with respect to a change in individual model input parameter selected for sensitivity analysis. Detailed results of the sensitivity analysis are presented in Chapter 7. Flow chart of the methodology adopted for the sensitivity analysis has been presented in Figure 5.5.

5.6 CALIBRATION OF MODEL

Model calibration was performed to derive important model input parameter values at which simulated SEB components will be closed to the observed SEB fluxes. Calibration has been completed through iteratively trying different values of the parameter (± 40% change in the input parameters with respect to base value) and determining the closeness of the model response with the observed data. Calibration was completed along with the sensitivity analysis. The model was run for a range of input variable values, one parameter at a time and model results were simultaneously compared with hourly observed data of net all-wave radiation and SEB fluxes for the summer season (90 days) of the year 1999. Comparison of simulated and observed SEB fluxes has been done only for summer of year 1999 for which observed data were available. Selected input values have been used in the calibration of model to determine SEB fluxes i.e., net all-wave radiation, storage heat flux, sensible heat flux and latent heat flux.

Calibrated model parameters for both the locations are those input parameters to which model has been found to be sensitive and calibrated parameter values are that values at which simulated results are closest to the corresponding observed value for the different location of Delhi.

The optimum value of an individual parameter selected for calibration has been determined after careful examination of relative variation in model results and their nearness to the observed values corresponding to the different value of that particular parameter. Final calibrated parameters of the model where model results have been found to closest with observed SEB fluxes have been presented in the Table 7.3.

5.7 VALIDATION OF MODEL

After model conceptualization and sensitivity analysis, efforts have been made to validate the results by comparing the model results corresponding to a range to model input parameters to observed data for different locations of Delhi. Validation using the observed data of heat fluxes for a different location in Delhi for the year 1998 and 1999 (summer and winter season) has been performed. Simulated energy balance components i.e., heat fluxes corresponding to different ranges of model input parameters have been compared with the observed heat fluxes for different locations in Delhi for year 1998 & 1999. The observed fluxes values have been taken from published research articles by (Goodhead, 1988; Das and Padmanabhamurty, 2009; Das et al., 2014). The observed fluxes values have been taken

from six sites in Delhi such as, Okhla (Industrial site), Connaught Place (Commercial site), Greater Kailash-II (residential site), Jawaharlal Nehru University (Rural site), Deer park, Safdarjung and Palam. Calibration is an inverse modelling problem, which involves estimation of the selected model parameter through matching of simulated and observed data of surface energy balance components. Simulated surface energy fluxes values at seasonal average, monthly average and at particular days of the season have been calculated for Palam and Safdarjung areas. Observed and simulated data have been compared to judge the closeness of simulated model results with observed fluxes during validation phase at different temporal scales. The steps involved in validation process are presented in Figure 5.6. Results of the validation have been presented in Chapter 7.

5.8 ASSESSMENT OF IMPACTS OF LULC CHANGES ON MICRO-CLIMATE

To investigate the impacts of LULC changes on the micro-climate in term of changes in surface energy balance corresponding to changes in LULC, three scenarios have been framed.

- Scenario-A: surface energy balance (annual fluxes) was simulated corresponding to actual meteorology and LULC for different years,
- Scenario-B: simulation of the surface energy balance (annual) for different years, corresponding to meteorology of the base year (1973) and LULC of respective years, and
- Scenario-C: surface energy balance (annual) was simulated for different years, corresponding to LULC of the base year (1973) and meteorology of different years.

The validated model has been used for the three scenarios as mentioned above. The model was run for different years, for three scenarios corresponding to respective input parameters. The first case was conceptualized to consider all climate change forcing (LULC and other anthropogenic forcing) while simulating the surface energy balance for different years. Results revealed the changes in surface energy fluxes over the years as a result of alterations in LULC and other climate change forcing. In Case-B, where, meteorology was kept at the base year values and results of surface energy balance were obtained corresponding to LULC of different years to ascertain the change in energy fluxes corresponding to change in LULC over the years.

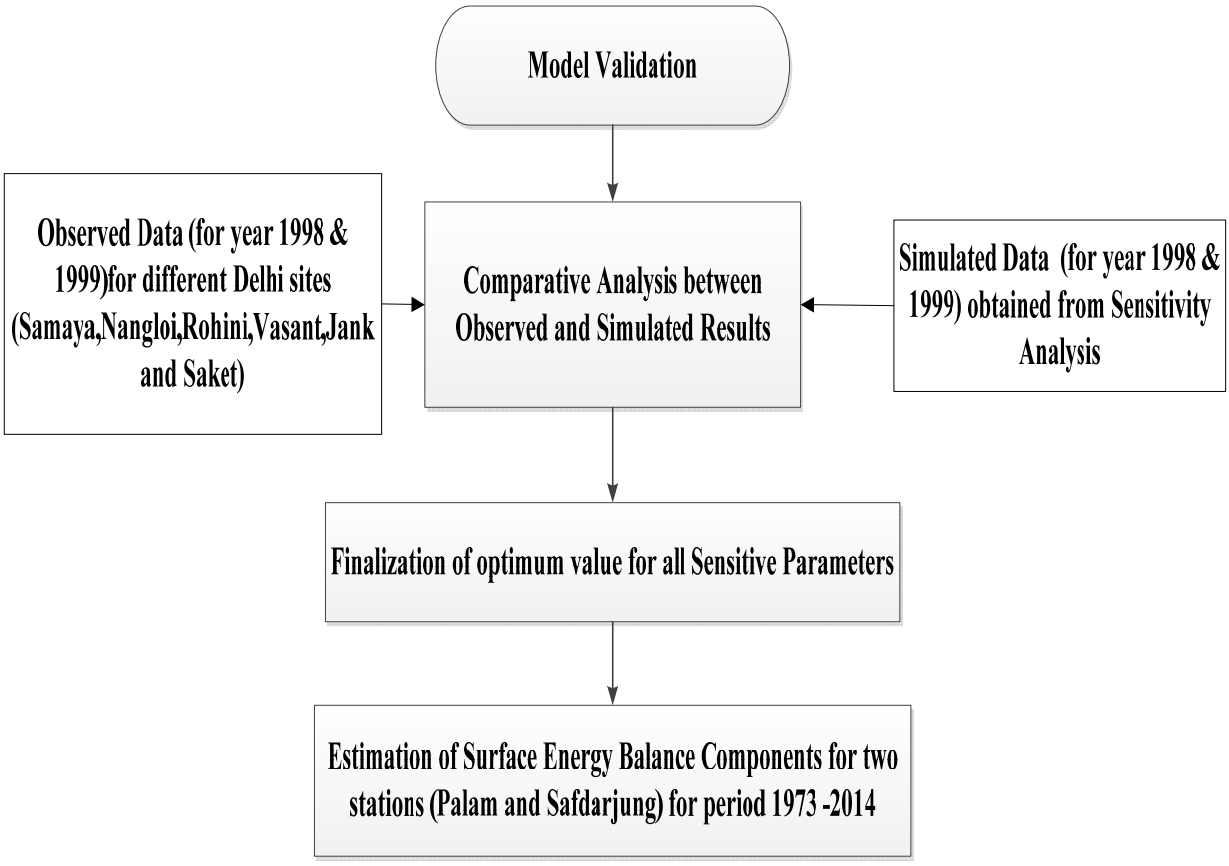

Figure 5.6 : Methodology adopted for model validation

Results of the Case-B revealed the impact of LULC change effects on surface energy balance components and surface temperature, which are indicative of change in micro-climate. In Case-C, surface energy balance was simulated considering climate change forcing other than LULC change like gaseous pollution and other anthropogenic activities. Case-C results indicate effect of other climate change factors (forcing) excluding LULC changes on surface energy balance components & surface temperature. Therefore, through comparative changes in surface energy balance components corresponding to change in LULC in Case B and C, relative contribution of LULC on change in micro-climate in term of change in surface energy fluxes and surface temperature has been ascertained.

Further, quantitative relationships have been developed between relative change in surface energy balance fluxes (% change in net & storage heat flux as compared to base year) with respect to base year (1973) and relative change in dominant LULC classes (% change in area of LULC class) through non-linear regression technique. Detailed results have been presented in Chapter 7. The workflow for the analysis has been presented in Figure 5.7.

5.9 OPTIMUM ADAPTATION MEASURES

Understanding the relationship between urbanization and micro-climate is necessary for urban environmental planning to determine effective design strategies, e.g. altering the land use regime, in order to improve urban climate. The knowledge of how to purposefully manipulate the SEB by changing urban land use and land cover is crucial to urban climate adaptation. After determining the relative effect of LULC in changing micro-climate in term of relative change in surface energy balance components, potential of different LULC related adaptation measures in limiting the adverse changes in surface energy fluxes have been explored through simulating the energy balance using calibrated SUEWS model corresponding to different possible alterations in LULC.

Although, the rather low sense of urgency regarding these two-climate change induced risks, urban planners are investing in more open water and public green areas. So far, most research has concentrated on the identification and quantification of these threats as well as the development of adaptation measures. Adaptations are explored to determine the methods by which urban climate can be pleasant for the habitants means to maintain the temperature at sustainable level. Therefore, sustainable adaptation measure is required to reduce these impacts. Analytical framework for analyzing and explaining effects in heat fluxes by transforming land use /land cover class has been explored.

Different adaptation measures in term of purposeful alterations in LULC classes like barren to forest, barren to water, building to vegetation, and all possible LULC conversions simultaneously (mixed land use) are considered as Case-1, Case-2, Case-3, and Case-4, respectively. Change in surface energy balance corresponding to above mentioned LULC adaptations have been determined by simulating the SEB using SUEWS model for proposed alterations in LULC, keeping other model parameters as constant. For each scenario, LULC values are changed in different percentages (10%, 25%, and 50%) and change in surface energy balance are quantified. Potential of proposed LULC related adaptation measures is determined by calculating the favorable changes in surface energy balance components. Further, optimum adaptation measures have been identified corresponding to highest favorable changes in SEB. The detailed description of the results are presented in Chapter 8 and methodology adopted to investigate the adaptations is presented in Figure 5.8.

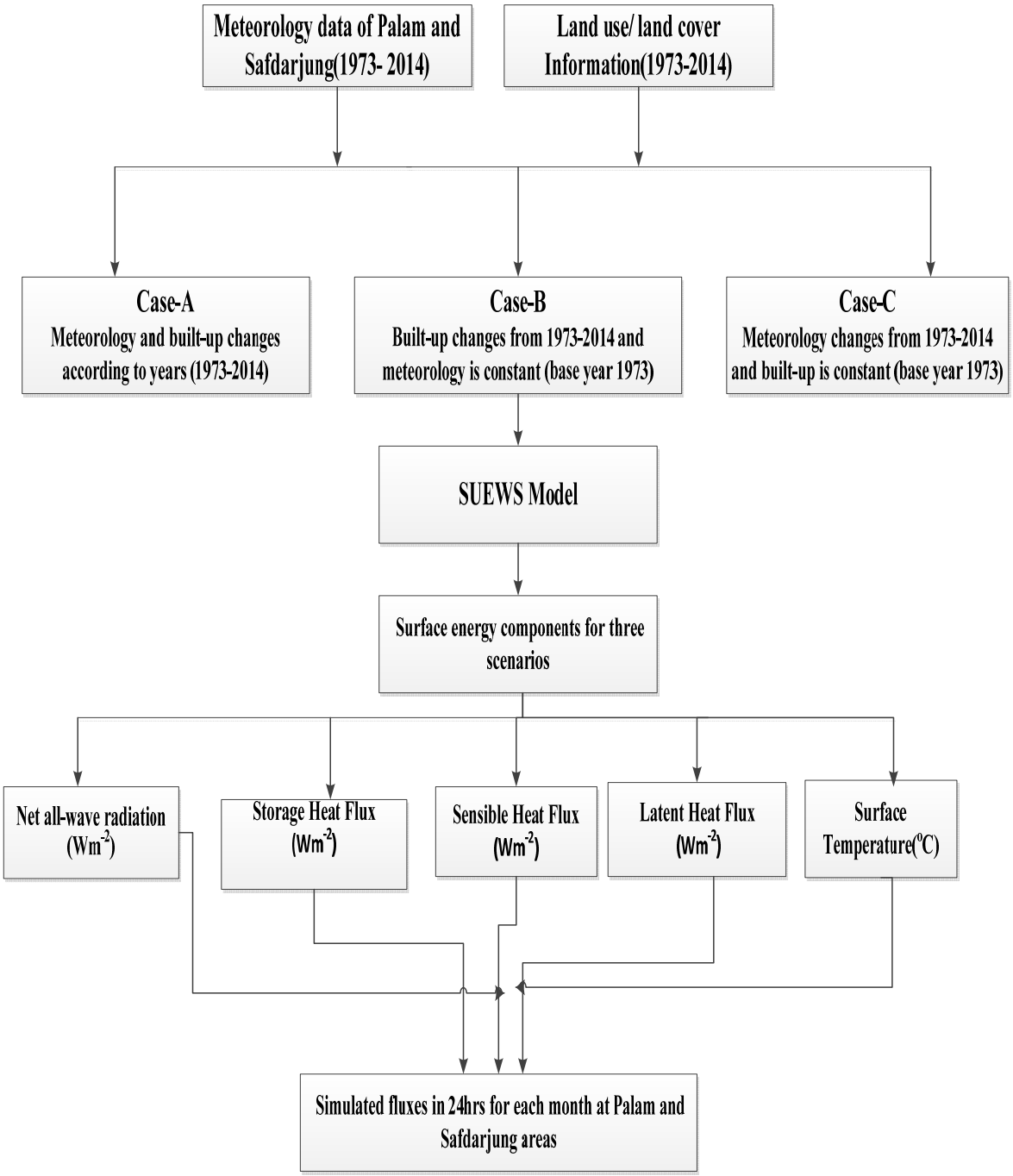

Figure 5.7 : Workflow for the simulation of surface energy fluxes for different scenarios using SUEWS model

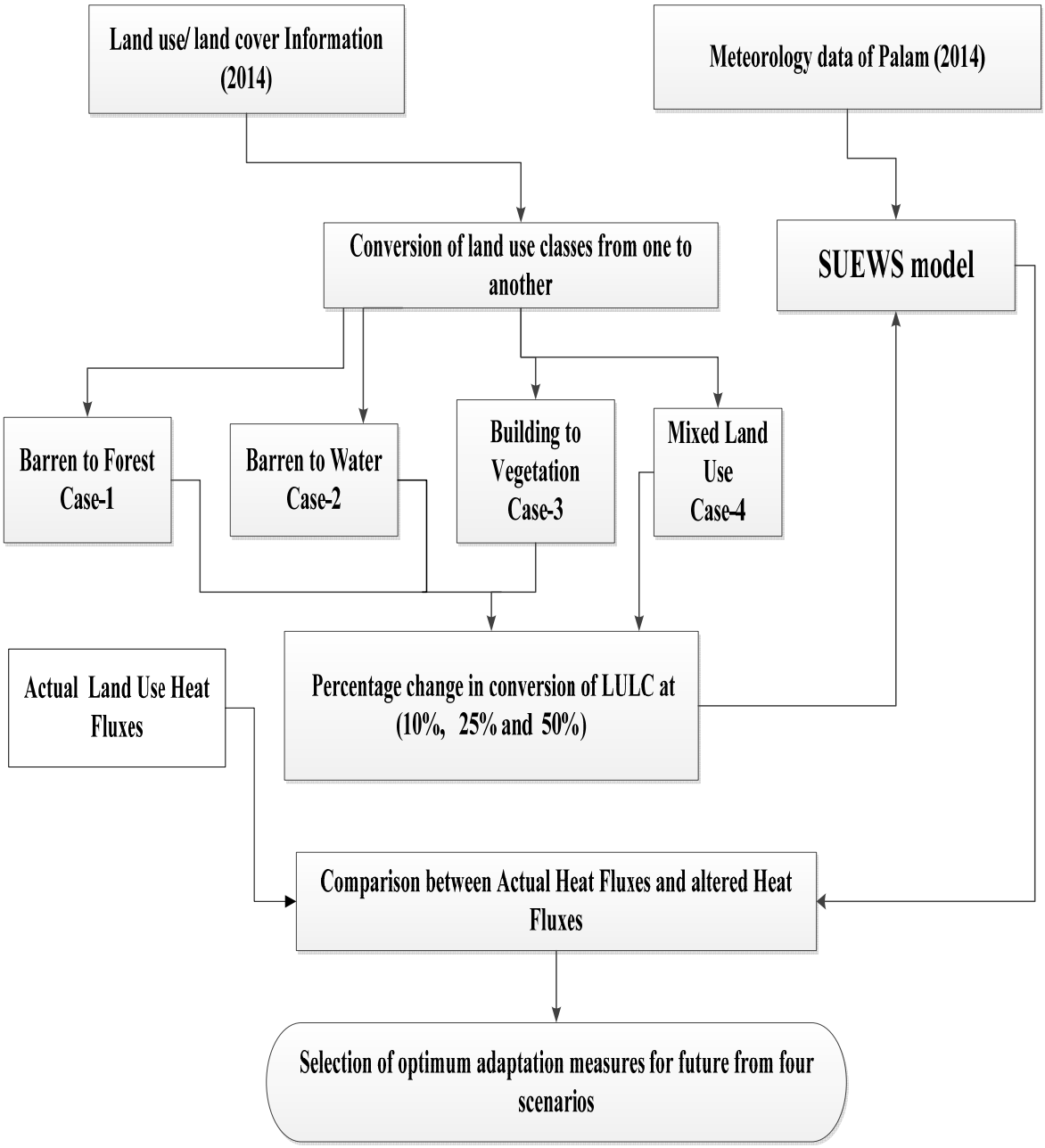

Figure 5.8 : Methodology adopted for identification of optimum adaptation measures

CHAPTER 6

CLIMATE CHANGE ASSESSMENT

6.1 INTRODUCTION

In the present study, assessment of climate change for Delhi has been carried out using trend analysis of representative climatic variables i.e., temperature and rainfall time series data. Detailed trend analysis of temperature and rainfall has been carried out for average daily, seasonal and extreme values at monthly, and annual temporal resolutions using temperature and rainfall data of 44 years (i.e., 1969–2012). Parametric and non-parametric Mann-Kendall (MK), Modified Mann-Kendall (MMK), Sen's slope estimator and Pettit-Mann-Whiteney (PMW) shift detection tests have been used for trend and shift detection analysis. Further, statistical downscaling of rainfall and temperature have been performed using SDSM model and newly developed RCP scenarios for Delhi region. Results have been discussed in detail in subsequent sections.

6.2 AVERAGE DAILY RAINFALL AT ANNUAL AND SEASONAL SCALE

The MK and MMK tests have been used for the trend analysis of average daily rainfall over 44 years. The results of these trend tests were derived at the 5% level of significance. The test statistics (S), Z_{mk} and Z_{mmk} derived for average daily rainfall at different temporal resolutions (i.e., seasonal and annual) are presented in Table 6.1 to 6.2. The positive values of Z_{mk} statistics indicate the increasing trends in climatic variables while, negative values of Z_{mk} and Z_{mmk} shows decreasing trends of climatic variables at 5% level of significance. After the MK test, the Sen's estimator of the slope was employed to find out the change per unit time of the trends observed in the time series of average daily & total rainfall. The corresponding results for Delhi region on the above-mentioned time scales are presented in Figure 6.1 & Figure 6.2 and Table 6.1 & Table 6.2, where a negative sign indicates a downward slope and a positive sign indicates an upward slope.

6.2.1 Average Daily Rainfall

Trend analysis was carried out for average daily rainfall at annual and seasonal temporal scales (i.e., winter, spring, summer, autumn, monsoon and non-monsoon).

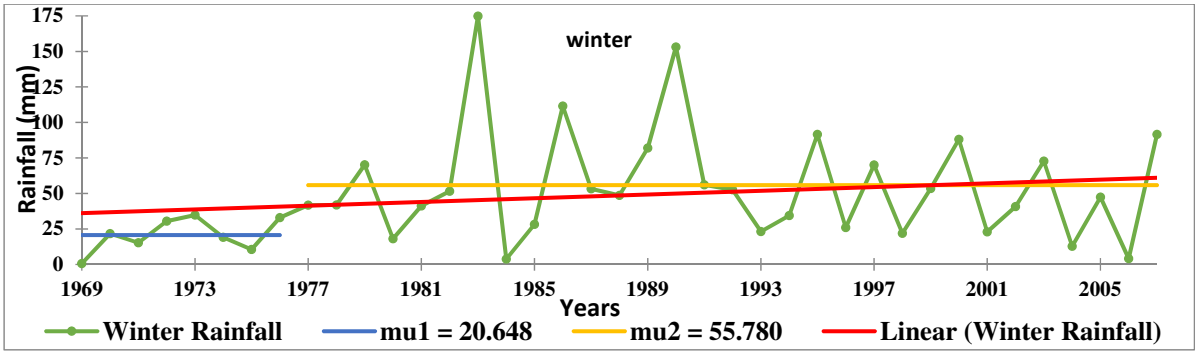

Figure 6.1 : Significant trend in winter season rainfall (mm) at daily time step for Palam

Table 6.1: Trend in mean annual and seasonal rainfall (mm) at daily time step for Palam

Variable	Mean	MK test Z_{mk}	Sen's slope p-value	% Change	MMK Test	Shift Detection Test Z_{mmk}	p-value	t	p-value
Annual	1.8	0.03	0.78	0.003	7.65	*	*	1989	0.84
Winter	48.6	*	*	0.82	66.05	2.11	0.03	1976	0.08
Spring	58.2	*	*	0.86	57.7	1.39	0.16	1981	0.17
Summer	436.5	0.07	0.66	1.73	15.49	*	*	1989	0.56
Autumn	125.4	-0.13	0.4	-1.24	-38.47	*	*	1976	0.1
Monsoon	529.4	0.1	0.5	2.82	20.77	*	*	1989	0.56
Non-monsoon	110.5	0.24	0.128	1.43	50.56	*	*	1981	0.04

Table 6.2 : Trend in mean annual and seasonal rainfall (mm) at daily time step for Safdarjung

Variable	Mean	MK test	Sen's slope (mm/year)	% Change		MMK test		Shift Detection Test	
		Z_{mk}	p-value			Z_{mk}	p-value	t	p-value
Annual	1.85	0.05	0.627	0.003	7.45	*	*	1989	0.6
Winter	57.4	0.15	0.148	0.58	44.46	*	*	1985	0.22
Spring	83.6	*	*	2.02	106.26	3.5	0.0001	1995	0.002
Summer	443.7	0.11	0.297	2.36	23.41	*	*	1989	0.47
Autumn	99.6	*	*	-3.31	-46.08	-3.7	0.001	1991	0.001
Monsoon	513.4	-0.01	0.927	-0.12	-1.06	*	*	1998	0.51
Non-monsoon	170.8	0.14	0.160	1.43	36.72	*	*	1996	0.14

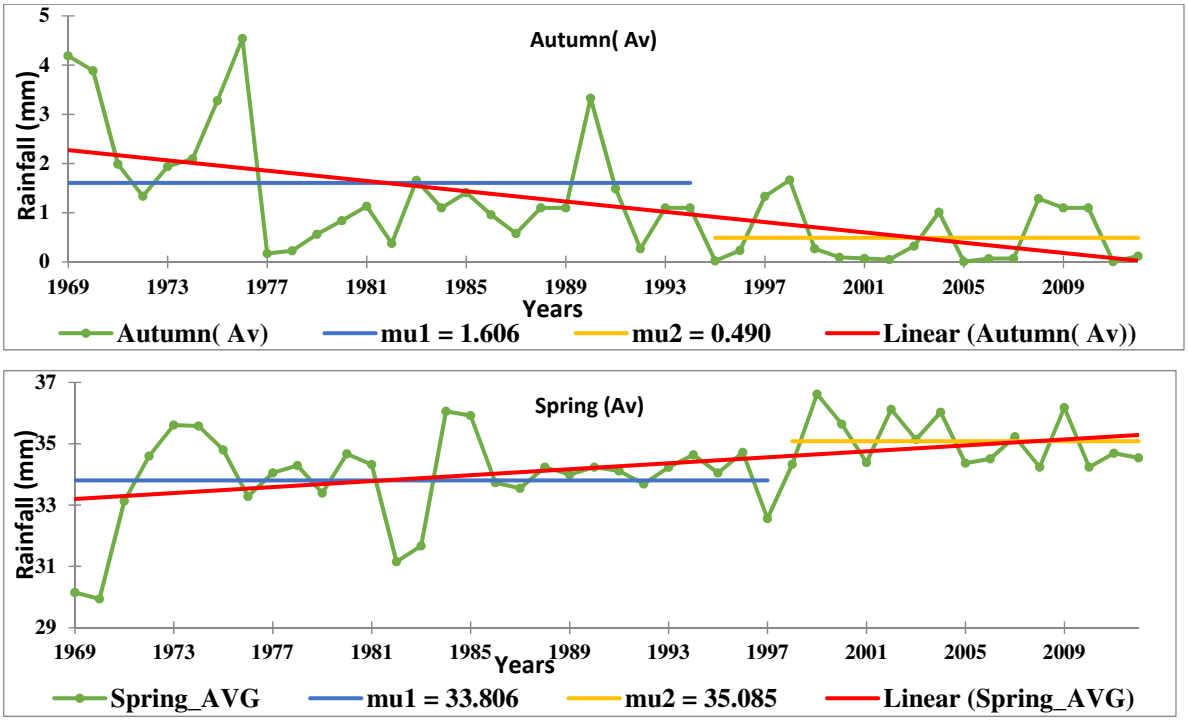

Figure 6.2 : Significant trend in seasonal (autumn and spring) rainfall (mm) at daily time step for Safdarjung

Significant increasing trends have been observed in winter and spring season average daily rainfall for Delhi region in last 44 years with Z_{mmk} = 2.11 & 3.5 at 95% significance level (Table 6.1 & 6.2 and Figure 6.1 & 6.2).

But the significant decreasing trend in autumn season average daily rainfall has been found at 95% significance level for Safdarjung (Table 6.2 and Figure 6.2). Sen's slope magnitude also indicates significant increasing/decreasing trend in average daily rainfall at winter, spring, and autumn season (0.82, 2.02 and -3.31mm/year), respectively (Figure 6.1 and Figure 6.2). Similarly, the change in percentage has been found to be 66.05%, 106.26% and -146.08% over a period of time. The PMW test was used to calculate the shift in average daily rainfall trend. A clear shift has been observed in the years 1995, 1991 and 1981for spring, autumn and non-monsoon season, respectively (Table 6.2 and Figure 6.2). Land use changes affect several atmospheric properties and processes such as boundary layer dynamics convection mesoscale circulations, cloud properties, and precipitation. A significant impact of urbanization on the spatiotemporal patterns of precipitation was also highlighted in the literature (Marshall, 2004). It can be concluded that significant increasing and decreasing trends have been observed in average daily rainfall at winter, spring and autumn seasonal scales. However, increasing and decreasing trend (but not statistically significant at 95% confidence level) in average daily rainfall at remaining temporal scales

has been observed over last 44 years. Therefore, it can be concluded that climate change is happening in Delhi. A similar study on analysis of rainfall during different seasons indicated decreasing tendency in the summer monsoon rainfall over the Indian landmass and increasing trend in the rainfall during pre-monsoon and post-monsoon months and also found decreasing trend in monsoon rainfall over northwest and central India during 1941–2002 (Kothawale et al., 2010).

6.2.2 Average Daily Temperature

The MK and MMK tests have been used for the trend analysis of average daily maximum and minimum temperature over 44 years. The results of these trend tests were derived at the 5% level of significance. The test statistics (S), $Z_{mk,}$ and Z_{mmk} derived for average daily maximum & minimum temperature at different temporal resolutions i.e., seasonal (winter, spring, summer, autumn and annual) are presented in Table 6.3 to 6.6. The positive values of Z_{mk} and Z_{mmk} statistics indicate the increasing trends in temperature while, negative values of Z_{mk} and Z_{mmk} shows decreasing trends at the significant and non-significant level. After the MK test, the Sen's estimator of the slope was employed to find out the change per unit time for the trends observed in the time series of average daily maximum & minimum temperature. The corresponding results for Delhi on the above mentioned time scales are presented in Figure 6.3 to Figure 6.6 and Table 6.3 to Table 6.6, where a negative sign indicates a downward slope and a positive sign indicates an upward slope.

6.2.3 Minimum Average Daily Temperature

Trend analysis was carried out for the average daily minimum temperature at annual and seasonal temporal scales (i.e. winter, spring, summer, autumn, monsoon and non-monsoon). Significant increasing trends have been observed in average daily temperature at these time scales for Delhi region in last 44 years with Z_{mmk}= 2.69, 3.67, 5.24, 2.72, 3.13 at 95% significance level (Table 6.3 & Figure 6.3). But statistically significant decreasing trend found at the autumn season with Z_{mmk} = -6.73 at 95% significance level in minimum temperature data series at Palam (Table 6.3 & Figure 6.3). Similarly, statistically significant increasing trends in minimum average daily temperature has been observed at annual, spring, summer, monsoon and non-monsoon season for Safdarjung in Delhi region with Z_{mmk} = 2.94, 2.68, 5.58, 3.03, 2.42 at 95% significance level (Table 6.4 and Figure 6.4) .

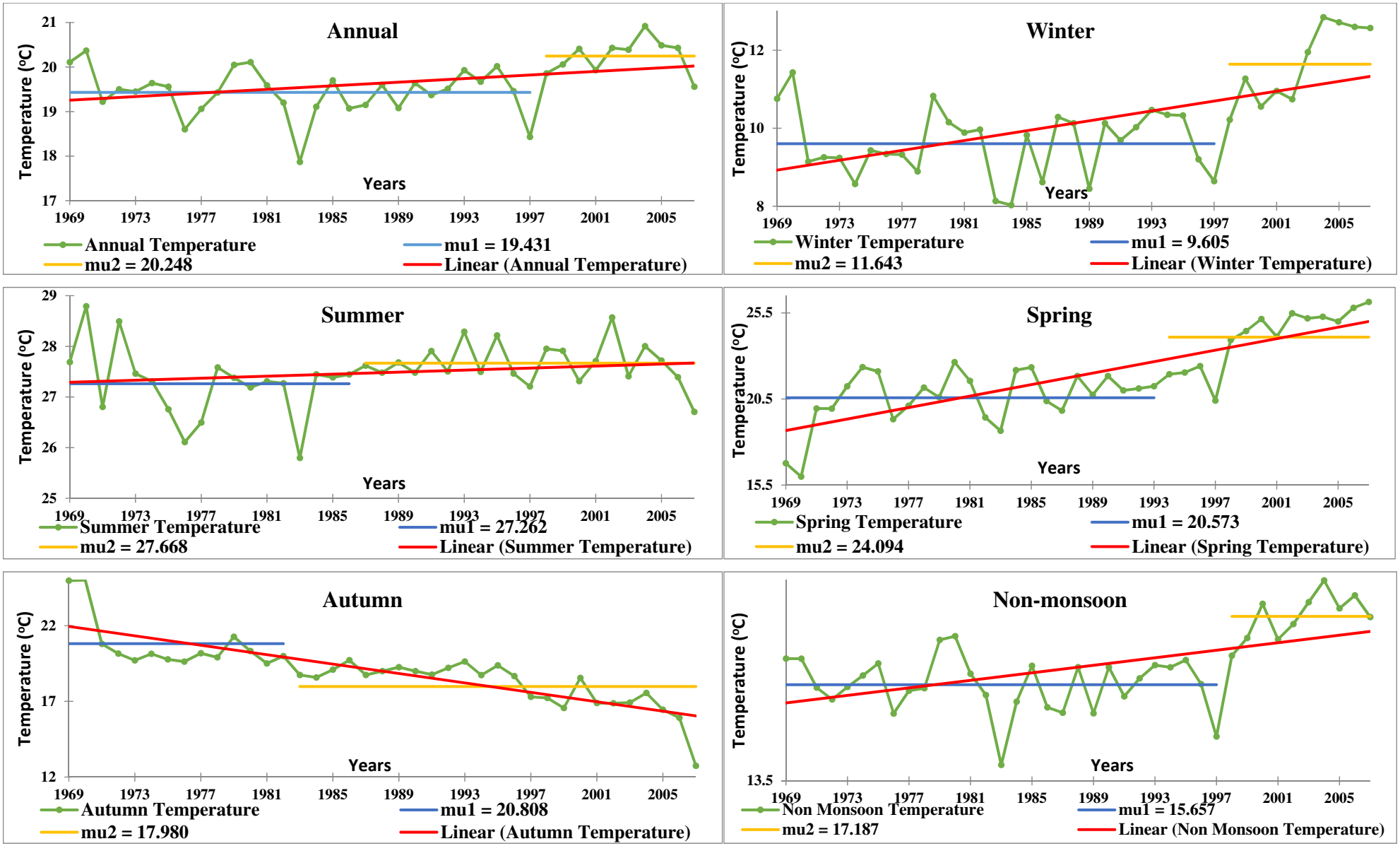

Figure 6.3 : Significant trend in mean, annual and seasonal minimum temperature (°C) at daily time step for Palam

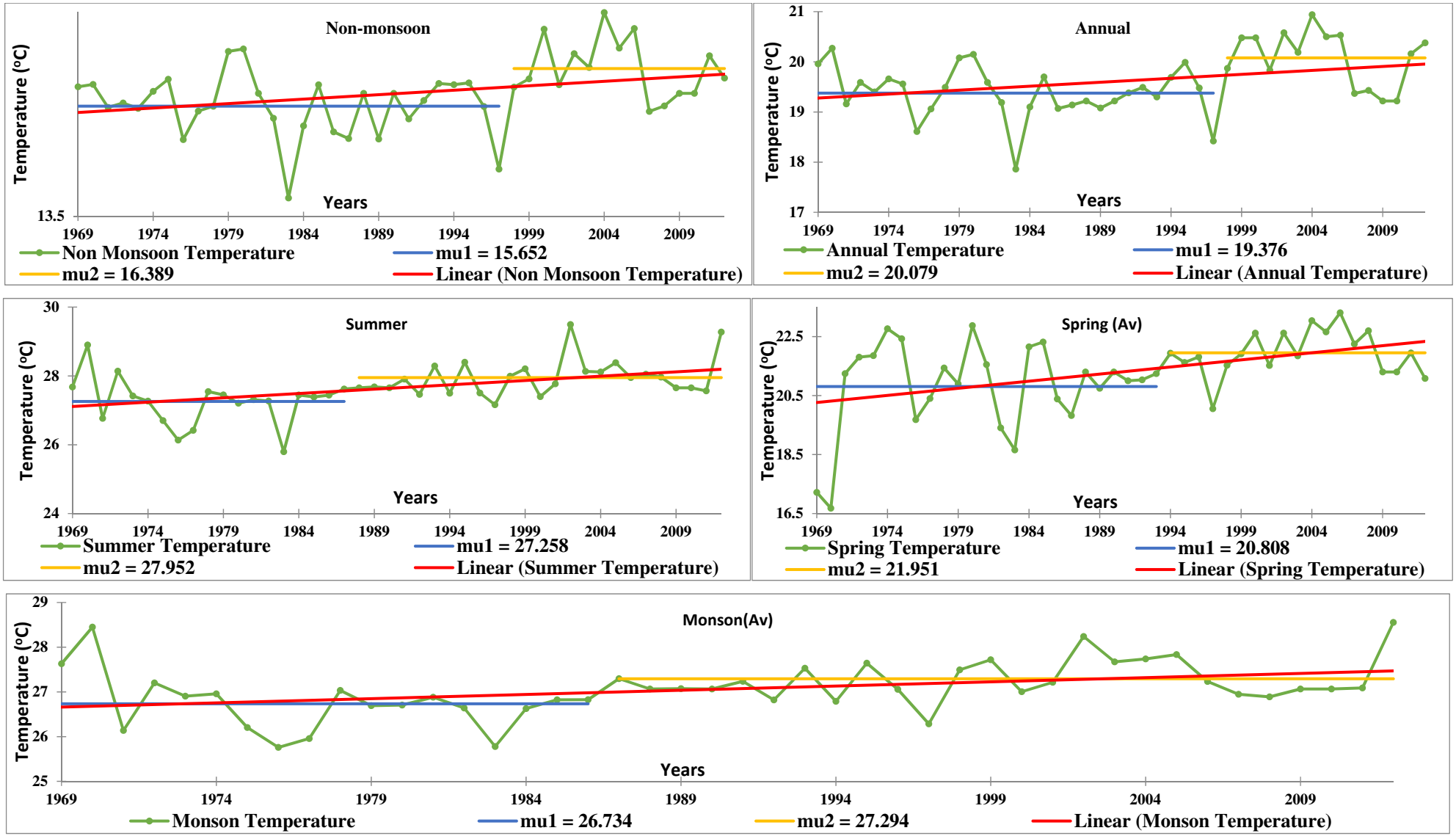

Figure 6.4 : Significant trend in mean, annual and seasonal minimum temperature (°C) at daily time step for Safdarjung

Table 6.3 : Trend in mean annual and seasonal minimum temperature (°C) at daily time step for Palam

Variable	Mean	MK test		Sen's slope (°C/year)	% Change	MMK test		Shift detection Test	
		Z_{mk}	p-value			Z_{mmk}	p-value	t	p-value
Annual	19.64	*	*	0.022	4.37	2.698	0.007	1997	0.001
Winter	10.1	*	*	0.06	23.11	3.67	0.0001	1997	0.0001
Spring	21.8	*	*	0.172	30.72	5.24	0.0001	1993	0.0001
Summer	27.5	*	*	0.01	1.56	2.72	0.01	1986	0.027
Autumn	19.0	*	*	-0.125	-25.66	-6.73	0.0001	1982	0.0001
Monsoon	26.7	-0.18	0.097	-0.013	-1.90	*	*	1996	0.169
Non-monsoon	16.0	*	*	0.041	9.96	3.13	0.0017	1997	0.0001

Table 6.4 : Trend in mean annual and seasonal minimum temperature (°C) at daily time step for Safdarjung

Variable	Mean	MK test Z_{mk}	Sen's slope (°C/year) p-value	% Change	MMK test	Shift Detection Test Z_{mk}	p-value	t	p-value
Annual	19.61	*	*	0.015	3.40	2.94	0.003	1997	0.005
Winter	9.74	*	*	0.015	6.62	1.57	0.117	1991	0.120
Spring	21.30	*	*	0.039	7.97	2.68	0.007	1993	0.015
Summer	27.65	*	*	0.023	3.74	5.58	0.0001	1987	0.0001
Autumn	19.80	0.08	0.42	0.01	2.27	*	*	1997	0.100
Monsoon	27.06	*	*	0.019	3.13	3.03	0.002	1986	0.001
Non-monsoon	15.90	*	*	0.016	4.46	2.42	0.016	1997	0.007

Sen's slope magnitude also indicates significant increasing and decreasing trend in average daily minimum temperature for Palam and Safdarjung (0.022, 0.060, 0.172, 0.01, -0.125, and 0.041°C/year) & (0.015, 0.039, 0.023, 0.019 and 0.016°C/year, respectively) (Figure 6.3 and Figure 6.4). Similarly, the percentage change has been found to be 4.37, 23.11, 30.72, 1, 56, -25.66, 9.96 & 3.40, 7.97, 3.74, 3.13, 4.46, respectively. PMW test was used to calculate the shift in average daily minimum temperature trend. A clear shift in trend has been observed in the years 1997, 1997, 1993, 1986, 1982 and 1997 in annual, winter, spring, summer, autumn, and non-monsoon season, respectively (Table 6.3 and Figure 6.3).

Similarly, in minimum average daily temperature at Safdarjung station shift has been found in the years 1997, 1993, 1987, 1986 and 1997 for annual, spring, summer, monsoon, non-monsoon, respectively (Table 6.4 and Figure 6.4). Several studies were undertaken to analyze the trends in long term temperature, its inter-annual, seasonal and decadal variability at different spatial scales such as local, regional, national and continental scales (Lu et al., 2003; Gadgil and Dhorde, 2005; Tomozeiu et al., 2007; Kothawale et al., 2010).

6.2.4 Maximum Average Daily Temperature

Trend analysis was carried out for the average daily maximum temperature at annual and seasonal temporal scales (i.e. winter, spring, summer, autumn, monsoon and non-monsoon). Significant increasing trends have been observed in average daily temperature at spring, non-monsoon scales for Delhi region with Z_{mmk}= 4.11, 3.41 at 95% significance level (Table 6.5 & Figure 6.5). But the statistically significant decreasing trend in maximum temperature was found at autumn scale with Z_{mmk} = -4.54 at 95% significance level in Palam (Table 6.5 and Figure 6.5). Similarly, statistically significant increasing trends have been observed in spring season average daily maximum temperature at Safdarjung in Delhi region over a period of 46 years with Z_{mmk}= 2.73 at 95% significance level (Table 6.6 and Figure 6.6), respectively. Sen's slope magnitude also indicates significant increasing and decreasing trend in average daily maximum temperature for Palam and Safdarjung (0.134, -0.093, 0.027°C/year) and (0.03°C/year), respectively (Figure 6.5 and Figure 6.6). Similarly, the change in percentage has been found to be 18.28%, -11.87%, 3.03% and 4.30%, respectively. PMW test was used to calculate the shift in average daily maximum temperature trend.

Table 6.5 : Trend in mean annual and seasonal maximum temperature (°C) at daily time step for Palam

Variable	Mean	MK test		Sen's slope (°C/year)	% Change	MMK test		Shift Detection Test	
		Z_{mk}	p-value			Z_{mmk}	p-value	t	p-value
Annual	30.62	0.15	0.17	0.011	1.35	*	*	1983	0.150
Winter	22.16	*	*	0.025	4.42	1.50	0.13	1998	0.08
Spring	28.56	*	*	0.134	18.28	4.11	0.001	1997	0.001
Summer	35.11	-0.19	0.08	-0.024	-2.69	*	*	1995	0.03
Autumn	30.42	*	*	-0.093	-11.87	-4.54	0.001	1995	0.001
Monsoon	34.63	*	*	-0.027	-3.05	-1.85	0.06	1995	0.04
Non-monsoon	34.61	*	*	0.027	3.03	3.41	0.001	1998	0.001

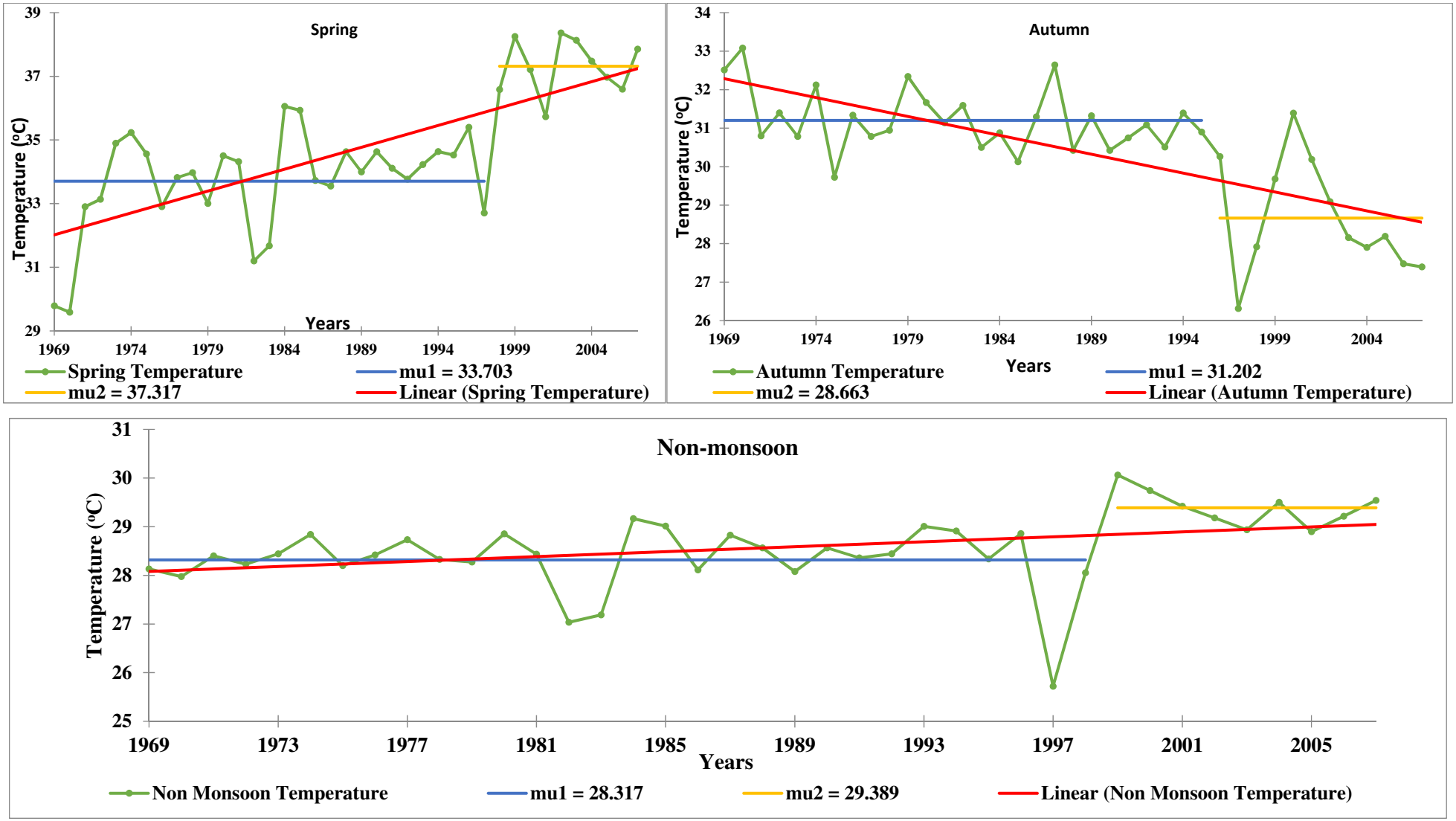

Figure 6.5 : Significant trend in mean, annual and seasonal maximum temperature (°C) at daily time step for Palam

Table 6.6 : Trend in mean annual and seasonal maximum temperature (°C) at daily time step for Safdarjung

Variable	Mean	MK test		Sen's slope (°C/year)	% Change	MMK test		Shift Detection Test	
		Z_{mk}	p-value			Z_{mmk}	p-value	t	p-value
Annual	30.62	0.15	0.145	0.008	1.20	*	*	1998	0.138
Winter	21.83	*	*	-0.008	1.68	-0.39	0.69	1971	0.66
Spring	34.24	0.29	0.05	0.03	4.30	2.73	0.01	1997	0.0001
Summer	35.35	0.10	0.3	0.013	1.56	*	*	1978	0.48
Autumn	30.96	-0.12	0.237	-0.012	-1.70	*	*	2001	0.34
Monsoon	34.84	0.09	0.407	0.009	1.13	*	*	1978	0.59
Non-monsoon	28.47	0.18	0.084	0.009	1.37	*	*	1998	0.10

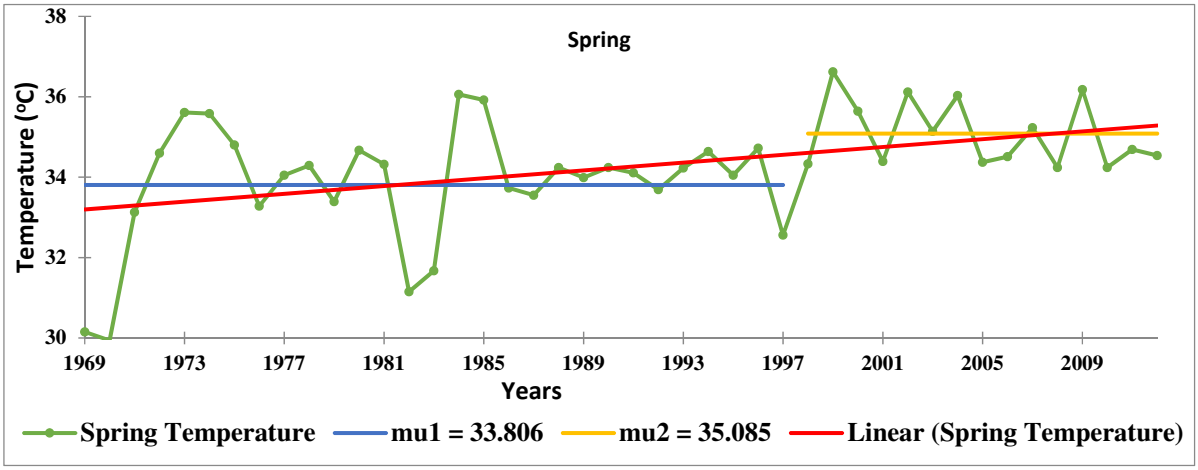

Figure 6.6 : Significant trend in mean, annual and seasonal maximum temperature (°C) at daily time step for Safdarjung

A clear shift in trend has been observed in the years 1997, 1995, 1995, 1995, 1998 during spring, summer, autumn, monsoon and non-monsoon season, respectively (Table 6.5 and Figure 6.5). Similarly, spring season maximum temperature has shown a shift in the years 1997 at Safdarjung (Table 6.6 and Figure 6.6).

6.2.5 Extreme Daily Maximum and Minimum Temperature at Annual Scale

Trend analysis has been carried out for the annual extreme daily maximum and minimum temperature which shows non-significant increasing trend at 95% significance level (Table 6.7 and Figure 6.7) in Palam. Similarly, Safdarjung station has shown statistically non-

significant trend at 95% significance level (Table 6.8 and Figure 6.8). The Sen's slope results also indicate increasing trends for extreme daily maximum and minimum temperature for Palam and Safdarjung (0.03 & 0.02°C/year and 0.025 & 0.012 °C/year) (Table 6.7 and Figure 6.7) (Table 6.8 and Figure 6.8), respectively. Similarly, the change in percentage has been found to 2.98% & 19.9% and 2.5% & 11.58%. Shift in trend by PMW test has been observed in years (1991 & 1978) at both stations, respectively (Table 6.7 and Table 6.8).

The extreme daily minimum and maximum temperatures have been found to 2.0°C and 45.1°C, respectively. The results clearly indicate the warming trends in the extreme annual minimum daily temperature in Delhi, which indicates attribution of anthropogenic influence on climate. This may be due to several natural and anthropogenic activities such as land use/land cover, urbanization and industrialization (Chase et al., 2000; Feddema, 2005; Christy et al., 2006; Wichansky et al., 2006; Betts et al., 2007; Nayak and Mandal, 2012). Various anthropogenic activities like the conversion of pervious areas into impervious results in significant increase in extreme daily minimum temperature (Arora and Boer, 2010; Kothawale et al., 2010; Kumar et al., 2010; Pal and Al-Tabbaa, 2011a; b, Subash et al., 2011a; b). Long wave radiations emanated from hard surfaces during night time leads to increase in minimum temperature (Das and Padmanabhamurty, 2008). Results indicate a change in minimum and maximum temperature in Delhi over last 44 years. Urban areas (comprising of Industrial, Commercial and Residential sites) with concrete, asphalt and paved surfaces show higher values of storage heat flux due to high heat capacity, thermal conductivity and surface temperature as compared to their rural counterparts (Das and Padmanabhamurty, 2009).

6.2.6 Extreme Daily Maximum and Minimum Temperature at Monthly Scale

Trend analysis has been done at monthly scale to ascertain the possible climate change. The MK and MMK analysis techniques have been used to find the trend in maximum and daily minimum temperature at monthly scale for Palam and Safdarjung (Table 6.9 to Table 6.12 and Figure 6.9 (a, b) to Figure 6.12 (a, b)). It is interesting to note that significant increasing trends are observed for daily maximum temperature in Palam and Safdarjung for 4 months i.e., in February, March April, and May over the 44 year with Z_{mmk} = 4.20, 3.60, 3.64 and 3.48 & for 2 months i.e., April, and May with Z_{mmk} = 2.4, 2.71. Trends have been found to be statistically significant at 95% confidence level. The Sen's slopes reveal increasing trend in daily maximum temperature for the respective months (Table 6.9 & Table 6.11).

A significant decreasing trend has been observed in daily maximum temperature in Palam station for 5 months (i.e. June, July, October, November and December) with Z_{mk} and Z_{mmk} = -3.12, -0.26, -4.02, -3.74 and -3.36. However, this trend is found to be statistically significant at 95% confidence level. The Sen's slope (-0.08, -0.08, -0.09, -0.13 and -0.10°C/month) and percentage change (-7.12, -8.41, -10.50, -15.83 and -14.95%) also indicates decreasing trend in daily maximum temperature in these months. PMW test was applied to detect the shift in the daily maximum trend at monthly scale. Significant shift has been observed in daily maximum temperature for different months (Figure 6.9 (a, b)).

Table 6.7 : Trend in extreme annual (Tmax and Tmin) (°C) at daily time step for Palam

Variable	Mean	MK test		Sen's slope	% Change	MMK Test		Shift Detection Test	
		Z_{mk}	p-value			Z_{mmk}	p-value	t	p-value
Ext. Annual Max.	43.6	*	*	0.025	2.5	1.7	0.1	1991	0.1
Ext. Annual Min	4.4	*	*	0.012	11.58	0.89	0.37	1978	0.3

Table 6.8 : Trend in extreme annual (Tmax and Tmin) (°C) at daily time step for Safdarjung

Variable	Mean	MK test		Sen's slope	% Change	MMK test		Shift Detection test	
		Z_{mk}	p-value			Z_{mmk}	p-value	t	p-value
Ext. Annual Max.	43.56	0.20	0.075	0.03	2.98	1.8	0.1	1991	0.05
Ext. Annual Min	4.3	0.147	0.199	0.02	19.9	*	*	1978	0.197

Similarly, in both Palam and Safdarjung increasing trend have been observed in daily minimum temperature for most of the months except (August, September, October, November and December) & (September and December) (Table 6.10. & Table 6.12 and Figure 6.10 (a), (b) and (c) & Figure 6.12 (a), (b)). The statistically significant increasing trend in extreme daily minimum temperature has been found in the months of January to July & February, March and June months at 95% confidence interval, respectively (Table 6.10 & Table 6.12 and Figure 6.10 (a, b, c) & Figure 6.12 (a,b)).

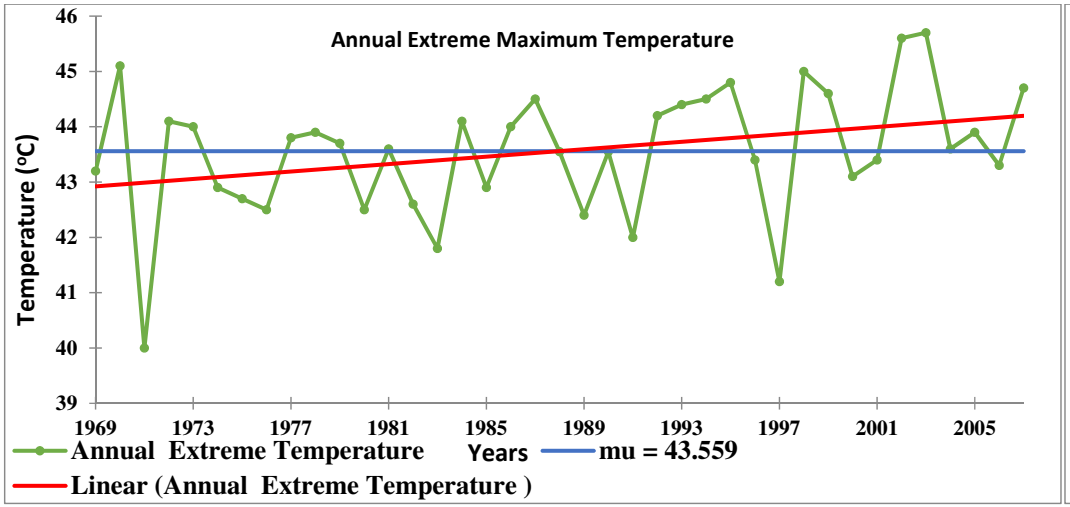

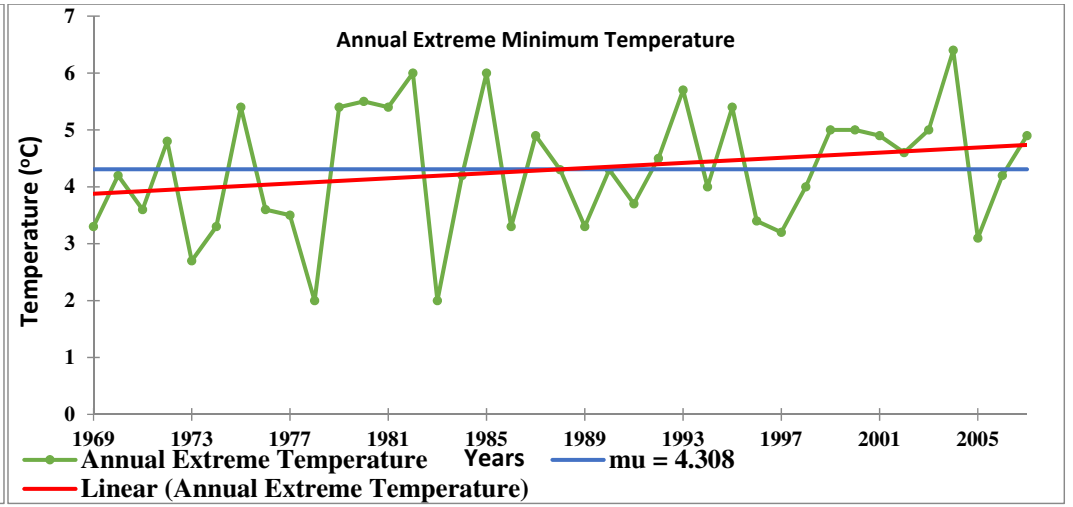

Figure 6.7 : Trend in extreme annual (Tmax and Tmin) temperature (°C) at daily time step for Palam

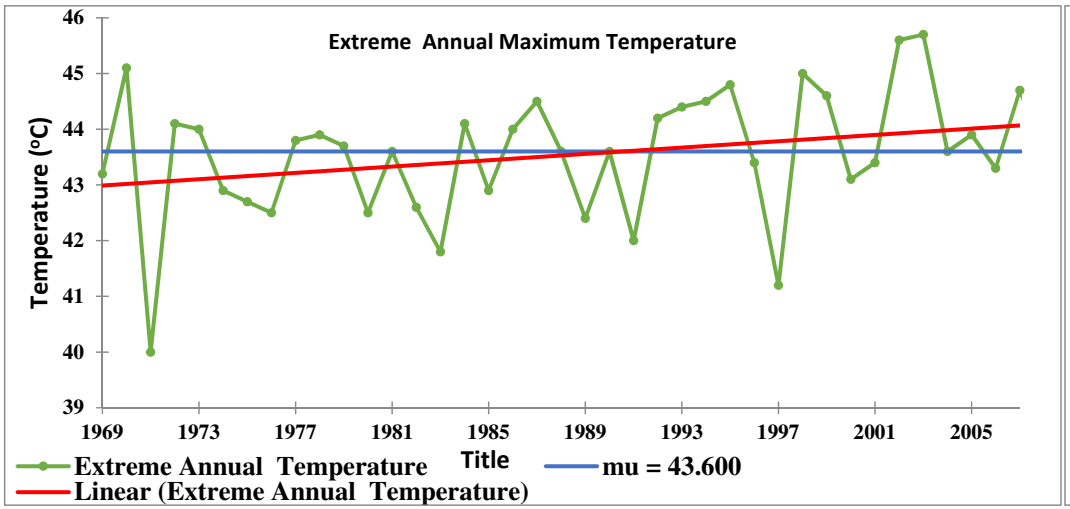

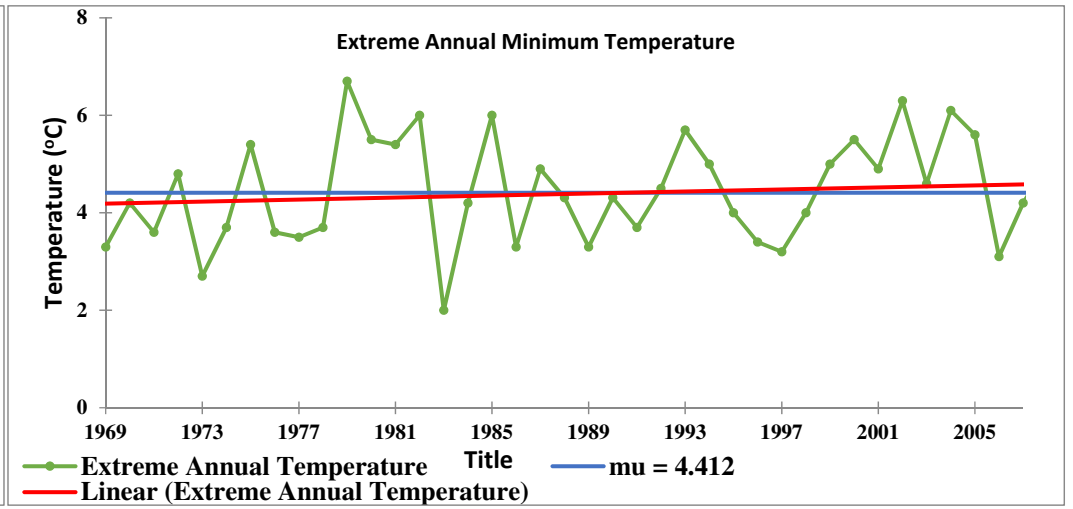

Figure 6.8 : Trend in extreme annual (Tmax and Tmin) temperature (°C) at daily time step for Safdarjung

Significant decreasing trend has been observed in Palam time series data for daily extreme minimum temperature in the months of September to December, respectively (Table 6.10 and Figure 6.10 (a), (b) and (c)). The Sen's slope (-0.13, -0.20, -0.14 and -0.08°C/month, respectively) and percentage change (-23.73, -55.67, -57.97 and -50.21) results also confirms the similar trends. Similarly, PMW test was used to detect the shift in trend in extreme daily minimum temperature over 44 years in Delhi (Figure 6.10 (a), (b), (c) and Table 6.12 (a), (b)). Decreasing trend but not statistically significant for Safdarjung time series data has been observed in daily extreme minimum temperature for September, November and December (Table 6.12). The Sen's slope and percentage change results also confirm the similar trends. Trend analysis results at different temporal scales indicate that climate change is happening in Delhi. Significant increasing trends in average daily minimum temperature has been found which indicates warmer nights (Dash and Hunt, 2007; Kothawale et al., 2010; Jain and Kumar, 2012). Similar, increasing trends have been observed at annual and seasonal temporal scales. Increasing trends have been observed in average daily maximum temperature, however, not statistically significant. Increase in night time temperature indicates warming due to a possible change in land use/land cover (LULC) in last 44 years. This study is successful in demonstrating the use of trend analysis techniques for climate change assessment at the local scale.

6.2.7 Annual Extreme Daily Rainfall

Trend analysis has been carried out for the extreme daily maximum rainfall at annual scale shows increasing trend over the 44 year period but not statistically significant 95% significance level (Table 6.13) in Palam and Safdarjung station. The Sen’s slope results also indicate increasing trend over 44 years for extreme daily maximum rainfall for Palam & Safdarjung (0.34 & 0.162 mm/year) (Table 6.13 and Figure 6.13). Similarly, the change in percentage has been found to 15.2 & 7.98 over a period of time. Both stations, shift in trend has been observed in the year 1980.

6.2.8 Monthly Extreme Daily Maximum Rainfall

The trend analysis has been done at monthly temporal scale to ascertain the possible climate change. The MK and MMK trend analysis techniques have been used to find the trend in daily maximum rainfall at monthly temporal scale for Palam and Safdarjung stations. The results are presented in Table 6.14 & Table 6.15 and shown in Figure 6.14 & Figure 6.15. It is interesting to note that significant increasing trends are observed for the daily

maximum in Palam and Safdarjung for May and June month over the 44 year with Z_{mmk} = 2.27 and 3.58 & in April, May, June and December with Z_{mk} and Z_{mmk} = 0.21, 3.1, 3.0 and 0.23. Trends have been found to be statistically significant at 95% confidence level. The Sen's slope and percentage change indicating an increase in trend for extreme daily maximum rainfall in these months (Table 6.14 & Table 6.15).

Table 6.9 : Trend in extreme monthly daily maximum temperature (°C) for Palam

Variable	Mean	MK test		Sen's slope (°C/year)	% Change	MMK Test		Shift Detection Test	
		Zmk	p-value			Zmmk	p-value	t	p-value
January	25.9	*	*	0.06	9.03	1.75	0.1	1989	0.006
February	29.8	*	*	0.19	24.62	4.20	0.001	1996	0.0001
March	35.7	*	*	0.18	20.02	3.60	0.001	1997	0.0001
April	40.9	*	*	0.10	9.53	3.64	0.001	1997	0.0001
May	42.7	*	*	0.06	5.76	3.48	0.001	1992	0.001
June	42.2	*	*	-0.08	-7.12	-3.12	0.00	1995	0.0001
July	38.9	-0.26	0.02	-0.08	-8.41	*	*	1993	0.095
August	36.8	0.019	0.875	0.003	0.32	*	*	1983	0.802
September	36.3	0.042	0.716	0.007	0.75	*	*	1978	0.468
October	34.9	*	*	-0.09	-10.50	-4.02	0.000	1992	0.002
November	30.8	*	*	-0.13	-15.83	-3.74	0.000	1993	0.001
December	26.1	*	*	-0.10	-14.95	-3.36	0.001	1995	0.002

Table 6.10 : Trend in extreme monthly daily maximum temperature (°C) for Safdarjung

Variable	Mean	MK test		Sen's slope (°C/year)	% Change	MMK test		Shift Detection Test	
		Z_{mk}	p-value			Z_{mmk}	p-value	t	p-value
January	5.09	*	*	0.058	44.68	2.8	0.01	1998	0.03
February	7.63	*	*	0.16	82.80	5.7	0.00	1989	0.001
March	11.87	*	*	0.24	78.05	5.6	0.00	1984	0.001
April	17.30	*	*	0.15	34.31	3.3	0.00	1997	0.001
May	21.21	*	*	0.09	16.45	3.3	0.00	1990	0.004
June	22.85	0.18	0.110	0.04	7.11	*	*	1997	0.04
July	24.33	*	*	0.05	8.01	3.21	0.001	1992	0.006
August	23.75	-0.15	0.187	-0.02	-3.79	*	*	1982	0.33
September	21.23	*	*	-0.13	-23.73	-4.72	0.00	1993	0.001
October	14.32	*	*	-0.20	-55.67	-5.82	0.00	1992	0.002
November	9.25	*	*	-0.14	-57.97	-3.29	0.001	1994	0.005
December	6.13	*	*	-0.08	-50.21	-2.9	0.0	1981	0.02

Table 6.11 : Trend in extreme monthly maximum temperature (°C) at daily time step for Safdarjung

Variable	Mean	MK test		Sen's slope (°C/year)	% Change	MMK test		Shift Detection Test	
		Zmk	p-value			Zmmk	p-value	t	p-value
January	25.2	-0.032	0.780	-0.01	-1.79	*	*	1974	0.45
February	28.82	0.13	0.244	0.04	6.11	*	*	2000	0.44
March	35.15	*	*	0.067	8.34	1.9	0.1	1998	0.03
April	40.55	*	*	0.051	5.49	2.4	0.02	1997	0.00
May	42.69	*	*	0.053	5.50	2.71	0.01	1992	0.001
June	42.92	0.008	0.953	0.0001	0.0001	*	*	2002	0.6
July	39.19	-0.035	0.762	-0.014	-1.63	*	*	1976	0.9
August	36.95	*	*	0.019	2.31	0.88	0.38	1983	0.6
September	36.41	*	*	0.017	2.01	1.06	0.29	1978	0.4
October	35.47	-0.127	0.258	-0.024	-2.94	*	*	2002	0.4
November	31.56	-0.147	0.188	-0.033	-4.65	*	*	2001	0.3
December	26.49	-0.021	0.861	-0.004	-0.58	*	*	1971	0.7

Table 6.12 : Trend in extreme monthly minimum temperature (°C) at daily time step for Safdarjung

Variable	Mean	MK test		Sen's slope (oC/year)	% Change	MMK test		Shift Detection Test	
		Zmk	P-value			Zmk	p-value	t	P-value
January	4.75	0.06	0.624	0.008	7.00	*	*	1998	0.89
February	6.81	*	*	0.08	51.71	3.51	0.001	1984	0.01
March	10.91	*	*	0.08	33.61	3.51	0.001	1984	0.01
April	16.71	*	*	0.06	15.80	1.26	0.21	1997	0.00
May	20.91	*	*	0.03	6.33	1.70	0.09	1989	0.26
June	22.69	*	*	0.04	7.76	2.56	0.01	1997	0.19
July	24.50	*	*	0.044	7.99	0.48	0.63	1992	0.00
August	24.25	*	*	0.007	1.32	0.63	0.53	1991	0.48
September	21.96	-0.071	0.529	-0.017	-3.34	*	*	1980	0.84
October	15.76	0.027	0.816	0.007	1.93	*	*	1998	0.24
November	9.72	*	*	-0.013	-5.66	-0.66	0.50	1981	0.39
December	6.08	-0.058	0.608	-0.009	-6.82	*	*	1981	0.57

Table 6.13 : Trend in extreme annual maximum rainfall (mm) at daily time step for Palam and Safdarjung

Variable	Mean	MK test		Sen's slope	% Change	MMK test		Shift Detection Test	
		Z_{mk}	p-value			Z_{mmk}	p-value	T	Z_{mk}
Ex_Annual Palam	87.2	0.06	0.6	0.34	15.2	*	*	1980	0.45
Ex_Annual Safdarjung	89.3	0.73	0.7	0.162	7.98	*	*	1980	0.40

Table 6.14 : Trend in extreme daily monthly rainfall (mm) at daily time step for Palam

Variable	Mean	MK test		Sen's slope (^oC/year)	% Change	MMK test		Shift Detection Test	
		Z_{mk}	p-value			Z_{mmk}	p-value	t	p-value
January	14.1	0.09	0.40	0.12	33.01	*	*	1985	0.25
February	10.4	0.07	0.54	0.07	26.33	*	*	1975	0.63
March	6.6	*	*	-0.03	-15.18	-0.56	0.58	1990	0.77
April	10.9	*	*	-0.02	-8.28	-0.60	0.55	1994	0.52
May	12.4	*	*	0.30	94.60	2.27	0.02	1981	0.05
June	33.2	*	*	0.94	110.50	3.58	0.001	1992	0.001
July	47.3	0.01	0.96	0.05	3.88	*	*	1994	0.90
August	68.0	0.11	0.33	0.43	24.76	*	*	1981	0.31
September	37.2	-0.07	0.54	-0.18	-19.14	*	*	1976	0.62
October	14.4	-0.26	0.02	-0.29	-77.22	*	*	1976	0.04
November	2.1	0.11	0.36	0	0.00	*	*	1977	0.18
December	4.4	*	*	0	0.00	-0.16	0.87	1991	0.56

A significant decreasing trend has been observed in extreme daily maximum rainfall in Palam and Safdarjung time series data for October and September and October months over the 44 years with Z_{mk} = -0.26 and Z_{mk} and Z_{mmk}=-3.73 and -0.34. However, this trend is found to be statistically significant at 95% confidence level. The Sen's slope [(-0.29) and (-2.71, and 0.27) mm/month, respectively] (Figure 6.14 & Figure 6.15) and percentage change (-77.22)% and (-171.25, and -54.57)%, respectively indicates decreasing trend in extreme daily maximum rainfall in these months. PMW test was applied to detect the shift

in the maximum daily trend at monthly temporal scale. A significant shift has been observed in extreme daily maximum rainfall for different months (Figure 6.14 & Figure 6.15). But in the month of February and March no trend (Table 6.15) has been observed.

Table 6.15 : Trend in extreme monthly rainfall (mm) at daily time step for Safdarjung

Variable	Mean	MK test		Sen's slope	% Change	MMK test		Shift Detection Test	
		Zmk	p-value			Zmmk	p-value	t	p-value
January	22.92	0.15	0.16	0.28	54.40	1.4	0.16	1999	0.34
February	20.72	0.00	1.00	0.00	0.00	*	*	1992	0.71
March	12.21	0.02	0.88	0.00	1.09	*	*	1978	0.98
April	23.82	0.21	0.05	0.29	52.83	*	*	1981	0.08
May	47.55	*	*	1.67	154.51	3.1	0.01	1986	0.001
June	105.24	*	*	2.79	116.67	3.0	0.001	1987	0.00
July	169.24	0.15	0.17	1.44	37.46	*	*	1979	0.27
August	169.20	-0.09	0.40	-1.22	-31.77	*	*	1976	0.26
September	69.73	*	*	-2.71	-171.25	-3.73	0.001	1991	0.003
October	21.61	-0.34	0.001	-0.27	-54.57	*	*	1989	0.001
November	8.24	0.23	0.04	0.00	0.00	*	*	1986	0.21
December	13.77	0.23	0.03	0.19	59.65	*	*	1984	0.001

Urbanization plays an important role in human induced climate change at the regional scale through altered land atmosphere interactions over urban areas (Oke et al., 1978; Das and Padmanabhamurty, 2008). Previous studies have demonstrated the possible effects of urbanization on both temperature and precipitation (Arora and Boer, 2010; Kothawale et al., 2010; Kumar et al., 2010; Srivastava et al., 2010; Pal and Al-tabbaa, 2011; Subash et al., 2011a; Chakraborty et al., 2015).

6.3 DOWNSCALED CLIMATE PROJECTIONS USING COUPLED MODEL INTERCOMPARISON PROJECT 5 (CMIP5) MODEL

Statistical downscaling involves the establishment of empirical relationships between historical large-scale atmospheric and local climate characteristics. Once a relationship has been determined and validated, future large-scale atmospheric conditions projected by GCMs are used to predict future local climate characteristics. In other words, large-scale GCM outputs are used as predictors to obtain local variables called as predictands. Statistical downscaling includes a heterogeneous group of methods that vary in sophistication and applicability. Statistical downscaling methods are computationally inexpensive in comparison to RCMs that require complex modelling of physical processes.

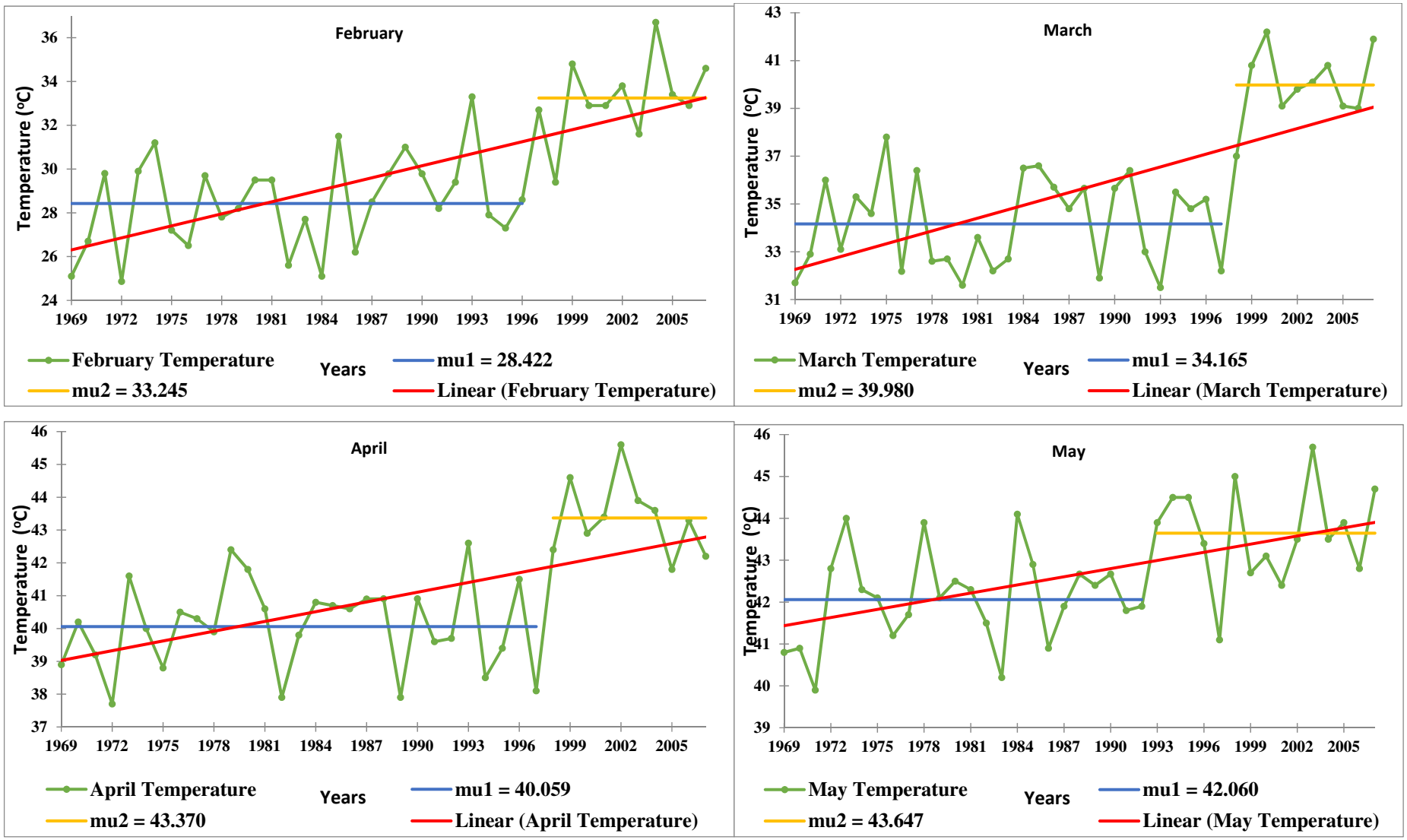

Figure 6.9 (a): Significant trend in extreme monthly maximum temperature (°C) at daily time step for Palam

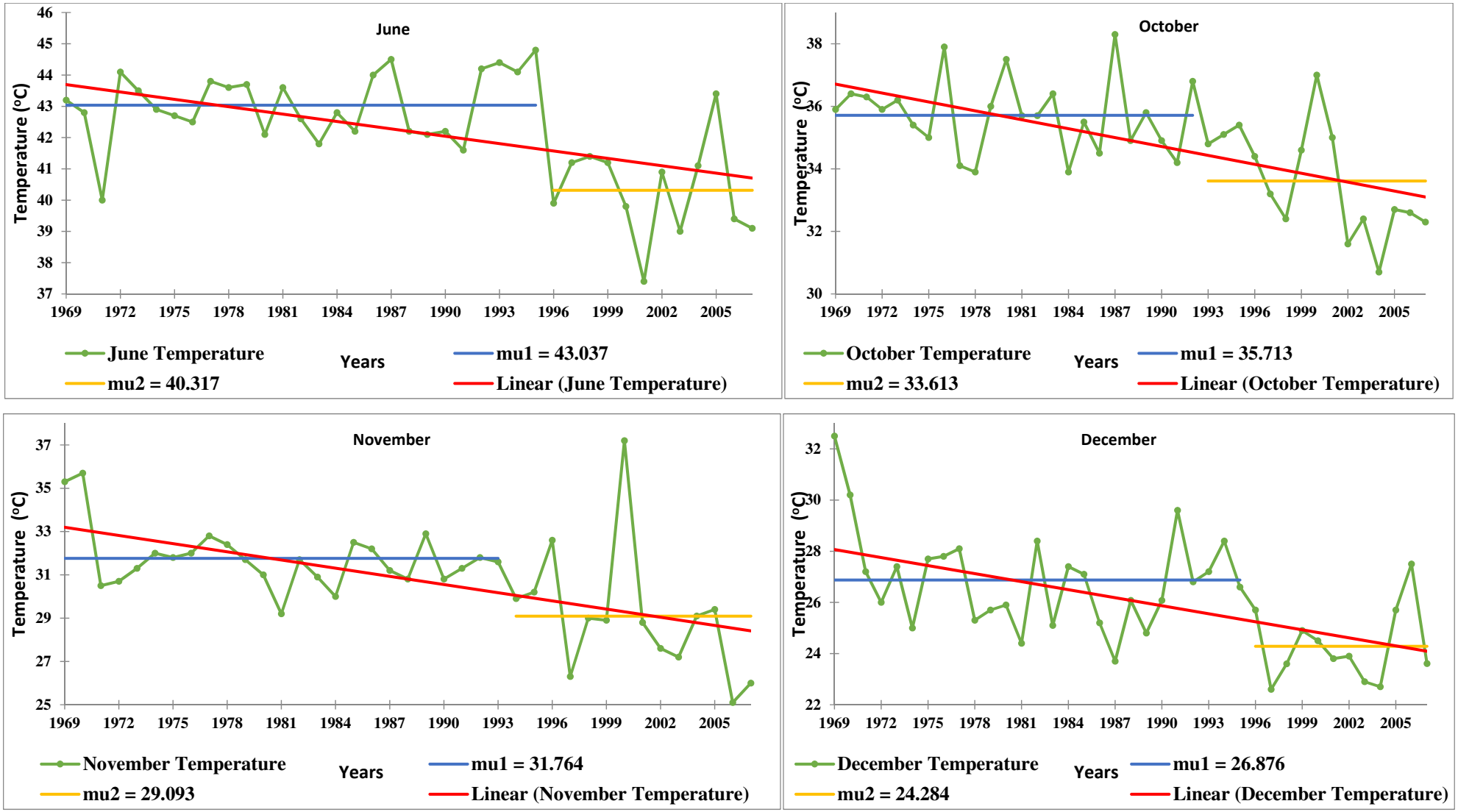

Figure 6.9 (b): Significant trend in extreme monthly maximum temperature (°C) at daily time step for Palam

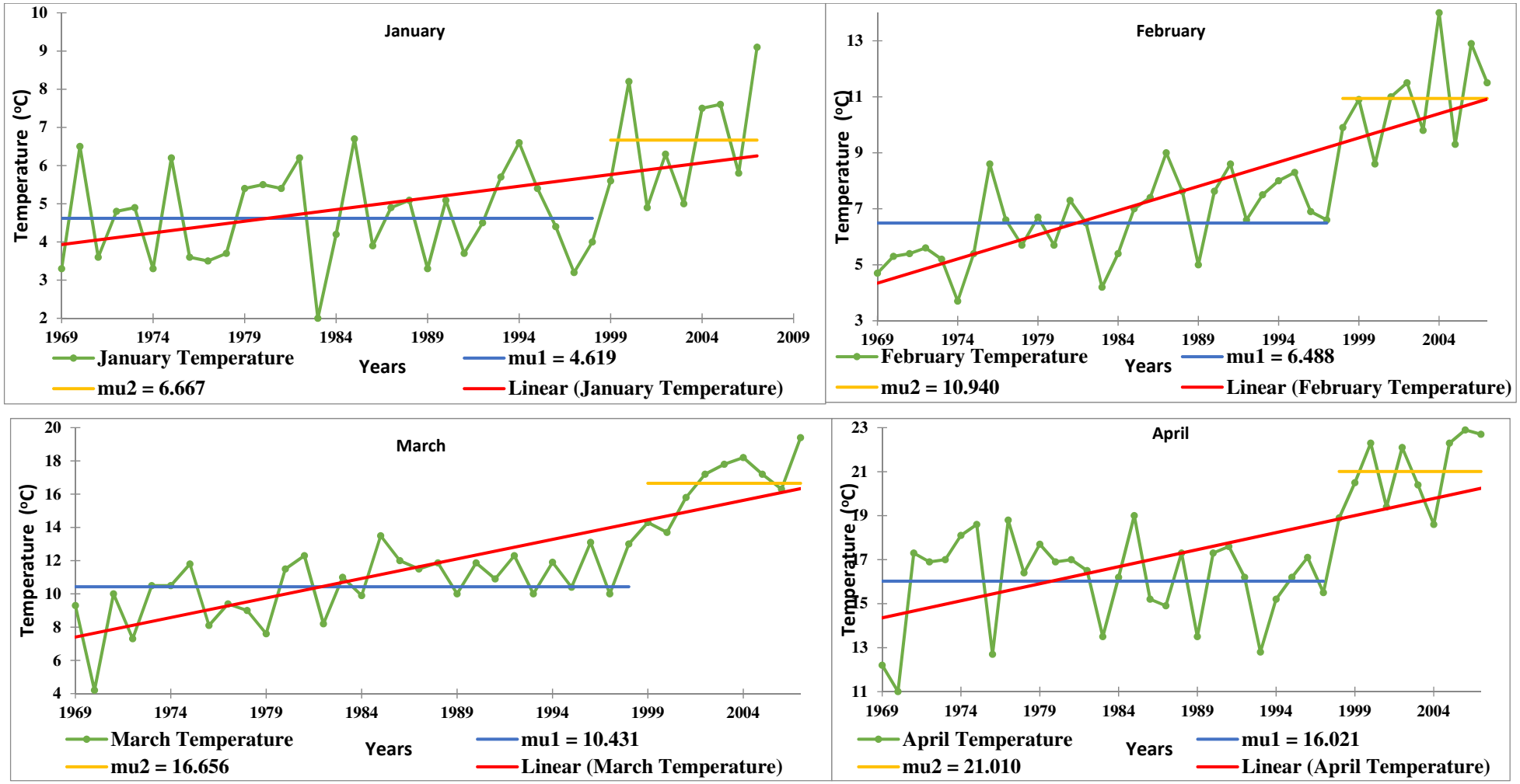

Figure 6.10 (a): Significant trend in extreme monthly minimum temperature (°C) at daily time step for Palam

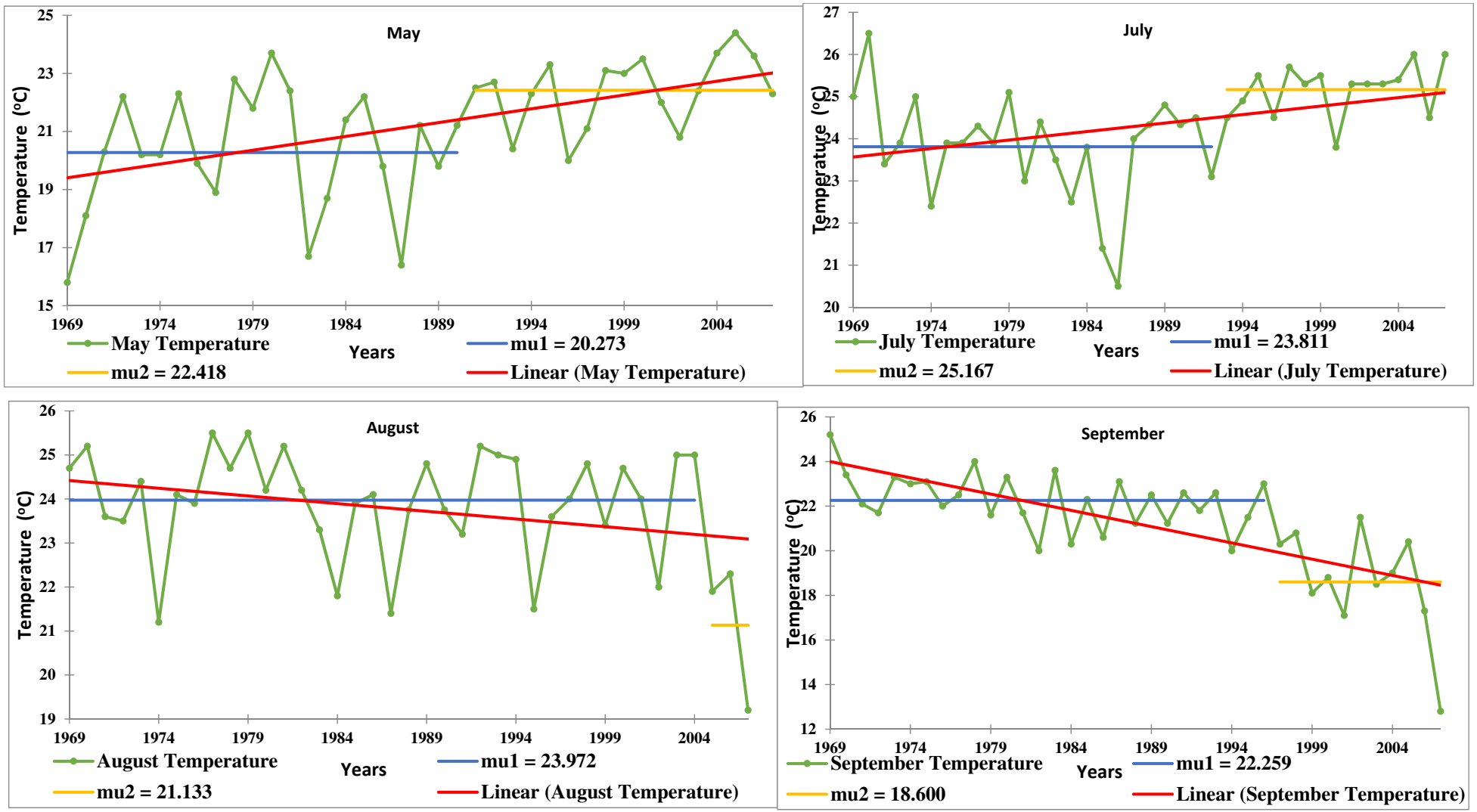

Figure 6.10 (b): Significant trend in extreme monthly minimum temperature (°C) at daily time step for Palam

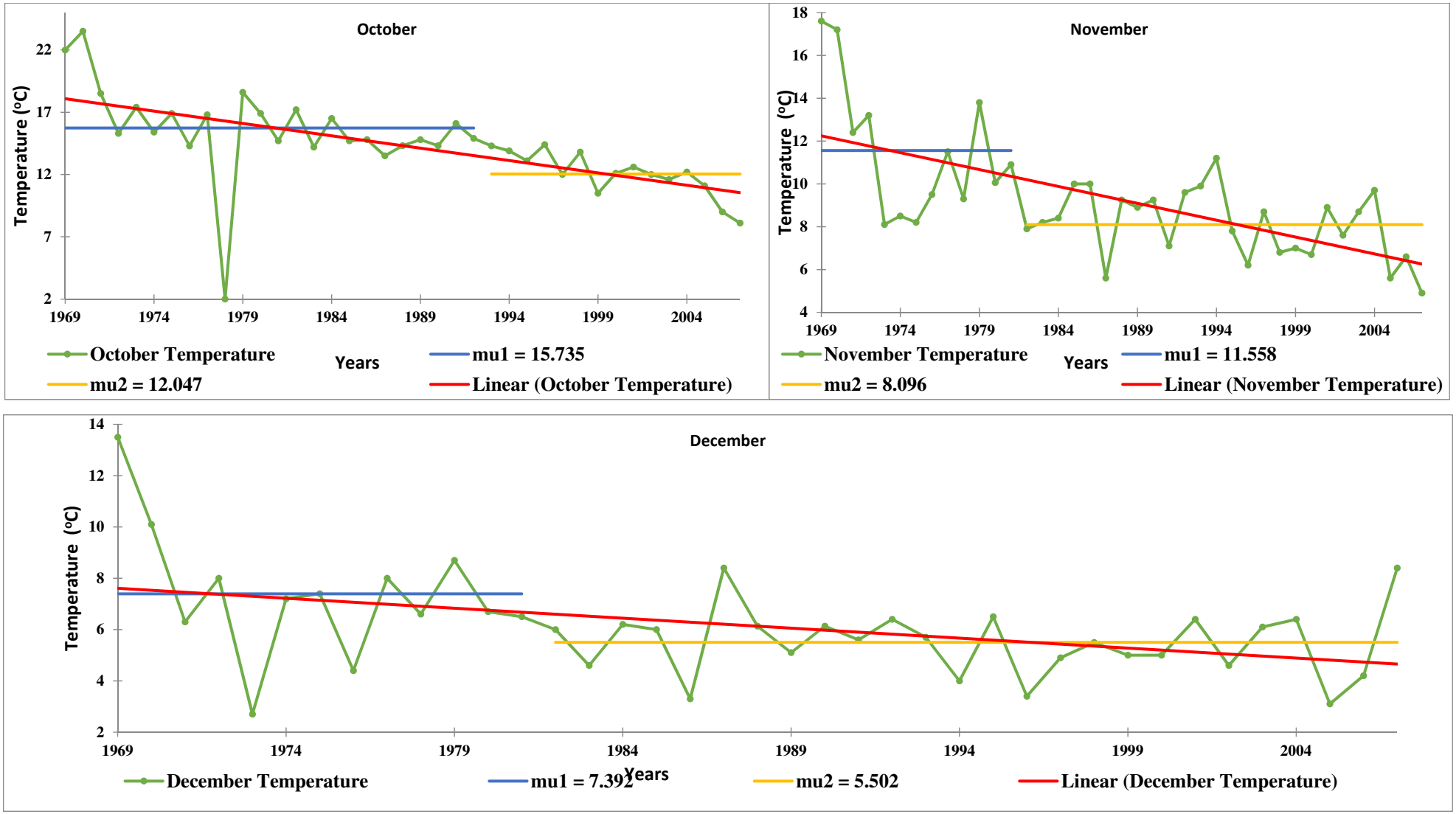

Figure 6.10 (c): Significant trend in extreme monthly minimum temperature (°C) at daily time step for Palam

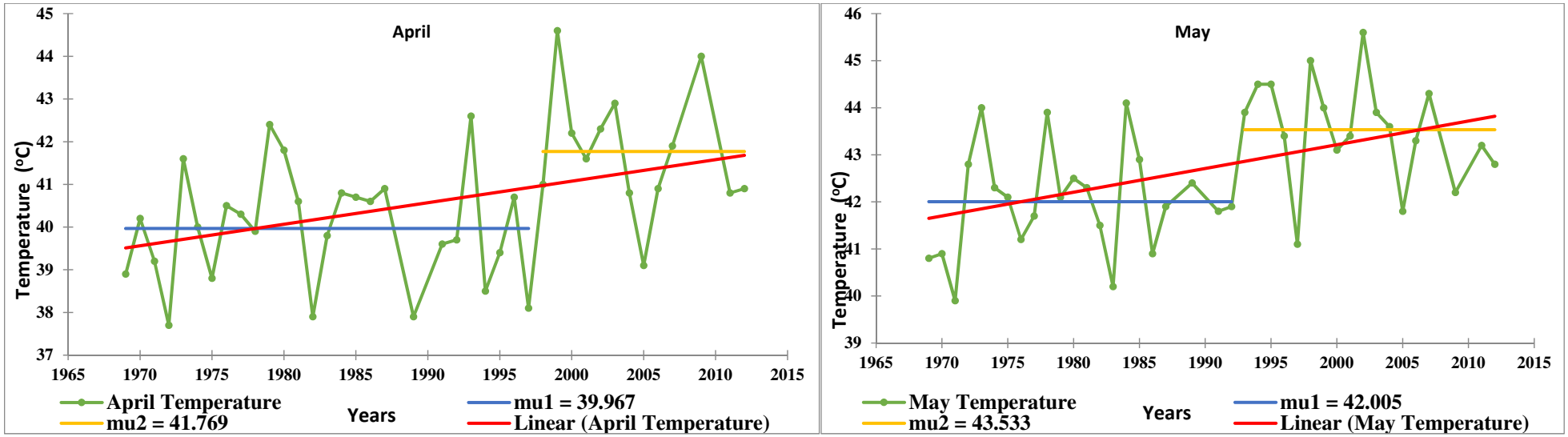

Figure 6.11: Significant trend in extreme monthly maximum temperature (°C) at daily time step for Safdarjung

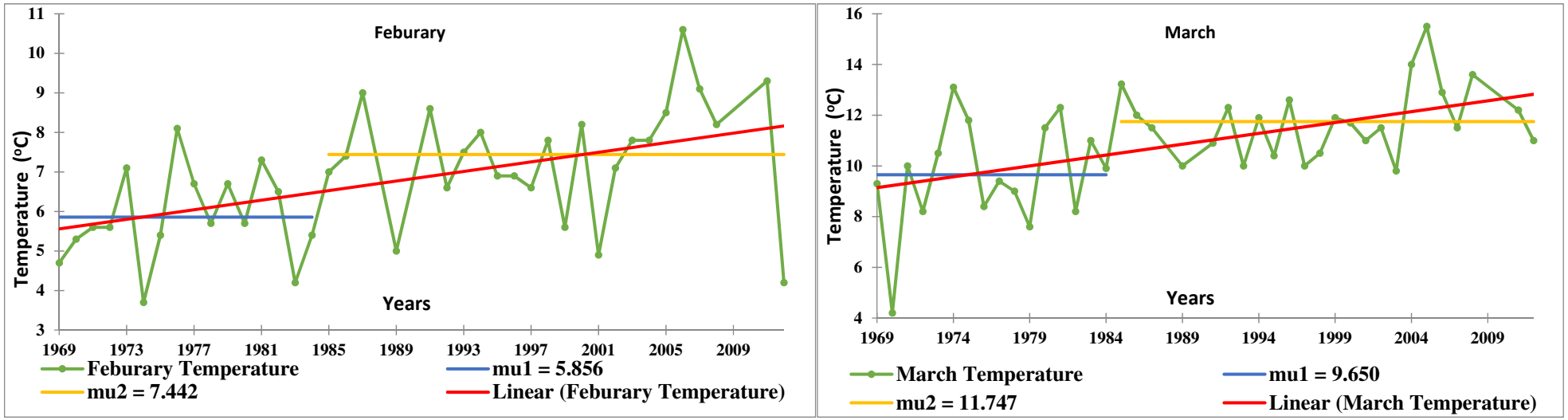

Figure 6.12 (a): Significant trend in extreme monthly minimum temperature (°C) at daily time step for Safdarjung

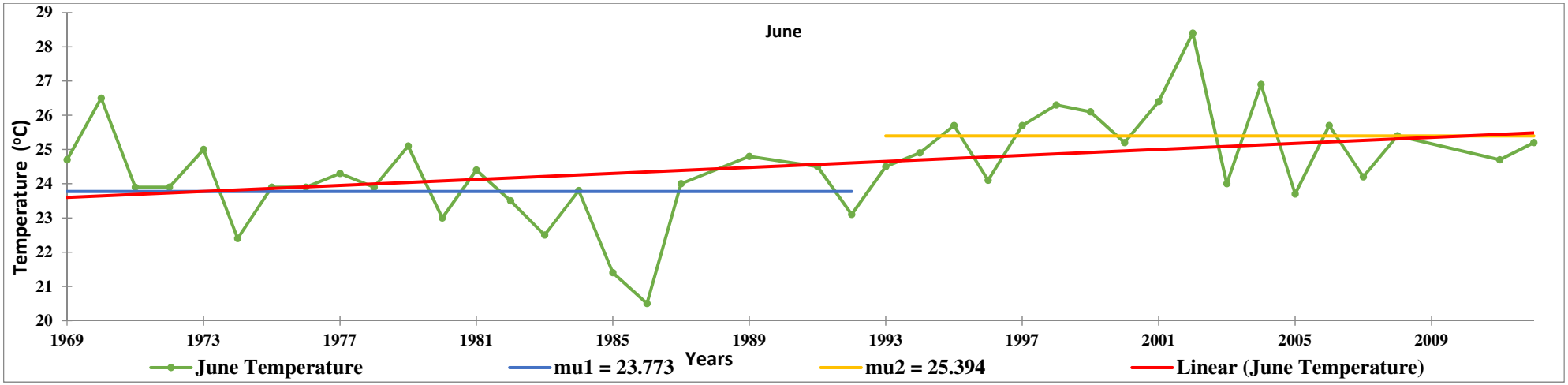

Figure 6. 12 (b): Significant trend in extreme monthly minimum temperature (°C) at daily time step for Safdarjung

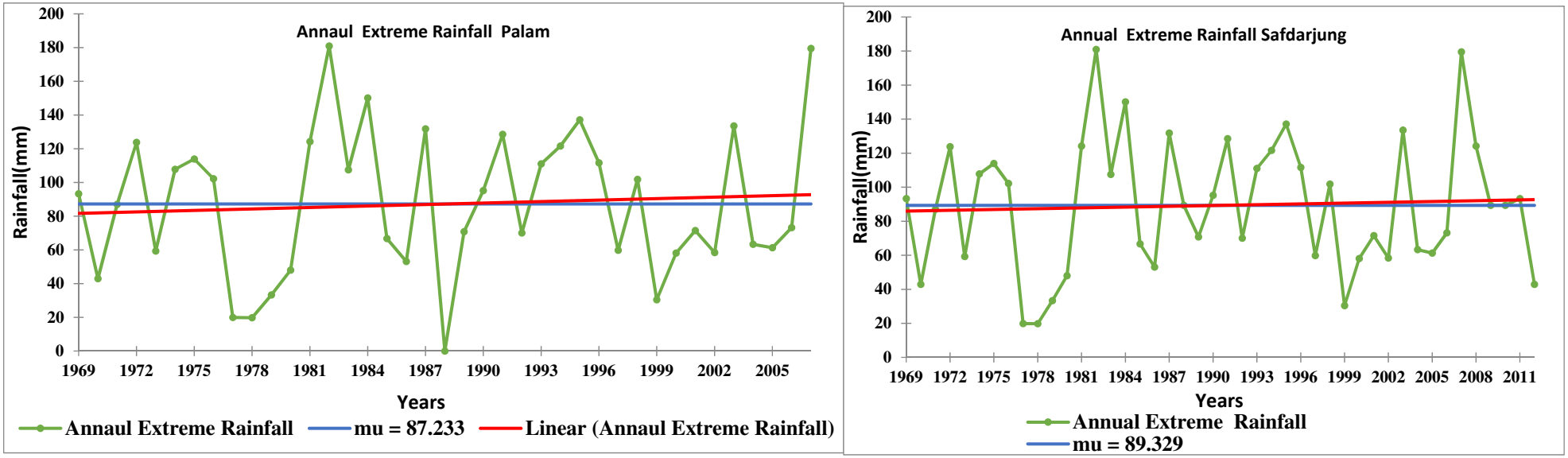

Figure 6.13: Significant trend in extreme annual rainfall (mm) at daily time step for Palam and Safdarjung

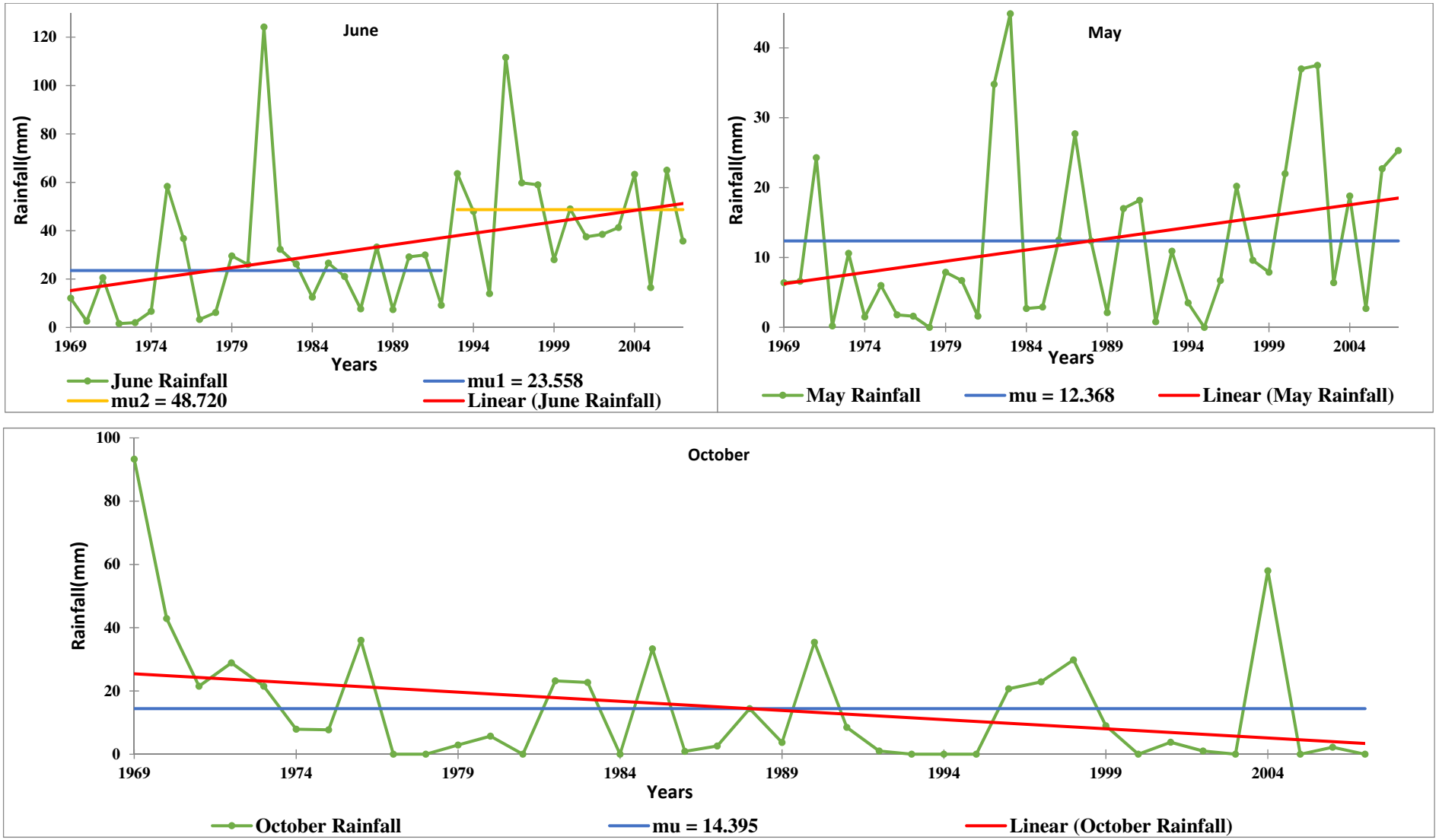

Figure 6.14: Significant trend in extreme monthly rainfall (mm) at daily time step for Palam

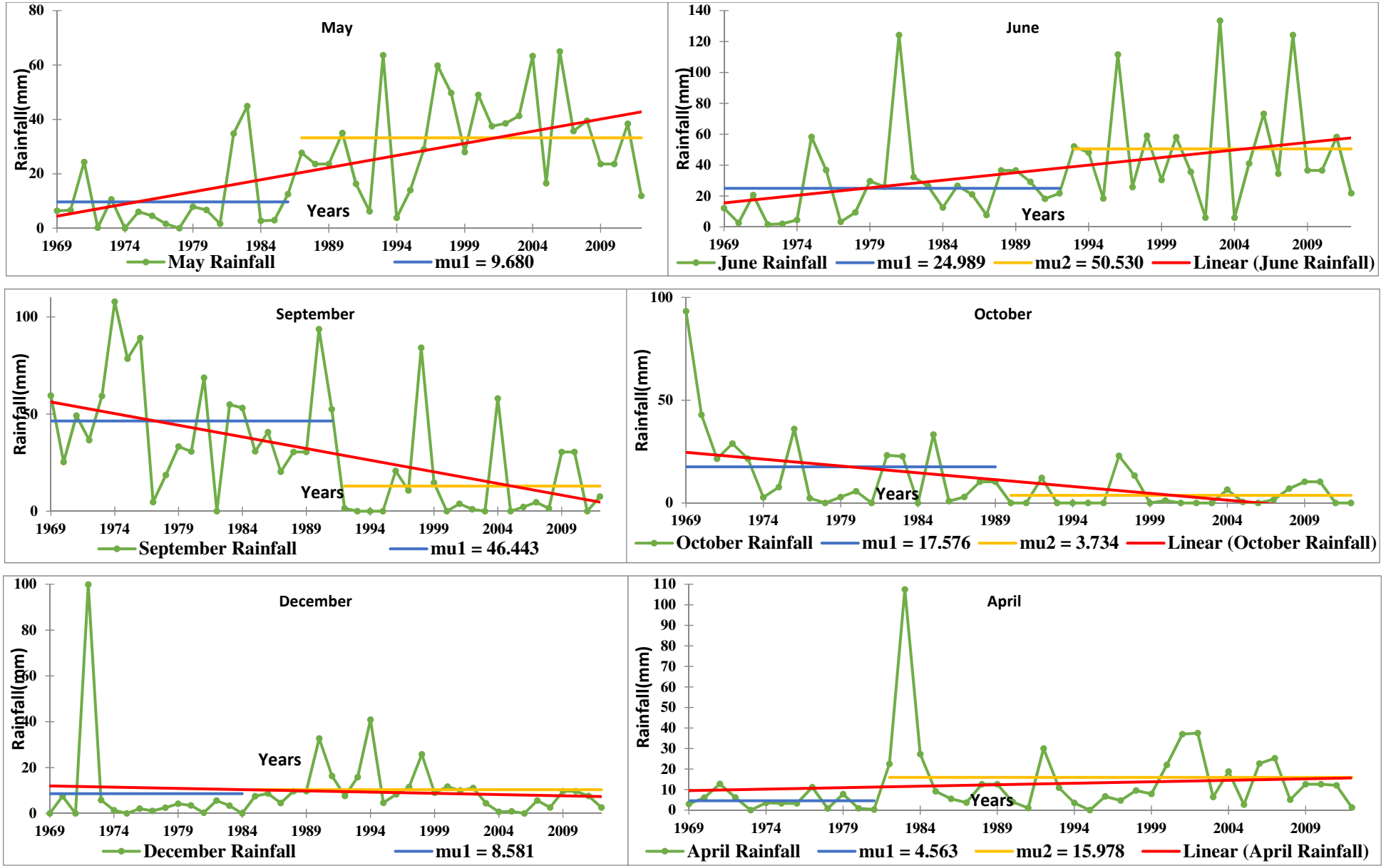

Figure 6.15: Significant trend in extreme monthly rainfall (mm) at daily time step for Safdarjung

Thus, they are viable and sometimes advantageous alternative for institutions that do not have the computational capacity and technical expertise required for dynamical downscaling. Unlike RCMs, which produce downscaled projections at a spatial scale of 20–50 km, statistical methods can provide station scale climate information (Giorgi, 1999).

6.3.1 Statistical Downscaling Model (SDSM)

The SDSM is freely available software in which multiple linear regression methods are used to spatially downscale daily predictor-predictand and their relationships (Wilby et al., 2002). SDSM provides climate information at specific locations for which there is daily data adequate to calibrate the model, as well as archived GCM output (Wilby and Dawson, 2013). Key inputs include quality observed daily data for both local-scale and large-scale climate variables as well as daily GCM outputs for large-scale variables for future climate (SED, 2015). Outputs can be applied over a range of climate impact sectors and include site-specific daily scenarios for maximum and minimum temperature, and precipitation.

6.3.2 Results and Discussion

To investigate the future impact of climate change, the outputs of the CanESM2 model was used to downscale the future climate at the study area. The comparison between the intra-annual variability of monthly statistics of precipitation (mean, maximum, wet days , mean dry spell, mean wet precipitation, maximum dry spell , maximum wet spell, maximum total precipitation) and in the case of temperature (minimum and maximum) were carried out. The downscaling of precipitation and temperature has been carried out for both the stations in Safdarjung and Palam. The future climate conditions were determined using different RCPs scenarios (RCP2.6, RCP4.5, and RCP8.5) and NCEP for Canadian (CanESM2) model at a different temporal scales (annual, seasonal and monthly). Observed data used to calibrate the model for the period of 1969 to 2005.

6.3.2.1 Projection of precipitation under different RCP's for different temporal scales

The mean distributions of the daily precipitation frequency and amount for the different temporal scales categories derived from observations (1969–2005) and the GCM model ensemble simulations for the present (1961–2005, historical) and future (2080–2099) climate under the RCP2.6, RCP4.5 and RCP8.5 scenarios. Analysis indicates that the rainfall events in

Delhi region are projected to be considerably more extreme under global warming scenarios. The number of days of intense precipitation is reported to significantly decrease with respect to the present day, and its contribution to the annual precipitation change is also obviously decreased. This magnitude of change is scaled to the emission scenarios, with a greater decrease in the magnitude of RCP8.5 and a smaller decrease in RCP4.5 in the both stations Palam and Safdarjung.

This change suggests an increased risk of drought in Delhi region from decreased levels of intense precipitation under the RCP emission scenarios. The amount of precipitation in Delhi region is significantly decreased under global warming scenario (Jain & Kumar, 2012). Similar results can be found in the CMIP5 simulations. It shows the distribution of the percentage changes in the annual precipitation by the end of the 21st century under the RCP4.5 and RCP8.5 scenario with respect to the present-day simulation. On comparing the trace rain in the months of June to September which is considered as the monsoon season of the Delhi region (IMD, 2005). According to the projected results, rainfall has been found to be decreased in both the stations. For Palam station, the rainfall values in the month June (2.26, 1.99 mm), July (4.84, 4.54 mm), August (6.13, 6.33 mm) and September (3.20, 3.01mm) have been determined under the RCP4.5 and RCP8.5 respectively when the observed values are 2.31 mm (June), 5.42 mm (July), 6.32 mm (August) and 3.09 mm (September). Similarly, in Safdarjung station, rainfall values in June (2.86, 2.63 mm), July (4.16, 4.72 mm), August (6.47, 5.45 mm) and September (2.76, 2.73 mm) under the RCP4.5 and RCP8.5 respectively have been determined and the observed values are 3.14 mm (June), 5.35 mm (July), 5.42 mm (August) and 2.66mm (September). Results are shown in Table 6.16 and Figure 6.16 and Annexure A1 and Figure 6.18 for Palam and Safdarjung stations respectively.

Annual change in percentage (%) mean precipitation in three scenarios RCPs (2.6, 4.5, and 8.5) as compared to the observed climatic condition has shown a downward trend for both the stations. For Palam station, the values are 1.82, 1.74 and 1.71mm (RCP2.6, RCP4.5 and RCP 8.5) with change in percentage values are -0.09, -4.56 and -6.05 % and the observed value is 1.82 mm. Similarly, for Safdarjung station, the values are 1.82, 1.71 and 1.72 mm (RCP2.6, RCP4.5 and RCP 8.5) with change in percentage values are -1.04, -6.98 and -6.51% with observed value is 1.84 mm. In the future, prediction of mean annual rainfall at both stations

Palam and Safdarjung have been found decreasing (Table 6.16, Figure 6.16, Annexure A1 and Figure 6.18).

In the case of maximum precipitation, annual change in values are 162.53, 141.31 and 152.27, 165.92 mm with change in percentage -10.16, -21.88 % and -15.88 -8.33% under the RCP4.5 and RCP8.5 respectively with respect to observed values which are 180.90 and 181.00 mm at both stations Palam and Safdarjung, respectively. In the future, prediction of maximum precipitation at both stations Palam and Safdarjung have been found decreasing. Details results are shown in Table 6.17, Figure 6.16, Annexure A2 and Figure 6.18.

In case of an average number of wet days (%) change in scenarios under three RCPs (2.6, 4.5 and 8.5) have been determined. Annual wet day's percentage change in scenarios the values are -37.48,-37.29, -38.07 and -28.37,-27.67, -26.88 % with respect to the observed values which are 0.22 and 0.16 at Palam and Safdarjung, respectively. On comparing the results, it can be observed that wet days (%) in Palam and Safdarjung have been decreased from the present situation. Detailed results are shown in Table 6.18, Figure 6.16 and Annexure A3 and Figure 6.18.

In the case (mean dry spell) of average length of spells with amounts less than the wet-day threshold and mean wet spell average length of spells with amounts greater than or equal to the wet-day threshold annual changes in values under two RCPs (4.5 and 8.5), the values are 8.68, 8.52 and 9.87, 9.52 with respect to observed values are 8.57 and 9.46 in Palam and Safdarjung, respectively. Similarly, for the case of mean wet spell the RCP values are 1.42, 1.37 and 1.37, 1.34 with respect to observed values are 2.45 and 1.92 at Palam and Safdarjung station, respectively. Results when compared with present climate mean dry spell length increased but mean wet spell decreased, this situation may create a drought condition in future for Delhi region. Detailed results are shown in Table 6.19, 6.20, Figure 6.16, 6.17 and Annexure A4, Annexure A5 and Figure 6.18, 6.19 for both Palam and Safdarjung.

In the case (maximum dry spell length) of longest spell with amounts less than the wet-day threshold and (maximum wet spell length) longest spell with amounts greater than or equal to wet-day threshold the annual changes in maximum dry spell length values under two RCPs (4.5 and 8.5) the values are 97.35, 94.55 and 117.80, 108.75 with respect to observed values 116.00, 129.00 for both the stations respectively.

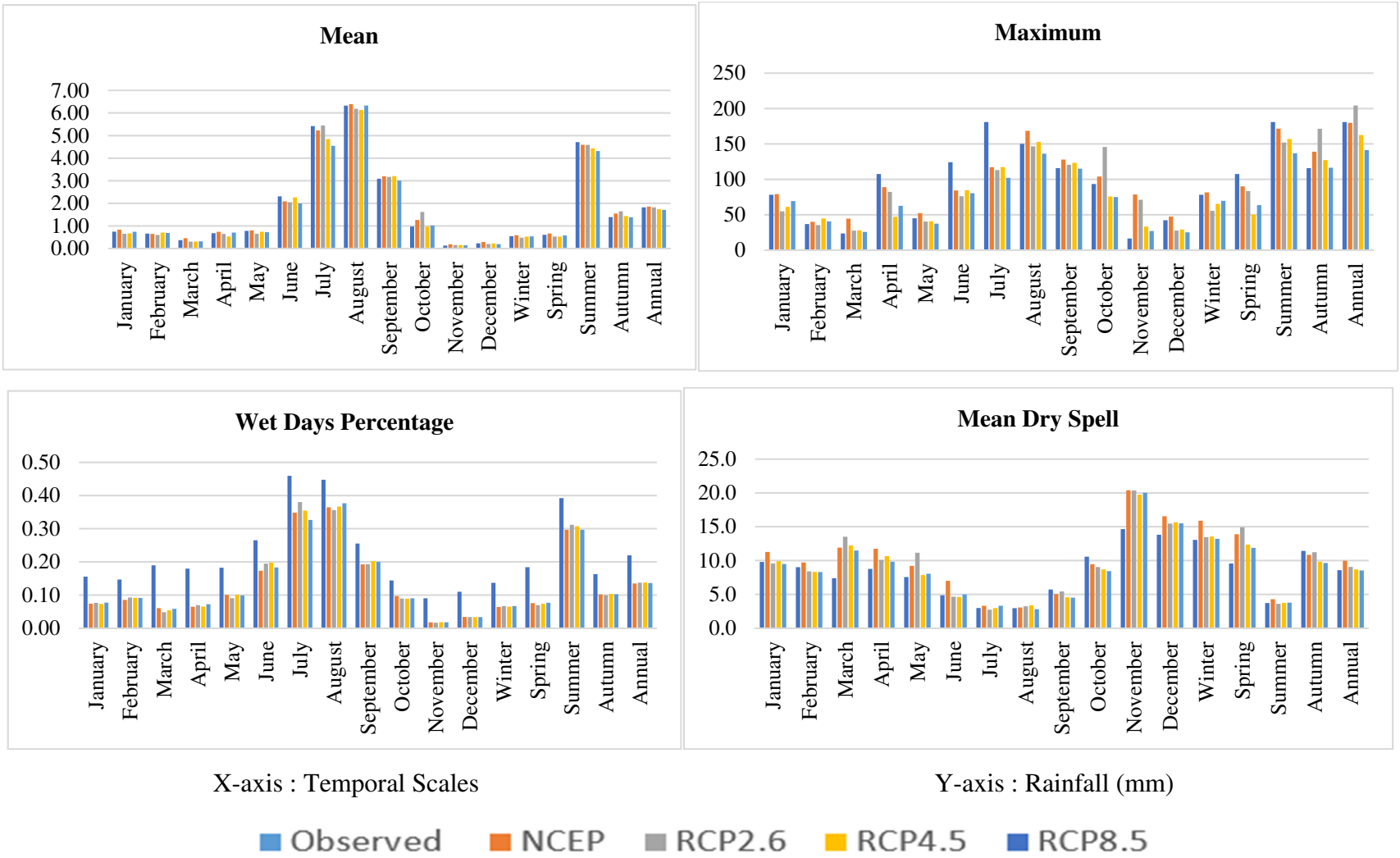

Figure 6.16: Comparison of observed and downscaled rainfall corresponding to different RCP scenarios at different temporal for Palam (1)

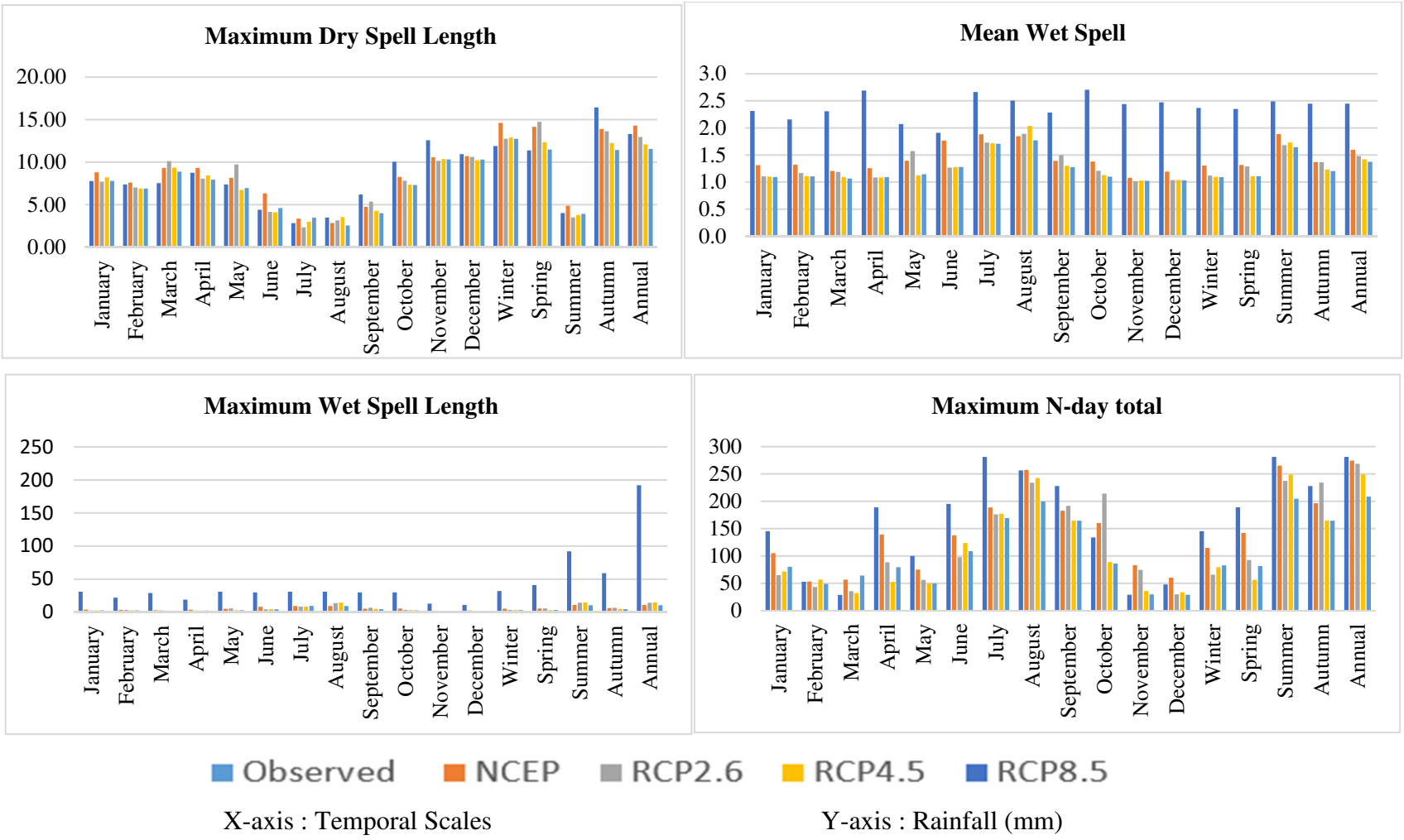

Figure 6.17: Comparison of observed and downscaled rainfall for different RCP scenarios at different temporal scales for Palam (2)

Table 6.16 : Comparison of observed and projected mean precipitation for different RCP scenarios at different temporal scales for Palam Station

Temporal scale	Observed	NCEP	RCP 2.6	RCP 4.5	RCP 8.5	NCEP %	RCP 2.6%	RCP 4.5%	RCP 8.5%
January	0.74	0.83	0.65	0.67	0.74	11.74	-11.87	-10.03	-0.14
February	0.66	0.65	0.60	0.70	0.69	-1.80	-9.04	6.38	4.17
March	0.37	0.45	0.30	0.30	0.31	23.40	-17.47	-17.33	-14.39
April	0.68	0.74	0.65	0.53	0.71	9.32	-4.55	-21.86	4.28
May	0.78	0.80	0.65	0.74	0.72	2.40	-16.61	-5.53	-7.93
June	2.31	2.09	2.04	2.26	1.99	-9.46	-11.32	-1.89	-13.54
July	5.42	5.22	5.44	4.84	4.54	-3.58	0.46	-10.64	-16.13
August	6.32	6.38	6.18	6.13	6.33	0.96	-2.27	-3.07	0.05
September	3.09	3.20	3.17	3.20	3.01	3.57	2.58	3.65	-2.64
October	0.97	1.26	1.62	0.97	1.02	29.50	66.39	-0.35	4.53
November	0.13	0.19	0.16	0.15	0.14	42.77	19.10	15.36	5.98
December	0.23	0.29	0.20	0.22	0.19	28.04	-12.36	-1.48	-15.05
Winter	0.54	0.59	0.48	0.53	0.54	8.89	-10.86	-2.51	-0.63
Spring	0.61	0.66	0.53	0.52	0.58	9.18	-12.40	-13.85	-4.81
Summer	4.71	4.59	4.58	4.43	4.31	-2.46	-2.66	-5.81	-8.40
Autumn	1.39	1.54	1.65	1.43	1.38	10.95	18.28	3.06	-0.67
Annual	1.82	1.85	1.82	1.74	1.71	1.91	-0.09	-4.56	-6.05

Table 6.17 : Comparison of observed and projected maximum precipitation for different RCP scenarios at different temporal scales for Palam

Temporal scale	Observed	NCEP	RCP 2.6	RCP 4.5	RCP 8.5	NCEP %	RCP 2.6%	RCP 4.5%	RCP 8.5%
January	78.10	79.10	54.67	61.08	69.25	1.27	-30.00	-21.80	-11.33
February	36.70	39.91	35.22	44.68	40.54	8.75	-4.03	21.74	10.47
March	23.40	44.37	27.55	27.82	25.59	89.60	17.72	18.88	9.36
April	107.50	88.97	82.28	47.04	62.48	-17.24	-23.46	-56.24	-41.87
May	44.90	52.23	40.38	40.64	37.25	16.32	-10.07	-9.48	-17.03
June	124.20	84.27	76.17	84.44	80.30	-32.15	-38.67	-32.01	-35.35
July	180.90	117.01	112.99	117.28	102.05	-35.32	-37.54	-35.17	-43.59
August	150.10	168.44	146.59	152.64	136.09	12.22	-2.34	1.69	-9.33
September	115.70	127.81	120.49	123.23	115.02	10.47	4.14	6.51	-0.59
October	93.30	103.94	145.64	75.72	74.98	11.40	56.10	-18.84	-19.63
November	16.30	78.56	71.15	33.27	26.91	381.94	336.47	104.12	65.09
December	42.10	47.42	27.43	28.93	25.17	12.65	-34.85	-31.29	-40.22
Winter	78.10	81.52	55.52	65.35	69.69	4.38	-28.91	-16.32	-10.77
Spring	107.50	90.04	83.39	50.08	63.51	-16.24	-22.42	-53.42	-40.92
Summer	180.90	171.56	151.92	156.94	136.69	-5.16	-16.02	-13.25	-24.44
Autumn	115.70	138.91	171.47	127.10	116.39	20.06	48.21	9.85	0.59
Annual	180.90	179.72	204.22	162.53	141.31	-0.65	12.89	-10.16	-21.88

Table 6.18 : Comparison of observed and projected wet day's for different RCP scenarios at different temporal scales for Palam

Temporal scale	Observed	NCEP	RCP 2.6	RCP 4.5	RCP 8.5	NCEP %	RCP 2.6%	RCP 4.5%	RCP 8.5%
January	0.16	0.07	0.08	0.07	0.08	-52.45	-50.90	-52.86	-50.53
February	0.15	0.09	0.09	0.09	0.09	-41.67	-37.05	-37.85	-37.69
March	0.19	0.06	0.05	0.05	0.06	-68.10	-74.52	-71.43	-69.20
April	0.18	0.06	0.07	0.06	0.07	-63.93	-61.35	-63.76	-59.76
May	0.18	0.10	0.09	0.10	0.10	-45.06	-50.39	-44.86	-45.93
June	0.26	0.17	0.19	0.20	0.18	-34.63	-26.52	-25.58	-30.88
July	0.46	0.35	0.38	0.35	0.33	-24.13	-17.25	-22.87	-29.02
August	0.45	0.36	0.36	0.37	0.38	-18.58	-20.40	-18.03	-15.80
September	0.25	0.19	0.19	0.20	0.20	-24.68	-24.40	-20.61	-21.53
October	0.14	0.10	0.09	0.09	0.09	-32.78	-37.93	-38.28	-37.51
November	0.09	0.02	0.02	0.02	0.02	-80.64	-81.66	-80.18	-80.60
December	0.11	0.03	0.03	0.03	0.03	-69.20	-69.53	-69.56	-69.49
Winter	0.14	0.06	0.07	0.07	0.07	-53.46	-51.40	-52.44	-51.46
Spring	0.18	0.08	0.07	0.07	0.08	-59.07	-62.26	-60.11	-58.41
Summer	0.39	0.30	0.31	0.31	0.30	-24.31	-20.50	-21.61	-24.35
Autumn	0.16	0.10	0.10	0.10	0.10	-37.33	-38.93	-36.80	-37.12
Annual	0.22	0.13	0.14	0.14	0.14	-38.54	-37.48	-37.29	-38.07

Table 6.19 : Comparison of observed and projected mean dry spell precipitation for different RCP scenarios at different temporal scales for Palam

Temporal scale	Observed	NCEP	RCP2.6	RCP4.5	RCP8.5	NCEP%	RCP2.6%	RCP4.5%	RCP8.5%
January	9.79	11.27	9.57	9.91	9.48	15.13	-2.22	1.22	-3.18
February	9.01	9.70	8.39	8.31	8.28	7.71	-6.92	-7.82	-8.05
March	7.38	11.89	13.52	12.22	11.48	61.15	83.21	65.50	55.55
April	8.76	11.74	10.09	10.65	9.83	33.99	15.14	21.57	12.22
May	7.56	9.20	11.15	7.84	8.03	21.62	47.37	3.65	6.21
June	4.86	6.99	4.65	4.61	4.99	44.00	-4.30	-5.14	2.80
July	2.98	3.31	2.72	2.96	3.31	11.02	-8.86	-0.76	11.11
August	2.95	3.06	3.23	3.36	2.81	3.74	9.42	13.85	-4.82
September	5.70	5.02	5.42	4.56	4.52	-11.91	-5.03	-20.08	-20.80
October	10.56	9.45	9.04	8.67	8.43	-10.47	-14.42	-17.87	-20.18
November	14.64	20.38	20.35	19.73	20.01	39.21	39.02	34.79	36.69
December	13.80	16.53	15.45	15.65	15.49	19.81	12.00	13.44	12.25
Winter	13.04	15.88	13.45	13.53	13.19	21.77	3.16	3.76	1.18
Spring	9.55	13.88	14.90	12.34	11.86	45.35	56.04	29.26	24.23
Summer	3.72	4.27	3.60	3.73	3.76	14.87	-3.26	0.27	1.29
Autumn	11.41	10.84	11.23	9.83	9.63	-5.06	-1.59	-13.85	-15.60
Annual	8.57	9.96	9.05	8.68	8.52	16.20	5.65	1.29	-0.58

Table 6.20 : Comparison of observed and projected mean wet precipitation for different RCP scenarios at different temporal scales for Palam

Temporal scale	Observed	NCEP	RCP2.6	RCP4.5	RCP8.5	NCEP%	RCP2.6%	RCP4.5%	RCP8.5%
January	2.31	1.31	1.10	1.10	1.09	-43.32	-52.27	-52.50	-52.80
February	2.15	1.32	1.16	1.11	1.10	-38.80	-45.99	-48.58	-48.75
March	2.31	1.20	1.19	1.09	1.07	-47.82	-48.61	-52.74	-53.86
April	2.69	1.26	1.08	1.08	1.09	-53.28	-59.70	-59.72	-59.53
May	2.07	1.39	1.57	1.12	1.14	-32.69	-24.05	-45.80	-44.81
June	1.91	1.76	1.27	1.27	1.28	-7.61	-33.74	-33.35	-33.10
July	2.66	1.88	1.73	1.72	1.71	-29.28	-35.11	-35.52	-35.93
August	2.50	1.84	1.89	2.04	1.77	-26.29	-24.51	-18.63	-29.35
September	2.28	1.39	1.50	1.30	1.27	-39.14	-34.45	-43.12	-44.15
October	2.70	1.38	1.21	1.13	1.10	-49.04	-55.44	-58.30	-59.36
November	2.44	1.08	1.02	1.03	1.02	-55.88	-58.36	-57.96	-58.14
December	2.47	1.19	1.04	1.04	1.03	-51.81	-58.07	-58.02	-58.27
Winter	2.37	1.31	1.12	1.09	1.09	-44.88	-52.75	-53.85	-54.06
Spring	2.35	1.31	1.29	1.11	1.11	-44.12	-45.26	-52.97	-52.92
Summer	2.49	1.88	1.68	1.73	1.64	-24.29	-32.45	-30.58	-33.99
Autumn	2.45	1.37	1.37	1.23	1.20	-44.10	-44.13	-49.81	-50.86
Annual	2.45	1.60	1.48	1.42	1.37	-34.82	-39.64	-42.04	-43.92

Table 6.21 : Comparison of observed and projected maximum dry spell length precipitation for different RCP scenarios at different temporal scales for Palam

Temporal scale	Observed	NCEP	RCP 2.6	RCP 4.5	RCP 8.5	NCEP %	RCP 2.6%	RCP 4.5%	RCP 8.5%
January	31.00	31.00	30.95	31.00	31.00	0.00	-0.16	0.00	0.00
February	29.00	28.85	28.65	28.20	28.35	-0.52	-1.21	-2.76	-2.24
March	31.00	31.00	31.00	31.00	31.00	0.00	0.00	0.00	0.00
April	30.00	30.00	30.00	30.00	29.95	0.00	0.00	0.00	-0.17
May	31.00	30.90	31.00	30.80	30.80	-0.32	0.00	-0.65	-0.65
June	20.00	29.70	24.05	24.90	25.95	48.50	20.25	24.50	29.75
July	19.00	23.60	15.75	22.15	24.15	24.21	-17.11	16.58	27.11
August	24.00	19.55	20.45	22.45	19.70	-18.54	-14.79	-6.46	-17.92
September	30.00	26.05	29.60	25.35	25.45	-13.17	-1.33	-15.50	-15.17
October	31.00	31.00	31.00	30.90	31.00	0.00	0.00	-0.32	0.00
November	30.00	30.00	30.00	30.00	30.00	0.00	0.00	0.00	0.00
December	31.00	31.00	31.00	31.00	31.00	0.00	0.00	0.00	0.00
Winter	53.00	80.30	71.70	74.00	74.05	51.51	35.28	39.62	39.72
Spring	67.00	78.35	84.80	74.40	67.70	16.94	26.57	11.04	1.04
Summer	25.00	41.15	26.10	29.90	30.80	64.60	4.40	19.60	23.20
Autumn	85.00	77.70	75.20	66.70	67.35	-8.59	-11.53	-21.53	-20.76
Annual	116.00	105.50	105.25	97.35	94.55	-9.05	-9.27	-16.08	-18.49

Table 6.22 : Comparison of observed and projected maximum wet spell precipitation for different RCP scenarios at different temporal scales for Palam

Temporal scale	Observed	NCEP	RCP 2.6	RCP 4.5	RCP 8.5	NCEP %	RCP 2.6%	RCP 4.5%	RCP 8.5%
January	31.00	4.05	2.60	2.75	2.70	-86.94	-91.61	-91.13	-91.29
February	22.00	3.65	3.40	2.80	2.75	-83.41	-84.55	-87.27	-87.50
March	29.00	3.05	2.80	2.35	2.35	-89.48	-90.34	-91.90	-91.90
April	19.00	3.75	2.30	2.35	2.50	-80.26	-87.89	-87.63	-86.84
May	31.00	5.10	5.70	2.95	2.95	-83.55	-81.61	-90.48	-90.48
June	30.00	8.10	4.45	4.55	4.35	-73.00	-85.17	-84.83	-85.50
July	31.00	9.30	8.50	8.30	9.65	-70.00	-72.58	-73.23	-68.87
August	31.00	9.30	13.85	14.65	9.40	-70.00	-55.32	-52.74	-69.68
September	30.00	5.40	6.70	5.20	4.50	-82.00	-77.67	-82.67	-85.00
October	30.00	5.60	3.60	3.15	2.70	-81.33	-88.00	-89.50	-91.00
November	13.00	1.90	1.35	1.45	1.45	-85.38	-89.62	-88.85	-88.85
December	11.00	2.60	1.80	1.85	1.70	-76.36	-83.64	-83.18	-84.55
Winter	32.00	5.45	3.50	3.10	3.15	-82.97	-89.06	-90.31	-90.16
Spring	41.00	5.65	5.70	3.10	3.30	-86.22	-86.10	-92.44	-91.95
Summer	92.00	10.90	14.45	14.95	10.55	-88.15	-84.29	-83.75	-88.53
Autumn	59.00	6.20	6.70	5.20	4.50	-89.49	-88.64	-91.19	-92.37
Annual	192.00	10.90	14.45	14.95	10.55	-94.32	-92.47	-92.21	-94.51

Table 6.23 : Comparison of observed and projected maximum N-Total precipitation for different RCP scenarios at different temporal scales for Palam

Temporal scale	Observed	NCEP	RCP 2.6	RCP 4.5	RCP 8.5	NCEP %	RCP 2.6%	RCP 4.5%	RCP 8.5%
January	145.1	104.9	64.8	71.6	80.0	-27.69	-55.37	-50.63	-44.86
February	52.6	53.0	43.3	56.9	48.8	0.79	-17.68	8.14	-7.27
March	28.6	56.5	35.5	31.9	64.0	97.39	23.99	11.64	123.78
April	188.8	139.1	88.2	52.4	79.2	-26.32	-53.28	-72.25	-58.03
May	100.0	74.9	56.0	49.8	49.6	-25.06	-44.00	-50.17	-50.37
June	195.2	137.6	97.8	123.7	108.6	-29.52	-49.88	-36.61	-44.37
July	281.0	188.6	175.9	177.3	169.2	-32.87	-37.40	-36.91	-39.78
August	256.4	257.3	233.9	242.3	199.7	0.34	-8.76	-5.51	-22.12
September	227.8	182.5	191.6	164.6	164.2	-19.90	-15.90	-27.76	-27.90
October	133.9	160.3	214.0	88.9	85.8	19.68	59.84	-33.63	-35.93
November	28.9	83.1	74.5	35.7	29.6	187.39	157.77	23.58	2.54
December	47.8	60.3	29.5	33.4	28.8	26.09	-38.25	-30.09	-39.76
Winter	145.1	114.7	65.8	79.2	82.7	-20.94	-54.63	-45.41	-42.98
Spring	188.8	142.1	92.4	56.4	81.6	-24.74	-51.07	-70.14	-56.78
Summer	281.0	265.1	237.3	248.8	204.5	-5.65	-15.55	-11.44	-27.24
Autumn	227.8	196.3	234.0	164.6	164.2	-13.81	2.73	-27.72	-27.90
Annual	281.0	274.4	268.6	249.2	208.5	-2.35	-4.41	-11.32	-25.81

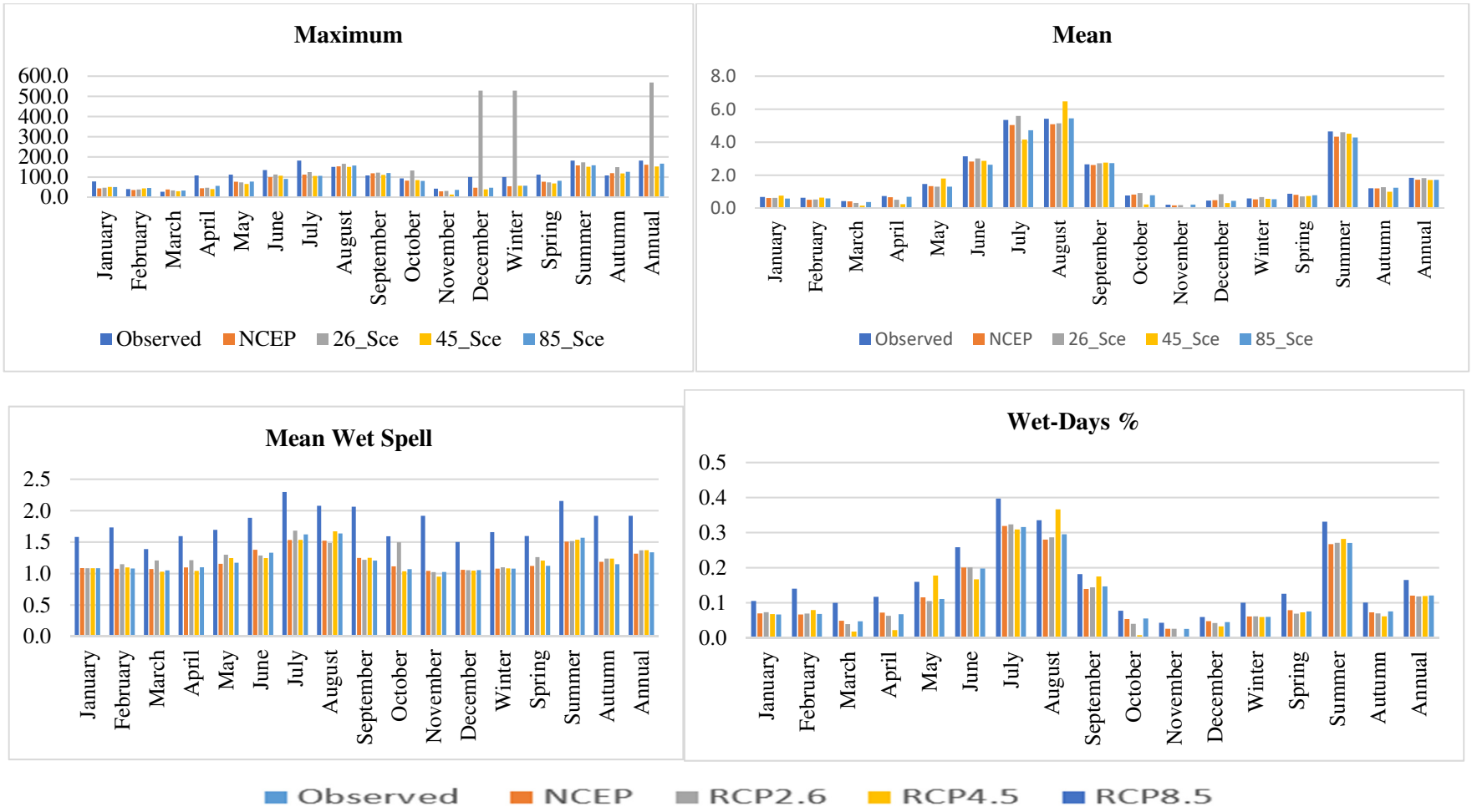

X-axis: Temporal Scales

Y-axis : Rainfall (mm)

Figure 6.18: Comparison of observed and projected rainfall for different RCP scenarios at different temporal scales for Safdarjung (1)

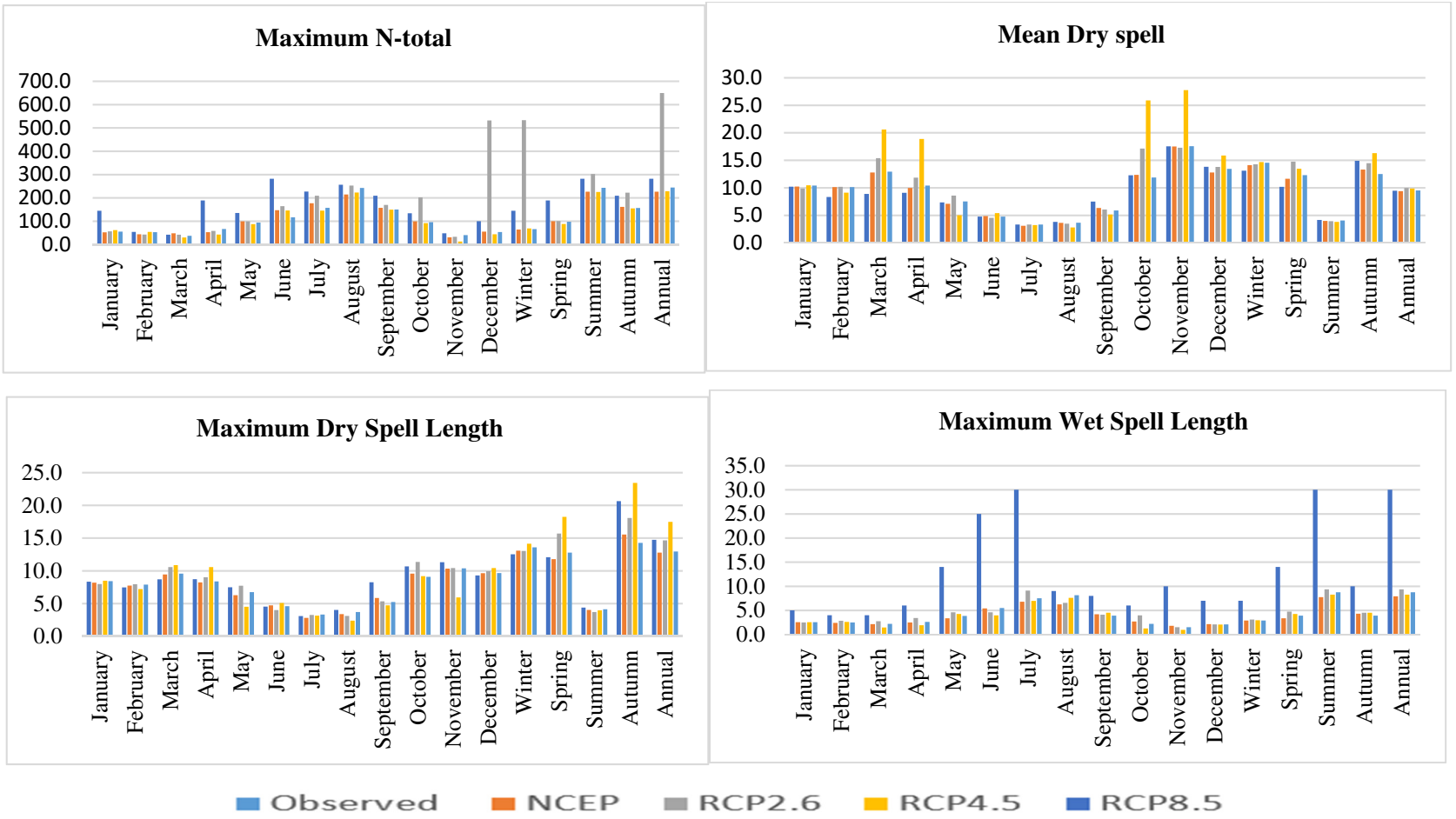

X-axis : Temporal Scales

Y-axis : Rainfall (mm)

Figure 6.19: Comparison of observed and projected rainfall for different RCP scenarios at different temporal scales for Safdarjung (2)

Similarly, for maximum wet spell length RCPs values are 14.95, 10.55 and 8.25, 8.75 with respect to observed values are 192.00 and 30.00 at Palam and Safdarjung station, respectively. Details results are shown in Table 6.21, 6.22, Annexure A6, Annexure A7, and Figure 6.17 and Figure 6.19.

While maximum total accumulated over N-days (Maximum N-day total) in both stations annual change under three RCPs (2.6, 4.5 and 8.5) and the values are 268.6, 249.2, 208.5 and 649.4, 228.34, 244.55 with respect to observed 281.0 and 282.0 in Palam and Safdarjung, respectively. Detailed results are shown in Table 6.23, Annexure A8 and Figure 6.17 and 6.19.

6.3.3 Projection of maximum and minimum temperature in different RCP scenarios

In the case of mean maximum temperature for different temporal scales monthly (January to December) and seasonal (winter, spring, summer, autumn), annual under three RCPs (2.6, 4.5 and 8.5) scenarios have been compared with the observed values in both the stations Palam and Safdarjung. In the winter season, the values are 21.93, 21.97 and 21.94 ℃ and 21.69, 21.69 and 21.65 ℃ with respect to observed 21.98 and 21.71 ℃ at Palam and Safdarjung station, respectively. Similarly, summer season, the RCPs values are 35.16, 35.20 and 35.19 ℃ and 35.29, 35.32 and 35.23 ℃ with respect to observed values 35.28 and 35.10℃. Annual mean maximum temperature under three different RCPs scenarios are 30.57, 30.60, 30.58 ℃ and 30.56, 30.56, 30.53℃ and change in percentage (-0.03, 0.06 and 0.01%) and (-0.08, -0.05 and -0.17 %) with respect to the observed values 30.58 and 30.58 ℃ in the both stations Palam and Safdarjung, respectively. Detailed results are shown in Table 6.24, Figure 6.20 and Annexure A 9 and Figure 6.22.

Mean minimum temperature for different temporal scales such as monthly (January to December), seasonal (winter, spring, summer, autumn) and annual scale under three RCPs (2.6, 4.5 and 8.5) have been compared with respect to the observed values in both stations Palam and Safdarjung. Winter season the scenarios values for three different RCPs are 9.98, 9.99 and 9.99 ℃ and 9.62, 9.61 and 9.64 ℃ with change in percentage (-0.28, -0.11 and -0.12 %) and (-0.09,-0.025 and 0.08 %) with respect to observed values are 10.0 and 9.63 ℃ for both the station Palam and Safdarjung, respectively. Similarly, summer season the scenarios values for three different RCPs the values are 27.51, 27.49 and 27.44℃ and 27.48, 27.56 and 27.47

ºC with change in percentage (0.07, -0.01 and -0.18) and (-0.32, -0.06 and -0.37)% with respect to the observed values are 27.49 and 27.57. Annual mean minimum temperature under three different RCPs values are 19.62, 19.62 and 19.60 ℃ and 19.57, 19.60 and 19.55 ºC and change in percentage (-0.13, -0.13, -0.21) and (-0.22, -0.07, -0.31) % with respect to the observed values 19.64 and 19.61 ℃ at both station Palam and Safdarjung, respectively. Detailed results are shown in Table 6.29, Figure 6.21 and Annexure A 14, Figure 6.23.

In the case of extreme maximum temperature winter season scenarios under two RCPs (4.5 and 8.5) values are 36.52, 36.69 and 34.18, 33.89ºC with respect to observed value 37.40 and 33.30 ℃ at Palam and Safdarjung, respectively. Similarly, for summer season RCPs values are 49.26, 49.42 ºC and 49.32, 49.54 ºC with respect to observed value 45.10 and 45.70 ºC for both the stations Palam and Safdarjung, respectively.

Annual extreme maximum temperature under two RCPs (4.5 and 8.5) values are 49.76, 49.89 and 49.68, 49.72 ℃ and change in percentage 8.89 and 9.16 and 8.72 and 8.80 with respect to observed value 45.70 and 45.70 ºC at Palam and Safdarjung, respectively.

In the case of extreme minimum temperature in winter season under RCP 4.5 and 8.5 scenarios are expected to 0.12, 0.09 ℃ and 0.57, 0.30 ℃ with respect to observed value 2.00 and 2.0℃ at Palam and Safdarjung, respectively. Similarly, for summer season RCPs values are 19.29, 19.43 and 19.13, 19.32 ºC with respect to observed value 12.80 and 12.80 ℃ for both the station Palam and Safdarjung, respectively. Annual extreme maximum temperature under two RCPs (4.5 and 8.5) value is 0.12, 0.09 ℃ and 0.57, 0.30 ℃ with respect to observed value 2.00 and 2.00 ℃ at Palam and Safdarjung, respectively. Detailed results are shown in Table 6.25, 6.26 6.30, 6.31, Figure 6.20, 6.21 and Annexure A 10, Annexure A 11, Annexure A 15, Annexure A 16 and Figure 6.22 & 6.23.

Maximum range of values within a given period for temperature under three RCPs (2.6, 4.5 and 8.5) annual change in values are 37.54, 37.80 and 37.45 ℃ and 36.37, 37.26 and 37.06 ºC with respect to observed values are 34.50 and 34.60ºC in both Palam and Safdarjung station, respectively. Similarly, minimum range of values within a given period and for temperature under three RCPs (2.6, 4.5 and 8.5) the values are 28.17, 28.33 and 28.10℃ and 32.59, 34.76 and 33.68ºC with respect to present climate values are 20.40 and 20.87ºC. Detailed results are shown in Table 6.27, 6.28, 6.32, 6.33 and Figure 6.20, 6.21 and Annexure A 12. Annexure A 13, Annexure A 17, Annexure A 18 and Figure 6.22 & 6.23.

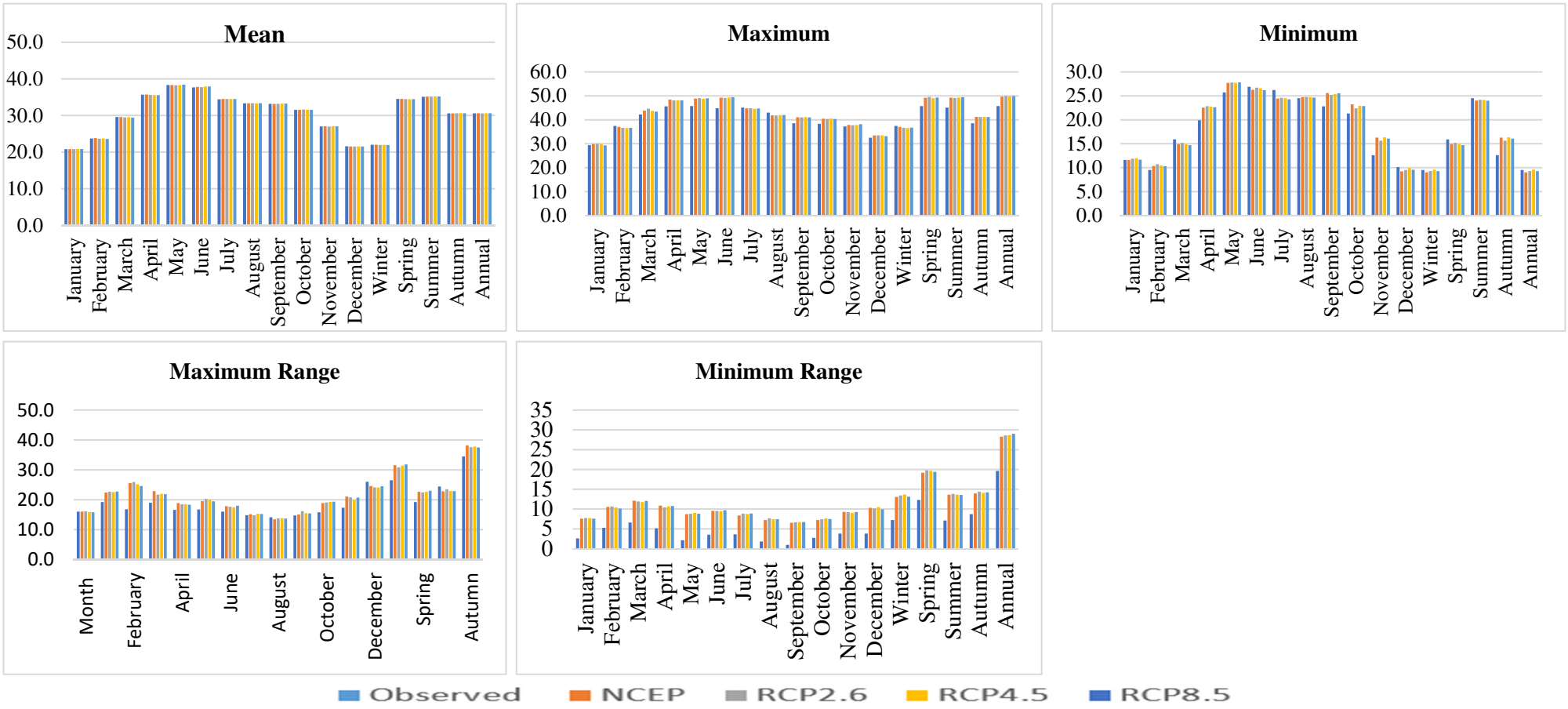

Figure 6.20: Comparison of observed and projected max. temperature (ºC) for different RCP scenarios at different temporal scale for Palam (1)

Table 6.24: Comparison of observed and projected mean maximum temperature corresponding to different RCP scenarios at different temporal scales for Palam

Temporal scale	Observed	NCEP	RCP 2.6	RCP 4.5	RCP 8.5	NCEP %	RCP 2.6%	RCP 4.5%	RCP 8.5%
January	20.81	20.81	20.79	20.83	20.84	0.01	-0.11	0.07	0.15
February	23.72	23.82	23.65	23.70	23.59	0.43	-0.28	-0.11	-0.57
March	29.56	29.56	29.48	29.52	29.41	-0.02	-0.30	-0.15	-0.53
April	35.67	35.70	35.60	35.56	35.52	0.11	-0.18	-0.31	-0.41
May	38.31	38.27	38.25	38.28	38.41	-0.09	-0.16	-0.07	0.25
June	37.67	37.80	37.73	37.89	37.88	0.34	0.16	0.57	0.56
July	34.41	34.52	34.50	34.52	34.46	0.31	0.26	0.32	0.13
August	33.31	33.29	33.34	33.29	33.33	-0.06	0.08	-0.05	0.06
September	33.16	33.14	33.17	33.23	33.24	-0.05	0.03	0.22	0.24
October	31.52	31.53	31.63	31.57	31.51	0.01	0.35	0.14	-0.04
November	27.02	27.04	26.96	27.02	27.05	0.08	-0.19	0.02	0.11
December	21.57	21.52	21.50	21.54	21.53	-0.22	-0.31	-0.13	-0.17
Winter	21.98	22.00	21.93	21.97	21.94	0.07	-0.24	-0.06	-0.20
Spring	34.50	34.50	34.43	34.44	34.43	0.00	-0.20	-0.17	-0.20
Summer	35.10	35.17	35.16	35.20	35.19	0.20	0.17	0.29	0.26
Autumn	30.58	30.58	30.60	30.62	30.61	0.01	0.08	0.14	0.10
Annual	30.58	30.60	30.57	30.60	30.58	0.07	-0.03	0.06	0.01

Table 6.25: Comparison of observed and projected extreme maximum of maximum temperature for different RCP scenarios at different temporal scales for Palam

Temporal scale	Observed	NCEP	RCP 2.6	RCP 4.5	RCP 8.5	NCEP %	RCP 2.6%	RCP 4.5%	RCP 8.5%
January	29.40	29.81	29.92	29.87	29.29	1.40	1.78	1.61	-0.38
February	37.40	37.01	36.62	36.51	36.65	-1.03	-2.07	-2.37	-2.00
March	42.20	43.80	44.65	43.70	43.42	3.78	5.81	3.56	2.88
April	45.60	48.41	48.08	48.13	48.12	6.16	5.44	5.55	5.54
May	45.70	48.85	49.06	48.75	48.95	6.90	7.35	6.67	7.12
June	44.80	49.21	49.09	49.26	49.42	9.84	9.58	9.95	10.32
July	45.10	44.76	44.83	44.53	44.70	-0.76	-0.59	-1.26	-0.89
August	43.00	41.84	41.79	41.93	41.97	-2.69	-2.80	-2.48	-2.40
September	38.50	41.05	41.00	41.09	41.00	6.63	6.49	6.72	6.49
October	38.30	40.38	40.32	40.47	40.32	5.44	5.28	5.67	5.28
November	37.20	37.86	37.67	37.78	38.17	1.77	1.28	1.56	2.62
December	32.50	33.45	33.49	33.48	33.14	2.93	3.05	3.01	1.97
Winter	37.40	37.01	36.64	36.52	36.69	-1.03	-2.02	-2.35	-1.90
Spring	45.70	49.14	49.51	48.99	49.28	7.54	8.33	7.19	7.84
Summer	45.10	49.21	49.09	49.26	49.42	9.11	8.85	9.22	9.58
Autumn	38.50	41.20	41.16	41.22	41.14	7.02	6.91	7.06	6.86
Annual	45.70	49.63	49.88	49.76	49.89	8.60	9.14	8.89	9.16

Table 6.26: Comparison of observed and projected extreme minimum of maximum temperature for different RCP scenarios at different temporal scales for Palam

Temporal scale	Observed	NCEP	RCP 2.6	RCP 4.5	RCP 8.5	NCEP %	RCP 2.6%	RCP 4.5%	RCP 8.5%
January	11.60	11.61	11.87	11.98	11.66	0.12	2.37	3.28	0.49
February	9.50	10.35	10.72	10.46	10.29	8.97	12.85	10.10	8.28
March	15.90	14.90	15.18	14.88	14.69	-6.29	-4.54	-6.40	-7.59
April	19.90	22.53	22.83	22.75	22.61	13.21	14.74	14.32	13.61
May	25.70	27.71	27.79	27.73	27.81	7.81	8.12	7.91	8.22
June	26.90	26.26	26.71	26.58	26.18	-2.37	-0.71	-1.18	-2.69
July	26.20	24.43	24.58	24.49	24.27	-6.77	-6.20	-6.51	-7.38
August	24.50	24.72	24.76	24.72	24.65	0.88	1.07	0.88	0.60
September	22.80	25.57	25.17	25.36	25.54	12.16	10.41	11.24	12.01
October	21.30	23.21	22.37	22.92	22.85	8.99	5.03	7.59	7.27
November	12.60	16.26	15.63	16.31	16.05	29.07	24.08	29.47	27.42
December	10.10	9.23	9.52	9.91	9.56	-8.64	-5.77	-1.92	-5.38
Winter	9.50	9.01	9.28	9.58	9.26	-5.19	-2.27	0.86	-2.55
Spring	15.90	14.90	15.18	14.88	14.69	-6.29	-4.54	-6.40	-7.59
Summer	24.50	24.01	24.16	24.13	23.97	-1.99	-1.39	-1.49	-2.16
Autumn	12.60	16.26	15.63	16.31	16.05	29.07	24.08	29.47	27.42
Annual	9.50	9.01	9.28	9.58	9.26	-5.19	-2.27	0.86	-2.55

Table 6.27: Comparison of observed and projected maximum range of maximum temperature for different RCP scenarios at different temporal scales for Palam.

Temporal scale	Observed	NCEP	RCP 2.6	RCP 4.5	RCP 8.5	NCEP %	RCP 2.6%	RCP 4.5%	RCP 8.5%
January	16.00	16.01	16.07	15.82	15.80	0.07	0.46	-1.13	-1.25
February	19.20	22.38	22.70	22.56	22.71	16.55	18.22	17.48	18.29
March	16.80	25.56	25.93	25.18	24.59	52.13	54.36	49.86	46.37
April	19.00	22.87	21.73	21.98	21.85	20.36	14.39	15.71	14.98
May	16.60	18.86	18.47	18.47	18.31	13.61	11.27	11.28	10.28
June	16.70	19.54	20.25	20.03	19.43	17.03	21.23	19.96	16.37
July	16.00	17.80	17.65	17.41	17.99	11.24	10.34	8.83	12.41
August	14.80	15.17	14.78	15.31	15.22	2.51	-0.16	3.42	2.87
September	14.10	13.45	13.72	13.72	13.69	-4.61	-2.71	-2.70	-2.92
October	14.70	15.05	16.17	15.48	15.40	2.38	9.99	5.30	4.77
November	15.80	18.85	19.05	19.24	19.32	19.29	20.59	21.76	22.26
December	17.30	21.06	20.81	19.92	20.72	21.73	20.30	15.13	19.78
Winter	26.00	24.58	24.11	24.06	24.49	-5.48	-7.26	-7.47	-5.81
Spring	26.50	31.54	30.83	31.37	31.80	19.00	16.34	18.39	20.00
Summer	19.20	22.64	22.45	22.65	22.96	17.89	16.91	17.96	19.57
Autumn	24.40	22.79	23.50	22.88	22.85	-6.60	-3.70	-6.23	-6.36
Annual	34.50	38.14	37.54	37.80	37.45	10.55	8.81	9.58	8.56

Table 6.28: Comparison of observed and projected minimum range of maximum temperature for different RCP scenarios at different temporal scales for Palam Station

Temporal scale	Observed	NCEP	RCP 2.6	RCP 4.5	RCP 8.5	NCEP %	RCP 2.6%	RCP 4.5%	RCP 8.5%
January	2.60	7.57	7.73	7.68	7.57	191.32	197.43	195.31	191.15
February	5.24	10.53	10.64	10.39	10.08	100.93	103.08	98.36	92.45
March	6.59	12.09	11.89	11.75	12.03	83.51	80.49	78.35	82.59
April	5.10	10.87	10.41	10.65	10.77	113.12	104.15	108.80	111.21
May	2.10	8.71	8.80	9.03	8.80	314.71	318.93	330.14	319.28
June	3.50	9.52	9.48	9.42	9.69	172.09	170.96	169.22	176.96
July	3.60	8.36	8.84	8.73	8.86	132.26	145.42	142.46	146.11
August	1.78	7.21	7.67	7.41	7.42	305.05	330.85	316.11	316.79
September	0.94	6.50	6.66	6.70	6.69	591.45	608.13	612.88	611.82
October	2.70	7.22	7.41	7.62	7.45	167.36	174.47	182.29	175.96
November	3.80	9.28	9.22	9.02	9.25	144.19	142.69	137.32	143.50
December	3.80	10.27	10.13	10.46	9.92	170.31	166.52	175.37	160.97
Winter	7.20	13.03	13.41	13.64	13.10	81.00	86.27	89.44	81.92
Spring	12.30	19.17	19.75	19.65	19.39	55.85	60.60	59.77	57.61
Summer	7.10	13.63	13.82	13.61	13.55	91.90	94.61	91.69	90.87
Autumn	8.70	13.93	14.38	14.09	14.21	60.15	65.32	61.95	63.37
Annual	19.60	28.27	28.56	28.69	28.98	44.25	45.73	46.36	47.87

Table 6.29: Comparison of observed and projected mean minimum temperature for different RCP scenarios at different temporal scales for Palam

Temporal scale	Observed	NCEP	RCP 2.6	RCP 4.5	RCP 8.5	NCEP %	RCP 2.6%	RCP 4.5%	RCP 8.5%
January	8.96	8.95	8.92	9.00	9.02	-0.19	-0.46	0.39	0.67
February	11.70	11.75	11.67	11.65	11.58	0.41	-0.27	-0.38	-1.00
March	16.71	16.69	16.59	16.68	16.51	-0.12	-0.70	-0.17	-1.16
April	22.36	22.39	22.28	22.33	22.25	0.11	-0.38	-0.15	-0.49
May	26.17	26.16	26.11	25.97	26.14	-0.04	-0.24	-0.74	-0.12
June	28.12	28.19	28.17	28.26	28.13	0.25	0.18	0.52	0.03
July	27.53	27.56	27.53	27.46	27.50	0.10	0.01	-0.26	-0.10
August	26.85	26.87	26.85	26.77	26.73	0.06	0.01	-0.29	-0.46
September	24.67	24.76	24.64	24.78	24.69	0.37	-0.10	0.47	0.10
October	19.33	19.49	19.36	19.22	19.32	0.87	0.18	-0.56	-0.05
November	13.43	13.47	13.41	13.40	13.43	0.33	-0.11	-0.16	0.05
December	9.50	9.52	9.49	9.47	9.51	0.26	-0.11	-0.29	0.11
Winter	10.00	10.02	9.98	9.99	9.99	0.18	-0.28	-0.11	-0.12
Spring	21.74	21.74	21.65	21.65	21.63	-0.01	-0.40	-0.39	-0.52
Summer	27.49	27.53	27.51	27.49	27.44	0.14	0.07	-0.01	-0.18
Autumn	19.14	19.24	19.14	19.14	19.15	0.53	-0.01	-0.03	0.04
Annual	19.64	19.68	19.62	19.62	19.60	0.20	-0.13	-0.13	-0.21

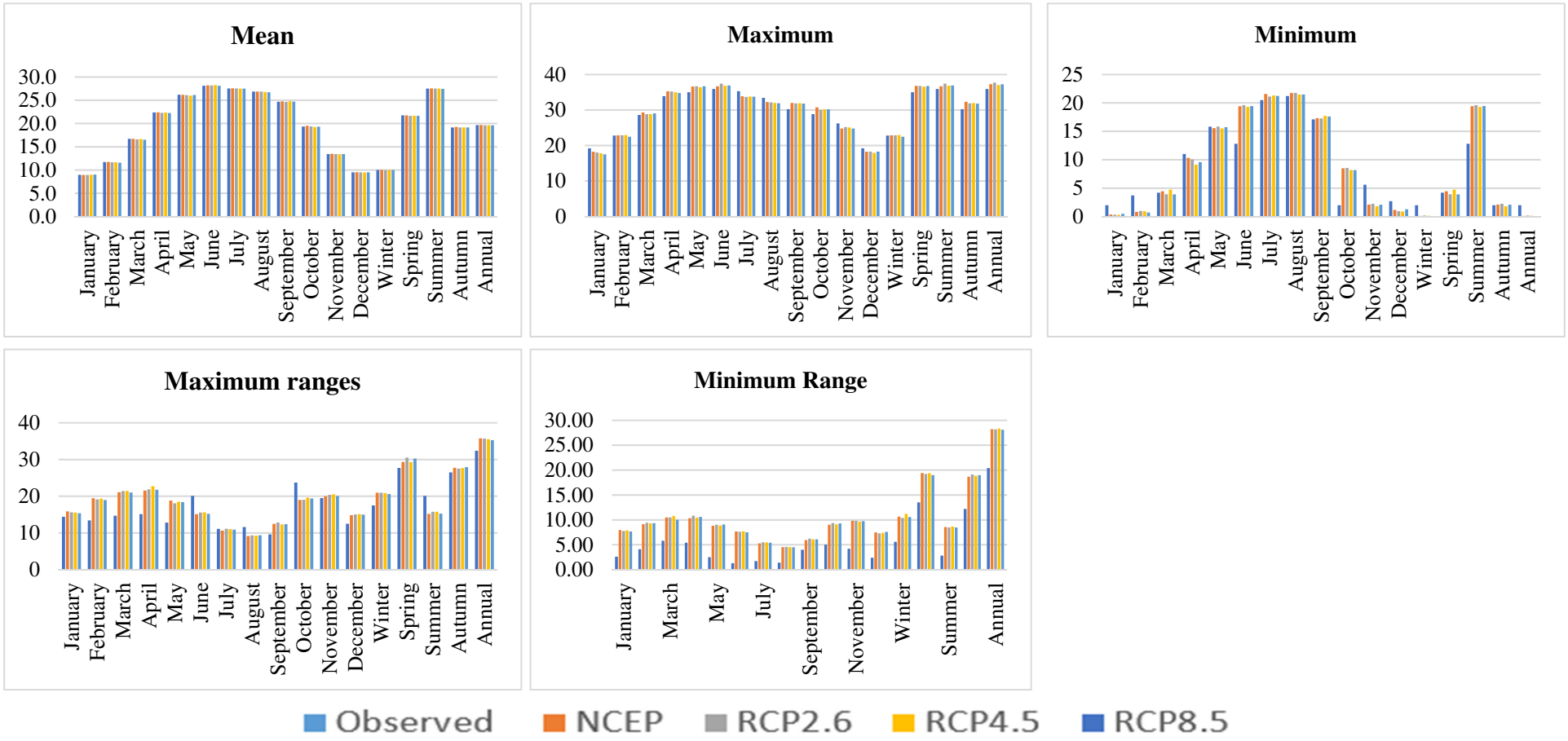

X-axis : Temporal Scales

Y-axis : Temperature (°C)

Figure 6.21: Comparison of observed and projected minimum temperature (°C) for different RCP scenarios at different temporal scales for Palam (2)

Table 6.30: Comparison of observed and projected extreme maximum of minimum temperature for different RCP scenarios at different temporal scales for Palam

Temporal scale	Observed	NCEP	RCP 2.6	RCP4.5	RCP 8.5	NCEP%	RCP 2.6%	RCP 4.5%	RCP 8.5%
January	19.20	18.26	18.02	17.82	17.52	-4.92	-6.17	-7.21	-8.74
February	22.80	22.89	22.85	22.93	22.47	0.38	0.24	0.57	-1.46
March	28.60	29.30	28.83	28.83	29.02	2.46	0.80	0.80	1.48
April	33.90	35.26	35.20	34.97	34.78	4.00	3.82	3.16	2.61
May	35.00	36.59	36.68	36.39	36.67	4.54	4.81	3.98	4.78
June	35.90	36.69	37.40	36.83	36.90	2.20	4.17	2.58	2.78
July	35.30	33.86	33.66	33.78	33.72	-4.08	-4.66	-4.32	-4.47
August	33.40	32.24	32.14	31.99	31.91	-3.48	-3.78	-4.23	-4.47
September	30.20	31.99	31.86	31.89	31.80	5.92	5.50	5.61	5.31
October	28.80	30.74	29.95	30.16	30.17	6.74	3.99	4.71	4.76
November	26.20	24.78	25.18	25.06	24.78	-5.41	-3.87	-4.36	-5.42
December	19.20	18.24	18.27	17.92	18.28	-4.98	-4.83	-6.67	-4.80
Winter	22.80	22.89	22.85	22.93	22.47	0.38	0.24	0.57	-1.46
Spring	35.00	36.81	36.75	36.58	36.76	5.16	5.00	4.51	5.03
Summer	35.90	36.69	37.40	36.83	36.90	2.20	4.17	2.58	2.78
Autumn	30.20	32.30	31.86	31.95	31.80	6.96	5.50	5.81	5.31
Annual	35.90	37.28	37.72	37.01	37.24	3.84	5.08	3.10	3.72

Table 6.31: Comparison of observed and projected extreme minimum of minimum temperature (°C) for different RCP scenarios at different temporal scales for Palam

Temporal scale	Observed	NCEP	RCP 2.6	RCP 4.5	RCP 8.5	NCEP %	RCP 2.6%	RCP 4.5%	RCP 8.5%
January	2.00	0.35	0.32	0.30	0.48	-82.43	-84.22	-85.23	-76.14
February	3.70	0.81	0.99	0.93	0.69	-78.15	-73.30	-74.89	-81.29
March	4.20	4.45	3.92	4.72	3.89	5.93	-6.67	12.40	-7.47
April	11.00	10.31	10.05	9.13	9.56	-6.25	-8.65	-16.98	-13.13
May	15.80	15.55	15.84	15.50	15.72	-1.61	0.22	-1.90	-0.50
June	12.80	19.41	19.60	19.29	19.43	51.65	53.12	50.71	51.81
July	20.50	21.57	21.11	21.29	21.22	5.20	2.97	3.85	3.51
August	21.20	21.74	21.76	21.45	21.47	2.53	2.64	1.18	1.27
September	17.10	17.30	17.25	17.71	17.60	1.18	0.89	3.58	2.93
October	2.00	8.49	8.54	8.19	8.15	324.60	327.23	309.61	307.74
November	5.60	2.11	2.24	1.80	2.08	-62.36	-59.93	-67.93	-62.91
December	2.70	1.15	0.93	0.89	1.27	-57.26	-65.66	-67.10	-53.04
Winter	2.00	0.11	0.18	0.12	0.09	-94.61	-91.10	-93.85	-95.68
Spring	4.20	4.45	3.92	4.72	3.89	5.93	-6.67	12.40	-7.47
Summer	12.80	19.41	19.59	19.29	19.43	51.65	53.07	50.71	51.81
Autumn	2.00	2.11	2.24	1.80	2.08	5.39	12.20	-10.19	3.85
Annual	2.00	0.11	0.17	0.12	0.09	-94.61	-91.47	-93.85	-95.68

Table 6.32: Comparison of observed and projected maximum range of minimum temperature for different RCP scenarios at different temporal scales for Palam

Temporal scale	Observed	NCEP	RCP 2.6	RCP 4.5	RCP 8.5	NCEP %	RCP 2.6%	RCP 4.5%	RCP 8.5%
January	14.40	15.84	15.63	15.53	15.36	10.03	8.51	7.85	6.65
February	13.40	19.44	19.12	19.33	18.95	45.06	42.69	44.26	41.43
March	14.70	21.08	21.39	21.45	21.02	43.41	45.51	45.91	42.98
April	15.10	21.55	21.85	22.71	21.77	42.72	44.69	50.40	44.19
May	12.80	18.82	18.06	18.48	18.36	47.03	41.09	44.36	43.47
June	20.10	15.12	15.55	15.60	15.18	-24.77	-22.64	-22.41	-24.49
July	11.10	10.64	11.14	11.04	10.89	-4.16	0.33	-0.58	-1.85
August	11.60	9.14	9.32	9.25	9.36	-21.24	-19.64	-20.26	-19.35
September	9.60	12.44	12.85	12.30	12.37	29.60	33.83	28.11	28.90
October	23.70	18.97	19.00	19.64	19.37	-19.95	-19.81	-17.14	-18.28
November	19.50	19.99	20.36	20.53	20.05	2.51	4.42	5.28	2.83
December	12.50	14.82	15.03	15.10	14.96	18.59	20.23	20.81	19.64
Winter	17.50	20.93	20.94	20.83	20.58	19.60	19.68	19.01	17.61
Spring	27.70	29.31	30.49	29.29	30.25	5.81	10.06	5.76	9.20
Summer	20.10	15.17	15.75	15.74	15.24	-24.51	-21.64	-21.72	-24.18
Autumn	26.50	27.72	27.50	27.67	27.91	4.59	3.78	4.43	5.32
Annual	32.40	35.76	35.68	35.50	35.27	10.36	10.12	9.57	8.87

Table 6.33: Comparison of observed and projected minimum range of minimum temperature for different RCP scenarios at different temporal scales for Palam

Temporal scale	Observed	NCEP	RCP 2.6	RCP 4.5	RCP 8.5	NCEP %	RCP 2.6%	RCP 4.5%	RCP 8.5%
January	2.60	7.94	7.77	7.87	7.66	205.33	198.69	202.78	194.61
February	4.10	9.14	9.42	9.28	9.33	122.85	129.88	126.30	127.51
March	5.80	10.49	10.48	10.77	10.01	80.89	80.76	85.61	72.64
April	5.40	10.33	10.82	10.45	10.59	91.23	100.36	93.43	96.07
May	2.50	8.81	9.03	8.86	9.08	252.37	261.05	254.29	263.18
June	1.30	7.65	7.62	7.69	7.50	488.57	486.03	491.43	476.78
July	1.70	5.27	5.48	5.46	5.41	210.05	222.23	221.38	218.01
August	1.40	4.52	4.58	4.52	4.48	222.50	227.15	222.98	220.30
September	4.00	5.93	6.21	6.08	6.09	48.24	55.27	52.04	52.16
October	5.00	9.03	9.36	9.09	9.29	80.58	87.24	81.84	85.78
November	4.20	9.81	9.81	9.66	9.72	133.60	133.69	129.88	131.48
December	2.40	7.47	7.30	7.39	7.58	211.33	204.11	207.99	215.93
Winter	5.60	10.64	10.38	11.20	10.57	90.06	85.36	100.06	88.67
Spring	13.50	19.41	19.21	19.37	18.99	43.74	42.33	43.46	40.64
Summer	2.80	8.54	8.48	8.64	8.46	205.13	202.70	208.66	202.28
Autumn	12.20	18.66	19.10	18.85	18.99	52.93	56.58	54.52	55.65
Annual	20.40	28.20	28.17	28.33	28.10	38.23	38.10	38.88	37.73

6.4 CONCLUDING REMARKS

In the present study, the trends in mean and extreme events of total rainfall and average temperature (seasonal/annual) were analysed using MK and MMK test for national capital territory Delhi region in India. The Sen's slope, percentage changes and shift detection were estimated in rainfall and temperature. The trend analysis results revealed that average temperature (i.e. minimum, average and maximum) shows increasing trend (@ 0.008 to 0.05^{o}C/year) in most of the temporal scales. The total rainfall has shown significant increasing trends in the winter season (@ 0.82 mm/hydrologic year) at Palam station as well as spring season (@ 2.02 mm/hydrologic year) at Safdarjung station. Similarly, total rainfall has shown a significant decreasing trend in Safdarjung meteorological station (@ -3.31 mm/hydrologic year). The extreme annual daily minimum temperature has shown significant increasing trends (@0.015^{o}C to 0.0022^{o}C/year) in Palam and Safdarjung station, respectively. However, significant trends were not found in the case of maximum temperature, at both stations of Delhi region in the northern part of India.

Similarly, in case of non-monsoon, the significant increasing trend has been shown in maximum temperature (@0.0027^{o}C/year) and the significant decreasing trend has been shown in autumn season (@-0.093^{o}C/year) at Palam metrological station. Similarly, in Safdarjung station increasing or decreasing trend has been found but not significant were not found in the case of maximum temperature except spring season. The extreme annual daily minimum and maximum temperature in these stations were found to be -2.0 to 6.7^{o}C and 40.0 to 47.5^{o}C, respectively. While extreme maximum and minimum annual daily rainfall found to be 1145.35 mm and 176.4 mm respectively at Delhi reason.

The results of Sen's slope and percentage change of mean and extreme average rainfall and temperature (annual/seasonal) has shown predominant changes in Delhi region. Significant warming in minimum temperatures was associated with a dominant LULC conversion of forest to urban and barren land to urban cover at nearly twice the rate expected from chance alone. This conversion type also was strongly associated with significant warming in maximum temperatures. While there is a strong correlation between increases in temperature trends at normal stations and nearby LULC changes, this does not necessarily imply that the LULC changes are the causative factor. The assessment of average and extreme events of rainfall and temperature are necessary for preparation of suitable adaptation strategies in uncertain changing climate and extreme weather events.

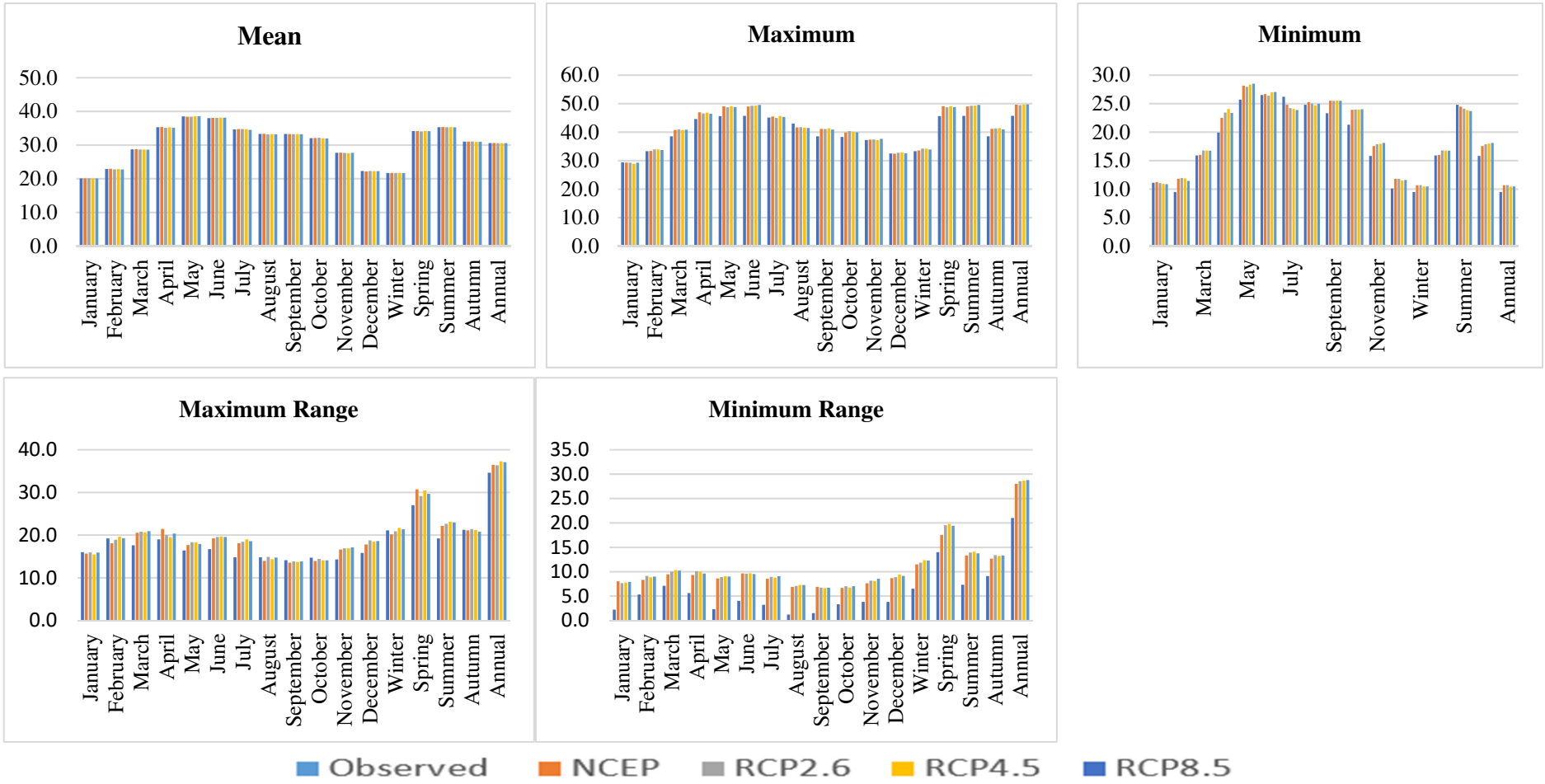

X-axis : Temporal Scales

Y-axis : Temperature (oC)

Figure 6.22: Comparison of observed and projected maximum temperature (°C) for different RCP scenarios at different temporal scales for Safdarjung (1)

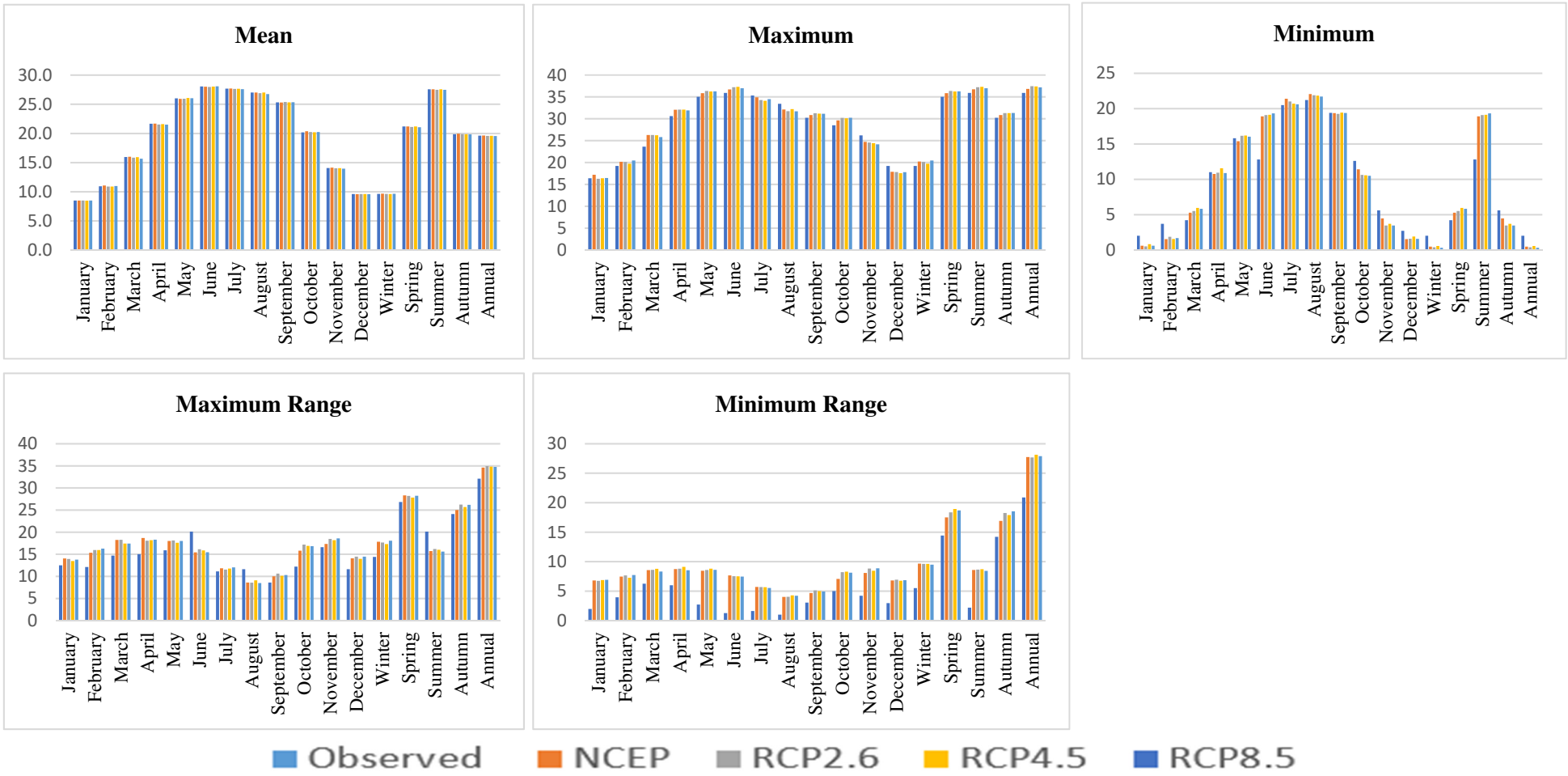

X-axis : Temporal Scales Y-axis : Temperature (°C)

Figure 6.23: Comparison of observed and projected minimum temperature (°C) for different RCP scenarios at different temporal scales for Safdarjung (2)

This will provide information to the policy makers, hydrologists and water resources planners regarding the climate change in Delhi region in the northern part of India for the sustainable development and planning the resources.

Public awareness of climate change and extreme events has increased sharply across the world recently but knowledge of climate change is still insufficient (Souch and Grimmond, 2006). This work presents future projections of climate change (i.e. temperature and precipitation) in the Delhi region over the 21st century from the CMIP5 model under three RCPs (2.6, 4.5 and 8.5) emission scenarios using SDSM. Change of extreme temperature and precipitation are addressed for a better understanding of future changes in climate extremes of this region. Although the automated procedures such as stepwise multiple regressions are helpful in identifying best predictors in the downscaling study, it is still hard to select physical variables. For instance, specific humidity does not always correlate strongly with precipitation in the present climate, but is expected to change considerably with climate and will significantly affect future precipitation scenarios (Charles et al., 1999). However, capability in modelling drought indices like the maximum number of consecutive dry days was insufficient. Because the extreme precipitation events always occur under the condition of abnormal climate in special terrain, the ability to simulate heavy rainfall should be improved if the terrain factors can be considered in SDSM. This provided an essential need for the model improvement. For most precipitation and evaporation related indices, the performance in summer was worse than in winter. This was partly because the study region is dominated by local climate processes in summer, when statistical links between the large-scale predictors and the local climate variables are weak (Toggweiler and Key, 2001). Meanwhile, the predictors in this study were selected at annual scale. (Fealy and Sweeney, 2008) indicated that there is a strong seasonal consistency for a number of predictors (e.g. geopotential heights and humidity), while the seasonal specific predictors also play an important role (e.g. surface divergence during the summer months). So the predictors selected at seasonal scale (or month scale) may improve the downscaling performance to some extent in summer. Bias correction for the single GCM as well as the development of SDSM predictor data sets from other GCMs is helpful in dealing with these issues to generate more reliable projections in response to future climate change.

Projection of precipitation in the 21st century (2011–2099) indicated a decreased in the monsoon precipitation and shifted toward the winter side with respect to the present climate. Annual maximum precipitation in both stations shows a downward trend in three

RCPs with a negative value of the change in percentage with respect to the observed values. An average number of wet days (%) changes in scenarios compared results show that Wet days (%) in Palam and Safdarjung are decreased from the present situation. Mean Dry Spell average length of spells with amounts less than the wet-day threshold future projected values is highest and Mean wet Spell is lowest with respect to observed values. It means to develop the situation of drought in future. Projection of temperature daily mean of maximum temperature and daily mean minimum temperature under three RCPs the change in percentage is a negative sign its shows decreasing trend in the 21st century (2011–2099). Extreme Temp (Max) summer season scenarios under two RCPs (4.5 and 8.5) RCPs values are (49.26, 49.42) ^{o}C and (49.32, 49.54) ^{o}C with respect to observed value 45.10 and 45.70 ^{o}C for both the station Palam and Safdarjung, respectively. Extreme Temperature (Min) summer season RCPs values are 19.29, 19.43 and 19.13, 19.32 ^{o}C with respect to observed value 12.80 and 12.80℃ for both the station Palam and Safdarjung, respectively. In the case of extreme values the minimum and maximum in both areas are increased with respect to observed values. The simultaneously significant increases trend in the found in the minimum and maximum ranges of the temperature in both station under three RCPs.

Various changes in these variables were projected over summer and autumn season. The projected changes in temperature were likely to impact the hydrological processes in the study area. The projections of precipitation extremes were not consistent with temperature extremes. Seasonal precipitation and most precipitation extremes showed consistency among various seasons except in summer and monsoon. In autumn, when the significant increase in mean and extreme precipitation the intensity of the autumn floods may be intensified in future.

CHAPTER 7

LAND USE LAND COVER CHANGE AND SURFACE ENERGY BALANCE

7.1 INTRODUCTION

The demand of development have caused rapid changes in LULC and this is still going on. With the increase in population and industrialization lot of waste land & forest areas have been converted into agriculture land and put under built-up activities. Such LULC change are more in urban areas causing severe stress on natural resources and climate. Rapid urbanization has contributed to change in local and regional scale meteorology significantly. LULC transition will have an impact on the surface energy balance through the alteration of surface properties affecting net all-wave radiation and heat storage, and consequently affects local climate (Oke, 1988). Understanding the relationship between urbanization and micro-climate is necessary for urban environmental planning to determine effective design strategies, e.g. altering the land use like vegetation and irrigation regime, in order to improve the urban climate. The knowledge of how to purposefully manipulate the SEB by changing urban land cover is crucial to urban climate adaptation. Very limited investigations (Morris *et al.*, 2015; Morris and Deavin, 2016) have been performed to establish a relationship between LULC changes and micro-climate representing surface energy fluxes (Omran, 2012; Deng et. al., 2013). Various models are available, as discussed in Chapter 5, which can simulate the climate of urban areas but lacks a better description of the factors affecting the energy partitioning into sensible and latent heat fluxes. Recently, to overcome such limitation, SUEWS (Surface Urban Energy and Water Balance Model) model has been developed which simulates both energy and water fluxes (Järvi, et al., 2011). Unlike other models, SUEWS model requires relatively less input data which are available and can provide results of surface energy balance at the local scale. SUEWS model has been discussed in detail in Chapter 5.

Therefore, in the present study, an attempt has been made to conceptualize SUEWS model for selected study areas to model the surface energy balance (SEB) in different scenarios of LULC changes over a period of 41 years i.e., 1973 to 2014. Change in SEB components indirectly indicates changes in micro-climate of the areas. Details of input data used in the present study have been discussed in Chapter 3 and Chapter 4. The SUEWS model has been conceptualized and parameterized to simulate the surface energy balance. Model sensitivity analysis has been performed to determine the sensitivity of the model results to constants/coefficients and few selected model variables. The model has been

calibrated through an iterative procedure in which model was run for no. of times corresponding to a range of different values of selected model parameters and results were compared with observed hourly data of SEB fluxes of summer 1999. Validation of the model has been performed by comparing SEB components obtained from the calibrated model and observed hourly data of SEB fluxes for selected sites of Delhi for summer 1999 and seasonal maximum & minimum values of SEB fluxes for summer and winter seasons of the year 1998 & 1999. Further, to investigate the influence of LULC characteristics on micro-climate in term of change in SEB fluxes, three scenarios have been proposed, as discussed in Chapter 5. In the first Scenario (Scenario-A), SUEWS model is conceptualized for actual conditions i.e., actual LULC and meteorology are considered in the model for different years. In Scenario-B, the influence of a change in LULC is considered by considering constant meteorology corresponding to base year i.e., 1973 and LULC of different years. This case has been proposed to determine the relative impact of the change in LULC over the years on the surface energy fluxes for the study areas. In Scenario-C, the influence of climate change forcing other than LULC change have been conceptualized by considering constant LULC of the base year (1973) and meteorology of respective years. The relative difference in SEB fluxes in Scenario-B and C represents the change in different surface energy balance over the years as compared to the base year due to change in LULC characteristics. To determine the quantitative relationship between relative change in LULC fractions and their effect on SEB, linear and non-linear regression analysis has been performed. Detailed results of the SEB modelling have been discussed in subsequent sections of this Chapter.

7.2 CONCEPTUALIZATION OF SUEWS MODEL

In SUEWS model, it is very important to extract each input variable for the selected study area. The SUEWS has been conceptualized through parameterization of model with the required input data of the study areas in a suitable format. In addition to the study area characteristics, LULC information and hourly meteorological data, other model coefficients have been adopted from the literature, as mentioned in Table 7.1. The details of the model conceptualization have been discussed in subsequent sections. Few model parameters have been adopted from the reference literature, as suggested by the model developers and mentioned in Model Manual (Grimmond et al., 2011; Järvi, Grimmond and Christen, 2011; Järvi et al., 2014). Model input parameters have been selected from above mentioned literature as per the study area characteristics.

7.2.1 Land Use and Land Cover Information

The SUEWS model requires fractional LULC information for the study area. LULC fractions for respective years have been provided to the model for different LULC classes. Preparation of LULC maps has been discussed in detail in Chapter 4. Different LULC classes found in the area and supplied to model are built-up areas (settlement), paved surfaces, trees, forest, irrigated and non-irrigated surfaces.

Table 7.1 : Important input parameter values for the conceptualization of model for the study area

S. No.	Input Parameters	Used for	Assigned Values	References
1	Interval	Results	60 min	Recommended by SUEWS model literature
2	Wind speed is measured at Height	Input Data	22.5 m	Gomathinayagam and Harikrishna, 2009
3	Growing degree days for leaf) Base GDD = 5 (°C) Or (41 F)	Calculation of Leaf Area Index	300 (°C)	Jarvi et al. 2011
4	Growing degree days for senescence growth Needs to be a negative number or 0	Calculation of Leaf Area Index	0 (°C)	Jarvi et al. 2011
5	Leaf area index initial coniferous forest	Water Use	5.23 (m2 m-2)	Champion and Seth, 1968; Asner and Scurlock, 2003
6	Leaf area index initial Deciduous forest	Water Use	5.23 (m2 m-2)	Champion and Seth, 1968; Asner and Scurlock, 2003
7	LAI initial irrigated grass	Water Use	1.6 (m2 m-2)	Everitt and Ritchie, 2003
8	Porosity of deciduous vegetation	Evaporation	0.05 No unit	Chianucci and Cutini, 2013
9	Mean building height	(m)	15.9	MCD Delhi
10	Mean tree height	(m)	15	Forest Dept. Delhi
11	Altitude mean topographic height	(m)	233 (Palam) 216 (Safdarjung)	(IMD, 2005)

7.2.2 Meteorological Parameters

Hourly meteorological data such as air temperature, air pressure, wind speed, relative humidity and precipitation along with incoming solar radiation have been provided to the model. Details of the data used have been discussed in Chapter 3.

7.2.3 Additional Important Input Parameters

The model was fully parameterized using measured data for the study areas and from the references available from the literature. Some model input parameters which have not been available for the study area are adopted from the literature as suggested by the Model developers (Jarvi et. al., 2011, 2014). Drainage equations, coefficients and vegetation canopy cover have been specified in the input files based on the recent literature for the Delhi (Das et. al., 2009, 2014). Information related to outdoor water usage for irrigation has been adopted from the Delhi Jab Board website and official circulars. As per the available information, most of the outdoor water usage such as lawn irrigation is done from April to mid-June and least usage have been reported from August to November. Outdoor water usage is required for evapotranspiration calculations within the model. According to the survey, Delhi comes under Level 0 category of the model. Level 0 represents 'Careful Use' of water supplies based on no serious storage, rainfall or stream flow. Delhi has limited water supply and the hours of water supply in a day are restricted. In most of the areas in Delhi, water is supplied (obtained from Delhi Jal Board) in two slots that are 6-8 am and 6-8 pm. The SUEWS model accounts for the movement of water in both vertical and horizontal direction. Storm water generated during the rainy season has been collected and drained off through storm water drainage system.

According to survey and information available in the literature, 71% of runoff generated from buildings is disposed to Lawns, 14 % of precipitation is directed to the roadways and 15 % discharged directly into the storm drainage network. In case of paved surfaces, 96% of the precipitation is discharged into drainage system as surface runoff and 4% is discharged on grass areas. A major portion of the surface runoff generated from areas having grass or dense vegetation infiltrated into the underlying soil. Surface runoff generated from buildings, paved, trees and grass surfaces have been used in the calculation in the model in term of runoff coefficient. Population density has been calculated for different years based on decadal population information and used in the model for calculating anthropogenic heat flux. Population growth and related information have been presented in Table 7.2.

Table 7.2 : Population density for Palam and Safdarjung areas

Year	Population density for Palam (persons per hectare)	Population density for Safdarjung (persons per hectare)
1973	12	26
1977	14	30
1986	28	43
1991	33	48
1998	49	65
1999	49	65
2002	53	68
2006	59	71
2009	64	73
2011	66	75
2013	70	77
2014	72	79

7.3 SENSITIVITY ANALYSIS

The purpose of sensitivity analysis is to determine the model sensitivity with model coefficients and variables. Sensitivity analysis helps in determining the level of uncertainties in the model results due to uncertainties of model coefficients and variables. Sensitivity analysis has been performed by altering the values of selected model parameters within a range of ±40% from the base value, iteratively. Each selected parameter has been changed within the range keeping other parameters at the base value and SEB has been simulated respectively. Analysis has been carried out for the one study area i.e., Palam out of two considered in the study i.e., Palam and Safdarjung for the year 1999 for two seasons (summer and winter). Parameters selected for sensitivity analysis are albedo, emissivity, drainage, maximum conductance, conductance parameters, storage capacity minimum, and storage capacity maximum. The model has been run for a number of times in continuous simulation mode for each selected parameters. At a given time, the value of one parameter has been changed sequentially, while other parameters are kept constant. We have also tried for other inputs parameters but not found any significant changes in the outputs components of the heat fluxes other than above selected parameters. Detailed theoretical information about the sensitivity analysis has been discussed in Chapter 5. Sensitivity of the model have been determine as % change in model response (change in SEB fluxes) corresponding to % change in a particular model parameter selected for sensitivity analysis. Model

sensitivity to each selected input parameters on the SEB fluxes have been discussed in the following subsections.

7.3.1 Albedo

Model has been found to be sensitive to the albedo for both the seasons i.e., winter and summer. Net all-wave radiation is linearly varying with respect to changes in albedo. In winter season at Palam (Figure 7.1), with reduction in albedo from -10 to -40 % increase in net all-wave radiation have been observed. The maximum values of net all-wave radiation have increased from 379.6 Wm^{-2} to 399.0 Wm^{-2} as compared to base value of 373.2 Wm^{-2}. However, when albedo values are increased by 10% to 40% as compared to base value, decrease in net all-wave radiation have been observed from 366.7 Wm^{-2} to 347.3 Wm^{-2} as compared to base value of 373.2 Wm^{-2}. As presented in Figure 7.1, change in net all-wave radiation is inversely proportional to the change in albedo values with respect to base value during day in winter time and no significant changes have been observed during the night time.

In case of storage heat flux in winter season (Figure 7.1), linear relationship has been observed between % change in albedo and resulting % change in storage heat flux. During day time model results for storage heat flux are indicating inverse relationship with % change in albedo values from the base value, whereas for night time relationship is proportional, with increase in albedo from the base value storage flux is increasing but relatively less. During day time, there is gradual increase in the values of storage flux from 113.3Wm^{-2} to 119.69 Wm^{-2} with reduction in albedo from 10% to 40 %, from the base value. However, during day time, when albedo values are increased from 10% to 40%, decrease in storage heat flux from 109.17 Wm^{-2} to 102.87 Wm^{-2}has been observed. For the night time decrease in storage heat flux has been observed as compared to value corresponding to base value of albedo with % decrease in albedo. Similarly, increase in storage heat flux has been observed with increase in albedo for night time as compared to values at base value of albedo.

In case of sensible heat flux in the winter season, a linear relationship has been observed between % change in albedo and resulting % change in sensible heat flux. The relationship is significant during day time and relatively very less effect has been observed during night time. During day time relationship is inversely proportional and significant where as for the night time sensible heat flux exhibiting very less impact with a change in albedo from the base value (Figure 7.1). Sensible heat flux in winter has been found to increase linearly

from 298.83 Wm^{-2} to 312.55 $Wm^{-2}$with a decrease in albedo by 10% to 40% from the adopted base value during day time. However, a decrease in sensible heat flux has been observed during day time from 289.68 Wm^{-2} to 275.96 $Wm^{-2}$with an increase in albedo from 10% to 40% from the base value. No significant trend has been observed during the night time.

In case of latent heat flux also linear relationship has been found with the albedo as shown in Figure 7.1, however, not so significant. It is difficult to draw any inferences about the trend in latent heat with a change in values of albedo, as value of latent heat flux is also function of the moisture availability. However, in general, for day time inversely proportional relationship has been found between % change in latent heat flux and % change in albedo from the base value. Similarly trends are opposite for night time. The marginal increase in sensible heat flux from 5.23 Wm^{-2} to 5.30 Wm^{-2} has been found with % decrease in albedo value from 10% to 40 % respectively, from the base value during day time. However, when albedo values are increased from 10% to 40% from the base value during day time, no significant change has been observed in latent heat values in absolute terms.

For the summer season also model results have been found to be sensitive to the changes in albedo, as shown in Figure 7.2. Relatively, net all-wave radiation, storage heat flux and sensible heat flux are more sensitive to changes in albedo as compared to latent heat flux. The model response in term of change in SEB fluxes has been found to be linear with % change in albedo from the base value.

Model response with respect to net all-wave radiation is inversely proportional to the % change in albedo from the base value during day time and proportional but relatively less, for night time during summer season (Figure 7.2). Net all-wave radiation has increased from 560.74 Wm^{-2} to 590.24 Wm^{-2} with 10% and 40% change in albedo values respectively, as compared to base value during day time. At base value of albedo net all-wave radiation is 552.75 Wm^{-2}. However, when albedo values are increased from 10% to 40%, net all-wave radiation has decreased from 544.75 Wm^{-2} to 516.07 Wm^{-2} respectively, during day time. For the night time just opposite variations have been observed, however less significant.

In case of storage heat flux in summer season (Figure 7.2), model sensitivity has been found to be similar to winter season, as discussed above. Increase in the storage heat flux from 164.07 Wm^{-2} to 172.97 Wm^{-2} has been observed during day time with respect

to 10% to 40% decrease in albedo values respectively from the base value. Value of the storage heat flux at base value of albedo in summer season has been found to be 161.66 Wm^{-2}. However, during day time when albedo values are increased from 10% to 40% from the base value, then decrease in storage heat flux has been observed from 159.2 Wm^{-2} to 150.6 Wm^{-2}. During day time model results for storage heat flux are indicating inverse relationship with % change in albedo values from the base value, whereas for night time relationship is proportional, with increase in albedo from the base value, storage flux is increasing but relatively less.

In case of sensible heat flux for summer season, linear relationship has been observed between % change in albedo and resulting % change in sensible heat flux, which is similar to the winter season. Relationship is significant during day time and relatively very less effect has been observed during night time. During day time relationship is inversely proportional and significant whereas for the night time sensible heat flux exhibiting very less impact with change in albedo from the base value (Figure 7.2). In case of sensible heat flux during day time, there is gradual increase in the values of sensible heat flux from 432.98 Wm^{-2} to 454.14 $Wm^{-2}$when albedo is decreased from -10 to -40 % from the base value. However, when albedo values are increased from 10% to 40%, decrease in sensible heat flux has been observed during day time from 421.52 Wm^{-2} to 400.94 Wm^{-2} respectively, which is similar to the behavior in winter season. For the night time, model sensitivity with respect to sensible heat flux has been found to be opposite as compared to day time, as shown in Figure 7.2.

In case of latent heat flux for the summer season, model sensitivity has been found to be similar to the winter season as discussed above. In general, for day time inversely proportional relationship has been found between % change in latent heat flux and % change in albedo from the base value. Similarly trends are opposite for night time. Sensible heat has been found to be increasing marginally from 45.84 Wm^{-2} to 47.8 $Wm^{-2}$with decrease in albedo from 10% to 40% respectively during day time.

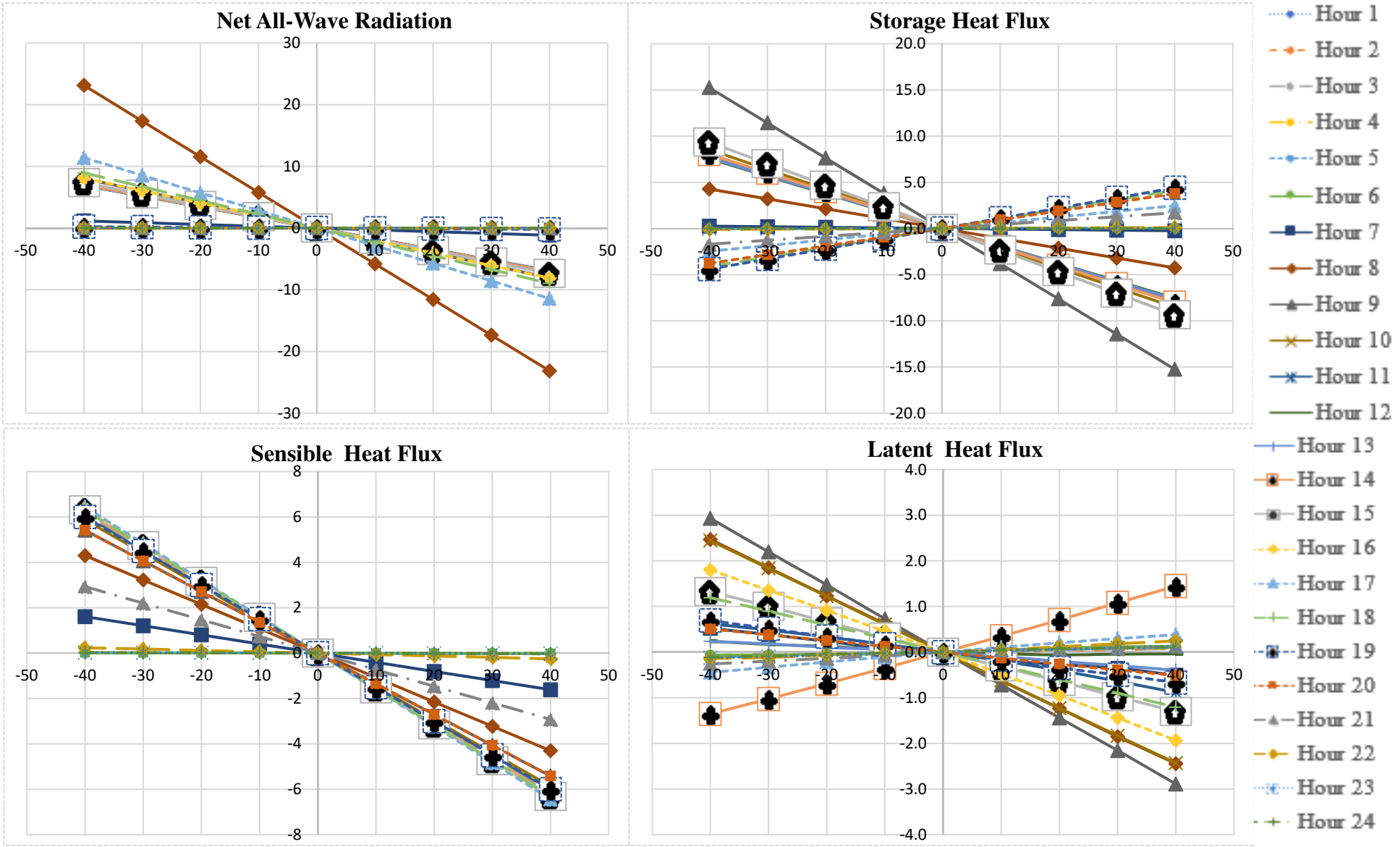

X-axis : Percentage Change in Input Parameter	Y- axis : Percentage Change in Fluxes Value

Figure 7.1: Model sensitivity corresponding to albedo (±40%) for Palam area for winter of year 1999

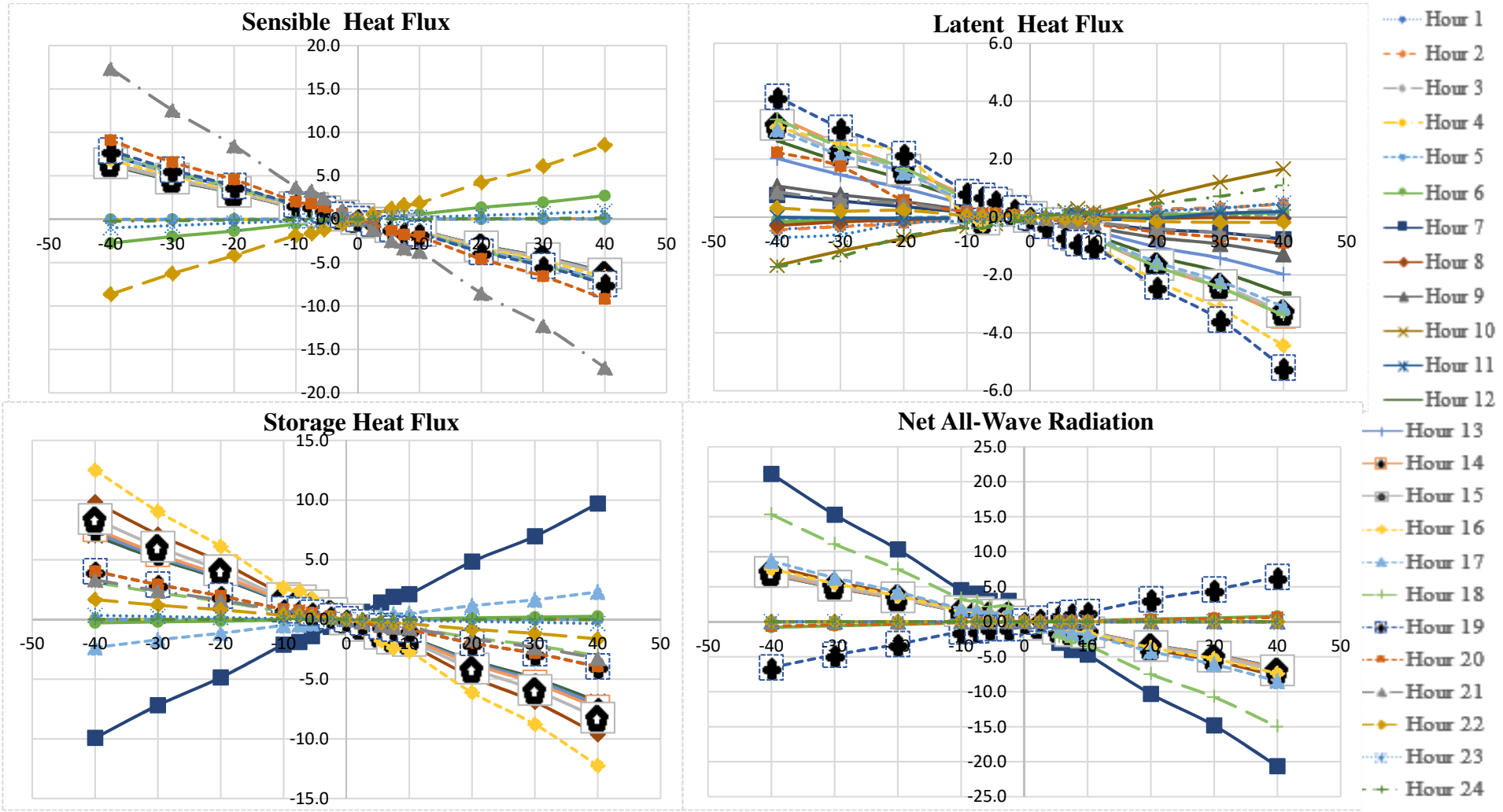

X–axis : Percentage Change in Input Parameter	Y–axis : Percentage Change in Fluxes Value

Figure 7.2: Model sensitivity corresponding to albedo (±40%) for Palam area for summer of year 1999

However, when albedo values are increased from 10% to 40% there is decrease in latent heat flux values from 45.31 Wm^{-2} to 44.21 Wm^{-2} during day time. Opposite sensitivity has been observed, but relatively less significant during the night time. Therefore, it can be concluded from the above discussion that SEB fluxes except latent heat flux are inversely proportional to the change in albedo. Latent heat flux is less sensitive to the albedo. Albedo is affecting surface energy balance significantly during day time as compared to night time.

7.3.2 Conductance

Conductance is one of the controlling parameter which govern transfer of water vapor in the atmosphere, which means it affects the energy partitioning into latent heat and sensible heat. That's why in the present study, net all-wave radiation and storage heat flux have not been found to be significantly sensitive to the conductance. Sensible and latent heat fluxes have been found to be sensitive to the conductance parameter.

In winter season (Figure 7.3), when conductance values are reduced from -10 to -40% from the base value, no significant change in the values of sensible heat flux has been observed. Sensible heat flux has not found to be sensitive up to 10% increase in the conductance. However, it has shown some sensitivity when conductance was increased from 10% to 20% as compared to base value (Figure 7.3). Similar behavior has been observed during the summer season also (Figure 7.4). Sensible heat flux is less sensitive to the change in conductance. Variation in sensible heat flux is not more than 4% (at 20% increase or decrease in conductance) with change in conductance both in negative and positive directions. Latent heat flux has been found to be sensitive to the conductance both in winter and summer seasons (Figure 7.3 and 7.4). When conductance values are reduced from -10 to -40% there is no change in the values of latent heat flux in winter season (Figure 7.3). However in winter season, when conductance values are increased from 10 to 40% from the base value, there is significant increase in the latent heat flux values for the day time and negligible change during night time (Figure 7.3). Similarly, latent heat is found to be sensitive to the conductance during day time in summer season (Figure 7.4). The maximum relative change in percentage of latent heat flux values have been found when conductance is decreased from 0 to 10 %. Latent heat flux has been found to decrease significantly with increase in conductance from 0% to 10% from the base value. However, when conductance is further increased from 10% to 20%, significant increase in latent heat flux has been observed during day time (Figure 7.4). By investigating these results, it has been identified that changing conductance parameter values does not show significant changes on surface energy components. It can be concluded that

conductance is important parameter for the latent heat flux and increase in its value from 10% to 20% as compared to the base value will increase the latent heat flux significantly.

7.3.3 Drainage

Similar to the conductance, drainage is also one of the parameter which affects energy partitioning into sensible and latent heat flux. Drainage parameter indicate moisture availability into the system and any change in its value will affect latent heat flux significantly. In the present study ground heat flux and net all-wave radiation have not been found to be sensitive to the drainage parameter. Therefore, sensitivity of these two SEB components has not discussed in detail here.

In winter season, sensible heat flux has not found to be sensitive when drainage parameter is decreases by 30% to 40% and increase from 0% to 30% from the adopted base value (Figure 7.5). Sensible heat flux has been found to be sensitive (decrease) to decrease in drainage parameter from 0% to 10% and also sensitive (increase) to increase in drainage parameter from 30% to 40% from the base value. The change in maximum values of sensible heat flux has been found to be from 294.26 Wm^{-2} to 284.56 Wm^{-2} with 0% to 10% decrease in drainage parameter. With increase in drainage parameter from the base value, no significant increase in sensible heat flux has been observed (Figure 7.5). In summer season during day time, sensible heat flux has not been found to be sensitive to increase or decrease in drainage parameter from the base value (Figure 7.6). For the night time, sensible heat flux has been found to be sensitive to decrease in drainage parameter but not significantly.

Latent heat flux has been found to be sensitive to the drainage parameter both in winter as well as in summer season. In winter season, latent heat flux is very sensitive to the reduction in drainage parameter from 0% to 10 % of the base value. Further decrease in values of drainage parameter beyond 10% have no significant effects. Latent heat flux has been found to be increasing from 5.20 Wm^{-2} to 11.62 Wm^{-2} with a reduction in drainage parameter from 0% to 10% from the base value. However, when drainage parameter values are increased from 0 to 30% there is no change in latent heat flux. The maximum relative change in percentage of sensible heat flux has been found when percentage change in drainage parameter values have varied from -30 to -40% in case of negative side. Whereas, in case of positive side no significant changes have been found in sensible heat flux with increase in drainage parameter (Figure 7.5). In summer season also similar behavior has been observed in latent heat flux (Figure 7.6). With increase in drainage parameter value from the base value, no significant change in latent heat flux has been observed.

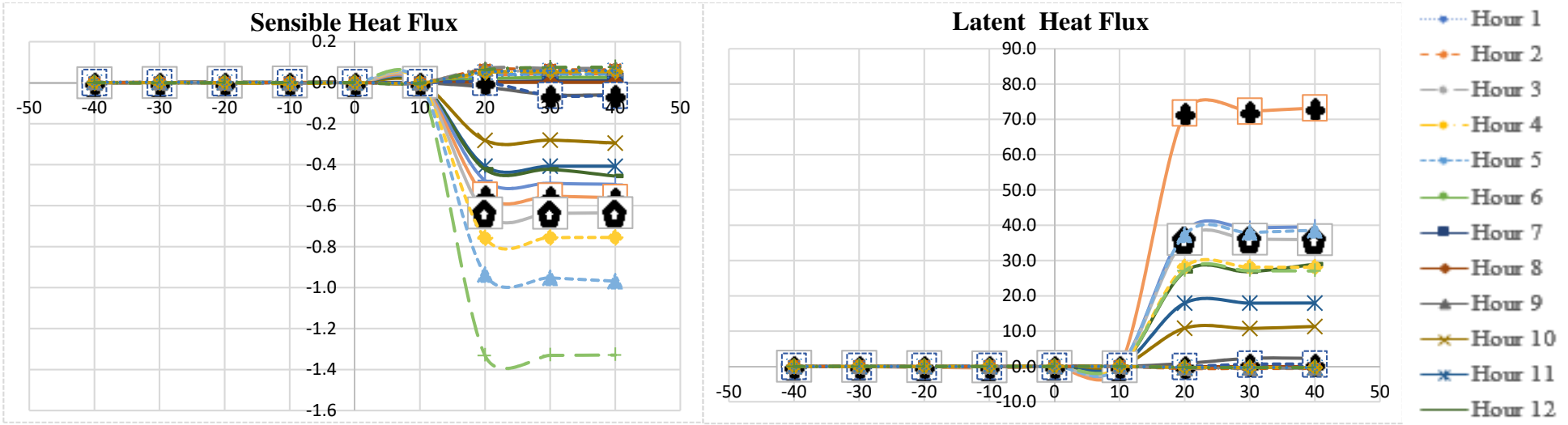

Figure 7.3: Sensitivity of turbulent heat fluxes to model conductance parameter (±40%) for Palam area for winter of year 1999

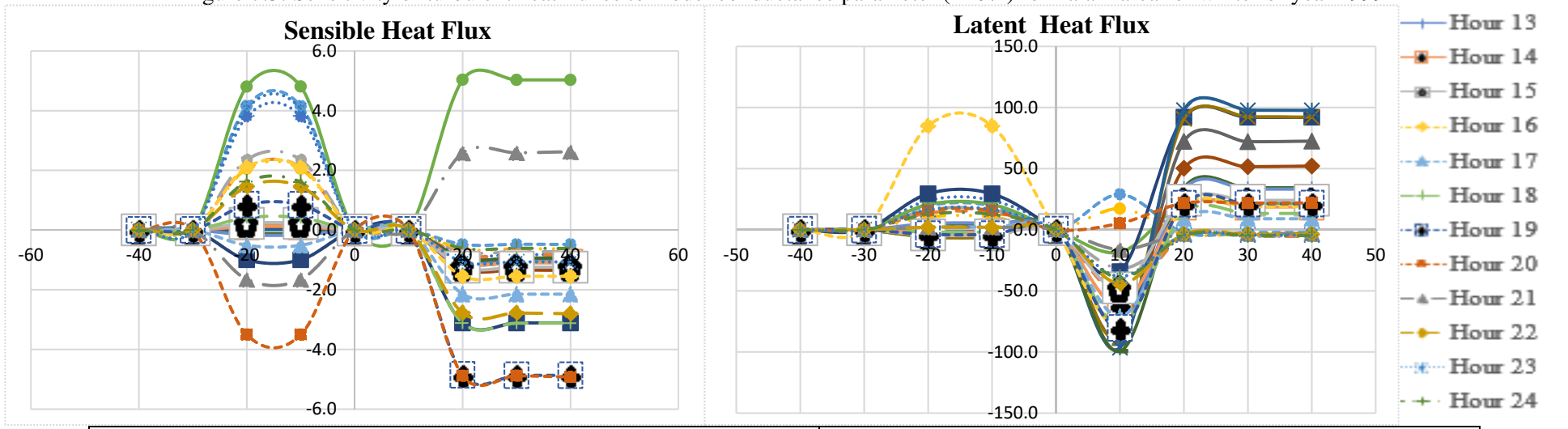

Figure 7.4: Sensitivity of turbulent heat fluxes to model conductance parameter (±40%) for Palam area for summer of year 1999

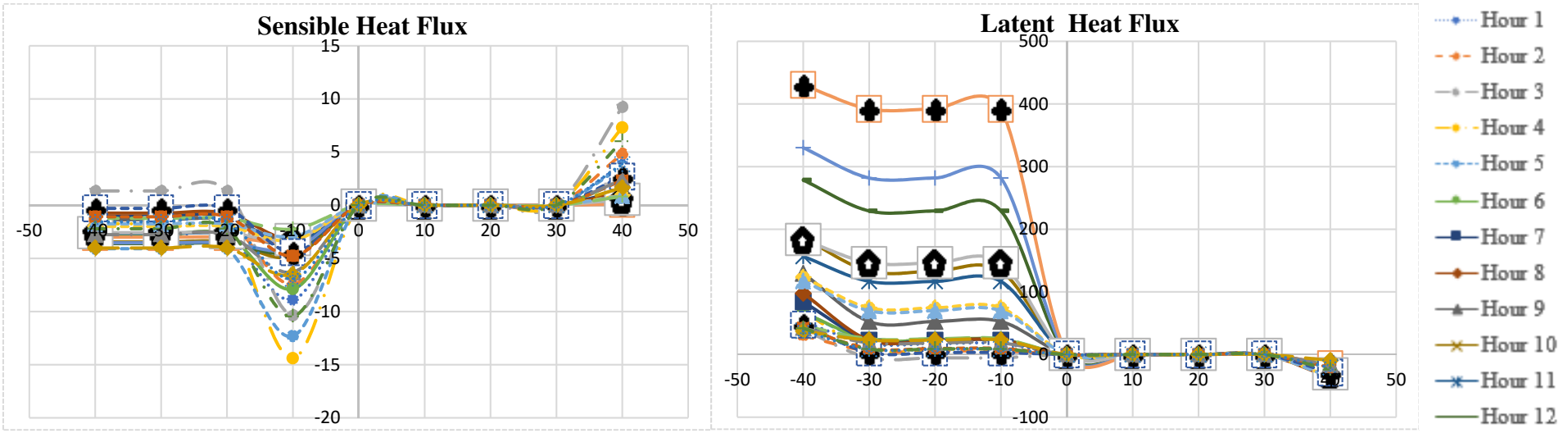

Figure 7.5: Sensitivity of turbulent heat fluxes to model drainage parameter (±40%) at Palam for winter of year 1999

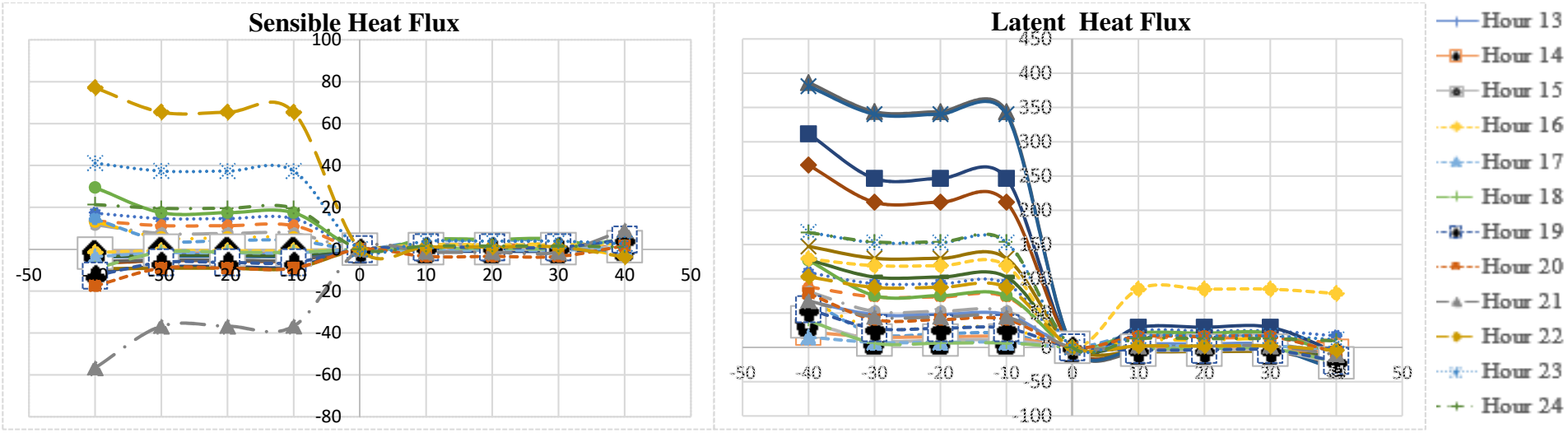

Figure 7.6: Sensitivity of turbulent heat fluxes to model drainage parameter (±40%) at Palam area for summer of year 1999

However, with reduction in drainage parameter from 0% to 10%, significant increase in latent heat flux has been found during day time. Latent heat flux has been found to be increasing from 45.62 Wm^{-2} to 52.44 Wm^{-2} with decrease in drainage parameter during day time from 0% to 10% respectively from the base value. It can be concluded from this study that latent heat flux is sensitive to changes in drainage parameter during day time as compared to night time. Sensible heat flux has been found to less significant with respect to drainage parameter.

7.3.4 Emissivity

Emissivity is one of the important parameter which affects surface energy balance. Emissivity affects short and long wave radiations emitted from the different type of surfaces, thus affecting the net radiation and net available energy for partitioning into sensible and latent heat fluxes. Sensitivity analysis has been performed by altering the values of emissivity from +2.55 to -7.5% with respect to base values adopted in the model for different type of surfaces (0.96 to 0.98). Emissivity value cannot be more than 1, that's why variation in +ve side has been restricted to 2.5%.

In winter, net all-wave radiation has been found to be inversely proportional to emissivity, with respect to base value. With decrease in emissivity, net all-wave radiation is increasing and with increase in emissivity net all-wave radiation is decreasing, however relatively less (Figure 7.7). In winter season (Figure 7.7), when emissivity values are reduced from 0 to 7.5 % from the base value, increase in net all-wave radiation has been found from 440.17 Wm^2 to 446.98 Wm^{-2}. Such a variation is more significant during day time and less during night time. With increase in emissivity marginal decrease in net all-wave radiation has been observed. Similarly in case of summer season (Figure 7.8), when emissivity values are reduced from 0 to 7.5 % during day time, increase in net all-wave radiation has been observed from 552.75 Wm^2 to 558.22 Wm^{-2}, respectively. During the night time reverse relationship has been found.

Storage heat flux has been to be sensitive to the emissivity both in summer and winter seasons. In winter, storage heat flux is inversely proportional to the emissivity. Storage heat flux is increasing during day time from 136.88 Wm^{-2} to 138.69 Wm^{-2} with decrease in emissivity from 0 to 7.5% from the base value. Storage heat flux marginally decreased with increase in emissivity from 0 to 2.5% (Figure 7.7). Storage heat flux in summer also exhibit inverse linear relation during day time and linear relationship during night time. Storage heat flux has been found to be increasing from 161.66 Wm^{-2} to 162.84 Wm^{-2} with decrease in emissivity from 0 to 7.5% from the base value (Figure 7.8) during day time.

Sensible heat flux also has been found to be sensitive to emissivity. In winter season, sensible heat flux is having inverse relationship with the emissivity. Increase in sensible heat flux from 354.98 Wm^{-2} to 359.98 Wm^{-2} has been observed with decrease in emissivity from 0 to 7.5% from the base value. Storage heat flux marginally decreased with increase in emissivity from 0 to 2.5% (Figure 7.7). Sensible heat flux during day time in summer season has been found to be sensitive to emissivity (Figure 7.8). For the day time sensible heat flux is increasing with decrease in emissivity. Sensible heat flux is increasing from 427.25 Wm^{-2} to 431.31 Wm^{-2} with decrease in emissivity from 0 to 7.5% from the base value. For the night time in summer season sensible heat flux is decreasing with decreasing emissivity, however marginally.

For latent heat flux also, emissivity have similar type of relationships as it have with storage and sensible heat fluxes for the winter season. Latent heat flux in winter season is exhibiting inverse relationship with the emissivity (Figure 7.7). Latent heat flux increases marginally from 13.54 Wm^{-2} to 13.56 Wm^{-2} with decrease in emissivity values by 0 to 7.5% from the base value in winter season. In summer also latent heat flux has been found to be sensitive to the emissivity. Variations in the latent heat flux have inverse linear relationship with emissivity. With decrease in emissivity from 0 to 7.5% latent heat flux is increasing from 45.62 Wm^{-2} to 45.90 Wm^{-2}, respectively during day time (Figure 7.8). During night time behavior is opposite but less significant. From the sensitivity results, it can be concluded that for both winter and summer seasons, all SEB fluxes are sensitive to the emissivity. SEB fluxes have inverse relationship with emissivity. All fluxes are increasing with decrease in emissivity 0 to 7.5% from the base value except few night hours.

7.3.5 Maximum Conductance

Similar to the surface conductance, maximum conductance parameter also governs partitioning of available energy into turbulent fluxes i.e., sensible and latent heat fluxes. Maximum conductance parameter affects surface conductance in the model and it represents stomatal resistance, which indirectly affects evapotranspiration and thus energy partitioning into latent and sensible heat fluxes. Other SEB fluxes, storage heat flux and net all-wave radiation has not been found to be significantly sensitive to maximum conductance parameter. In winter season (Figure 7.9), when maximum conductance values are reduced from 0 to 40% there is a negligible change in the values of sensible heat flux. Also, when maximum conductance values are increased from 10 to 30%, no change in the sensible heat flux has been found as compared to its base values.

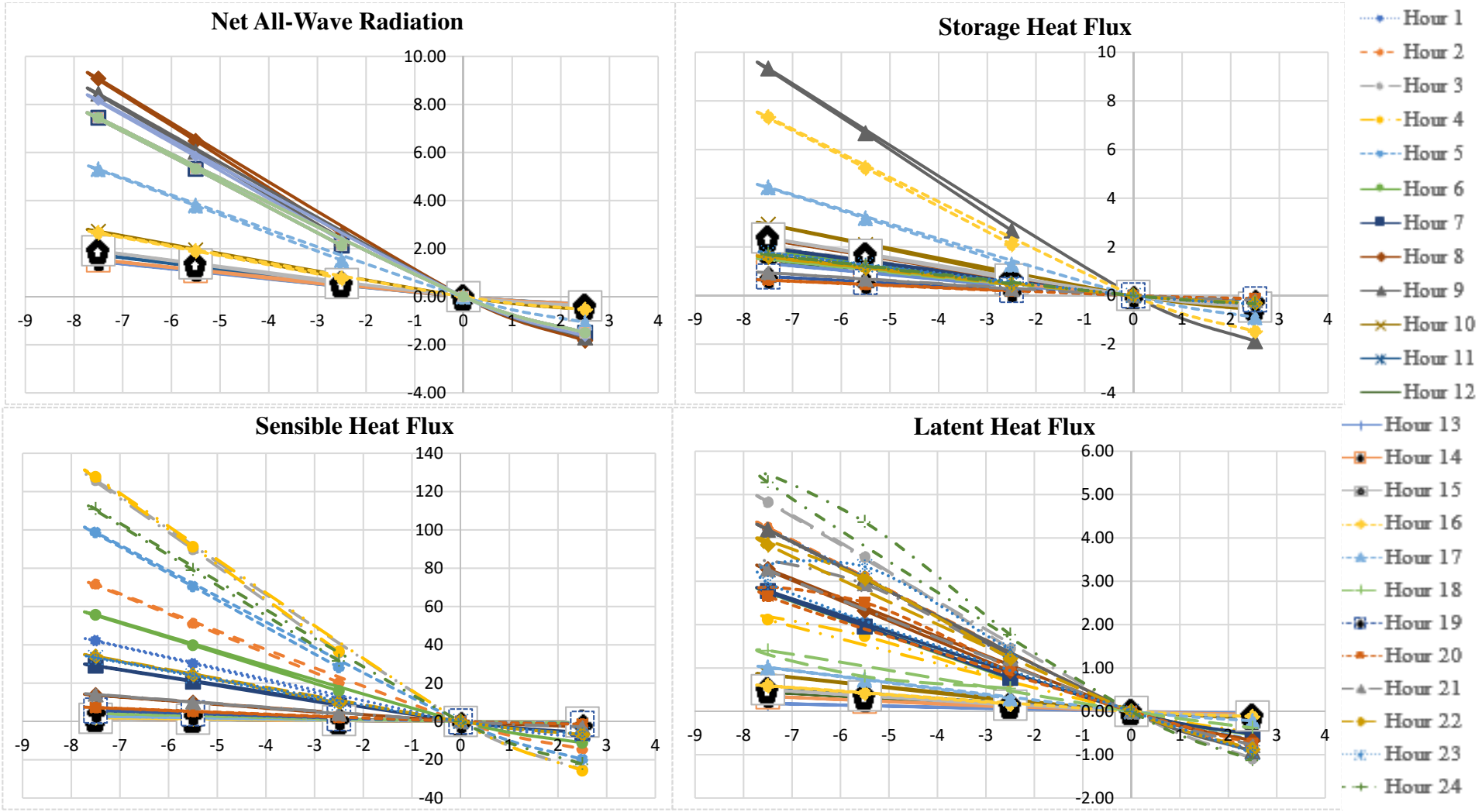

X: Percentage Change in Input Parameter	Y: Percentage Change in Fluxes Value

Figure 7.7: Sensitivity of SEB fluxes with emissivity parameter (±40%) for Palam area for winter of year 1999

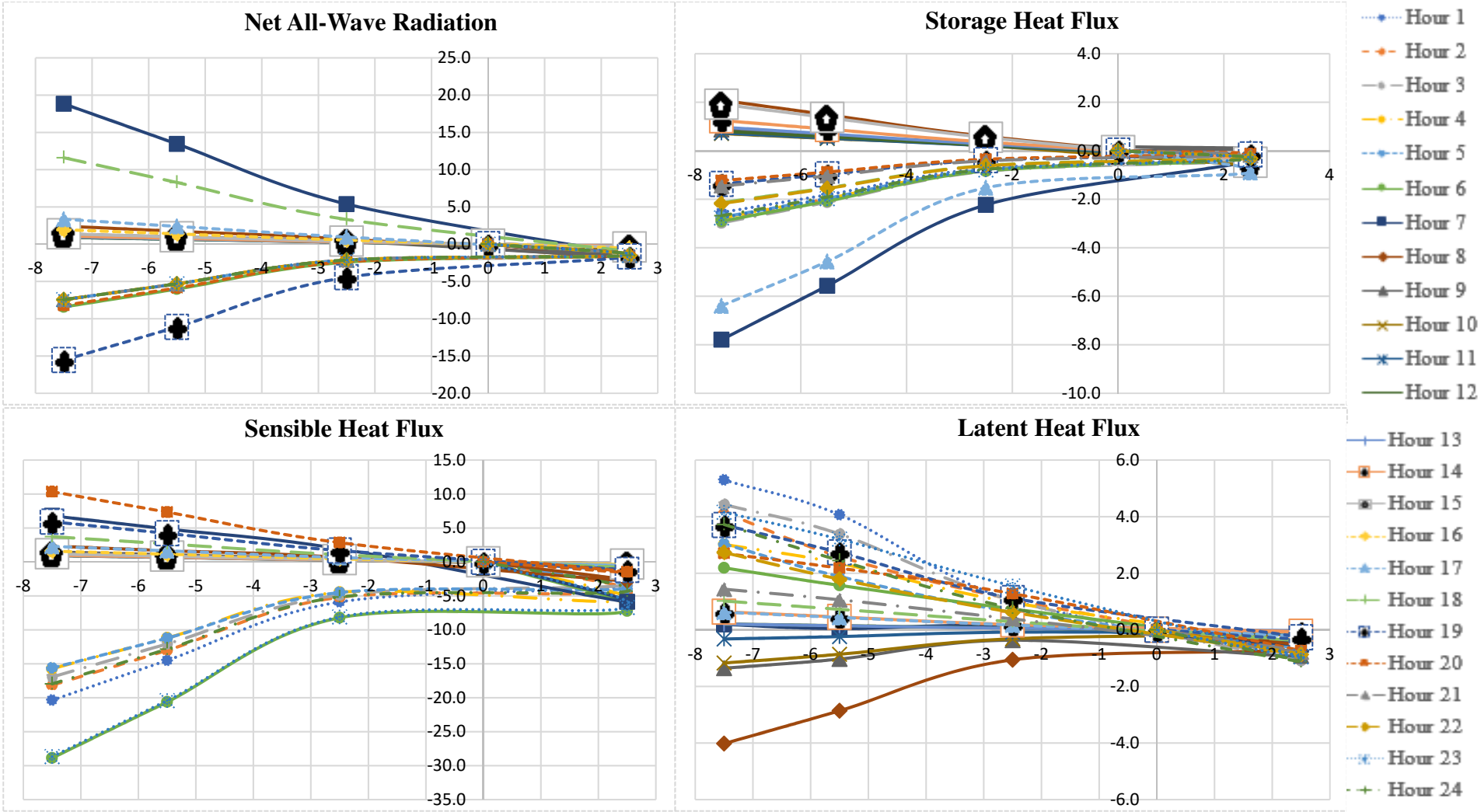

X: Percentage Change in Input Parameter	Y: Percentage Change in Fluxes Value

Figure 7.8: Sensitivity of SEB fluxes with emissivity parameter (±40%) for Palam area for summer of year 1999

In summer season (Figure 7.10) also similar behavior, as in case of winter season, has been observed in the sensible heat flux with change in maximum conductance parameter. Variation in sensible heat flux has been found to be very less (< 5%) when max conductance parameter decreases from 0 to 10%. However, when maximum conductance values are increased from 0 to 10%, small change in the sensible heat flux has been observed for few hours of the day on further increasing the values. Maximum conductance parameter have very negligible effect on latent heat flux.

As presented in Figure 7.9, latent heat flux is linearly increasing and decreasing with increase and decrease in maximum conductance parameter, however not so significant. The negligible change in maximum values of latent heat flux (3.84 $Wm^{-2}$to 3.83 Wm^{-2}) has been observed with increase in maximum conductance parameter from 10 to 40%. In case summer season, when maximum conductance is decreased from 0 to 30 % there is no significant change in the values of latent heat flux has been observed (Figure 7.10). Minor variation in latent heat flux has been observed when maximum conductance is reduced from 0 to 10%. The change in maximum values of latent heat flux has been observed from 45.62 Wm^{-2} to 52.44 Wm^{-2}. However, when maximum conductance values are increased from 10 to 30%, no change has been observed in latent heat flux values.

Both sensible and latent heat fluxes are not found to be sensitive (significantly) to the change in maximum conductance. Both fluxes have a very small variation when values of maximum conductance varies from 0 to 10% in both negative and positive side.

7.3.6 Maximum Storage Capacity

In this analysis, net all wave radiation and storage heat flux are not shown because no change was observed in their values when storage capacity maximum values were changed during the sensitivity analysis. In winter season (Figure 7.11), when maximum storage capacity values are reduced from 0 to 40% from the base value, no significant change in the values of sensible heat flux has been observed. Also similar behavior has been observed in the positive side also i.e., sensible heat flux is not significantly sensitive to the maximum storage value. In summer season (Figure 7.12), sensible heat flux is not showing any sensitivity to the maximum storage when its values are changed from +20 % to -40%. However, sensible heat flux in summer season has been found to be sensitive to increase in maximum storage values beyond 30%. Sensible heat flux values are found to be increasing from 0 to 5% with increase in maximum storage value from 30 to 40% during day time. For night time opposite behavior has been observed.

Latent heat flux in winter season have linear relationship with the change in maximum storage value, however not so significant (Figure 7.11). Latent heat values are exhibiting increasing/decreasing trend with increase and decrease in maximum storage values, respectively, however change is even less than 1%. In summer season (Figure 7.12), latent heat flux is not showing any sensitivity to the maximum storage when its values are changed from +30% to -40%. However, latent heat flux in summer season has been found to be sensitive with increase in maximum storage values beyond 30%. Latent heat flux values are found to be increasing from 0 to 30% with increase in maximum storage value from 30 to 40% during day time. For night time relatively less opposite behavior has been observed.

7.3.7 Minimum Storage Capacity

Minimum storage capacity parameter affects and found to be sensitive to only turbulent heat fluxes. In this analysis, net all wave radiation and storage heat flux are not shown because no change was observed in their values when minimum storage capacity values were changed during sensitivity analysis.

In winter season (Figure 7.13), sensible heat flux is exhibiting linear relationship with change in minimum storage capacity parameter. Sensible heat flux is increasing and decreasing with increase and decrease in minimum storage capacity parameter respectively. With an increase and decrease in minimum storage capacity parameter from 0 to 40%, sensible heat flux in winter season increasing and decreasing by 0 to 4% respectively (Figure 7.13).
In winter season (Figure 7.13), latent heat flux is exhibiting inverse linear relationship with change in minimum storage capacity parameter. Latent heat flux is decreasing with increase in value of parameter and increasing with decrease in minimum storage capacity parameter. With an increase in minimum storage capacity parameter from 0 to 40%, latent heat flux in winter season is decreasing by 0 to 12% (Figure 7.13). With decrease in minimum storage capacity parameter from 0 to 40%, latent heat flux in winter season is increasing by 0 to 20% (Figure 7.13). In summer season during day time (Figure 7.14), when minimum storage capacity values are reduced from 0 to 20%, values of sensible heat flux decreases by 2%. Further, decrease in parameter value do not change the sensible heat flux in summer season. During night time just opposite behavior has been observed in summer season. Similarly, during day time sensible heat flux is increasing from 0 to 2.5% with increase in value of minimum storage capacity from 0 to 40%. During night time opposite behavior was observed. In summer, latent heat flux is exhibiting inverse linear relationship with minimum storage capacity parameter.

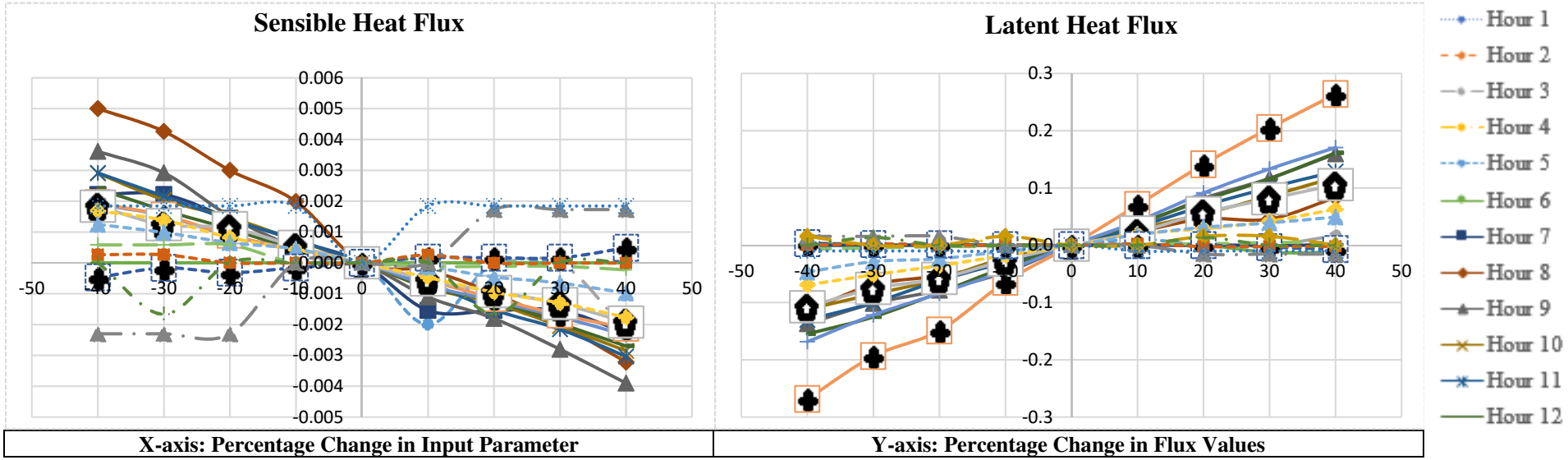

Figure 7.9: Sensitivity of turbulent heat fluxes with max. conductance parameter (±40%) for Palam area for winter of year 1999

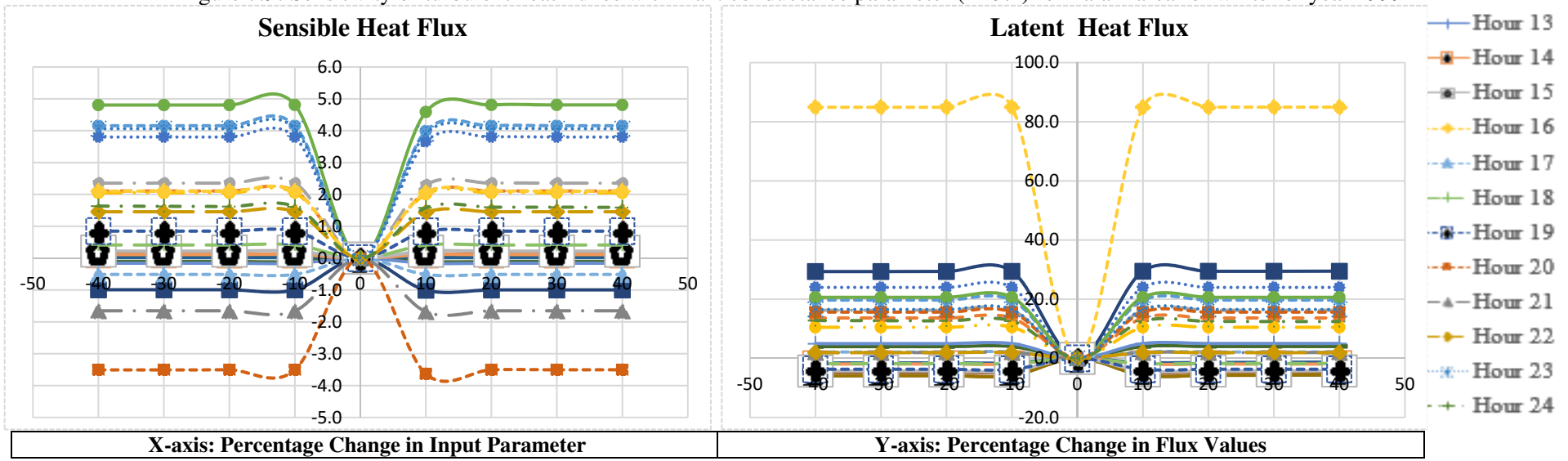

Figure 7.10: Sensitivity of turbulent heat fluxes with max. conductance parameter (±40%) for Palam area for summer of year 1999

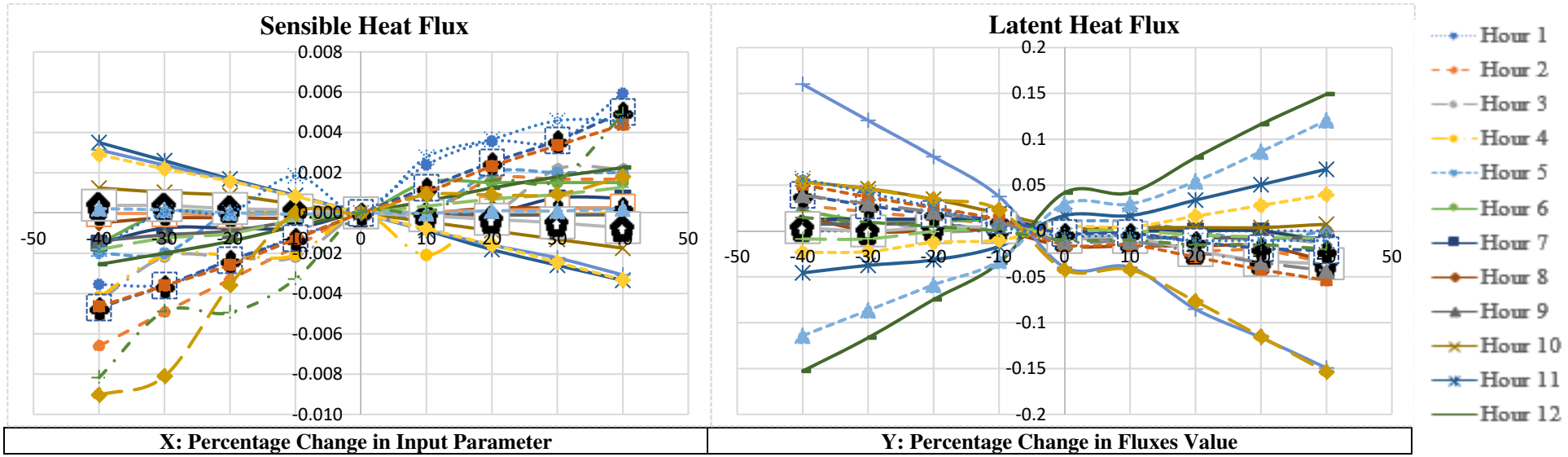

Figure 7.11: Sensitivity of turbulent heat fluxes with maximum storage capacity parameter (± 40%) for Palam area for winter of year 1999

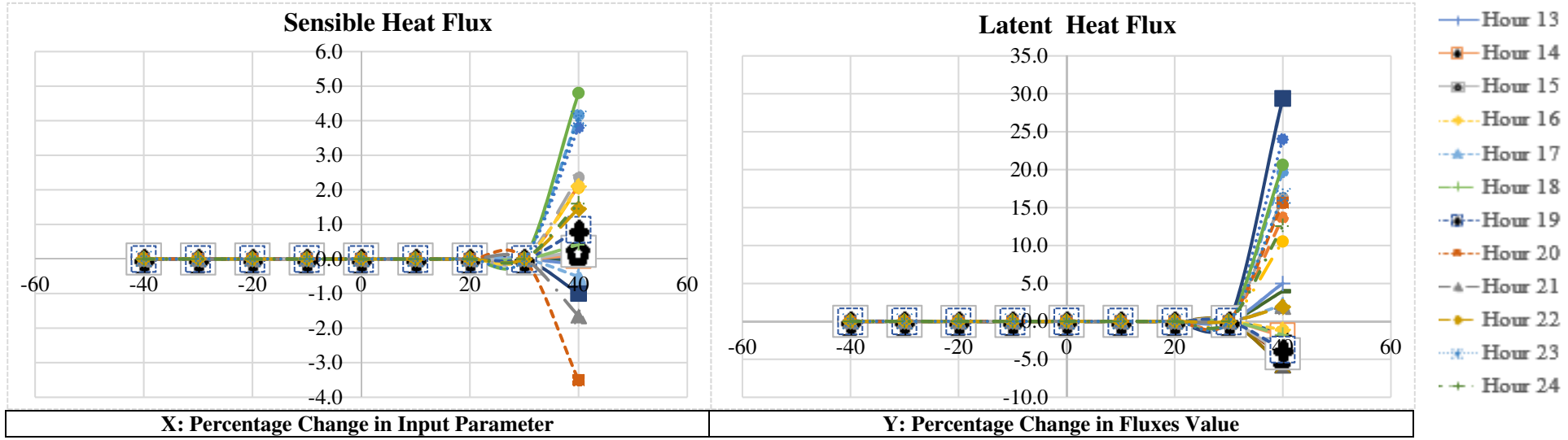

Figure 7.12: Sensitivity of turbulent heat fluxes with maximum storage capacity parameter (± 40%) for Palam area for summer of year 1999

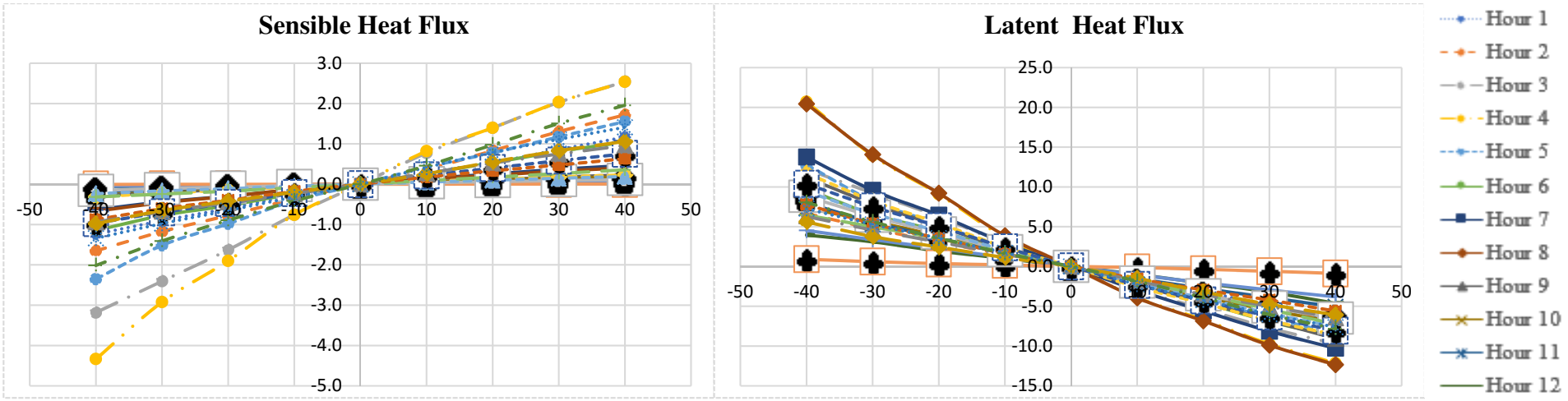

X-axis: Percentage Change in Input Parameter	Y-axis: Percentage Change in Fluxes Value

Figure 7.13: Sensitivity of turbulent heat fluxes with minimum storage capacity parameter (± 40%) for Palam area for winter of year 1999

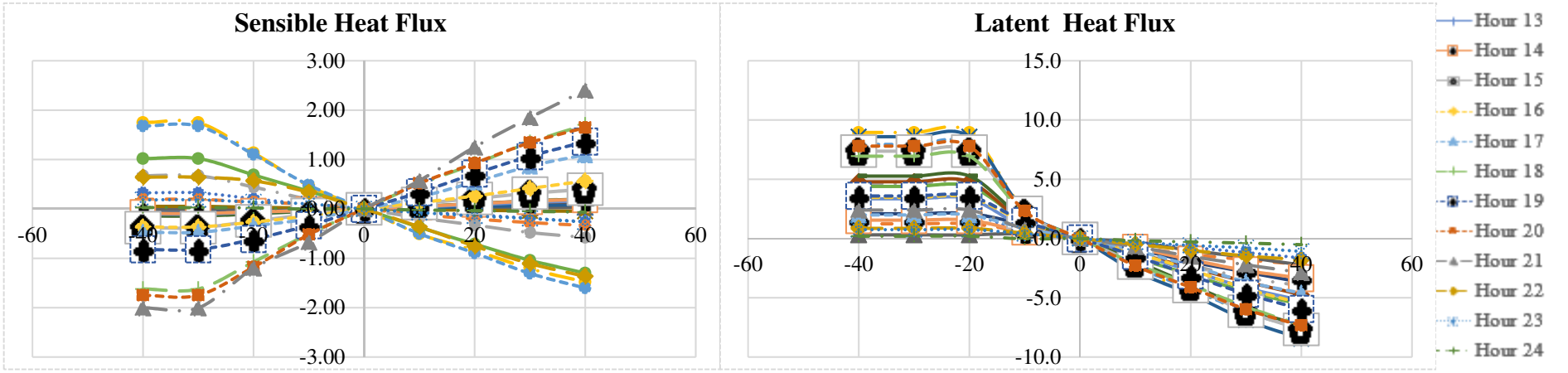

X: Percentage Change in Input Parameter	Y: Percentage Change in Fluxes Value

Figure 7.14: Sensitivity of turbulent heat fluxes with minimum storage capacity parameter (± 40%) for Palam area for summer of year 1999

For different hours, latent heat flux is increasing from 0 to 8% with decrease in minimum storage capacity from 0 to 10%, whereas latent heat flux is decreasing by 0 to 9% with increase in minimum storage capacity parameter from 0 to 40% for different hour (Figure 7.14). It can be concluded from the above discussion that both turbulent heat fluxes are sensitive to a smaller extent with minimum storage capacity parameter. Latent heat flux and minimum storage capacity are having inverse linear relationship, whereas during day time, sensible heat flux have linear (positive) relationship with the minimum storage capacity parameter.

7.4 MODEL CALIBRATION AND VALIDATION

7.4.1 Model Calibration

Model calibration has been achieved by determining values of important model input parameters at which simulated SEB components are closest to the observed SEB fluxes. Calibration has been completed through iteratively trying different values of parameter (± 40% change in the input parameters with respect to base value) and determining closeness of the model response with the observed data. Calibration was completed along with the sensitivity analysis. Model was run for a range of input variable values, one parameter at a time and model results were simultaneously compared with hourly observed data of net all-wave radiation and SEB fluxes for summer season (90 days) of year 1999. Comparison of simulated and observed SEB fluxes has been done only for summer of year 1999 for which observed data were available. Selected input values have been used in the calibration of model to determine SEB fluxes i.e., net all-wave radiation, storage heat flux, sensible heat flux and latent heat flux.

Calibrated model parameters for both the locations are those input parameters to which model has been found to be sensitive and calibrated parameter values are that values at which simulated results are closest to the corresponding observed value for different location of Delhi. Typical comparison of the simulated and observed SEB fluxes during calibration process for the different selected parameters have been presented in Figure 7.15 to 7.22. Optimum value of individual parameter selected for calibration have been determine after careful examination of relative variation in model results and their nearness to the observed values corresponding to different value of that particular parameter. Final calibrated parameters of the model where model results have been found to closest with observed SEB fluxes have been presented in the Table 7.3.

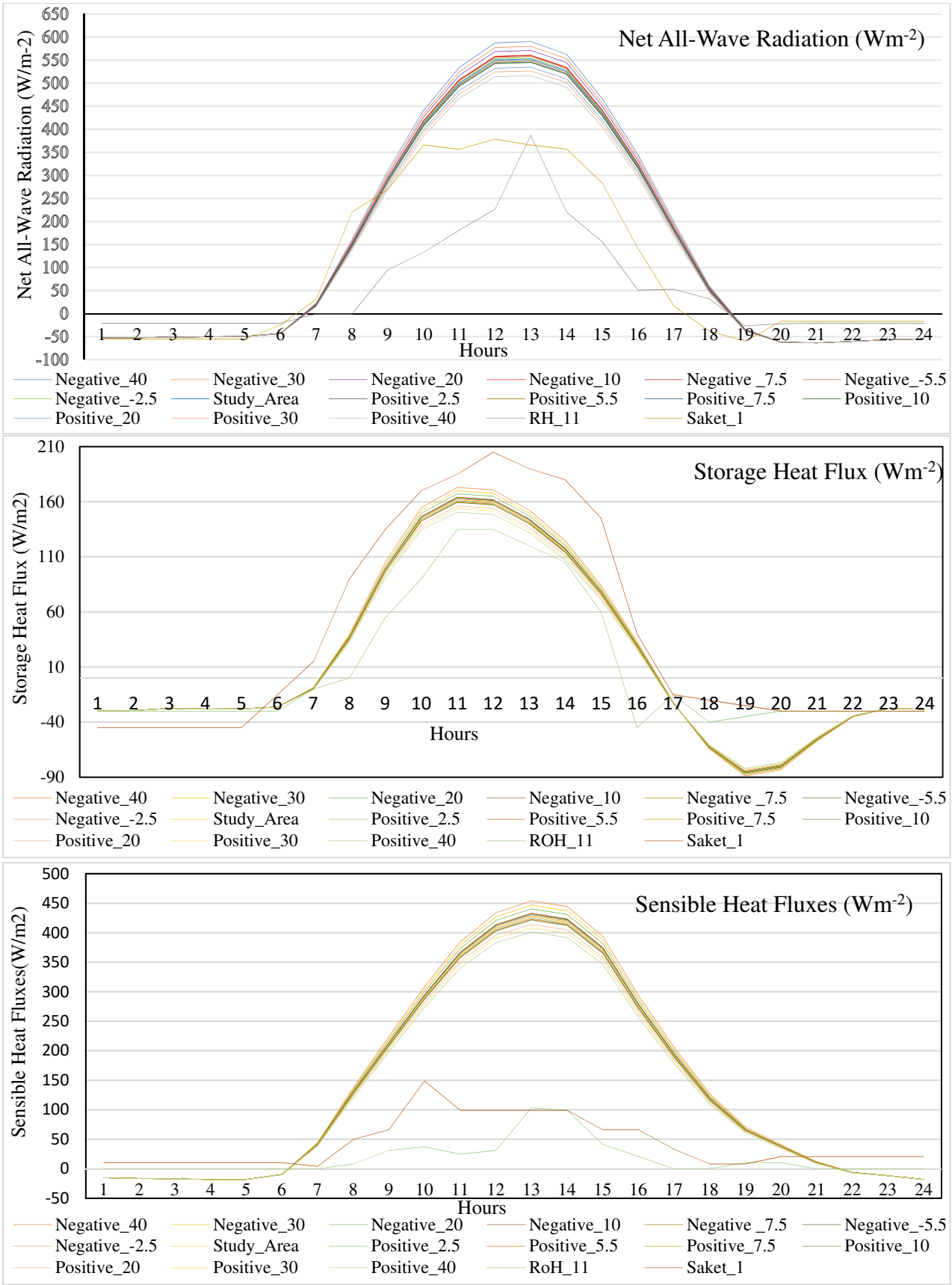

Figure 7.15: Calibration of model for albedo using data of Palam for summer of year 1999

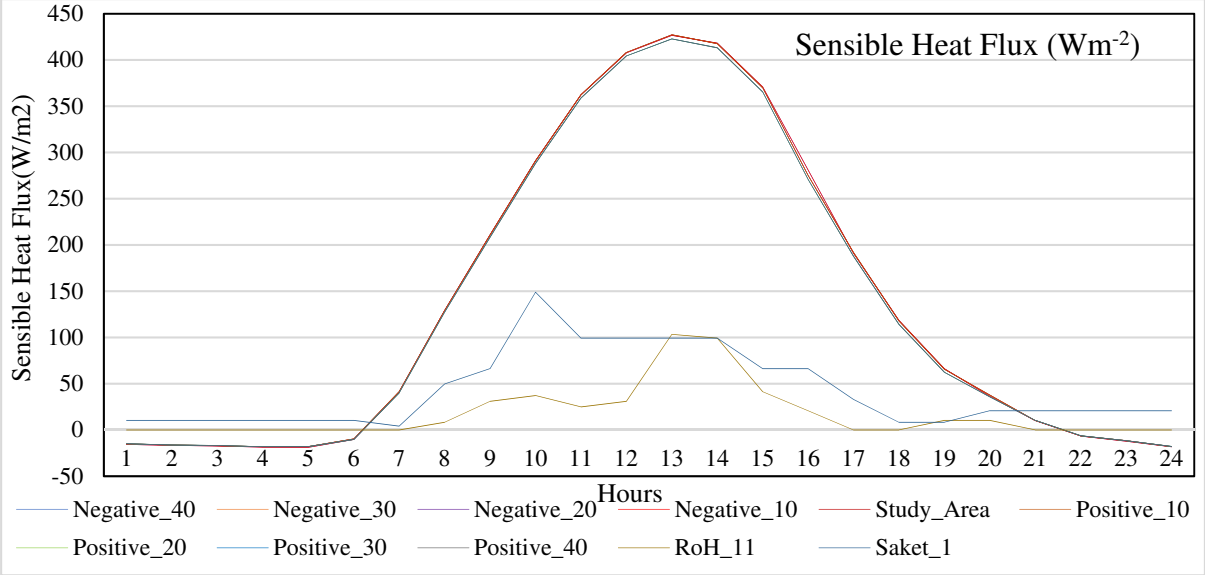

Figure 7.16: Model calibration for conductance using data of Palam for summer of year 1999

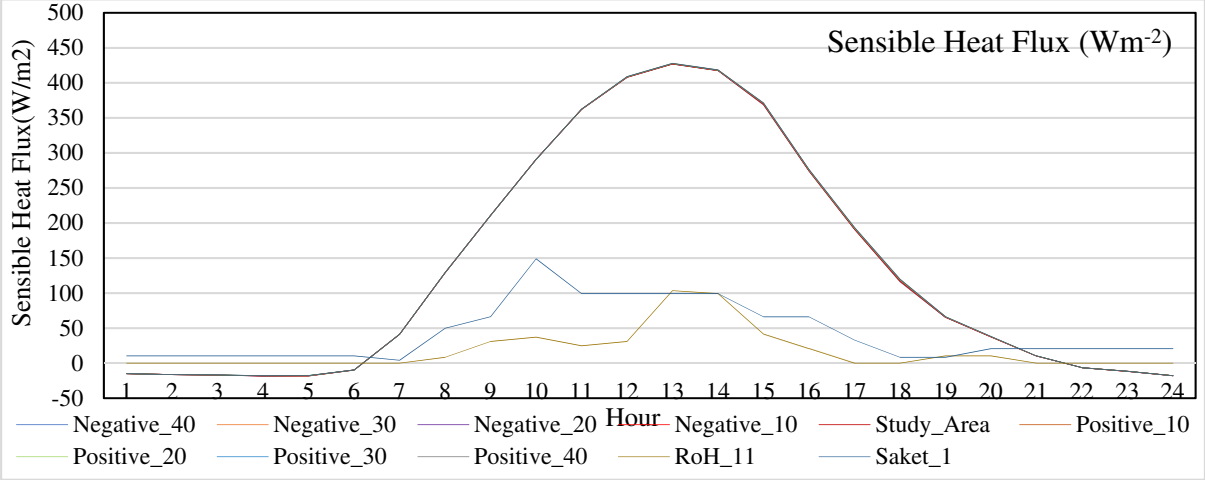

Figure 7.17: Model calibration for min. storage capacity using data of Palam for summer of year 1999

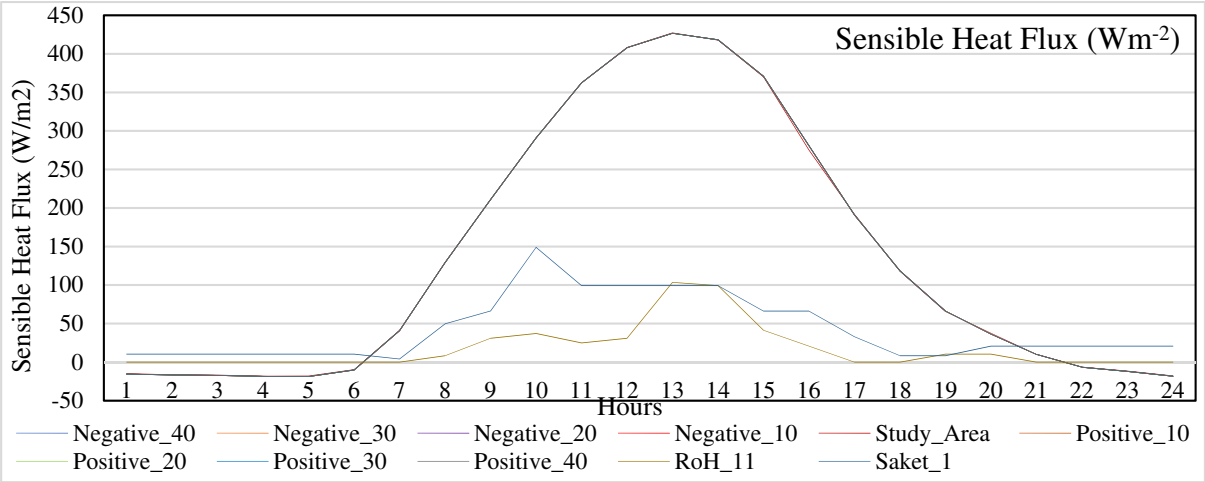

Figure 7.18: Model calibration for max. conductance using data of Palam for summer of year 1999

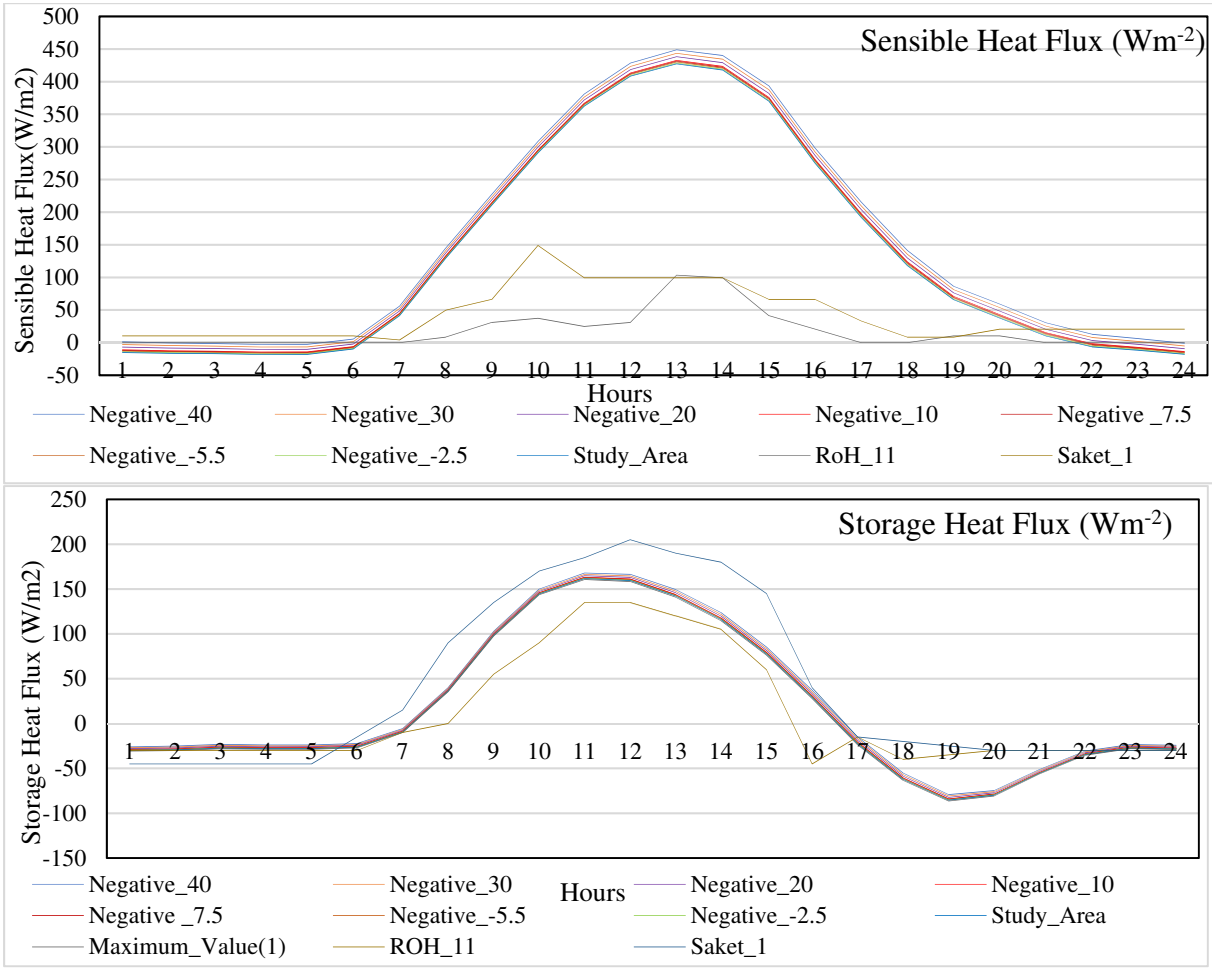

Figure 7.19: Model calibration for emissivity using data of Palam for summer of year 1999

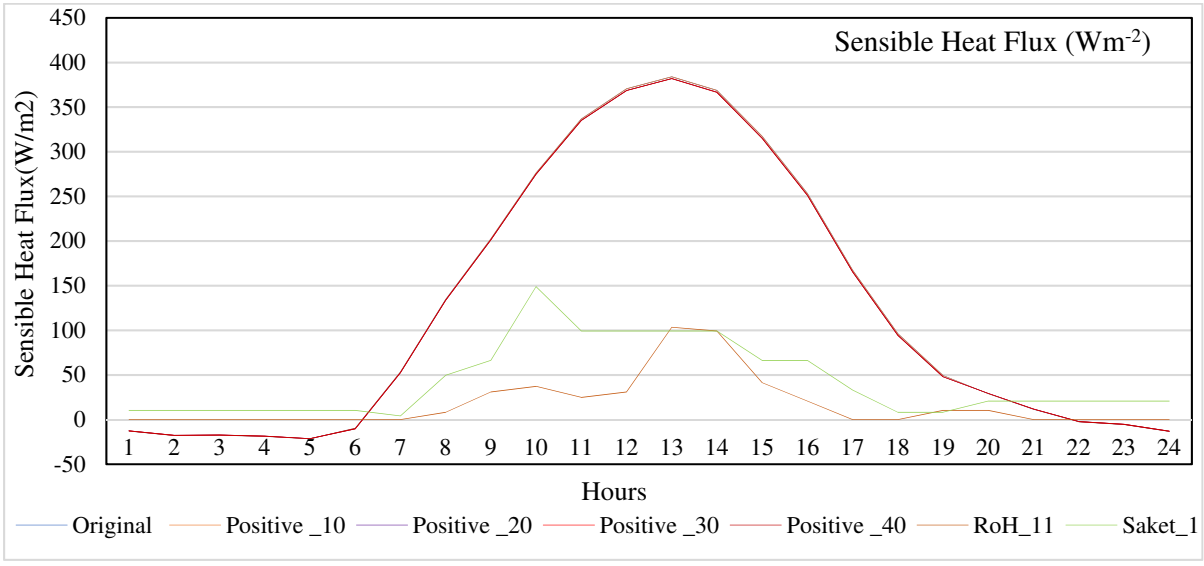

Figure 7.20: Model calibration for conductance using data of Safdarjung for summer of year 1999

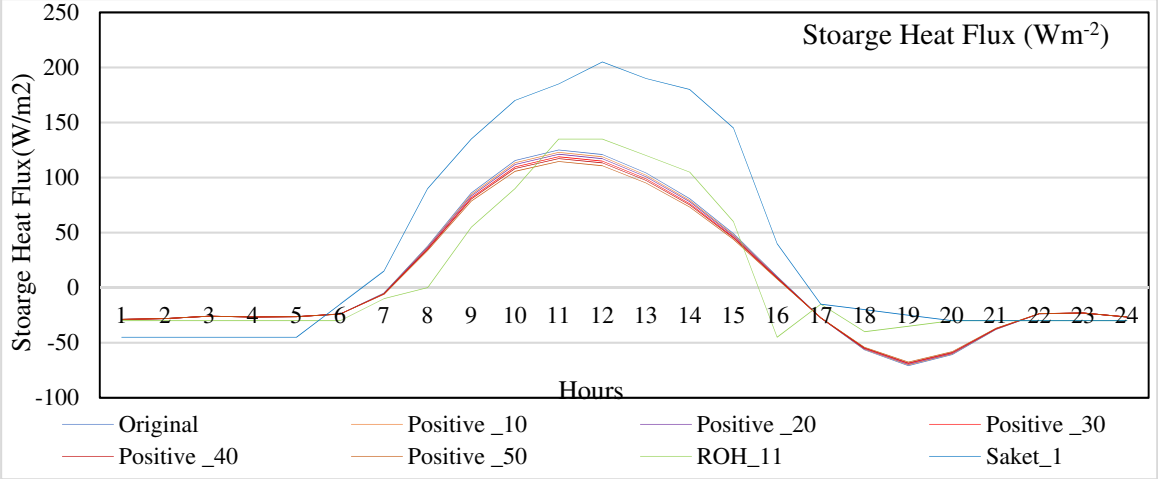

Figure 7.21: Model calibration for albedo using data of Safdarjung for summer of year 1999

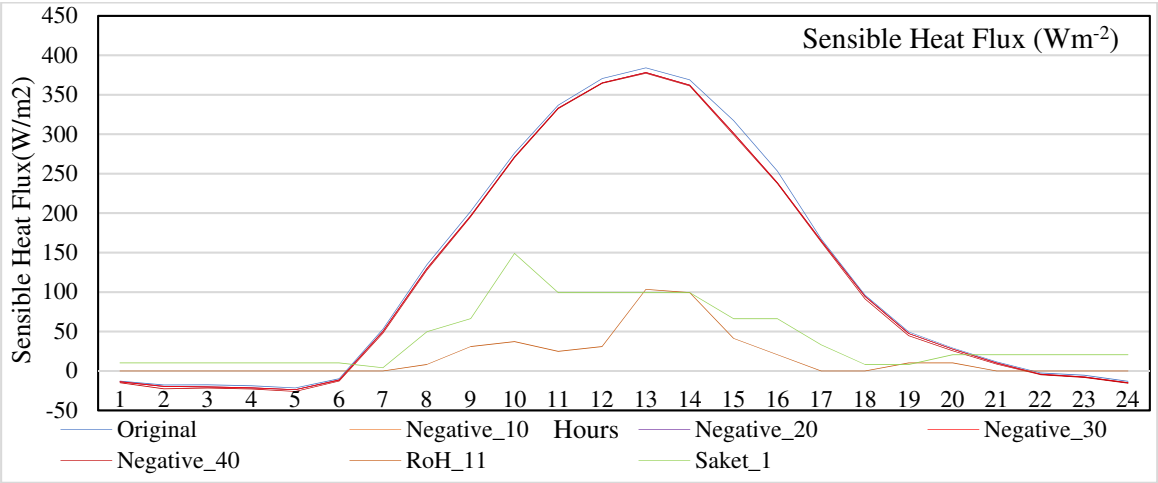

Figure 7.22: Model calibration for drainage parameter using data of Safdarjung for summer of year 1999

Table 7.3: Calibrated model parameters for different LULC classes

Model Parameter/ LULC Class	Albedo	Emissivity	Drainage	Max. Storage Capacity	Min. Storage Capacity Min	Conductance Parameter	Max. Conductance
Paved	0.12	0.95	2.7	0.48	0.48	16.5	-
Buildings	0.15	0.91	2.7	0.25	0.25	566.1	-
Forest	0.1	0.98	1.8	1.3	1.3	0.2	7.4
Trees	0.18	0.98	1.8	0.8	0.3	3.4	11.7
Irrigated Grass	0.21	0.93	2.7	1.9	1.9	11.1	40
Unirrigated Grass	0.21	0.93	1.8	1.9	1.9	0.0176	33.1
Water	0.1	0.95	0	2000	0.5	NA	-

7.4.2 Model Validation

After model calibration, model was run with calibrated parameters to validate the model. Model validation has been done by comparing the simulated results of net all-wave radiation and SEB fluxes with observed data from different locations of Delhi.

Model results have been validated corresponding to two set of observed data.

(1) Hourly observed net all-wave radiation and storage heat flux for three months (April, May and June) for year 1999 for different locations in Delhi (Padmanabhamurthy, 1999b; Das, et al., 2009; Das et al., 2014).
(2) Observed seasonal maximum and minimum values of net all-wave radiation for summer and winter season of year 1998 and 1999 for different locations in Delhi (Das, et al., 2009; Das et al., 2014).

Model is producing areal average values of net all-wave radiation and SEB fluxes for the study areas as a whole, whereas, reference (observed) values of fluxes are point observations. In the absence of appropriate observed data i.e., areal averages, model results were compared with observed point observations of SEB fluxes of different locations in Delhi. Observed data of net all-wave radiation & storage heat flux is available at hourly time step only for three months of summer season for years 1999. Reference data of hourly turbulent sensible and latent heat fluxes are also available for validation (Padmanabhamurty B., 1999b - DST Project Report-Ref. No. ES/048/319/95) for summer 1999 at hourly scale. Also reference data for seasonal minimum and maximum values of net all-wave radiation for different sites of Delhi, for year 1998 & 1999 is available and used for model validation. Model results at different temporal resolutions like summer season (90 days), randomly selected individual dates, and monthly have been compared with observed/reference data. Model results produced at hourly temporal scale were generalized by taking means corresponding to different temporal scales. The observed SEB component values have been adopted from literature (Das, Padmanabhamurty and Murty, 2009; Das, Padmanabhamurty and Murty, 2014). Authors have reported 5 to 12% uncertainties in the observed results. Available observed data includes only point observations of hourly net all-wave radiation and storage heat flux from the different sites in Delhi for three months of summer 1999. Turbulent sensible and latent heat flux were calculated from available equations and models (Das et al., 2009a, 2009b, 2014).

Model results are validated by comparing simulated SEB fluxes and observed/reference hourly SEB Flux values at different temporal resolutions and also by comparing seasonal maximum and minimum values of fluxes. Minimum values have been adopted as the values corresponding to 6:00 - 7:00 hr in morning and 18:00 to 20:00 hrs in evening. Maximum values have been adopted as the values corresponding to 12:30 to 13:00 hrs. The comparison of seasonal maximum and minimum modelled and measured SEB fluxes have been presented in Table 7.4 and Table 7.5. Comparison of seasonal minimum and maximum SEB fluxes indicate satisfactory agreement between simulated and observed SEB fluxes for different locations. According to the modelled and measured net all-wave radiation values (seasonal minimum & maximum), it can be observed that the modelled values are within the close range of measured values at different sites for summer 1999 and winter 1998 for both the study areas i.e., Palam and Safdarjung. Observed seasonal minimum net all-wave radiation for summer 1999 ranges from – 48 W/m^2 to -90 W/m^2 in morning 6 to 7 hrs and model output ranges from 39.1 and -63.5 W/m^2 for Safdarjung and -43.0 and -62.2 W/m^2 for Palam areas. Similarly model results of seasonal maximum net all-wave radiation for summer 1999 ranges from 453.1 W/m^2 (Safdarjung) to 550.40 W/m^2 (Palam), which is very near to the observed values of similar sites in Delhi i.e., 386 W/m^2 to 560 W/m^2. Comparison of model results and observed net all-wave radiation indicate satisfactory agreement and hence can be concluded that model is producing good results.

Table 7.4: Model results v/s observed net all-wave radiation for summer of year 1999

Site Name	Type of Results (Summer)	Minimum Net All-wave Radiation (Wm^{-2}) (6:00–7:00 hr)* and (18:00 - 20:00 hr)	Maximum Net All-wave Radiation (Wm^{-2}) (12:30-13:00 hr)
Okhla (Industrial site)	Measured	-90*	560
Connaught Place (Commercial site)	Measured	-78*	450
Greater Kailash –II (residential site)	Measured	-48.2 and -50	402
Jawaharlal Nehru University (Rural site)	Measured	-48*	386
Deer park	Measured	-54*	392
Safdarjung	Modelled	-39.1 and -63.5	453.1
Palam	Modelled	-43.0 and -62.2	550.4

Table 7.5: Model results v/s observed net all-wave radiation for winter of year 1998

Site Name	Type of Results (Winter)	Minimum Net All-wave Radiation (Wm^{-2}) (6:00–7:00 hr)* and (18:00-20:00 hr)	Maximum Net All-wave Radiation (Wm^{-2}) (12:30-13:00 hr)
Okhla (Industrial site)	Measured	-66*	372
Connaught Place (Commercial site)	Measured	-60*	390
Greater Kailash –II (residential site)	Measured	-30 and -54	338
Jawaharlal Nehru University (Rural site)	Measured	-36 and -54	264
Deer park	Measured	-18*	110
Safdarjung	Modelled	-32.63 and -52.49	390.31
Palam	Modelled	-30.68 and -50.10	438.44

Surface energy fluxes at seasonal (90 days), monthly temporal scales and at particular days of the season have been simulated and compared with corresponding observed values for Palam and Safdarjung areas to validate the model results. Particular days values are the average values of that particular day for three months of summer season. For the Palam area, selected particular days are 7th, 8th, 17th, 25th and 30th whereas for Safdarjung area, selected particular days of the summer season are 2th, 12th, 22th, 28th and 30th day. These dates have been chosen randomly to compare the simulated and observed fluxes to ascertained match. Measured fluxes values at two sites such as Samaya and Rohini have been selected for comparison from available six sites because these two sites have surface characteristics similar to the selected study areas. Due to space constraint in tables, results of alternate hours have been shown in the tables. For each flux, root mean squared error (RMSE) has also been calculated to ascertain the closeness of simulated and observed results. Detailed discussion of validation with respect to net all-wave radiation and each SEB fluxes has been presented in the following sections.

7.4.3 Net All-wave Radiation

On comparing, reference and modelled values of hourly net all-wave radiation for Palam area, for summer 1999, it has been found that modelled values of net all-wave radiation at different temporal scale are following trend similar to observed values (Figure 7.23 and 7.24) for both Palam and Safdarjung areas. The minimum difference between measured

and modelled values of net all-wave radiation has been found during 1:00 to 7:00 hr and 19:00 to 23:00 hr. Peak value of measured and modelled net all-wave radiation has been found at the same time period, that is, 12:00 to 13:00 hr. The range of observed seasonal minimum values of net all-wave radiation at Rohini and Samaya, during summer 1999 varies from -0.8 to -26.8 Wm^{-2} and -10.7 to -18.3 Wm^{-2} respectively, whereas range of observed seasonal day time values of net all-wave radiation at Rohini and Samaya during same time period varies from 32.0 to 387 $Wm^{-2}$and 14.6 to 359.3Wm^{-2} for Palam area (Table 7.6 and Figure 7.23). The range of modelled minimum values of net all-wave radiation at seasonal scale (90 days) varies from -36.1 to -63.5 Wm^{-2}whereas day time values of net all-wave radiation varies from 154 to 552. 8 Wm^{-2}. Comparison of modelled and observed net all-wave radiation at seasonal scale indicate satisfactory matching (Table 7.6 and Figure 7.23).

On comparing monthly values of simulated net all-wave radiation in month of May & June for Palam area are better matched with measured values as compared April month for year 1999. Simulated net all-wave radiation for Palam area and observed seasonal net all-wave radiations at Rohini & Samaya sites are also matching in trend at individual days. Simulated values for 30th May has been found to be the closest to the observed data at Saket area in Delhi. The range of minimum values of simulated net all-wave radiation for Palam on 30th May 1999 varies from -35.6 to -66.0 Wm^{-2} which is very near Saket location of Delhi (-48 Wm^{-2} to -59.7 Wm^{-2}). Range of simulated day time net all-wave radiation on 30th May 1999 varies from 31 to 591.7 Wm^{-2}, which is near to the observed seasonal values (14.6 Wm^{-2} to 439.3 Wm^{-2}) of Samaya area of Delhi (Table 7.6 and Figure 7.23).

Similarly, simulated results of net all-wave radiation at different temporal scales for Safdarjung have been compared with the seasonal observed data of different locations of Delhi (Table 7.7 and Figure 7.24). Similar trends have been observed in simulated and observed data of net all-wave radiation for Safdarjung for summer 1999, which indicates that model is simulating the surface energy balance of the area satisfactorily. The range of modelled minimum values of net all-wave radiation at seasonal scale (90 days) varies from -39.1 to -63.5 Wm^{-2} , which are comparable with minimum values of observed values at Janak & Saket areas of the Delhi. Similarly, day time seasonal simulated values of net all-wave radiation varies from 2.9 to 453.1Wm^{-2}, which are comparable with the observed values of 29.5 to 439.3 Wm^{-2} of Samaya. On comparing monthly values of simulated net all-wave radiation, values in month of June are comparable with measured values at Janak

& Samaya areas of Delhi. The range of minimum simulate values of net all-wave radiation for June month varies from -14.9 to -40.2 Wm^{-2} which are comparable with -16.6 to -54.8.2 Wm^{-2} for the Saket area of Delhi. Similarly, positive values of monthly simulated values of net all-wave radiation for June month (43.5 to 452.2 Wm^{-2}) are comparable with observed seasonal net all-wave radiation of Samaya (29.5 to 439.3 Wm^{-2}). Also simulated net all-wave radiation values for 12th day are comparable with the observed seasonal values of net all-wave radiation of Samaya area.

Root mean square errors (RMS) have also been calculated to determine the closeness of the simulated and observed values of net all-wave radiation at different temporal scale. RMS errors has been found to be 116 – 198.71 Wm^{-2} for the summer season for both the areas. Similarly RMS error have been found to be between 116 – 178.74 Wm^{-2} at monthly scale, between 41.76 – 187.57 Wm^{-2} at daily temporal scale. Looking at the satisfactory matching of trends of simulated and observed average hourly net all-wave radiation, it can be concluded that model is simulating the net all-wave radiations satisfactory. Ranges of the minimum and day time values of simulated and observed values have also been found to be comparable. RMS errors at different temporal scales are also not very high. Model is overestimating net all-wave radiation peak values during day time however, trend is matching well.

7.4.4 Storage Heat flux

On comparing, measured and modelled values of storage heat flux for Palam area in summer of 1999, it has been found that modelled values of storage heat flux at different temporal scale are following trend similar to measured values. The minimum difference between measured and modelled values of storage heat flux has been found during 1:00 am to 7:00 am. Peak value of measured and modelled storage heat flux has been found at the same time period, that is, 12:00 pm to 15:00 pm. The range of simulated minimum seasonal storage heat flux has been found to be between -9.6 to -85.4 Wm^{-2} which is comparable with observed minimum seasonal storage heat flux at Rohini during summer 1999 i. e, -10.0 to -45.0 Wm^{-2}. Positive seasonal simulated storage flux has been found to be 29.2 to 161.7 Wm^{-2}which is comparable with the range of observed positive storage heat flux (15 to 145 Wm^{-2}) at Samaya (Table 7.8 and Figure 7.23). On comparing monthly scale values of storage heat flux, values in month of June are better matched with measured values as compared to values in April and May months.

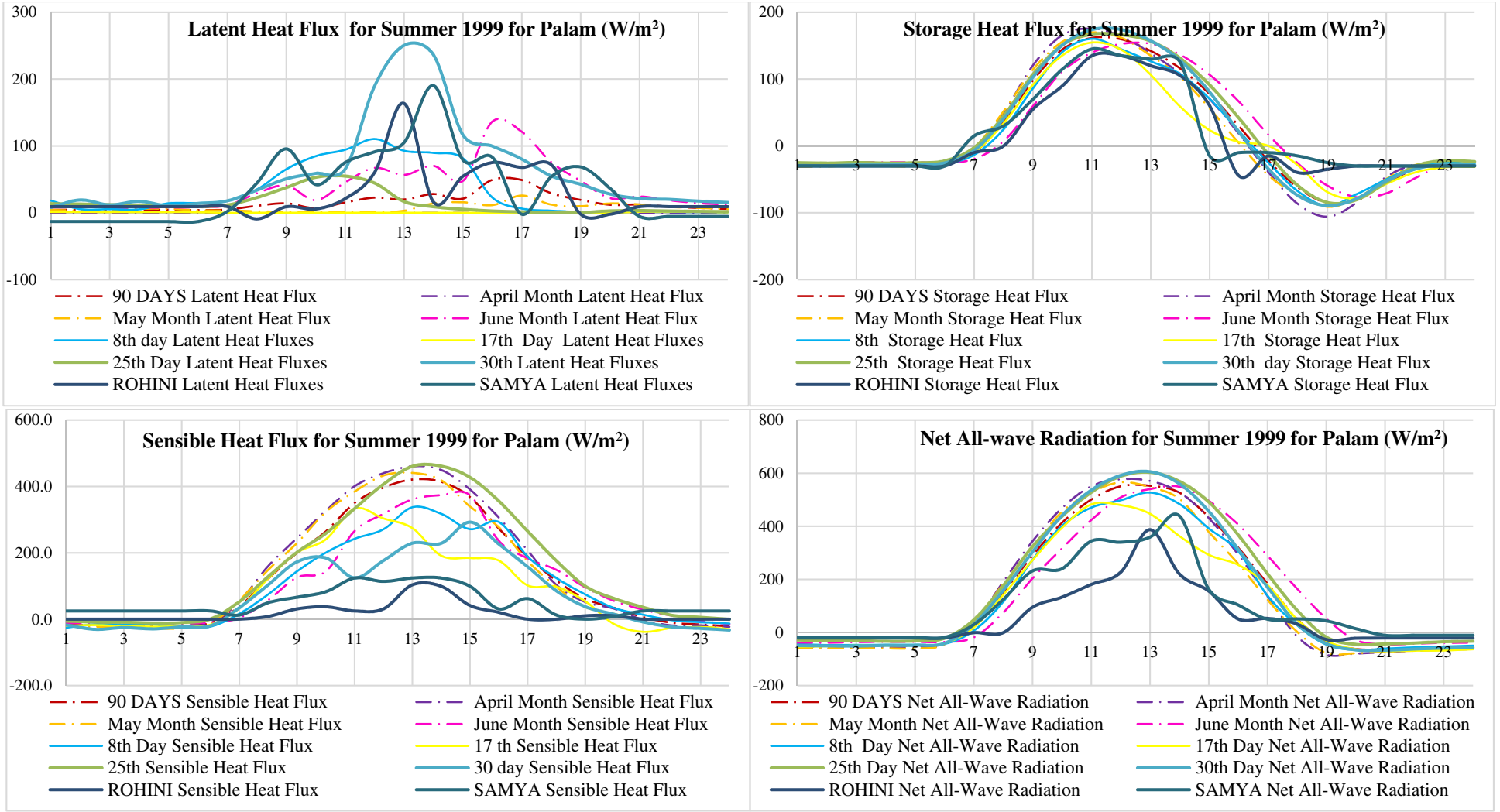

Figure 7.23: Seasonal measured and modelled values of SEB fluxes for summer of year 1999 for Palam area

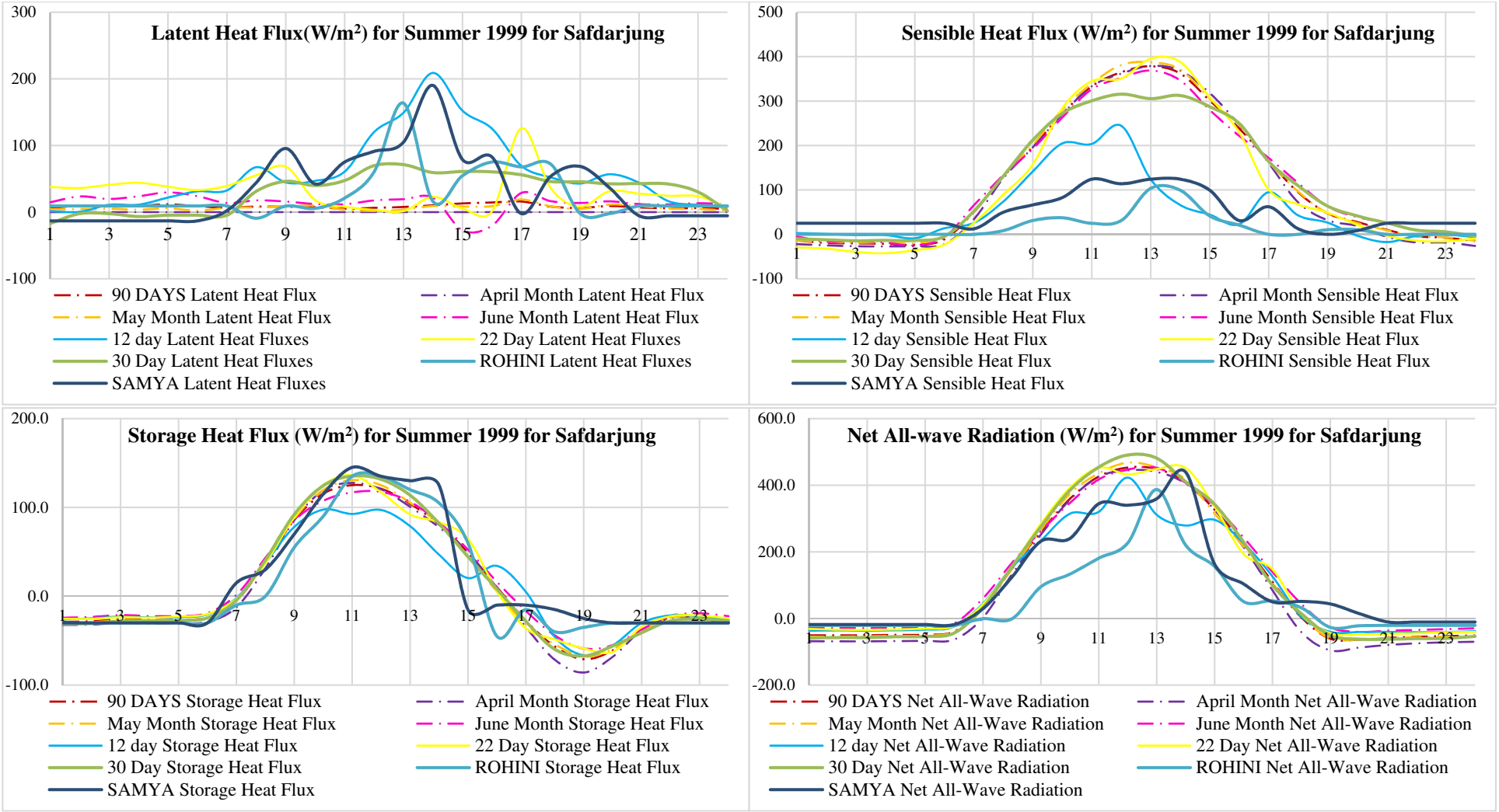

X-axis: Time in Hours	Y-axis: Fluxes (W/m^2)

Figure 7.24: Seasonal measured and modelled values of SEB fluxes for summer of year 1999 for Safdarjung area

Table 7.6: Seasonal measured and modelled values of net all-wave radiation for summer of year 1999 for Palam area

Time	Seasonal	April	June	May	30th Day	7th Day	8th Day	17th Day	25th Day	Nangloim	Rohini	Vasantm	Jank	Samaya	Saket
1	-53.1	-59.5	-59.8	-39.9	-66	-45.5	-53.9	-28.1	-49.5	-3.3	-20.8	-41.1	-47.7	-18.3	-54.8
3	-50.9	-57.2	-59.3	-36.4	-61.5	-47	-49.6	-31.2	-51.3	-26.9	-20.8	-20.2	-47.7	-18.3	-54.8
5	-49.7	-53.4	-60.2	-35.6	-58.3	-46.2	-48.2	-32.1	-48.2	-26.9	-20.8	-20.5	-47.7	-18.3	-54.8
7	18.9	33.2	42.3	-18.8	5.5	6.8	19.3	47.4	31	-16.9	-0.8	-10.5	43	29.5	31.2
9	289.8	343.7	321.9	203.7	295	273.6	272.1	323.6	303.6	48.4	95.1	61.8	197.4	231.8	269.1
11	500.5	550.7	527.1	423.6	505.8	470.3	482.4	527.8	536.2	182.9	181	173.1	303.9	344.3	356.6
13	552.8	570.7	547.5	540.1	563.3	527	446.8	603.3	605.7	227.1	387	193.6	224.4	359.3	365.7
15	435.1	431	378.5	495.9	461.7	392.1	292.6	491.7	456.8	241.1	155.9	109.4	142.6	163.4	283.1
17	183.5	137.7	123.5	289.2	200.7	138.7	178.3	221.2	171	45.3	52.9	28.9	91.4	49.9	16.9
19	-36.1	-83.8	-77.1	52.6	-35.6	-45.1	-31.5	-17	-41.8	-1.3	-26.8	-8.2	-52.5	43.6	-59.7
21	-63.5	-73.8	-71.8	-44.8	-61.7	-61	-70.4	-43	-67	-8.4	-20.8	-41.1	-48	-10.7	-16.6
23	-56.6	-65.3	-65.5	-39.1	-52.3	-52.7	-67.9	-35	-58.9	-8.4	-20.8	-41.1	-48	-10.7	-16.6
RMSE	198.71	178.74	164.84	164.17	41.76	171.37	144.74	127.59	187.57						

Table 7.7: Seasonal measured and modelled values of net all-wave radiation for summer of year 1999 for Safdarjung area

Time	Seasonal	April	May	June	12th day	22nd Day	30th Day	28th Day	2nd Day	Nangloim	Rohini	Vasantm	Jank	Samaya	Saket
1	-50.5	-68.2	-54.5	-29	-36.9	-31.3	-58.4	-52.3	-47.9	-3.3	-20.8	-41.1	-47.7	-18.3	-54.8
3	-50.3	-68.6	-53.4	-28.9	-36.5	-34.4	-57.1	-56.6	-52.9	-26.9	-20.8	-20.2	-47.7	-18.3	-54.8
5	-48.8	-66.9	-51.6	-27.7	-33.4	-30.3	-54	-53.6	-51.2	-26.9	-20.8	-20.5	-47.7	-18.3	-54.8
7	32.4	2.6	34.2	60.5	44.8	42.9	32.5	25.3	15.5	-16.9	-0.8	-10.5	43	29.5	31.2
9	259.9	251.9	265.5	262.2	233.5	284	276	225.3	236.4	48.4	95.1	61.8	197.4	231.8	269.1
11	426.1	425.3	435.6	417.4	320.1	452.6	454.2	376.9	421.2	182.9	181	173.1	303.9	344.3	356.6
13	448.7	440	453.8	452.2	311.3	448.5	481.1	419.4	447.5	227.1	387	193.6	224.4	359.3	365.7
15	326.5	325.8	315	338.6	296.1	336.2	342.8	313.3	332.9	241.1	155.9	109.4	142.6	163.4	283.1
17	110	84.4	105.8	139.8	126.1	147.7	100	107.8	111.6	45.3	52.9	28.9	91.4	49.9	16.9
19	-60.9	-95.8	-60.4	-26.5	-40.3	-44.3	-51	-63.5	-51.9	-1.3	-26.8	-8.2	-52.5	43.6	-59.7
21	-58.2	-79.6	-58.6	-36.6	-40.3	-45.9	-62.3	-56.5	-50.4	-8.4	-20.8	-41.1	-48	-10.7	-16.6
23	-52.8	-71.5	-54.9	-32	-40.8	-41.7	-59.8	-50.8	-44.8	-8.4	-20.8	-41.1	-48	-10.7	-16.6
RMSE	116.99	117.52	120.22	116.99	92.34	123.96	128.37	103.97	112.39						

The range of minimum values of storage heat flux in June varies from -19.3 to -76.7 Wm^{-2} which are comparable with seasonal observed values of storage heat flux (-10.0 to -45 Wm^{-2}) for Rohini area. Simulated positive values of storage heat flux for June varies from 7.2 to 152.8 Wm^{-2}. When storage heat flux values were calculated at particular days, values at 17th day were found nearer to the values at selected sites. The range of simulated negative/minimum values of storage heat flux varies from -9.3 to -69.0 Wm^{-2} which are comparable with Rohini areas of Delhi. Similarly, range of simulated positive storage heat flux values varies from 5.8 to 154.7 Wm^{-2} which is comparable with observed values of Samaya areas.

Similar investigation has been carried out for Safdarjung area for summer season of year 1999 (Table 7.8 and Figure 7.24). The range of modelled minimum values of storage heat flux at seasonal scale (90 days) varies from -4.9 to -70.9 Wm^{-2}whereas positive values of storage heat flux varies from 10.3 to 125.1 Wm^{-2}, which are comparable with respective range of minimum and positive values of observed storage heat flux of Rohini and Samaya. On comparing monthly scale values of storage heat flux, values in month of June are better matched with measured values as compared to values for April and May. The range of simulated minimum values of storage heat flux in June month varies from -18.9 to -58.7 Wm^{-2} whereas day time values of storage heat flux varies from 1.6 to 117.5 Wm^{-2}. Simulated values of June month are comparable with the seasonal observed values of Rohini area. has been with in the When storage heat flux values were calculated at particular days, values at 12th day was found nearer to the values at selected sites. The range of minimum values of storage heat flux varies from -2.1 to -66.5 Wm^{-2} whereas day time values of storage heat flux varies from 5.0 to 97.1Wm^{-2}.

Root mean square errors (RMS) have also been calculated to determine the closeness of the simulated and observed values of storage heat flux at different temporal scale. RMS errors has been found to be between 20.72 to 28.99 Wm^{-2} for the summer season, for both the areas. Similarly at monthly scale, RMS error have been found to be between 20.17 to 35.64 Wm^{-2} and at daily scale between 19.95 – 33.70 Wm^{-2} for both the areas i.e., Palam and Safdarjung. Ranges of the minimum (night time) and day time values of simulated and observed values have also been found to be comparable. RMS errors at different temporal scales are also quite satisfactory. Therefore, it can be concluded that calibrated model is performing well in simulating the storage heat flux.

Table 7.8: Seasonal measured and modelled values of storage heat flux (Wm^{-2}) for summer of year 1999 for Palam area

Time	Seasonal	April	June	May	30th Day	7th Day	8th Day	17th Day	25th Day	Nangloim	Rohini	Vasantm	Jank	Samaya	Saket
1	-30	-31.2	-31.2	-27.6	-33.9	-29.8	-27.9	-25.1	-29.3	-15	-30	-20	-30	-30	-45
3	-27.5	-28.5	-29.4	-24.6	-29.4	-27	-27.4	-24.8	-28.6	-15	-30	-20	-30	-30	-45
5	-28	-28.5	-30.8	-24.5	-29.4	-27.5	-27.5	-25.2	-27.6	-15	-30	-20	-30	-30	-45
7	-9.6	-6.3	-2.8	-19.6	-11.7	-9.3	-13.2	-2.3	-6.7	-5	-10	-10	10	15	15
9	98.3	120.8	114.6	59.6	100.5	91.7	86.5	107.3	103.2	15	55	15	70	70	135
11	161.7	175.6	169.8	139.7	166.1	154.7	160.3	167.1	174.1	90	135	100	110	145	185
13	142.1	138.6	134.9	152.8	142	106.2	126.5	156.6	157.3	95	120	110	105	130	190
15	77.5	70	56	106.4	87	23.5	70.4	91.2	80.5	60	60	45	10	-15	145
17	-22.5	-39.5	-44.4	16.3	-15.6	0	-25.3	-12.9	-34.6	15	-15	-5	-10	-10	-15
19	-85.4	-105.8	-91	-59.5	-91.5	-69	-89.9	-84.6	-89.4	-15	-35	-20	-35	-25	-25
21	-55.5	-46.3	-49.2	-71	-54.2	-57	-50.1	-54.7	-52.3	-15	-30	-20	-30	-30	-30
23	-27.4	-27.3	-27.4	-27.5	-26.2	-31.9	-24.8	-22	-27.6	-15	-30	-20	-30	-30	-30
RMSE	28.99	35.64	30.98	31.37	32.17	25.58	31.81	25.77	33.70						

Table 7.9: Seasonal measured and modelled values of storage heat flux (Wm^{-2}) for summer of year 1999 for Safdarjung area

Time	Seasonal	April	May	June	12th day	22nd Day	30th Day	28th Day	2nd Day	Nangloim	Rohini	Vasantm	Jank	Samaya	Saket
1	-28.8	-32.3	-29.8	-24.2	-25.9	-25.3	-31.1	-28.8	-27.7	-15	-30	-20	-30	-30	-45
3	-25.9	-29.9	-26.8	-21.2	-22.9	-23.7	-27.9	-28.1	-25.8	-15	-30	-20	-30	-30	-45
5	-26.3	-30.3	-26.6	-22.1	-23.4	-22.7	-27.1	-27.9	-28.8	-15	-30	-20	-30	-30	-45
7	-4.9	-12.4	-3.8	1.6	-2.1	-2.8	-4.5	-6.1	-9.2	-5	-10	-10	10	15	15
9	86.1	85.6	87.4	85.3	78	88.7	92.1	75.8	78.8	15	55	15	70	70	135
11	125.1	127.6	130.7	116.9	92.6	136.2	135.3	109.7	124.8	90	135	100	110	145	185
13	104.1	100.8	105.3	106.4	78.9	92.1	113.7	97.7	109.8	95	120	110	105	130	190
15	49.1	49.3	45.4	52.5	20.5	64.7	44.5	60.1	41.1	60	60	45	10	-15	145
17	-27.5	-34.4	-31.7	-16.5	5	-36.1	-28.3	-24.6	-19.6	15	-15	-5	-10	-10	-15
19	-70.9	-85.8	-68	-58.7	-66.5	-58.7	-67.2	-77.6	-72	-15	-35	-20	-35	-25	-25
21	-38.2	-38.4	-38.7	-37.4	-30.2	-34.5	-41.1	-36.5	-32.5	-15	-30	-20	-30	-30	-30
23	-23	-26	-23.7	-19.2	-22.6	-21.7	-25.7	-21.9	-21.6	-15	-30	-20	-30	-30	-30
RMSE	20.72	23.09	20.17	20.63	29.37	20.99	20.77	21.66	19.95						

7.4.5 Sensible Heat flux

On comparing, measured and modelled values of sensible heat flux for Palam and Safdarjung areas in summer 1999, it has been found that modelled values of sensible heat flux at different temporal scale are following trend similar to measured values (Figure 7.23 and 7.24). The minimum difference between measured and modelled values of sensible heat flux has been found during 1:00 am to 7:00 am and 21:00 pm to 23:00 pm. Peak value of measured and modelled sensible heat flux has been found at the same time period that is 12:00 pm to 1:00 pm. However the difference between the peak value of measured and modelled sensible heat flux has been found quite large because in SUEWS model sensible heat flux is calculated as the residual of the energy balance and therefore accumulates the error in all other terms (Ward et al., 2016).

The range of measured seasonal minimum (negative during night time) values of sensible heat flux at Nangloi and Vasantm in Delhi, during summer 1999 varies from -4.1 to -10.3 Wm^{-2} and 0 to -8.30 Wm^{-2} respectively. For Palam area during same time, (Table 7.10 and Figure 7.23) the range of modelled minimum values of sensible heat flux at seasonal scale (90 days) has been found to be between -10.7 to -21.4 Wm^{-2}, which indicates match in trend only. Similarly for Palam range of simulated seasonal sensible heat flux during day time (positive values) varies from 6.5 to 420.9 Wm^{-2} whereas measured values of seasonal sensible flux for Samaya area of Delhi varies from 8.3 to 124.1 Wm^{-2}, which indicate similarity at lower values but have differences in peak values. Similar trend has been observed when monthly values are compared. Good agreement has been observed between simulated sensible heat flux on 30th day (14.8 to 292.5 Wm^{-2}) and seasonal observed values of Samaya area (8.3 to 124.1 Wm^{-2}).

Similar comparison can be found for the Safdarjung area also (Figure 7.24 and Table 7.11). For Safdarjung area simulated results are following the general trend of observed seasonal sensible heat flux (Figure 7.24). Range of the modelled night time sensible heat flux values (negative) varying from -4.2 to -23.2 Wm^{-2} which are following similar trend when compared with observed values (-4.1 to -8.3 Wm^{-2}) of Vasantm area Delhi, however have different in peak value. Similarly, seasonal sensible heat flux during day time (positive) varies of 10.1 to 378.3Wm^{-2} which are following trend of observed seasonal sensible heat flux values of Samaya area of Delhi, however, peak values are quite different. On comparing results at monthly scale, simulated values of seasonal sensible heat flux in month of June are better matching with measured values of Samaya area of Delhi.

The range of night time values of sensible heat flux have been found between -4.7 to -24.7 Wm^{-2} in month of June whereas day time values of sensible heat flux varies from 2.6 to 368.8 Wm^{-2}. When sensible heat flux values were calculated at particular days, values at 28th day were found be comparable with observed values of different locations in Delhi (Figure 7.24 and Table 7.11).

Root mean square errors (RMS) have also been calculated to determine the closeness of the simulated and observed values of sensible heat flux at different temporal scale. At seasonal scale, RMS errors has been found to be between 158.90 to 177.90 Wm^{-2} for the summer season, for both the areas. Similarly RMS error have been found to be between to 140.40 to 201.74 Wm^{-2} at monthly scale, between 75.31 to 200.64 Wm^{-2} at daily temporal scale for both the areas i.e., Palam and Safdarjung. Simulated sensible heat flux, except peak values during day time are comparable with the observed values. Model is overestimating sensible heat flux. However the difference between the peak value of measured and modelled sensible heat flux has been found quite large because in SUEWS model sensible heat flux is calculated as the residual of the energy balance and therefore accumulates the error in all other terms (Ward et al., 2016).

7.4.6 Latent Heat Flux

On comparing, measured and modelled values of latent heat flux for Palam and Safdarjung areas for summer of 1999, it has been found that modelled values of latent heat flux at different temporal scale are following trend similar to measured values (Figure 7.23, 7.24 and Table 7.12, 7.13). The minimum difference between measured and modelled values of latent heat flux has been found during 1:00 am to 7:00 am and 15:00 pm to 23:00 pm. Peak value of measured and modelled latent heat flux has been found at the same time period, that is, 15:00 pm to 17:00 pm. However the difference between the peak value of measured and modelled latent heat flux has been found quite large because when SUEWS model is executed with 0% to 14% water as an input variable, this model underestimates latent heat flux and thus reducing the performance of the model (Ward et al., 2016).

For Palam (Table 7.12 and Figure 7.23) the range of modelled latent heat flux at seasonal scale (90 days) varies from 3.7 to 49.0 Wm^{-2} which comparable with measured seasonal latent heat flux at Nagloi and Rohini areas of Delhi, except peak values during day time. On comparing monthly scale values of latent heat flux, values in month of June are better matched with measured values as compared to values in April and May.

Table 7.10: Seasonal measured and modelled values of sensible heat flux (Wm^{-2}) for summer of year 1999 for Palam area

Time	Seasonal	April	June	May	30th Day	7th Day	8th Day	17th Day	25th Day	Nangloim	Rohini	Vasantm	Jank	Samaya	Saket
1	-17.2	-18.4	-21.8	-11.5	-22.7	-25.6	-19.6	-5.8	-17.4	4.1	0.0	-4.1	2.1	24.8	10.3
3	-18.2	-20.1	-24.4	-10.1	-24.2	-16.2	-20.9	-9.3	-25.1	4.1	0.0	2.1	2.1	24.8	10.3
5	-18.8	-17.7	-27.5	-11.2	-22.4	-25.4	-21.4	-10.3	-23.1	4.1	0.0	4.1	2.1	24.8	10.3
7	37.9	53.0	56.6	4.0	30.6	16.2	32.8	52.7	34.5	4.1	0.0	4.1	0.0	12.4	4.1
9	199.8	244.2	229.2	126.0	217.2	144.0	200.5	201.6	172.8	12.4	31.0	24.8	66.2	66.2	66.2
11	350.3	400.8	384.5	265.7	317.0	242.2	333.0	333.6	124.4	43.5	24.8	24.8	115.9	124.1	99.3
13	420.9	460.7	440.9	361.0	354.4	337.3	274.5	460.7	229.0	37.2	103.4	37.2	74.5	124.1	99.3
15	368.0	390.9	339.6	373.6	287.4	271.3	184.4	427.6	292.4	91.0	41.4	31.0	57.9	99.3	66.2
17	188.7	207.3	175.1	183.6	63.7	188.8	101.8	265.1	158.0	14.5	0.0	12.4	31.0	62.1	33.1
19	61.5	51.8	36.8	96.0	-4.4	74.6	53.7	99.6	37.8	-10.3	10.3	-4.1	-4.1	0.0	8.3
21	6.5	-2.2	-7.1	28.7	-22.3	13.6	-37.9	36.0	-8.2	-4.1	0.0	-4.1	4.1	24.8	20.7
23	-16.0	-18.6	-24.0	-5.4	-26.9	-8.8	-23.8	5.9	-27.6	-4.1	0.0	-4.1	4.1	24.8	20.7
RMSE	177.90	201.74	188.36	148.40	146.06	134.9	123.21	200.64	104.12						

Table 7.11: Seasonal measured and modelled values of sensible heat flux (Wm^{-2}) for summer of year 1999 for Safdarjung area

Time	Seasonal	April	May	June	12th day	22nd Day	30th Day	28th Day	2nd Day	Nangloim	Rohini	Vasantm	Jank	Samaya	Saket
1	-13.7	-22.1	-14.3	-4.8	2.9	-29.5	-10.0	-60.2	-5.9	4.1	0.0	-4.1	2.1	24.8	10.3
3	-20.2	-26.9	-18.8	-14.9	-1.7	-39.5	-14.6	-85.9	-14.7	4.1	0.0	2.1	2.1	24.8	10.3
5	-23.8	-26.7	-20.0	-24.7	-8.7	-35.6	-13.8	-103.1	-12.1	4.1	0.0	4.1	2.1	24.8	10.3
7	50.2	33.8	51.6	65.2	25.7	25.6	52.0	14.2	44.2	4.1	0.0	4.1	0.0	12.4	4.1
9	196.6	195.9	201.3	192.5	141.5	157.4	212.2	150.0	188.4	12.4	31.0	24.8	66.2	66.2	66.2
11	333.1	333.3	339.3	326.6	203.5	344.8	300.6	265.7	333.4	43.5	24.8	24.8	115.9	124.1	99.3
13	378.3	379.0	387.3	368.8	124.1	395.6	305.5	294.9	379.2	37.2	103.4	37.2	74.5	124.1	99.3
15	301.3	318.2	305.7	280.0	44.4	308.7	287.5	238.9	335.3	91.0	41.4	31.0	57.9	99.3	66.2
17	165.2	160.5	163.1	172.0	94.8	100.8	164.0	116.9	-10.1	14.5	0.0	12.4	31.0	62.1	33.1
19	47.3	31.8	47.2	62.9	26.3	48.8	63.6	13.2	2.7	-10.3	10.3	-4.1	-4.1	0.0	8.3
21	10.1	-5.6	9.2	26.7	-17.4	-2.6	25.7	-24.1	6.5	-4.1	0.0	-4.1	4.1	24.8	20.7
23	-7.6	-18.4	-6.9	2.6	-1.0	-16.0	5.6	-41.8	-21.8	-4.1	0.0	-4.1	4.1	24.8	20.7
RMSE	158.93	159.95	163.59	153.95	75.31	157.60	145.28	128.05	157.16						

The range of values of latent heat flux in June moth varies from 7.32 to 136.4 Wm^{-2}, which are comparable with seasonal latent heat flux at Rohini and Nagloi. When simulated values of latent heat flux were calculated at particular days, values at 8th day (0.8 to 110.3 Wm^{-2}) were found nearer to the measured values of latent heat flux at Rohini.

Model validation for the latent heat flux has also been carried out for the Safdarjung area using observed data of summer 1999. In summer 1999 (Table 7.13 and Figure 7.24) the modelled values of latent heat flux at seasonal scale (90 days) varies from 6.2 to 15.90 Wm^{-2} which are found to be comparable with observed seasonal latent heat flux of Rohini area. On comparing monthly scale values of latent heat flux, values in month of June are better matched with measured values as compared to values at April and May. The range of values of latent heat flux varies from -20.4 to 29.6 Wm^{-2} which are comparable with seasonal latent heat flux at Nangloim. When latent heat flux values were calculated at particular days, values at 12th day were found be nearer to the values at Rohini area. The range of values of latent heat flux varies from 0.52 to 208.9 Wm^{-2}.

The RMSE error has been calculated to determine the agreement between simulated and observed values. For both the study areas RMSE error has been found as 33.83 to 40.95 Wm^{-2}. Trend of simulated latent heat flux has been found to be matching with trend of observed values. Model seems to under estimating the peak latent heat flux values.

7.4.7 Validation with Respect to SEB Flux Ratios

In addition to the validation of simulated results through matching the hourly trend, peak values during day time and night time of observed data at corresponding temporal scales, different ratios of simulated SEB fluxes as suggested by Grimmond and Oke (1999) and Middle et. al. 2012 have be calculated for day time seasonal mean, night time seasonal mean and seasonal daily mean temporal scales and compared with respective observed SEB flux ratios. Four ratios which include ratio of sensible heat flux to net all-wave radiation (QH/Q), ratio of latent heat flux to net all-wave radiation (QE/Q), ratio of storage heat flux to net all-wave radiation (QS/Q) and ratio of sensible heat flux to storage heat flux (QH/QS). These ratios have been calculated for modelled values and measured values at different sites. Ratio of simulated values have been found very close to the measured values at Nangloi and Rohini areas in Delhi (Table 7.14). Therefore, our modelled results have been successfully validated. Ratio of simulated sensible heat flux to net all-wave radiation QH/Q (0.39) has been found to be comparable with observed ratio (0.40) of Nagloi and Rohini (0.34) at daily temporal scale.

Table 7.12: Seasonal measured and modelled values of latent heat flux (Wm^{-2}) for summer of year 1999 for Palam area

Time	Seasonal	April	June	May	30th Day	7th Day	8th Day	17th Day	25th Day	Nangloim	Rohini	Vasantm	Jank	Samaya	Saket
1	4.6	0	4.1	9.7	1.3	18.2	1.1	13.5	8	7.6	9.2	-17	-19.7	-13.1	-20.2
3	3.7	0	3.9	7.3	1.2	5.4	1	12.1	11.7	-16	9.2	-2.3	-19.7	-13.1	-20.2
5	4.6	0	6	7.8	1.2	14.1	0.9	11.1	10.3	-16	9.2	-4.6	-19.7	-13.1	-20.2
7	4.8	0	3.4	11.1	1.1	17.9	0	11.6	17.9	-16	9.2	-4.6	33	2.1	12
9	14.1	0	1.6	40.8	0	65.1	0	37.7	50.7	21	9	22	61.2	95.6	67.9
11	15.5	0	1.1	45.5	50.1	94.3	0	54.8	65.6	49.5	21.2	48.2	78.1	75.2	72.3
13	19.9	0	3.1	56.7	97.6	92.8	0	16.8	250.5	94.9	163.5	46.4	44.9	105.1	76.4
15	21.1	0	15.7	47.7	119.5	81.5	0	5.3	116.5	90	54.5	33.4	74.6	79.1	71.9
17	49	0	25.8	121.2	184.7	6.3	0	1.4	80.3	15.8	67.9	21.5	70.3	-2.2	-1.2
19	19.2	0	9.9	47.7	92.5	1.3	0	0.4	42.5	24	-2.1	16	-13.3	68.6	-43
21	12.3	0	12.4	24.4	42.2	1.9	1.5	3.3	21.4	10.8	9.2	-17	-22.1	-5.5	-7.3
23	7.2	0	7.3	14.4	21.6	1.1	1.3	2.1	17.5	10.8	9.2	-17	-22.1	-5.5	-7.3
RMSE	33.83	45.95	41.56	33.97	55.05	41.90	45.86	43.06	61.07						

Table 7.13: Seasonal measured and modelled values of latent heat flux (Wm^{-2}) for summer of year 1999 for Safdarjung area

Time	Seasonal	April	May	June	12th day	22nd Day	30th Day	28th Day	2nd Day	Nangloim	Rohini	Vasantm	Jank	Samaya	Saket
1	6.4	0	4.4	14.8	1.4	37.6	-17	26.1	0	7.6	9.2	-17	-19.7	-13.1	-20.2
3	8.2	0	4.9	19.8	11	41	-2.3	26.8	0	-16	9.2	-2.3	-19.7	-13.1	-20.2
5	11.8	0	5.6	29.6	21.8	38.2	-4.6	20.5	0	-16	9.2	-4.6	-19.7	-13.1	-20.2
7	6.7	0	6.5	13.7	32.6	39.3	-4.6	44	0	-16	9.2	-4.6	33	2.1	12
9	8.1	0	8.3	15.9	44.6	68.3	46.3	33	0	21	9	22	61.2	95.6	67.9
11	5.2	0	3.7	11.9	60.8	8.1	47.4	55.4	0	49.5	21.2	48.2	78.1	75.2	72.3
13	7.7	0	3.8	19.4	149.4	1.6	71.3	44.9	0	94.9	163.5	46.4	44.9	105.1	76.4
15	13.1	0	8.5	-27.2	152.3	5.5	61	74.6	0	90	54.5	33.4	74.6	79.1	71.9
17	15.9	0	18.9	28.7	69.5	125.8	56.1	70.3	110	15.8	67.9	21.5	70.3	-2.2	-1.2
19	6.2	0	5	13.7	43	8.4	45.5	16.6	60.9	24	-2.1	16	-13.3	68.6	-43
21	7	0	9	12	44.1	27.7	42.9	26.6	12.8	10.8	9.2	-17	-22.1	-5.5	-7.3
23	6	0	4.6	13.4	10.7	23.7	30.3	13.4	26.8	10.8	9.2	-17	-22.1	-5.5	-7.3
RMSE	40.95	45.95	42.34	43.70	54.76	49.25	32.40	39.87	45.04						

Table 7.14: Validation of model through comparison of SEB flux ratios

Ratio	QH/Q	QH/Q	QH/Q	QE/Q	QE/Q	QS/Q	QS/Q	QS/Q	QH/QS	QH/QS	QH/QS
Temporal Scale	Modelled	Nangloi	Rohini	Modelled	Rohini	Modelled	Nangloi	Rohini	Modelled	Nangloi	Rohini
Day time mean	0.63	0.82	0.59	35.55	41.34	0.33	0.32	0.30	1.11	0.58	0.24
Night time mean	-0.29	0.61	-0.08	2.30	1.23	0.81	1.00	1.44	0.07	0.04	-0.06
Daily mean	0.39	0.40	0.34	20.52	22.66	0.42	1.03	1.32	0.74	0.30	0.12

Ratio of simulated storage heat flux and net all-wave radiation QS/Q (0.33) has been found to be close to observed ratio for Nagloi (0.32) and Rohini (0.30) areas for day time. Similarly other ratios corresponding to different fluxes have been found to be in close agreement, which indicate that model is simulating SEB for both the areas satisfactorily. Similarly ration have been compared with other published studies (Grimmond and Oke 1999, Middle et al., 2012) and found to be in line with their conclusions.

7.5 SIMULATED SURFACE ENERGY BALANCE FOR DIFFERENT LULC CHANGE SCENARIOS

Results of the surface energy balance modelling for different scenarios conceptualized to study the effects of LULC change for the two study areas Palam and Safdarjung in Delhi have been discussed in this section. The effect of urbanization (LULC changes) on the local climate of Palam and Safdarjung has been studied in term of estimation of changes in surface energy balance constituents corresponding to different scenarios of LULC and meteorology for different years i.e., 1973, 1977, 1986, 1991, 1999, 2002, 2006, 2009, 2011, 2013, and 2014. This is a period during which Delhi became more urbanized. Three cases (Scenario-A, Scenario-B and Scenario-C) were conceptualized, which are discussed in Chapter 5.

- Scenario-A: surface energy balance (annual fluxes) was simulated corresponding to actual meteorology and LULC for different years,
- Scenario-B: simulation of surface energy balance (annual) for different years corresponding to meteorology of base year (1973) and LULC of respective years, and

- Scenario-C: surface energy balance (annual) was simulated for different year's corresponding to LULC of base year (1973) and meteorology of different years.

Corresponding to above mentioned scenarios, calibrated model has been run for different years using input data of respective years for Palam and Safdarjung area. SEB fluxes have been simulated at hourly temporal scale, for above mentioned years, for three scenarios and then transformed into results at different temporal resolution like monthly average hourly fluxes, seasonal hourly fluxes and annual hourly fluxes. Further relative change in SEB fluxes corresponding to base year i.e., 1973 have been determined for different LULC scenarios using equation 7.1. In this equation V_1 is the flux value in base year 1973 and V_2 is the flux value in different years. The relative percentage change in these fluxes is defined as the negative and positive change of the absolute value from the base value i.e., fluxes value in year 1973 in percentage.

$$\text{Relative Percentage Change from } V_1 \text{ to } V_2 = \frac{(V_2 - V_1)}{V_1} * 100 \qquad 7.1$$

Also, impact of LULC on each surface energy component have been investigated in term of change in peak values of these components over the years 1973-2014 for three scenarios. Also, annual mean values of anthropogenic heat flux calculated by LUCY model have shown increasing trend from 1973 (1.12 $\mathrm{Wm^{-2}}$) to 2014 (3.82 $\mathrm{Wm^{-2}}$) and this is occurring due to the impact of rapid and continuous urbanization. The detailed results of SEB modelling has been presented in subsequent sections.

7.5.1 Net All-Wave Radiation

Monthly, seasonal and annual average of net all-wave radiation at hourly temporal scale have been calculated for both the study areas i.e., Palam and Safdarjung from hourly model results for different Scenarios (A, B and C) for different years. Annual extreme hourly values have also been calculated to ascertain the effects of LULC change scenario on extreme values of net all-wave radiation.

Net all-wave radiation is an algebraic sum of all fluxes and indicates changes in other fluxes with change in surface and other environmental conditions. For Palam area in Scenario-A, peak value of monthly average hourly net all-wave radiation during night time in different years have been found to be increasing means negative values are decreasing over the years from -90.60 $\mathrm{Wm^{-2}}$ in year 1973 to -59.30 $\mathrm{Wm^{-2}}$ in year 2014. Similarly, hourly peak values of net all-wave radiation during day time have been found to be

decreasing over the years from 622 Wm^{-2} in year 1973 to 481.30 Wm^{-2} in year 2014, as shown in Table 7.15 and Figure 7.25. For Palam area in Scenario-A, relative percentage change in peak value of net all-wave radiation during night time as compared to the base year is showing decreasing trend over the years from 11.04% in year 1977 to 34.55% in year 2014. Similarly, relative percentage change in peak value of net all-wave radiation during day time, from the base year, is showing decrease in net all-wave radiation from year 1977 (0.58%) to 2014 (22.62%). For Safdarjung area in Scenario-A, peak values of monthly average hourly net all-wave radiation has been calculated. According to the results, monthly average hourly peak values of net all-wave radiation during night and day time over the years from 1973 to 2014 are increasing and decreasing, respectively. Monthly mean hourly peak value of net all-wave radiation during night time in different years found to be increasing i.e., means negative values are decreasing over the years from -91 Wm^{-2} (1973) to -60.8 Wm^{-2} (2014) and during day time found to be decreasing from 638.3 Wm^{-2} (1973) to 488.80 Wm^{-2} (2014), as shown in Table 7.18 and Figure 7.28. Relative percentage change in night time net all-wave radiation from the base year is showing decrease in negative values from 1977 (4.07%) to 2014 (33.19%). Similarly, relative percentage change in day time monthly average hourly net all-wave radiation from the base year is showing decreasing trend from year 1977 (2.29%) to 2014 (23.42%).

In Scenario-B, for Palam station, monthly average hourly net all-wave radiation have been calculated from the hourly simulated results. According to the results (Table 7.16 and Figure 7.26), peak value of monthly average hourly net all-wave radiation during night time are increasing (means negative values are decreasing) from year 1973 to 2014 whereas during day time trend is increasing over the years, which indicate effect of urbanization. Peak values of monthly average hourly net all-wave radiation during night time increasing (means negative values are reducing) over the years from -90.60 Wm^{-2} (1973) to -88.40 Wm^{-2} (2014) whereas during the day time values are increasing over the years from 622.0 Wm^{-2} (1973) to 629.60 Wm^{-2} (2014), as shown in Table 7.16 and Figure 7.26. Relative percentage change in monthly average hourly net all-wave radiation during night time from the base year is showing decreasing trend in negative values from year 1977 (0.11%) to 2014 (2.43%). Similarly, relative percentage change in peak monthly average hourly net all-wave radiation during day time from the base year is showing increasing trend from year 1977 (0.53%) to 2014 (1.22%). In case of Safdarjung area in Scenario-B, monthly average of net all-wave radiation at hourly basis has been calculated from hourly simulated results. According to the results (Table 7.19 and Figure 7.29), peak values of monthly

average hourly net all-wave radiation during night time have shown decreasing trend from -91 Wm^{-2} (1973) to -89.10 Wm^{-2} (2014) over the years, whereas results exhibit increasing trend in peak values from 638.3 Wm^{-2} (1973) to 642.80 Wm^{-2} (2014) during day time over the years. Relative percentage change in peak values of monthly average hourly net all-wave radiation during night time, from the base year, is showing decreasing trend in negative values from year 1977 (0.11%) to 2014 (2.09%). Similarly, relative percentage change in peak values of monthly average hourly net all-wave radiation during day time, from the base year, is showing increasing trend from year 1977(0.13%) to 2014 (0.70%).

Due to urbanization over the years high albedo LULC areas like irrigated & unirrigated (0.21), trees (0.18) have been converted into LULC classes of low albedo like settlement and built-up surface (0.12 to 0.15). Also high emissivity areas like irrigated & unirrigated grass (0.93), forest & trees areas (0.98) have been converted into low emissivity areas like buildings (0.91) and paved areas (0.95). Such a conversion of LULC classes due to urbanization leads to reduction in reflected radiation and outward flow of short & long wave radiations, which results in increase in net radiation over the years. The overall net all-wave radiation are found to be increasing in Scenario-B due to change in pervious & vegetative LULC classes into impervious built-up LULC classes over the years which leads to decrease in overall vegetation, evaporative cooling and resulting warmer urban areas. Results are in line with conclusions drawn in similar studies in different parts of the world (Abdellah et al., 2015; Arnfield & Grimmond, 1998; Das et al., 2009a; Das & Padmanabhamurty, 2008; Das et al., 2014; Dash & Hunt, 2007; Diffenbaugh, 2009; Nagar et. al., 2002).

In Scenario-C, for Palam area, peak values of monthly average net all-wave radiation at hourly temporal scale have been calculated from hourly simulated results. According to the results (Table 7.17 and Figure 7.27), peak value of monthly average hourly net all-wave radiation during night time is increasing (means negative values are decreasing) from year 1973 to 2014 whereas during day time trend is increasing over the years. During night time peak values of monthly average hourly net all-wave radiation are showing decreasing trend in negative values from -90.60 Wm^{-2} (1973) to -60.80 Wm^{-2} (2014) over the years where as during day time net all-wave radiation values are showing decreasing trend from 622.0 Wm^{-2} (1973) to 475.60 Wm^{-2} (2014) over the years (Table 7.17 and Figure 7.27). Relative percentage change in monthly average hourly net all-wave radiation, during night time, with respect to base year value is showing decreasing trend in negative values from 1977 (11.15%) to 2014 (32.89%). Similarly, during day time relative

percentage change in peak values of monthly average hourly net all-wave radiation with respect to base year value, is showing decreasing trend from 1977 (1.91%) to 2014 (23.54%). For Safdarjung area also, results indicate trends in net all-wave radiation similar to the Palam area. During night time, peak values of monthly average hourly net all-wave radiation are showing decreasing trend in negative values over the years from -91Wm^{-2} (1973) to -62.10 Wm^{-2} (2014), also during day time decreasing trends in net all-wave radiation have been observed from 638.3 Wm^{-2} (1973) to 485.40 Wm^{-2} (2014) over the years (Table 7.20 and Figure 7.30). Relative percentage change in peak values of monthly average hourly net all-wave radiation, during night time, with respect to base year value, is showing decreasing trend in negative values from 1977 (3.96%) to 2014 (31.76%). Similarly, during day time, relative percentage change in monthly average hourly net all-wave radiation with respect to base year value, is showing decreasing trend from 1977 (-2.55%) to 2014 (-23.95%). The overall peak values of monthly average hourly net all-wave radiation during night and day time are decreasing over the years due to change in effects of climate change forcing other than LULC changes.

Annual extreme hourly values of net all-wave radiation have also been calculated from the hourly simulated results in different Scenarios i.e., A, B and C to study the effect of LULC changes on extreme values for both areas i.e., Palam and Safdarjung (Table 7.21). Annual extreme hourly values of net all-wave radiation during night time for Palam area have decreased (negative values) for Scenario-A (-155.64 to -121.15 Wm^{-2}), Scenario-B (-155.64 to -123.97 Wm^{-2}) and Scenario-C (-155.64 to -123.97 Wm^{-2}). Further for Palam area, results indicate that annual extreme hourly values of net all-wave radiation during day time have decreased for Scenario-A (728.88 to 533.37 Wm^{-2}) and Scenario-C (728.88 to 528.86 Wm^{-2}) whereas in Scenario-B, values have increased from 728.88 to 734.74 Wm^{-2} over the years from 1973 to 2014 (Table 7.21).

Trends similar to Palam area have been found in extreme values of annual hourly net all-wave radiation for Safdarjung area. Annual extreme hourly values of net all-wave radiation during night time for Safdarjung areas have decreased (negative values) for Scenario-A (-161.14 to -107.01 Wm^{-2}), Scenario-B (-161.14 to -157.97 Wm^{-2}) and Scenario-C (-161.14 to -109.16 Wm^{-2}). Further for Safdarjung area, results indicate that annual extreme hourly values of net all-wave radiation during day time have decreased (negative values) significantly for Scenario-A (741.61 to 548.51 Wm^{-2}) and Scenario-C (741.61 to 545.5 Wm^{-2}) over the years from 1973 to 2014, whereas in Scenario-B, values have increased from 741.61 to 744.52 Wm^{-2} during the same period (Table 7.21).

This is happening due to conversion of vegetation into paved surfaces caused by rapid urbanization. On comparing these three cases, it is found that maximum change in net all-wave radiation has been observed in Scenario-B which indicates more impact of LULC changes as compared to the impact of meteorological changes (Scenario-C). The results of present study are showing similar conclusions to other studies held in Delhi, Anand region in Gujarat and two UK sites (Nagar S.G., 2002;Y Das et al., 2009b; Yashvant Das et al., 2014; Mohan & Kandya, 2015; Ward H. C., 2016). Trends in annual extreme hourly net all-wave radiation are also indicating the effect of urbanization. Decreasing trend have been found for Scenario-A and C whereas trend of annual extreme hourly net all-wave radiation is increasing for Scenario-B, where LULC effects have been considered while simulating the net all-wave radiations using calibrated SUEWS model. Therefore, it can be concluded that net all-wave radiation in Scenario-B has increased over the years due to change in pervious & vegetative LULC classes into impervious built-up LULC classes leading to decrease in overall vegetation, evaporative cooling, less reflection of radiation resulting warmer urban areas. Results are in line with conclusions drawn in similar studies in different parts of the world (Abdellah et al., 2015; Arnfield & Grimmond, 1998; Y Das et al., 2009a; Yashvant Das & Padmanabhamurty, 2008; Yashvant Das et al., 2014; Dash & Hunt, 2007; Diffenbaugh, 2009; Nagar, Seetaramayya, Tyagi, & Singh, 2002).

7.5.2 Storage Heat Flux

Monthly, seasonal and annual average of storage heat flux at hourly temporal scale has been calculated for both the study areas Palam and Safdarjung from hourly model results for different Scenarios (A, B and C) for different years. Annual extreme hourly values have also been calculated to ascertain the effects of LULC change scenario on extreme values of storage flux. For Palam area in Scenario-A, peak value of monthly average hourly storage heat flux during night time in different years found to be increasing means negative values are decreasing over the years from -97.20 Wm^{-2} in year 1973 to -101.0 Wm^{-2} in year 2014. Similarly, hourly peak values of storage heat flux during day time have been found to be decreasing over the years from 157.0 Wm^{-2} in year 1973 to 161.50 Wm^{-2} in year 2014, as shown in Table 7.22 and Figure 7.31. Relative percentage change in peak value of storage heat flux during night time, as compared to the base year values is showing decreasing trend over the years ranging from 13.58 % in year 1977 to -3.91 % in year 2014.

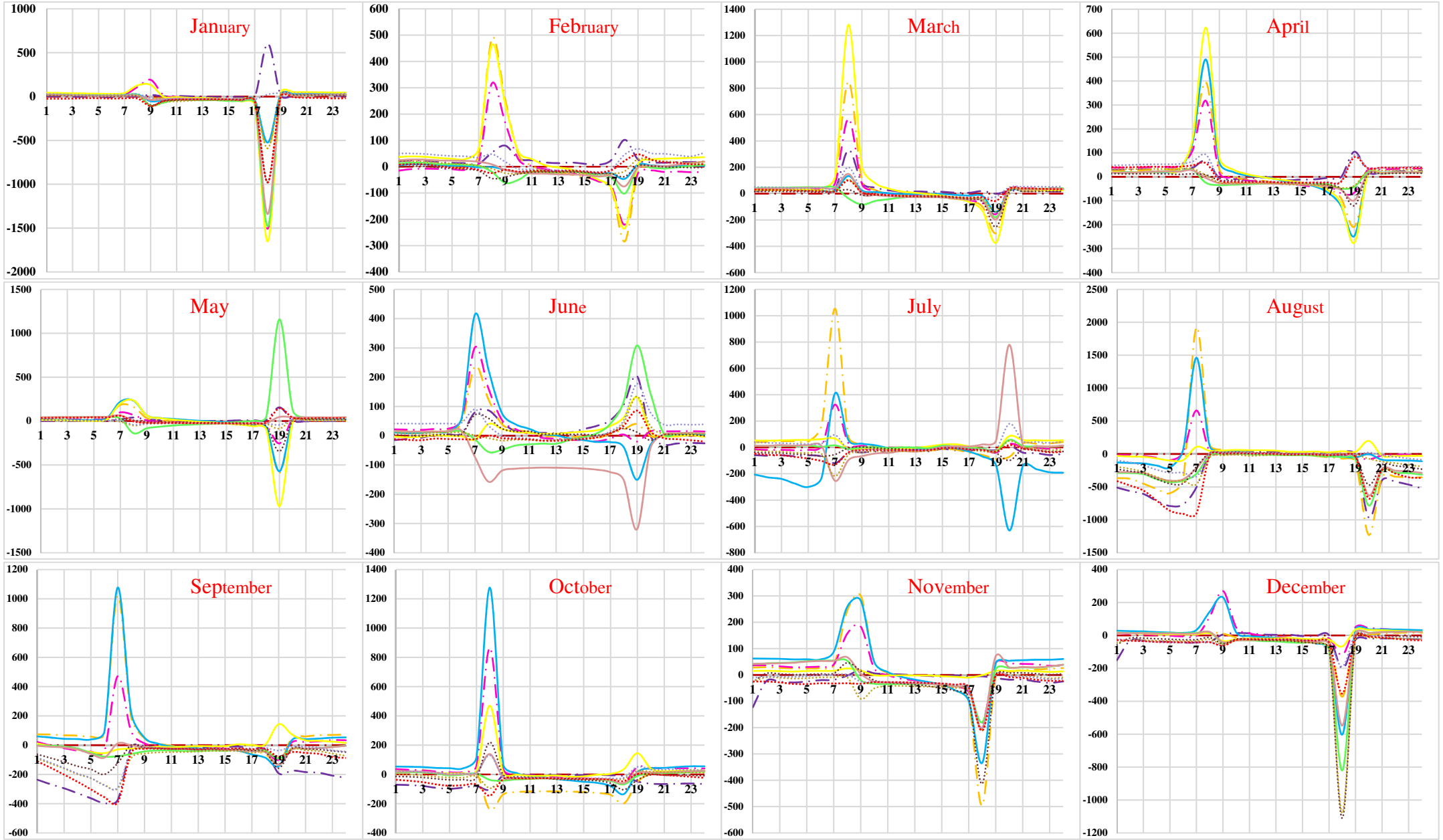

1973	1977	1986	1991	1998	1999	2002	2006	2009	2011	2013	2014	X-axis - Time in Hours
												Y-axis -% change in Heat Flux
Note: Percentage change in values of heat flux are very high because of the values in base year are very small which are used in denominator while calculating percentage change for different years.												

Figure 7.25: Percentage change in values of monthly average hourly net all-wave radiation for Scenario-A for Palam area

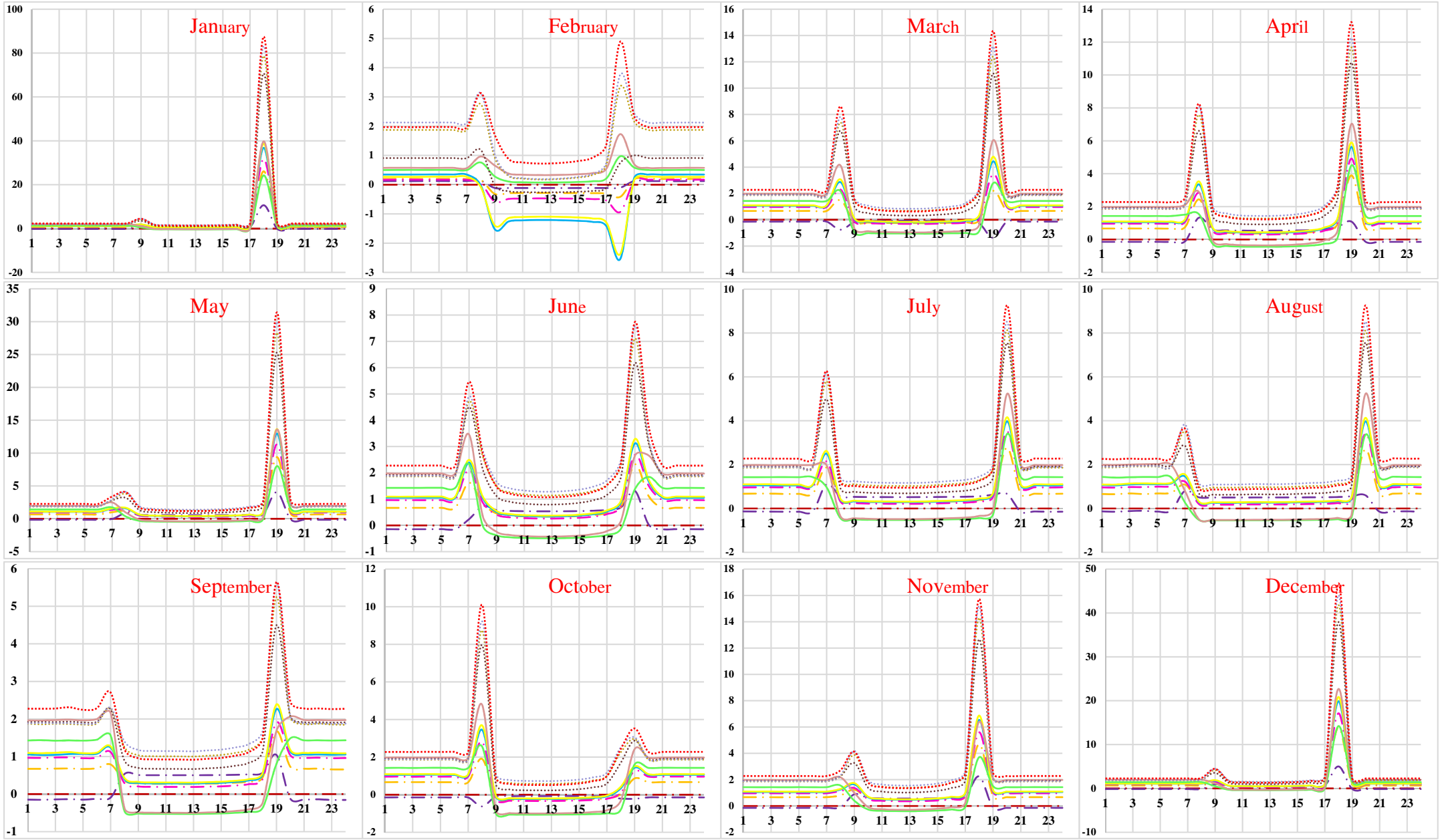

1973	1977	1986	1991	1998	1999	2002	2006	2009	2011	2013	2014	X-axis - Time in Hours
												Y-axis -% change in Heat Flux
Note: Percentage change in values of heat flux are very high because of the values in base year are very small which are used in denominator while calculating percentage change for different years.												

Figure 7.26: Percentage change in values of monthly average hourly net all-wave radiation for Scenario-B for Palam area

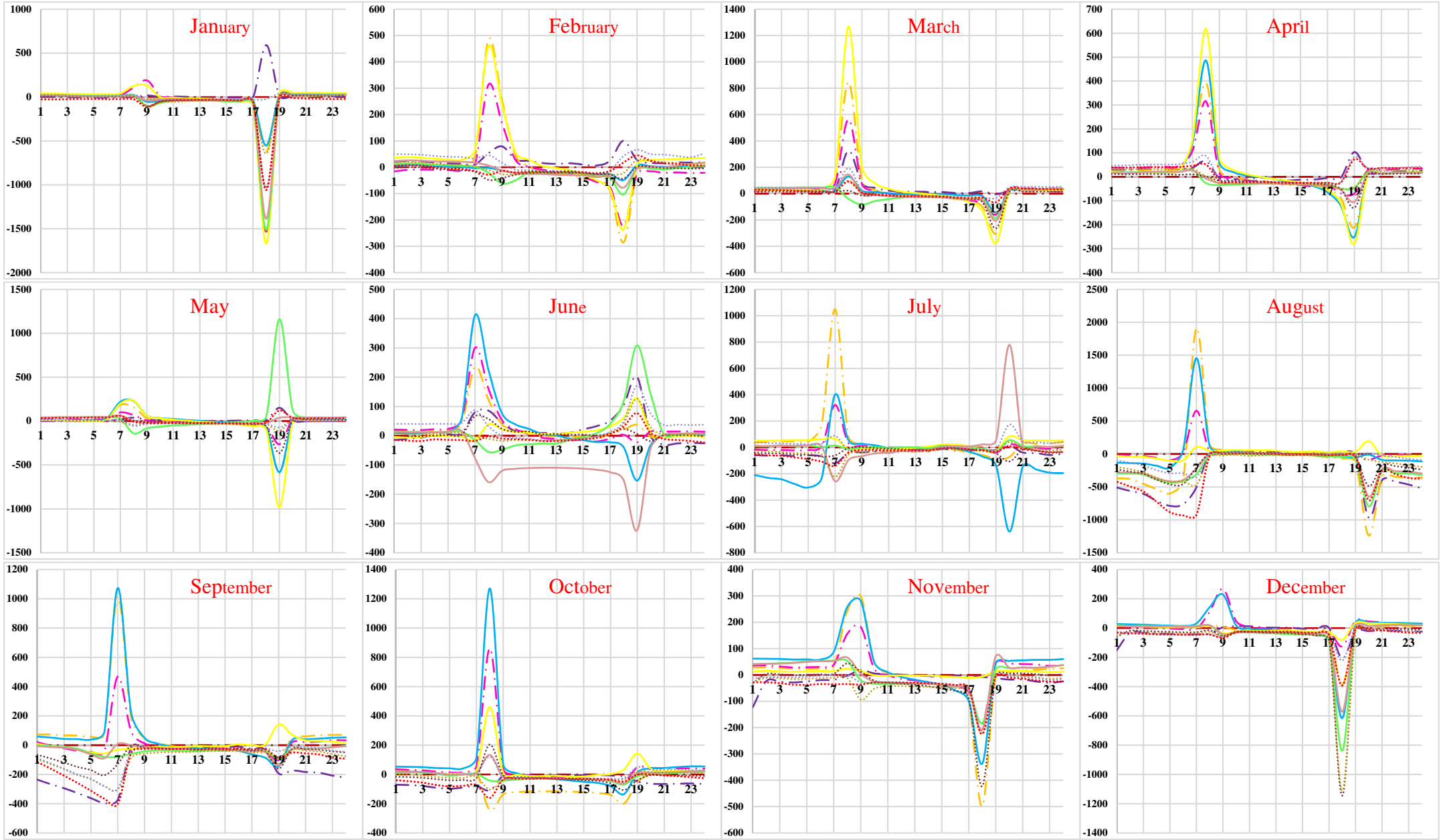

1973	1977	1986	1991	1998	1999	2002	2006	2009	2011	2013	2014	X-axis - Time in Hours
												Y-axis -% change in Heat Flux
Note: Percentage change in values of heat flux are very high because of the values in base year are very small which are used in denominator while calculating percentage change for different years.												

Figure 7.27: Percentage change in values of monthly average hourly net all-wave radiation for Scenario-C for Palam area

Table 7.15: Simulated peak values of monthly average hourly net all-wave radiation for Scenario-A for Palam area

Year	Time	Jan	Feb	Mar	Apr	May	Jun	Jul	Aug	Sep	Oct	Nov	Dec
1973	Min	-57.7	-52.1	-74.9	-90.6	-78.8	-44.1	-20.3	-6.5	-19.0	-39.8	-49.7	-47.1
	Min_Hr	19	19	20	20	21	21	21	21	20	20	19	19
	Max	411.9	445.8	536.8	622.0	595.4	506.4	491.3	407.5	565.3	523.5	423.6	373.0
	Max_Hr	14	13	14	13	13	13	13	14	13	13	13	13
1977	Min	-48.9	-43.2	-59.4	-73.3	-80.6	-57.5	-28.3	-32.4	-52.1	-65.1	-76.5	-73.5
	Min_Hr	19	20	20	21	21	21	21	21	20	20	1	1
	Max	394.0	512.3	618.4	594.9	608.9	550.3	362.9	515.0	478.3	498.0	417.4	385.3
	Max_Hr	14	14	13	13	13	13	13	14	13	13	13	13
1986	Min	-54.6	-63.6	-57.5	-82.8	-73.3	-45.7	-14.2	-32.0	-9.6	-94.4	-53.9	-49.3
	Min_Hr	19	18	20	20	20	21	21	20	20	15	18	19
	Max	316.3	345.1	438.5	487.5	491.8	499.7	438.7	398.0	450.3	-15.7	354.6	292.8
	Max_Hr	13	12	12	12	13	13	12	12	12	3	12	13
1991	Min	-47.6	-65.1	-46.2	-65.0	-62.5	-37.4	-19.6	-8.0	-15.1	-22.2	-27.5	-27.1
	Min_Hr	19	19	20	20	21	21	21	21	20	20	19	6
	Max	303.6	378.4	441.0	467.1	447.9	453.4	427.2	356.8	430.0	408.9	336.1	331.7
	Max_Hr	13	13	13	12	13	13	13	14	14	13	13	13
1998	Min	-43.7	-49.2	-59.3	-78.5	-63.0	-42.5	-51.1	-12.1	-12.2	-27.4	-31.8	-30.7
	Min_Hr	19	20	20	20	20	20	20	21	20	19	18	19
	Max	285.5	361.9	522.6	573.2	616.8	512.3	451.8	405.5	444.7	371.6	354.0	320.3
	Max_Hr	14	13	14	13	13	13	13	13	12	12	12	13
1999	Min	-37.4	-47.1	-66.2	-83.8	-78.2	-44.8	-9.0	-8.1	-11.1	-27.1	-42.3	-30.3
	Min_Hr	18	19	19	19	20	21	21	21	21	21	19	19
	Max	339.6	434.0	562.0	576.9	565.7	549.0	516.3	568.2	529.1	481.3	414.5	306.5
	Max_Hr	13	13	12	12	12	14	14	13	13	13	13	14
2002	Min	-58.0	-53.9	-52.1	-76.1	-48.2	-41.5	-18.0	-22.9	-24.4	-36.9	-39.2	-42.5
	Min_Hr	19	20	20	21	21	21	21	21	20	20	19	19
	Max	244.1	367.1	436.8	449.6	437.3	424.8	489.7	333.2	335.1	373.8	276.4	238.8
	Max_Hr	14	14	14	13	15	14	13	14	14	13	14	13
2006	Min	-57.7	-53.6	-55.0	-78.8	-44.8	-54.8	-17.6	-20.9	-24.6	-34.6	-33.5	-41.6
	Min_Hr	19	19	20	20	21	16	21	21	20	20	20	19
	Max	291.9	316.2	390.1	440.7	448.4	-28.7	393.1	419.2	395.9	376.0	290.2	267.5
	Max_Hr	14	13	14	13	13	6	14	13	13	13	13	13
2009	Min	-49.5	-50.3	-62.9	-82.2	-67.8	-42.5	-23.0	-17.1	-23.1	-44.3	-50.5	-51.4
	Min_Hr	19	20	20	20	20	21	21	21	20	19	19	19
	Max	267.1	357.3	420.4	491.9	483.0	539.1	405.8	429.7	389.5	351.9	266.2	255.4
	Max_Hr	13	14	13	13	13	13	13	13	13	13	13	13
2011	Min	-42.4	-39.2	-51.2	-67.3	-69.4	-41.3	-20.4	-14.0	-23.5	-32.4	-51.1	-52.8
	Min_Hr	19	20	20	20	21	21	21	21	20	20	19	19
	Max	244.2	345.9	424.1	455.3	432.9	447.9	354.2	346.4	320.1	367.4	239.9	258.9
	Max_Hr	13	13	14	13	13	14	14	14	13	13	13	13
2013	Min	-34.3	-25.5	-38.4	-57.3	-75.2	-27.3	-10.9	-8.3	-20.8	-26.7	-50.3	-43.7
	Min_Hr	19	20	20	20	21	21	21	4	20	20	19	19
	Max	306.9	386.0	434.2	489.8	445.7	436.6	397.2	401.6	416.3	393.8	301.6	285.7
	Max_Hr	14	14	13	13	13	14	13	13	13	13	13	13
2014	Min	-59.3	-37.9	-45.4	-57.8	-54.7	-47.8	-22.4	-22.3	-28.1	-39.3	-50.9	-48.0
	Min_Hr	19	20	20	20	21	21	21	21	20	20	20	19
	Max	286.7	373.9	435.4	481.3	455.2	421.3	385.7	380.3	409.9	379.6	300.3	282.6
	Max_Hr	14	14	14	13	13	14	13	13	13	13	13	13

Table 7.16: Simulated peak values of monthly average hourly net all-wave radiation for Scenario-B for Palam area

Year	Time	Jan	Feb	Mar	Apr	May	Jun	Jul	Aug	Sep	Oct	Nov	Dec
1973	Min	-57.7	-52.1	-74.9	-90.6	-78.8	-44.1	-20.3	-6.5	-19.0	-39.8	-49.7	-47.1
	Min_Hr	19	19	20	20	21	21	21	21	20	20	19	19
	Max	411.9	445.8	536.8	622.0	595.4	506.4	491.3	407.5	565.3	523.5	423.6	373.0
	Max_Hr	14	13	14	13	13	13	13	14	13	13	13	13
1977	Min	-57.8	-52.1	-75.0	-90.7	-78.9	-44.1	-20.4	-6.5	-19.1	-39.9	-49.8	-47.2
	Min_Hr	19	19	20	20	21	21	21	21	20	20	19	19
	Max	414.2	448.2	536.2	625.3	598.7	509.1	493.8	409.6	568.1	523.2	426.0	375.1
	Max_Hr	14	13	14	13	13	13	13	14	13	13	13	13
1986	Min	-57.3	-51.7	-74.4	-90.0	-78.3	-43.8	-20.2	-6.4	-18.9	-39.6	-49.4	-46.8
	Min_Hr	19	19	20	20	21	21	21	21	20	20	19	19
	Max	413.6	447.5	535.4	624.2	597.6	508.1	492.7	408.6	566.8	522.1	425.4	374.4
	Max_Hr	14	13	14	13	13	13	13	14	13	13	13	13
1991	Min	-57.1	-51.5	-74.2	-89.7	-78.0	-43.6	-20.1	-6.4	-18.8	-39.4	-49.2	-46.7
	Min_Hr	19	19	20	20	21	21	21	21	20	20	19	19
	Max	413.3	447.2	535.1	623.9	597.2	507.7	492.3	408.3	566.3	521.8	425.1	374.2
	Max_Hr	14	13	14	13	13	13	13	14	13	13	13	13
1998	Min	-57.1	-51.4	-74.1	-89.6	-78.0	-43.6	-20.1	-6.4	-18.8	-39.4	-49.2	-46.6
	Min_Hr	19	19	20	20	21	21	21	21	20	20	19	19
	Max	413.8	447.7	535.7	624.5	597.7	508.1	492.7	408.6	566.8	522.3	425.6	374.7
	Max_Hr	14	13	14	13	13	13	13	14	13	13	13	13
1999	Min	-57.1	-51.4	-74.1	-89.6	-77.9	-43.6	-20.1	-6.4	-18.8	-39.4	-49.1	-46.6
	Min_Hr	19	19	20	20	21	21	21	21	20	20	19	19
	Max	414.0	447.8	535.9	624.7	597.9	508.3	492.8	408.7	567.0	522.5	425.8	374.8
	Max_Hr	14	13	14	13	13	13	13	14	13	13	13	13
2002	Min	-56.9	-51.3	-73.8	-89.3	-77.7	-43.4	-20.1	-6.4	-18.8	-39.3	-49.0	-46.5
	Min_Hr	19	19	20	20	21	21	21	21	20	20	19	19
	Max	410.3	443.9	531.1	619.2	592.7	503.9	488.7	405.3	562.3	518.0	422.0	371.5
	Max_Hr	14	13	14	13	13	13	13	14	13	13	13	13
2006	Min	-56.6	-51.0	-73.4	-88.8	-77.2	-43.2	-19.9	-6.4	-18.7	-39.0	-48.7	-46.2
	Min_Hr	19	19	20	20	21	21	21	21	20	20	19	19
	Max	410.7	444.3	531.6	619.7	593.2	504.3	488.9	405.4	562.4	518.3	422.4	371.8
	Max_Hr	14	13	14	13	13	13	13	14	13	13	13	13
2009	Min	-56.6	-50.9	-73.5	-88.8	-77.3	-43.2	-20.0	-6.4	-18.6	-39.1	-48.7	-46.2
	Min_Hr	19	19	20	20	21	21	21	21	20	20	19	19
	Max	416.1	450.0	538.5	627.7	600.7	510.4	494.7	410.2	569.0	524.7	428.0	376.6
	Max_Hr	14	13	14	13	13	13	13	14	13	13	13	13
2011	Min	-56.6	-50.9	-73.5	-88.8	-77.3	-43.2	-20.0	-6.4	-18.7	-39.1	-48.7	-46.2
	Min_Hr	19	19	20	20	21	21	21	21	20	20	19	19
	Max	417.6	451.6	540.5	629.9	602.8	512.2	496.3	411.5	570.9	526.6	429.5	378.0
	Max_Hr	14	13	14	13	13	13	13	14	13	13	13	13
2013	Min	-56.6	-50.9	-73.5	-88.8	-77.3	-43.2	-20.0	-6.4	-18.6	-39.1	-48.7	-46.2
	Min_Hr	19	19	20	20	21	21	21	21	20	20	19	19
	Max	418.3	452.3	541.3	630.9	603.7	512.9	497.0	412.1	571.7	527.3	430.2	378.6
	Max_Hr	14	13	14	13	13	13	13	14	13	13	13	13
2014	Min	-56.3	-56.3	-73.2	-88.4	-77.0	-43.1	-19.9	-6.3	-18.6	-38.9	-48.5	-46.0
	Min_Hr	19	19	20	20	21	21	21	21	20	20	19	19
	Max	417.4	417.4	540.2	629.6	602.4	511.9	495.9	411.1	570.4	526.2	429.3	377.8
	Max_Hr	14	14	14	13	13	13	13	14	13	13	13	13

Table 7.17: Simulated peak values of monthly average hourly net all-wave radiation for Scenario-C for Palam area

Year	Time	Jan	Feb	Mar	Apr	May	Jun	Jul	Aug	Sep	Oct	Nov	Dec
1973	Min	-57.7	-52.1	-74.9	-90.6	-78.8	-44.1	-20.3	-6.5	-19.0	-39.8	-49.7	-47.1
	Min_Hr	19	19	20	20	21	21	21	21	20	20	19	19
	Max	411.9	445.8	536.8	622.0	595.4	506.4	491.3	407.5	565.3	523.5	423.6	373.0
	Max_Hr	14	13	14	13	13	13	13	14	13	13	13	13
1977	Min	-48.9	-43.2	-59.3	-73.2	-80.5	-57.4	-28.3	-32.4	-52.1	-65.0	-76.4	-73.4
	Min_Hr	19	20	20	21	21	21	21	21	20	20	1	1
	Max	391.8	509.6	610.1	591.6	605.6	547.3	361.0	512.2	475.7	491.0	415.2	383.3
	Max_Hr	14	14	13	13	13	13	13	14	13	13	13	13
1986	Min	-55.0	-64.2	-57.9	-83.4	-73.8	-46.0	-14.2	-32.2	-9.7	-95.1	-54.3	-49.6
	Min_Hr	19	18	20	20	20	21	21	20	20	15	18	19
	Max	314.7	343.5	436.7	485.4	489.8	498.0	437.5	396.6	449.0	-15.8	353.0	291.3
	Max_Hr	13	12	12	12	13	13	12	12	12	3	12	13
1991	Min	-48.1	-65.7	-46.7	-65.6	-63.1	-37.8	-19.8	-8.1	-15.2	-22.4	-27.8	-27.4
	Min_Hr	19	19	20	20	21	21	21	21	20	20	19	6
	Max	302.4	377.0	439.5	465.7	446.5	452.2	426.2	356.0	429.0	407.8	335.0	330.8
	Max_Hr	13	13	13	12	13	13	13	14	14	13	13	13
1998	Min	-44.2	-49.7	-60.0	-79.4	-63.7	-43.0	-51.6	-12.3	-12.3	-27.7	-32.2	-31.0
	Min_Hr	19	20	20	20	20	20	20	21	20	19	18	19
	Max	284.1	360.3	520.5	570.9	614.6	510.7	450.2	404.4	443.5	370.3	352.6	318.9
	Max_Hr	14	13	14	13	13	13	13	13	12	12	12	13
1999	Min	-37.8	-47.6	-66.9	-84.8	-79.1	-45.3	-9.1	-8.2	-11.2	-27.4	-42.8	-30.7
	Min_Hr	18	19	19	19	20	21	21	21	21	21	19	19
	Max	338.3	432.2	556.0	574.4	563.3	546.9	514.9	566.6	527.6	476.1	412.7	305.2
	Max_Hr	13	13	12	12	12	14	14	13	13	13	13	14
2002	Min	-58.8	-54.6	-52.9	-77.2	-48.9	-42.1	-18.2	-23.3	-24.8	-37.5	-39.8	-43.1
	Min_Hr	19	20	20	21	21	21	21	21	20	20	19	19
	Max	244.9	368.6	435.5	451.5	439.3	426.8	492.4	334.9	336.7	372.8	277.5	239.7
	Max_Hr	14	14	14	13	15	14	13	14	14	13	14	13
2006	Min	-58.9	-54.8	-56.1	-80.4	-45.8	-55.9	-17.9	-21.4	-25.1	-35.3	-34.2	-42.4
	Min_Hr	19	19	20	20	21	16	21	21	20	20	20	19
	Max	292.4	316.9	389.5	442.0	450.2	-29.3	395.1	421.2	397.7	375.6	291.0	268.1
	Max_Hr	14	13	14	13	13	6	14	13	13	13	13	13
2009	Min	-50.5	-51.3	-64.1	-83.8	-69.1	-43.3	-23.5	-17.4	-23.5	-45.2	-51.5	-52.4
	Min_Hr	19	20	20	20	20	21	21	21	20	19	19	19
	Max	264.1	353.7	414.3	487.0	478.6	535.1	403.0	426.8	386.7	346.9	263.2	252.4
	Max_Hr	13	14	13	13	13	13	13	13	13	13	13	13
2011	Min	-43.3	-39.9	-52.2	-68.7	-70.7	-42.0	-20.8	-14.3	-24.0	-33.0	-52.1	-53.8
	Min_Hr	19	20	20	20	21	21	21	21	20	20	19	19
	Max	240.6	341.5	416.4	449.4	427.2	442.7	350.3	342.9	316.6	361.3	236.1	254.9
	Max_Hr	13	13	14	13	13	14	14	14	13	13	13	13
2013	Min	-35.0	-26.0	-39.2	-58.4	-76.6	-27.9	-11.1	-8.5	-21.2	-27.2	-51.4	-44.6
	Min_Hr	19	20	20	20	21	21	21	4	20	20	19	19
	Max	303.0	381.0	425.9	483.2	439.0	431.0	392.8	397.4	411.4	386.8	296.9	281.4
	Max_Hr	14	14	13	13	13	14	13	13	13	13	13	13
2014	Min	-60.8	-38.8	-46.4	-59.2	-55.9	-48.9	-22.9	-22.8	-28.7	-40.2	-52.2	-49.1
	Min_Hr	19	20	20	20	21	21	21	21	20	20	19	19
	Max	282.4	369.4	428.6	475.6	449.6	416.3	381.8	376.6	405.9	373.8	296.1	278.8
	Max_Hr	14	14	14	13	13	14	13	13	13	13	13	13

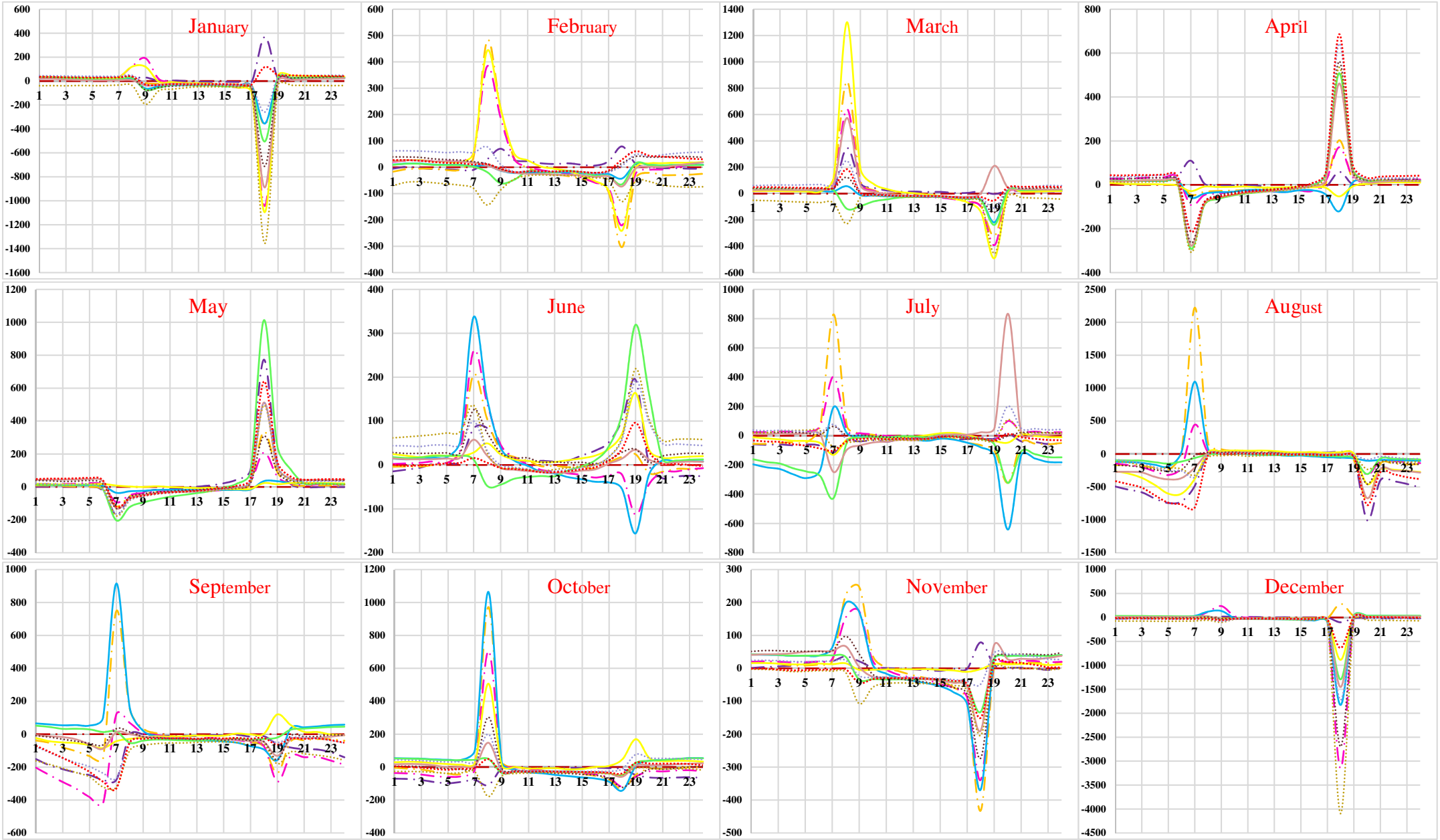

1973	1977	1986	1991	1998	1999	2002	2006	2009	2011	2013	2014	X-axis - Time in Hours
												Y-axis -% change in Heat Flux
Note: Percentage change in values of heat flux are very high because of the values in base year are very small which are used in denominator while calculating percentage change for different years.												

Figure 7.28: Percentage change in values of monthly average hourly net all-wave radiation for Scenario-A for Safdarjung area

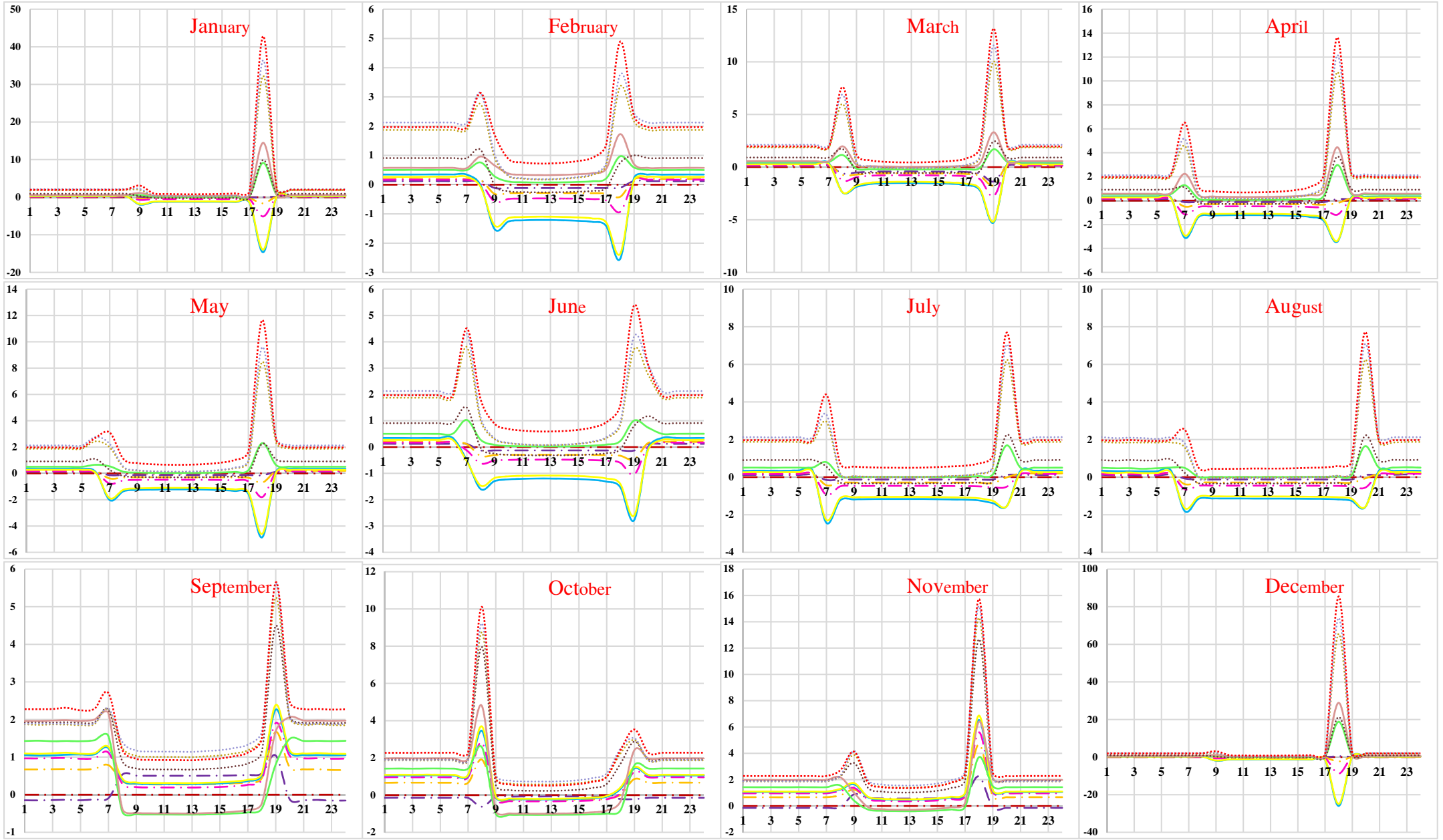

1973	1977	1986	1991	1998	1999	2002	2006	2009	2011	2013	2014	X-axis - Time in Hours
												Y-axis -% change in Heat Flux
Note: Percentage change in values of heat flux are very high because of the values in base year are very small which are used in denominator while calculating percentage change for different years.												

Figure 7.29: Percentage change in values of monthly average hourly net all-wave radiation for Scenario-B for Safdarjung area

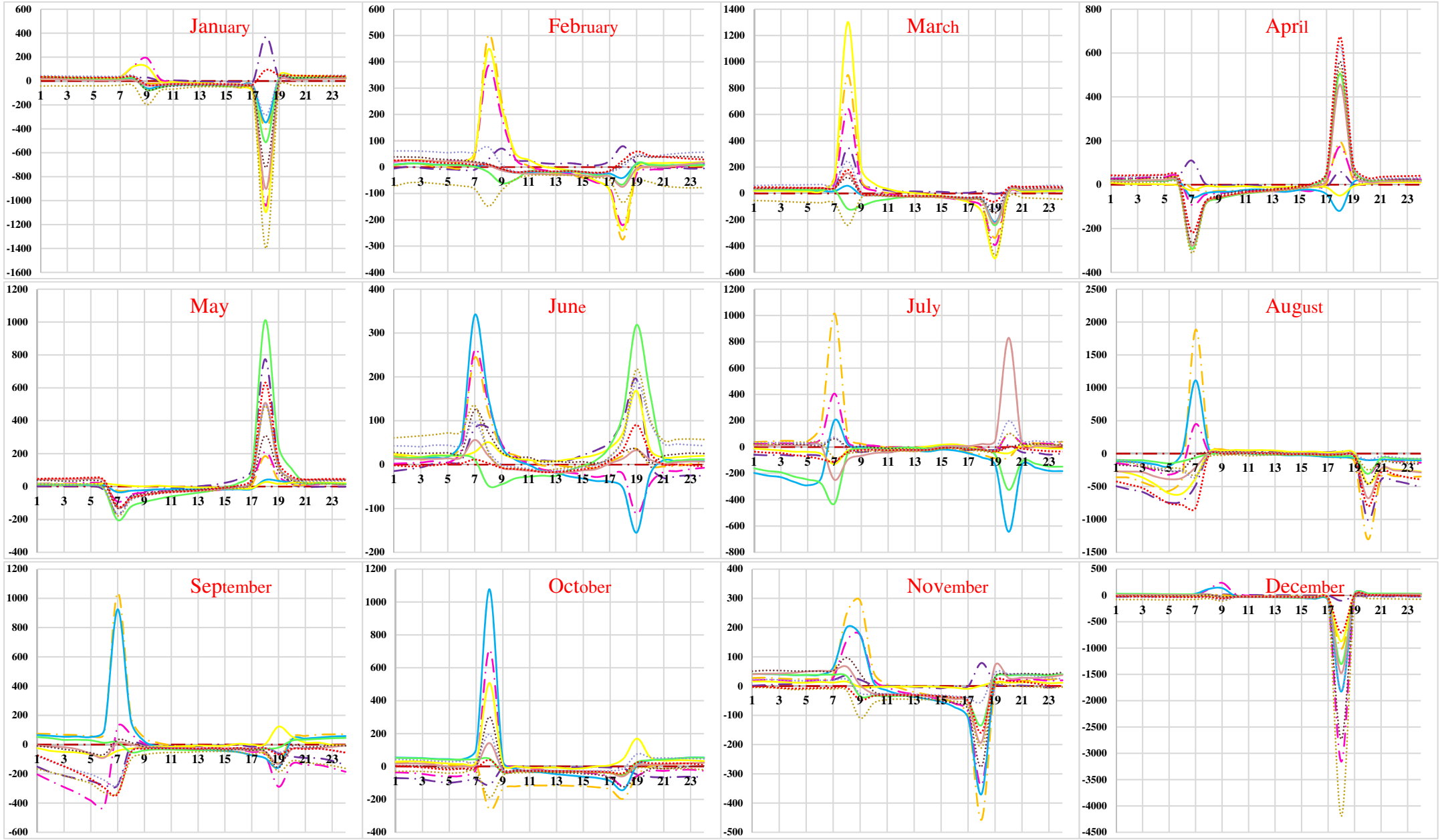

1973	1977	1986	1991	1998	1999	2002	2006	2009	2011	2013	2014	X-axis - Time in Hours
												Y-axis -% change in Heat Flux
Note: Percentage change in values of heat flux are very high because of the values in base year are very small which are used in denominator while calculating percentage change for different years.												

Figure 7.30: Percentage change in values of monthly average hourly net all-wave radiation for Scenario-C for Safdarjung area

Table 7.18: Simulated peak values of monthly average hourly net all-wave radiation for Scenario-A for Safdarjung area

Year	Time	Jan	Feb	Mar	Apr	May	Jun	Jul	Aug	Sep	Oct	Nov	Dec
1973	Min	-57.6	-51.8	-74.8	-91.0	-82.5	-44.0	-20.3	-6.5	-19.0	-39.7	-49.6	-46.3
	Min_Hr	19	19	20	20	20	21	21	21	20	20	19	19
	Max	420.4	454.8	545.9	638.3	610.2	516.1	500.3	414.8	575.5	532.0	432.4	381.9
	Max_Hr	14	13	14	13	13	13	13	14	13	13	13	13
1977	Min	-46.7	-52.2	-59.0	-87.3	-80.2	-57.2	-28.2	-32.2	-34.4	-64.7	-45.8	-54.2
	Min_Hr	19	20	20	19	21	21	21	21	20	20	20	19
	Max	393.7	518.0	623.7	609.9	617.0	557.3	367.4	521.3	508.9	502.3	418.1	383.8
	Max_Hr	14	14	13	12	13	13	13	14	13	13	13	13
1986	Min	-51.8	-74.2	-57.9	-87.2	-73.1	-50.8	-29.8	-18.3	-27.3	-46.5	-50.3	-32.0
	Min_Hr	19	18	20	20	21	21	21	20	20	19	18	19
	Max	317.2	334.3	446.2	504.5	468.7	505.6	427.5	410.9	435.5	385.9	352.4	314.4
	Max_Hr	13	13	12	12	13	13	12	12	12	13	12	13
1991	Min	-48.9	-64.9	-69.2	-77.8	-70.2	-51.4	-14.2	-13.1	-44.1	-50.3	-44.3	-51.4
	Min_Hr	19	19	20	20	21	21	21	21	20	19	19	18
	Max	303.9	374.8	424.1	445.9	441.1	438.9	444.4	370.2	414.2	377.2	312.9	287.1
	Max_Hr	13	13	13	12	13	13	13	14	13	13	13	13
1998	Min	-44.0	-46.9	-61.1	-79.6	-63.1	-39.5	-49.4	-12.2	-12.4	-29.7	-40.7	-31.7
	Min_Hr	19	20	20	19	20	21	20	21	20	19	18	19
	Max	286.4	365.1	414.3	490.3	496.8	415.9	364.1	328.5	360.7	293.9	274.6	242.0
	Max_Hr	14	13	14	12	12	13	13	13	12	12	12	13
1999	Min	-37.5	-53.5	-76.0	-95.4	-63.1	-36.7	-18.7	-21.4	-14.1	-22.0	-43.2	-36.1
	Min_Hr	18	19	19	19	20	21	21	21	21	21	19	19
	Max	338.4	428.1	554.4	563.1	584.3	561.5	508.3	559.2	527.5	498.6	419.7	293.2
	Max_Hr	13	13	12	12	12	14	14	13	13	13	13	13
2002	Min	-42.1	-47.1	-58.2	-73.3	-62.0	-38.1	-41.8	-10.8	-13.8	-24.5	-34.8	-32.1
	Min_Hr	19	20	20	21	21	21	21	21	20	20	19	19
	Max	267.6	389.4	444.0	457.9	435.3	441.8	478.0	352.4	353.1	394.8	287.5	251.8
	Max_Hr	14	14	14	13	15	14	13	14	14	13	14	13
2006	Min	-58.4	-54.2	-45.1	-79.8	-45.1	-42.9	-17.8	-21.1	-24.9	-35.0	-33.9	-42.1
	Min_Hr	19	19	21	20	21	21	21	21	20	20	20	19
	Max	300.1	325.0	460.4	452.8	460.4	425.0	403.2	430.0	406.3	387.5	298.3	274.9
	Max_Hr	14	13	13	13	13	13	14	13	13	13	13	13
2009	Min	-49.0	-31.9	-45.9	-71.6	-51.7	-35.0	-16.0	-14.7	-20.9	-51.7	-34.3	-50.9
	Min_Hr	19	20	20	20	20	21	21	21	20	19	19	19
	Max	263.1	376.8	438.8	509.2	499.1	552.7	410.6	434.0	388.2	332.8	269.9	257.5
	Max_Hr	13	14	13	13	13	13	13	13	13	13	13	13
2011	Min	-77.8	-79.7	-92.8	-68.9	-61.5	-19.2	-16.1	-14.4	-39.4	-41.6	-49.6	-72.8
	Min_Hr	19	20	20	20	21	21	21	21	20	20	19	19
	Max	217.3	314.9	400.3	459.9	445.5	473.5	357.0	330.1	291.4	348.4	235.3	246.1
	Max_Hr	13	13	14	13	13	14	14	14	13	13	13	13
2013	Min	-37.7	-30.6	-44.6	-67.2	-54.2	-22.5	-10.2	-9.0	-23.0	-17.7	-26.6	-53.2
	Min_Hr	19	20	20	20	21	21	21	21	20	20	20	19
	Max	297.3	376.8	434.3	476.9	454.7	450.6	402.5	397.5	413.0	398.5	313.1	273.4
	Max_Hr	14	14	14	13	13	14	13	13	13	13	13	13
2014	Min	-28.8	-28.9	-39.4	-60.8	-43.9	-42.8	-22.5	-24.4	-24.0	-31.1	-39.9	-40.1
	Min_Hr	19	20	20	20	21	21	21	21	20	20	19	19
	Max	317.0	386.3	446.4	488.8	472.3	435.7	391.8	385.0	414.3	385.3	303.4	287.1
	Max_Hr	14	14	14	13	13	14	13	13	13	13	13	13

Table 7.19: Simulated peak values of monthly average hourly net all-wave radiation for Scenario-B for Safdarjung area

Year	Time	Jan	Feb	Mar	Apr	May	Jun	Jul	Aug	Sep	Oct	Nov	Dec
1973	Min	-57.6	-51.8	-74.8	-91.0	-82.5	-44.0	-20.3	-6.5	-19.0	-39.7	-49.6	-46.3
	Min_Hr	19	19	20	20	20	21	21	21	20	20	19	19
	Max	420.4	454.8	545.9	638.3	610.2	516.1	500.3	414.8	575.5	532.0	432.4	381.9
	Max_Hr	14	13	14	13	13	13	13	14	13	13	13	13
1977	Min	-57.5	-51.8	-74.7	-90.9	-82.4	-43.9	-20.3	-6.5	-19.0	-39.7	-49.5	-46.2
	Min_Hr	19	19	20	20	20	21	21	21	20	20	19	19
	Max	420.0	454.2	543.6	637.5	609.5	515.5	499.6	414.3	574.8	529.8	431.9	381.5
	Max_Hr	14	13	14	13	13	13	13	14	13	13	13	13
1986	Min	-57.5	-51.7	-74.6	-90.8	-82.3	-43.9	-20.3	-6.5	-18.9	-39.7	-49.5	-46.2
	Min_Hr	19	19	20	20	20	21	21	21	20	20	19	19
	Max	419.2	453.5	542.6	636.4	608.4	514.6	498.8	413.7	573.9	529.0	431.2	380.8
	Max_Hr	14	13	14	13	13	13	13	14	13	13	13	13
1991	Min	-57.5	-51.8	-74.6	-90.8	-82.4	-43.9	-20.3	-6.5	-18.9	-39.7	-49.5	-46.2
	Min_Hr	19	19	20	20	20	21	21	21	20	20	19	19
	Max	418.4	452.6	541.6	635.2	607.3	513.6	498.0	413.0	572.9	528.0	430.4	380.1
	Max_Hr	14	13	14	13	13	13	13	14	13	13	13	13
1998	Min	-57.4	-51.7	-74.5	-90.7	-82.2	-43.8	-20.2	-6.4	-18.9	-39.6	-49.4	-46.1
	Min_Hr	19	19	20	20	20	21	21	21	20	20	19	19
	Max	415.3	449.3	537.5	630.5	602.8	509.9	494.5	410.1	568.9	524.2	427.1	377.3
	Max_Hr	14	13	14	13	13	13	13	14	13	13	13	13
1999	Min	-57.4	-51.8	-74.6	-90.8	-82.3	-43.9	-20.3	-6.5	-18.9	-39.6	-49.4	-46.1
	Min_Hr	19	19	20	20	20	21	21	21	20	20	19	19
	Max	415.8	449.8	538.2	631.2	603.5	510.5	495.0	410.6	569.6	524.8	427.6	377.7
	Max_Hr	14	13	14	13	13	13	13	14	13	13	13	13
2002	Min	-57.3	-51.5	-74.4	-90.5	-82.1	-43.8	-20.2	-6.4	-18.9	-39.5	-49.3	-46.0
	Min_Hr	19	19	20	20	20	21	21	21	20	20	19	19
	Max	420.8	455.1	544.7	638.7	610.5	516.2	500.3	414.9	575.6	530.7	432.8	382.2
	Max_Hr	14	13	14	13	13	13	13	14	13	13	13	13
2006	Min	-57.2	-51.5	-74.3	-90.4	-43.7	-20.2	-6.4	-18.9	-39.5	-49.2	-46.0	-46.0
	Min_Hr	19	19	20	20	21	21	21	20	20	19	19	19
	Max	421.9	456.2	546.1	640.3	517.5	501.5	415.8	576.9	532.0	434.0	383.2	383.2
	Max_Hr	14	13	14	13	13	13	14	13	13	13	13	13
2009	Min	-57.0	-51.3	-74.1	-90.1	-81.7	-43.6	-20.1	-6.4	-18.8	-39.4	-49.1	-45.8
	Min_Hr	19	19	20	20	20	21	21	21	20	20	19	19
	Max	419.4	453.6	542.8	636.5	608.4	514.5	498.6	413.4	573.6	528.9	431.4	380.9
	Max_Hr	14	13	14	13	13	13	13	14	13	13	13	13
2011	Min	-56.4	-50.7	-73.4	-89.2	-80.9	-43.2	-19.9	-6.3	-18.6	-39.0	-48.5	-45.4
	Min_Hr	19	20	20	20	20	21	21	21	20	20	19	19
	Max	421.4	455.6	545.4	639.3	611.0	516.5	500.3	414.7	575.4	531.0	433.5	382.7
	Max_Hr	14	13	14	13	13	13	13	14	13	13	13	13
2013	Min	-56.3	-50.6	-73.2	-89.0	-80.7	-43.0	-19.9	-6.3	-18.5	-38.9	-48.4	-45.3
	Min_Hr	19	20	20	20	20	21	21	21	20	20	19	19
	Max	421.5	455.6	545.4	639.4	611.1	516.5	500.3	414.7	575.4	531.1	433.6	382.7
	Max_Hr	14	13	14	13	13	13	13	14	13	13	13	13
2014	Min	-56.4	-50.7	-73.3	-89.1	-80.8	-43.1	-19.9	-6.3	-18.6	-39.0	-48.5	-45.3
	Min_Hr	19	20	20	20	20	21	21	21	20	20	19	19
	Max	423.8	458.1	548.4	642.8	614.3	519.2	502.8	416.7	578.2	533.8	435.9	384.8
	Max_Hr	14	13	14	13	13	13	13	14	13	13	13	13

Table 7.20: Simulated peak values of monthly average hourly net all-wave radiation for Scenario-C for Safdarjung area

Year	Time	Jan	Feb	Mar	Apr	May	Jun	Jul	Aug	Sep	Oct	Nov	Dec
1973	Min	-57.6	-51.8	-74.8	-91.0	-82.5	-44.0	-20.3	-6.5	-19.0	-39.7	-49.6	-46.3
	Min_Hr	19	19	20	20	20	21	21	21	20	20	19	19
	Max	420.4	454.8	545.9	638.3	610.2	516.1	500.3	414.8	575.5	532.0	432.4	381.9
	Max_Hr	14	13	14	13	13	13	13	14	13	13	13	13
1977	Min	-46.7	-52.2	-59.1	-87.4	-80.3	-57.3	-28.2	-32.3	-34.4	-64.8	-45.8	-54.3
	Min_Hr	19	20	20	19	21	21	21	21	20	20	20	19
	Max	394.2	519.1	622.0	610.7	617.8	558.0	367.9	521.9	509.5	500.9	418.6	384.3
	Max_Hr	14	14	13	12	13	13	13	14	13	13	13	13
1986	Min	-54.8	-63.8	-57.8	-83.2	-73.5	-45.9	-14.2	-32.1	-9.7	-94.9	-54.0	-49.5
	Min_Hr	19	18	20	20	20	21	21	20	20	15	18	19
	Max	321.5	350.8	445.7	495.6	499.9	507.7	445.4	404.2	457.1	-15.8	360.4	297.9
	Max_Hr	13	12	12	12	13	13	12	12	12	3	12	13
1991	Min	-49.0	-65.0	-69.3	-77.9	-70.3	-51.5	-14.2	-13.1	-44.2	-50.3	-44.3	-51.5
	Min_Hr	19	19	20	20	21	21	21	21	20	19	19	18
	Max	305.5	376.7	426.2	448.1	443.3	441.1	446.5	371.9	416.1	379.0	314.5	288.6
	Max_Hr	13	13	13	12	13	13	13	14	13	13	13	13
1998	Min	-44.1	-47.1	-61.3	-79.8	-63.3	-39.6	-49.6	-12.3	-12.4	-29.8	-40.8	-31.8
	Min_Hr	19	20	20	19	20	21	20	21	20	19	18	19
	Max	290.1	369.7	419.5	496.4	502.9	420.9	368.6	332.4	365.0	297.5	278.1	245.2
	Max_Hr	14	13	14	12	12	13	13	13	12	12	12	13
1999	Min	-37.6	-53.7	-76.2	-95.6	-63.3	-36.8	-18.7	-21.5	-14.1	-22.0	-43.3	-36.2
	Min_Hr	18	19	19	19	20	21	21	21	21	21	19	19
	Max	342.2	432.9	555.5	569.4	590.7	567.6	513.7	565.1	533.0	499.8	424.5	296.7
	Max_Hr	13	13	12	12	12	14	14	13	13	13	13	13
2002	Min	-42.3	-47.3	-58.5	-73.6	-62.3	-38.3	-42.0	-10.9	-13.9	-24.6	-34.9	-32.3
	Min_Hr	19	20	20	21	21	21	21	21	20	20	19	19
	Max	267.4	389.2	439.6	457.5	435.0	441.6	478.0	352.3	353.0	391.3	287.3	251.6
	Max_Hr	14	14	14	13	15	14	13	14	14	13	14	13
2006	Min	-58.7	-54.6	-56.0	-80.2	-45.3	-43.2	-17.9	-21.3	-25.1	-35.2	-34.1	-42.3
	Min_Hr	19	19	20	20	21	21	21	21	20	20	20	19
	Max	299.0	323.8	397.6	451.2	459.1	423.8	402.3	429.0	405.2	383.1	297.3	274.0
	Max_Hr	14	13	14	13	13	13	14	13	13	13	13	13
2009	Min	-49.5	-32.2	-46.3	-72.3	-52.2	-35.4	-16.1	-14.8	-21.1	-52.2	-34.6	-51.4
	Min_Hr	19	20	20	20	20	21	21	21	20	19	19	19
	Max	263.8	377.9	436.3	510.6	500.6	554.6	411.9	435.4	389.4	333.5	270.6	258.1
	Max_Hr	13	14	13	13	13	13	13	13	13	13	13	13
2011	Min	-79.3	-81.2	-94.6	-70.3	-62.7	-19.6	-16.4	-14.7	-40.1	-42.4	-50.5	-74.2
	Min_Hr	19	20	20	20	21	21	21	21	20	20	19	19
	Max	216.1	313.6	396.9	459.1	444.8	473.4	356.8	329.7	290.6	346.0	234.2	244.9
	Max_Hr	13	13	14	13	13	14	14	14	13	13	13	13
2013	Min	-38.5	-31.3	-45.6	-68.7	-55.5	-23.0	-10.4	-9.2	-23.5	-18.1	-27.1	-54.4
	Min_Hr	19	20	20	20	21	21	21	21	20	20	20	19
	Max	296.6	376.1	432.1	476.0	453.8	450.5	402.6	397.6	412.8	397.1	312.4	272.4
	Max_Hr	14	14	14	13	13	14	13	13	13	13	13	13
2014	Min	-29.5	-29.4	-40.2	-62.1	-44.8	-43.6	-22.9	-24.8	-24.4	-31.8	-40.8	-40.9
	Min_Hr	19	20	20	20	21	21	21	21	20	20	19	19
	Max	314.8	383.8	441.9	485.4	469.2	432.9	389.7	382.9	412.0	382.8	300.8	284.8
	Max_Hr	14	14	14	13	13	14	13	13	13	13	13	13

Table 7.21: Annual extreme hourly values net all-wave radiation for different scenario

Year	Data	Palam Area			Safdarjung Area		
		Scenario-A	Scenario-B	Scenario-C	Scenario-A	Scenario-B	Scenario-C
1973	Max	728.88	728.88	728.88	741.61	741.61	741.61
	Min	-155.64	-155.64	-155.64	-161.14	-161.14	-161.14
1977	Max	777.16	732.52	773.12	786.38	740.68	787.37
	Min	-127.15	-155.84	-126.99	-126.47	-160.95	-126.63
1986	Max	619.01	730.69	617.45	610.49	739.51	628.10
	Min	-132.67	-154.54	-133.56	-132.89	-160.83	-133.29
1991	Max	711.85	730.04	710.54	742.49	738.27	745.84
	Min	-118.2	-154.07	-119.35	-118.30	-160.87	-118.50
1998	Max	741.27	730.55	739.67	602.92	733.26	609.81
	Min	-116.58	-153.92	-117.83	-115.77	-160.59	-116.17
1999	Max	730.44	730.73	728.43	714.53	734.08	722.04
	Min	-130.68	-153.86	-132.12	-121.66	-160.71	-121.97
2002	Max	577.28	724.77	580.62	577.91	741.50	577.99
	Min	-118.34	-153.36	-120.08	-111.35	-160.33	-111.91
2006	Max	561.63	724.86	564.59	575.91	743.10	574.62
	Min	-114.3	-152.48	-116.6	-115.69	-160.22	-116.36
2009	Max	653.1	733.07	648.7	648.25	738.95	650.40
	Min	-107.28	-152.52	-109.37	-91.12	-159.68	-91.96
2011	Max	562.61	735.43	557.07	595.37	741.04	595.96
	Min	-131.29	-152.58	-133.83	-112.77	-18.53	-114.92
2013	Max	535.32	736.39	528.62	537.57	740.91	537.17
	Min	-115.6	-152.54	-117.83	-113.58	-157.72	-116.05
2014	Max	533.37	734.74	528.86	548.51	744.52	545.50
	Min	-121.15	-151.92	-123.97	-107.01	-157.97	-109.16

Similarly, relative percentage change in peak value of storage heat flux, during day time, from the base year, is showing decreasing trend in storage heat flux by 7.99% in year 1977 to increase by 1.57% in year 2014.

In case of Safdarjung area for Scenario-A, monthly average hourly storage heat flux has been calculated. According to the results, monthly average hourly peak values of storage heat flux during night and day time over the years from 1973 to 2014 are decreasing (in negative values) and increasing respectively. Monthly mean hourly peak value of storage heat flux during night time in different years found to be increasing i.e., means negative values are decreasing over the years from -102 Wm^{-2} (1973) to -99.70 Wm^{-2} (2014) and during day time found to be increasing from 168.70 Wm^{-2} (1973) to 170.80 Wm^{-2} (2014) as shown in Table 7.25 and Figure 7.34. Relative percentage change in night time storage heat flux from the base year is showing decreasing trend in negative values (increasing) from 1977 (6.27%) to 2006 (21.18%) then increasing to

2.25% in year 2014. Similarly, relative percentage change in day time monthly average hourly storage heat flux from the base year is showing decreasing trend from 1977 (1.96%) to 2006 (21.70%) and then increasing till year 2014 (1.24%).

In Scenario-B, for Palam station, monthly average hourly storage heat flux have been calculated from the hourly simulated results. According to the results (Table 7.23 and Figure 7.32), peak value of monthly average hourly storage heat flux during night time is decreasing (means negative values are increasing) from year 1973 to 2014, whereas during day time trend is increasing over the years, which indicate effect of urbanization. Peak values of monthly average hourly storage heat flux during night time decreasing (means negative values are increasing) over the years from -97.20 Wm^{-2} (1973) to -140.0 Wm^{-2} (2014) whereas during the day time values are increasing over the years from 159.0 Wm^{-2} (1973) to 209.50 Wm^{-2} (2014), as shown in Table 7.23 and Figure 7.32. Relative percentage change in monthly average hourly storage heat flux during night time from the base year is showing decreasing trend in negative values from year 1973 (0.0 %) to 2014 (44.03%). Similarly, relative percentage change in peak monthly average hourly storage heat flux during day time from the base year is showing increasing trend from 1973 (0 %) to 2014 (31.76%). In case of Safdarjung area, monthly average hourly values of storage heat flux has been calculated from hourly simulated results. According to the results (Table 7.26 and Figure 7.35), peak values of monthly average hourly storage heat flux during night time have shown decreasing trend from -102.0 Wm^{-2} (1973) to -144.30 Wm^{-2} (2014) over the years, whereas results exhibit increasing trend in peak values from 168.70 Wm^{-2} (1973) to 218.10 Wm^{-2} (2014) during day time over the years. Relative percentage change in peak values of monthly average hourly storage heat flux during night time, from the base year, is showing increasing trend in negative values from 1977 (1.96%) to 2014 (41.47%). Similarly, relative percentage change in peak values of monthly average hourly storage heat flux during day time, from the base year, is showing increasing trend from 1977 (0.95%) to 2014 (29.28%) (Table 7.26 and Figure 7.35).

In Scenario-C, for Palam station, peak values of monthly average storage heat flux at hourly temporal scale have been calculated from hourly simulated results. According to the results (Table 7.24 and Figure 7.33), peak values of monthly average hourly storage heat flux during night time are increasing (means negative values are decreasing) from year 1973 to 2014 whereas during day time, trend is decreasing over the years. During night time peak values of monthly average hourly storage heat flux

values are showing decreasing trend in negative values from -97.20 Wm^{-2} (1973) to -72.80 Wm^{-2} (2014) over the years also during day time storage heat flux values are showing decreasing trend from 159.0 Wm^{-2} (1973) to 118.30 Wm^{-2} (2014) over the years (Table 7.24 and Figure 7.33). Relative percentage change in monthly average hourly storage heat flux, during night time, with respect to base year value is showing decreasing trend in negative values from 1977 (9.67%) to 2014 (25.10%). Similarly, during day time relative percentage change in peak values of monthly average hourly storage heat flux with respect to base year value, is showing decreasing trend from 1977 (2.89%) to 2014 (25.60%).

For Safdarjung area also, results indicate trends in storage heat flux similar to the Palam area. During night time, peak values of monthly average hourly storage heat flux are showing decreasing trend in negative values over the years from -102.0 Wm^{-2} (1973) to -76.40 Wm^{-2} (2014), also during day time results are showing decreasing trends from 168.70 Wm^{-2} (1973) to 125.80 Wm^{-2} (2014) over the years (Table 7.27 and Figure 7.36). Relative percentage change in peak values of monthly average hourly storage heat flux, during night time, with respect to base year value, is showing decreasing trend in negative values from 1977 (7.75%) to 2014 (25.10%). Similarly, during day time, relative percentage change in monthly average hourly storage heat flux with respect to base year value, is showing decreasing trend from 1977 (3.5%) to 2014 (25.43%). The overall peak values of monthly average hourly storage heat flux during night and day time are decreasing over the years due to change in effects of climate change forcing other than LULC changes.

Annual extreme hourly values of storage heat flux have also been calculated from the hourly simulated results for different Scenarios i.e., A, B and C to study the effect of LULC changes on extreme values for both areas i.e., Palam and Safdarjung (Table 7.28). Annual extreme hourly values of storage heat flux during night time in Palam area have decreased (negative values) in Scenario-A (-129.66 to -119.88 Wm^{-2}), Scenario-B (-129.66 to –218.93 Wm^{-2}) and Scenario-C (-129.66 to - 82.747 Wm^{-2}). Further for Palam area, results indicate that annual extreme hourly values of storage heat flux during day time have increased first up to year 2011 and then decreases for Scenario-A (204.32 – 184.33 Wm^{-2}) and for Scenario-C storage heat flux extreme values have shown increasing trend (204.32 to 133.85 Wm^{-2}) whereas in Scenario-B, values have increased from 204.32 to 268.27 Wm^{-2} over the years from 1973 to 2014 (Table 7.28).

Trends similar to Palam area have been found in extreme values of annual hourly storage heat flux for Safdarjung area. Annual extreme hourly values of storage heat flux during night time for Safdarjung areas have decreased (negative values) for Scenario-A initially increase in negative values have been found and then decreasing trends in negative values have been observed (-144.10 to -111.17 Wm^{-2}). In Scenario-B, annual extreme values of storage heat flux have been found to be deceasing (means increase in negative values) (-144.10 to -230.06 Wm^{-2}) and in Scenario-C extreme values of hourly storage heat flux negative values are decreasing over the years (-144.10 to -84.55 Wm^{-2}). Further for Safdarjung area, results indicate that annual extreme hourly values of storage heat flux during day time have decreased in Scenario-A (214.79 to 187.01 Wm^{-2}) and Scenario-C (214.79 to 140.67 Wm^{-2}) over the years from 1973 to 2014, whereas in Scenario-B, values have increased from 214.79 to 278.16 Wm^{-2} during the same period (Table 7.28).

Due to urbanization over the years high albedo LULC areas like irrigated & unirrigated (0.21), trees (0.18) have been converted into LULC classes of low albedo like settlement and built-up surface (0.12 to 0.15) resulting less reflection and more absorption leading to increase in storage heat flux over the years. Also high emissivity areas like irrigated & unirrigated grass (0.93), forest & trees areas (0.98) have been converted into low emissivity areas like buildings (0.91) and paved areas (0.95) leading less outflow of radiations from the surfaces. Such conditions will leads to increase in surface temperature. Such a conversion of LULC classes due to urbanization leads to reduction in reflected radiation and outward flow of short & long wave radiations, which results in increase in storage heat flux during day time and increase in negative values of storage heat flux during the night time, over the years. Decrease in storage flux in night leads to increase in night time air temperature. The overall storage heat flux are found to be increasing in Scenario-B due to change in pervious & vegetative LULC classes into impervious built-up LULC classes over the years which leads to decrease in overall vegetation, evaporative cooling and thus results in warmer urban surfaces. Results are in line with conclusions drawn in similar studies in different parts of the world (Das et al., 2009b; Das et al., 2014; Grimmond & Oke, 1995, 1999; Mohan & Kandya, 2015; Nagar et al., 2002).

This is happening due to conversion of vegetation into paved surfaces caused by rapid urbanization.

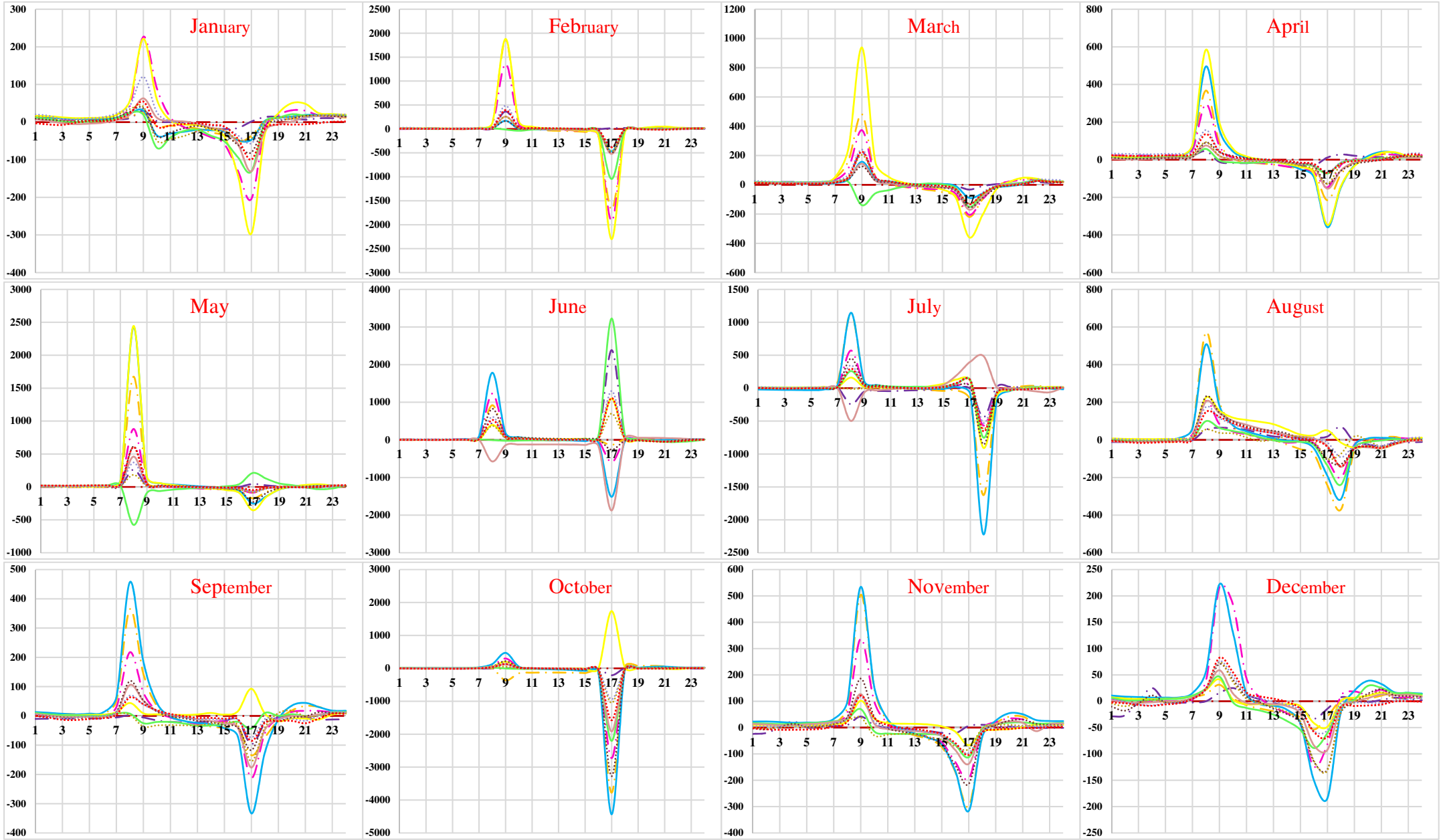

1973	1977	1986	1991	1998	1999	2002	2006	2009	2011	2013	2014	X-axis - Time in Hours
												Y-axis -% change in Heat Flux

Note: Percentage change in values of heat flux are very high because of the values in base year are very small which are used in denominator while calculating percentage change for different years.

Figure 7.31: Percentage change in values of monthly average hourly storage heat flux for Scenario-A for Palam area

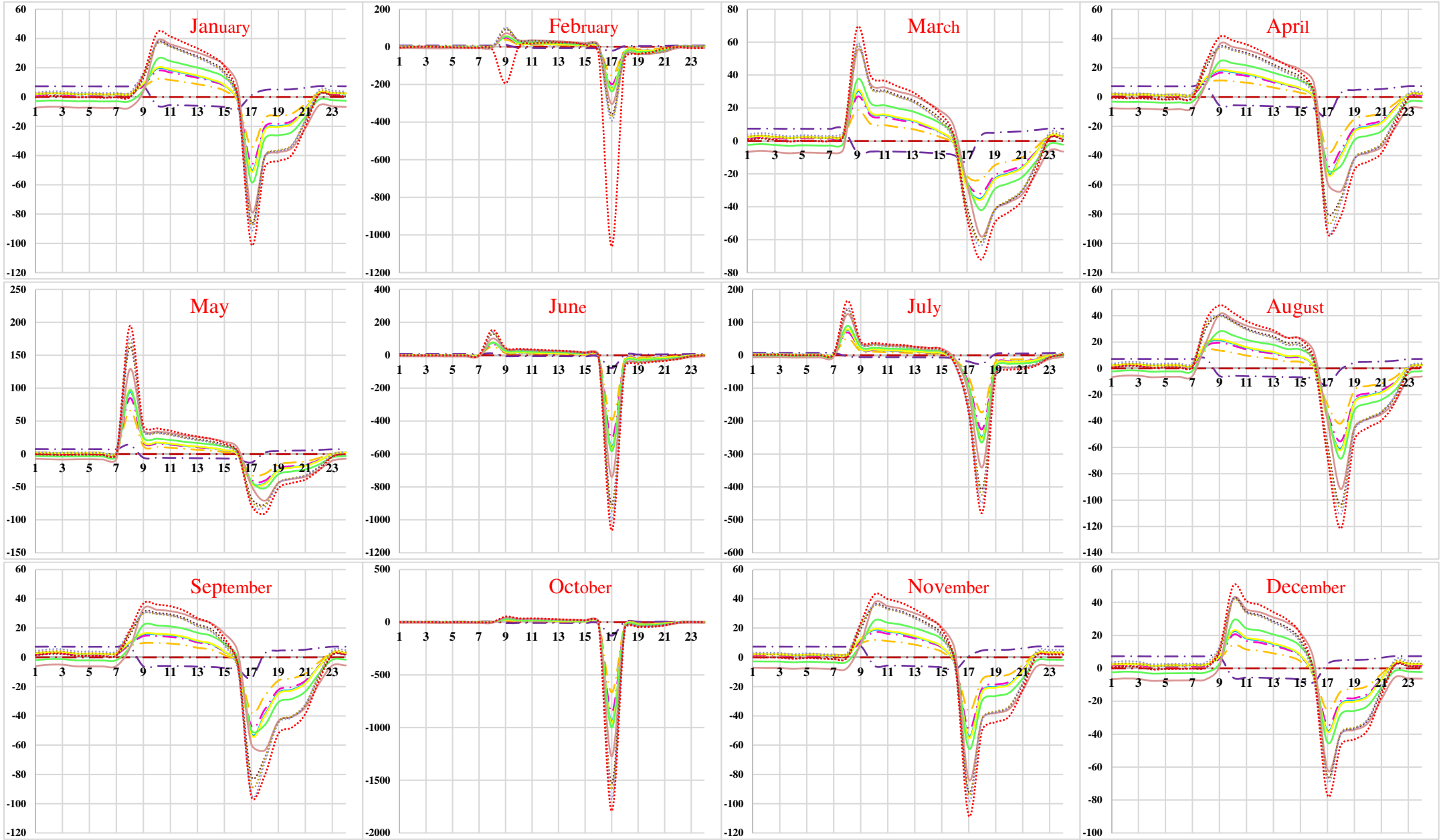

1973	1977	1986	1991	1998	1999	2002	2006	2009	2011	2013	2014	X-axis - Time in Hours
												Y-axis -% change in Heat Flux

Note: Percentage change in values of heat flux are very high because of the values in base year are very small which are used in denominator while calculating percentage change for different years.

Figure 7.32: Percentage change in values of monthly average hourly storage heat flux for Scenario-B for Palam area

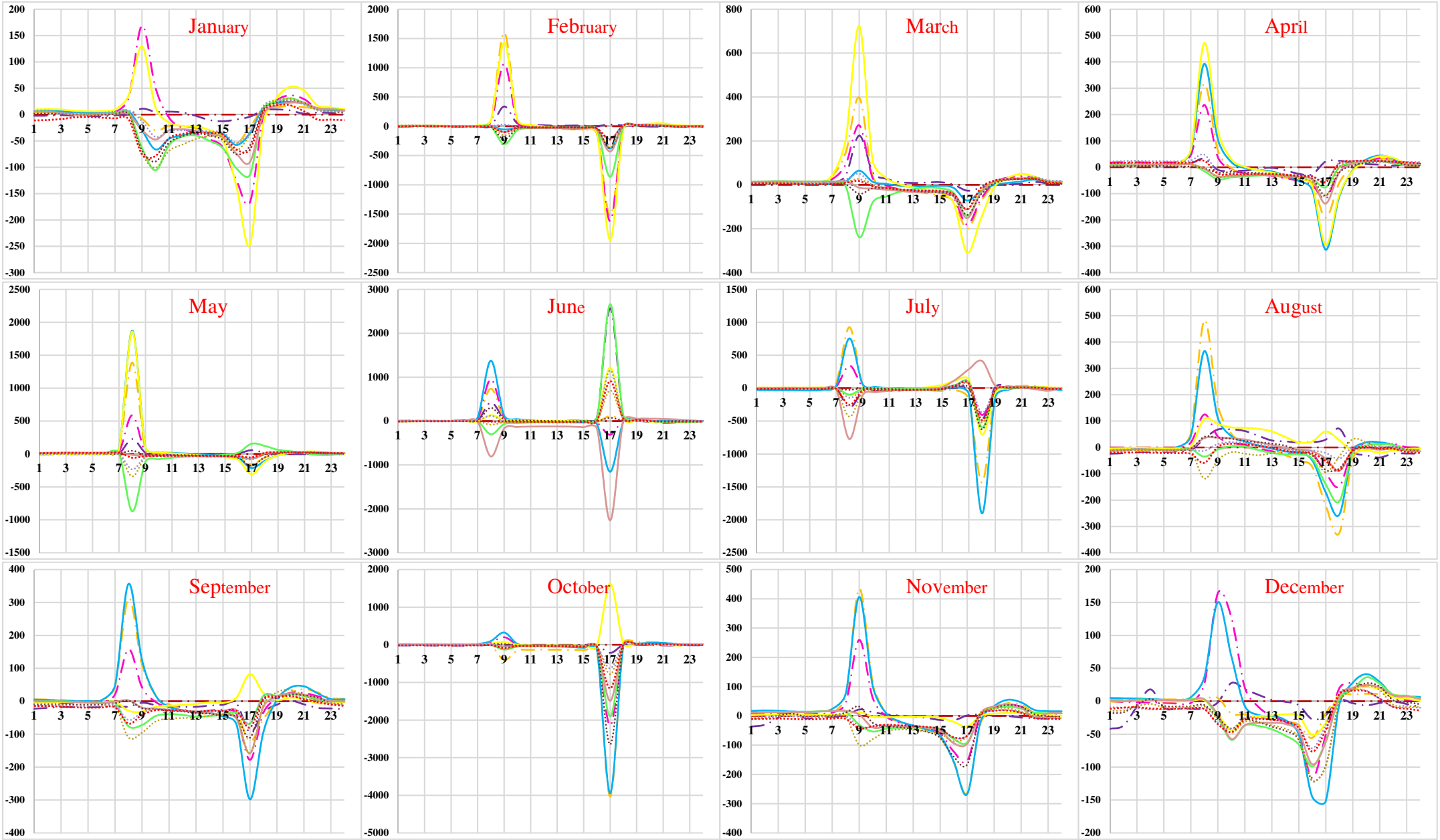

1973	1977	1986	1991	1998	1999	2002	2006	2009	2011	2013	2014	X-axis - Time in Hours
												Y-axis -% change in Heat Flux

Note: Percentage change in values of heat flux are very high because of the values in base year are very small which are used in denominator while calculating percentage change for different years.

Figure 7.33: Percentage change in values of monthly average hourly storage heat flux for Scenario-C for Palam area

Table 7.22: Simulated peak values of monthly average hourly storage heat flux for Scenario-A for Palam area

Year	Time	Jan	Feb	Mar	Apr	May	Jun	Jul	Aug	Sep	Oct	Nov	Dec
1973	Min	-78.4	-81.8	-88.4	-97.2	-86.7	-60.9	-54.7	-52.6	-69.6	-76.3	-75.3	-71.1
	Min_Hr	19	19	20	20	20	20	21	20	20	19	19	19
	Max	106.2	115.5	140.1	159.0	147.1	126.3	116.7	87.5	140.4	132.0	111.1	96.9
	Max_Hr	13	12	13	12	13	13	12	13	12	13	13	13
1977	Min	-67.2	-72.3	-83.5	-81.7	-84.0	-70.8	-47.7	-65.4	-65.7	-74.8	-71.5	-69.5
	Min_Hr	19	19	20	20	20	21	21	20	20	19	19	19
	Max	100.4	127.1	146.3	141.7	136.1	127.5	80.3	113.3	109.4	117.7	104.6	94.5
	Max_Hr	12	12	12	13	12	13	13	12	12	12	12	12
1986	Min	-73.8	-78.6	-83.8	-90.3	-82.1	-68.8	-56.1	-56.2	-69.5	-39.8	-75.3	-69.7
	Min_Hr	19	18	19	19	20	20	19	19	19	15	18	19
	Max	90.1	100.4	119.2	128.5	130.3	129.3	112.1	96.2	123.8	-17.4	97.6	78.8
	Max_Hr	12	11	12	12	11	12	12	12	11	20	11	13
1991	Min	-66.6	-74.9	-80.0	-88.4	-86.9	-65.6	-64.0	-51.8	-64.9	-69.7	-59.8	-58.0
	Min_Hr	18	18	19	20	20	20	20	20	19	19	18	19
	Max	89.3	104.8	124.7	132.0	126.7	122.7	119.1	93.3	118.0	119.6	97.9	97.5
	Max_Hr	12	12	12	11	11	11	12	11	11	12	12	12
1998	Min	-69.4	-78.3	-96.0	-104	-93.7	-69.9	-79.7	-48.6	-67.7	-62.4	-74.8	-69.1
	Min_Hr	19	19	20	19	19	20	19	20	19	18	18	18
	Max	84.5	107.2	153.2	167.3	178.7	143.5	120.0	105.3	121.9	109.0	106.0	88.8
	Max_Hr	13	13	12	11	12	11	11	11	11	11	11	13
1999	Min	-76.5	-87.2	-102	-107	-93.2	-80.4	-71.9	-71.0	-75.6	-73.7	-81.8	-66.2
	Min_Hr	18	18	19	19	19	20	20	20	20	20	19	19
	Max	97.0	132.0	168.5	174.2	168.3	151.2	133.9	164.4	146.1	132.0	126.9	90.8
	Max_Hr	13	11	11	11	11	13	14	12	13	13	13	13
2002	Min	-69.6	-80.8	-84.2	-96.3	-81.1	-80.1	-68.9	-59.1	-65.7	-73.6	-65.6	-68.8
	Min_Hr	19	19	19	20	21	21	20	20	20	19	19	19
	Max	84.5	123.3	142.0	135.4	125.1	114.6	141.9	96.7	104.2	116.6	84.4	75.1
	Max_Hr	13	13	13	12	13	12	13	11	12	12	13	12
2006	Min	-83.0	-83.7	-86.1	-99.6	-84.1	-27.5	-67.9	-73.7	-70.2	-79.2	-65.4	-71.9
	Min_Hr	19	19	20	20	20	20	21	20	20	19	19	19
	Max	104.2	110.5	135.0	150.8	148.4	-14.3	117.6	134.1	135.1	129.7	97.7	91.6
	Max_Hr	12	12	12	12	12	9	13	12	12	12	12	13
2009	Min	-75.9	-88.6	-94.8	-108	-91.2	-85.5	-67.3	-70.5	-73.3	-81.8	-68.7	-72.7
	Min_Hr	19	19	19	20	20	20	20	20	20	19	19	19
	Max	95.4	122.8	144.6	163.5	158.1	172.2	127.9	130.6	128.9	123.4	92.9	89.4
	Max_Hr	13	12	12	12	12	12	11	12	12	12	12	12
2011	Min	-69.8	-79.5	-90.7	-96.2	-85.9	-74.5	-61.2	-60.6	-57.0	-74.9	-68.4	-72.0
	Min_Hr	19	19	20	20	20	21	20	21	20	19	19	19
	Max	80.4	119.7	141.6	146.7	141.4	133.2	107.0	102.0	95.1	120.1	83.9	88.2
	Max_Hr	13	12	12	12	12	13	12	14	12	12	12	12
2013	Min	-73.0	-77.1	-84.8	-97.2	-91.4	-71.4	-63.8	-64.8	-76.3	-75.7	-77.3	-72.9
	Min_Hr	19	19	20	20	20	20	20	20	20	19	19	19
	Max	101.4	130.7	141.5	155.5	140.2	132.5	116.8	122.5	134.0	126.6	102.0	96.4
	Max_Hr	13	12	12	12	12	12	12	12	12	12	12	13
2014	Min	-83.6	-83.5	-92.5	-101	-90.1	-81.3	-69.6	-70.9	-81.4	-82.4	-81.2	-77.5
	Min_Hr	19	19	20	20	20	20	20	20	20	19	19	19
	Max	103.1	132.9	150.6	161.5	148.8	137.5	120.5	123.5	139.2	130.5	108.2	101.6
	Max_Hr	13	12	12	12	12	12	12	12	12	12	12	13

Table 7.23: Simulated peak values of monthly average hourly storage heat flux for Scenario-B for Palam area

Year	Time	Jan	Feb	Mar	Apr	May	Jun	Jul	Aug	Sep	Oct	Nov	Dec
1973	Min	-78.4	-81.8	-88.4	-97.2	-86.7	-60.9	-54.7	-52.6	-69.6	-76.3	-75.3	-71.1
	Min_Hr	19	19	20	20	20	20	21	20	20	19	19	19
	Max	106.2	115.5	140.1	159.0	147.1	126.3	116.7	87.5	140.4	132.0	111.1	96.9
	Max_Hr	13	12	13	12	13	13	12	13	12	13	13	13
1977	Min	-74.4	-77.7	-83.6	-92.2	-82.3	-57.8	-51.9	-50.0	-66.3	-72.3	-71.5	-67.5
	Min_Hr	19	19	20	20	20	20	21	20	20	19	19	19
	Max	99.9	108.8	130.7	149.4	137.9	118.5	109.6	82.0	132.0	123.0	104.4	91.2
	Max_Hr	13	12	13	12	13	13	12	13	12	13	13	13
1986	Min	-88.5	-92.9	-99.5	-109	-98.0	-68.4	-61.3	-59.6	-79.7	-86.8	-85.1	-80.1
	Min_Hr	19	19	20	20	20	20	21	20	20	19	19	19
	Max	115.5	126.8	150.2	172.2	157.0	135.4	126.3	93.9	152.2	142.2	120.7	105.7
	Max_Hr	13	12	13	12	12	13	12	13	12	12	12	13
1991	Min	-92.8	-97.6	-104	-115	-102	-71.6	-64.2	-62.6	-83.8	-91.3	-89.3	-84.0
	Min_Hr	19	19	20	20	20	20	21	20	20	19	19	19
	Max	120.1	132.2	155.8	178.9	162.9	140.2	131.2	97.3	158.2	148.0	126.0	110.0
	Max_Hr	13	12	13	12	12	13	12	13	12	12	12	13
1998	Min	-94.1	-99.0	-105	-116.	-104	-72.5	-65.1	-63.5	-85.1	-92.7	-90.5	-85.2
	Min_Hr	19	19	20	20	20	20	20	20	20	19	19	19
	Max	121.3	133.6	157.2	180.5	164.3	141.3	132.3	98.1	159.7	149.5	127.4	111.2
	Max_Hr	13	12	13	12	12	13	12	13	12	12	12	13
1999	Min	-94.5	-99.4	-106.	-117.	-104.	-72.8	-65.3	-63.7	-85.5	-93.1	-90.9	-85.5
	Min_Hr	19	19	20	20	20	20	20	20	20	19	19	19
	Max	121.8	134.1	157.7	181.1	164.8	141.8	132.8	98.4	160.2	150.1	127.9	111.6
	Max_Hr	13	12	13	12	12	13	12	13	12	12	12	13
2002	Min	-98.9	-104.	-111.	-122.	-109.	-76.3	-68.4	-66.7	-89.4	-97.4	-95.2	-89.5
	Min_Hr	19	19	20	20	20	20	20	20	20	19	19	19
	Max	127.6	140.5	165.3	189.8	172.7	148.6	139.2	103.2	167.9	157.3	134.0	116.9
	Max_Hr	13	12	13	12	12	13	12	13	12	12	12	13
2006	Min	-108.	-113.	-121.	-134.	-119.	-83.1	-74.7	-72.9	-98.0	-106.	-104.	-97.7
	Min_Hr	19	19	20	20	20	20	20	20	20	19	19	19
	Max	138.5	152.9	179.0	205.7	187.0	160.6	150.8	111.6	182.0	170.8	145.9	127.0
	Max_Hr	13	12	13	12	12	13	12	13	12	12	12	13
2009	Min	-107.	-113.	-120.	-133.	-119.	-82.5	-74.4	-72.6	-97.9	-106.	-103.	-97.1
	Min_Hr	19	19	20	20	20	20	20	20	20	19	19	19
	Max	135.9	150.6	175.1	201.5	182.8	156.6	147.6	108.8	178.2	167.9	143.9	124.7
	Max_Hr	13	12	13	12	12	13	12	13	12	12	12	13
2011	Min	-106.	-113.	-120.	-132.	-118.	-82.1	-74.1	-72.3	-97.6	-106.	-103.	-96.7
	Min_Hr	19	19	20	20	20	20	20	20	20	19	19	19
	Max	134.8	149.5	173.6	199.8	181.2	155.1	146.4	107.8	176.8	166.6	142.9	123.8
	Max_Hr	13	12	12	12	12	13	12	13	12	12	12	13
2013	Min	-107.	-113.	-121.	-133.	-119.	-82.7	-74.5	-72.8	-98.3	-106.	-103.	-97.2
	Min_Hr	19	19	20	20	20	19	20	20	20	19	19	19
	Max	135.0	149.9	173.8	200.0	181.2	155.0	146.5	107.7	176.9	166.9	143.3	124.0
	Max_Hr	13	12	12	12	12	12	12	13	12	12	12	13
2014	Min	-112.	-112.	-126.	-140.	-124.	-86.7	-78.1	-76.3	-103.	-112.	-108.	-101.
	Min_Hr	19	19	20	20	20	19	20	20	20	19	19	19
	Max	141.5	141.5	182.2	209.5	189.9	162.4	153.5	112.8	185.4	175.0	150.4	130.0
	Max_Hr	13	13	12	12	12	12	12	13	12	12	12	13

Table 7.24: Simulated peak values of monthly average hourly storage heat flux for Scenario-C for Palam area

Year	Time	Jan	Feb	Mar	Apr	May	Jun	Jul	Aug	Sep	Oct	Nov	Dec
1973	Min	-78.4	-81.8	-88.4	-97.2	-86.7	-60.9	-54.7	-52.6	-69.6	-76.3	-75.3	-71.1
	Min_Hr	19	19	20	20	20	20	21	20	20	19	19	19
	Max	106.2	115.5	140.1	159.0	147.1	126.3	116.7	87.5	140.4	132.0	111.1	96.9
	Max_Hr	13	12	13	12	13	13	12	13	12	13	13	13
1977	Min	-70.8	-75.9	-86.9	-85.5	-87.8	-73.9	-49.8	-68.2	-68.6	-78.2	-75.3	-73.2
	Min_Hr	19	19	20	20	20	21	21	20	20	19	19	19
	Max	106.6	135.1	154.4	150.9	145.1	135.9	85.4	120.7	116.5	123.9	111.1	100.2
	Max_Hr	12	12	12	13	12	13	13	12	12	12	12	12
1986	Min	-67.2	-71.9	-75.4	-81.4	-74.4	-61.9	-50.4	-51.4	-61.8	-41.2	-68.8	-63.7
	Min_Hr	19	18	19	19	20	20	19	19	19	15	18	19
	Max	79.8	89.7	109.3	118.7	119.6	118.6	103.5	88.9	112.1	-19.9	86.8	70.6
	Max_Hr	12	11	12	12	12	12	12	12	11	20	11	13
1991	Min	-59.0	-65.8	-68.8	-76.2	-74.7	-56.9	-54.6	-45.2	-55.7	-60.0	-52.7	-51.4
	Min_Hr	18	19	19	20	20	20	20	20	19	19	19	19
	Max	76.3	91.4	108.8	116.5	111.1	106.4	104.8	80.8	101.5	104.1	84.2	83.6
	Max_Hr	12	12	12	12	12	11	12	12	12	12	12	12
1998	Min	-61.1	-68.0	-81.0	-89.5	-79.8	-60.7	-68.5	-42.6	-58.2	-55.9	-65.5	-60.9
	Min_Hr	19	19	20	19	19	20	19	20	19	18	18	18
	Max	70.1	91.0	131.5	143.5	157.1	123.6	101.1	90.0	103.5	90.9	88.9	75.1
	Max_Hr	13	13	12	11	12	12	11	12	11	11	12	13
1999	Min	-67.0	-75.4	-86.3	-91.6	-80.5	-66.8	-59.1	-58.2	-62.0	-61.2	-69.8	-57.6
	Min_Hr	18	18	19	19	19	20	20	20	20	20	19	19
	Max	82.1	112.0	143.4	149.8	144.0	132.3	118.3	143.0	128.1	114.3	108.2	75.8
	Max_Hr	13	12	11	11	11	13	14	12	13	13	13	13
2002	Min	-59.8	-67.5	-69.1	-78.2	-65.6	-64.5	-55.1	-48.9	-53.8	-61.3	-55.9	-58.4
	Min_Hr	19	19	19	20	21	21	20	20	20	19	19	19
	Max	64.0	97.4	112.5	109.3	100.4	91.4	117.2	75.6	82.2	93.0	66.1	57.0
	Max_Hr	13	13	13	13	14	12	13	12	12	13	13	12
2006	Min	-64.7	-64.9	-65.0	-75.1	-62.9	-30.3	-50.6	-54.8	-52.9	-60.5	-50.8	-56.6
	Min_Hr	19	19	19	20	20	16	21	20	20	19	19	19
	Max	74.0	79.8	99.0	112.2	110.7	-24.1	85.6	100.1	100.4	94.6	69.7	65.3
	Max_Hr	12	12	12	12	12	8	13	12	12	12	13	13
2009	Min	-60.4	-68.5	-72.3	-81.4	-69.8	-64.0	-50.9	-52.8	-55.2	-63.8	-55.9	-58.6
	Min_Hr	19	19	19	20	20	20	20	20	20	19	19	19
	Max	68.0	90.5	107.1	124.6	121.6	132.4	95.8	100.5	97.3	91.0	66.6	62.5
	Max_Hr	13	13	12	12	12	12	12	12	12	12	12	12
2011	Min	-56.5	-62.1	-68.2	-73.2	-66.3	-57.1	-46.5	-46.3	-45.3	-58.4	-56.2	-58.6
	Min_Hr	19	19	20	20	20	21	20	21	20	19	19	19
	Max	57.1	88.4	106.9	112.0	107.0	103.2	79.5	77.7	70.7	88.6	58.6	61.9
	Max_Hr	13	12	12	12	12	13	12	14	13	12	12	12
2013	Min	-58.0	-58.9	-63.4	-72.9	-69.8	-52.9	-47.2	-48.4	-57.0	-58.1	-61.7	-58.5
	Min_Hr	19	19	20	20	20	20	20	20	20	19	19	19
	Max	74.2	97.6	106.8	119.7	106.0	101.3	88.9	93.6	101.5	93.9	73.3	69.7
	Max_Hr	13	12	12	12	12	12	12	12	12	12	12	13
2014	Min	-64.3	-61.6	-66.2	-72.8	-65.1	-58.6	-49.9	-51.6	-58.5	-61.5	-62.1	-59.8
	Min_Hr	19	19	20	20	20	20	20	20	20	19	19	19
	Max	70.3	93.8	108.0	118.3	107.8	99.6	86.6	89.0	100.1	91.5	73.8	69.6
	Max_Hr	13	13	12	12	12	12	12	12	12	12	12	13

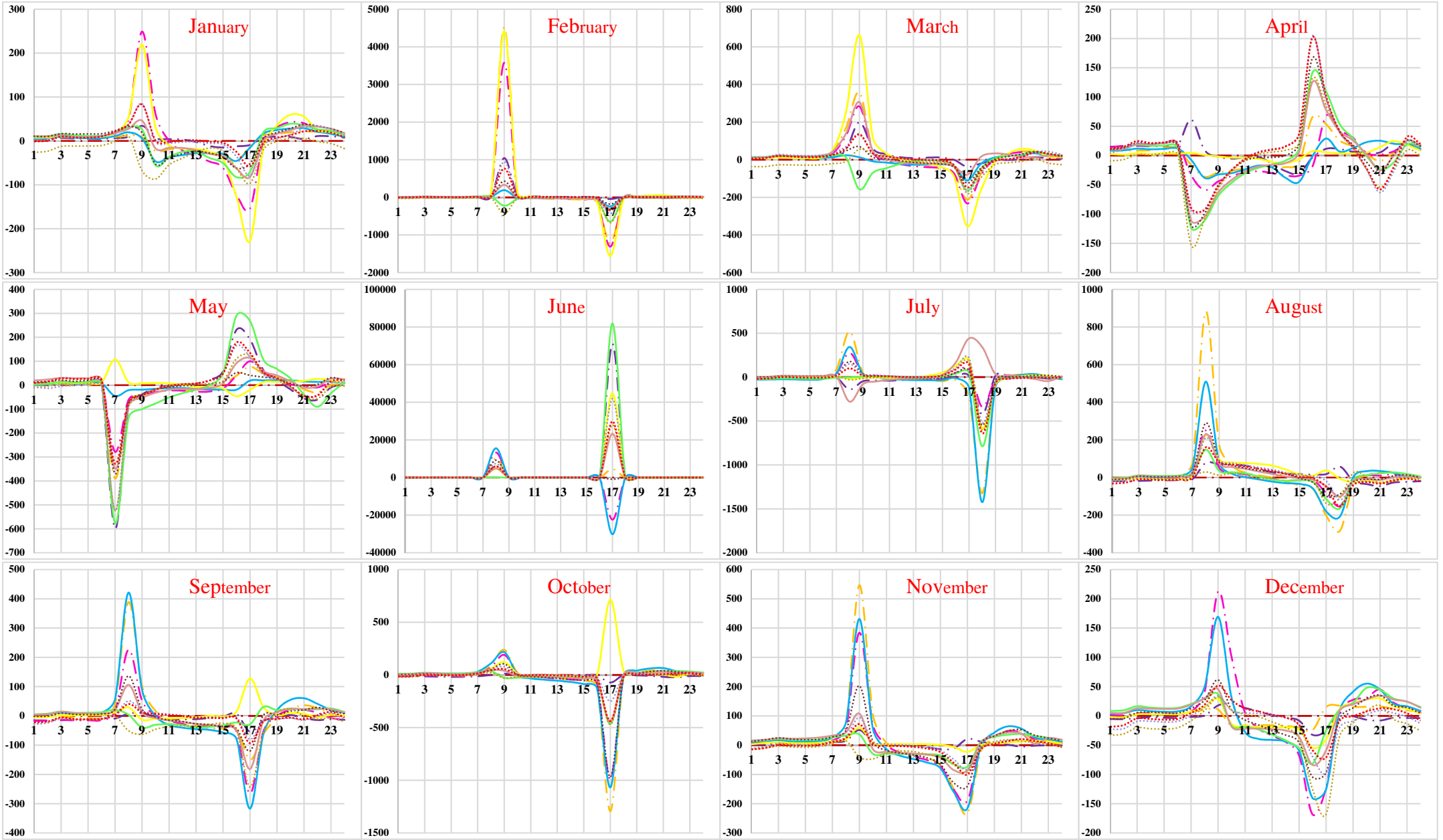

1973	1977	1986	1991	1998	1999	2002	2006	2009	2011	2013	2014	X-axis - Time in Hours
												Y-axis -% change in Heat Flux

Note: Percentage change in values of heat flux are very high because of the values in base year are very small which are used in denominator while calculating percentage change for different years.

Figure 7.34: Percentage change in values of monthly average hourly storage heat flux for Scenario-A for Safdarjung area

1973	1977	1986	1991	1998	1999	2002	2006	2009	2011	2013	2014	X-axis - Time in Hours
												Y-axis -% change in Heat Flux

Note: Percentage change in values of heat flux are very high because of the values in base year are very small which are used in denominator while calculating percentage change for different years.

Figure 7.35: Percentage change in values of monthly average hourly storage heat flux for Scenario-B for Safdarjung area

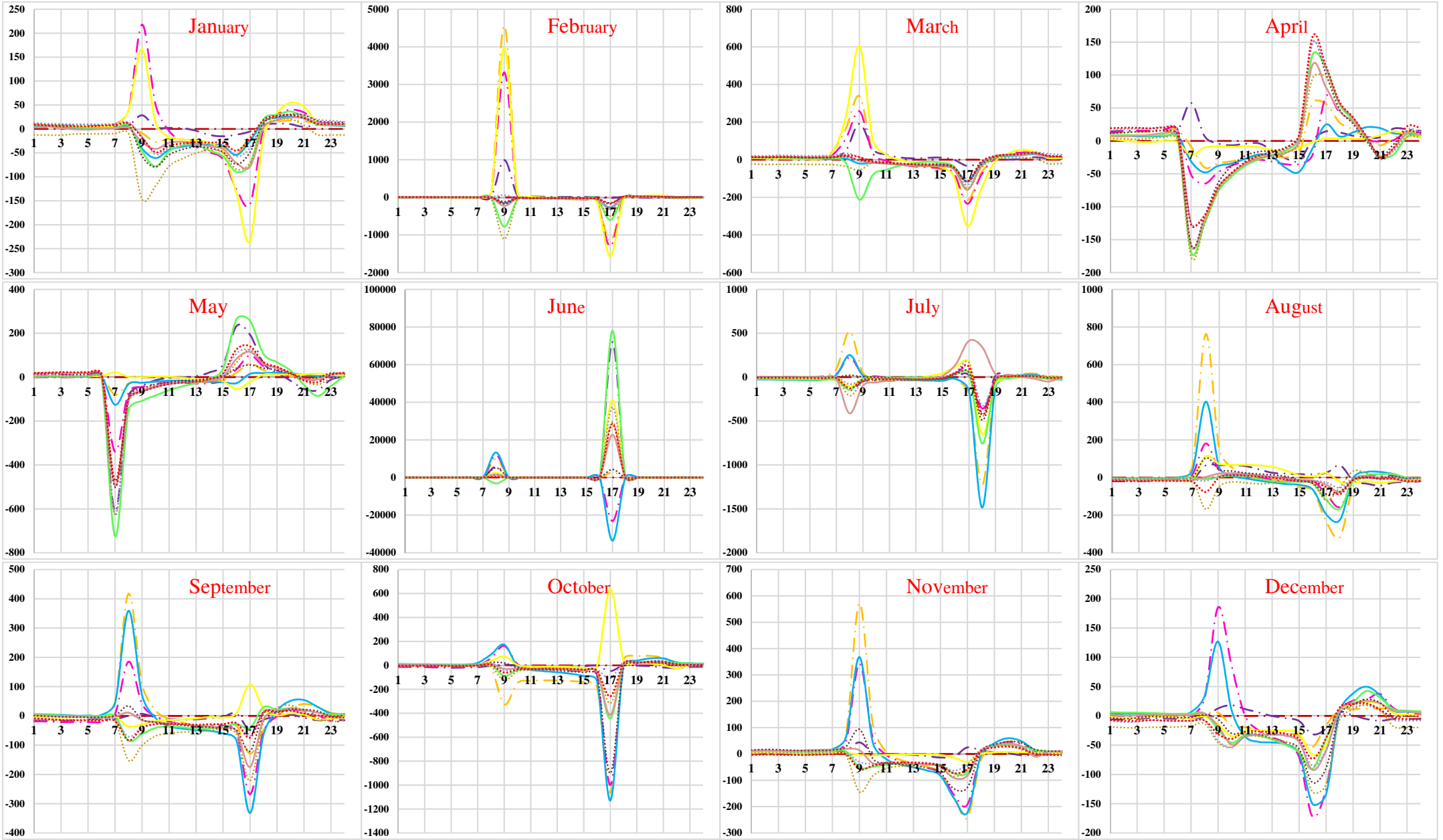

1973	1977	1986	1991	1998	1999	2002	2006	2009	2011	2013	2014	X-axis - Time in Hours
												Y-axis -% change in Heat Flux
Note: Percentage change in values of heat flux are very high because of the values in base year are very small which are used in denominator while calculating percentage change for different years.												

Figure 7.36: Percentage change in values of monthly average hourly storage heat flux for Scenario-C for Safdarjung area

Table 7. 25: Simulated peak values of monthly average hourly storage heat flux for

Year	Time	Jan	Feb	Mar	Apr	May	Jun	Jul	Aug	Sep	Oct	Nov	Dec
1973	Min	-81.8	-85.9	-92.2	-102.	-90.9	-62.0	-55.9	-53.9	-72.7	-80.0	-78.6	-73.8
	Min_Hr	19	19	20	19	19	20	21	20	20	19	19	19
	Max	113.2	123.8	147.4	168.7	154.6	133.4	124.2	92.9	149.0	139.3	118.2	104.3
	Max_Hr	13	12	13	11	12	13	12	13	12	12	13	13
1977	Min	-73.8	-83.7	-93.8	-95.6	-94.0	-78.6	-51.7	-73.0	-70.6	-83.9	-75.6	-74.1
	Min_Hr	19	19	20	19	20	21	21	20	20	19	19	19
	Max	114.0	145.9	165.4	163.1	154.5	143.8	91.9	129.3	131.3	134.5	118.5	107.1
	Max_Hr	12	12	12	11	12	13	13	12	12	12	12	12
1986	Min	-68.5	-77.0	-79.4	-86.1	-70.2	-65.0	-54.5	-49.0	-69.1	-65.8	-71.4	-62.4
	Min_Hr	19	18	19	19	20	20	19	19	19	18	18	19
	Max	89.5	94.7	121.1	132.6	121.3	130.5	109.6	99.7	119.2	104.2	95.7	87.5
	Max_Hr	12	11	12	12	12	12	12	12	11	12	12	13
1991	Min	-60.7	-68.0	-77.3	-78.4	-76.8	-58.7	-55.0	-47.6	-63.9	-68.4	-59.0	-55.5
	Min_Hr	18	18	19	20	20	20	20	20	19	19	18	18
	Max	86.3	99.6	114.7	119.7	119.2	114.8	117.5	91.9	111.6	107.3	88.3	77.9
	Max_Hr	12	11	11	11	12	11	12	12	11	12	12	12
1998	Min	-61.4	-69.4	-74.1	-88.9	-72.1	-51.5	-61.0	-35.7	-52.7	-50.3	-60.9	-54.7
	Min_Hr	19	19	20	19	19	20	19	20	18	18	18	18
	Max	81.5	102.9	114.0	134.6	136.5	109.6	90.7	80.2	92.4	80.2	76.0	61.5
	Max_Hr	13	13	12	12	12	11	11	12	11	11	11	13
1999	Min	-69.5	-79.9	-93.9	-98.7	-78.4	-67.8	-63.5	-63.5	-65.7	-63.4	-73.8	-57.8
	Min_Hr	18	18	19	19	19	20	20	20	20	20	19	19
	Max	92.5	125.2	156.6	161.9	163.7	147.2	127.1	154.5	138.6	131.2	122.3	83.4
	Max_Hr	13	11	11	11	11	13	14	12	13	12	13	13
2002	Min	-58.1	-70.5	-76.9	-82.8	-73.3	-68.6	-63.6	-47.1	-54.3	-63.3	-56.6	-57.2
	Min_Hr	19	19	19	20	21	21	20	20	20	19	19	19
	Max	85.2	120.5	133.4	128.5	116.5	111.4	129.0	95.2	101.6	114.5	83.0	76.1
	Max_Hr	13	13	13	12	13	12	12	11	12	12	12	12
2006	Min	-68.6	-69.4	-66.8	-80.4	-66.8	-62.7	-53.8	-58.4	-55.6	-65.6	-53.8	-59.2
	Min_Hr	19	19	20	20	20	20	21	20	19	19	19	19
	Max	92.5	97.6	130.3	132.1	130.3	118.2	102.8	117.8	118.6	114.5	86.8	80.4
	Max_Hr	12	12	12	12	12	12	13	12	12	12	12	13
2009	Min	-66.2	-73.9	-80.1	-91.0	-74.1	-70.8	-54.2	-58.9	-61.7	-71.5	-55.3	-63.7
	Min_Hr	19	19	19	20	20	20	20	20	19	19	18	19
	Max	86.5	118.7	138.3	157.3	151.0	163.8	120.2	123.6	119.8	110.1	86.0	84.0
	Max_Hr	13	12	12	12	12	12	11	12	12	12	12	12
2011	Min	-82.8	-96.1	-107.	-101.	-86.2	-71.2	-59.5	-58.4	-57.4	-77.9	-69.7	-82.4
	Min_Hr	19	19	20	20	20	21	20	21	19	19	19	19
	Max	84.6	127.4	154.3	166.3	161.6	153.2	120.7	108.4	98.7	130.0	94.5	97.9
	Max_Hr	13	12	12	12	12	12	12	14	12	12	12	12
2013	Min	-77.7	-85.3	-90.3	-101.	-86.6	-71.6	-64.2	-64.9	-78.2	-76.9	-73.1	-80.3
	Min_Hr	19	19	20	20	20	20	20	20	20	19	19	19
	Max	110.8	140.8	158.9	173.2	161.1	154.3	134.7	137.4	151.2	144.8	119.6	104.9
	Max_Hr	13	12	12	12	12	12	12	12	12	12	12	13
2014	Min	-75.9	-82.9	-89.7	-99.7	-82.9	-76.3	-65.6	-67.1	-77.0	-80.2	-75.7	-74.1
	Min_Hr	19	19	20	20	20	20	20	20	20	19	19	19
	Max	114.9	140.8	158.2	170.8	160.6	147.8	128.7	131.1	148.1	138.0	113.9	107.1
	Max_Hr	13	12	12	12	12	12	12	12	12	12	12	12

Scenario-A for Safdarjung area

Table 7.26: Simulated peak values of monthly average hourly storage heat flux for Scenario-B for Safdarjung area

Year	Time	Jan	Feb	Mar	Apr	May	Jun	Jul	Aug	Sep	Oct	Nov	Dec
1973	Min	-81.8	-85.9	-92.2	-102.	-90.9	-62.0	-55.9	-53.9	-72.7	-80.0	-78.6	-73.8
	Min_Hr	19	19	20	19	19	20	21	20	20	19	19	19
	Max	113.2	123.8	147.4	168.7	154.6	133.4	124.2	92.9	149.0	139.3	118.2	104.3
	Max_Hr	13	12	13	11	12	13	12	13	12	12	13	13
1977	Min	-83.4	-87.7	-93.9	-104.	-92.8	-63.2	-57.0	-55.1	-74.3	-81.7	-80.2	-75.2
	Min_Hr	19	19	20	19	19	20	21	20	20	19	19	19
	Max	114.4	125.3	148.2	170.3	155.6	134.3	125.4	93.6	150.5	140.4	119.4	105.4
	Max_Hr	13	12	13	11	12	13	12	13	12	12	12	13
1986	Min	-84.6	-89.0	-95.2	-105.	-94.1	-64.1	-57.7	-55.9	-75.4	-82.8	-81.3	-76.3
	Min_Hr	19	19	20	19	19	20	21	20	20	19	19	19
	Max	115.7	126.8	149.8	172.2	157.2	135.7	126.8	94.6	152.2	142.1	120.9	106.6
	Max_Hr	13	12	13	11	12	13	12	13	12	12	12	13
1991	Min	-84.4	-88.8	-94.9	-105.	-93.8	-63.9	-57.5	-55.8	-75.4	-82.8	-81.1	-76.0
	Min_Hr	19	19	20	19	19	20	21	20	20	19	19	19
	Max	114.0	125.3	147.5	169.8	154.5	133.5	124.9	93.0	150.1	140.3	119.5	105.1
	Max_Hr	13	12	13	11	12	13	12	13	12	12	12	13
1998	Min	-85.5	-90.0	-96.2	-106.	-95.2	-64.8	-58.3	-56.5	-76.4	-83.9	-82.2	-77.1
	Min_Hr	19	19	20	19	19	20	21	20	20	19	19	19
	Max	115.0	126.4	148.8	171.3	155.7	134.6	126.0	93.8	151.4	141.6	120.6	106.0
	Max_Hr	13	12	13	11	12	13	12	13	12	12	12	13
1999	Min	-85.4	-90.0	-96.1	-106.	-95.1	-64.7	-58.3	-56.5	-76.4	-83.9	-82.1	-77.0
	Min_Hr	19	19	20	19	19	20	21	20	20	19	19	19
	Max	115.1	126.5	148.9	171.4	155.8	134.7	126.1	93.9	151.5	141.6	120.6	106.1
	Max_Hr	13	12	13	11	12	13	12	13	12	12	12	13
2002	Min	-90.4	-95.6	-101.	-113.	-100.	-68.3	-61.5	-60.1	-81.5	-89.4	-87.1	-81.5
	Min_Hr	19	19	20	19	19	20	21	20	20	19	19	19
	Max	118.7	131.3	152.8	176.4	159.0	137.5	129.7	95.9	156.0	146.5	125.5	109.6
	Max_Hr	13	12	13	11	11	13	12	13	12	12	12	13
2006	Min	-91.4	-96.7	-102.	-114.	-69.0	-62.1	-60.8	-82.6	-90.5	-88.0	-82.4	-82.4
	Min_Hr	19	19	20	19	20	21	20	20	19	19	19	19
	Max	119.5	132.4	153.7	177.5	138.2	130.4	96.3	156.9	147.6	126.6	110.4	110.4
	Max_Hr	13	12	13	11	12	12	13	12	12	12	13	13
2009	Min	-96.7	-102.3	-108.7	-121.1	-107.8	-73.0	-65.7	-64.2	-87.4	-95.8	-93.1	-87.1
	Min_Hr	19	19	20	19	19	19	20	20	20	19	19	19
	Max	126.2	139.8	162.2	187.4	168.7	145.8	137.7	101.7	165.7	155.9	133.8	116.6
	Max_Hr	13	12	12	11	11	12	12	13	12	12	12	13
2011	Min	-116.0	-123.0	-130.5	-145.4	-129.4	-88.6	-78.8	-77.2	-105.4	-115.5	-111.8	-104.4
	Min_Hr	19	19	20	19	19	19	20	20	20	19	19	19
	Max	149.3	166.3	192.2	221.1	198.8	171.8	162.5	119.4	195.5	184.8	159.4	138.1
	Max_Hr	13	12	12	11	11	12	12	13	12	12	12	13
2013	Min	-117.1	-124.3	-131.8	-146.9	-130.7	-89.5	-79.6	-77.9	-106.5	-116.7	-112.9	-105.4
	Min_Hr	19	19	20	19	19	19	20	20	20	19	19	19
	Max	150.9	168.0	194.2	223.3	200.8	173.6	164.1	120.6	197.5	186.7	161.1	139.6
	Max_Hr	13	12	12	11	11	12	12	13	12	12	12	13
2014	Min	-115.	-122.1	-129.4	-144.3	-128.4	-88.3	-78.3	-76.6	-104.8	-114.8	-110.9	-103.6
	Min_Hr	19	19	20	19	19	19	20	20	20	19	19	19
	Max	147.5	164.4	189.8	218.1	195.9	169.4	160.2	117.6	192.8	182.5	157.6	136.4
	Max_Hr	12	12	12	11	11	12	12	13	12	12	12	13

Table 7.27: Simulated peak values of monthly average hourly storage heat flux for Scenario-C for Safdarjung area

Year	Time	Jan	Feb	Mar	Apr	May	Jun	Jul	Aug	Sep	Oct	Nov	Dec
1973	Min	-81.8	-85.9	-92.2	-102.	-90.9	-62.0	-55.9	-53.9	-72.7	-80.0	-78.6	-73.8
	Min_Hr	19	19	20	19	19	20	21	20	20	19	19	19
	Max	113.2	123.8	147.4	168.7	154.6	133.4	124.2	92.9	149.0	139.3	118.2	104.3
	Max_Hr	13	12	13	11	12	13	12	13	12	12	13	13
1977	Min	-72.7	-82.3	-91.9	-94.1	-92.4	-77.4	-51.1	-71.7	-69.5	-82.3	-74.4	-73.1
	Min_Hr	19	19	20	19	20	21	21	20	20	19	19	19
	Max	112.2	143.9	162.8	161.2	152.8	142.5	90.7	127.8	129.7	132.0	116.6	105.3
	Max_Hr	12	12	12	11	12	13	13	12	12	12	12	12
1986	Min	-69.1	-74.7	-78.5	-84.5	-76.0	-63.2	-51.8	-52.3	-64.5	-38.2	-71.6	-65.4
	Min_Hr	19	18	19	19	20	20	19	19	19	15	18	19
	Max	87.2	96.8	116.0	125.4	126.7	125.9	109.6	94.3	119.5	-16.0	94.0	76.5
	Max_Hr	12	11	12	12	12	12	12	12	11	20	11	13
1991	Min	-61.2	-68.1	-77.4	-78.6	-77.2	-59.8	-55.4	-48.5	-64.4	-68.8	-59.6	-56.5
	Min_Hr	18	18	19	20	20	20	20	20	19	19	18	18
	Max	83.0	96.0	111.0	116.0	115.9	110.9	114.4	88.7	107.6	103.9	85.1	74.7
	Max_Hr	12	11	11	12	12	11	12	12	11	12	12	12
1998	Min	-62.5	-69.8	-74.2	-89.0	-73.2	-53.6	-62.3	-38.0	-53.8	-51.9	-61.8	-56.0
	Min_Hr	19	19	20	19	19	20	19	20	18	18	18	18
	Max	76.3	97.9	108.3	129.1	130.5	103.4	84.6	74.8	86.5	74.5	71.1	56.9
	Max_Hr	13	13	12	12	12	11	11	12	11	11	12	13
1999	Min	-70.3	-80.0	-93.1	-98.8	-79.6	-68.6	-64.3	-64.4	-66.3	-63.6	-74.2	-59.3
	Min_Hr	18	18	19	19	19	20	20	20	20	20	19	19
	Max	87.1	118.9	148.5	154.7	156.2	141.0	121.4	147.5	132.8	124.3	116.4	77.8
	Max_Hr	13	11	11	11	11	13	14	12	13	13	13	13
2002	Min	-57.7	-68.2	-73.3	-80.0	-71.0	-66.1	-62.3	-47.4	-53.4	-61.2	-56.0	-56.5
	Min_Hr	19	19	19	20	21	21	20	20	20	19	19	19
	Max	74.7	108.9	120.2	116.7	104.9	99.9	118.9	83.7	90.8	102.2	72.9	65.7
	Max_Hr	13	13	13	12	13	12	13	11	12	12	13	12
2006	Min	-66.8	-67.1	-67.5	-77.7	-65.0	-60.9	-52.3	-54.8	-54.5	-62.9	-52.5	-58.2
	Min_Hr	19	19	19	20	20	20	21	20	20	19	19	19
	Max	80.7	86.3	105.9	119.6	117.8	106.9	91.6	100.1	107.0	101.5	75.8	70.8
	Max_Hr	12	12	12	12	12	12	13	12	12	12	12	13
2009	Min	-61.6	-66.6	-71.3	-82.2	-68.3	-64.9	-50.7	-54.5	-56.7	-66.0	-52.0	-59.8
	Min_Hr	19	19	19	20	20	20	20	20	19	19	18	19
	Max	71.2	100.2	116.8	135.8	130.8	141.9	102.3	106.4	101.8	92.3	70.8	67.8
	Max_Hr	13	12	12	12	12	12	12	12	12	12	12	12
2011	Min	-66.3	-74.5	-81.9	-77.2	-66.8	-54.5	-46.7	-46.2	-46.5	-60.3	-56.0	-65.6
	Min_Hr	19	19	20	20	20	21	20	21	19	19	19	19
	Max	56.3	87.9	109.0	120.1	116.1	112.7	84.6	77.7	67.4	90.1	62.6	64.8
	Max_Hr	13	12	12	12	12	13	12	14	13	12	12	12
2013	Min	-60.2	-63.9	-67.9	-77.0	-66.5	-54.3	-49.1	-50.1	-59.5	-57.8	-56.3	-62.7
	Min_Hr	19	19	20	20	20	21	20	20	20	19	19	19
	Max	76.4	98.7	112.6	124.2	114.3	110.4	95.5	97.7	106.9	101.3	81.6	71.7
	Max_Hr	13	12	12	12	12	12	12	12	12	13	12	13
2014	Min	-59.2	-63.0	-68.1	-76.4	-64.3	-59.6	-51.5	-53.4	-59.7	-61.9	-59.8	-58.9
	Min_Hr	19	19	20	20	20	20	20	20	20	19	19	19
	Max	81.9	101.5	114.9	125.8	117.1	107.5	92.8	94.6	107.0	98.3	79.1	74.9
	Max_Hr	13	13	12	12	12	12	12	12	12	12	13	13

Table 7.28: Annual extreme values of hourly storage heat flux for different Scenarios

Year	Data	Palam Area			Safdarjung Area		
		Scenario-A	Scenario-B	Scenario-C	Scenario-A	Scenario-B	Scenario-C
1973	Max	204.32	204.32	204.32	214.79	214.79	214.79
	Min	-129.66	-129.66	-129.66	-144.10	-144.10	-144.10
1977	Max	229.44	191.87	242.93	262.91	216.69	258.87
	Min	-124.08	-124.9	-130.87	-146.74	-149.07	-143.78
1986	Max	205.01	220.28	184.43	205.16	219.08	197.03
	Min	-138.78	-157.83	-120.99	-122.70	-151.65	-130.48
1991	Max	195.53	228.54	176.37	193.64	215.91	191.33
	Min	-135.26	-168.32	-111.73	-123.96	-152.93	-119.07
1998	Max	226.77	230.47	191.81	172.66	217.89	162.91
	Min	-152.27	-172.06	-126.11	-139.88	-155.33	-136.29
1999	Max	258.47	231.21	217.16	248.15	218.02	237.46
	Min	-144.61	-173.05	-112.83	-129.24	-155.15	-124.86
2002	Max	224.18	242.38	176.29	213.39	223.66	190.70
	Min	-125.89	-180.98	-102.07	-112.97	-171.45	-104.67
2006	Max	202.87	262.2	156.07	174.63	225.24	158.79
	Min	-135.91	-201.4	-94.12	-116.40	-174.71	-102.43
2009	Max	236.64	257.46	172.43	223.08	237.87	190.40
	Min	-176.65	-205.17	-128.36	-163.73	-185.50	-140.23
2011	Max	252.18	255.52	182.38	263.00	281.71	184.70
	Min	-143.96	-205.49	-99.54	-165.81	-122.49	-113.16
2013	Max	167.32	255.97	129.04	196.08	284.57	143.07
	Min	-117.19	-208.05	-88.02	-114.60	-232.60	-85.76
2014	Max	184.33	268.27	133.85	187.01	278.16	140.67
	Min	-119.88	-218.93	-82.74	-111.17	-230.06	-84.55

Trend in extreme annual values of storage heat flux values in different scenarios are also indicating impacts of LULC changes in affecting the micro-climate of Delhi. Extreme values of storage heat flux values are increasing during day time in Scenario-B and reducing in Scenario-C reveals the LULC change impacts. Increase in storage heat flux indicates increase in urban surface temperature over the years. Extreme values of storage heat flux values in Scenario-B are decreasing over the years which indicates outflow of radiations during night leading to increase in night time air temperature. These effects are clearly indicating that LULC changes are increasing the temperature in urban areas and thus affecting the micro-climate. Study results are in line with results of other experimental & modelling studies for different type of urban surfaces (Scenario-C) (Kircsi et al., 2005; Pielke et al., 2000; Barron & Pollard, 2005; Miller et al., 2005; Mölders & Olson, 2004; Voldoire & Royer, 2004).

7.5.3 Sensible Heat Flux

Monthly, seasonal and annual average of sensible heat flux at hourly temporal scale has been calculated for both the study areas Palam and Safdarjung from hourly model results for different Scenarios (A, B and C) and for different years. Annual extreme hourly values have also been calculated to ascertain the effects of LULC change scenario on extreme values of sensible heat flux.

For Palam area in Scenario-A, peak value of monthly average hourly sensible heat flux during night time in different years found to be increasing means negative values are decreasing over the years from -42.0 Wm^{-2} in year 1973 to -9.20 Wm^{-2} in year 2014. Similarly, peak values of monthly average hourly sensible heat flux during day time have been found to be decreasing over the years from 491.20 Wm^{-2} in year 1973 to 382.40 Wm^{-2} in year 2014, as shown in Table 7.29 and Figure 7.37. Relative percentage change in peak value of sensible heat flux during night time, as compared to the base year values is showing decreasing trend over the years ranging from 2.14 % in year 1986 to 9.20 % in year 2014. Similarly, relative percentage change in peak value of sensible heat flux, during day time, from the base year, is showing decreasing trend in sensible heat flux by 0.45 % in year 1977 to increase by 22.15 % in year 2014.

In case of Safdarjung area for Scenario-A, peak values of monthly average hourly sensible heat flux has been calculated. According to the results, monthly average hourly peak values of sensible heat flux during night and day time over the years from 1973 to 2014 are decreasing (in negative values) respectively. Monthly mean hourly peak value of sensible heat flux during night time in different years found to be increasing i.e., means negative values are decreasing over the years from -39.50 Wm^{-2} (1973) to -3.80 Wm^{-2} (2014) and also during day time found to be deceasing from 510.10 Wm^{-2} (1973) to 388.50 Wm^{-2} (2014) as shown in Table 7.32 and Figure 7.40. Relative percentage change in night time sensible heat flux from the base year is showing decreasing trend in negative values from 1986 (32.91 %) to 2014 (90.38 %). Similarly, relative percentage change in day time monthly average hourly sensible heat flux from the base year is showing decreasing trend from 1977 (4.20%) to 2014 (25.43%).

In Scenario-B, for Palam station, monthly average hourly sensible heat flux have been calculated from the hourly simulated results. According to the results (Table 7.30 and Figure 7.38), peak value of monthly average hourly sensible heat flux during night

time is decreasing (means negative values are decreasing) from year 1973 to 2014, also during day time trend is decreasing over the years, which indicates the less availability of available energy for partitioning into sensible and latent heat due to urbanization. Peak values of monthly average hourly sensible heat flux during night time decreasing (means negative values are decreasing) over the years from -42 Wm^{-2} (1973) to -39.10 Wm^{-2} (2014) whereas during the day time values are decreasing over the years from 491.20 Wm^{-2} (1973) to 469.10 Wm^{-2} (2014), as shown in Table 7.30 and Figure 7.38.

Relative percentage change in monthly average hourly sensible heat flux during night time from the base year is showing decreasing trend in negative values from year 1973 (0.0 %) to 2014 (6.90%). Similarly, relative percentage change in peak monthly average hourly sensible heat flux during day time from the base year is showing decreasing trend from 1973 (0 %) to 2014 (4.50 %). In case of Safdarjung area, peak value of monthly average hourly sensible heat flux has been calculated from hourly simulated results. According to the results (Table 7.33 and Figure 7.41), peak values of monthly average hourly sensible heat flux during night time have shown decreasing trend from -39.50 Wm^{-2} (1973) to -36.60 Wm^{-2} (2014) over the years, also results exhibit increasing trend in peak values from 510.10 Wm^{-2} (1973) to 484.70 Wm^{-2} (2014) during day time over the years. Relative percentage change in peak values of monthly average hourly sensible heat flux during night time, from the base year, is showing decreasing trend in negative values from 1977 (0.51%) to 2014 (7.34 %). Similarly, relative percentage change in peak values of monthly average hourly sensible heat flux during day time, from the base year, is showing decreasing trend from 1977 (0.24%) to 2014 (4.98%) (Table 7.33 and Figure 7.41).

In Scenario-C, for Palam area, peak values of monthly average sensible heat flux at hourly temporal scale have been calculated from hourly simulated results. According to the results (Table 7.31 and Figure 7.39), peak values of monthly average hourly sensible heat flux during night time are decreasing (means negative values are increasing) from year 1973 to 2014 whereas during day time, trend is decreasing over the years. During night time peak values of monthly average hourly sensible heat flux values are showing decreasing trend in negative values from -42 Wm^{-2} (1973) to -51 Wm^{-2} (2014) over the years also during day time sensible heat flux values are showing decreasing trend from 491.20 Wm^{-2} (1973) to 376 Wm^{-2} (2014) over the years (Table 7.31 and Figure 7.39). Relative percentage change in monthly average hourly sensible heat flux, during night time, with respect to base year value is showing decreasing trend

in negative values from 1973 (0.0 %) to 2014 (21.43 %) except in few years in which trends are opposite. Similarly, during day time relative percentage change in peak values of monthly average hourly sensible heat flux with respect to base year value, is showing decreasing trend from 1977 (3.87 %) to 2014 (23.45 %).

For Safdarjung area also, results indicate trends in sensible heat flux similar to the Palam area. During night time, peak values of monthly average hourly sensible heat flux are showing decreasing trend in negative values over the years from -39.50Wm^{-2} (1973) to -28.10 Wm^{-2} (2014), also during day time results are showing decreasing trends from 510.10 Wm^{-2} (1973) to 376 Wm^{-2} (2014) over the years (Table 7.34 and Figure 7.42). Relative percentage change in peak values of monthly average hourly sensible heat flux, during night time, with respect to base year value, is showing decreasing trend in negative values from 1973 (0.0%) to 2014 (28.86 %). Similarly, during day time, relative percentage change in monthly average hourly sensible heat flux with respect to base year value, is showing decreasing trend from 1977 (4.29%) to 2014 (26.29%). The overall peak values of monthly average hourly sensible heat flux during night and day time are decreasing over the years due to less availability of available energy to partition in sensible and latent heat fluxes because of increase in storage heat flux.

In the results, relative percentage change in simulated values of sensible heat flux from the base year 1973 over the study period, for Scenario-A (Figure 7.37) and Scenario-C (Figure 7.39) at Palam area are very high in the month of November. For Safdarjung area, percentage change values for Scenario–A (Figure 7.40) are very high in the month July and October. Also, in Scenario-C (Figure 7.42) percentage change values are very high in the month of January, July, October and November. The relative percentage change in the above mentioned months are very high because the flux values in base year is very small which has been used in equation 7.1 to compute percentage change for different years.

Annual extreme hourly values of sensible heat flux have also been calculated from the hourly simulated results for different Scenarios i.e., A, B and C to study the effect of LULC changes on extreme values for both areas i.e., Palam and Safdarjung (Table 7.35). Annual extreme hourly values of sensible heat flux during night time in Palam area have decreased (negative values) in Scenario-A (-900.45 to -388.16 Wm^{-2}), Scenario-B (-900.45 to -264.87 Wm^{-2}) and in Scenario-C values are increasing (-900.45 to -959.48 Wm^{-2}). Further for Palam area, results indicate that annual extreme hourly

values of sensible heat flux during day time have decreased in Scenario-A (555.91 to 413.49 Wm^{-2}) and Scenario-C (555.91 to 409.42 Wm^{-2}) whereas in Scenario-B, values have not changed much 555.91 to 555.95 Wm^{-2} over the years from 1973 to 2014 (Table 7.35). This is happening due to conversion of vegetation into paved surfaces caused by rapid urbanization. On comparing these three cases, it is found that maximum change in net all-wave radiation has been observed in Scenario-C showing that the impact of meteorological changes is more as compared to the impact of LULC changes (Scenario-B). This is caused by the availability of water may be due to rainfall since in Scenario-C meteorology has been changed and thus affecting the sensible heat flux.

Trends similar to Palam area have been found in extreme values of annual hourly sensible heat flux for Safdarjung area. Annual extreme hourly values of sensible heat flux during night time for Safdarjung areas have decreased (negative values) for Scenario-A initially increase in negative values have been found and then decreasing trends in negative values have been observed (-997.38 to -365.86 Wm^{-2}). In Scenario-B, annual extreme values of sensible heat flux have been found to be deceasing (-997.38 to -292.77 Wm^{-2}) and in Scenario-C extreme values of hourly sensible heat flux negative values are marginally increasing over the years from 1973 to 2014 (-997.38 to -989.26 Wm^{-2}).

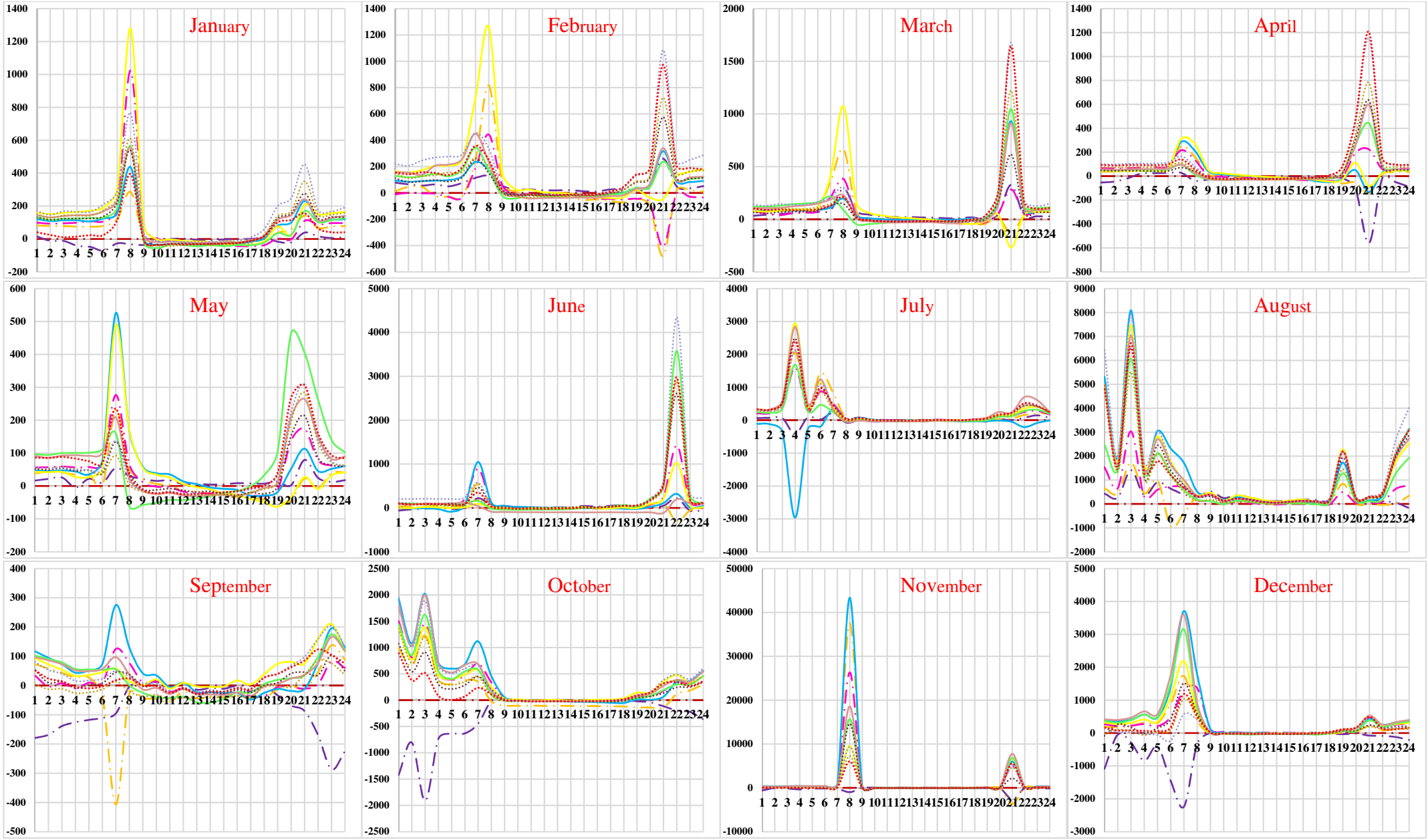

1973	1977	1986	1991	1998	1999	2002	2006	2009	2011	2013	2014	X-axis - Time in Hours
												Y-axis -% change in Heat Flux

Note: Percentage change in values of heat flux are very high because of the values in base year are very small which are used in denominator while calculating percentage change for different years.

Figure 7.37: Percentage change in values of monthly average hourly sensible heat flux for Scenario-A for Palam area

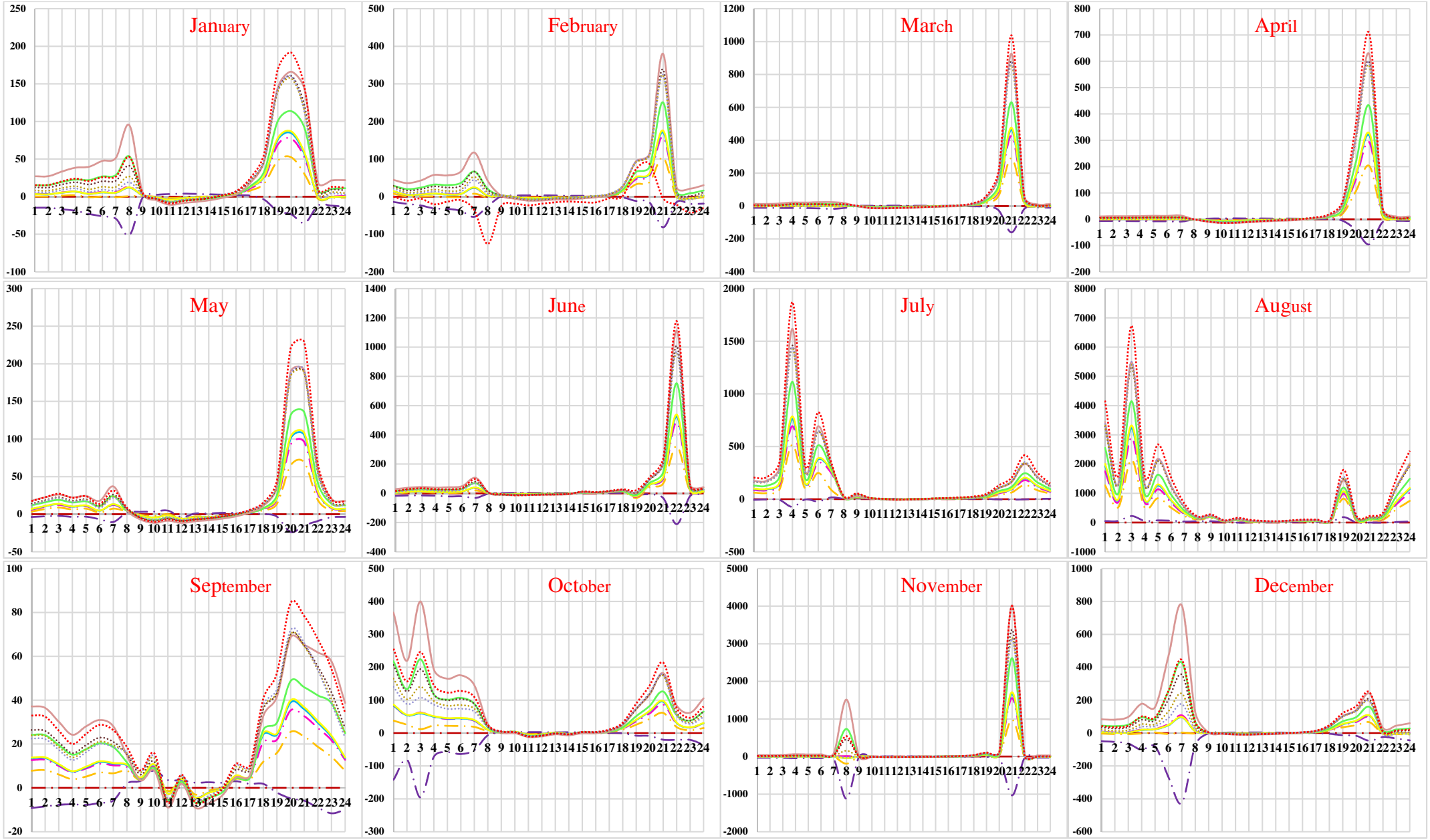

1973	1977	1986	1991	1998	1999	2002	2006	2009	2011	2013	2014	X-axis - Time in Hours
												Y-axis -% change in Heat Flux

Note: Percentage change in values of heat flux are very high because of the values in base year are very small which are used in denominator while calculating percentage change for different years.

Figure 7.38: Percentage change in values of monthly average hourly sensible heat flux for Scenario-B for Palam area

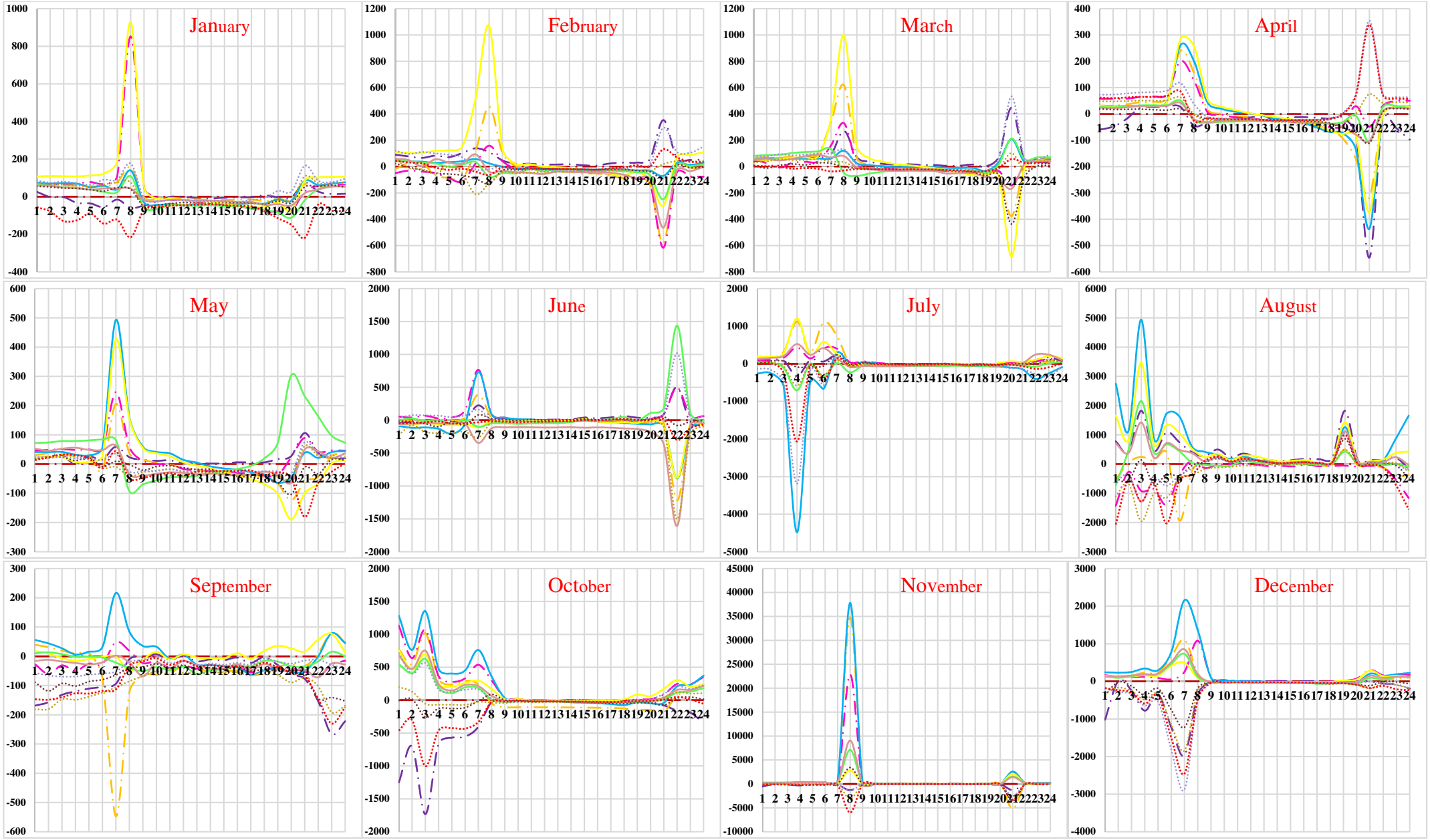

1973	1977	1986	1991	1998	1999	2002	2006	2009	2011	2013	2014	X-axis - Time in Hours
												Y-axei -% change in Heat Flux

Figure 7.39: Percentage change in values of monthly average hourly sensible heat flux for Scenario-C for Palam area

Table 7.29: Simulated peak values of monthly average hourly sensible heat flux for Scenario-A for Palam area

Year	Time	Jan	Feb	Mar	Apr	May	Jun	Jul	Aug	Sep	Oct	Nov	Dec
1973	Min	-16.9	-12.6	-27.1	-41.2	-42.0	-11.9	-10.9	-1.0	7.1	-6.1	-9.1	-7.3
	Min_Hr	22	22	23	23	24	24	24	6	23	22	22	22
	Max	301.7	340.4	419.3	491.2	464.2	380.7	348.0	189.8	412.3	381.0	329.8	273.3
	Max_Hr	14	14	14	14	14	14	13	14	13	14	14	14
1977	Min	-14.5	-6.2	-19.5	-75.6	-37.9	-18.2	-2.7	-0.4	-13.2	-18.9	-41.3	-39.5
	Min_Hr	23	22	23	24	4	24	24	24	23	23	1	1
	Max	281.7	413.4	489.0	435.3	485.4	441.7	244.7	411.1	361.9	396.6	327.9	308.8
	Max_Hr	14	14	14	13	14	15	15	14	14	14	14	14
1986	Min	-5.5	-12.5	-11.9	-28.0	-28.5	-14.5	6.3	-9.8	-42.9	-40.6	-8.5	-1.0
	Min_Hr	22	21	22	23	6	23	23	6	7	15	21	22
	Max	249.6	236.1	342.5	375.9	378.9	379.7	275.5	204.5	247.5	11.7	265.5	225.2
	Max_Hr	14	13	13	13	13	13	12	13	14	8	12	14
1991	Min	-2.1	-13.7	-11.5	-15.7	-17.8	-2.3	6.6	3.4	9.4	10.1	5.4	2.2
	Min_Hr	22	22	3	23	24	2	2	5	2	5	4	5
	Max	214.6	271.6	333.9	369.2	359.8	334.5	323.9	149.4	309.7	330.5	264.4	260.5
	Max_Hr	14	14	13	13	14	14	14	15	13	14	13	13
1998	Min	0.5	-1.6	-7.1	-22.2	-23.6	-15.9	-13.9	14.5	18.2	14.4	14.1	7.3
	Min_Hr	5	23	23	22	5	5	5	4	4	5	2	5
	Max	198.9	286.5	414.9	452.8	479.3	392.0	325.5	304.3	330.4	291.5	284.0	252.4
	Max_Hr	14	14	14	13	13	13	13	13	12	13	13	13
1999	Min	5.4	1.8	-10.6	-23.7	-28.4	-11.0	13.6	14.1	16.6	9.9	1.9	4.8
	Min_Hr	5	21	22	22	22	2	5	2	5	2	2	5
	Max	242.0	323.5	443.2	457.9	437.8	368.4	310.2	392.2	399.8	372.5	324.7	246.1
	Max_Hr	14	13	13	13	13	15	14	13	13	13	14	14
2002	Min	0.3	-0.5	1.9	-19.5	-2.3	-3.1	5.0	7.8	18.6	10.4	9.7	6.2
	Min_Hr	22	22	23	24	2	5	6	1	2	5	22	22
	Max	187.8	286.3	328.7	351.0	349.0	306.2	271.9	229.6	228.2	290.3	229.9	186.6
	Max_Hr	14	14	14	14	15	16	14	14	16	14	14	13
2006	Min	2.5	-0.4	-2.9	-17.6	-7.0	-9.4	13.7	13.1	18.2	12.8	12.4	9.2
	Min_Hr	22	22	23	24	23	15	4	2	2	5	2	2
	Max	237.6	218.7	299.2	351.0	334.3	12.4	238.1	301.6	288.5	292.7	228.8	208.8
	Max_Hr	14	15	14	14	14	9	14	13	13	14	14	14
2009	Min	1.9	-1.6	-9.5	-20.0	-21.1	-2.5	9.1	10.4	10.7	6.5	-7.3	-6.2
	Min_Hr	5	2	23	2	2	4	5	4	2	5	1	1
	Max	208.8	282.3	330.5	377.0	389.9	416.5	323.4	294.1	303.4	291.0	205.2	204.8
	Max_Hr	14	14	14	13	14	14	14	14	14	14	14	14
2011	Min	3.3	1.1	-2.1	-9.9	-19.1	-10.1	9.0	9.7	8.5	8.1	-5.1	-4.2
	Min_Hr	5	2	2	2	5	1	5	4	2	5	1	1
	Max	196.2	255.9	347.4	356.6	338.6	332.7	276.4	201.6	233.2	289.9	197.2	212.8
	Max_Hr	15	14	14	14	13	14	14	15	14	15	14	14
2013	Min	4.9	8.5	5.5	-1.2	-19.3	9.1	10.3	15.2	14.3	12.6	-1.3	-3.1
	Min_Hr	5	6	2	24	2	5	3	5	5	5	2	5
	Max	249.9	288.7	353.6	394.2	367.8	346.6	306.6	277.4	332.8	305.2	242.7	232.2
	Max_Hr	14	14	14	14	14	14	14	13	14	14	14	14
2014	Min	-9.2	1.9	-2.6	-4.1	-8.9	-3.0	11.2	9.2	11.1	2.2	-5.4	-0.8
	Min_Hr	23	5	5	2	5	5	5	5	5	5	5	5
	Max	212.6	295.9	345.8	382.4	362.5	349.3	314.3	293.1	315.2	301.0	240.6	225.0
	Max_Hr	14	14	14	14	14	14	14	14	14	14	14	14

Table 7.30 : Simulated peak values of monthly average hourly sensible heat flux for Scenario-B for Palam area

Year	Time	Jan	Feb	Mar	Apr	May	Jun	Jul	Aug	Sep	Oct	Nov	Dec
1973	Min	-16.9	-12.6	-27.1	-41.2	-42.0	-11.9	-10.9	-1.0	7.1	-6.1	-9.1	-7.3
	Min_Hr	22	22	23	23	24	24	24	6	23	22	22	22
	Max	301.7	340.4	419.3	491.2	464.2	380.7	348.0	189.8	412.3	381.0	329.8	273.3
	Max_Hr	14	14	14	14	14	14	13	14	13	14	14	14
1977	Min	-18.9	-14.5	-29.4	-43.9	-43.5	-13.3	-10.5	-0.4	6.3	-7.3	-11.0	-9.1
	Min_Hr	22	22	23	23	24	24	24	2	23	22	22	22
	Max	311.0	348.6	427.6	503.8	468.9	391.2	357.5	211.1	422.1	390.9	338.2	281.4
	Max_Hr	14	14	14	14	14	14	13	14	13	14	14	14
1986	Min	-17.4	-12.7	-27.6	-41.4	-40.2	-10.9	-5.2	3.5	8.1	-5.4	-9.5	-7.7
	Min_Hr	22	22	23	23	24	24	24	2	23	23	22	22
	Max	302.6	334.1	411.6	487.1	450.8	379.1	350.3	229.5	400.0	371.0	325.3	272.1
	Max_Hr	14	14	14	14	14	14	14	14	13	14	14	14
1991	Min	-17.1	-12.3	-27.2	-40.8	-39.2	-10.2	-3.4	5.0	8.6	-4.9	-9.2	-7.4
	Min_Hr	22	22	23	23	24	24	24	2	23	23	22	22
	Max	300.6	331.1	407.0	482.3	447.3	375.9	348.9	235.7	394.8	369.8	321.5	269.7
	Max_Hr	14	15	14	14	14	14	14	14	13	14	14	14
1998	Min	-17.1	-12.4	-27.3	-40.9	-39.0	-10.2	-2.6	5.6	8.7	-4.9	-9.3	-7.5
	Min_Hr	22	22	23	23	24	1	24	2	23	23	22	22
	Max	301.0	331.4	406.7	482.3	447.6	376.0	349.8	239.9	394.5	370.8	321.2	269.9
	Max_Hr	14	15	14	14	14	14	14	14	13	14	14	14
1999	Min	-17.1	-12.3	-27.3	-40.9	-38.9	-10.2	-2.4	5.8	8.8	-4.8	-9.3	-7.5
	Min_Hr	22	22	23	23	24	1	24	2	23	23	22	22
	Max	301.1	331.3	406.5	482.1	447.6	375.9	350.0	240.9	394.3	370.9	321.1	269.8
	Max_Hr	14	15	14	14	14	14	14	14	13	14	14	14
2002	Min	-15.5	-10.9	-25.7	-38.9	-37.0	-8.9	-0.4	7.4	9.8	-3.6	-7.9	-6.3
	Min_Hr	22	22	23	23	24	1	24	2	23	23	22	22
	Max	293.9	324.1	395.2	469.3	436.6	366.5	343.5	243.4	384.7	362.5	312.2	263.0
	Max_Hr	14	15	14	14	14	14	14	14	13	14	14	14
2006	Min	-13.8	-9.4	-24.2	-36.9	-34.6	-7.5	2.8	10.0	11.2	-2.2	-6.6	-5.0
	Min_Hr	22	22	23	23	24	1	24	2	23	23	22	22
	Max	287.7	318.1	384.5	458.3	427.3	358.4	339.3	250.5	375.2	355.6	303.8	256.7
	Max_Hr	14	15	14	14	14	14	14	14	13	14	14	14
2009	Min	-15.7	-11.3	-26.4	-39.4	-36.4	-9.0	2.4	9.7	10.2	-3.7	-8.5	-6.8
	Min_Hr	22	22	23	23	24	1	24	2	23	23	22	22
	Max	296.5	326.2	395.9	472.0	440.0	368.7	347.6	259.2	385.9	366.2	312.4	264.2
	Max_Hr	14	15	14	14	14	14	14	14	13	14	14	14
2011	Min	-16.3	-11.8	-27.0	-40.1	-36.8	-9.5	2.4	9.8	10.0	-4.0	-9.0	-7.3
	Min_Hr	22	22	23	23	24	1	24	2	23	23	22	22
	Max	299.5	328.7	399.5	476.2	444.0	372.1	350.5	262.9	389.4	369.7	315.2	266.7
	Max_Hr	14	15	14	14	14	14	14	14	13	14	14	14
2013	Min	-16.6	-12.0	-27.4	-40.5	-37.0	-9.8	2.6	10.0	9.8	-4.2	-9.3	-7.6
	Min_Hr	22	22	23	23	24	1	24	2	23	23	22	22
	Max	300.6	329.8	400.7	477.7	445.5	373.4	351.6	265.8	390.8	371.1	316.0	267.7
	Max_Hr	14	15	14	14	14	14	14	14	13	14	14	14
2014	Min	-15.3	-15.3	-26.3	-39.1	-35.0	-8.9	5.3	12.4	10.9	-3.1	-8.4	-6.6
	Min_Hr	22	22	23	23	24	1	24	2	23	23	22	22
	Max	296.6	296.6	392.8	469.1	438.6	367.5	350.1	275.7	385.0	366.3	309.7	263.6
	Max_Hr	14	14	14	14	14	14	14	14	13	14	14	15

Table 7.31: Simulated peak values of monthly average hourly sensible heat flux for Scenario-C for Palam area

Year	Time	Jan	Feb	Mar	Apr	May	Jun	Jul	Aug	Sep	Oct	Nov	Dec
1973	Min	-16.9	-12.6	-27.1	-41.2	-42.0	-11.9	-10.9	-1.0	7.1	-6.1	-9.1	-7.3
	Min_Hr	22	22	23	23	24	24	24	6	23	22	22	22
	Max	301.7	340.4	419.3	491.2	464.2	380.7	348.0	189.8	412.3	381.0	329.8	273.3
	Max_Hr	14	14	14	14	14	14	13	14	13	14	14	14
1977	Min	-13.3	-4.7	-17.5	-79.2	-36.4	-18.0	-2.8	-0.3	-11.8	-17.0	-39.2	-37.5
	Min_Hr	23	23	23	24	4	24	24	24	23	23	1	1
	Max	273.5	402.2	472.1	418.9	472.2	429.3	241.2	398.5	351.6	381.9	319.2	300.5
	Max_Hr	14	14	14	13	14	15	15	14	14	14	14	14
1986	Min	-8.6	-15.8	-15.3	-31.0	-37.4	-21.1	-2.7	-19.3	-62.5	-46.9	-12.3	-3.8
	Min_Hr	22	21	22	23	22	23	23	6	7	15	21	22
	Max	247.2	200.9	341.9	374.4	370.8	378.8	268.0	231.2	231.5	8.1	271.7	220.9
	Max_Hr	14	14	13	13	13	13	12	13	13	7	12	14
1991	Min	-7.1	-18.4	-19.7	-21.3	-22.7	-7.4	0.0	-6.5	3.8	7.8	2.9	-0.3
	Min_Hr	22	22	3	22	24	4	1	4	22	5	3	6
	Max	202.3	278.0	328.1	369.2	354.9	322.8	311.6	90.4	238.1	327.4	263.5	259.8
	Max_Hr	13	13	13	13	14	14	14	16	13	14	13	13
1998	Min	-6.6	-9.4	-13.6	-31.9	-25.4	-26.6	-23.2	8.4	12.4	5.3	6.4	3.6
	Min_Hr	22	22	23	22	5	5	1	4	22	21	21	22
	Max	172.8	281.4	412.3	449.3	475.8	375.5	308.4	284.9	318.9	287.1	279.4	250.4
	Max_Hr	13	14	14	13	13	13	13	13	12	13	13	13
1999	Min	-1.0	-6.5	-18.0	-32.1	-43.1	-20.9	5.2	2.9	10.1	5.0	-4.0	0.7
	Min_Hr	21	21	22	22	22	24	2	24	24	24	22	2
	Max	221.4	309.1	438.2	453.0	431.6	373.2	273.9	378.8	394.9	369.5	322.4	240.1
	Max_Hr	14	13	13	13	13	14	16	13	13	13	14	14
2002	Min	-10.1	-11.6	-8.2	-31.3	-11.5	-13.4	-72.4	-1.9	8.2	0.9	-0.3	-4.1
	Min_Hr	22	22	23	24	24	5	8	1	23	22	22	22
	Max	169.2	277.4	333.9	350.0	341.6	320.2	146.5	227.4	213.2	288.3	227.6	181.4
	Max_Hr	14	14	14	14	15	15	14	14	15	14	14	13
2006	Min	-10.4	-16.5	-16.5	-32.0	-32.0	-42.6	0.5	0.3	3.5	3.3	2.9	-0.6
	Min_Hr	22	22	23	23	23	15	24	24	22	23	23	22
	Max	239.2	204.3	286.2	355.3	309.9	-11.4	183.4	263.6	289.2	295.1	230.3	210.9
	Max_Hr	14	14	14	14	14	7	13	13	13	14	14	14
2009	Min	-7.7	-11.1	-32.0	-32.8	-36.5	-20.0	-6.8	-5.7	-5.6	-4.4	-19.6	-15.4
	Min_Hr	22	22	22	24	24	4	5	2	22	22	1	1
	Max	197.0	272.6	324.0	377.0	381.7	401.6	298.4	228.8	241.1	279.1	191.9	196.3
	Max_Hr	14	14	14	13	14	13	13	13	14	14	13	14
2011	Min	-4.9	-10.1	-22.5	-22.8	-32.7	-33.7	-5.6	-11.7	-7.9	0.0	-14.3	-14.0
	Min_Hr	22	2	22	24	6	1	6	8	2	23	1	1
	Max	181.7	224.5	337.3	350.7	333.0	300.7	222.0	125.6	172.8	267.3	180.4	202.0
	Max_Hr	13	14	14	13	13	14	14	14	15	14	14	14
2013	Min	-3.4	-3.8	-12.1	-14.8	-33.1	-6.4	-27.1	-4.6	3.4	4.2	-11.8	-12.5
	Min_Hr	23	7	23	23	24	1	23	6	3	23	22	4
	Max	229.8	242.6	339.4	381.5	351.9	306.4	264.8	213.7	297.1	286.6	232.1	222.1
	Max_Hr	14	14	14	14	14	14	14	13	14	14	14	14
2014	Min	-27.0	-6.6	-20.0	-17.2	-51.0	-20.5	-12.1	-9.3	-9.2	-6.7	-13.9	-16.2
	Min_Hr	23	5	2	24	23	23	23	5	23	5	22	22
	Max	179.0	280.2	330.6	376.0	347.0	337.6	279.3	244.0	275.0	293.8	233.8	209.1
	Max_Hr	14	14	14	14	14	14	14	14	14	14	14	14

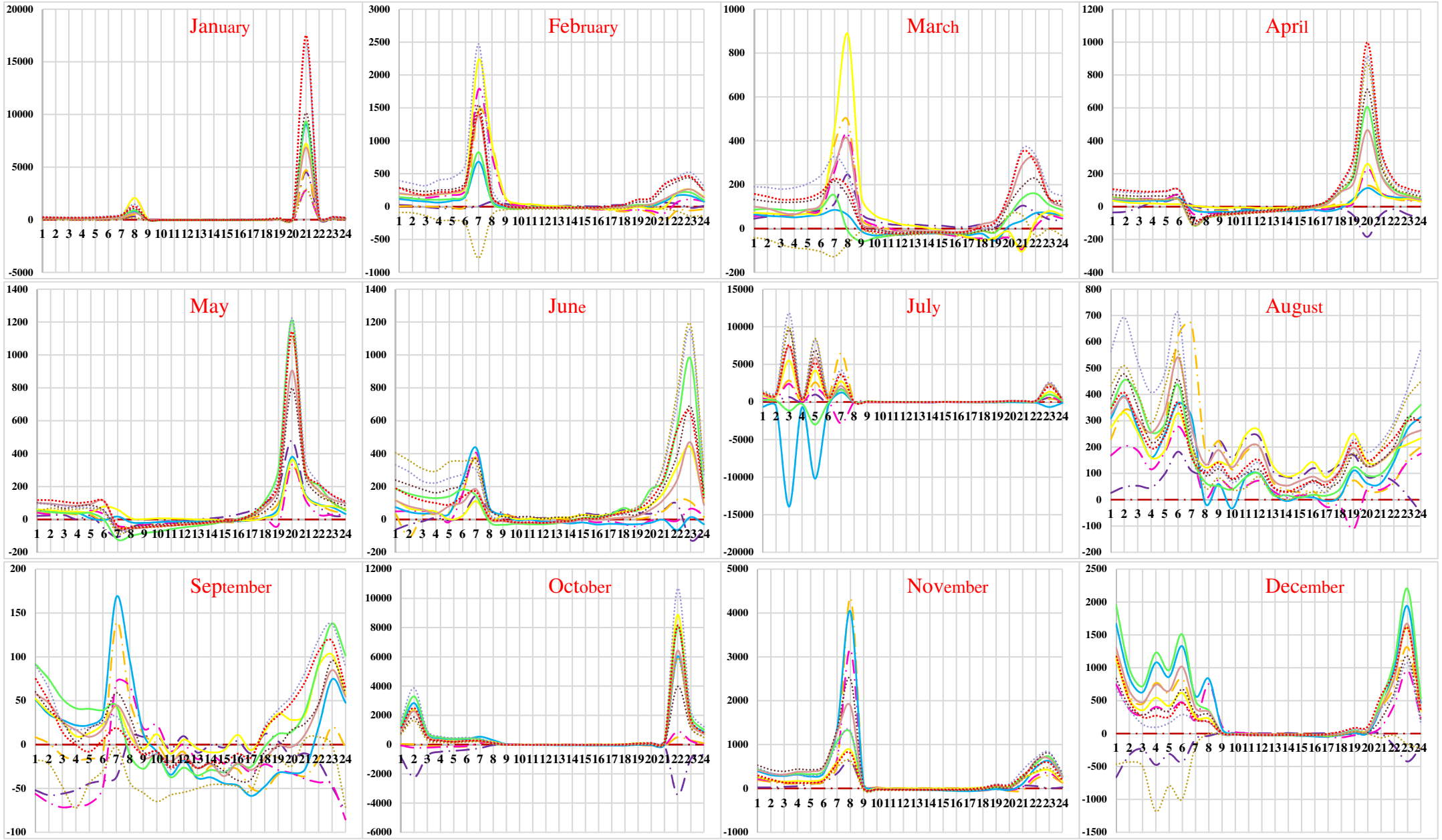

1973	1977	1986	1991	1998	1999	2002	2006	2009	2011	2013	2014	X-axis - Time in Hours
												Y-axis -% change in Heat Flux

Figure 7.40: Percentage change in values of monthly average hourly sensible heat flux for Scenario-A for Safdarjung area

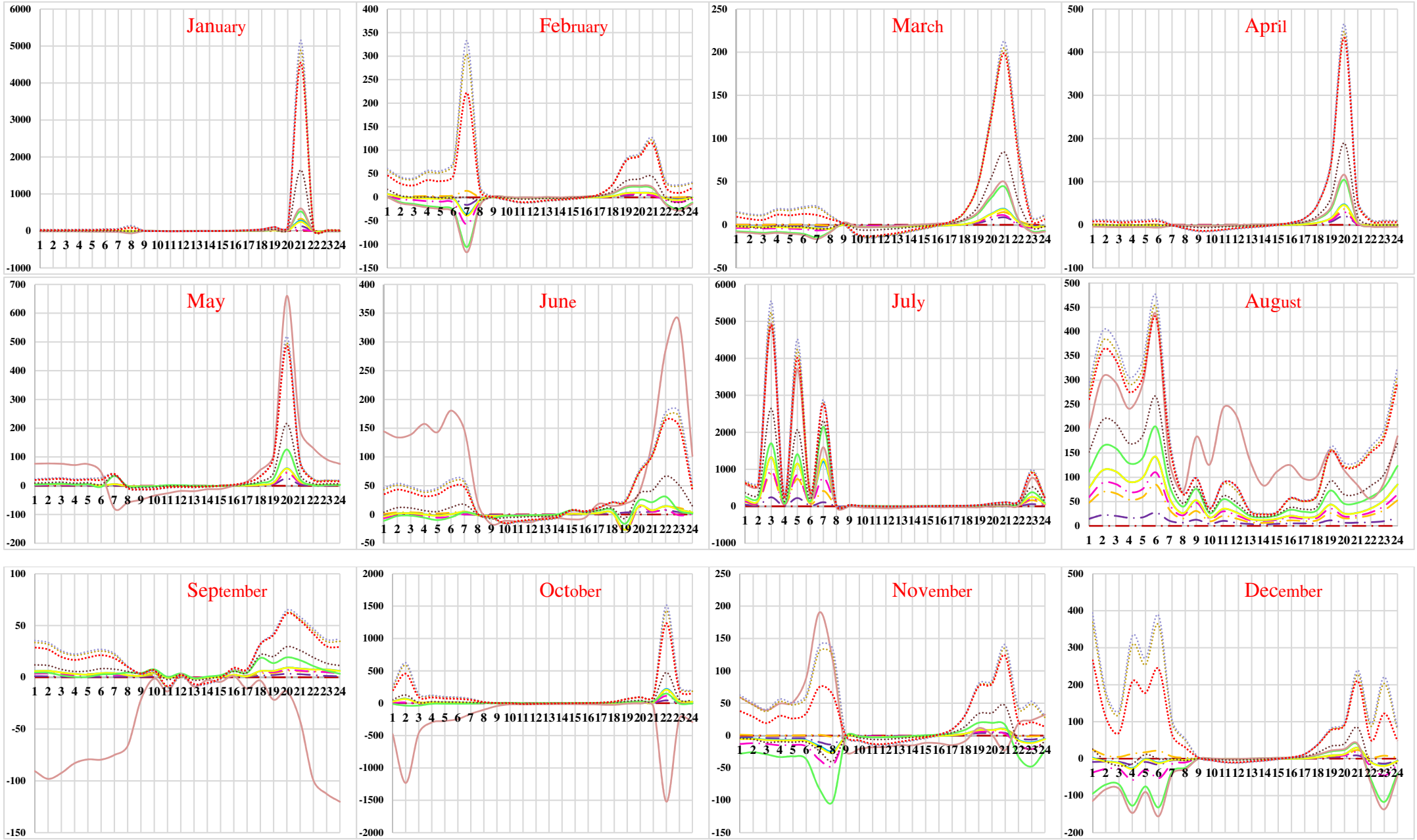

1973	1977	1986	1991	1998	1999	2002	2006	2009	2011	2013	2014	X-axis - Time in Hours
												Y-axis -% change in Heat Flux
Note: Percentage change in values of heat flux are very high because of the values in base year are very small which are used in denominator while calculating percentage change for different years.												

Figure 7.41: Percentage change in values of monthly average hourly sensible heat flux for Scenario-B for Safdarjung area

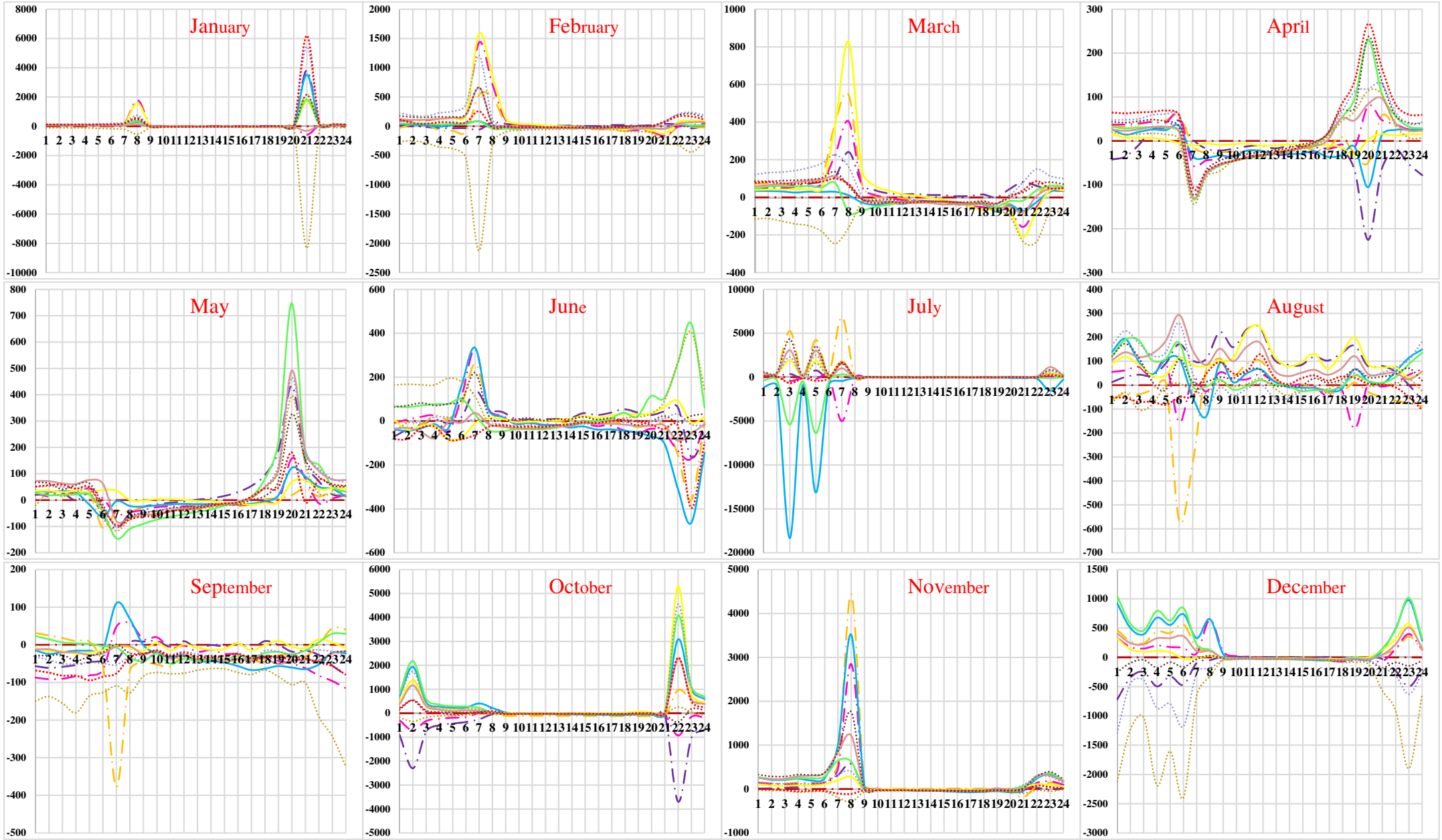

1973	1977	1986	1991	1998	1999	2002	2006	2009	2011	2013	2014	X-axis - Time in Hours
												Y-axis -% change in Heat Flux
Note: Percentage change in values of heat flux are very high because of the values in base year are very small which are used in denominator while calculating percentage change for different years.												

Figure 7.42: Percentage change in values of monthly average hourly sensible heat flux for Scenario-C for Safdarjung area

Table 7.32: Simulated peak values of monthly average hourly sensible heat flux for Scenario-A for Safdarjung area

Year	Time	Jan	Feb	Mar	Apr	May	Jun	Jul	Aug	Sep	Oct	Nov	Dec
1973	Min	-13.0	-8.3	-23.2	-39.0	-39.5	-9.7	-6.1	2.8	10.8	-2.0	-6.1	-2.8
	Min_Hr	24	24	23	24	24	24	24	6	24	24	24	24
	Max	315.6	350.4	431.8	510.1	474.6	397.1	363.8	223.5	419.1	387.6	341.7	286.8
	Max_Hr	14	14	14	13	13	14	14	14	13	14	14	14
1977	Min	-5.4	-7.3	-14.7	-67.3	-34.3	-15.6	-0.1	2.0	2.6	-15.5	-4.7	-8.4
	Min_Hr	22	24	24	24	4	24	24	24	24	24	24	24
	Max	288.1	397.6	488.7	439.9	488.5	450.4	250.4	417.1	403.5	380.7	326.6	307.0
	Max_Hr	14	14	14	12	14	15	13	14	14	14	14	14
1986	Min	-0.3	-13.1	-10.0	-26.5	-25.4	-16.9	1.2	11.8	10.5	-1.6	0.3	5.3
	Min_Hr	24	21	24	24	24	2	24	24	24	5	5	5
	Max	235.4	278.6	339.0	399.4	385.1	404.6	327.8	308.5	306.0	275.5	281.8	250.7
	Max_Hr	14	13	14	13	13	13	12	14	14	13	13	14
1991	Min	-0.2	-2.3	-12.5	-23.7	-28.4	-8.7	-27.8	-4.8	1.6	-2.6	2.2	2.4
	Min_Hr	3	22	24	24	24	5	7	19	24	24	4	4
	Max	245.4	305.7	352.6	357.7	369.5	334.6	227.4	240.0	358.9	320.6	265.8	243.2
	Max_Hr	13	13	13	13	14	13	15	14	14	14	13	13
1998	Min	1.3	-2.0	-9.5	-23.1	-31.4	-12.5	-24.9	10.6	16.0	13.7	7.1	7.8
	Min_Hr	4	24	24	24	5	24	5	4	24	3	5	4
	Max	246.4	286.6	334.7	369.0	413.0	329.0	257.1	224.5	259.7	227.0	219.8	211.9
	Max_Hr	14	15	14	13	13	13	13	13	13	12	13	13
1999	Min	3.0	4.3	-9.1	-27.6	-19.4	-7.5	9.1	10.1	15.2	11.1	2.5	3.3
	Min_Hr	5	24	24	4	3	5	4	5	4	4	5	5
	Max	260.5	344.6	455.6	466.5	471.7	450.9	358.5	421.5	400.7	401.2	346.0	254.3
	Max_Hr	14	13	13	13	13	14	14	14	13	13	14	14
2002	Min	1.3	-0.3	-3.7	-20.7	-22.7	2.6	-7.5	13.6	19.2	16.2	9.2	8.9
	Min_Hr	5	24	24	24	3	4	5	5	3	4	4	4
	Max	237.1	319.6	356.0	383.0	354.4	368.3	396.6	261.3	288.0	327.1	254.8	210.8
	Max_Hr	14	14	14	14	15	14	13	14	14	14	14	13
2006	Min	-0.3	3.2	-5.7	-23.1	-5.7	-5.8	12.9	13.2	15.0	9.7	10.3	5.1
	Min_Hr	4	24	4	24	4	4	4	3	5	5	3	4
	Max	266.9	281.8	379.9	391.5	379.9	337.0	290.0	342.7	315.7	327.4	256.3	229.3
	Max_Hr	14	14	14	14	14	14	14	14	14	14	14	14
2009	Min	7.3	7.7	1.6	-14.9	-12.2	5.6	16.4	12.9	14.3	8.2	13.1	2.2
	Min_Hr	4	5	24	24	3	4	5	4	4	24	4	4
	Max	219.1	313.5	360.9	415.4	412.3	445.5	345.5	292.8	319.3	289.3	223.9	222.7
	Max_Hr	14	14	14	14	14	14	14	14	14	14	13	14
2011	Min	-12.3	-19.6	-30.7	-18.9	-19.6	17.4	17.4	15.8	3.1	6.7	0.6	-10.1
	Min_Hr	24	24	24	3	1	4	3	4	24	3	4	4
	Max	181.0	234.7	326.0	358.9	353.3	365.0	259.7	226.2	219.9	285.3	200.1	205.5
	Max_Hr	15	15	14	14	15	14	14	13	14	15	14	14
2013	Min	11.6	14.5	11.1	-8.0	-9.9	11.0	19.7	20.2	15.6	17.7	7.9	0.0
	Min_Hr	4	3	24	24	5	4	4	3	3	5	5	4
	Max	241.6	287.6	333.4	377.8	373.6	336.2	281.5	268.8	316.7	303.5	249.3	218.9
	Max_Hr	14	14	14	14	14	15	14	13	14	15	14	14
2014	Min	7.7	5.3	5.3	-3.8	-0.2	-0.8	12.2	12.0	12.7	9.2	1.1	1.4
	Min_Hr	4	3	4	24	4	5	4	4	5	5	4	4
	Max	255.3	302.1	352.7	388.5	378.3	360.3	303.5	288.3	323.6	308.1	245.6	232.9
	Max_Hr	14	14	14	14	14	14	15	14	14	14	14	14

Table 7.33: Simulated peak values of monthly average hourly sensible heat flux for Scenario-B for Safdarjung area

Year	Time	Jan	Feb	Mar	Apr	May	Jun	Jul	Aug	Sep	Oct	Nov	Dec
1973	Min	-13.0	-8.3	-23.2	-39.0	-39.5	-9.7	-6.1	2.8	10.8	-2.0	-6.1	-2.8
	Min_Hr	24	24	23	24	24	24	24	6	24	24	24	24
	Max	315.6	350.4	431.8	510.1	474.6	397.1	363.8	223.5	419.1	387.6	341.7	286.8
	Max_Hr	14	14	14	13	13	14	14	14	13	14	14	14
1977	Min	-13.1	-8.5	-23.4	-39.1	-39.3	-9.5	-5.2	3.6	10.9	-1.9	-6.3	-2.9
	Min_Hr	24	24	23	24	24	24	24	6	24	24	24	24
	Max	315.6	349.1	429.3	508.9	473.6	396.4	364.1	230.5	416.9	385.5	340.6	286.4
	Max_Hr	14	14	14	13	13	14	14	14	13	14	14	14
1986	Min	-12.8	-8.2	-23.3	-38.9	-38.5	-9.2	-3.6	5.2	11.4	-1.5	-6.1	-2.7
	Min_Hr	24	24	23	24	24	24	24	6	24	24	24	24
	Max	315.2	347.8	427.1	506.5	471.7	395.5	364.6	237.5	415.6	385.2	338.8	285.9
	Max_Hr	14	14	14	13	13	14	14	14	13	14	14	14
1991	Min	-13.3	-8.7	-24.0	-39.7	-38.8	-9.6	-3.0	5.9	11.2	-1.9	-6.7	-3.3
	Min_Hr	24	24	23	24	24	24	24	6	24	24	24	24
	Max	317.1	348.8	428.6	508.2	473.4	397.3	366.5	246.2	417.6	387.6	339.8	287.6
	Max_Hr	14	14	14	13	13	14	14	14	13	14	14	14
1998	Min	-12.8	-8.4	-23.7	-39.2	-38.2	-9.3	-2.1	6.7	11.5	-1.5	-6.4	-3.0
	Min_Hr	24	24	23	24	24	24	24	2	24	24	24	24
	Max	314.3	345.1	423.6	502.5	468.3	393.3	363.8	250.0	413.9	384.4	335.9	284.8
	Max_Hr	14	14	14	13	13	14	14	14	13	14	14	14
1999	Min	-12.9	-8.4	-23.8	-39.3	-38.2	-9.3	-2.1	6.7	11.5	-1.6	-6.4	-3.0
	Min_Hr	24	24	23	24	24	24	24	2	24	24	24	24
	Max	314.6	345.4	424.1	503.1	468.9	393.8	364.0	250.1	414.3	384.8	336.3	285.2
	Max_Hr	14	14	14	13	13	14	14	14	13	14	14	14
2002	Min	-14.2	-9.3	-25.0	-40.5	-38.6	-9.5	-0.3	8.3	11.2	-2.1	-7.5	-3.9
	Min_Hr	24	24	23	24	24	4	24	2	24	24	24	24
	Max	319.9	349.3	428.8	509.7	475.6	399.3	371.0	262.9	416.1	392.9	339.6	289.1
	Max_Hr	14	15	14	13	13	14	14	14	13	14	14	14
2006	Min	-14.5	-9.5	-25.2	-40.8	-9.6	0.2	8.6	11.1	-2.2	-7.7	-4.1	-4.1
	Min_Hr	24	24	23	24	4	24	2	24	24	24	24	24
	Max	321.1	350.1	429.8	511.0	400.4	372.7	265.7	416.9	394.4	340.3	289.9	289.9
	Max_Hr	14	15	14	13	14	14	14	13	14	14	14	14
2009	Min	-13.2	-8.3	-23.9	-39.1	-36.9	-8.4	1.8	10.0	12.0	-1.1	-6.7	-3.1
	Min_Hr	24	24	23	24	24	4	24	2	24	24	24	24
	Max	314.2	343.4	419.5	499.5	466.7	391.7	366.4	266.0	407.4	386.4	332.1	283.4
	Max_Hr	14	15	14	13	13	14	14	14	13	14	14	14
2011	Min	-10.1	-5.8	-21.2	-35.5	-32.4	-5.5	7.7	14.9	14.6	1.7	-4.4	-0.6
	Min_Hr	24	24	23	24	24	4	24	5	24	24	24	24
	Max	301.8	332.7	399.0	477.8	447.5	375.5	355.4	277.8	391.0	371.9	315.6	272.0
	Max_Hr	14	15	14	13	13	14	14	14	15	14	14	15
2013	Min	-9.8	-5.7	-21.0	-35.2	-32.0	-5.3	8.5	15.5	14.8	1.9	-4.3	-0.5
	Min_Hr	24	24	23	24	24	4	24	5	24	24	24	24
	Max	301.3	332.3	397.5	476.3	446.3	374.4	355.9	280.8	389.7	371.2	314.4	271.5
	Max_Hr	14	15	14	13	13	14	14	14	15	14	14	15
2014	Min	-10.9	-6.7	-22.1	-36.6	-33.4	-6.2	7.2	14.2	14.0	0.9	-5.3	-1.4
	Min_Hr	24	24	23	24	24	4	24	5	24	24	24	24
	Max	306.0	336.8	404.8	484.7	453.9	380.4	359.4	276.1	394.3	376.8	320.0	275.2
	Max_Hr	14	15	14	13	13	14	14	14	15	14	14	15

Table 7.34: Simulated peak values of monthly average hourly sensible heat flux for Scenario-C for Safdarjung area

Year	Time	Jan	Feb	Mar	Apr	May	Jun	Jul	Aug	Sep	Oct	Nov	Dec
1973	Min	-13.0	-8.3	-23.2	-39.0	-39.5	-9.7	-6.1	2.8	10.8	-2.0	-6.1	-2.8
	Min_Hr	24	24	23	24	24	24	24	6	24	24	24	24
	Max	315.6	350.4	431.8	510.1	474.6	397.1	363.8	223.5	419.1	387.6	341.7	286.8
	Max_Hr	14	14	14	13	13	14	14	14	13	14	14	14
1977	Min	-6.6	-7.8	-15.1	-69.4	-34.5	-16.1	-0.7	1.5	2.1	-15.8	-5.0	-8.7
	Min_Hr	22	24	24	24	4	24	24	24	24	24	24	24
	Max	286.2	396.5	486.8	439.6	488.2	448.9	247.8	415.6	402.6	379.9	326.3	306.7
	Max_Hr	14	14	14	12	14	15	15	14	14	14	14	14
1986	Min	-4.6	-10.5	-10.0	-27.7	-29.9	-14.7	5.8	-16.7	-46.8	-41.1	-6.4	0.9
	Min_Hr	24	21	22	24	6	23	23	7	7	16	21	22
	Max	258.1	231.0	353.6	388.1	385.9	387.6	282.3	238.0	271.9	9.9	267.1	231.6
	Max_Hr	14	13	13	13	13	13	12	13	13	7	12	14
1991	Min	-2.8	-8.2	-16.9	-26.9	-36.4	-11.3	-47.8	-32.8	-1.7	-5.5	0.0	0.8
	Min_Hr	2	22	22	23	22	5	7	19	24	24	24	5
	Max	235.9	296.2	345.9	347.4	359.6	321.7	189.3	217.1	349.9	312.6	259.4	236.8
	Max_Hr	13	13	13	13	14	13	15	14	14	14	13	13
1998	Min	-2.0	-6.9	-16.2	-29.3	-39.6	-23.6	-32.0	-9.9	8.4	9.7	3.9	4.6
	Min_Hr	24	24	23	2	5	24	5	8	24	3	5	4
	Max	237.7	274.6	328.0	378.6	402.4	315.8	225.3	209.1	236.3	215.7	207.3	203.2
	Max_Hr	14	15	14	12	13	13	13	13	13	13	12	13
1999	Min	-0.7	-2.2	-19.0	-33.0	-26.1	-13.9	3.5	5.0	9.9	6.5	-2.4	-0.1
	Min_Hr	5	21	22	24	3	5	3	5	24	24	24	5
	Max	244.0	336.7	444.1	456.6	460.6	432.1	326.3	402.3	385.7	389.6	337.3	244.1
	Max_Hr	13	13	13	13	13	14	13	14	13	13	14	14
2002	Min	-3.1	-6.6	-10.2	-27.7	-30.5	-3.7	-15.7	7.0	13.4	11.6	5.6	5.5
	Min_Hr	24	24	1	24	2	24	5	7	3	24	24	4
	Max	217.8	294.9	339.3	363.1	317.3	342.1	376.8	222.3	250.2	307.2	239.5	194.9
	Max_Hr	14	14	14	14	15	14	13	14	14	14	14	13
2006	Min	-5.2	-4.2	-12.3	-30.0	-13.8	-16.1	4.7	6.1	9.0	5.6	4.5	1.6
	Min_Hr	22	22	23	24	3	4	24	24	24	24	24	24
	Max	249.0	264.8	303.9	369.1	359.2	308.3	236.9	307.9	263.7	305.0	239.7	213.0
	Max_Hr	14	14	14	14	14	14	14	14	14	14	14	13
2009	Min	-0.5	2.8	-6.9	-23.7	-22.1	-6.5	7.7	2.8	8.0	-1.7	7.7	-4.4
	Min_Hr	22	5	24	24	3	24	3	5	4	22	24	24
	Max	202.3	299.7	345.9	401.3	389.9	427.6	319.5	218.3	288.0	273.0	214.8	208.2
	Max_Hr	14	14	14	13	14	14	14	14	14	14	13	14
2011	Min	-24.1	-32.4	-42.8	-36.6	-44.9	3.7	-3.0	-0.1	-24.2	-3.5	-6.7	-20.9
	Min_Hr	22	22	24	24	1	24	24	3	24	24	4	22
	Max	175.3	209.5	321.8	360.5	337.8	344.0	224.3	157.9	149.1	280.8	195.5	200.0
	Max_Hr	14	15	14	13	15	14	13	13	14	14	14	14
2013	Min	3.9	4.9	0.0	-22.4	-20.0	-11.6	3.6	3.9	6.2	9.5	0.8	-11.1
	Min_Hr	24	3	24	24	5	24	5	8	3	3	5	1
	Max	229.7	254.5	330.7	376.2	372.6	324.0	231.7	138.2	314.4	299.6	249.0	211.7
	Max_Hr	14	14	13	14	14	13	14	15	13	13	14	14
2014	Min	0.6	-3.9	-12.2	-15.9	-28.1	-18.8	-2.4	-0.1	0.8	1.4	-6.0	-5.7
	Min_Hr	3	3	23	24	21	24	24	24	5	5	3	4
	Max	247.6	281.8	335.2	376.0	358.9	335.0	275.4	244.9	285.2	305.1	240.5	215.6
	Max_Hr	14	14	14	14	14	14	13	15	13	14	14	14

Table 7.35: Annual extreme values of hourly sensible heat flux for different Scenarios

Year	Data	Palam Area			Safdarjung Area		
		Scenario-A	Scenario-B	Scenario-C	Scenario-A	Scenario-B	Scenario-C
1973	Max	555.91	555.91	555.91	583.83	583.83	583.83
	Min	-900.45	-900.45	-900.45	-997.38	-997.38	-997.38
1977	Max	616.69	580.84	603.93	630.64	585.29	628.15
	Min	-724.59	-975.33	-878.26	-571.31	-959.68	-602.15
1986	Max	482.37	567.41	475.86	502.91	583.04	493.39
	Min	-933.15	-985.3	-994.55	-985.35	-988.55	-995.06
1991	Max	523.9	564.31	525.81	530.43	587.22	520.16
	Min	-761.51	-875.42	-921.17	-912.41	-949.04	-952.55
1998	Max	659.93	564.91	625.87	559.43	583.85	543.17
	Min	-977.42	-824.95	-872.49	-980.46	-893.11	-989.47
1999	Max	602.87	564.82	591.27	605.13	582.94	595.32
	Min	-811.58	-820.49	-990	-815.44	-890.22	-744.47
2002	Max	471.86	551.55	463.65	503.34	592.94	477.23
	Min	-919.86	-715.96	-994	-879.65	-849.91	-991.96
2006	Max	446.78	541.71	465.68	490.74	594.80	468.23
	Min	-700.58	-554.71	-982.95	-881.30	-826.64	-934.61
2009	Max	510.99	557.27	494.6	538.32	583.61	523.03
	Min	-851.7	-528.96	-880.07	-974.18	-690.37	-959.23
2011	Max	502.16	562.24	447.34	547.86	565.12	479.35
	Min	-736.33	-502.13	-967.03	-660.39	-18.55	-816.80
2013	Max	440.49	564.19	426.52	421.59	563.72	433.08
	Min	-284.73	-471.13	-773.34	-735.63	-215.62	-978.73
2014	Max	413.49	555.95	409.42	423.62	572.72	419.94
	Min	-388.16	-264.87	-959.48	-365.86	-292.77	-989.26

7.5.4 Latent Heat Flux

Monthly, seasonal and annual average of latent heat flux at hourly temporal scale has been calculated for Palam and Safdarjung areas from hourly model results for different Scenarios (A, B and C) and for different years. Annual extreme hourly values have also been calculated to ascertain the effects of LULC change on extreme values of latent heat flux. In both the study areas in all three Scenarios-A, B and C minimum latent heat flux has been found to be zero in different years i.e., 1973 to 2014, which is obvious. In some month of a year latent heat flux may be zero. Latent heat flux has been varying during day time and general trend in different scenarios is decreasing over the years at both the study areas i.e., Palam and Safdarjung. Such a trend indicates that available energy for partitioning into sensible and latent heat flux is less and also moisture availability became less and less over the years due to conversion of pervious surfaces into impervious, reduction in vegetation and reduction of water bodies.

For Palam area, in Scenario-A, minimum peak value of monthly average hourly latent heat flux, in different years, have been found as zero, whereas, peak values of monthly average hourly latent heat flux during day (positive values) time have been found to be decreasing over the years from 175 Wm^{-2} in year 1973 to 35.50 Wm^{-2} in year 2014, as shown in Table 7.36 and Figure 7.43. Relative percentage change in peak value of latent heat flux during day time, from the base year, is showing decreasing trend from 10.11 % in year 1991 to increase by 79.71 % in year 2014. In case of Safdarjung area for Scenario-A, peak values of monthly average hourly latent heat flux has been calculated. Monthly mean hourly peak value of latent heat flux during day time found to be deceasing from 141.30 Wm^{-2} (1973) to 49.40 Wm^{-2} (2014) as shown in Table 7.39 and Figure 7.46. Relative percentage change in day time monthly average hourly latent heat flux, from the base year is showing decreasing trend from year 1991 (62.05 %) to 2014 (90.32 %).

In Scenario-B, for Palam station, monthly average hourly latent heat flux have been calculated from the hourly simulated results of different years. According to the results (Table 7.37 and Figure 7.44), minimum peak value of monthly average hourly latent heat flux has been found as zero in different years, whereas, during day time (positive) decreasing trend is observed over the years from 175Wm^{-2} (1973) to 67.30 Wm^{-2} (2014), which indicates the less availability of available energy for partitioning into sensible and latent heat and less availability of moisture due to urbanization (Table 7.37 and Figure 7.44). Relative percentage change in monthly average hourly latent heat flux during day time, from the base year, is showing decreasing trend from 1973 (0 %) to 2014 (61.54 %). In case of Safdarjung area in Scenario-B, trends in latent heat flux has been found to be similar to the Palam area. Peak value of monthly average hourly latent heat flux has been calculated from hourly simulated results. According to the results (Table 7.40 and Figure 7.47), peak values of monthly average hourly latent heat flux during day time (positive) have shown decreasing trend over the years from 141.30 Wm^{-2} (1973) to 69.80 Wm^{-2} (2014). Relative percentage change in peak values of monthly average hourly latent heat flux during day time, from the base year, is showing decreasing trend from 1986 (5.52 %) to 2014 (50.60 %) (Table 7.40 and Figure 7.47).
In Scenario-C, for both the areas i.e., Palam and Safdarjung, peak values of monthly average latent heat flux at hourly temporal scale have been calculated from hourly simulated results. For both the areas minimum latent heat flux in Scenario-C for both areas have been found as zero. According to the results for Palam in Scenario-C (Table

7.38 and Figure 7.45), peak values of monthly average hourly latent heat flux is found to be increasing in few months and decreasing in other months from 175.0 Wm^{-2} (1973) to 73.50 Wm^{-2} (2014) (Table 7.38 and Figure 7.45). For Safdarjung area also in Scenario-C, results indicate trends in latent heat flux similar to the Palam area. Minimum peak values of monthly average hourly latent heat flux in Safdarjung also found as zero, whereas, during day time results are showing increase during few years and decrease in other years ranging from 141.0 Wm^{-2} (1973) to 78.5 Wm^{-2} (2014) (Table 7.41 and Figure 7.48). Relative percentage change in peak values of monthly average hourly latent heat flux during day time, with respect to base year value, is showing decreasing trend from 1986 (7.36 %) to 2014 (44.44 %).

In the results, relative percentage change in simulated values of latent heat flux from the base year 1973 over the study period, for Scenario-A at Palam area (Figure 7.43) have shown very high percentage value of fluxes in the month of March, April, May and November. Also, percentage change values of latent heat flux for Scenario-C (Figure 7.45) are very high in the month of March, April and November. For Safdarjung area, percentage change values for Scenario-A (Figure 7.46) are very high in the month March, April, May and November and percentage change values in Scenario-B (Figure 7.47) are very high in the month of February and October. Also, in Scenario-C (Figure 7.48) percentage change values are very high in the month of March, April, May and November. The relative percentage change in the above mentioned months are very high because the flux values in base year is very small (close to zero), which has been used in equation 7.1 to compute percentage change for different years.

Annual extreme hourly values of latent heat flux have also been calculated from the hourly simulated results for different Scenarios i.e., A, B and C to study the effect of LULC changes on extreme values for both areas i.e., Palam and Safdarjung (Table 7.42). Annual extreme hourly values of latent heat flux during night time in Palam area have decreased (negative values) in Scenario-A (-377.0 to -0.04 Wm^{-2}), Scenario-B (-377.0 to 0.18 Wm^{-2}) and also in Scenario-C (-377.0 to - 0 Wm^{-2}) over the years from 1973 to 2014. Further for Palam area, results indicate that annual extreme hourly values of latent heat flux during day time have decreased for Scenario-A (924.24 to 588.03 Wm^{-2}) and Scenario-B (924.24 to 486.32 Wm^{-2}) (Table 7.42). Trends similar to Palam area have been found in extreme values of annual hourly latent heat flux for Safdarjung area also.

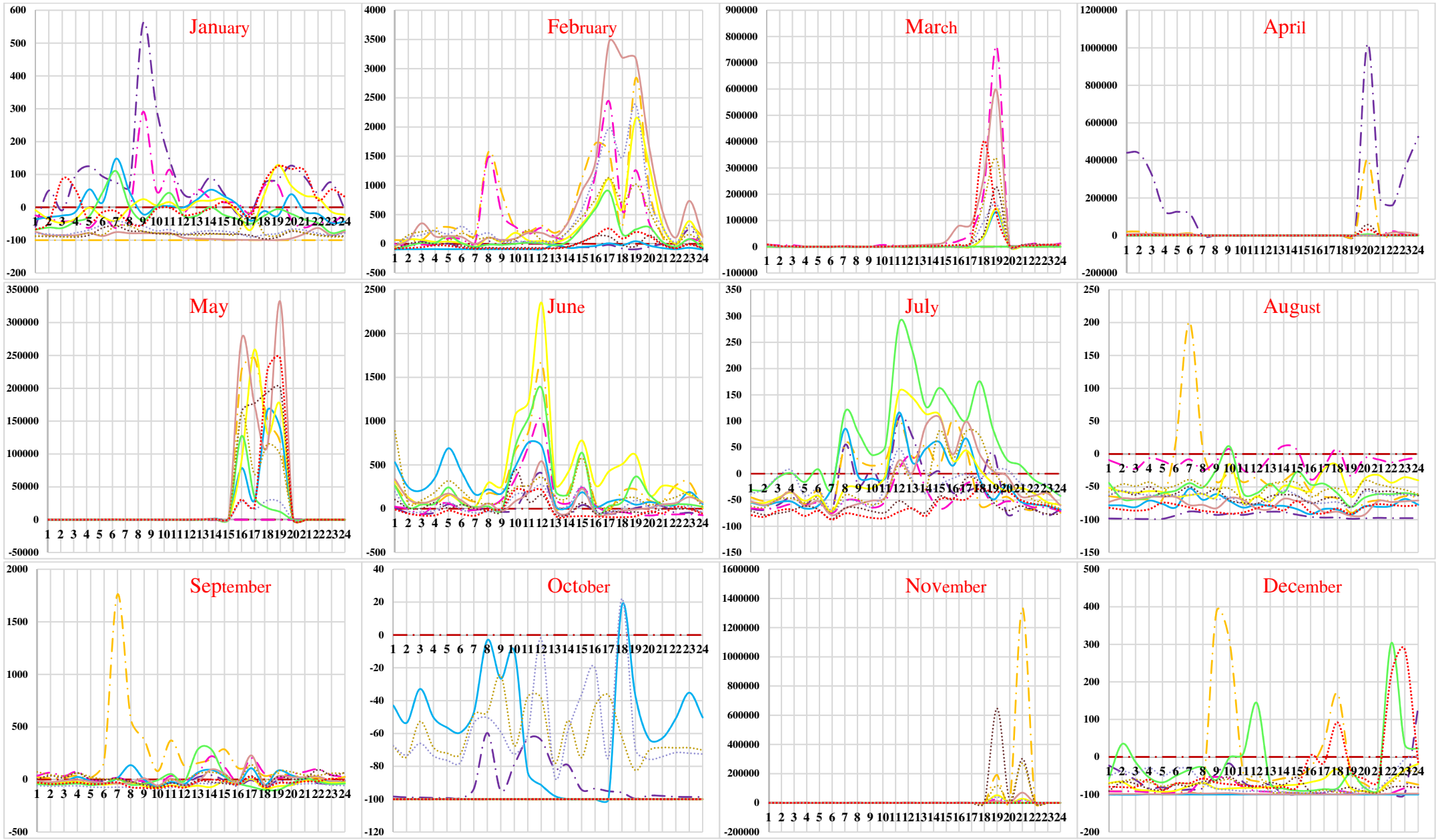

1973	1977	1986	1991	1998	1999	2002	2006	2009	2011	2013	2014	X-axis - Time in Hours
												Y-axis -% change in Heat Flux
Note: Percentage change in values of heat flux are very high because of the values in base year are very small which are used in denominator while calculating percentage change for different years.												

Figure 7.43: Percentage change in values of monthly average hourly latent heat flux for Scenario-A for Palam area

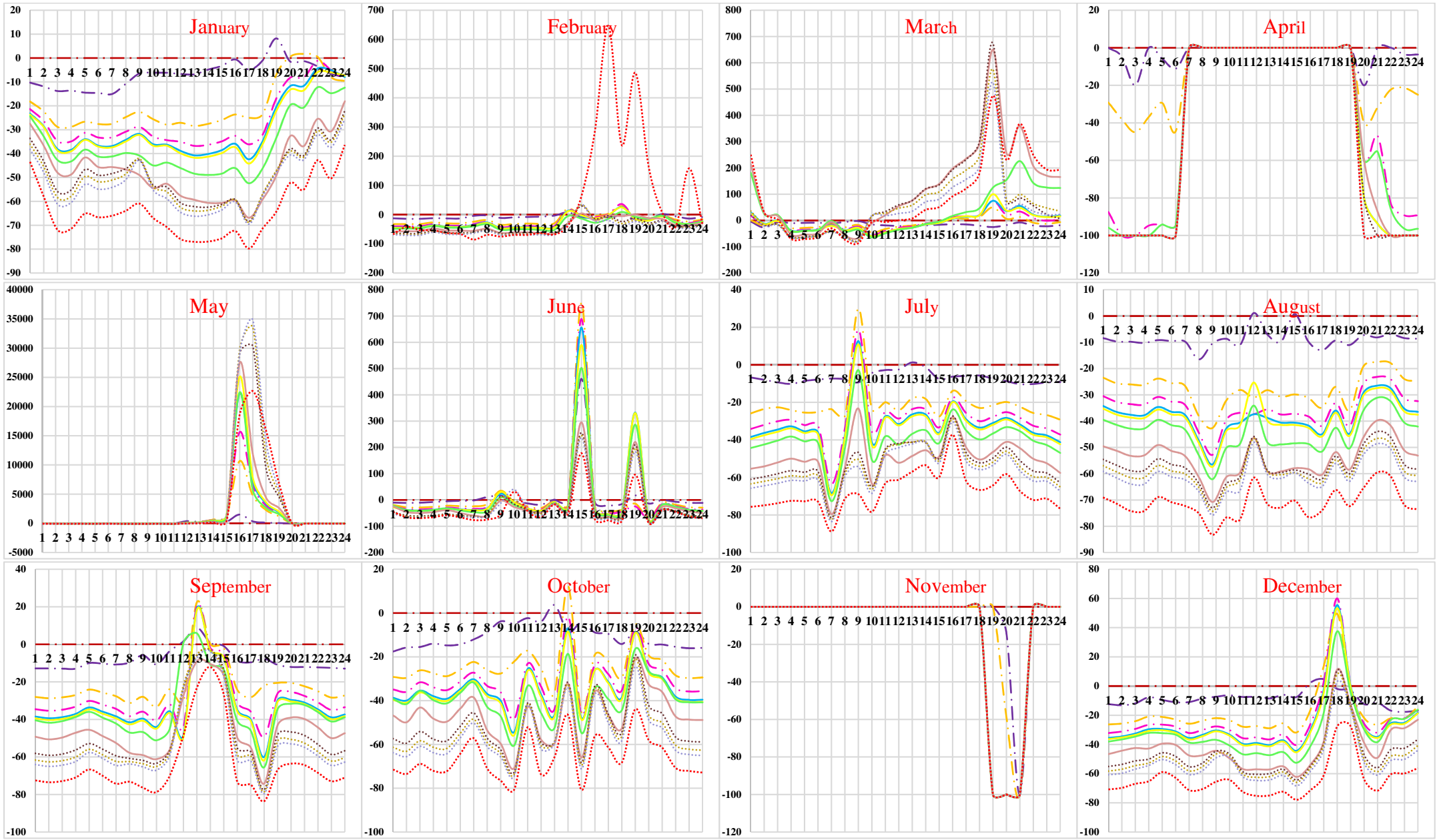

1973	1977	1986	1991	1998	1999	2002	2006	2009	2011	2013	2014	X-axis - Time in Hours
												Y-axis -% change in Heat Flux

Note: Percentage change in values of heat flux are very high because of the values in base year are very small which are used in denominator while calculating percentage change for different years.

Figure 7.44: Percentage change in values of monthly average hourly latent heat flux for Scenario-B for Palam area

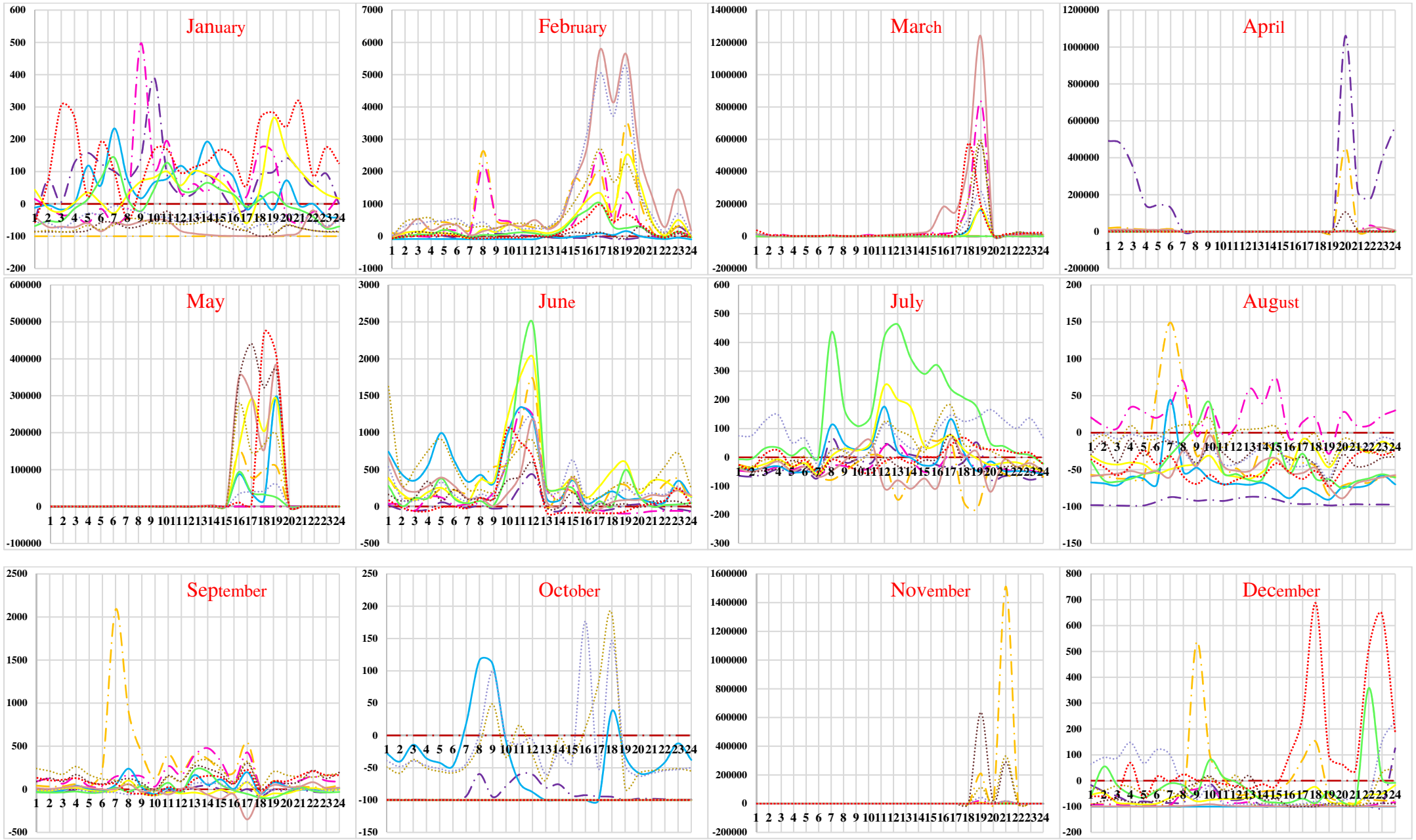

1973	1977	1986	1991	1998	1999	2002	2006	2009	2011	2013	2014	X-axis - Time in Hours
												Y-axis -% change in Heat Flux

Note: Percentage change in values of heat flux are very high because of the values in base year are very small which are used in denominator while calculating percentage change for different years.

Figure 7.45: Percentage change in values of monthly average hourly latent heat flux for Scenario-C for Palam area

Table 7.36: Simulated peak values of monthly average hourly latent heat flux for Scenario-A for Palam area

Year	Time	Jan	Feb	Mar	Apr	May	Jun	Jul	Aug	Sep	Oct	Nov	Dec
1973	Min	1.1	0.2	0.0	0.0	0.0	1.6	11.8	18.3	3.7	2.2	0.0	0.7
	Min_Hr	7	19	19	7	19	1	4	4	4	3	1	24
	Max	25.6	17.2	8.0	0.0	24.5	23.7	63.8	175.0	67.9	44.2	0.0	16.1
	Max_Hr	12	13	9	21	11	16	11	12	10	13	20	13
1977	Min	0.9	0.0	0.0	6.9	0.0	1.5	3.9	0.2	2.7	0.0	0.0	0.0
	Min_Hr	1	19	19	6	19	3	23	4	3	19	1	18
	Max	40.8	16.6	3.4	58.4	9.1	18.8	65.7	18.5	28.1	8.3	0.0	5.3
	Max_Hr	14	12	20	11	9	16	12	12	14	13	20	10
1986	Min	0.0	1.9	0.0	0.1	3.3	4.6	5.5	5.7	5.1	0.0	0.0	0.1
	Min_Hr	2	3	18	15	5	4	24	4	4	1	17	2
	Max	0.0	67.4	7.6	18.9	36.0	46.5	88.0	112.2	129.9	0.0	25.3	25.8
	Max_Hr	4	12	9	17	8	12	16	12	11	1	13	10
1991	Min	0.4	0.9	2.5	0.0	0.0	1.2	5.0	14.4	4.4	0.0	0.0	0.0
	Min_Hr	7	22	1	18	2	23	4	3	5	1	3	22
	Max	36.6	61.5	51.1	2.7	0.0	32.5	46.4	157.3	63.6	0.0	3.4	2.7
	Max_Hr	13	12	10	22	21	16	13	14	14	19	12	10
1998	Min	1.3	0.0	0.0	0.0	0.6	6.3	5.5	3.5	3.2	0.0	0.0	0.0
	Min_Hr	24	24	17	1	12	22	4	3	2	17	1	2
	Max	32.9	14.9	1.9	0.0	25.2	40.2	75.5	40.4	38.0	27.7	0.0	0.0
	Max_Hr	14	13	18	20	14	17	15	12	14	10	1	4
1999	Min	0.7	1.1	0.0	0.0	1.2	5.5	7.5	7.2	2.7	0.0	0.0	0.1
	Min_Hr	7	7	17	1	12	6	4	6	6	1	6	5
	Max	28.2	28.0	2.0	0.0	24.2	117.9	99.9	99.6	19.1	0.0	9.9	3.4
	Max_Hr	13	10	18	19	17	17	15	17	16	20	16	14
2002	Min	0.6	0.7	0.0	0.0	0.3	3.7	11.9	5.7	0.1	0.0	0.0	0.2
	Min_Hr	23	1	19	3	20	2	4	3	19	1	2	18
	Max	21.5	17.7	5.7	2.2	16.4	43.4	124.0	106.5	81.3	0.0	0.0	35.5
	Max_Hr	14	12	10	8	16	13	15	10	13	20	4	12
2006	Min	0.0	2.3	1.7	0.0	5.7	5.1	6.3	2.5	3.2	0.0	0.0	0.0
	Min_Hr	19	2	6	19	4	7	5	20	7	1	8	19
	Max	3.0	46.7	27.9	3.4	35.5	18.5	97.8	47.9	42.5	0.0	8.6	0.2
	Max_Hr	11	12	16	9	16	15	15	11	17	20	17	10
2009	Min	0.2	0.1	0.3	0.0	0.1	2.3	3.5	6.7	4.7	0.0	0.9	0.1
	Min_Hr	4	19	16	7	14	5	4	24	1	1	7	1
	Max	4.7	4.9	5.9	12.3	23.7	24.2	29.8	53.4	20.3	0.0	7.1	5.6
	Max_Hr	13	12	22	14	15	10	17	14	16	1	16	15
2011	Min	0.2	1.3	0.4	0.0	0.3	5.3	6.1	7.1	5.4	0.8	0.4	0.1
	Min_Hr	3	23	16	1	14	2	2	24	7	2	19	18
	Max	18.9	45.9	8.5	0.0	21.4	38.4	85.6	80.6	37.2	13.2	6.4	8.0
	Max_Hr	17	11	18	1	15	15	15	14	12	12	13	12
2013	Min	0.3	2.0	0.5	0.0	0.1	2.4	9.5	6.4	1.3	0.7	0.0	0.1
	Min_Hr	3	24	16	1	15	3	5	24	6	6	6	19
	Max	6.1	26.5	6.2	0.0	3.6	20.2	47.0	62.1	17.9	21.0	0.9	1.4
	Max_Hr	14	14	11	1	16	15	11	14	16	12	10	13
2014	Min	0.7	0.4	1.6	0.0	1.8	0.4	3.1	2.6	2.6	0.0	0.0	0.2
	Min_Hr	5	8	19	19	17	18	2	3	4	1	1	2
	Max	23.4	4.0	19.5	2.6	21.3	14.1	25.3	35.5	19.5	0.0	0.0	8.2
	Max_Hr	15	14	18	8	21	10	18	15	14	1	1	16

Table 7. 37: Simulated peak values of monthly average hourly latent heat flux for Scenario-B for Palam area

Year	Time	Jan	Feb	Mar	Apr	May	Jun	Jul	Aug	Sep	Oct	Nov	Dec
1973	Min	1.1	0.2	0.0	0.0	0.0	1.6	11.8	18.3	3.7	2.2	0.0	0.7
	Min_Hr	7	19	19	7	19	1	4	4	4	3	1	24
	Max	25.6	17.2	8.0	0.0	24.5	23.7	63.8	175.0	67.9	44.2	0.0	16.1
	Max_Hr	12	13	9	21	11	16	11	12	10	13	20	13
1977	Min	1.0	0.2	0.0	0.0	0.0	1.4	10.6	16.4	3.2	1.9	0.0	0.6
	Min_Hr	7	19	19	7	19	1	4	4	4	3	1	24
	Max	23.8	16.6	7.8	0.0	32.2	31.7	62.1	177.0	60.6	45.8	0.0	14.8
	Max_Hr	12	13	9	21	12	15	11	12	10	13	20	13
1986	Min	0.8	0.2	0.0	0.0	0.1	1.3	8.9	13.5	2.7	1.7	0.0	0.5
	Min_Hr	7	19	19	7	19	1	4	4	4	3	1	23
	Max	18.6	12.1	6.6	0.0	16.3	48.0	54.2	120.8	45.2	28.1	0.0	11.5
	Max_Hr	12	13	9	21	12	15	9	12	10	13	20	13
1991	Min	0.7	0.2	0.0	0.0	0.1	1.2	8.3	12.2	2.5	1.5	0.0	0.5
	Min_Hr	7	19	19	2	19	1	4	4	4	3	1	23
	Max	16.6	10.5	6.1	0.0	15.5	44.6	49.5	109.7	40.3	24.8	0.0	10.2
	Max_Hr	12	13	9	21	21	15	9	12	10	13	1	13
1998	Min	0.7	0.2	0.0	0.0	0.1	1.2	7.9	11.4	2.3	1.4	0.0	0.5
	Min_Hr	7	19	19	1	19	1	4	4	4	3	1	23
	Max	15.6	9.8	5.8	0.0	15.1	42.7	47.0	109.6	38.0	23.6	0.0	9.6
	Max_Hr	12	13	9	21	21	15	9	12	10	13	1	13
1999	Min	0.7	0.2	0.0	0.0	0.1	1.2	7.8	11.2	2.3	1.4	0.0	0.5
	Min_Hr	7	19	19	1	19	1	4	4	4	3	1	23
	Max	15.4	9.6	5.7	0.0	15.0	39.0	46.2	130.7	37.4	23.3	0.0	9.5
	Max_Hr	12	13	9	21	21	15	9	12	10	13	1	13
2002	Min	0.7	0.2	0.0	0.0	0.1	1.3	7.3	10.5	2.3	1.4	0.0	0.5
	Min_Hr	7	19	19	2	19	1	4	4	4	3	1	23
	Max	13.8	8.2	5.2	0.0	14.8	34.0	40.5	115.4	40.1	21.0	0.0	8.5
	Max_Hr	12	13	9	21	21	15	9	12	12	13	1	13
2006	Min	0.6	0.2	0.0	0.0	0.1	1.2	5.9	8.6	2.0	1.3	0.0	0.5
	Min_Hr	7	19	19	1	19	20	4	24	4	3	1	23
	Max	10.8	6.1	2.6	0.0	13.9	25.1	33.1	93.8	28.9	17.9	0.0	6.9
	Max_Hr	12	13	9	21	21	19	11	12	12	13	1	13
2009	Min	0.6	0.2	0.0	0.0	0.2	0.9	5.1	7.6	1.6	1.0	0.0	0.4
	Min_Hr	7	19	19	1	19	1	4	4	4	3	1	23
	Max	10.1	5.9	1.9	0.0	13.0	24.2	35.2	94.7	30.5	18.2	0.0	6.5
	Max_Hr	12	13	9	20	21	19	11	12	12	13	1	13
2011	Min	0.5	0.2	0.0	0.0	0.3	0.8	4.8	7.1	1.5	0.9	0.0	0.4
	Min_Hr	7	19	19	1	19	1	4	4	4	3	1	23
	Max	9.6	5.8	1.8	0.0	12.5	23.3	34.7	93.5	31.1	18.1	0.0	6.1
	Max_Hr	12	13	9	1	21	19	11	12	12	13	1	13
2013	Min	0.5	0.2	0.0	0.0	0.3	0.8	4.5	6.6	1.4	0.9	0.0	0.3
	Min_Hr	7	19	19	1	19	1	4	4	4	3	1	23
	Max	9.0	5.5	1.7	0.0	12.3	22.2	33.3	90.9	30.7	17.8	0.0	5.8
	Max_Hr	12	13	9	1	21	19	11	12	12	13	1	13
2014	Min	0.4	0.4	0.0	0.0	0.3	0.8	3.2	4.7	1.1	0.7	0.0	0.3
	Min_Hr	7	7	19	1	19	20	4	4	4	3	1	23
	Max	6.2	6.2	1.1	0.0	11.1	15.7	27.3	67.3	20.5	15.1	0.0	4.0
	Max_Hr	12	12	9	1	21	15	16	12	12	13	1	13

Table 7.38: Simulated peak values of monthly average hourly latent heat flux for Scenario-C for Palam area

Year	Time	Jan	Feb	Mar	Apr	May	Jun	Jul	Aug	Sep	Oct	Nov	Dec
1973	Min	1.1	0.2	0.0	0.0	0.0	1.6	11.8	18.3	3.7	2.2	0.0	0.7
	Min_Hr	7	19	19	7	19	1	4	4	4	3	1	24
	Max	25.6	17.2	8.0	0.0	24.5	23.7	63.8	175.0	67.9	44.2	0.0	16.1
	Max_Hr	12	13	9	21	11	16	11	12	10	13	20	13
1977	Min	1.0	0.0	0.0	7.8	0.0	1.7	4.2	0.2	2.9	0.0	0.0	0.0
	Min_Hr	1	19	19	6	19	3	23	4	3	19	1	18
	Max	43.9	17.2	2.4	63.1	10.3	20.0	54.5	19.5	28.1	8.5	0.0	5.6
	Max_Hr	10	12	20	11	9	16	10	13	14	13	20	10
1986	Min	0.0	2.1	0.0	0.0	3.8	5.8	-24.5	6.9	5.9	0.0	0.0	0.1
	Min_Hr	2	22	18	15	3	24	19	4	4	1	17	2
	Max	0.0	60.5	10.1	25.8	43.0	62.1	71.7	118.0	150.9	0.0	36.6	19.3
	Max_Hr	19	11	9	17	8	9	15	14	10	19	10	9
1991	Min	0.4	1.0	3.5	0.0	0.0	0.4	7.7	19.7	6.3	0.0	0.0	0.0
	Min_Hr	7	23	1	18	7	19	3	3	5	1	3	22
	Max	41.6	53.7	60.7	4.1	0.0	48.8	51.6	235.5	114.7	0.0	4.6	5.0
	Max_Hr	11	10	10	22	21	13	13	13	14	20	11	10
1998	Min	1.3	0.0	0.0	0.0	0.5	7.0	7.6	5.3	3.6	0.0	0.0	0.0
	Min_Hr	24	24	17	6	12	22	6	3	1	17	6	2
	Max	62.7	16.4	2.2	0.0	31.0	49.2	90.7	53.9	56.1	28.2	0.0	0.0
	Max_Hr	14	13	9	20	14	17	11	12	13	10	19	4
1999	Min	0.8	1.4	0.0	0.0	1.1	7.2	10.8	9.3	3.9	0.0	0.0	0.2
	Min_Hr	7	7	17	6	12	3	3	6	6	4	12	4
	Max	48.2	44.6	2.2	0.0	27.3	82.6	110.6	117.8	26.3	0.0	15.6	5.7
	Max_Hr	13	10	19	20	17	17	12	17	8	21	16	14
2002	Min	0.6	0.8	0.0	0.0	0.6	3.5	15.7	6.3	0.2	0.0	0.0	0.1
	Min_Hr	23	19	15	3	20	2	4	3	19	2	1	18
	Max	37.4	30.7	11.1	3.4	23.7	67.9	196.0	134.2	68.5	0.0	0.0	13.8
	Max_Hr	12	12	10	8	13	12	13	10	13	20	20	12
2006	Min	0.0	3.3	2.3	0.0	9.7	10.3	-4.7	3.8	-32.2	0.0	0.0	0.0
	Min_Hr	19	4	6	17	4	9	20	20	17	8	8	18
	Max	6.8	99.2	65.0	9.6	58.4	34.1	99.5	92.4	63.1	0.0	14.1	0.6
	Max_Hr	11	12	16	9	11	12	11	10	10	20	17	10
2009	Min	0.0	0.1	0.3	0.0	0.0	3.9	7.1	11.2	8.5	0.0	0.6	0.0
	Min_Hr	18	19	16	7	14	5	4	3	3	7	17	18
	Max	12.5	13.1	14.8	17.7	44.1	30.0	58.5	120.9	78.0	0.0	19.1	19.2
	Max_Hr	14	12	22	14	16	17	17	14	12	20	14	13
2011	Min	0.3	2.2	0.1	0.0	0.2	13.0	10.5	12.5	10.6	1.1	0.4	0.1
	Min_Hr	6	23	16	7	14	2	1	24	7	19	19	18
	Max	10.2	71.8	24.3	0.0	35.9	54.6	98.6	178.5	87.7	24.2	15.2	17.6
	Max_Hr	15	12	9	21	16	16	16	12	14	18	13	12
2013	Min	0.5	3.4	1.0	0.0	0.2	6.6	24.9	16.5	3.3	1.4	0.0	0.2
	Min_Hr	3	24	16	7	15	2	5	24	7	3	4	19
	Max	16.4	66.1	17.4	0.0	4.4	44.4	85.2	116.8	36.0	31.6	2.0	5.1
	Max_Hr	14	13	11	20	16	14	16	14	13	16	10	10
2014	Min	0.8	0.5	2.5	0.0	0.6	0.9	10.4	7.9	8.1	0.0	0.0	0.4
	Min_Hr	8	8	19	19	17	18	2	3	6	8	3	2
	Max	53.9	20.3	27.8	20.7	60.5	50.4	59.1	73.5	61.9	0.0	0.0	15.5
	Max_Hr	15	12	18	8	21	10	18	15	16	20	19	16

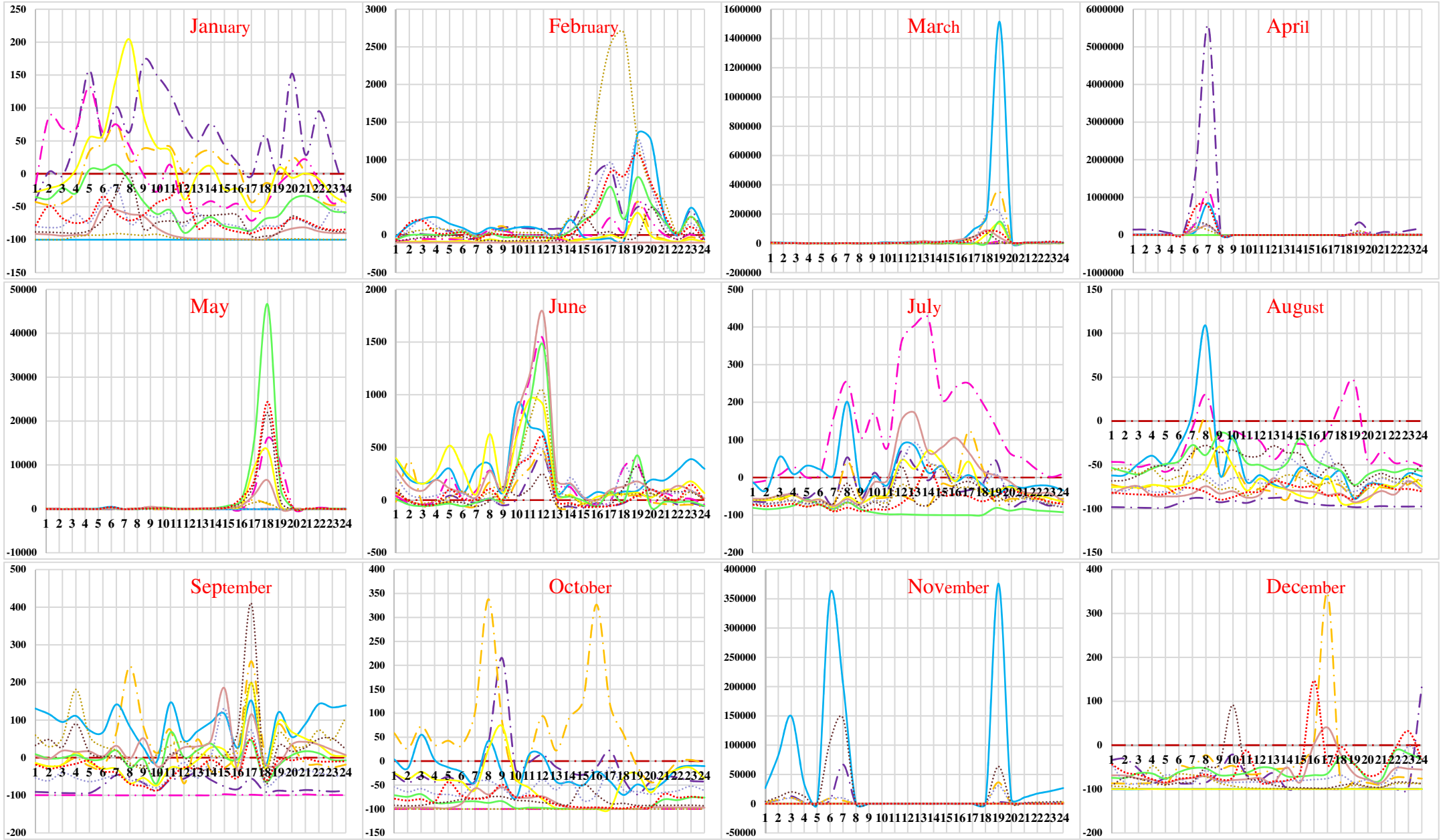

1973	1977	1986	1991	1998	1999	2002	2006	2009	2011	2013	2014	X-axis - Time in Hours
												Y-axis -% change in Heat Flux
Note: Percentage change in values of heat flux are very high because of the values in base year are very small which are used in denominator while calculating percentage change for different years.												

Figure 7.46: Percentage change in values of monthly average hourly latent heat flux for Scenario-A for Safdarjung area

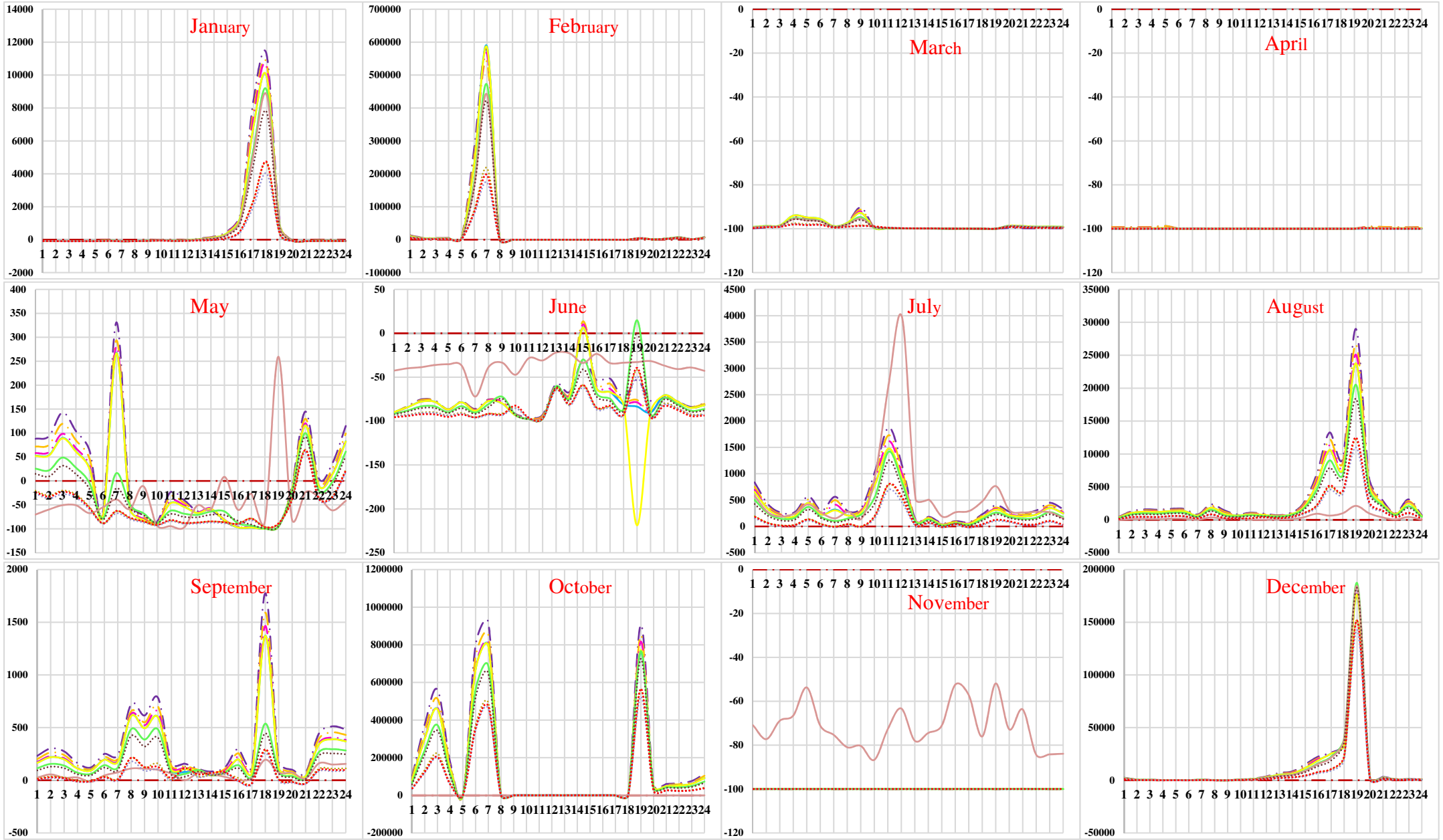

1973	1977	1986	1991	1998	1999	2002	2006	2009	2011	2013	2014	X-axis - Time in Hours
												Y-axis -% change in Heat Flux
Note: Percentage change in values of heat flux are very high because of the values in base year are very small which are used in denominator while calculating percentage change for different years.												

Figure 7.47: Percentage change in values of monthly average hourly latent heat flux for Scenario-B for Safdarjung area

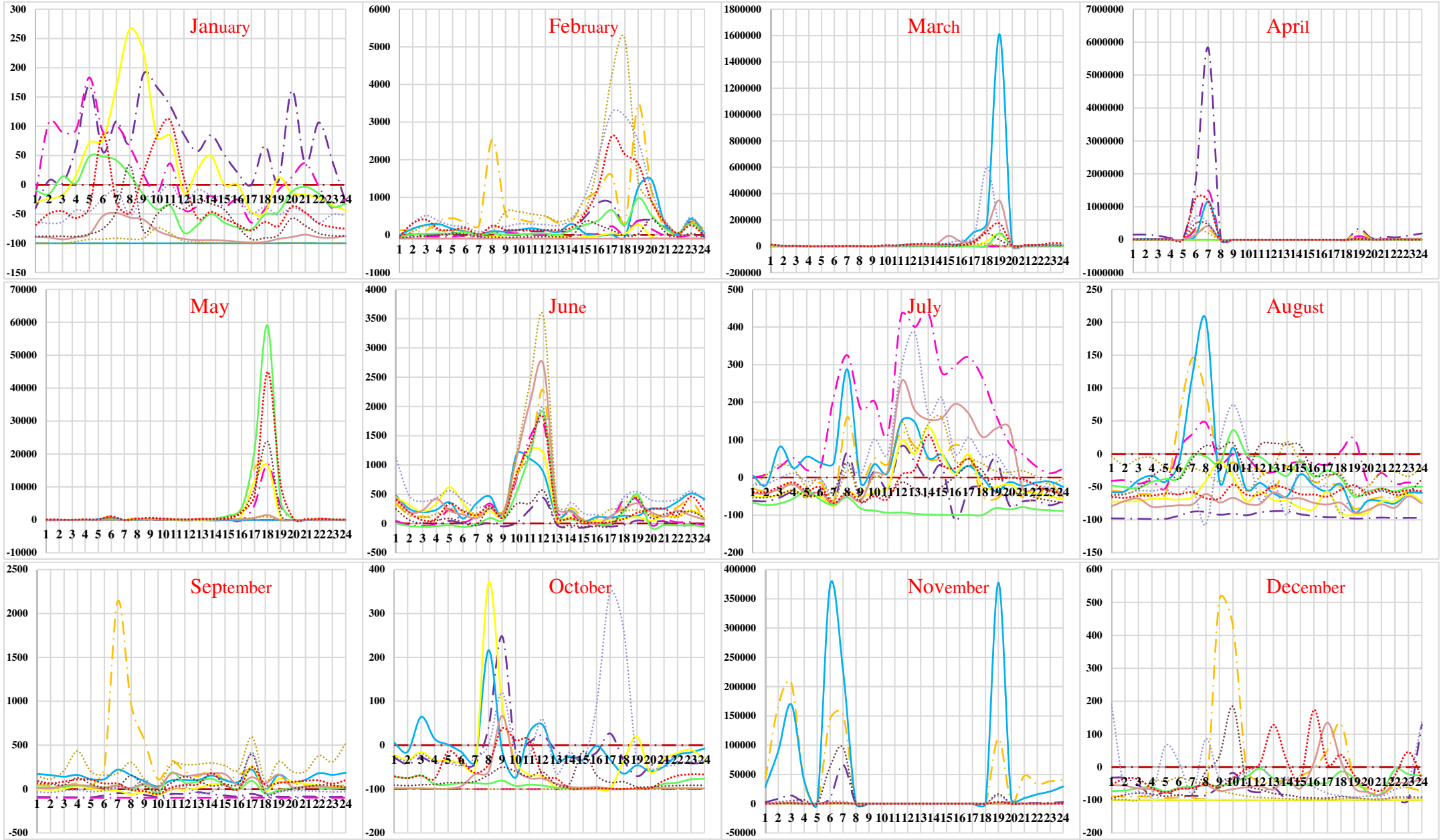

1973	1977	1986	1991	1998	1999	2002	2006	2009	2011	2013	2014	X-axis - Time in Hours
												Y-axis -% change in Heat Flux

Note: Percentage change in values of heat flux are very high because of the values in base year are very small which are used in denominator while calculating percentage change for different years.

Figure 7.48: Percentage change in values of monthly average hourly latent heat flux for Scenario-C for Safdarjung area

Table 7.39: Simulated peak values of monthly average hourly latent heat flux for Scenario-A for Safdarjung area

Year	Time	Jan	Feb	Mar	Apr	May	Jun	Jul	Aug	Sep	Oct	Nov	Dec
1973	Min	1.0	0.2	0.0	0.0	0.1	1.5	10.1	15.8	3.2	2.0	0.0	0.6
	Min_Hr	7	19	19	8	18	1	4	4	4	3	5	24
	Max	21.3	15.1	7.5	0.0	22.4	23.5	62.7	141.3	52.6	33.5	0.0	13.3
	Max_Hr	12	13	9	20	11	15	9	11	10	13	20	13
1977	Min	1.2	0.4	0.0	5.7	0.0	1.5	4.3	0.2	0.2	1.4	0.0	0.0
	Min_Hr	1	6	19	6	19	3	23	4	4	3	19	18
	Max	37.3	27.8	2.5	56.2	8.1	14.8	59.5	16.2	16.8	29.4	10.5	4.8
	Max_Hr	12	13	20	10	9	16	10	13	13	13	11	13
1986	Min	0.9	0.2	1.6	0.0	0.0	1.3	4.4	3.6	3.1	2.8	0.0	0.1
	Min_Hr	3	2	5	7	14	1	6	6	5	24	13	18
	Max	26.3	9.4	31.6	0.0	16.1	25.3	67.6	47.6	59.0	53.4	30.1	18.8
	Max_Hr	13	9	13	20	16	17	17	15	10	14	16	17
1991	Min	1.6	0.3	0.0	0.0	0.0	1.9	13.0	7.0	0.0	0.0	0.0	0.0
	Min_Hr	24	6	18	18	16	3	4	5	8	1	1	1
	Max	13.7	12.0	6.1	16.8	44.4	38.0	193.6	115.8	0.7	0.0	0.0	0.0
	Max_Hr	11	12	10	11	19	11	14	11	15	20	19	19
1998	Min	0.0	0.2	2.8	0.0	0.0	5.2	9.9	6.0	6.8	1.8	0.1	0.0
	Min_Hr	1	18	5	19	19	6	2	24	4	7	18	2
	Max	0.0	29.8	44.1	18.9	19.0	43.6	67.7	74.4	62.3	22.0	17.4	0.0
	Max_Hr	1	14	10	10	10	10	8	8	11	11	13	4
1999	Min	1.3	0.1	0.0	0.0	1.6	6.5	5.2	3.4	3.1	0.0	0.0	0.0
	Min_Hr	24	5	17	4	12	24	5	20	3	16	1	2
	Max	21.1	11.5	2.7	0.0	21.0	40.8	63.4	53.1	30.4	17.8	0.0	0.0
	Max_Hr	14	13	18	20	17	8	14	9	17	10	20	19
2002	Min	1.0	0.9	0.0	0.0	2.4	1.3	0.0	6.4	3.4	0.0	0.0	0.2
	Min_Hr	24	4	18	2	6	5	18	3	4	18	1	2
	Max	6.5	15.5	3.2	0.0	36.2	36.1	9.6	89.0	42.2	1.5	0.0	6.2
	Max_Hr	14	14	1	21	10	12	9	15	11	9	18	13
2006	Min	0.0	0.0	0.2	0.0	0.2	4.1	5.3	2.4	3.7	0.0	0.0	0.2
	Min_Hr	18	2	20	19	20	5	6	5	4	19	20	3
	Max	1.4	0.0	35.7	4.3	35.7	43.1	90.6	45.3	68.0	6.9	0.0	7.7
	Max_Hr	10	4	9	9	9	12	13	13	15	10	21	16
2009	Min	0.2	0.2	0.2	0.1	2.8	1.6	3.8	5.3	4.6	0.2	0.0	0.1
	Min_Hr	5	19	19	18	2	5	24	1	5	3	18	24
	Max	7.3	13.8	12.0	6.3	20.7	28.9	39.5	93.2	54.3	10.2	9.8	10.8
	Max_Hr	13	15	12	10	11	9	12	13	16	15	16	10
2011	Min	0.0	1.4	0.1	0.0	0.1	2.2	3.2	5.2	5.4	0.0	0.0	0.0
	Min_Hr	3	1	19	17	20	3	5	23	7	1	1	18
	Max	0.7	34.1	3.8	8.3	15.1	31.3	48.8	45.9	57.1	0.0	0.0	0.6
	Max_Hr	10	14	13	18	1	13	14	14	10	20	1	4
2013	Min	0.3	1.0	0.4	0.3	0.0	3.6	3.8	3.1	1.5	0.8	0.0	0.1
	Min_Hr	5	1	6	17	1	5	24	4	5	5	18	3
	Max	8.2	16.3	16.4	9.6	0.0	39.6	64.3	67.9	55.1	17.5	0.9	2.3
	Max_Hr	13	13	14	18	21	14	13	14	15	14	11	14
2014	Min	0.3	0.8	1.2	0.6	3.5	1.6	3.0	2.5	2.7	0.1	0.0	0.3
	Min_Hr	5	1	19	19	3	4	7	4	7	18	1	4
	Max	18.2	10.6	15.5	5.4	30.1	17.9	49.4	40.7	22.3	6.7	0.0	18.6
	Max_Hr	12	14	13	12	21	10	14	13	12	10	19	16

Table 7.40: Simulated peak values of monthly average hourly latent heat flux for Scenario-B for Safdarjung area

Year	Time	Jan	Feb	Mar	Apr	May	Jun	Jul	Aug	Sep	Oct	Nov	Dec
1973	Min	1.0	0.2	0.0	0.0	0.1	1.5	10.1	15.8	3.2	2.0	0.0	0.6
	Min_Hr	7	19	19	8	18	1	4	4	4	3	5	24
	Max	21.3	15.1	7.5	0.0	22.4	23.5	62.7	141.3	52.6	33.5	0.0	13.3
	Max_Hr	12	13	9	20	11	15	9	11	10	13	20	13
1977	Min	1.0	0.2	0.0	0.0	0.1	1.4	9.6	15.0	3.0	1.9	0.0	0.6
	Min_Hr	7	19	19	8	18	1	4	4	4	3	1	24
	Max	20.3	14.2	7.2	0.0	19.4	27.9	60.0	144.2	49.6	32.2	0.0	12.6
	Max_Hr	12	13	9	20	7	15	9	12	10	13	20	13
1986	Min	0.9	0.2	0.0	0.0	0.1	1.5	8.7	13.6	2.7	1.7	0.0	0.5
	Min_Hr	7	19	19	8	18	1	4	4	4	3	1	24
	Max	18.3	13.1	6.5	0.0	17.7	45.8	55.2	133.5	45.0	29.8	0.0	11.3
	Max_Hr	12	13	9	20	7	15	9	12	10	13	20	13
1991	Min	0.8	0.2	0.0	0.0	0.1	1.4	8.1	12.5	2.5	1.6	0.0	0.5
	Min_Hr	7	19	19	8	18	12	4	4	4	3	1	24
	Max	17.1	12.4	5.9	0.0	17.1	44.4	52.6	125.1	42.0	28.1	0.0	10.3
	Max_Hr	12	13	9	20	7	15	9	12	10	13	20	13
1998	Min	0.7	0.2	0.0	0.0	0.1	1.1	7.7	11.8	2.4	1.5	0.0	0.5
	Min_Hr	7	19	19	1	18	12	4	4	4	3	1	24
	Max	16.1	11.6	5.4	0.0	16.5	43.0	49.5	108.7	39.3	26.7	0.0	9.6
	Max_Hr	12	13	9	1	7	15	9	12	10	13	1	13
1999	Min	0.7	0.2	0.0	0.0	0.1	32.9	7.7	11.8	2.4	1.5	0.0	0.5
	Min_Hr	7	19	19	6	18	19	4	4	4	3	1	24
	Max	16.1	11.6	5.4	0.0	16.5	42.9	49.4	117.5	39.2	26.6	0.0	9.5
	Max_Hr	12	13	9	20	7	15	9	12	10	13	20	13
2002	Min	0.7	0.2	0.0	0.0	0.2	0.8	6.8	9.5	2.0	1.2	0.0	0.5
	Min_Hr	7	19	19	2	18	12	4	4	4	3	1	24
	Max	13.2	9.8	4.0	0.0	12.9	31.8	45.5	96.8	32.7	23.1	0.0	7.7
	Max_Hr	12	14	9	20	21	19	11	12	10	13	1	13
2006	Min	0.6	0.2	0.0	0.0	0.7	6.5	8.9	1.9	1.2	0.0	0.5	0.5
	Min_Hr	7	19	19	2	12	4	4	4	3	1	24	24
	Max	12.7	9.6	3.5	0.0	30.6	44.6	93.8	31.4	22.5	0.0	7.4	7.4
	Max_Hr	16	14	9	20	19	11	12	10	13	1	13	13
2009	Min	0.6	0.2	0.0	0.0	0.2	0.7	5.9	8.3	1.8	1.1	0.0	0.5
	Min_Hr	7	19	19	2	18	12	4	4	4	3	1	24
	Max	11.5	8.4	3.0	0.0	12.4	27.9	40.6	86.0	28.4	20.8	0.0	6.7
	Max_Hr	12	14	9	20	21	19	11	12	10	13	1	13
2011	Min	0.5	0.2	0.0	0.0	0.5	0.7	3.4	4.9	1.1	0.7	0.0	0.3
	Min_Hr	7	19	19	2	6	12	4	4	4	3	1	24
	Max	6.5	4.5	1.2	0.0	10.7	16.5	28.5	75.9	27.3	15.9	0.0	3.9
	Max_Hr	16	14	9	20	21	15	16	12	12	13	1	13
2013	Min	0.4	0.2	0.0	0.0	0.5	0.8	3.0	4.3	1.0	0.7	0.0	0.3
	Min_Hr	7	19	19	1	6	12	4	4	4	3	1	24
	Max	5.6	3.8	0.9	0.0	10.3	15.4	28.2	66.6	23.6	15.2	0.0	3.5
	Max_Hr	16	14	9	20	21	15	16	12	12	13	1	13
2014	Min	0.4	0.2	0.0	0.0	0.5	0.7	3.3	4.9	1.0	0.7	0.0	0.3
	Min_Hr	7	19	19	1	6	5	4	4	4	3	1	24
	Max	6.6	4.5	1.0	0.0	10.6	16.8	29.7	69.8	25.7	16.6	0.0	4.1
	Max_Hr	12	14	9	20	21	19	16	12	12	13	1	13

Table 7.41: Simulated peak values of monthly average hourly latent heat flux for Scenario-C for Safdarjung area

Year	Time	Jan	Feb	Mar	Apr	May	Jun	Jul	Aug	Sep	Oct	Nov	Dec
1973	Min	1.0	0.2	0.0	0.0	0.1	1.5	10.1	15.8	3.2	2.0	0.0	0.6
	Min_Hr	7	19	19	8	18	1	4	4	4	3	5	24
	Max	21.3	15.1	7.5	0.0	22.4	23.5	62.7	141.3	52.6	33.5	0.0	13.3
	Max_Hr	12	13	9	20	11	15	9	11	10	13	20	13
1977	Min	1.2	0.5	0.0	6.0	0.0	1.7	-6.0	0.2	0.2	1.4	0.0	0.0
	Min_Hr	1	6	19	6	19	3	16	4	4	3	19	18
	Max	39.6	29.1	2.0	58.2	8.6	15.2	60.9	17.0	17.3	31.9	11.1	5.0
	Max_Hr	12	13	20	10	9	16	10	13	13	9	12	13
1986	Min	0.0	2.0	0.0	0.0	3.4	5.1	6.0	6.2	5.3	0.0	0.0	0.1
	Min_Hr	2	3	18	15	5	4	24	4	4	8	17	5
	Max	0.0	79.6	8.4	21.3	40.4	54.6	84.0	107.3	130.9	0.0	31.2	29.7
	Max_Hr	20	12	9	17	8	12	11	11	9	20	10	10
1991	Min	1.6	0.3	0.0	0.0	0.0	2.0	15.2	8.0	0.0	0.0	0.0	0.0
	Min_Hr	1	2	18	18	16	3	1	5	8	8	2	3
	Max	16.4	14.5	9.4	19.3	26.2	47.3	198.7	135.5	0.6	0.0	0.0	0.0
	Max_Hr	11	12	10	11	22	11	14	11	15	20	20	19
1998	Min	0.0	0.4	3.3	0.0	0.0	5.7	12.1	5.9	8.4	2.0	0.2	0.0
	Min_Hr	2	18	7	19	19	6	2	22	4	7	18	3
	Max	0.0	39.2	46.2	23.8	22.5	55.4	87.0	108.7	68.3	27.7	24.8	0.0
	Max_Hr	20	14	12	10	10	10	8	8	10	12	13	19
1999	Min	1.3	0.1	0.0	0.0	2.5	7.7	6.4	3.7	3.6	0.0	0.0	0.0
	Min_Hr	24	5	17	7	6	24	6	20	7	17	8	3
	Max	28.3	11.4	1.8	0.0	25.3	41.1	86.4	66.7	37.0	18.5	0.0	0.0
	Max_Hr	14	13	8	20	17	11	14	9	17	8	20	20
2002	Min	1.5	1.2	0.0	0.0	2.5	1.3	0.0	7.8	4.4	0.0	0.0	0.3
	Min_Hr	7	3	18	8	6	6	18	3	24	19	9	2
	Max	9.5	24.1	3.7	0.0	46.2	46.1	11.0	141.9	73.0	2.0	0.0	11.4
	Max_Hr	14	14	1	21	17	12	9	11	11	11	20	12
2006	Min	0.1	0.0	2.4	0.0	0.1	6.2	7.5	3.1	4.5	0.0	0.0	0.3
	Min_Hr	3	8	5	19	20	5	6	4	2	19	20	3
	Max	1.8	0.0	51.1	7.2	64.4	65.1	123.9	53.8	74.4	15.3	0.0	9.9
	Max_Hr	10	20	15	9	11	11	16	13	12	9	21	17
2009	Min	0.2	0.3	0.6	0.2	3.5	3.2	5.9	6.3	4.7	0.2	0.0	0.1
	Min_Hr	5	19	4	18	20	7	24	1	24	3	18	24
	Max	15.2	18.4	19.2	10.3	48.1	30.3	42.8	159.0	72.3	17.1	19.4	15.9
	Max_Hr	13	15	9	10	10	18	16	12	12	15	16	10
2011	Min	0.0	1.9	0.1	0.0	0.1	6.6	10.5	11.8	9.0	0.0	0.0	0.0
	Min_Hr	3	4	3	17	20	3	5	23	2	8	8	3
	Max	2.1	82.3	8.7	37.4	44.8	84.0	104.3	141.5	113.7	0.0	0.0	1.1
	Max_Hr	10	12	10	9	11	12	15	14	12	20	20	11
2013	Min	0.6	2.4	0.7	0.3	0.0	12.9	10.3	-2.4	2.5	1.5	0.0	0.2
	Min_Hr	5	24	7	17	7	5	24	8	2	5	18	18
	Max	18.7	53.6	25.3	18.9	0.0	63.7	161.9	166.2	52.9	36.5	2.5	12.3
	Max_Hr	13	13	18	8	21	15	13	11	17	17	12	12
2014	Min	0.6	1.6	2.8	0.6	12.1	4.7	8.8	5.6	6.7	0.0	0.0	0.4
	Min_Hr	24	24	19	19	15	4	4	2	4	18	10	5
	Max	25.1	36.5	46.0	20.3	60.1	44.0	78.5	67.0	64.0	30.2	0.0	30.4
	Max_Hr	11	13	10	10	21	12	14	13	14	10	19	13

No significant trend has been observed in minimum annual extreme hourly values of latent heat flux for Safdarjung areas in different scenarios. Further for Safdarjung area, results indicate that annual extreme hourly values of latent heat flux during day time have decreased in Scenario-A (961.27 to 554.62 Wm^{-2}) and Scenario-B (961.27 to 592.48 Wm^{-2}) (Table 7.42). The overall peak values of monthly average hourly latent heat flux during day time are decreasing over the years due to less availability of available energy to partition in sensible and latent heat fluxes because of increase in storage heat flux. Latent heat flux is also decreasing due to conversion of pervious areas into impervious, conversion of vegetative areas into hard surfaces and reduction in moisture availability.

Table 7.42: Extreme annual hourly values of latent heat flux for different scenario

Year	Data	Palam Area			Safdarjung Area		
		Scenario-A	Scenario-B	Scenario-C	Scenario-A	Scenario-B	Scenario-C
1973	Max	924.24	924.24	924.24	961.27	961.27	961.27
	Min	-377	-377	-377	-0.10	-0.10	-0.10
1977	Max	853.18	987.01	920.33	602.03	927.01	621.19
	Min	-0.14	-0.11	-0.12	-0.18	-0.12	-0.17
1986	Max	994.16	958.93	998.72	987.78	920.39	996.91
	Min	-121.5	-0.15	-0.08	-0.15	-0.12	-0.11
1991	Max	929.58	881.88	959.41	998.64	861.60	932.75
	Min	-0.19	-0.16	-0.1	-58.88	-0.14	-0.11
1998	Max	885.52	997.07	962.22	963.79	816.40	907.69
	Min	-0.2	-0.17	-0.15	-0.11	-0.14	-0.12
1999	Max	983.9	994.66	979.49	918.31	813.57	964.59
	Min	-24.88	-0.18	-24.66	-25.87	-0.14	-33.40
2002	Max	947.88	889.66	968.98	892.56	946.93	918.79
	Min	-0.14	-0.17	-0.1	-0.18	-0.19	-0.15
2006	Max	884.07	734.62	978.85	997.36	911.59	990.27
	Min	-2.19	-0.18	-1.38	-1.43	-0.20	-1.50
2009	Max	732.26	711.82	949.14	955.05	830.03	996.37
	Min	-0.17	-0.23	-0.08	-0.19	-0.21	-0.12
2011	Max	950.72	721.22	897.46	805.64	669.69	990.86
	Min	-0.21	-0.24	-0.12	-0.17	0.00	-0.06
2013	Max	572.21	719.88	889.34	996.18	559.14	997.75
	Min	-0.24	-0.25	-0.15	-0.27	-0.26	-0.17
2014	Max	588.03	486.32	959.6	554.62	592.48	939.34
	Min	-0.04	-0.18	0	-0.22	-0.27	-350.14

Therefore, it can be concluded that decrease in latent heat flux in Scenario-B over the years indicates effect of urbanization. Study results are in agreement with other similar studies in different parts of the world. The results of present study are showing patterns

similar to other studies held in Delhi, Anand region in Gujarat and two UK sites (Nagar, 2002; Das et al., 2009b; Das et al., 2014; Mohan & Kandya, 2015; Ward H. C., 2016)

7.5.5 Surface Temperature

Annual, seasonal, and monthly average surface temperature at hourly temporal scale has been calculated for Palam and Safdarjung areas from hourly model results for different Scenarios (A, B and C) and for different years i.e., 1973 to 2014. Annual extreme hourly surface temperature have also been calculated to ascertain the effects of LULC change on extremes.

According to the results for Scenario-A for Palam area, peak values of minimum and maximum monthly average hourly surface temperature at a particular hour from year 1973 to 2014 is increasing over the years because of LULC due to urbanization. General trend in peak value of minimum monthly average hourly surface temperature has been found to be increasing over the years from 8.10 ^{o}C (1973) to 8.50 ^{o}C (2014), whereas, no significant changes have been fund in peak value of maximum monthly average hourly surface temperature. In few years it value increased and in other years it has found to be decreasing (Table 7.43). Relative percentage change in peak value of minimum monthly average hourly surface temperature, with respect to base year, has been found to be varying from 2.47 % in year 1977 to 4.94 % in year 2014. In case of Safdarjung area in Scenario-A, peak value of monthly average of surface temperature at hourly basis has been calculated and trends have been found to be similar to Palam area. According to the results, peak values of minimum and maximum monthly average hourly surface temperature at a particular hour from the year 1973 to 2014 are increasing and decreasing, respectively. In case of peak value of minimum monthly average hourly surface temperature has increased from 8.10 ^{o}C (1973) to 9.90 ^{o}C (2014), however, there is no specific trend has been found in peak values of maximum monthly average hourly surface temperature, as shown in Table 7.46. Relative percentage change in peak values of minimum monthly average hourly surface temperature, from the base year, is increased from 1973 (0 %) to 2014 (22.22%).

In Scenario-B, for both study areas i.e., Palam and Safdarjung, peak values of monthly average hourly surface temperature has been calculated for different Scenarios in different years i.e., 1973 to 2014 from the hourly simulated results. According to the results, no significant trend has been observed in peak values of minimum monthly average hourly surface temperature from the year 1973 to 2014 however, increasing

trend has been observed in peak values of maximum monthly average hourly surface temperature over the years from 1973 to 2014. For Palam area in Scenario-B, peak values of maximum monthly average hourly surface temperature have increased from 47.10 ^{o}C in year 1973 to 47.40 ^{o}C in year 2014, as shown in Table 7.44. Percentage increase in peak value of maximum monthly average hourly surface temperature, from year 1973 to 2014 has been found to be 0. 64%. Similar trends have been observed for Safdarjung area also. According to the results, no significant trend has been observed in peak values of minimum monthly average hourly surface temperature from the year 1973 to 2014 in Safdarjung area, however, increasing trend has been observed in peak values of maximum monthly average hourly surface temperature over the years from 1973 to 2014. For Safdarjung area in Scenario-B, peak values of maximum monthly average hourly surface temperature have increased from 46.90 ^{o}C in year 1973 to 47.10 ^{o}C in year 2014, as shown in Table 7.47. Percentage increase in peak value of maximum monthly average hourly surface temperature, from year 1973 to 2014 has been found to be 0. 43%.

Similar analysis has been carried out for Scenario-C also for both the areas. For Scenario-C, peak values of minimum & maximum monthly average hourly surface temperature has been calculated for both the areas. According to the results, in Scenario-C for Palam area, peak values of minimum monthly average hourly surface temperature are exhibiting increasing trend over the years from 8.10 ^{o}C (1973) to 8.50 ^{o}C (2014), whereas, no specific trend has been observed in peak values of maximum surface temperature, as shown in Table 7.45. In case of Safdarjung area, peak values of minimum hourly average hourly surface temperature are showing increasing trend and changed over the year from 8.10 ^{o}C (1973) to 9.90 ^{o}C (2014). Relative percentage change in peak values of minimum monthly average hourly surface temperature has been exhibiting increasing trend (Table 7.48). Annual hourly extreme values of surface temperature for different years have also been calculated to determine the trend in extreme values due to change in LULC for both the areas. In Palam area extreme values of minimum temperature is showing increasing trend in different Scenarios (Scenario-A: 2.8 to 3.2 ^{o}C, Scenario-B: 2.8 to 3 ^{o}C, Scenario-C: 2.8 to 3.2 ^{o}C) from year 1973 to 2014. No specific trend has been observed in extreme values of maximum surface temperature in Scenario-A and C for Palam area (Table 7.49), whereas increasing trends have been observed in peak values of maximum monthly average hourly surface temperature in Scenario-B (52.85 to 53.12 ^{o}C).

Table 7.43: Simulated peak values of monthly average hourly surface temperature for Scenario-A for Palam area

Year	Time	Jan	Feb	Mar	Apr	May	Jun	Jul	Aug	Sep	Oct	Nov	Dec
1973	Min	8.7	12.6	15.7	24.0	27.4	30.2	28.2	26.7	25.9	20.1	12.5	8.1
	Min_Hr	8	7	7	6	6	6	6	7	7	7	7	8
	Max	27.5	31.6	37.8	46.4	47.1	44.7	40.6	36.4	40.2	39.0	34.1	25.0
	Max_Hr	14	14	14	14	14	14	14	14	13	14	14	14
1977	Min	8.3	10.7	16.1	22.4	24.4	27.3	26.6	27.2	24.8	20.2	15.3	10.1
	Min_Hr	7	7	7	6	6	6	6	6	6	7	7	7
	Max	26.5	32.1	40.9	41.6	44.7	44.0	35.4	39.2	37.8	39.5	35.1	29.2
	Max_Hr	14	14	14	13	14	15	13	14	14	14	14	14
1986	Min	7.9	12.3	16.3	21.4	26.8	28.6	30.3	27.4	25.8	18.3	13.3	10.2
	Min_Hr	8	7	6	6	6	6	6	6	6	7	6	7
	Max	25.9	29.3	35.4	41.4	45.4	43.4	41.4	37.1	39.0	32.2	31.8	27.0
	Max_Hr	14	14	14	14	14	14	14	14	15	15	13	14
1991	Min	9.2	11.8	18.2	22.5	26.7	28.9	29.0	27.2	25.9	20.4	12.5	7.2
	Min_Hr	7	7	6	6	6	6	6	6	6	6	6	7
	Max	25.7	29.4	36.1	42.1	44.9	41.3	39.1	36.1	38.2	37.1	32.7	27.3
	Max_Hr	14	14	14	14	14	14	14	14	14	14	14	14
1998	Min	9.9	10.7	15.9	23.8	29.7	28.8	27.9	27.9	26.2	21.4	19.9	9.0
	Min_Hr	7	7	7	6	6	5	5	6	6	6	7	7
	Max	24.5	27.3	37.2	45.3	47.1	42.1	38.7	38.9	39.9	38.7	36.9	28.6
	Max_Hr	14	14	14	13	14	13	13	13	13	13	13	14
1999	Min	8.5	11.6	16.5	22.6	27.8	28.0	28.9	28.1	25.8	21.0	14.0	10.6
	Min_Hr	7	7	6	6	6	6	6	6	7	7	7	7
	Max	24.3	31.1	37.6	42.7	44.6	41.7	40.5	41.6	41.9	40.1	35.2	27.6
	Max_Hr	14	13	13	14	14	14	14	14	13	13	14	14
2002	Min	11.1	12.8	19.1	24.6	27.6	28.2	29.6	27.8	26.7	21.3	15.6	12.1
	Min_Hr	4	8	7	7	6	6	6	6	7	7	7	8
	Max	22.3	31.1	39.3	43.4	44.8	42.6	42.6	36.9	39.0	35.4	31.9	25.6
	Max_Hr	14	14	14	14	15	15	13	14	14	14	14	14
2006	Min	9.9	16.1	17.9	24.3	28.5	28.7	29.2	28.1	26.3	21.8	15.3	11.4
	Min_Hr	7	7	7	7	6	6	6	6	7	7	7	7
	Max	26.6	33.3	35.0	42.9	44.5	36.2	38.9	39.4	38.8	37.9	32.7	26.5
	Max_Hr	14	14	14	14	14	16	15	14	14	14	14	14
2009	Min	10.1	12.0	17.0	22.6	27.1	29.6	28.5	28.0	25.2	19.8	14.3	10.2
	Min_Hr	8	8	7	7	6	6	6	6	7	7	7	8
	Max	26.0	31.5	38.2	44.9	47.2	48.8	42.0	40.4	39.0	38.1	31.4	27.8
	Max_Hr	14	14	14	14	14	14	14	14	14	14	14	14
2011	Min	8.7	12.2	16.5	22.5	27.0	29.2	28.1	27.3	25.6	20.8	13.9	10.1
	Min_Hr	8	7	7	7	6	6	6	6	7	7	7	7
	Max	24.1	29.7	37.7	43.8	47.2	46.0	40.1	38.0	38.5	37.9	30.9	26.8
	Max_Hr	14	14	14	14	14	14	14	14	14	14	14	14
2013	Min	7.2	12.3	16.1	22.2	26.8	28.7	27.7	26.6	26.0	21.7	13.8	10.3
	Min_Hr	7	7	7	6	5	6	6	6	7	7	7	7
	Max	23.6	28.7	37.2	43.9	48.7	43.7	39.1	37.3	40.0	37.6	32.1	26.5
	Max_Hr	14	14	14	14	14	14	14	13	14	14	14	14
2014	Min	9.2	11.4	16.7	21.5	30.0	28.3	28.6	28.0	26.2	22.1	14.9	8.5
	Min_Hr	7	7	7	6	6	6	6	6	6	7	7	7
	Max	23.8	28.9	35.5	42.4	47.2	43.6	41.9	40.0	39.5	39.5	33.6	24.2
	Max_Hr	14	14	14	14	14	14	14	14	14	14	14	14

Table 7.44: Simulated peak values of monthly average hourly surface temperature for Scenario-B for Palam area

Year	Time	Jan	Feb	Mar	Apr	May	Jun	Jul	Aug	Sep	Oct	Nov	Dec
1973	Min	8.7	12.6	15.7	24.0	27.4	30.2	28.2	26.7	25.9	20.1	12.5	8.1
	Min_Hr	8	7	7	6	6	6	6	7	7	7	7	8
	Max	27.5	31.6	37.8	46.4	47.1	44.7	40.6	36.4	40.2	39.0	34.1	25.0
	Max_Hr	14	14	14	14	14	14	14	14	13	14	14	14
1977	Min	8.7	12.6	15.7	24.0	27.4	30.2	28.2	26.7	25.9	20.1	12.5	8.1
	Min_Hr	8	7	7	6	6	6	6	7	7	7	7	8
	Max	27.5	31.7	37.8	46.5	47.1	44.7	40.6	36.5	40.2	39.0	34.1	25.0
	Max_Hr	14	14	14	14	14	14	14	14	13	14	14	14
1986	Min	8.7	12.6	15.7	24.0	27.4	30.2	28.2	26.7	25.9	20.1	12.5	8.1
	Min_Hr	8	7	7	6	6	6	6	7	7	7	7	8
	Max	27.6	31.7	37.9	46.5	47.2	44.8	40.7	36.5	40.3	39.1	34.2	25.0
	Max_Hr	14	14	14	14	14	14	14	14	13	14	14	14
1991	Min	8.7	12.6	15.7	24.0	27.4	30.2	28.2	26.7	25.9	20.1	12.5	8.1
	Min_Hr	8	7	7	6	6	6	6	7	7	7	7	8
	Max	27.6	31.7	37.9	46.5	47.2	44.8	40.7	36.5	40.3	39.1	34.2	25.0
	Max_Hr	14	14	14	14	14	14	14	14	13	14	14	14
1998	Min	8.7	12.6	15.7	24.0	27.4	30.2	28.2	26.7	25.9	20.1	12.5	8.1
	Min_Hr	8	7	7	6	6	6	6	7	7	7	7	8
	Max	27.6	31.7	37.9	46.5	47.2	44.8	40.7	36.5	40.3	39.1	34.2	25.0
	Max_Hr	14	14	14	14	14	14	14	14	13	14	14	14
1999	Min	8.7	12.6	15.7	24.0	27.4	30.2	28.2	26.7	25.9	20.1	12.5	8.1
	Min_Hr	8	7	7	6	6	6	6	7	7	7	7	8
	Max	27.6	31.7	37.9	46.5	47.2	44.8	40.7	36.5	40.3	39.1	34.2	25.0
	Max_Hr	14	14	14	14	14	14	14	14	13	14	14	14
2002	Min	8.7	12.6	15.7	24.0	27.4	30.2	28.2	26.7	25.9	20.1	12.5	8.1
	Min_Hr	8	7	7	6	6	6	6	7	7	7	7	8
	Max	27.6	31.7	37.9	46.5	47.2	44.8	40.7	36.5	40.3	39.1	34.2	25.0
	Max_Hr	14	14	14	14	14	14	14	14	13	14	14	14
2006	Min	8.7	12.6	15.7	24.0	27.4	30.2	28.2	26.7	25.9	20.1	12.5	8.1
	Min_Hr	8	7	7	6	6	6	6	7	7	7	7	8
	Max	27.6	31.7	37.9	46.6	47.2	44.8	40.7	36.5	40.3	39.1	34.2	25.1
	Max_Hr	14	14	14	14	14	14	14	14	13	14	14	14
2009	Min	8.7	12.6	15.7	24.0	27.4	30.2	28.2	26.7	25.9	20.1	12.5	8.1
	Min_Hr	8	7	7	6	6	6	6	7	7	7	7	8
	Max	27.7	31.8	38.0	46.6	47.3	44.9	40.8	36.6	40.4	39.2	34.3	25.1
	Max_Hr	14	14	14	14	14	14	14	14	13	14	14	14
2011	Min	8.7	12.6	15.7	24.0	27.4	30.2	28.2	26.7	25.9	20.1	12.5	8.1
	Min_Hr	8	7	7	6	6	6	6	7	7	7	7	8
	Max	27.7	31.8	38.0	46.7	47.3	44.9	40.8	36.6	40.4	39.2	34.3	25.1
	Max_Hr	14	14	14	14	14	14	14	14	13	14	14	14
2013	Min	8.7	12.6	15.7	24.0	27.4	30.2	28.2	26.7	25.9	20.1	12.5	8.1
	Min_Hr	8	7	7	6	6	6	6	7	7	7	7	8
	Max	27.7	31.8	38.0	46.7	47.4	44.9	40.8	36.6	40.5	39.2	34.3	25.2
	Max_Hr	14	14	14	14	14	14	13	14	13	14	14	14
2014	Min	8.7	8.7	15.7	24.0	27.4	30.2	28.2	26.7	25.9	20.1	12.5	8.1
	Min_Hr	8	8	7	6	6	6	6	7	7	7	7	8
	Max	27.7	27.7	38.1	46.7	47.4	44.9	40.8	36.6	40.5	39.2	34.3	25.2
	Max_Hr	14	14	14	14	14	14	14	14	13	14	14	14

Table 7.45: Simulated peak values of monthly average hourly surface temperature for Scenario-C for Palam area

Year	Time	Jan	Feb	Mar	Apr	May	Jun	Jul	Aug	Sep	Oct	Nov	Dec
1973	Min	8.7	12.6	15.7	24.0	27.4	30.2	28.2	26.7	25.9	20.1	12.5	8.1
	Min_Hr	8	7	7	6	6	6	6	7	7	7	7	8
	Max	27.5	31.6	37.8	46.4	47.1	44.7	40.6	36.4	40.2	39.0	34.1	25.0
	Max_Hr	14	14	14	14	14	14	14	14	13	14	14	14
1977	Min	8.3	10.7	16.1	22.4	24.4	27.3	26.6	27.2	24.8	20.2	15.3	10.1
	Min_Hr	7	7	7	6	6	6	6	6	6	7	7	7
	Max	26.5	32.1	40.8	41.6	44.6	44.0	35.3	39.2	37.8	39.4	35.1	29.1
	Max_Hr	14	14	14	13	14	15	13	14	14	14	14	14
1986	Min	7.9	12.3	16.3	21.4	26.8	28.6	30.3	27.4	25.8	18.3	13.3	10.2
	Min_Hr	8	7	6	6	6	6	6	6	6	7	6	7
	Max	25.8	29.3	35.4	41.3	45.3	43.4	41.3	37.0	39.0	32.2	31.7	26.9
	Max_Hr	14	14	14	14	14	14	14	14	15	15	13	14
1991	Min	9.2	11.8	18.2	22.5	26.7	28.9	29.0	27.2	25.9	20.4	12.5	7.2
	Min_Hr	7	7	6	6	6	6	6	6	6	6	6	7
	Max	25.6	29.4	36.0	42.1	44.8	41.2	39.0	36.0	38.2	37.0	32.6	27.3
	Max_Hr	14	14	14	14	14	14	14	14	14	14	14	14
1998	Min	9.9	10.7	15.9	23.8	29.6	28.8	27.9	27.9	26.2	21.4	19.9	9.0
	Min_Hr	7	7	7	6	6	5	6	6	6	6	7	7
	Max	24.4	27.2	37.1	45.2	47.0	42.0	38.7	38.8	39.8	38.6	36.8	28.6
	Max_Hr	14	14	14	13	14	13	13	13	13	13	13	14
1999	Min	8.5	11.6	16.5	22.6	27.8	28.0	28.9	28.1	25.8	21.0	14.0	10.6
	Min_Hr	7	7	6	6	6	6	6	6	7	7	7	7
	Max	24.2	31.0	37.5	42.6	44.5	41.6	40.4	41.5	41.8	39.9	35.1	27.5
	Max_Hr	14	13	13	14	14	14	14	14	13	13	14	14
2002	Min	11.1	12.8	19.1	24.6	27.6	28.2	29.6	27.8	26.7	21.3	15.6	12.1
	Min_Hr	4	8	7	7	6	6	6	6	7	7	7	8
	Max	22.3	31.1	39.2	43.4	44.7	42.5	42.6	36.9	39.0	35.3	31.9	25.6
	Max_Hr	14	14	14	14	15	15	13	14	14	14	14	14
2006	Min	9.9	16.1	17.9	24.3	28.5	28.7	29.2	28.1	26.3	21.8	15.3	11.4
	Min_Hr	7	7	7	7	6	6	6	6	7	7	7	7
	Max	26.6	33.3	34.9	42.8	44.4	36.2	38.9	39.3	38.7	37.8	32.6	26.4
	Max_Hr	14	14	14	14	14	16	15	14	14	14	14	14
2009	Min	10.1	12.0	17.0	22.6	27.1	29.6	28.5	28.0	25.2	19.8	14.3	10.2
	Min_Hr	8	8	7	7	6	6	6	6	7	7	7	8
	Max	25.8	31.4	38.0	44.7	47.0	48.6	41.9	40.3	38.9	37.9	31.3	27.6
	Max_Hr	14	14	14	14	14	14	14	14	14	14	14	14
2011	Min	8.7	12.2	16.5	22.5	27.0	29.2	28.1	27.3	25.6	20.8	13.9	10.1
	Min_Hr	8	7	7	7	6	6	6	6	7	7	7	7
	Max	24.0	29.5	37.5	43.6	47.0	45.8	40.0	37.8	38.4	37.7	30.8	26.7
	Max_Hr	15	14	14	14	14	14	14	14	14	14	14	14
2013	Min	7.2	12.3	16.1	22.2	26.8	28.7	27.7	26.6	26.0	21.7	13.8	10.3
	Min_Hr	7	7	7	6	5	6	6	6	7	7	7	7
	Max	23.5	28.5	37.0	43.7	48.5	43.5	39.0	37.2	39.8	37.4	31.9	26.3
	Max_Hr	14	14	14	14	14	14	14	13	14	14	14	14
2014	Min	9.2	11.4	16.7	21.5	30.0	28.3	28.6	28.0	26.2	22.1	14.9	8.5
	Min_Hr	7	7	7	6	6	6	6	6	6	7	7	7
	Max	23.6	28.7	35.2	42.2	46.9	43.4	41.7	39.9	39.3	39.3	33.5	24.0
	Max_Hr	14	14	14	14	14	14	14	15	14	14	14	14

Table 7.46: Simulated peak values of monthly average hourly surface temperature for Scenario-A for Safdarjung area

Year	Time	Jan	Feb	Mar	Apr	May	Jun	Jul	Aug	Sep	Oct	Nov	Dec
1973	Min	8.7	12.6	15.7	24.1	27.6	30.2	28.2	26.6	25.9	20.1	12.5	8.1
	Min_Hr	8	7	7	6	6	6	6	6	7	7	7	8
	Max	27.6	31.8	38.0	46.3	46.9	44.8	40.7	36.6	40.4	39.1	34.2	25.1
	Max_Hr	14	14	14	13	13	14	14	14	13	14	14	14
1977	Min	8.3	5.1	15.9	22.5	24.4	27.3	26.6	27.2	27.3	20.2	20.2	10.1
	Min_Hr	7	3	7	6	6	6	6	6	7	7	7	7
	Max	26.6	27.3	41.0	41.2	44.8	44.1	35.5	39.3	39.2	39.6	38.2	29.3
	Max_Hr	14	14	14	12	14	15	13	14	14	14	14	14
1986	Min	7.7	10.0	16.0	20.7	27.2	28.8	28.4	27.5	25.5	19.7	13.5	9.2
	Min_Hr	7	7	6	6	6	6	6	6	6	7	7	7
	Max	24.9	28.4	34.7	41.3	45.7	43.7	40.2	38.2	39.1	38.8	32.8	25.4
	Max_Hr	14	14	14	14	14	14	13	13	13	13	13	14
1991	Min	10.7	12.0	18.5	20.9	27.5	29.7	27.8	27.4	25.3	19.1	13.3	10.3
	Min_Hr	7	7	6	6	6	6	6	6	6	6	7	7
	Max	25.8	29.1	37.0	39.8	45.8	44.0	38.0	36.9	39.9	38.5	33.1	28.5
	Max_Hr	14	14	14	14	14	14	14	14	14	14	14	14
1998	Min	8.4	12.4	15.0	23.2	28.0	29.6	28.8	27.8	26.9	21.9	15.0	9.5
	Min_Hr	8	7	7	6	6	6	6	6	6	6	7	6
	Max	24.2	28.8	33.2	41.6	45.5	42.3	38.5	36.3	37.3	34.2	30.8	25.1
	Max_Hr	14	14	14	15	14	13	15	14	14	13	14	14
1999	Min	10.1	12.2	17.0	22.6	28.1	28.8	29.2	28.3	26.8	20.5	13.9	8.8
	Min_Hr	7	6	6	6	6	6	6	6	7	7	7	7
	Max	23.2	30.1	39.3	46.3	46.4	45.2	42.0	41.6	39.7	39.3	35.4	27.7
	Max_Hr	14	14	14	14	14	14	14	14	13	13	14	14
2002	Min	9.4	11.7	17.3	23.9	28.9	30.2	31.8	28.5	25.1	21.4	14.9	10.5
	Min_Hr	7	7	7	7	6	6	6	6	7	7	7	7
	Max	24.9	29.8	37.3	44.2	46.6	43.9	44.2	37.9	36.5	37.8	32.1	26.7
	Max_Hr	14	14	14	14	15	15	13	14	14	14	14	14
2006	Min	9.9	16.1	28.8	24.3	28.8	28.8	29.2	28.1	26.3	21.8	15.3	11.4
	Min_Hr	7	7	6	7	6	6	6	6	7	7	7	7
	Max	26.7	33.4	44.7	42.9	44.7	42.1	39.0	39.5	38.8	38.0	32.7	26.6
	Max_Hr	14	14	14	14	14	14	15	14	14	14	14	14
2009	Min	10.4	12.6	17.1	23.6	27.3	29.9	29.5	28.3	26.1	20.1	14.4	10.2
	Min_Hr	8	7	7	7	6	6	6	6	7	7	7	7
	Max	26.4	31.5	37.5	44.4	45.8	47.1	40.8	39.9	38.6	37.4	30.7	27.6
	Max_Hr	14	14	14	14	14	14	14	14	14	14	14	14
2011	Min	8.1	12.5	17.2	22.3	28.5	27.7	28.6	27.9	25.5	21.3	16.1	9.1
	Min_Hr	8	8	7	7	6	6	6	6	7	7	7	7
	Max	23.2	29.5	36.6	41.9	44.7	40.2	38.5	37.1	36.0	37.8	32.6	27.6
	Max_Hr	15	14	14	14	15	14	14	14	14	14	14	14
2013	Min	8.5	13.2	17.4	23.2	27.9	29.4	29.1	28.2	27.3	23.0	14.1	11.0
	Min_Hr	7	7	7	6	6	6	6	7	7	7	7	7
	Max	23.8	28.7	36.8	43.0	47.4	42.5	39.3	37.5	39.6	37.4	31.3	27.0
	Max_Hr	14	14	14	14	14	14	14	13	14	14	14	14
2014	Min	10.5	11.8	17.2	22.1	30.6	30.1	28.9	28.8	27.0	22.0	14.2	9.9
	Min_Hr	7	7	7	6	6	6	6	6	7	7	7	7
	Max	24.1	28.1	34.7	41.7	45.1	45.0	40.4	40.2	39.6	38.2	33.0	25.8
	Max_Hr	14	14	14	14	15	14	14	14	14	14	14	14

Table 7.47: Simulated peak values of monthly average hourly surface temperature for Scenario-B for Safdarjung area

Year	Time	Jan	Feb	Mar	Apr	May	Jun	Jul	Aug	Sep	Oct	Nov	Dec
1973	Min	8.7	12.6	15.7	24.1	27.6	30.2	28.2	26.6	25.9	20.1	12.5	8.1
	Min_Hr	8	7	7	6	6	6	6	6	7	7	7	8
	Max	27.6	31.8	38.0	46.3	46.9	44.8	40.7	36.6	40.4	39.1	34.2	25.1
	Max_Hr	14	14	14	13	13	14	14	14	13	14	14	14
1977	Min	8.7	12.6	15.7	24.1	27.6	30.2	28.2	26.6	25.9	20.1	12.5	8.1
	Min_Hr	8	7	7	6	6	6	6	6	7	7	7	8
	Max	27.6	31.8	38.0	46.3	46.9	44.8	40.7	36.6	40.4	39.1	34.2	25.1
	Max_Hr	14	14	14	13	13	14	14	14	13	14	14	14
1986	Min	8.7	12.6	15.7	24.1	27.6	30.2	28.2	26.6	25.9	20.1	12.5	8.1
	Min_Hr	8	7	7	6	6	6	6	6	7	7	7	8
	Max	27.6	31.8	37.9	46.3	46.9	44.8	40.7	36.5	40.4	39.1	34.2	25.1
	Max_Hr	14	14	14	13	13	14	14	14	13	14	14	14
1991	Min	8.7	12.6	15.7	24.1	27.6	30.2	28.2	26.6	25.9	20.1	12.5	8.1
	Min_Hr	8	7	7	6	6	6	6	6	7	7	7	8
	Max	27.6	31.8	37.9	46.3	46.9	44.8	40.7	36.5	40.3	39.1	34.2	25.1
	Max_Hr	14	14	14	13	13	14	14	14	13	14	14	14
1998	Min	8.6	12.6	15.7	24.1	27.6	30.2	28.2	26.6	25.9	20.1	12.5	8.1
	Min_Hr	8	7	7	6	6	6	6	6	7	7	7	8
	Max	27.6	31.7	37.9	46.2	46.8	44.7	40.6	36.5	40.3	39.0	34.2	25.0
	Max_Hr	14	14	14	13	13	14	14	14	13	14	14	14
1999	Min	8.7	12.6	15.7	24.1	27.6	30.2	28.2	26.6	25.9	20.1	12.5	8.1
	Min_Hr	8	7	7	6	6	6	6	6	7	7	7	8
	Max	27.6	31.7	37.9	46.2	46.9	44.8	40.7	36.5	40.3	39.1	34.2	25.0
	Max_Hr	14	14	14	13	13	14	14	14	13	14	14	14
2002	Min	8.7	12.6	15.7	24.1	27.6	30.2	28.2	26.6	25.9	20.1	12.5	8.1
	Min_Hr	8	7	7	6	6	6	6	6	7	7	7	8
	Max	27.7	31.8	38.0	46.3	47.0	44.9	40.8	36.6	40.4	39.2	34.3	25.1
	Max_Hr	14	14	14	13	13	14	14	14	13	14	14	14
2006	Min	8.7	12.6	15.7	24.1	30.2	28.2	26.6	25.9	20.1	12.5	8.1	8.1
	Min_Hr	8	7	7	6	6	6	6	7	7	7	8	8
	Max	27.7	31.8	38.0	46.4	44.9	40.8	36.6	40.4	39.2	34.3	25.1	25.1
	Max_Hr	14	14	14	13	14	14	14	13	14	14	14	14
2009	Min	8.7	12.6	15.7	24.1	27.6	30.2	28.2	26.6	25.9	20.1	12.5	8.1
	Min_Hr	8	7	7	6	6	6	6	6	7	7	7	8
	Max	27.7	31.8	38.0	46.4	47.0	44.9	40.8	36.6	40.4	39.2	34.3	25.1
	Max_Hr	14	14	14	13	13	14	14	14	13	14	14	14
2011	Min	8.7	12.6	15.8	24.1	27.7	30.3	28.3	26.7	26.0	20.1	12.5	8.1
	Min_Hr	8	7	7	6	6	6	6	6	7	7	7	8
	Max	27.8	31.9	38.2	46.5	47.1	45.0	40.9	36.7	40.6	39.3	34.4	25.2
	Max_Hr	14	14	14	13	13	14	13	14	13	14	14	14
2013	Min	8.7	12.6	15.7	24.1	27.6	30.2	28.2	26.6	25.9	20.1	12.5	8.1
	Min_Hr	8	7	7	6	6	6	6	6	7	7	7	8
	Max	27.8	31.9	38.1	46.5	47.1	45.0	40.9	36.7	40.5	39.3	34.4	25.2
	Max_Hr	14	14	14	13	13	14	13	14	13	14	14	14
2014	Min	8.7	12.6	15.7	24.1	27.6	30.2	28.2	26.6	25.9	20.1	12.5	8.1
	Min_Hr	8	7	7	6	6	6	6	6	7	7	7	8
	Max	27.8	31.9	38.2	46.5	47.1	45.0	40.9	36.7	40.6	39.3	34.4	25.2
	Max_Hr	14	14	14	13	13	14	13	14	13	14	14	14

Table 7.48: Simulated peak values of monthly average hourly surface temperature for Scenario-C for Safdarjung area

Year	Time	Jan	Feb	Mar	Apr	May	Jun	Jul	Aug	Sep	Oct	Nov	Dec
1973	Min	8.7	12.6	15.7	24.1	27.6	30.2	28.2	26.6	25.9	20.1	12.5	8.1
	Min_Hr	8	7	7	6	6	6	6	6	7	7	7	8
	Max	27.6	31.8	38.0	46.3	46.9	44.8	40.7	36.6	40.4	39.1	34.2	25.1
	Max_Hr	14	14	14	13	13	14	14	14	13	14	14	14
1977	Min	8.3	5.1	15.9	22.5	24.4	27.3	26.6	27.2	27.3	20.2	20.2	10.1
	Min_Hr	7	3	7	6	6	6	6	6	7	7	7	7
	Max	26.6	27.3	40.9	41.2	44.8	44.1	35.5	39.3	39.2	39.5	38.2	29.3
	Max_Hr	14	14	14	12	14	15	13	14	14	14	14	14
1986	Min	7.9	12.3	16.3	21.4	26.8	28.6	30.3	27.4	25.8	18.3	13.3	10.2
	Min_Hr	8	7	6	6	6	6	6	6	6	7	6	7
	Max	25.9	29.4	35.5	41.5	45.4	43.5	41.4	37.2	39.1	32.2	31.9	27.0
	Max_Hr	14	14	14	14	14	14	14	14	15	15	13	14
1991	Min	10.7	12.0	18.5	20.9	27.5	29.7	27.8	27.4	25.3	19.1	13.3	10.3
	Min_Hr	7	7	6	6	6	6	6	6	6	6	7	7
	Max	25.8	29.2	37.0	39.8	45.8	44.0	38.0	36.9	40.0	38.6	33.1	28.5
	Max_Hr	14	14	14	14	14	14	14	14	14	14	14	14
1998	Min	8.4	12.4	15.1	23.2	28.0	29.6	28.8	27.8	27.0	21.9	15.0	9.5
	Min_Hr	8	7	7	6	6	6	6	6	6	6	6	7
	Max	24.3	28.9	33.3	41.6	45.6	42.4	38.6	36.4	37.3	34.3	30.8	25.2
	Max_Hr	14	14	14	13	14	13	15	14	14	13	14	14
1999	Min	10.1	12.2	17.0	22.6	28.1	28.8	29.2	28.3	26.8	20.5	13.9	8.8
	Min_Hr	7	6	6	6	6	6	6	6	7	7	7	7
	Max	23.2	30.2	39.3	46.3	46.5	45.2	42.1	41.7	39.8	39.3	35.4	27.8
	Max_Hr	14	14	14	14	14	14	14	14	13	13	14	14
2002	Min	9.4	11.7	17.3	23.9	28.9	30.2	31.8	28.5	25.1	21.4	14.9	10.5
	Min_Hr	7	7	7	7	6	6	6	6	7	7	7	7
	Max	24.9	29.7	37.2	44.2	46.5	43.9	44.2	37.9	36.5	37.8	32.0	26.7
	Max_Hr	14	14	14	14	15	15	13	14	14	14	14	14
2006	Min	9.9	16.1	17.9	24.3	28.8	28.8	29.2	28.1	26.3	21.8	15.3	11.4
	Min_Hr	7	7	7	7	6	6	6	6	7	7	7	7
	Max	26.7	33.4	35.0	42.9	44.6	42.0	39.0	39.5	38.8	37.9	32.7	26.5
	Max_Hr	14	14	14	14	14	14	15	14	14	14	14	14
2009	Min	10.4	12.6	17.1	23.6	27.3	29.9	29.5	28.3	26.1	20.1	14.4	10.2
	Min_Hr	8	7	7	7	6	6	6	6	7	7	7	7
	Max	26.3	31.4	37.4	44.3	45.7	47.1	40.8	39.9	38.6	37.4	30.7	27.5
	Max_Hr	14	14	14	14	14	14	14	14	14	14	14	14
2011	Min	8.1	12.4	17.2	22.3	28.5	27.7	28.6	27.9	25.5	21.3	16.0	9.0
	Min_Hr	8	8	7	7	6	6	6	6	7	7	7	7
	Max	23.1	29.3	36.4	41.7	44.6	40.0	38.3	36.9	35.9	37.7	32.5	27.5
	Max_Hr	15	14	14	14	15	14	14	14	14	14	14	14
2013	Min	8.5	13.2	17.4	23.2	27.9	29.4	29.1	28.2	27.3	23.0	14.1	11.0
	Min_Hr	7	7	7	6	6	6	6	7	7	7	7	7
	Max	23.7	28.6	36.6	42.8	47.2	42.3	39.2	37.3	39.5	37.2	31.2	26.9
	Max_Hr	14	14	14	14	14	14	14	13	14	14	14	14
2014	Min	10.5	11.8	17.2	22.1	30.6	30.1	28.9	28.8	27.0	22.0	14.2	9.9
	Min_Hr	7	7	7	6	6	6	6	6	7	7	7	7
	Max	24.0	28.0	34.5	41.5	45.0	44.9	40.3	40.0	39.5	38.0	32.9	25.6
	Max_Hr	14	14	14	14	15	14	14	14	14	14	14	14

In Safdarjung area extreme values of minimum temperature is showing increasing trend in Scenarios A and C (Scenario-A: 2.8 to 4.4 ºC, Scenario-C: 2.8 to 4.4 ºC) and no change has been observed for Scenario-B from year 1973 to 2014. No specific trend has been observed in extreme values of maximum surface temperature in Scenario-A and C for Safdarjung area also (Table 7.49), whereas increasing trends have been observed in peak values of maximum monthly average hourly surface temperature in Scenario-B (52.55 to 53.76 ºC).

Results revealed increase in maximum surface temperature in Scenario-B and increase in minimum temperature in Scenario-A and C. Increase in extreme values and average monthly values in Scenario-B indicates effects of LULC changes in increasing the peak temperature over the years. Increasing trend in minimum surface temperature in Scenario-A and C indicates the effect of other than LULC change climate change forcing. Results are matching with inferences drawn in other related studies about change in surface temperature (Das et al., 2014; Mohan and Kandya, 2015).

Table 7.49: Extreme annual values of surface temperature for different scenario

Year	Data	Palam Area			Safdarjung Area		
		Scenario-A	Scenario-B	Scenario-C	Scenario-A	Scenario-B	Scenario-C
1973	Max	52.85	52.85	52.85	52.55	52.55	52.55
	Min	2.8	2.8	2.8	2.80	2.80	2.80
1977	Max	52.49	52.88	52.46	52.63	52.55	52.63
	Min	3.6	2.8	3.6	0.00	2.80	0.00
1986	Max	48.67	52.93	48.6	49.48	52.55	48.74
	Min	3.73	2.8	3.73	3.33	2.80	3.73
1991	Max	49.53	52.95	49.46	50.62	52.53	50.64
	Min	4.03	2.8	4.03	5.00	2.80	5.00
1998	Max	51.08	52.96	50.97	51.99	52.45	52.08
	Min	5.5	2.8	5.5	4.06	2.80	4.07
1999	Max	50.13	52.97	50.03	51.96	52.49	52.02
	Min	5	2.8	5	5.00	2.80	5.00
2002	Max	50.22	52.93	50.16	51.91	52.60	51.88
	Min	6.1	2.8	6.1	6.37	2.80	6.37
2006	Max	49.74	52.97	49.64	49.82	52.63	49.77
	Min	3.1	2.8	3.1	3.10	2.80	3.10
2009	Max	53.6	53.07	53.43	52.18	52.61	52.13
	Min	5.9	2.8	5.9	5.00	2.80	5.00
2011	Max	50.72	53.09	50.53	49.55	52.77	49.37
	Min	4.9	2.8	4.9	3.40	25.73	3.40
2013	Max	52.45	53.1	52.26	50.88	52.73	50.76
	Min	2.4	2.8	2.4	3.80	2.80	3.80
2014	Max	51.35	53.12	51.17	50.51	52.76	50.36
	Min	3.2	3	3.2	4.40	2.80	4.40

7.6 QUANTITATIVE RELATIONSHIPS BETWEEN LULC AND SURFACE ENERGY BALANCE FLUXES

To investigate the relationship between LULC and surface energy fluxes, linear and non-linear regression techniques have been used. Quantitative relationship has been tried between LULC fractions and surface energy balance fluxes in corresponding years. The proposed null hypothesis is that there is no association existing between LULC and surface energy fluxes. Scenario-A to Scenario-C has been examined to determine the most significant relationship available between peak values of annual minimum and maximum hourly values of surface energy fluxes and LULC fractions.

In Scenario-B statistically significant relationship between LULC fractions and surface energy fluxes has been found whereas not statistically significant relationship has been found for Scenarios A and C. In this study, dependent variables are the annual minimum and maximum hourly values of net all-wave radiation, storage heat flux, sensible heat flux and latent heat flux. Independent variables are built-up area fractions (B), vegetation area fractions (V), open area fractions (O) and water body area fractions (W). In the beginning, different forms of the mathematical models/ distributions i.e., linear, power, exponential, and logarithmic have been tried to identify the form of relationship between LULC fractions and surface energy balance fluxes. The statistically significant relationships found for the Scenario-B have been shown in Table 50 and Table 51. Quantitative relationships have been determined for both the study areas when dependent variable was storage heat flux and net all-wave radiation. For Palam station, two strong relationship which are non-linear in nature have been identified based on the coefficient of determination (R^2) and error statistics (Standard errors, SSE and RMSE).

The relationship between minimum annual net all-wave radiation (Q*) (Table 51) is dependent variable and independent variables are B and V respectively. R^2 is very high for both relationships (0.94, 0.98) and very low error statistics (Standard errors, SSE and RMSE) have been found and therefore, rejecting the null hypothesis. According to the established relationships, when build-up fraction increases, Q* decreases because due to urbanization high albedo values are converted into low albedo values resulting less outflow of radiation and leading to reduction in net all-wave radiation. Also urbanization leads to conversion of high emissivity surface in to low emissivity surface which result in reduction in outflow of radiation from surfaces, result in increase in storage heat flux and reduction in net all-wave radiation. Therefore,

restricting the outward radiations in night (Y Das et al., 2009b; Grimmond & Oke, 1999). However, when vegetation fraction decreases Q* is also decreasing (Kurn, Bretz, Larsen, 2015; Simpson et al., 2011) . Two other strong associations were found, that are, annual minimum value of annual minimum hourly storage heat flux (ΔQS) (Table 50) with built-up fractions and annual maximum hourly value of storage heat flux (ΔQS) with vegetation fractions. According to the results when built-up fraction increases, (ΔQS) increases because the high thermal conductivity of the concrete surfaces allow the surface to respond rapidly and conduct more heat. Due to the deficiency of ground heat, during daytime ground heat storage is very high which supports the large negative ground heat fluxes at night and relatively high night time surface temperature is maintained (Cayan and DOUGLAS, 1984).When vegetation fraction increases (ΔQS) (Table 50) decreases because vegetation have low emissivity and high albedo which means less absorption and more reflection of radiation (Gillner et al., 2015; Larsen, 2015; Simpson et al., 2011). In both associations, R^2values are very high (0.95, 0.95) and very low error statistics (Standard errors, SSE and RMSE) and therefore, rejecting the null hypothesis.

For Safdarjung station, strong significant relationship has been found when dependent variable was min_ annual (Q*) and when independent variables were B and V respectively. The R^2value is very high for both associations (0.88, 0.89) and very low error statistics (Standard errors, SSE and RMSE) have been found and therefore, rejecting the null hypothesis. According to the established relationships, when build-up fraction increases, min_ annual (Q*) (Table 51) decreases because outward radiation at night would be less whereas when vegetation fraction increases, min_ annual (Q*) increases due to the cooling effect (Yashvant Das, 2015; Gillner et al., 2015; Kalyanapu, Burian, & McPherson, 2009; Larsen, 2015). Two other strong associations were found, that are, min_ annual (ΔQS) with B and, max_ annual (ΔQS) with V. According to the results, when built-up fraction increases, min_ annual (ΔQS) increases because in night time ground heat flux is negative which implies that heat is transferring in the outer surface but it is still less than net radiation. Therefore, resulting in negative storage flux (Cayan and DOUGLAS, 1984). When vegetation fraction increases, max_ annual (ΔQS) decreases because vegetation releases or dissipates this energy load in the form of latent heat flux rather than sensible heat flux (Offerle et al., 2006)**.** In both associations, $R^2$is very high (0.98, 0.93) and very low error statistics (Standard errors, SSE and RMSE) have been found and therefore, rejecting the null hypothesis. To test

the prediction accuracy of established equations, two equations have been selected with highest R^2 from Table 7.50 and Table 7.51 respectively. The first selected equation is when dependent variable is min_annual(ΔQS) and independent variable is B for Safdarjung station. The values are predicted using the equation and the actual and predicted values are plotted in Figure 7.49. Maximum number of predicted values are well matched and one outliner has been identified.

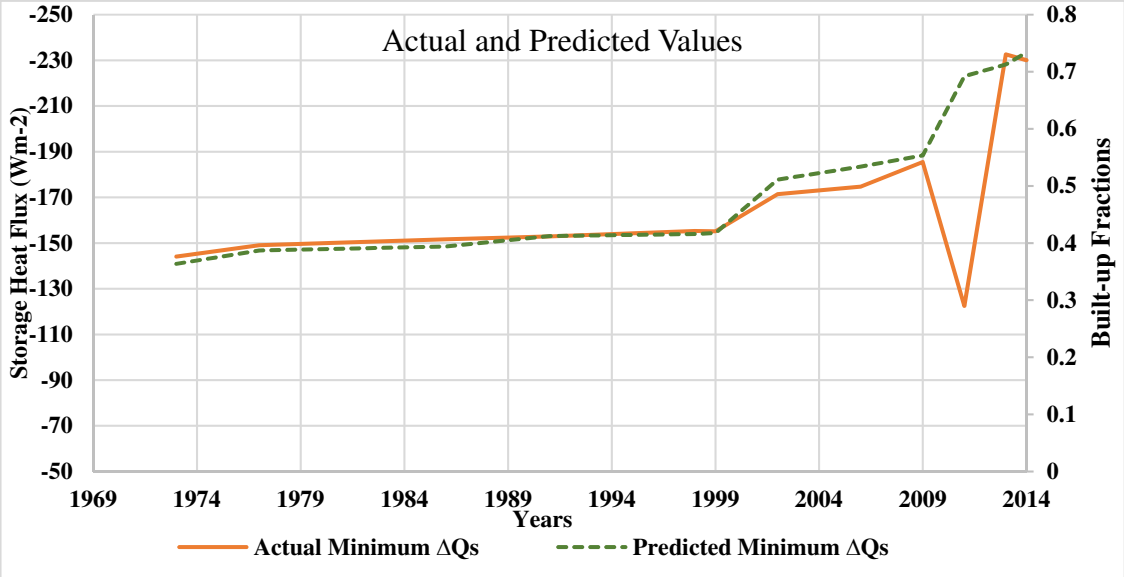

Figure 7.49: Actual and predicted values of minimum ΔQS for Safdarjung station

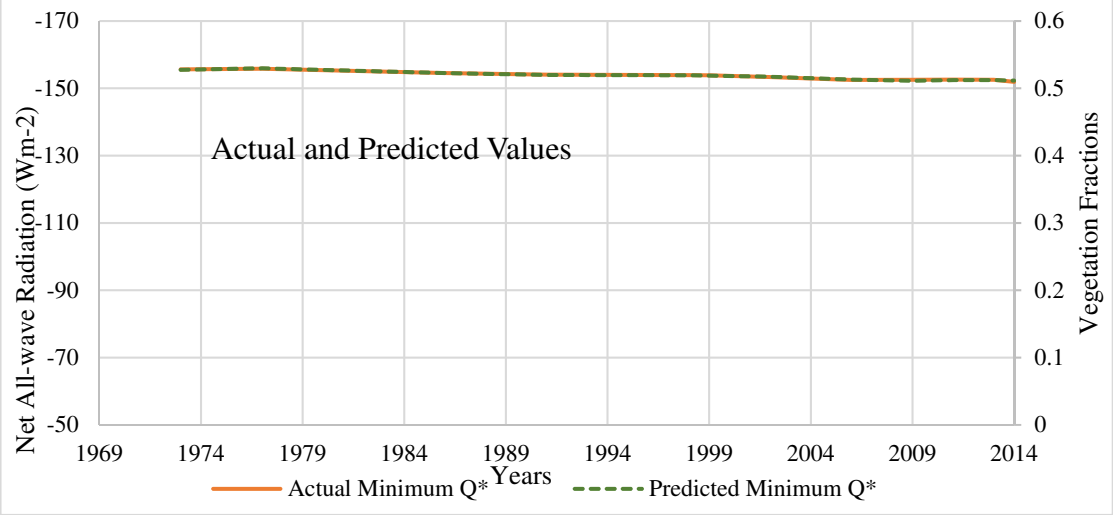

Figure 7.50: Actual and predicted values of minimum Q* for Palam station

The second selected equation is when dependent variable is min_annual(Q*) and independent variable is V for Palam station. The values are predicted using the equation and the actual and predicted values are plotted in Figure 7.50. All predicted values have well matched.

Table 7.50: Linear and non-linear regression analysis for storage heat flux (Scenario-B)

Storage Heat Flux: Scenario-B	Dependent Variable	Independent Variable	Type of Equation	form of Equation	Equation	Correlation Coefficient R-squared (R2)	Standard Error (pr1, pr2)	Sum of Squared Errors of Prediction (SSE)	Root Mean Squared Error (RMSE)
(Safdarjung Station)	min_annual (ΔQS)	B	Exponential	Y = pr1*Exp(pr2*X1)	t3 =-106.633*Exp(1.055*B)	0.98	2.636, 0.044	230.73	4.803
	max_annual (ΔQS)	V	Logarithmic	Y =pr1*Log10(X1)+pr2	t4 = -215.714*Log10(V)+153.466	0.93	19.311,7.754	642.59	8.016
(Palam Station)	min_annual (ΔQS)	B	Non-linear	Y = pr1*(X1^pr2)	t3 = -248.078*(B^0.381)	0.95	6.596,0.381	546.35	7.392
	max_annual (ΔQS)	V	Non-linear	Y = pr1*(X1^pr2)	t4 = 156.894*(V^-0.340)	0.95	5.157,0.026	322.15	5.675

Table 7.51: Linear and non-linear regression analysis for net all-wave radiation (Scenario-B)

Net all-wave radiation: Scenario-B	Dependent Variable	Independent Variable	Type of Equation	form of Equation	Equation	Correlation Coefficient R-squared (R2)	Standard Error (pr1, pr2)	Sum of Squared Errors of Prediction (SSE)	Root Mean Squared Error (RMSE)
(Safdarjung Station)	min_annual (Q*)	B	Logarithmic	Y = pr1*Ln(X1)+pr2	t3 = 3.211*Ln(B)-157.294	0.88	0.379,0.338	2.140	0.463
	min_annual (Q*)	V	Logarithmic	Y = pr1*Ln(X1)+pr2	t3 = -4.133*Ln(v)-163.576	0.89	0.457,0.422	1.905	0.436
(Palam Station)	min_annual (Q*)	B	Exponential	Y = pr1*Exp(pr2*X1)	t3 = -156.844*Exp(-0.047*B)	0.94	0.280,0.004	1.098	0.331
	min_annual (Q*)	V	Exponential	Y = pr1*Exp(pr2*X1)	t3 = -149.435*Exp(0.088*V)	0.98	0.187,0.004	0.333	0.183

7.7 CONCLUDING REMARKS

In this chapter, conceptualization of SUEWS model for our study area have been performed. To determine the model results sensitivity to selected model coefficients/parameters, sensitivity analysis has been performed. The results of sensitivity analysis have been used to determine most significant input parameters such as albedo and emissivity, so that model generated surface energy components have less uncertainty. Further, model was calibrated by running model iteratively for a range of input parameters and comparing simulated and observed SEB fluxes. Thereafter, validation of the model generated results have been performed by comparing these results by measured values of different surface energy components at different sites in Delhi for year 1998 and 1999. This comparison, have shown similar trend in modelled as well as measured values of fluxes at different temporal scales. Therefore, the model generated results have been successfully validated. Further, three scenarios, that are Scenario-A, Scenario-B and Scenario-C have been conceptualized to study the impact of LULC changes on SEB of the area. According to the results, the most significant change in fluxes have been observed in Scenario-B, where LULC changes over the years were considered while simulating the SEB for different years. Urbanization leads to conversion of pervious and vegetative surfaces into paved & impervious surfaces which leads to increase in storage heat flux, and surface temperature over the years, which indicates change in micro-climate of the study areas. In other Scenarios less significant change in fluxes have been observed which may be due to gradual effect of concentration of greenhouse gases and meteorology on surface energy components. Further empirical equations have been developed to establish relationship between LULC fractions and SEB fluxes, representing micro-climate of an area. The linear and non-linear association of components of surface energy with LULC classes have been determined and these equations can be used for the quantification of fluxes for the study area. In future, these proposed equations can be used in planning of adaptation measures for minimizing the impact of change in LULC on micro-climate.

Therefore, study has been successful in determining the relative impacts of LULC changes of micro-climate of study areas in term of changes in SEB fluxes and surface temperature. Also empirical equations have been developed to quantify the SEB fluxes corresponding to changes in LULC fractions.

CHAPTER 8

LAND USE/LAND COVER CHANGE ADAPTATION MEASURES

8.1 INTRODUCTION

In recent years, land use/land cover (LULC) changes are responsible for change in thermal heat fluxes, evapotranspiration and the exchange of greenhouse gasses from plants and soil into the atmosphere (Prentice et al., 2001) and thus causing rise in surface temperature. Additionally, changes in land cover due to rapid and unplanned urbanization affects the ecology, hydrology and thermal comfort of peoples (Bookhagen and Burbank, 2006; Sarkar et al., 2007). LULC changes due to urbanization affect local surface energy balance by changing the amount of solar energy reflected, the magnitude & duration over which absorbed energy is released as heat, and the amount of energy that is diverted to non-heating fluxes through evaporation consequently impact local climate adversely. To control these adverse effects of LULC changes, various measures have been proposed. Since, mitigation of LULC changes is not possible, there is a need for effective adaptation measures to minimize these harmful effects. Today, adaptation measures are very critical because increasing demands of people for better facilities is causing will cause continuous change in LULC. One of the most widely used adaptation measure is increase in vegetation in urban areas which reduces both urban air temperature and land surface temperature (Kurn et al., 1994; Weng and Yang, 2004; Simpson, et al., 2011; Gillner et al., 2015; Larsen, 2015).

Other measure includes wetting streets and roofs, open water and fountains, high albedo pavement instead of asphalt, constructing optimal shading in buildings, compact building and trees, warning systems, monitoring and inspection. Such changes in land surfaces will affects the local surface energy balance. Till now, qualitative methods have been proposed to minimize these adverse effects but these methods are incapable to determine how much change is required to minimize a specified quantity of heat flux components. Therefore, quantitative methods for adaptation are required to overcome this limitation (Grawe et al., 2007; Skelhorn et al., 2014; Klemm et al., 2015). Therefore, understanding the link between urbanization and micro-climate is vital for urban environmental sustainability to determine effective design strategies, e.g. altering the LULC like increasing vegetation and enhancing irrigation regime, using more reflective paved surfaces and materials in order to improve urban climate. The knowledge of how to

purposefully manipulate the SEB by changing urban land cover is crucial to urban climate adaptation.

In the present study, investigation of adverse effects of LULC has been performed. Additionally, potential of purposeful LULC alteration as possible adaptation measures have been investigated by determining how such alteration will change the SEB of an area. Different such adaptations measures have been explored and their performance in favorably altering the SEB fluxes have been quantified to identify a set of optimum measures for Palam areas. Study of adaptation has been done for Palam area corresponding the year 2014. This is performed by altering LULC classes like barren to forest, barren to water, partial covering of built-up surface to vegetation/grass and heat fluxes are simulated by using calibrated SEUWS model. Monthly relative changes in percentage of fluxes and surface temperature corresponding to different proposed adaptations have been quantified. Detailed results of adaptation study are presented below in subsequent sections.

8.2 QUANTIFICATION OF ADAPTATION MEASURES ON MICRO-CLIMATE

In this study, four cases of purposeful LULC transformation based adaptation measures have been proposed and their relative quantitative impact on SEB fluxes is determined. These four cases are Barren to Forest conversion (Case-1) in different percentages, barren to water (Case-2), building roof tops to vegetation (Case-3) and all three possible conversions considered simultaneously (mix land use class) (Case-4). The monthly relative % changes in hourly SEB fluxes and surface temperature as compared to actual condition with original land use class at different percentages (10%, 25% and 50%) have been quantified through simulations using SUEWS model and presented in Figures 8.1 to 8.15. Peak values during night time (negative values) and day time (positive) monthly average hourly fluxes for different Cases have been presented in Tables 8.1 to 8.5. Results are discussed in detail in the following sections.

8.2.1 Net All-Wave Radiation

Net all-wave radiation is the aggregation of storage heat flux, sensible heat flux and latent heat flux minus anthropogenic heat flux. Therefore, changes in all these fluxes directly reflects in net all-wave radiation. Monthly average net all-wave radiation at hourly temporal scale has been calculated from hourly simulated results for night time (negative values) as well as day time (positive) at proposed 10%, 25% and 50% transformation in LULC classes, as per the proposed adaptation measures in different Cases i.e., Case-1, Case-2, Case-3 and

Case-4. In Case-1, range of lowest values of net all-wave radiation occurring during night time (negative values) varies from -57.78 to -22.19 Wm^{-2} at 10%, -57.82 to -22.21 Wm^{-2} at 25% and -57.9 to -22.24 Wm^{-2} at 50% (Table 8.1) transformation level, as compared to (-57.78 to -21.40 Wm^{-2}) value in actual conditions of LULC. Also in Case-2, lowest values of net all-wave radiation during night time varies from -57.76 to -22.19 Wm^{-2} at 10%, -57.78 to -22.19 Wm^{-2} at 25% and -57.80 to -22.20 Wm^{-2} at 50% (Table 8.2) transformation level. Further, in Case 3, lowest values of net all-wave radiation at hourly time step obtained during night time has been found to vary from -57.81 to -22.21 Wm^{-2} at 10%, -57.91 to -22.24 Wm^{-2} at 25% and -58.07 to -22.31 Wm^{-2} at 50% (Table 8.3) level and in Case-4 lowest values of negative net all-wave radiation are varying from -57.87 to -22.23 Wm^{-2} at 10%, -58.06 to -22.30 Wm^{-2} at 25% and -58.38 to-22.43 Wm^{-2} at 50% (Table 8.1) transformation level.

In all cases of adaptations the highest negative value of net all-wave radiation (negative values obtained during night) are observed in the month of January and lowest negative value of minimum net all-wave radiation are observed in the month of August. In Case-4, lowest and highest value of negative values of net all-wave radiation has been observed when compared with other adaptation measures. When all measures are considered simultaneously (Case-4), lowest value of net all-wave radiation during night time (negative values) are increasing as compared to actual values (Table 8.1). Relative changes in percentage of net all-wave radiation during night time at 10%, 25% and 50% LULC transformations are shown in Figure 8.1, 8.2 and 8.3, respectively. The highest % increase in negative value of net all-wave radiation during night time has been found in Case-4 in the April month (-1.19 at 50%), as shown in Figure 8.3 and lowest % change (-0.03 at 10%) in monthly average hourly net all-wave radiation has been found in Case-2 in September month as shown in Figure 8.1.

Highest values of monthly average hourly net all-wave radiation occurring during day time in Case-1 varies from 473.64 to 275.01 Wm^{-2} at 10%, 474.68 to 275.63 Wm^{-2} at 25% and 476.36 to 276.65 Wm^{-2} at 50% level as compared to values in actual conditions of LULC (472.94 to 274.56 Wm^{-2}) as shown in Table 8.1, while in Case-2 values are varying from 473.66 to 275.03 Wm^{-2} at 10%, 474.74 to 275.68 Wm^{-2} at 25% and 476.49 to 276.75 Wm^{-2} at 50% (Table 8.2) level. Further, in Case 3 positive values of monthly average hourly net all-wave radiation obtained during day time varies from 470.88 to 273.31 Wm^{-2} at 10%, 467.77 to 271.38 Wm^{-2} at 25% and 462.60 to 268.18 Wm^{-2} at 50% level (Table 8.3) and in Case-4 values vary from 471.13 to 273.45 Wm^{-2} at 10%, 468.39 to

271.73 Wm^{-2} at 25% and 463.83 to 268.85 Wm^{-2} at 50% (Table 8.1) transformation level as compared to values in actual conditions of LULC (472.94 to 274.56 Wm^{-2}). In Case-1, Case-2, Case-3 and Case-4, the lowest value of positive net all-wave radiation (positive values obtained during day time) has been observed in the month of December and highest value of net all-wave radiation is observed in the month of April. Case-3 shows the lowest and Case-2 shows the highest value of positive net all-wave radiation when compared with other adaptation measures and values corresponding to actual condition without any adaptation (Table 8.1). When building to vegetation class conversion (Case-3) is considered, lowest value of positive net all-wave radiation in the month of January to June (279.76 to 470.88 Wm^{-2}) are increasing (rise in outward net radiation at daytime due to increase in surface from low albedo to higher albedo) (Baidya et al., 2003; Mahmood et al., 2010) whereas during October to December (402.11 to 268.18 Wm^{-2}) it is decreasing (reduction in outward net radiation at daytime).

Relative changes in percentage of values of net all-wave radiation corresponding to 10%, 25% and 50% proposed changes in LULC are shown in Figure 8.1, 8.2 and 8.3, respectively. The highest % change in value of positive net all-wave radiation as compared to values obtained in actual conditions without considering any adaptation has been obtained in September month for Case-3 (-2.54 at 50%) as shown in Figure 8.3. The lowest % change in value of positive net all-wave radiation w.r.t to values in actual condition has been found in the March month in Case-1 and Case-2 (-0.22 at 10%), as shown in Figure 8.1.

The four proposed adaptation measures have been analyzed and it has been found that in case of night time net all-wave radiation (negative values), barren to forest, building to vegetation and mixed land-use class (all possible conversions simultaneously) conversions (adaptation measures: Case-1, Case-3 and Case-4) have shown increasing trend in negative side of net all-wave radiation in all months (Table 8.1). This is happening due to proposed increase in vegetation cover having higher albedo result in increase in the outflow of radiation (Grawe et al., 2007; Klemm et al., 2015). However, in case of positive net all-wave radiation occurring during day time, barren to forest and barren to water adaptation measures (Case-1 and Case-2) have shown similar values in negative side of net all-wave radiation in all months. The decreasing trend in the reduction in negative values (obtained during night time) of net all-wave radiation has been observed in barren to water land use (LU) class conversion (adaptation measure: Case-2) due to increase in the net outflow of radiation (Figure 8.2). The decreasing trend in day time net all-wave radiation

(positive) has been observed in building to vegetation and mixed land use class conversion (adaptation measures: Case-3 and Case-4) due to transformation of impervious surface into pervious surfaces i.e., increase in high albedo surfaces (Table 8.1 and Figure 8.1 to 8.3). As shown in Table 8.1, negative values of net all-wave radiation occurring during night time are increasing from 10 to 50 % transformation in LULC classes thus showing that our proposed adaptation measures are effective (Figure 8.1 to 8.3). The most effective adaptation measure in case of lowest (negative) net all-wave radiation is the case-4, where all possible LULC transformations are considered simultaneously. Thus, increase in proportion of vegetation as compared to the other conversion classes is one of the possible effective adaptation measure. The most effective adaptation measure in case of day time (positive) net all-wave radiation is the conversion of building to vegetation (Case-3) because absorption of radiation is reduced due to change in surface characteristics. (Kurn et al., 1994; Weng and Yang, 2004; Simpson et al., 2011; Das, 2015; Gillner et al., 2015; Larsen, 2015).

8.2.2 Storage Heat Flux

In urban areas, storage heat flux plays a vital role in overall SEB and in impacting the urban climate. Increase in impervious and built-up surfaces due to urbanization, high emissivity & albedo LULC classes get converted into low emissivity and albedo values, which leads to increase in storage heat flux during day time and reduction in available energy for partitioning into sensible & latent heat fluxes, resulting increase in surface temperature and air temperature (Anuja; 2011; Noblet-Ducoudré et al., 2012; Yoshida et al., 2012, 2014). Monthly average storage heat flux at hourly temporal scale has been calculated from hourly simulated results obtained from calibrated SUEWS model for night time (negative values) as well as day time (positive) at proposed 10%, 25% and 50% transformation in LULC classes, as per the proposed adaptation measures in different Cases (Case-1 to 4).

In Case-1, range of lowest values of storage heat flux occurring during night time (negative values) varies from -100.26 to -63.1 Wm^{-2} at 10%, -99.27 to -62.49 Wm^{-2} at 25% and -97.69 to -61.53 Wm^{-2} at 50% (Table 8.2) transformation level, as compared to (-62.92 to -100.77 Wm^{-2}) value in actual conditions of LULC. Also in Case-2, lowest values of storage heat flux during night time varies from -100.77 to -63.37 Wm^{-2} at 10%, -100.56 to -63.17 Wm^{-2} at 25% and -100.33 to-62.92 Wm^{-2} at 50% (Table 8.2) transformation level.

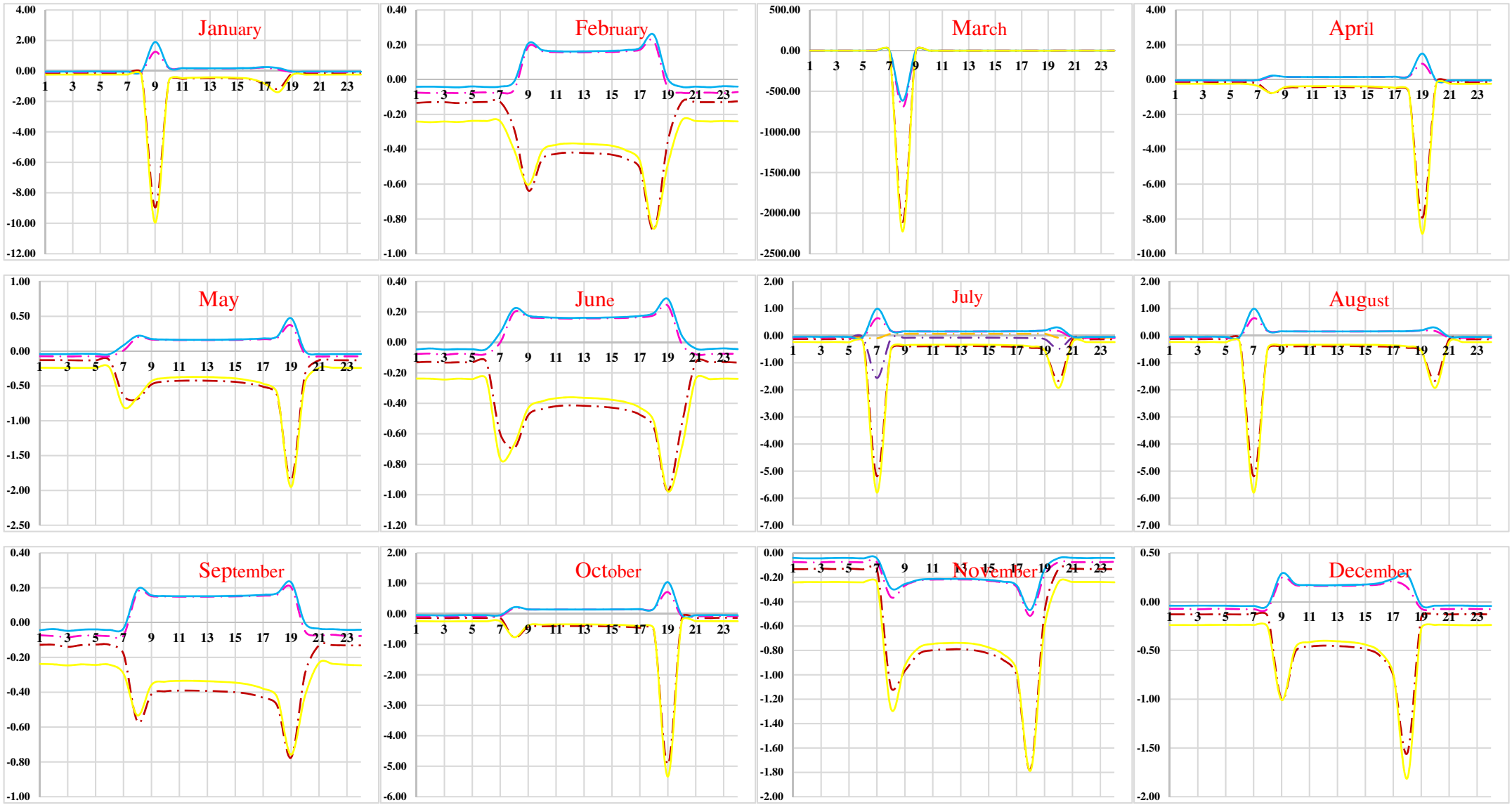

Building to Vegetation	Barren to Forest	Barren to water	Mixed Land Use	X-axis - Time in Hours
				Y-axis -% change in Net all-wave radiation

Figure 8.1 : Changes in net all-wave radiation (%) by transformation of LULC classes up to 10 % in different adaptation measures

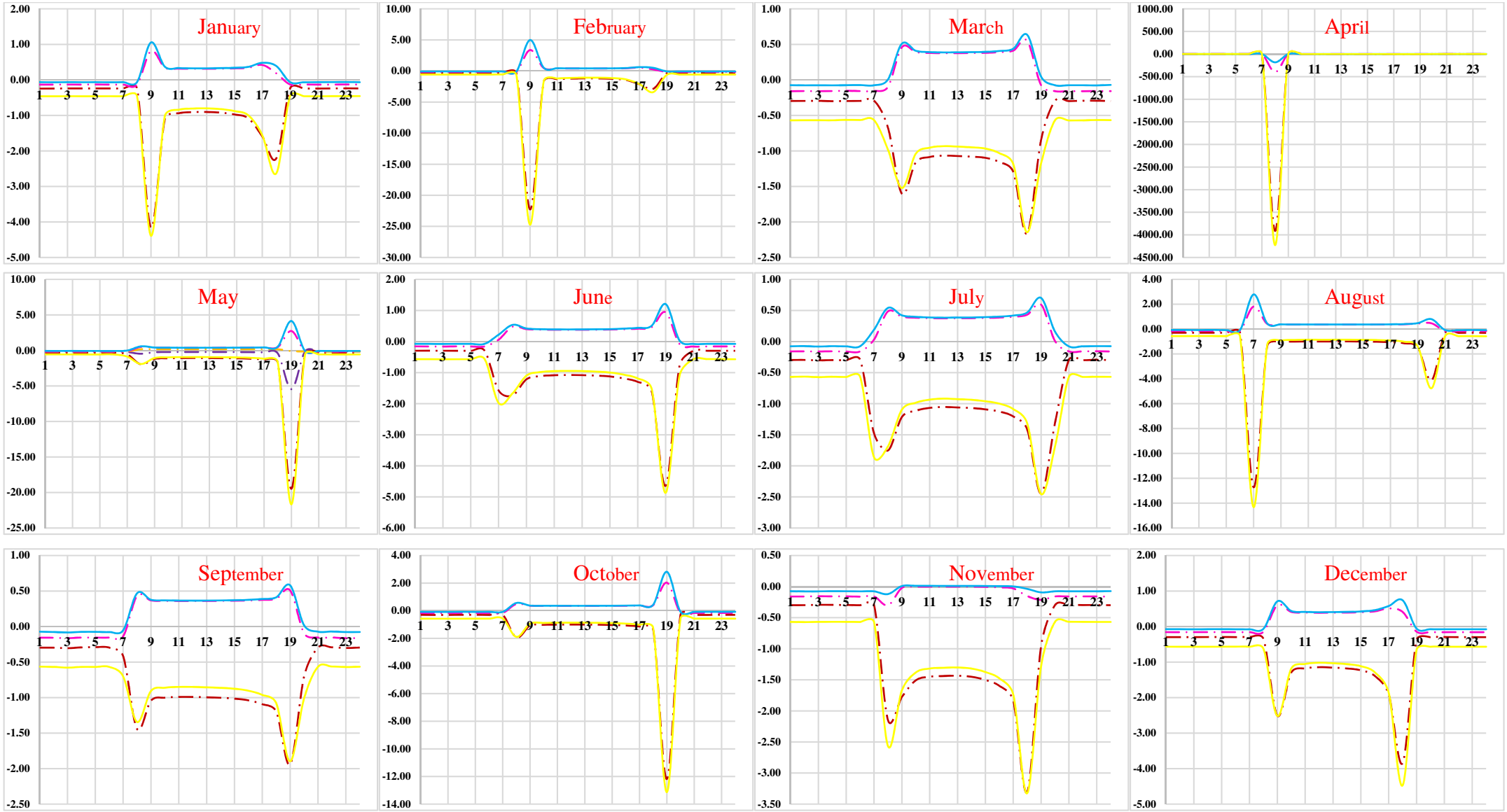

Building to Vegetation	Barren to Forest	Barren to water	Mixed Land Use	X-axis - Time in Hours
				Y-axis -% change in Net all-wave radiation

Figure 8.2 : Changes in net all-wave radiation (%) by transformation of LULC classes up to 25 % in different adaptation measures

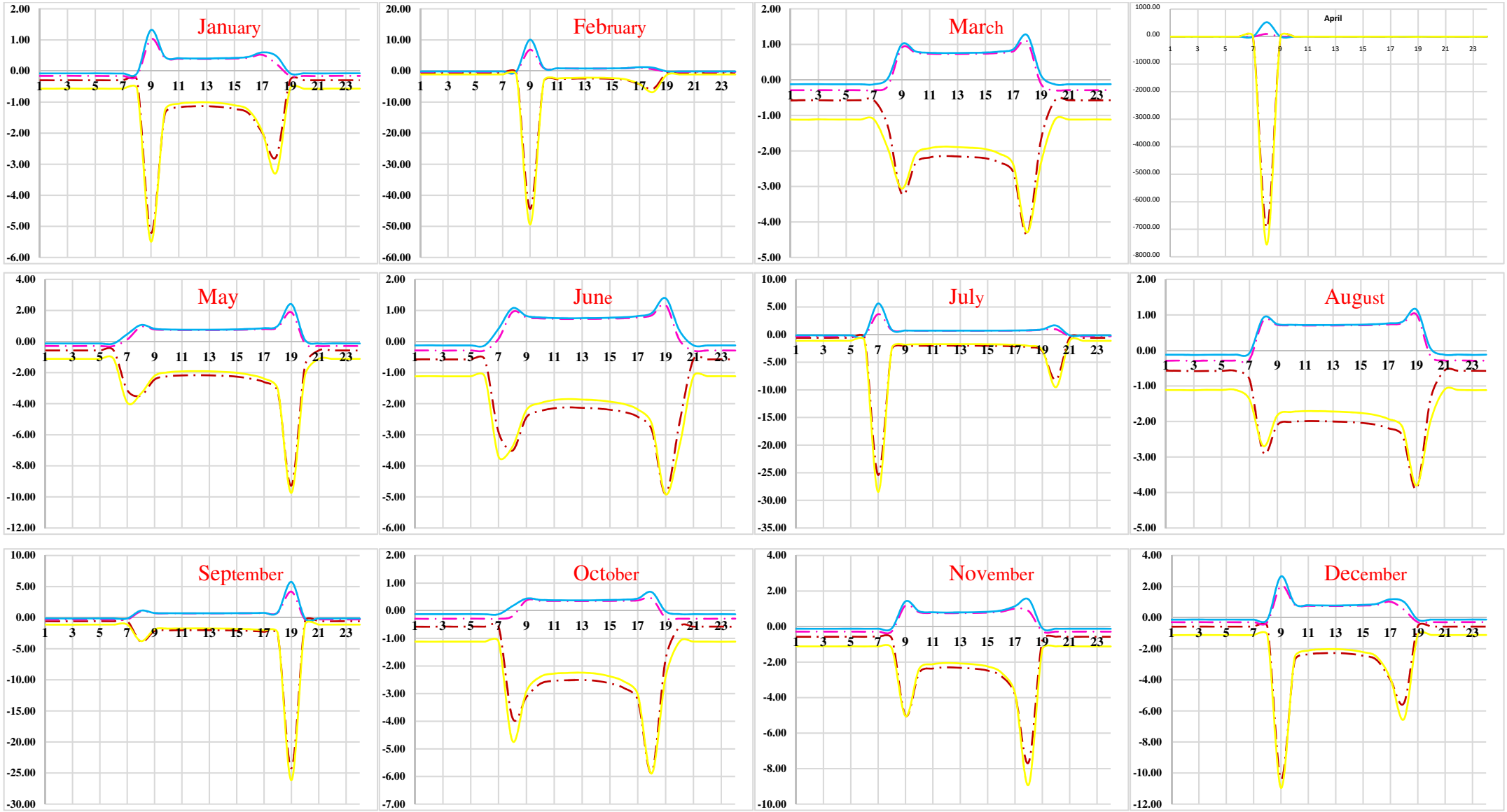

Building to Vegetation	Barren to Forest	Barren to water	Mixed Land Use	X-axis - Time in Hours
				Y-axis -% change in Net all-wave radiation

Figure 8.3 : Changes in net all-wave radiation (%) by transformation of LULC classes up to 50 % in different adaptation measures

Table 8.1 : Peak values of monthly average hourly net all-wave radiation (Wm^{-2}) corresponding to different adaption measures

Months	%	Original		Barren to Forest (Case-1)		Barren to water (Case 2)		Building Vegetation (Case-3)		Mixed Land Use (Case 4)	
		Max	Min	Max	Min	Max	Min	Max	Min	Max	Min
January	10	286.67	-57.73	287.14	-57.78	287.17	-57.76	285.31	-57.81	285.45	-57.87
	25	286.67	-57.73	287.81	-57.82	287.86	-57.78	283.23	-57.91	283.57	-58.06
	50	286.67	-57.73	288.88	-57.9	289.01	-57.8	279.76	-58.07	280.44	-58.38
February	10	373.92	-37.93	374.51	-37.96	374.53	-37.95	372.33	-37.98	372.53	-38.02
	25	373.92	-37.93	375.33	-37.99	375.38	-37.96	369.88	-38.05	370.37	-38.15
	50	373.92	-37.93	376.67	-38.05	376.77	-37.98	365.79	-38.15	366.77	-38.36
March	10	435.35	-45.35	434.38	-45.38	434.4	-45.37	431.87	-45.41	432.1	-45.46
	25	435.35	-45.35	435.33	-45.42	435.38	-45.38	429.05	-45.49	429.63	-45.61
	50	435.35	-45.35	436.87	-45.48	436.98	-45.41	424.35	-45.61	425.49	-45.86
April	10	472.94	-57.77	473.64	-57.81	473.66	-57.79	470.88	-57.85	471.13	-57.92
	25	472.94	-57.77	474.68	-57.86	474.74	-57.81	467.77	-57.96	468.39	-58.12
	50	472.94	-57.77	476.36	-57.93	476.49	-57.83	462.6	-58.15	463.83	-58.46
May	10	452.49	-50.09	453.21	-50.13	453.23	-50.11	450.54	-50.16	450.77	-50.21
	25	452.49	-50.09	454.21	-50.17	454.27	-50.13	447.53	-50.24	448.12	-50.37
	50	452.49	-50.09	455.84	-50.23	455.97	-50.15	442.51	-50.38	443.68	-50.65
June	10	421.33	-46.72	422	-46.76	422.01	-46.74	419.56	-46.79	419.78	-46.84
	25	421.33	-46.72	422.92	-46.8	422.96	-46.76	416.82	-46.86	417.38	-46.99
	50	421.33	-46.72	424.41	-46.86	424.52	-46.78	412.26	-46.99	413.38	-47.25
July	10	383.99	-21.4	384.58	-21.42	384.59	-21.41	382.5	-21.43	382.71	-21.46
	25	383.99	-21.4	385.39	-21.44	385.42	-21.42	380.18	-21.47	380.72	-21.53
	50	383.99	-21.4	386.71	-21.47	386.76	-21.43	376.31	-21.53	377.39	-21.64
August	10	371.37	-22.18	371.92	-22.19	371.94	-22.19	369.9	-22.21	370.11	-22.23
	25	371.37	-22.18	372.71	-22.21	372.74	-22.19	367.65	-22.24	368.16	-22.3
	50	371.37	-22.18	373.99	-22.24	374.04	-22.2	363.89	-22.31	364.92	-22.43
September	10	369.41	-39.28	368.6	-39.31	368.62	-39.29	366.46	-39.33	366.65	-39.37
	25	369.41	-39.28	369.41	-39.34	369.45	-39.31	364.05	-39.39	364.54	-39.5
	50	369.41	-39.28	370.72	-39.39	370.82	-39.32	360.04	-39.5	361.01	-39.72
October	10	403.74	-28.05	404.31	-28.08	404.32	-28.06	402.11	-28.09	402.33	-28.12
	25	403.74	-28.05	405.17	-28.1	405.2	-28.08	399.65	-28.14	400.21	-28.21
	50	403.74	-28.05	406.55	-28.14	406.62	-28.09	395.56	-28.21	396.68	-28.37
November	10	289.76	-50.93	290.24	-50.97	290.26	-50.96	288.42	-51	288.55	-51.06
	25	289.76	-50.93	290.9	-51.02	290.96	-50.97	286.34	-51.09	286.69	-51.22
	50	289.76	-50.93	291.98	-51.08	292.1	-51.00	282.89	-51.23	283.59	-51.5
December	10	274.56	-45.42	275.01	-45.45	275.03	-45.44	273.31	-45.48	273.45	-45.53
	25	274.56	-45.42	275.63	-45.49	275.68	-45.45	271.38	-45.56	271.73	-45.68
	50	274.56	-45.42	276.65	-45.55	276.75	-45.48	268.18	-45.68	268.85	-45.93

Further, in Case 3, lowest values of storage heat flux at hourly time step obtained during night time has been found to vary from -98.22 to - 63.37 Wm^{-2} at 10%, -94.21 to -59.22 Wm^{-2} at 25% and -87.62 to -55.03 Wm^{-2} at 50% (Table 8.3) level. In Case-4 lowest values of negative storage heat flux are varying from -98.00 to -61.66 Wm^{-2} at 10%, -93.63 to -58.92 Wm^{-2} at 25% and -86.49 to -54.44 Wm^{-2} at 50% (Table 8.2) transformation level.

In all cases of adaptations the negative value of storage heat flux (negative values obtained during night) are decreasing with increase in % conversion i.e., 10% to 50%. In Case-4 lowest values (-54.44 Wm^{-2}) and in Case-2 highest value (-100.77 Wm^{-2}) of negative storage heat flux has been observed as compared to the Case of actual LULC conditions (-62.92 to -100.77 Wm^{-2}) without any adaptation (Table 8.2). Decrease in negative values of storage heat flux indicates cooling effect which may be due to low surface temperature. Case-4 in which all possible LULC adaptations are considered has been found to be most effective at 50% conversion in reducing the negative storage heat flux as compared to other proposed adaptations (Table 8.2). Relative changes in percentage of storage heat flux during night time at 10%, 25% and 50% LULC transformations as compared to flux values in actual condition are shown in Figure 8.4, 8.5 and 8.6, respectively. The highest % decrease in negative value of storage heat flux during night time has been found in Case-4 in the July month (14.35 at 50%), as shown in Figure 8.6 and lowest % change (0.38 at 10%) in monthly average hourly storage heat flux has been found in Case-1 in December month as shown in Figure 8.1.

Highest values of monthly average hourly storage heat flux occurring during day time in Case-1 varies from 159.29 to 96.19 Wm^{-2} at 10%, 157.56 to 95.19 Wm^{-2} at 25% and 154.78 to 93.59 Wm^{-2} at 50% (Table 8.2) level as compared to values in actual conditions of LULC (97.48 to 161.47 Wm^{-2}) as shown in Table 8.2, while in Case-2 values are varying from 161.12 to 97.12 Wm^{-2} at 10%, 162.14 to 97.52 Wm^{-2} at 25% and 164.11 to 98.35 Wm^{-2} at 50% (Table 8.2) level. Further, in Case 3 positive values of monthly average hourly storage heat flux obtained during day time varies from 157.71 to 94.62 Wm^{-2} at 10%, 153.64 to 91.29 Wm^{-2} at 25% and 146.94 to 85.8 Wm^{-2} at 50% (Table 8.2) and in Case-4 values vary from 157.3 to 94.31 Wm^{-2} at 10%, 152.61 to 90.5 Wm^{-2} at 25% and 144.93 to 84.27 Wm^{-2} at 50% (Table 8.2) transformation level as compared to values in actual conditions of LULC (97.48 to 161.47 Wm^{-2}). In Case-1, Case-2, Case-3 and Case-4, the lowest value of positive storage heat flux (positive values obtained during day time) has been observed in month of January and highest value of maximum storage flux is observed in the month of April. Case-4 shows the lowest and Case-2 shows the highest value of

positive storage heat flux when compared with other adaptation measures and values corresponding to actual condition without any adaptation (Table 8.2). When all possible adaptations in Case-4 are considered as mixed land use class conversion, lowest value of positive storage flux in the month of January to June (84.27 to 123.68 Wm^{-2}) is increasing (rise in outward net radiation at daytime) whereas in October to December (124.45 to 86.5 Wm^{-2}) it is decreasing (reduction in outward net radiation at daytime). Relative changes in percentage of storage heat flux at proposed 10%, 25% and 50% changes in LULC as compared to storage heat flux corresponding to actual condition are shown in Figure 8.4, 8.5 and 8.6, respectively.

The highest % reduction in value of positive storage flux occurring during day time w.r.t. storage heat flux in actual condition, has been found in January month in Case-4 (13.55 at 50%) as shown in Figure 8.6. The lowest % reduction in value of positive storage flux w.r.t. storage heat flux in actual condition has been found in September month of Case-2 (0.15 at 10%) as shown in Figure 8.4.

Comparing the performance of four adaptation measures in altering the storage heat flux, it has been found that in case of storage heat flux during night time, barren to forest, building to vegetation and mixed land-use class conversions (adaptation measures: Case-1, Case-3 and Case-4) have shown decreasing trend in negative values means approaching toward zero side of storage flux in all months. This is happening due to proposed conversion of barren land and roof tops of the buildings into vegetation cover, which leads to reduction in surface temperature and storage heat flux during day time. Also due to increase in vegetation results in more outflow of radiation due to increase in high albedo surfaces and more partitioning of available energy into latent heat leading to cooling and less surface temperature and less radiation emission from surfaces in night time. (Baidya Roy et al., 2003; Mahmood et al., 2010). Barren to forest, building to vegetation and mixed land use (adaptation measures: Case-1, Case-3, Case-4) adaptations are reducing the monthly average hourly storage heat flux values in all months when compared with storage heat flux in actual condition.

Highest % reduction in monthly average hourly heat flux has been found from Case-4, where all adaptations have been proposed simultaneously. This happing because of proposed conversion of low albedo surfaces like built-up surfaces (0.15) into high albedo surfaces like grass covering on rooftops (0.21) resulting less absorption of radiations leading to reduction in storage heat flux during day time. Also such adaptations will increase the partitioning of available energy into latent heat results in cooling of surfaces.

In the negative values of monthly average hourly storage heat flux no significant decrease has been observed in barren to water adaptation measure (Case-2) from January to September. Significant decreasing trend in the reduction of storage flux has been observed in building to vegetation and mixed land use class conversion (adaptation measures: Case-3 and Case-4) due to proposed transformation of surface characteristics from low albedo to high albedo (Kurn et al., 1994; Das and Padmanabhamurty 2008; Gillner et al., 2015; Larsen 2015; Simpson et al., 2011; Weng and Yang, 2004). It can be concluded from the results shown in Figure 8.4 to 8.6 and Table 8.2, adaptation measures are successful in reducing the storage heat flux during day time significantly which can reduce surface temperature which will leads to cooler urban environment (Zhou et al., 2004; Christy et al., 2006; Chang et al., 2010; Calzadilla et al., 2013; Das, 2015; Liu et al., 2016). The most effective adaptation measure in w.r.t. storage heat flux is the mixed land use adaptation, where all possible adaptations are proposed simultaneously.

8.2.3 Sensible Heat Flux

Sensible heat flux is major component of surface energy and water balance. Sensible heat flux is one part of the energy available for partitioning into latent and sensible heat flux. The partitioning of available energy is influenced by the soil moisture, net radiation, vegetation condition, vapor pressure gradient and temperature. Increase or decrease in sensible heat flux affects the surface temperature. Minimum and maximum monthly average sensible heat fluxes at hourly time step at 10%, 25% and 50% transformation in LULC as per the proposed adaptation measures are calculated from the hourly simulated results obtained from SUEWS model for different Cases (Case-1 to 4).

In different months, range of minimum values of sensible flux found to vary from 11.77 to -9.33 Wm^{-2} at 10%, 11.47 to -9.7 Wm^{-2} at 25% and 10.98 to -10.30 Wm^{-2} at 50% (Table 8.11) transformation level while in Case-2 monthly average hourly sensible heat flux in different months varies from 12.03 to -8.95 Wm^{-2} at 10%, 12.06 to -8.77 Wm^{-2} at 25% and -12.16 to -8.42 Wm^{-2} at 50% LULC transformation level as compared to the value (-0.75 to 11.25 Wm^{-2}) in case of without any adaptation measure, as shown in Table 8.3. Further, in Case-3 minimum values of sensible heat flux in different months varies from 11.9 to -8.95 Wm^{-2} at 10%, 11.76 to -8.76 Wm^{-2} at 25% and 11.4 to -8.46 Wm^{-2} at 50% (Table 8.13) and in Case-4 values varies from 11.69 to -9.02 Wm^{-2} at 10%, 11.18 to -8.96 Wm^{-2} at 25% and 10.2 to -11.23 Wm^{-2} at 50% (Table 8.13) level of LULC conversion as compared to the value (-0.75 to 11.25 Wm^{-2}) in case of without any adaptation measure.

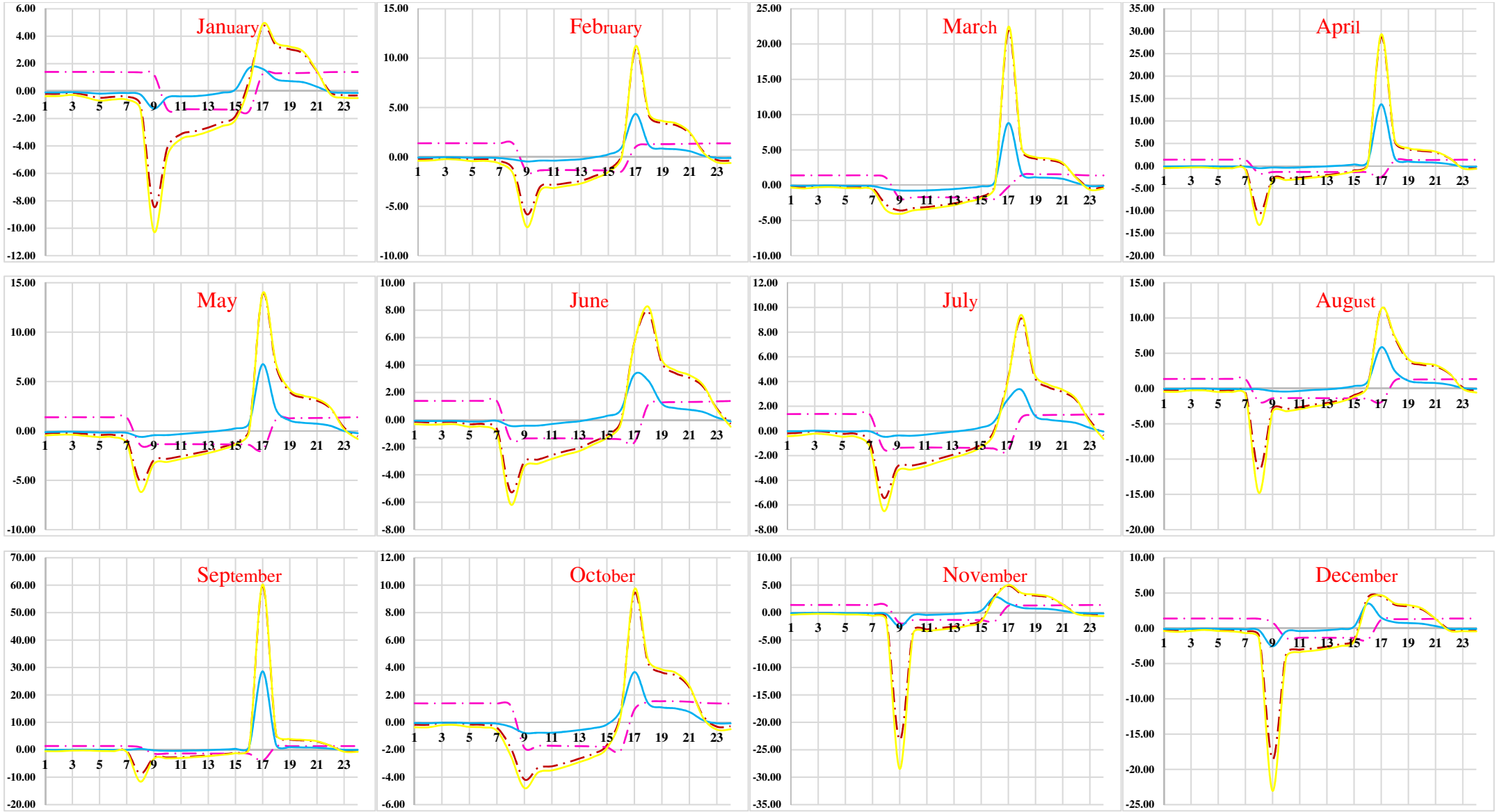

Building to Vegetation	Barren to Forest	Barren to water	Mixed Land Use	X-axis - Time in Hours
				Y-axis -% change in Storage Heat Flux

Figure 8.4 : Changes in storage heat flux (%) by transformation of LULC classes up to 10 % in different adaptation measures

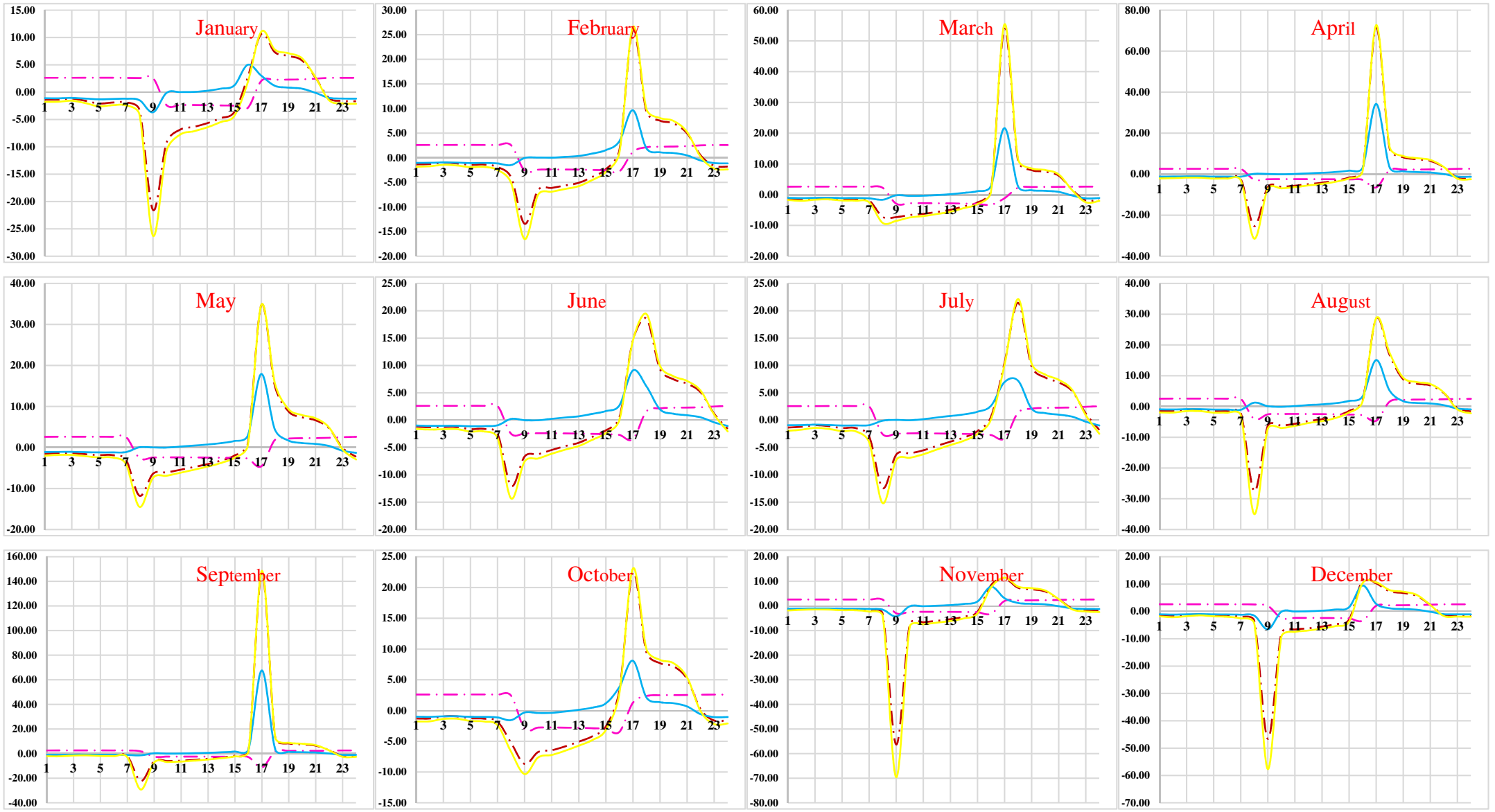

Building to Vegetation	Barren to Forest	Barren to water	Mixed Land Use	X-axis - Time in Hours
				Y-axis -% change in Storage Heat Flux

Figure 8.5 : Changes in storage heat flux (%) by transformation of LULC classes up to 25 % in different adaptation measures

Building to Vegetation	Barren to Forest	Barren to water	Mixed Land Use	X-axis - Time in Hours
				Y-axis -% change in Storage Heat Flux

Figure 8.6 : Changes in storage heat flux (%) by transformation of LULC classes up to 50 % in different adaptation measures

Table 8.2 : Peak values of monthly average hourly storage heat flux (Wm^{-2}) corresponding to different adaption measures

Months	%	Original		Barren to Forest (Case 1)		Barren to Water (Case 2)		Building to Vegetation (Case 3)		Mixed Land Use (Case 4)	
		Max	Min	Max	Min	Max	Min	Max	Min	Max	Min
January	10	97.48	-69.26	96.19	-68.79	97.12	-69.26	94.62	-67.81	94.31	-67.7
	25	97.48	-69.26	95.19	-68.08	97.52	-69.26	91.29	-65.66	90.5	-65.38
	50	97.48	-69.36	93.59	-66.95	98.35	-69.36	85.8	-62.13	84.27	-61.59
February	10	132.89	-79.21	131.12	-78.79	132.47	-79.21	129.38	-77.28	129	-77.12
	25	132.89	-79.06	129.72	-78.01	133.12	-79.06	125.41	-74.26	124.46	-73.85
	50	132.89	-78.93	127.49	-76.77	134.42	-78.93	118.88	-69.3	117.02	-68.5
March	10	150.59	-91.50	147.99	-91.04	149.6	-91.5	146.27	-89.19	145.87	-88.99
	25	150.59	-91.31	146.4	-90.14	150.43	-91.31	142.13	-85.55	141.12	-85.04
	50	150.59	-91.10	143.86	-88.72	152.05	-91.1	135.3	-79.59	133.33	-78.59
April	10	161.47	-100.77	159.29	-100.26	161.12	-100.77	157.71	-98.22	157.3	-98.0
	25	161.47	-100.56	157.56	-99.27	162.14	-100.56	153.64	-94.21	152.61	-93.63
	50	161.47	-100.33	154.78	-97.69	164.11	-100.33	146.94	-87.62	144.93	-86.49
May	10	148.81	-89.40	146.81	-88.96	148.5	-89.4	145.4	-87.11	145.01	-86.92
	25	148.81	-89.16	145.2	-88.09	149.49	-89.16	141.7	-83.49	140.72	-83.0
	50	148.81	-88.89	142.64	-86.7	151.36	-88.89	135.62	-77.55	133.72	-76.59
June	10	137.53	-80.61	135.68	-80.25	137.27	-80.61	134.4	-78.55	134.05	-78.37
	25	137.53	-80.36	134.19	-79.46	138.19	-80.36	131	-75.23	130.12	-74.78
	50	137.53	-80.07	131.81	-78.22	139.91	-80.07	125.41	-69.8	123.68	-68.92
July	10	120.54	-68.97	118.92	-68.71	120.32	-68.97	117.82	-67.15	117.5	-67.0
	25	120.54	-68.71	117.61	-68.05	121.13	-68.71	114.87	-64.17	114.07	-63.8
	50	120.54	-68.36	115.51	-67.01	122.68	-68.36	110.03	-59.28	108.46	-58.55
August	10	123.47	-70.31	121.8	-69.99	123.23	-70.31	120.66	-68.52	120.34	-68.37
	25	123.47	-71.10	120.44	-69.32	124.04	-70.1	117.62	-65.66	116.83	-65.28
	50	123.47	-69.85	118.31	-68.23	125.61	-69.85	112.63	-60.95	111.03	-60.24
September	10	130.47	-77.53	128.22	-77.11	129.59	-77.53	126.62	-75.64	126.26	-75.48
	25	130.47	-77.38	126.84	-76.35	130.27	-77.38	122.87	-72.69	121.96	-72.29
	50	130.47	-77.25	124.65	-75.14	131.63	-77.25	116.7	-67.85	114.92	-67.07
October	10	139.24	-80.75	137.35	-80.38	138.91	-80.75	135.9	-78.67	135.53	-78.5
	25	139.24	-80.54	135.86	-79.6	139.71	-80.54	132.26	-75.35	131.33	-74.9
	50	139.24	-80.27	133.46	-78.36	141.31	-80.27	126.26	-69.89	124.45	-69.01
November	10	108.23	-66.96	106.79	-66.51	107.86	-66.96	105.2	-65.54	104.87	-65.44
	25	108.23	-66.95	105.66	-65.83	108.35	-66.95	101.71	-63.43	100.88	-63.16
	50	108.23	-67.02	103.88	-64.74	109.34	-67.02	95.98	-59.98	94.35	-59.45
December	10	99.66	-63.37	98.33	-63.1	99.3	-63.37	96.8	-61.78	96.49	-61.66
	25	99.66	-63.17	97.3	-62.49	99.72	-63.17	93.49	-59.22	92.7	-58.92
	50	99.66	-62.92	95.66	-61.53	100.58	-62.92	88.05	-55.03	86.5	-54.44

In all adaptation measures (Case-1 to Case-4), the lowest value of minimum sensible flux are found to be reducing as compared to the value in case of without any adaptation measure. Lowest value of minimum sensible heat flux is observed in the month of May and highest value of minimum sensible heat flux is observed in the month of September. Highest value of minimum sensible heat flux has been found in Case-4 and lowest value has been found in Case-2. In Case-2, Case-3 and Case-4 adaptation measures, negative values of sensible heat flux are reducing with increase in % conversion from 10% to 50% where as in Case-1, negative values are increasing, however, in all Cases minimum values of sensible heat flux are reducing, when compared with the actual case where no adaptations are considered. Significant decrease in minimum values of sensible heat flux has been observed during monsoon season (Table 8.3) because of more consumption of available energy in latent heat of vaporization.

Relative percentage changes in the minimum values of sensible heat flux at 10%, 25% and 50% transformations in LULC for different adaptation scenarios have been shown in Figure 8.7 to 8.9, respectively. The highest % change in value of minimum sensible flux has been found in month of March in Case-4 (63.75 at 50%) as shown in Figure 8.9 and lowest % change in value of minimum sensible flux has been found in November month for Case-2 (0.21 at 10%) as shown in Figure 8.7.

In case of maximum monthly average hourly sensible heat flux, in different months, values have been found to vary 384.84 to 213.97 Wm^{-2} at 10%, 387.36 to 215.34 Wm^{-2} at 25% and 391.41 to 217.61 Wm^{-2} at 50% level of LULC transformation (Table 8.3) in Case-1 as compared to values (212.56 to 382.37 Wm^{-2}) in case of without any adaptation while in Case-2 maximum values varies from 383.04 to 211.72 Wm^{-2} at 10%, 382.83 to 209.70 Wm^{-2} at 25% and 382.20 to 206.13 Wm^{-2} at 50% level (Table 8.3). Further, in Case 3 maximum monthly average hourly sensible heat flux, in different months found to vary from 382.42 to 213.37 Wm^{-2} at 10%, 381.29 to 213.88 Wm^{-2} at 25% and 379.42 to 214.85 Wm^{-2} at 50% level (Table 8.13) and in Case-4 values are varying from 382.96 to 212.88 Wm^{-2} at 10%, 382.66 to 212.57 Wm^{-2} at 25% and 382.1 to 211.81 Wm^{-2} at 50% (Table 8.14) as compared to values (212.56 to 382.37 Wm^{-2}) in case of without any adaptation. In Case-1, Case-2, Case-3 and Case-4, the lowest value of maximum sensible flux is observed in the month of January and highest value of maximum sensible flux is observed in the month of April. Case-2 shows the lowest and Case-1 shows the highest value of maximum sensible flux when compared with other adaptation measures.

Relative percentage changes in the sensible heat flux as compared to case with actual LULC at 10%, 25% and 50% proposed LULC conversions in different adaptation have been shown in Figure 8.7, 8.8 and 8.9, respectively. The highest % change in value of maximum sensible heat flux as compared to original values has been observed in July month in Case-2 (7.46 at 25%) as shown in Figure 8.8. The lowest % change in value of maximum sensible heat flux has been observed in April month in Case-2 (0.04 at 10%) as shown in Figure 8.7.

The effect of four proposed adaptation measures on SEB have been simulated through calibrated SUEWS model and alterations in sensible heat flux values has been determined as compared to original values of sensible heat flux. As revealed from the comparison, minimum sensible heat flux is reducing in night time (negative values are reducing) for all adaptation measures i.e., barren to forest, building to vegetation and mixed land-use class conversions (adaptation measure: Case-1 and Case-4). This is happening due to inclusion of rainfall and more vegetation into the converted land-use classes. In adaptation measures Case-2, 3 and 4, peak values of monthly average hourly sensible heat flux are reducing in all months except in the month of May, November and December.

Highest reduction in maximum values of sensible heat flux have been found in monsoon season months i.e., July, August and September because of more consumption of available energy for evapotranspiration and vaporization (Table 8.3). Such a reduction in peak values of sensible heat flux indicates effectiveness of the adaptation measures in which impervious or built-up surfaces are proposed to be converted into vegetation (Table 8.3). In adaptation Case-1, sensible heat flux values are increased as compared to original values. It can be concluded from the results that proposed adaptation measures are effective in reducing the sensible heat flux in day time as well as in night time leading to reduction in surface temperature, which means adverse impacts of LULC conversions due to urbanization can be contained from these adaptation measures. Study results are in agreement with other published studies. (Nagar et al., 2002; Das and Padmanabhamurty, 2008, 2009a; Subash et al., 2011; Chakraborty et al., 2013, 2015; Mohan et al., 2013; Das et al., 2014; Das, 2015; Abeysingha et al., 2016b).

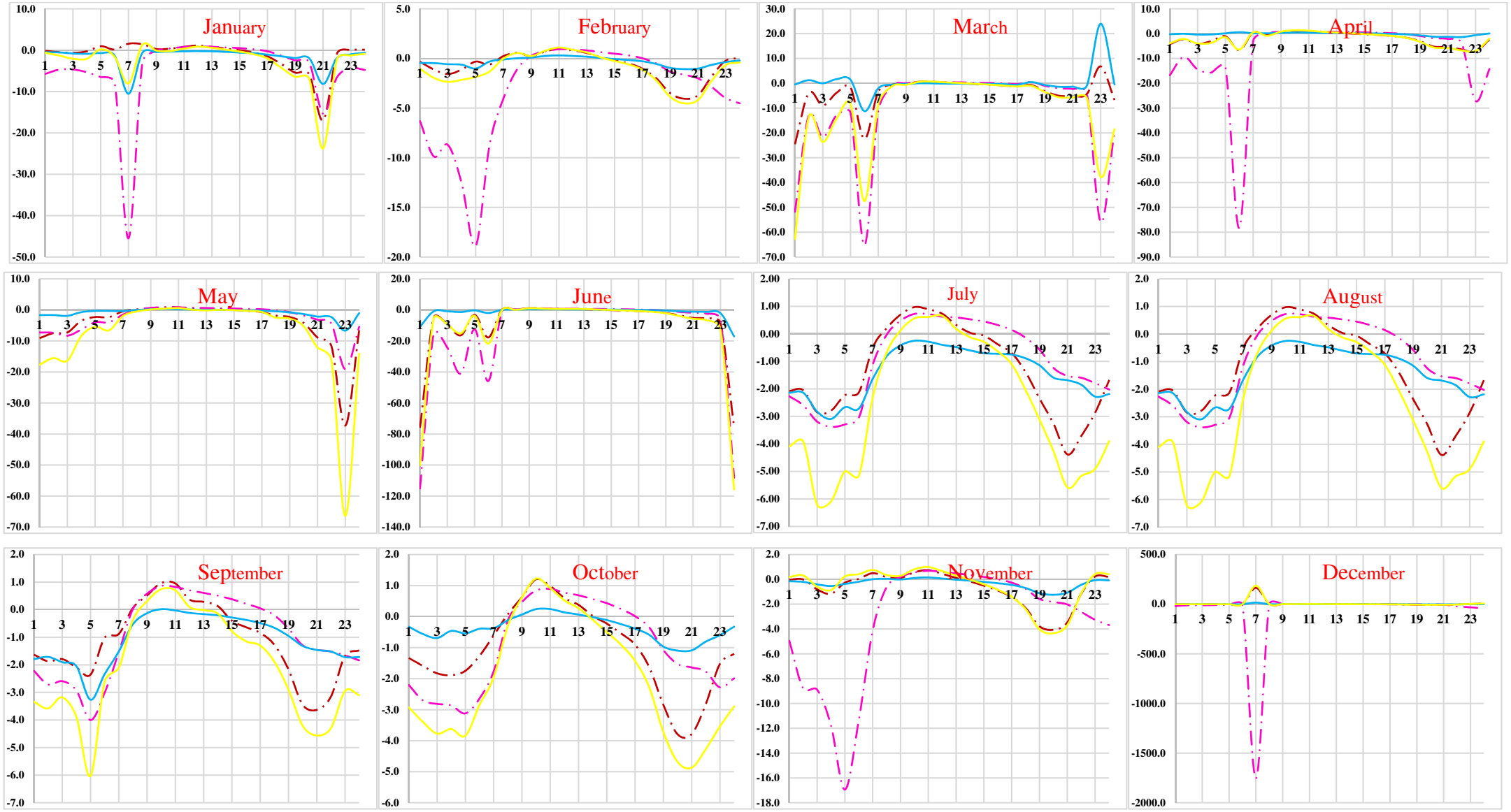

Building to Vegetation	Barren to Forest	Barren to water	Mixed Land Use	X-axis - Time in Hours
				Y-axis -% change in Sensible Heat Flux

Figure 8.7 : Changes in sensible heat flux (%) by transformation of LULC classes up to 10 % in different adaptation measures

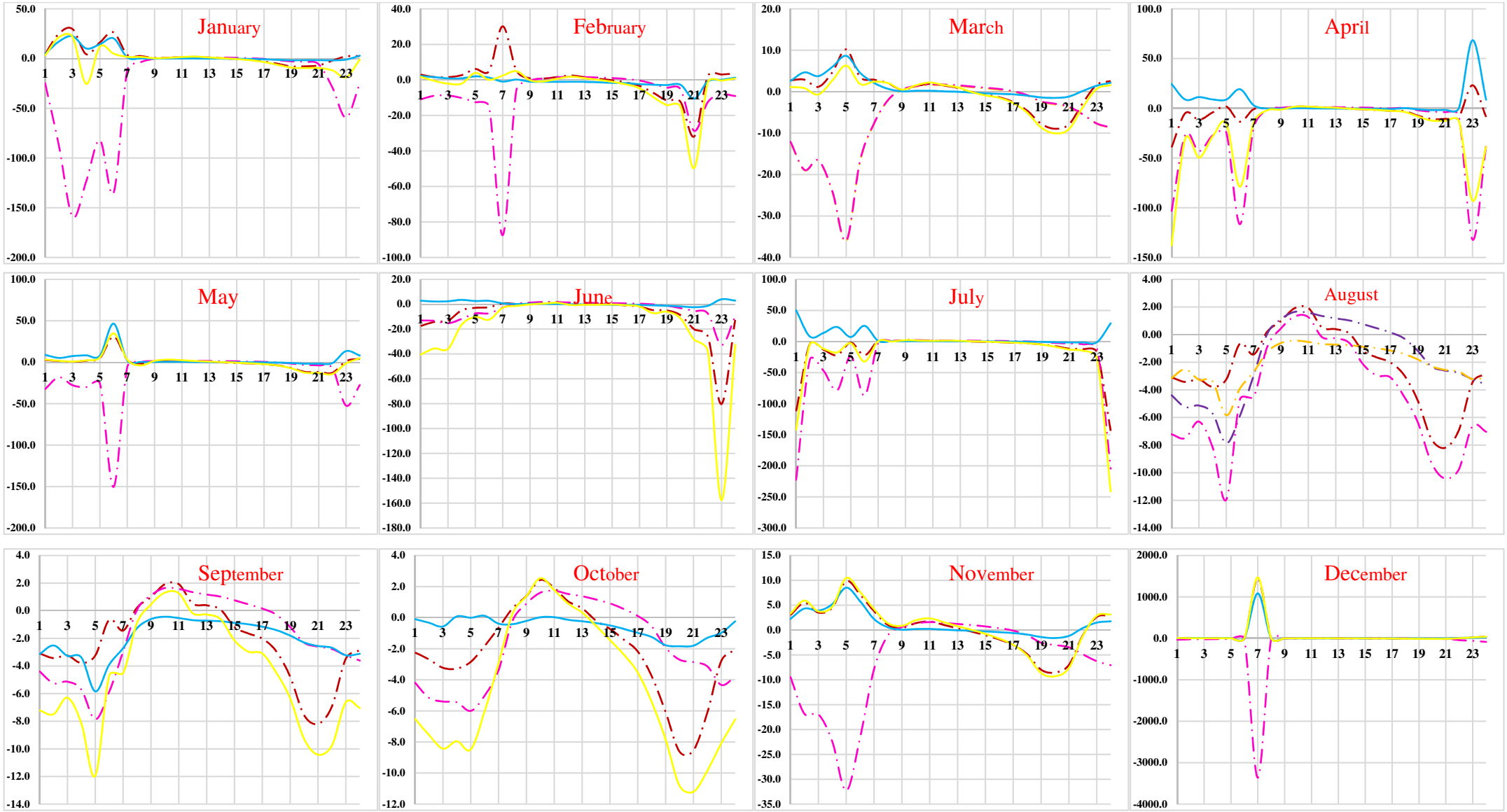

Building to Vegetation	Barren to Forest	Barren to water	Mixed Land Use	X-axis - Time in Hours
				Y-axis -% change in Sensible Heat Flux

Figure 8.8 : Changes in sensible heat flux (%) by transformation of LULC classes up to 25 % in different adaptation measures

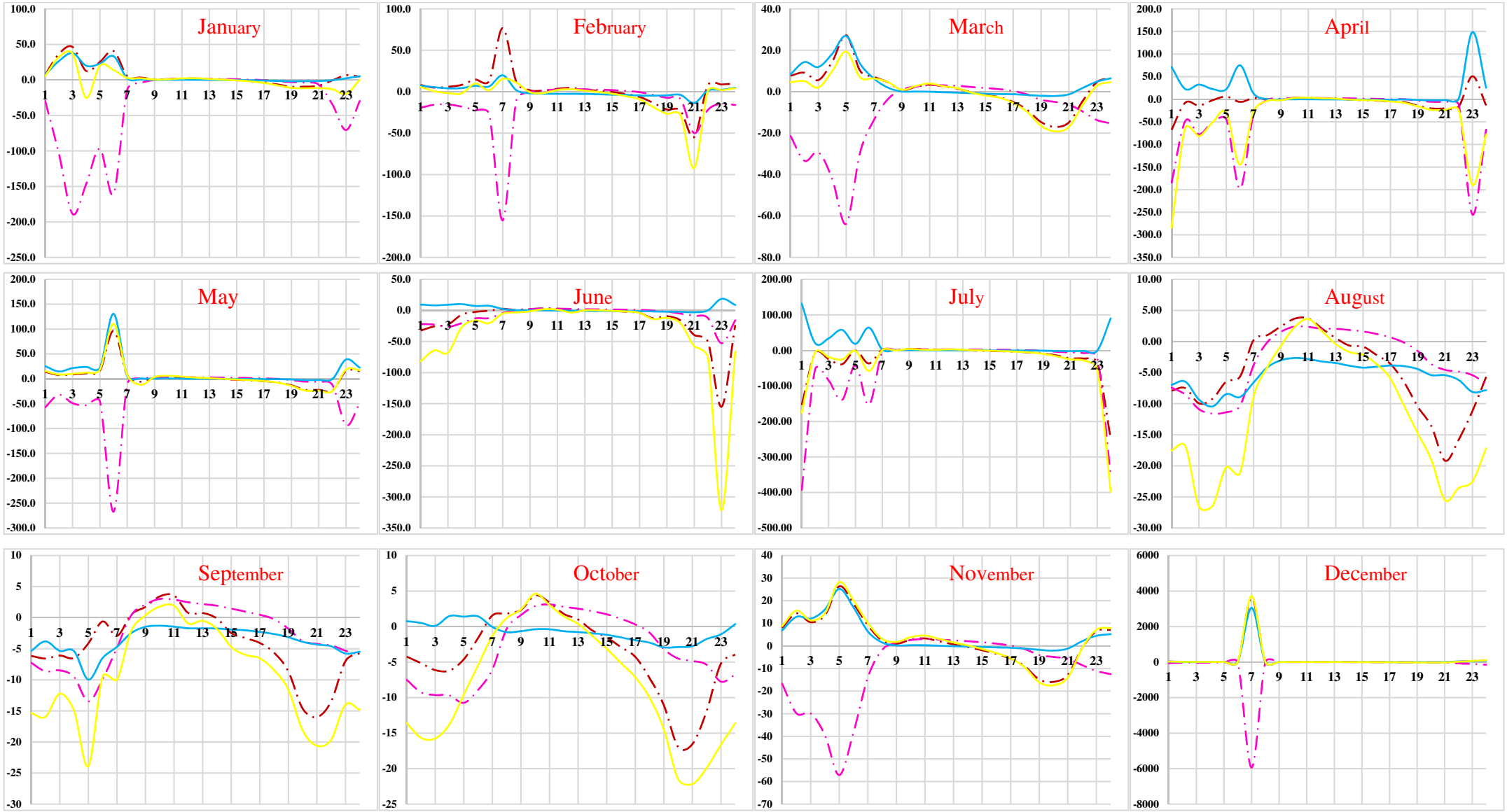

Building to Vegetation	Barren to Forest	Barren to water	Mixed Land Use	X-axis - Time in Hours
				Y-axis -% change in Sensible Heat Flux

Figure 8.9 : Changes in sensible heat flux (%) by transformation of LULC classes up to 50 % in different adaptation measures

Table 8.3 : Peak values of monthly average hourly sensible heat flux (Wm^{-2}) corresponding to different adaption measures

Months	%	Original		Barren to Forest (Case 1)		Barren to water (Case 2)		Building to vegetation (Case 3)		Mixed Land Use (Case 4)	
		Max	Min	Max	Min	Max	Min	Max	Min	Max	Min
January	10	212.56	-9.16	213.97	-9.56	211.72	-9.26	213.78	-9.53	212.88	-9.28
	25	212.56	-9.16	215.34	-9.92	209.70	-9.16	215.08	-9.92	212.57	-9.20
	50	212.56	-9.16	217.61	-10.49	206.13	-8.96	217.00	-10.49	211.81	-9.13
February	10	295.90	1.94	297.79	1.57	296.06	1.92	297.47	1.60	296.23	1.90
	25	295.90	1.94	299.63	1.24	295.29	2.11	299.14	1.24	295.70	2.06
	50	295.90	1.94	302.62	0.70	293.80	2.46	301.56	0.71	294.53	2.31
March	10	345.85	-2.62	346.47	-2.93	344.80	-2.58	346.16	-2.93	344.87	-2.84
	25	345.85	-2.62	348.67	-3.26	344.48	-2.39	348.23	-3.32	344.49	-3.13
	50	345.85	-2.62	352.20	-3.79	343.70	-2.04	351.27	-3.90	343.41	-3.93
April	10	382.37	-4.13	384.84	-4.52	383.04	-4.13	384.42	-4.49	382.96	-4.22
	25	382.37	-4.13	387.36	-4.88	382.83	-3.92	386.69	-4.88	382.66	-4.06
	50	382.37	-4.13	391.41	-5.46	382.20	-3.52	390.02	-5.45	382.10	-3.78
May	10	362.51	-8.91	364.40	-9.26	362.55	-8.94	364.18	-9.24	362.59	-9.39
	25	362.51	-8.91	366.12	-9.57	361.58	-8.68	365.81	-9.57	361.10	-9.83
	50	362.51	-8.91	369.04	-10.04	359.63	-8.27	368.23	-10.06	363.56	-11.23
June	10	349.26	-2.96	351.51	-3.33	349.94	-2.97	351.18	-3.30	349.98	-3.07
	25	349.26	-2.96	353.81	-3.66	349.95	-2.74	353.35	-3.66	349.94	-3.04
	50	349.26	-2.96	357.52	-4.20	349.54	-2.41	356.55	-4.20	349.71	-3.01
July	10	314.30	11.25	315.97	10.88	312.41	10.95	315.71	10.89	313.92	10.68
	25	293.07	9.19	296.07	8.47	290.84	8.65	295.71	8.43	291.27	8.09
	50	314.30	11.25	320.13	9.97	302.09	10.30	319.31	9.91	309.01	8.61
August	10	293.07	9.19	294.56	8.82	292.47	8.89	294.33	8.83	292.65	8.64
	25	293.07	9.19	296.07	8.47	290.84	8.65	295.71	8.43	291.27	8.09
	50	293.07	9.19	298.71	7.95	287.97	8.27	297.76	7.82	287.77	6.99
September	10	315.22	11.07	316.99	10.72	315.15	11.01	316.69	10.72	314.89	10.64
	25	315.22	11.07	318.89	10.40	314.11	11.07	318.41	10.36	313.57	10.13
	50	315.22	11.07	322.00	9.88	312.26	11.22	320.95	9.79	311.03	10.01
October	10	301.03	2.20	302.09	1.83	300.71	2.19	301.76	1.85	300.97	2.21
	25	301.03	2.20	304.08	1.49	300.58	2.39	303.56	1.49	301.25	2.43
	50	301.03	2.20	307.28	0.94	300.16	2.76	306.18	0.96	301.65	2.82
November	10	240.62	-5.43	242.21	-5.84	241.15	-5.43	241.93	-5.81	241.39	-5.44
	25	240.62	-5.43	243.78	-6.21	241.13	-5.19	243.34	-6.21	241.73	-5.21
	50	240.62	-5.43	246.32	-6.82	240.92	-4.75	245.40	-6.80	242.23	-4.82
December	10	224.98	-0.75	226.39	-1.14	225.14	-0.78	226.19	-1.11	225.52	-0.78
	25	224.98	-0.75	227.74	-1.48	224.59	-0.58	227.46	-1.49	225.50	-0.68
	50	224.98	-0.75	229.94	-2.05	223.52	-0.21	229.31	-2.04	225.21	-0.70

8.2.4 Latent Heat Flux

In urban areas, latent heat flux is one portion of energy available for partitioning into sensible and latent heat fluxes. Latent heat is also a function of available energy moisture availability in the system and vegetative & water surfaces. Decrease in latent heat flux means less consumption of heat for vaporization whereas increase in latent heat means increase in cooling effect and decrease in sensible heat flux which leads to lower surface and air temperature.

Monthly average latent heat flux at hourly time step has been calculated from hourly simulated results obtained from calibrated SUEWS model corresponding to actual conditions without adaptations and at proposed 10%, 25% and 50% transformation in LULC classes in different proposed adaptation measures in different Cases (Case-1 to 4). In Case-1, range of lowest values of monthly average hourly latent heat flux in different months varies from 4.3 to 0 Wm-2 at 10%, 4.58 to 0 Wm-2 at 25% and 4.98 to 0 Wm-2 at 50% (Table 8.4) transformation level, as compared to (0.0 to 4.02 Wm^{-2}) value in actual conditions of LULC. Also in Case-2, lowest values of monthly average hourly latent heat flux in different months varies from 4.6 to 0 Wm-2 at 10%, 5.48 to 0 Wm-2 at 25% and 6.19 to 0 Wm-2 at 50% (Table 8.4) transformation level. Further, in Case 3, lowest values of latent heat flux at hourly time step in different months has been found to vary from 3.45 to 0 Wm-2 at 10%, 3.8 to 0 Wm-2 at 25% and 4.61 to 0 Wm-2 at 50% (Table 8.3) level and in Case-4 lowest values of monthly average hourly latent heat flux in different months are varying from 3.63 to 0 Wm^{-2} at 10%, 4.51 to -8.96 Wm-2 at 25% and 5.96 to 0 Wm^{-2} at 50% (Table 8.4) transformation level.

In all cases of adaptations the minimum monthly average values of latent heat flux at hourly time step are increasing with increase in % conversions i.e., 10% to 50% except in dry months March to June. In Case-1 to Case-4, the lowest value of minimum latent flux in different months has been observed in the months of October, November and highest value of minimum latent heat flux is observed in the month of May. Case-4 shows highest value of minimum latent heat flux when compared with other adaptation measures (Das et al., 2014). Also highest relative changes as compared to original values have been found in Case-4. When mixed land use class (Case-4) is considered, lowest value of minimum latent heat flux has been found in drier months February, April and October to December. Highest minimum values of latent heat flux at hourly time step has been found in the rainy season

in moths July and August in adaptation Case-4 as compared to other adaptation Cases and actual values.

Relative increase in minimum values of latent heat flux observed during night time in different months due to proposed adaptations indicates that available energy is increasingly used in latent heat which may result in decrease in sensible heat flux which may leads to increase in cooling effect lower surface temperatures. Case-4 in which all possible LULC adaptations are considered has been found to be most effective at 50% conversion in increase the minimum latent heat flux values (obtained during night time) as compared to other proposed adaptations (Table 8.4). Relative changes in percentage of latent heat flux during night time at 10%, 25% and 50% LULC transformations as compared to flux values in actual condition are shown in Figure 8.10, 8.11 and 8.12, respectively. The highest % increase in minimum value of latent heat flux occurring during night time has been found in Case-4 in the July month (93.51 at 50%), as shown in Figure 8.12 and lowest % decrease (73.88 at 10%) in monthly average hourly latent heat flux has been found in Case-3 & Case-4 in April month as shown in Figure 8.10.

Maximum values of monthly average hourly latent heat flux in different months, occurring during day time, in Case-1 varies from 30.8 to 0 Wm^{-2} at 10%, 31.24 to 0 Wm^{-2} at 25% and 31.89 to 0 Wm^{-2} at 50% (Table 8.4) level as compared to values in actual conditions of LULC (0.0 to 30.35 Wm^{-2}) as shown in Table 8.4, while in Case-2 maximum values in different months are varying from 31.42 to 0 Wm^{-2} at 10%, 32.78 to 0 Wm^{-2} at 25% and 35.02 to 0 Wm^{-2} at 50% (Table 8.4) level. Further, in Case 3 maximum values of monthly average hourly latent heat flux in different months obtained during day time varies from 30.83 to 0 Wm^{-2} at 10%, 31.32 to 0 Wm^{-2} at 25% and 32.15 to 0 Wm^{-2} at 50% (Table 8.2) and in Case-4 values in different months vary from 32.02 to 0 Wm^{-2} at 10%, 34.44 to 0 Wm-2 at 25% and 38.93 to 0 Wm^{-2} at 50% (Table 8.4) transformation level as compared to values in actual conditions of LULC (0.0 to 30.35 Wm^{-2}). In Case-1 to 4, the lowest maximum value of latent heat flux (positive values obtained during day time) has been observed in month of October and November and highest value of maximum latent heat flux is observed in the month of August. Case-4 shows the highest value of maximum latent heat flux when compared with other adaptation measures and values corresponding to actual condition without any adaptation (Table 8.4).

When all possible adaptations in Case-4 are considered as mixed land use class conversion, lowest increase in values of maximum latent heat flux w.r.t. actual case has been found in February (4.11 to 4.40 Wm^{-2}) whereas highest increase in maximum latent

heat flux values have been found in the month of August (32.02 to 38.93Wm^{-2}) as compared to actual values (30.33 Wm^{-2}). Relative changes in percentage of latent heat flux at proposed 10%, 25% and 50% changes in LULC as compared to latent heat flux corresponding to actual condition are shown in Figure 8.10, 8.11 and 8.12, respectively.

The highest % increase in value of maximum storage flux occurring during day time w.r.t. latent heat flux in actual condition, has been found in August month in Case-4 (38.93 % at 50% conversion) as shown in Figure 8.12. In the Month of October and November latent heat flux has been found to be zero in all cases including case with actual LULC. Due to no change in these months, % change have not been shown in Figures for these months.

Comparing the performance of four adaptation measures in altering the latent heat flux, it has been found that in case of latent heat flux during night time, barren to forest, building to vegetation and mixed land-use class conversions (adaptation measures: Case-1, Case-3 and Case-4) have shown increasing trend in almost all months during day as well as night time. This is happening due to proposed conversion of barren land and roof tops of the buildings into vegetation cover, which leads to more energy consumption in evapotranspiration resulting reduction in sensible heat flux and surface temperature. Also increase in vegetation is increasing more outflow of radiation due to increase in high albedo surfaces and more partitioning of available energy into latent heat leading to cooling and less surface temperature. It can be concluded from the results shown in Figure 8.10 to 8.12 and Table 8.4, that adaptation measures are successful in increasing the latent heat flux during day time significantly which can reduce surface temperature which will leads to cooler urban environment. Study results found to be in line with conclusions of other similar studies (Hart and Sailor, 2009a; Coseo and Larsen, 2014; Feyisa et al., 2014; Petralli et al., 2014; Yan et al., 2014; Gillner et al., 2015; Huang et al., 2015a).

8.2.5 Surface Temperature

Surface temperature is a function of different constituents of SEB. Net all-wave radiation, storage heat flus and sensible heat flux affects the surface temperature. With increase in storage and sensible heat fluxes surface temperature also increases which may leads to warmer environment. Effects of different adaptation measures on surface temperature have been investigated by simulating the SEB corresponding to different adaptation proposed with different % of proposed purposeful LULC conversions.

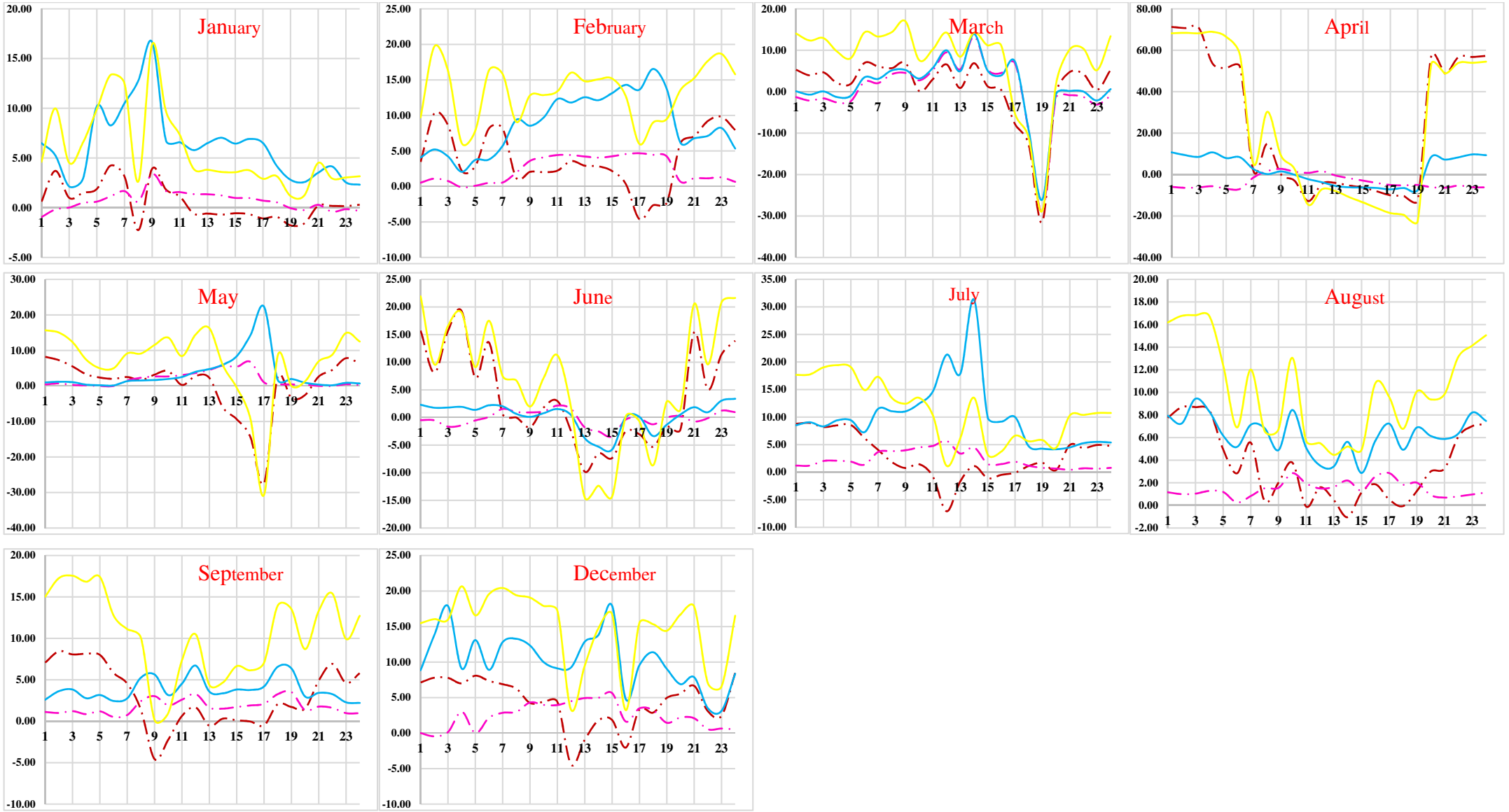

Building to Vegetation	Barren to Forest	Barren to water	Mixed Land Use	X-axis - Time in Hours
				Y-axis -% change in Latent Heat Flux

Figure 8.10 : Changes in latent heat flux (%) by transformation of LULC classes up to 10 % in different adaptation measures

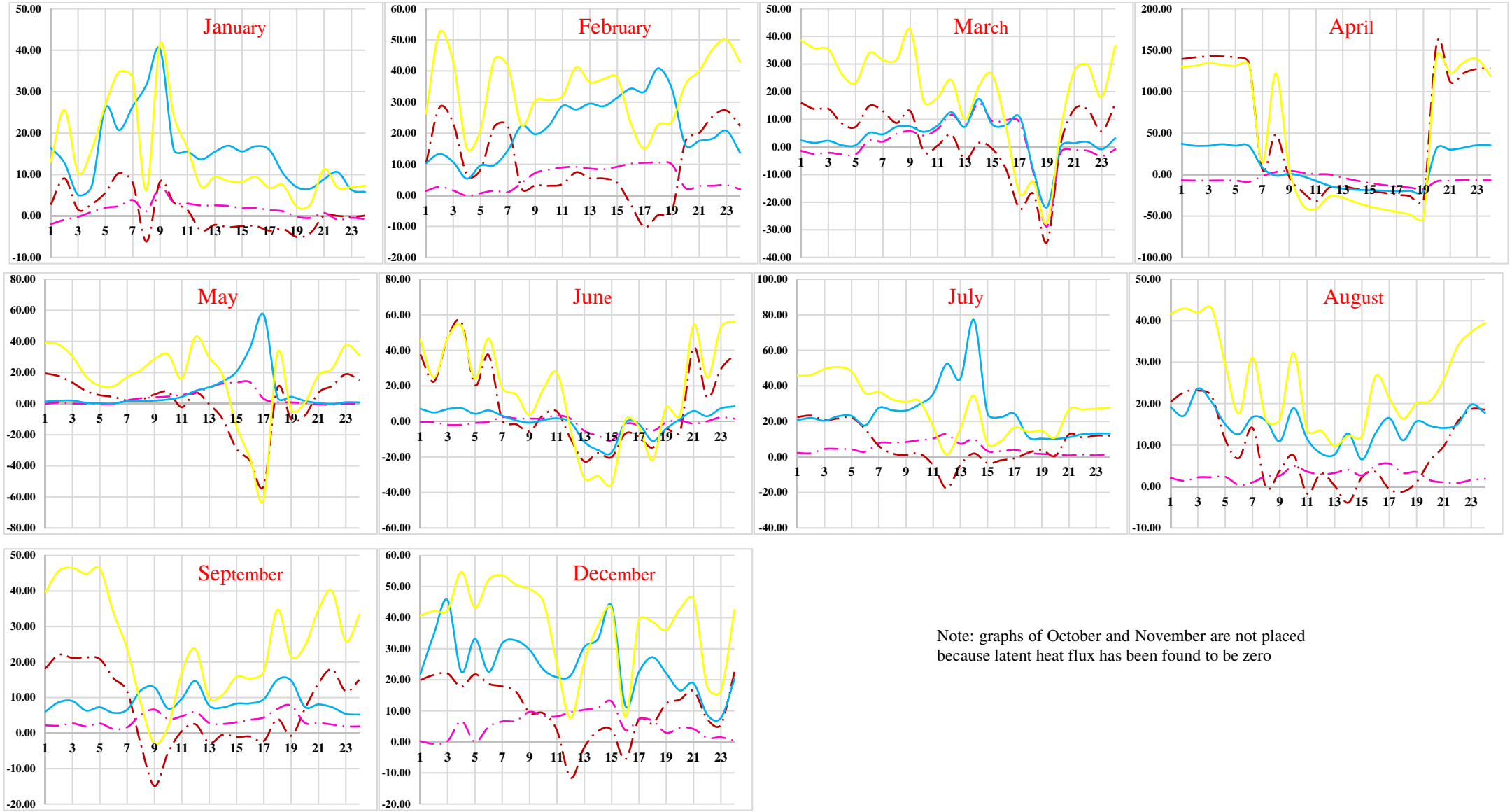

Note: graphs of October and November are not placed because latent heat flux has been found to be zero

Building to Vegetation	Barren to Forest	Mixed Land Use	Barren to water	X-axis - Time in Hours
				Y-axis -% change in Latent Heat Flux

Figure 8.11 : Changes in latent heat flux (%) by transformation of LULC classes up to 25 % in different adaptation measures

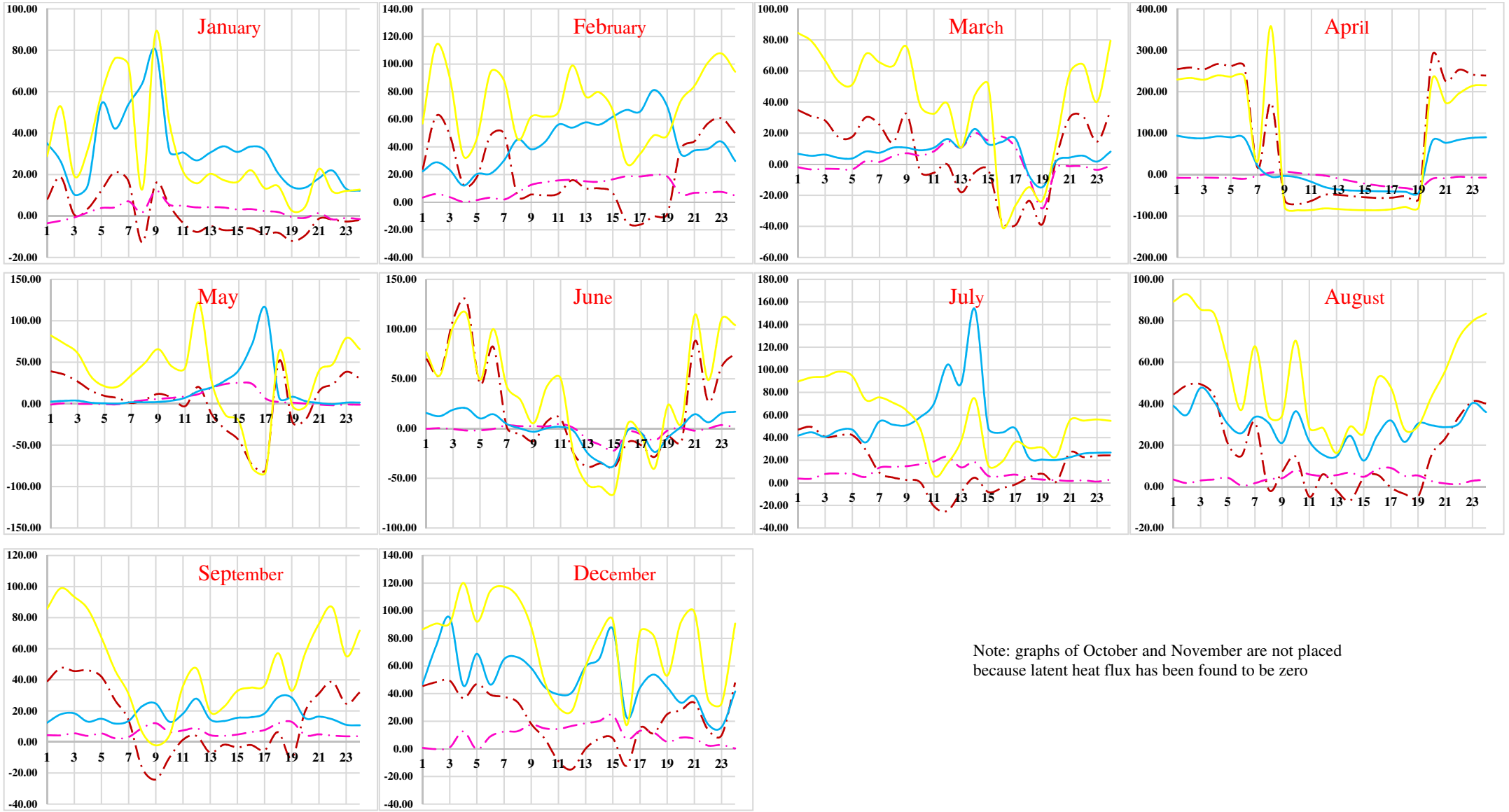

Note: graphs of October and November are not placed because latent heat flux has been found to be zero

Building to Vegetation	Barren to Forest	Barren to Water	Mixed Land Use	X-axis - Time in Hours
				Y-axis -% change in Latent Heat Flux

Figure 8.12 : Changes in latent heat flux (%) by transformation of LULC classes up to 50 % in different adaptation measures

Table 8.4 : Peak values of monthly average hourly latent heat flux (Wm^{-2}) corresponding to different adaption measures

Months	%	Original		Barren to Forest (Case 1)		Barren to Water (Case 2)		Building to Vegetation (Case 3)		Mixed Land Use (Case 4)	
		Max	Min	Max	Min	Max	Min	Max	Min	Max	Min
January	10	20.6	0.76	20.86	0.76	22.05	0.86	20.46	0.74	21.34	0.78
	25	20.6	0.76	21.1	0.77	24.1	1	20.04	0.71	22.34	0.81
	50	20.6	0.76	21.45	0.77	27.54	1.25	19.2	0.66	24.17	0.86
February	10	3.99	0.37	4.16	0.37	4.48	0.4	4.11	0.37	4.6	0.4
	25	3.99	0.37	4.33	0.38	5.14	0.44	4.21	0.37	5.49	0.45
	50	3.99	0.37	4.59	0.39	6.24	0.51	4.4	0.38	7.17	0.53
March	10	19.47	2.34	17.64	2.4	17.7	2.42	17.01	2.5	17.34	2.67
	25	19.47	2.34	17.69	2.4	17.84	2.46	16.18	2.49	17.01	2.91
	50	19.47	2.34	17.75	2.39	18.06	2.53	14.89	1.71	16.59	1.65
April	10	2.55	0.03	2.6	0.02	2.56	0.02	2.93	0.02	3.33	0.02
	25	2.55	0.03	2.63	0.02	2.53	0.02	3.78	0.02	5.67	0.01
	50	2.55	0.03	2.68	0.02	2.43	0.02	6.97	0.01	11.68	0.01
May	10	19.04	4.02	19.13	4.3	19.37	4.6	19.52	3.45	20.65	3.65
	25	19.04	4.02	19.25	4.58	19.8	5.48	20.99	2.54	25.27	2.6
	50	19.04	4.02	19.41	4.98	20.42	6.19	28.88	1.05	31.1	0.89
June	10	14.07	0.38	14.22	0.37	14.18	0.36	14.32	0.36	15.08	0.34
	25	14.07	0.38	14.3	0.36	14.17	0.34	14.56	0.32	16.62	0.3
	50	14.07	0.38	14.38	0.33	14.11	0.29	15.09	0.27	20.09	0.23
July	10	25.33	3.08	25.63	3.12	26.52	3.36	25.62	3.36	26.75	3.63
	25	25.33	3.08	25.92	3.15	28.16	3.76	25.92	3.8	28.9	4.51
	50	25.33	3.08	26.34	3.2	32.74	4.46	26.55	4.61	33.12	5.96
August	10	30.35	2.89	30.8	2.93	31.42	3.13	30.83	3.14	32.02	3.38
	25	30.35	2.89	31.24	2.95	32.78	3.41	31.32	3.52	34.44	4.14
	50	30.35	2.89	31.89	2.96	35.02	3.92	32.15	4.15	38.93	5.31
September	10	19.52	2.61	19.82	2.63	20.18	2.68	19.59	2.82	20.56	3.05
	25	19.52	2.61	20.09	2.66	20.99	2.77	19.44	3.16	22.34	3.61
	50	19.52	2.61	20.6	2.71	22.45	2.95	19.18	2.77	26.14	3.54
October	10	0	0	0	0	0.04	0	0	0	0	0
	25	0	0	0	0	0.12	0	0	0	0	0
	50	0	0	0	0	0.28	0	0	0	0	0
November	10	0	0	0	0	0.03	0	0	0	0	0
	25	0	0	0	0	0.09	0	0	0	0	0
	50	0	0	0	0	0.2	0	0	0	0	0
December	10	8.17	0.22	8.31	0.21	8.57	0.24	8.01	0.23	8.44	0.25
	25	8.17	0.22	8.49	0.21	9.13	0.29	7.71	0.26	8.83	0.31
	50	8.17	0.22	8.75	0.21	10.07	0.38	7.17	0.32	9.58	0.41

Minimum and maximum values of monthly average hourly surface temperature has been calculated from hourly simulated results for different scenarios for Palam area for year 2014. Results are presented in the form of % change in surface temperate w.r.t. to original values corresponding to no adaptation for different months and different adaptations at hourly time step as shown in Figure 8.13 to 8.15. Also peak values of monthly average hourly temperature in different months for different adaptation cases have been presented in Table 8.5.

In Case-1 to 4 in different months, range of minimum values of surface temperature changes from 30.03 to 8.63ºC at 10% and similar range has been observed at 25% and 50% (Table 8.21-8.24). In Case-1 to Case-4, the lowest value of minimum surface temperature is observed in the months of December and highest value of minimum surface temperature has been observed in the month of May. No significant changes have been observed after applying all the adaptation measures in minimum temperature except a very small decrease.

Maximum monthly average hourly surface temperature, in different months, have been found to vary from 47.16 to 23.79 ºC at 10%, 47.17 to 23.79 ºC at 25% and 47.18 to 23.80 ºC at 50% LULC transformation (Table 8.5) in Case-1 as compared to original surface temperature values (23.78 to 47.15 ºC) while in Case-2 maximum values of temperature have been found to vary from 47.16 to 23.79ºC at 10%, 47.17 to 23.80 ºC at 25% and 47.19 to 23.81 ºC at 50% level of LULC transformations as shown in Table 8.5. Further, in Case 3 maximum temperature values has been found to vary from 47.12 to 23.75 ºC at 10%, 47.07 to 23.71 ºC at 25% and 46.99 to 23.64 ºC at 50% (Table 8.5) and in Case-4 surface temperature values have been found to vary from 47.12 to 23.75 ºC at 10%, 47.07 to 23.71 ºC at 25% and 46.98 to 23.63 ºC at 50% LULC conversion (Table 8.24) as compared to original surface temperature values (23.78 to 47.15 ºC). In Case-1 to Case-4, the lowest value of maximum surface temperature is observed in the month of January and highest value of maximum surface is observed in the month of May.

Maximum values of monthly average hourly surface temperature has been found to reducing in Case-3 and Case-4 with increase in % LULC conversion from 10% to 50%. Case-3 and Case-4 adaptation measures where hard surfaces are proposed to be covered with vegetation have been fund to be effective in reducing surface temperature in tune of 0.03 ºC to 0.17 ºC with 10% to 50% proposed conversions (Figure 8.13 to 8.15). (Chakraborty et al., 2013, 2015; Das, 2015; Abeysingha et al., 2016a). Relative % changes in surface temperature at 10%, 25% and 50% in LULC conversions w.r.t. original values in no adaptation case are shown in Figure 8.13 to 8.15, respectively. It can be seen from

results (Figure 8.13 and Figure 8.14) that surface temperature is reducing during day time significantly whereas no significant change has been observed in night time temperature in Case-3 and Case-4. Surface temperature has been slightly increasing in adaptation Cases-1 and 2 during day time. In the case of maximum surface temperature, barren to forest and barren to water (adaptation measures: Case-1 and Case-2) class conversions have shown similar values in negative side of surface temperature from January to December.

The decreasing trend in the maximum surface temperature has been observed in building to vegetation and mixed land use class adaptations (adaptation measures: Case-3 and Case-4) due to transformation of impervious to pervious surfaces and increase in vegetation coverage. The most effective adaptation measure in case of surface temperature is the Case-4, mixed land use adaptation where all possible conversions are considered simultaneously. Thus, increases the proportion of vegetation as compared to the other conversion classes is the most effective adaptation measure in controlling the surface temperature. The second most effective adaptation measure in case of maximum surface temperature is the conversion of building to vegetation because absorption of heat radiation is reduced due to change in surface characteristics (Nagar et al., 2002; Das and Padmanabhamurty, 2008, 2009b; Mohan et al., 2013; Das et al., 2014).

8.3 CONCLUDING REMARKS

The partitioning of available energy is influenced by the soil moisture, net radiation, vapor pressure gradient, vegetation condition, and temperature. Land-atmosphere interactions always affects temperature or precipitation by influencing energy partitioning. The factors that influence the energy partitioning are closely related. On the one hand, soil moisture changes the upward shortwave and longwave radiation by influencing the albedo and emissivity, consequently changing the net radiation. There is also a close relationship between the soil moisture and vegetation. Also soil moisture can affect temperature through changes in the sensible and latent heat flux. On the other hand, changing the partitioning of energy can also influence these factors. The combination of an increasing sensible heat flux and decreasing latent heat flux would enhance the temperature. In this study, four adaptation measures have been proposed as discussed in the previous sections to determine the potential of proposed adaptation measures i.e., purposeful alterations in LULC in favorably changing the SEB constituents i.e., net all-wave radiation, storage heat flux, sensible heat flus, latent heat flux and surface temperature.

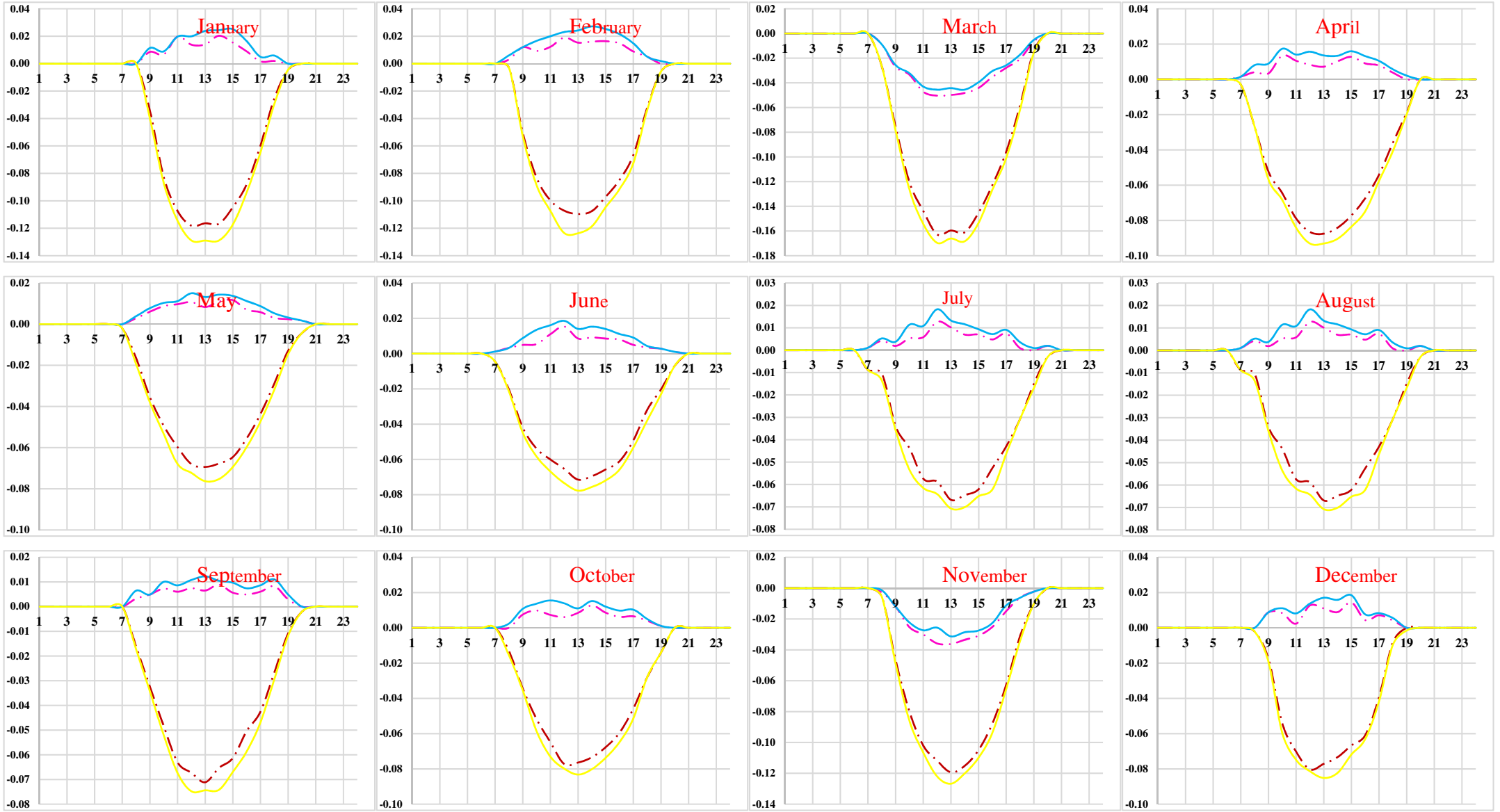

Building to Vegetation	Barren to Forest	Barren to water	Mixed Land Use	X-axis - Time in Hours
				Y-axis -% change in Surface Temperature

Figure 8.13 : Changes in surface temperature (%) by transformation of LULC classes Up To 10% in different cases

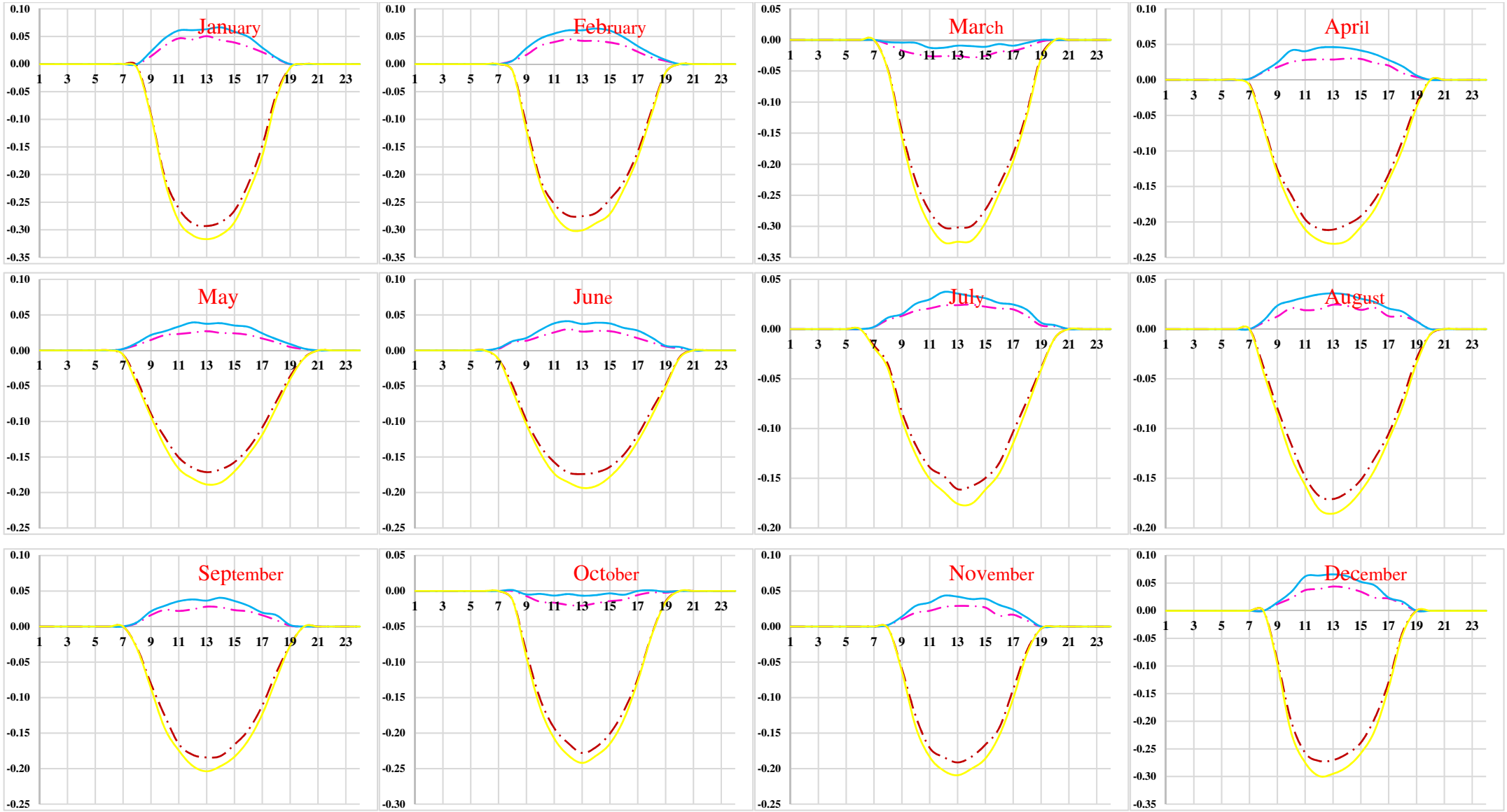

Building to Vegetation	Barren to Forest	Barren to water	Mixed Land Use	X-axis - Time in Hours
				Y-axis -% change in Surface Temperature

Figure 8.14 : Changes in surface temperature (%) by transformation of LULC classes up to 25% in different cases

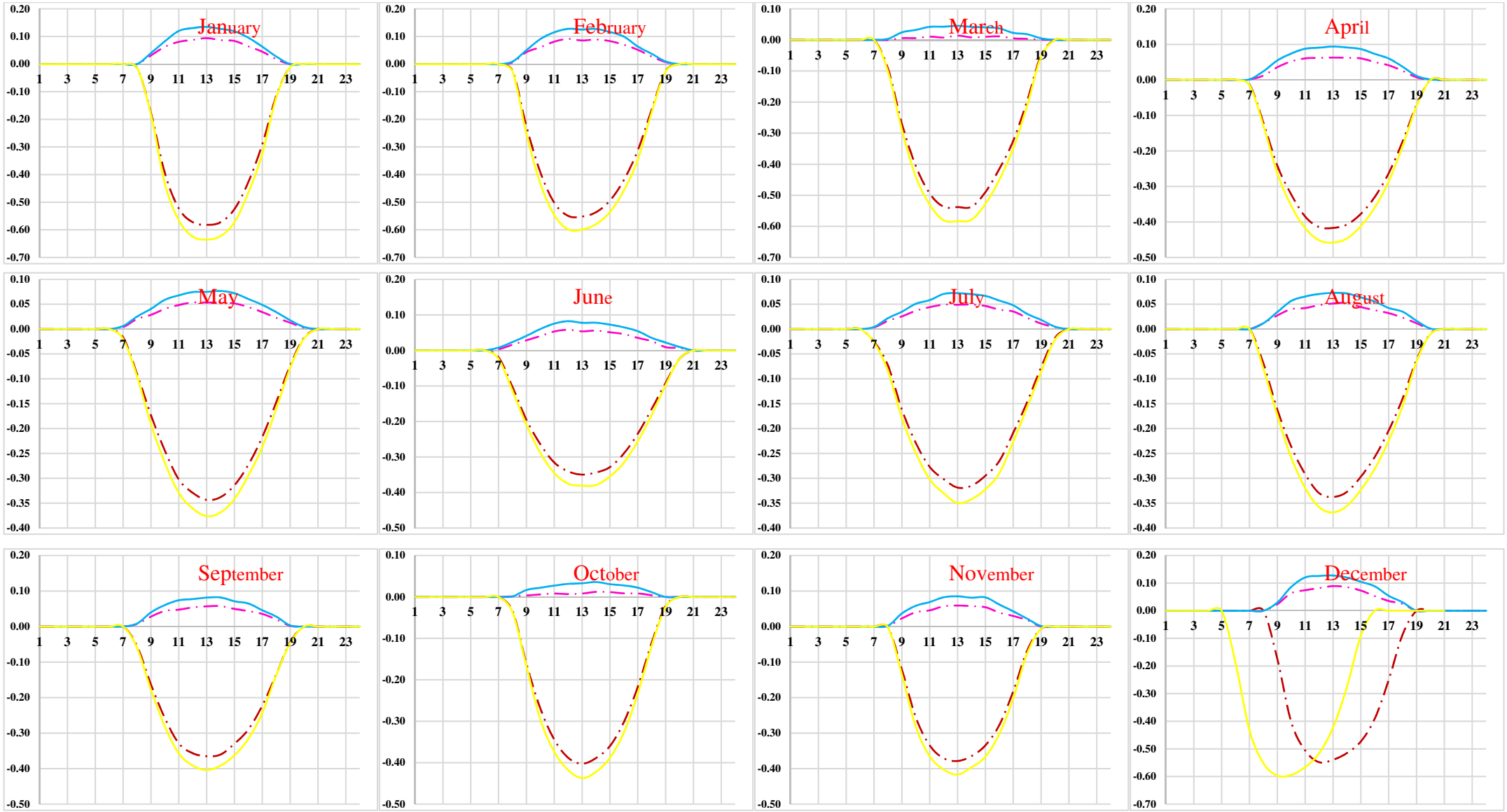

Building to Vegetation	Barren to Forest	Barren to water	Mixed Land Use	X-axis - Time in Hours
				Y-axis -% change in Surface Temperature

Figure 8.15 : Changes in surface temperature (%) by transformation of LULC classes up to 50% in different cases

Table 8.5 : Peak values of monthly average hourly surface temperature (°C) corresponding to different adaption measures

Months	%	Original		Barren to Forest (Case-1)		Barren to water (Case-2)		Building to Vegetation (Case-3)		Mixed Land Use (Case-4)	
		Max	Min	Max	Min	Max	Min	Max	Min	Max	Min
January	10	23.78	9.3	23.79	9.3	23.79	9.3	23.75	9.3	23.75	9.3
	25	23.78	9.3	23.79	9.3	23.8	9.3	23.71	9.3	23.71	9.3
	50	23.78	9.3	23.8	9.3	23.81	9.3	23.64	9.3	23.63	9.3
February	10	28.91	11.71	28.91	11.71	28.92	11.71	28.88	11.71	28.87	11.71
	25	28.91	11.71	28.92	11.71	28.93	11.71	28.83	11.71	28.83	11.71
	50	28.91	11.71	28.93	11.71	28.95	11.71	28.75	11.71	28.74	11.71
March	10	35.46	16.92	35.44	16.92	35.44	16.92	35.4	16.92	35.4	16.92
	25	35.46	16.92	35.45	16.92	35.45	16.92	35.35	16.92	35.34	16.92
	50	35.46	16.92	35.46	16.92	35.47	16.92	35.27	16.92	35.25	16.92
April	10	42.4	21.49	42.4	21.49	42.4	21.49	42.36	21.49	42.36	21.49
	25	42.4	21.49	42.41	21.49	42.42	21.49	42.31	21.49	42.3	21.49
	50	42.4	21.49	42.43	21.49	42.44	21.49	42.23	21.49	42.21	21.49
May	10	47.15	30.03	47.16	30.03	47.16	30.03	47.12	30.03	47.12	30.03
	25	47.15	30.03	47.17	30.03	47.17	30.03	47.07	30.03	47.07	30.03
	50	47.15	30.03	47.18	30.03	47.19	30.03	46.99	30.03	46.98	30.03
June	10	43.64	28.29	43.65	28.29	43.65	28.29	43.61	28.29	43.61	28.29
	25	43.64	28.29	43.65	28.29	43.66	28.29	43.57	28.29	43.56	28.29
	50	43.64	28.29	43.67	28.29	43.68	28.29	43.49	28.29	43.48	28.29
July	10	41.87	28.59	41.87	28.59	41.88	28.59	41.84	28.59	41.84	28.59
	25	41.87	28.59	41.88	28.59	41.89	28.59	41.81	28.59	41.8	28.59
	50	41.87	28.59	41.89	28.59	41.9	28.59	41.74	28.59	41.73	28.59
August	10	40.02	27.96	40.02	27.96	40.02	27.96	39.99	27.96	39.99	27.96
	25	40.02	27.96	40.03	27.96	40.03	27.96	39.95	27.96	39.94	27.96
	50	40.02	27.96	40.04	27.96	40.04	27.96	39.88	27.96	39.87	27.96
September	10	39.5	22.19	39.49	22.19	39.49	22.19	39.45	22.19	39.45	22.19
	25	39.5	22.19	39.49	22.19	39.5	22.19	39.41	22.19	39.41	22.19
	50	39.5	22.19	39.5	22.19	39.51	22.19	39.35	22.19	39.33	22.19
October	10	39.51	26.25	39.51	26.25	39.51	26.25	39.48	26.25	39.48	26.25
	25	39.51	26.25	39.52	26.25	39.52	26.25	39.44	26.25	39.43	26.25
	50	39.51	26.25	39.53	26.25	39.54	26.25	39.37	26.25	39.35	26.25
November	10	33.64	15.18	33.64	15.18	33.64	15.18	33.61	15.18	33.61	15.18
	25	33.64	15.18	33.65	15.18	33.65	15.18	33.58	15.18	33.57	15.18
	50	33.64	15.18	33.66	15.18	33.67	15.18	33.52	15.18	33.51	15.18
December	10	24.17	8.63	24.18	8.63	24.18	8.63	24.15	8.63	24.15	8.63
	25	24.17	8.63	24.18	8.63	24.19	8.63	24.11	8.63	24.11	8.63
	50	24.17	8.63	24.2	8.63	24.2	8.63	24.05	8.63	24.04	8.63

The relative changes in percentage in SEB fluxes and surface temperature corresponding to different proposed adaptations (with 10%, 25% and 50% proposed conversions) w.r.t. original land use class at different percentages have been determined to identify the relative influence of each proposed adaptation measures.

According to the results, the extreme change in maximum net all-wave radiation is observed when Case-3 (Building to vegetation) adaptation measure has been applied and net all-wave radiation is decreased by 11.0 Wm^{-2} from its original value. The most effective adaptation measure in case of lowest (negative) net all-wave radiation is the Case-4, where all possible LULC transformations are considered simultaneously. Thus, increase in proportion of vegetation as compared to the other conversion classes is one of the possible effective adaptation measure. The most effective adaptation measure in case of day time (positive) net all-wave radiation is the conversion of building to vegetation (Case-3) because absorption of radiation is reduced due to change in surface characteristics. This happing because of proposed conversion of low albedo surfaces like built-up surfaces (0.15) into high albedo surfaces like grass covering on rooftops (0.21) resulting less absorption of radiations leading to reduction in storage heat flux during day time. Also such adaptations will increase the partitioning of available energy into latent heat results in cooling of surfaces. In the negative values of monthly average hourly storage heat flux no significant decrease has been observed in barren to water adaptation measure (Case-2) from January to September.

Significant decreasing trend in the reduction of storage flux has been observed in building to vegetation and mixed land use class conversion (adaptation measures: Case-3 and Case-4) due to proposed transformation of surface characteristics from low albedo to high albedo. While in case of maximum storage flux, significant changes has been observed in Case-4 (Mixed land use) adaptation measure where it has decreased by 17.26 Wm^{-2} from its original value. Highest reduction in maximum values of sensible heat flux have been found in monsoon season months i.e., July, August and September because of more consumption of available energy for evapotranspiration and vaporization. Such a reduction in peak values of sensible heat flux indicates effectiveness of the adaptation measures in which impervious or built-up surfaces are proposed to be converted into vegetation. It can be concluded from the results that proposed adaptation measures are effective in reducing the sensible heat flux in day time as well as in night time leading to reduction in surface temperature, which means adverse impacts of LULC conversions due to urbanization can be contained from these adaptation measures.

Comparing the performance of four adaptation measures in altering the latent heat flux, it has been found that in case of latent heat flux during night time, barren to forest, building to vegetation and mixed land-use class conversions (adaptation measures: Case-1, Case-3 and Case-4) have shown increasing trend in almost all months during day as well as night time. This is happening due to proposed conversion of barren land and roof tops of the buildings into vegetation cover, which leads to more energy consumption in evapotranspiration resulting reduction in sensible heat flux and surface temperature. Also increase in vegetation is increasing more outflow of radiation due to increase in high albedo surfaces and more partitioning of available energy into latent heat leading to cooling and less surface temperature. It can be concluded from the results that adaptation measures are successful in increasing the latent heat flux during day time significantly which can reduce surface temperature which will leads to cooler urban environment.

The decreasing trend in the maximum surface temperature has been observed in building to vegetation and mixed land use class adaptations (adaptation measures: Case-3 and Case-4) due to transformation of impervious to pervious surfaces and increase in vegetation coverage. The most effective adaptation measure in case of surface temperature is the Case-4, mixed land use adaptation where all possible conversions are considered simultaneously. Thus, increases the proportion of vegetation as compared to the other conversion classes is the most effective adaptation measure in controlling the surface temperature. Proposed adaptation measures are found to be effective in reducing the adverse effects of urbanization on SEB fluxes and surface temperature which in turn directly influences the air temperature. Therefore, it can be concluded that adaptation measures are successful in favorably altering the SEB fluxes and surface temperature which will leads to cooler urban environment. Results are also in agreement with similar conclusions found out in different reported studies (Hart and Sailor, 2009b; Deng et al., 2013; Coseo and Larsen, 2014; Feyisa et al., 2014; Gillner et al., 2015; Huang et al., 2015b; Akbari et al., 2016).

Quantitative relationships established between LULC fractions and SEB fluxes further can be used to investigate the adaptations in different proportions. Quantitative relationships have been discussed in Chapter 7.

CHAPTER 9

CONCLUSIONS AND RECOMMENDATIONS

The conclusions of this study and recommendations for the future research work are presented in this chapter.

9.1 CONCLUSIONS

Present study has been successful in achieving targeted research objectives. Climate change has been assessed and impact of LULC changes on micro-climate in terms of changes in surface energy balance (SEB) fluxes has been determined. Further, quantitative relationship between micro-climate representing SEB fluxes and LULC fractions are established and potential of different purposeful LULC transformations related adaptation measures has been determined. Study is successful in finding the answers of research questions mentioned in Chapter 1 and the answers are mentioned below.

- Climate change assessment has been successfully carried out by determining changing trends in representative meteorological parameters i.e., temperature and rainfall using parametric & non-parametric statistical trend analysis techniques at different temporal scales. Possible future climatic trends have also been determined using statistical downscaling of CMIP5 data for different three RCP Scenarios.
- LULC changes are affecting micro-climate of any area. Surface energy balance of the study area has been modelled using SUEWS model to determine the effects of the change in LULC in altering SEB fluxes which represents micro-climate.
- Change in SEB fluxes due to change in LULC in different years have been studied by simulating the SEB in three different Scenarios where actual conditions, change in LULC along with constant meteorology and with constant LULC and changing meteorology are considered. Changes in SEB fluxes in three different Scenarios indicate the effects of LULC changes over the years. The mathematic relationships have been established between LULC fractions and SEB fluxes.
- Relative changes in SEB constituents in different years has been determined corresponding to the three different Scenarios of LULC and meteorology. Relative changes in SEB fluxes and surface temperature in three Scenarios revealed the relative contribution of LULC changes in altering the micro-climate.

- Potential of various adaptations i. e., purposeful LULC transformations in favorably changing the SEB fluxes and surface temperature has been studied and effective adaptation measures are identified.
- Relative changes in SEB fluxes and surface temperature corresponding to different adaptation measures in different degrees, as compared to existing condition have been determined, which indicate their effectiveness in restricting the adverse impacts of changing climate.

Salient findings and conclusions of the research work have been presented below –

1. LULC information for 12 years has been extracted from the LULC maps prepared from supervised classification of multispectral satellite images of different year from 1973 to 2014. Detailed GIS database has been prepared for LULC information of different years and transformed into format suitable for SUEWS model conceptualization. Over the years (1973 to 2014) significant urbanization has been observed in both the areas i.e., Palam and Safdarjung. In Palam, built-up areas have increased from 1546.20 ha to 7747.70 ha from year 1973 to 2014 and in Safdarjung area built-up areas have increased from 2910.90 to 8499 ha in same period.
2. Assessment of climate change has been done by performing time series analysis of rainfall and temperature using 44 years of historical meteorological data (i.e., 1969-2012) and by predicting climate for the future through downscaling of CMIP5 data. The main findings of this analysis are as follows:
    - Significant increasing trends for average temperature has been observed for both the locations i.e., Palam and Safdarjung. Minimum temperature in almost all the temporal resolution is showing significant increasing trend for both the station at 95% significance level. The range of extreme annual daily minimum and maximum temperature at Palam Station was found to be 2.0 to 6.4℃ and 40.0 to 45.7℃, respectively. Significant increasing trends have been observed in the extreme annual daily minimum temperature (@0.015 ºC to 0.0022 ºC /yr) at both Palam and Safdarjung meteorological station.
    - Results of shift detection test have also revealed clear shift in temperature trends during year 1982 to 1997 for Palam station. Similarly, for Safdarjung station, shift has been observed during year 1986 to 1997.
    - The total rainfall has been showing increasing trend in monsoon season but not significant at Palam station whereas decreasing trend has been observed for

Safdarjung, which is also not significant. The total rainfall has been showing significant increasing trends in winter season (@ 0.82 mm/hydrologic yr) and shift in trend has been observed in year 1976 at Palam station.

- Significant increasing trends have been found for total rainfall in spring season (@ 2.02 mm/hydrologic yr) for Safdarjung station and also shift in trend has been observed in year 1995. Similarly, significant decreasing trends have been found in total rainfall of autumn season at Safdarjung meteorological station (@ -3.31 mm/hydrologic yr) and shift in trend has been observed in year 1991.

The results of Sen's slope, percentage change in mean, extreme average rainfall & temperature (annual/seasonal) and shift detection results revealed changes in micro-climate at both the meteorological stations.

3. Future temperature and rainfall has been projected using CanESM2, GCM model corresponding to CMIP5 experiment for three different RCP Scenarios (i.e., RCP 2.6, RCP 4.5 and RCP 8.5) and downscaled using SDSM model for Delhi. The main findings of this study are as follows:
    - In RCP 4.5 and 8.5 scenarios, annual mean minimum and maximum rainfall have been projected to decrease as compared to observed mean (1969 – 2005) from 1.82 mm to 1.74 and 1.71 mm in case of minimum and from 180.90 mm to 162.53 and 141.31 mm respectively in case of annual mean maximum. Similar trend has been observed for Safdarjung station also.
    - In RCP 4.5 and 8.5 scenarios for Palam, annual mean minimum temperature have been projected to decrease as compared to observed mean (1969 – 2005) from 19.68 ^{o}C to 19.62 and 19.60 ^{o}C and annual mean maximum temperature have been found to increase from 30.58 ^{o}C to 30.60 and 30.58 ^{o}C respectively. Similar trend has been observed for Safdarjung station also.
    - In RCP 4.5 and 8.5 scenarios for Palam, annual extreme minimum temperature have been projected to decrease as compared to observed mean (1969 – 2005) from 2.0 ^{o}C to 0.12 and 0.09 ^{o}C and annual extreme maximum temperature have been found to increase from 45.70 ^{o}C to 49.67 and 49.89 ^{o}C respectively. Similar trend has been observed for Safdarjung station also.

Results indicate that extreme maximum temperature is projected to increase significantly in RCP 4.5 and 8.5 scenarios.

3. SUEWS model has been conceptualized for the different years and found to be successful in simulating the SEB of both the areas.
4. Sensitivity analysis has been performed for Palam area to determine the most important parameters to which SUEWS model is sensitive. Albedo and emissivity have significant inverse relationship with net all-wave radiation. Drainage parameter has been found to another parameter to which SUEWS is sensitive and have proportional linear relationship with sensible heat flux and inverse relationship with latent heat flux.
5. Model was calibrated for selected coefficients and parameters by comparing simulated results iteratively with the observed data. The calibrated model parameters have been determined for different LULC classes. Calibrated value albedo varies from 0.10 to 0.21, emissivity values varies from 0.91 to 0.99, drainage parameter varies from 0 to 2.7, maximum storage capacity values vary from 0.8 to 2000, minimum storage capacity varies from 0.25 to 1.90, conductance parameter varies from 0.01 to 567 and maximum conductance varies from 7.4 to 33.1 for different LULC classes.
6. Model results are validated by comparing simulated SEB fluxes and reference hourly SEB flux values at different temporal scales and also by comparing seasonal day time and night time values of fluxes. Ratios of simulated values of fluxes have also been compared the referenced flux ratios. RMSE has been calculated for each simulated flux with respect to the referenced flux values. RMSE values vary from 19.95 to 201.74 Wm^{-2}. The results of validation have shown modelled results following similar patterns as observed data. Also, the ratios of simulated flux values are very close to the referenced flux ratios. Thus, it can be concluded that modelled results are validated and found within the satisfactory limits which is in line with the reported studies.
7. To investigate the influence of LULC characteristics on micro-climate in terms of change in SEB fluxes, three scenarios were conceptualized. In Scenario-A, SUEWS model is conceptualized for actual conditions i.e., actual LULC and meteorology are considered in the model for different years. In Scenario-B, the influence of change in LULC over the years has been with constant meteorology i.e., not considering indirect enforcing parameters like greenhouse gases for different years. In Scenario-C, influence of climate change forcing other than LULC change have

been conceptualized by considering constant LULC of base year (1973) and meteorology of respective years.

8. In scenario-A, for Palam area, daytime values of sensible heat flux (491.20 to 382.40 Wm^{-2}), net all wave radiation (622 to 481.30Wm^{-2}) and latent heat flux (175 to 35.5Wm^{-2}) are decreasing while storage heat flux values (159 to 161.50Wm^{-2}) and surface temperature (47.10 to 47.20 ^{o}C) are increasing. For Safdarjung area, daytime values of sensible heat flux (510.10 to 388.50 Wm^{-2}), net all wave radiation (638.3 to 488.8Wm^{-2}), surface temperature (46.90 to 45.10 ^{o}C) and latent heat flux (141.30 to 49.40Wm^{-2}) are decreasing while storage heat flux values (168.70 to 170.80Wm^{-2}) are found to be increasing.
9. In scenario-B, for Palam area, daytime values of sensible heat flux (491.20 to 469.10 Wm^{-2}) and latent heat flux (175 to 67.3Wm^{-2}) are decreasing while storage heat flux values (159 to 209.50Wm^{-2}), net all wave radiation (622 to 629.20 Wm^{-2}) and surface temperature (47.10 to 47.40 ^{o}C) are increasing. For Safdarjung area, the daytime values of sensible heat flux (510.10 to 484.70 Wm^{-2}) and latent heat flux (141.30 to 69.80Wm^{-2}) are decreasing while storage heat flux values (168.70 to 170.80Wm^{-2}), net all wave radiation (638.3 to 642.8Wm^{-2}) and surface temperature (46.90 to 47.10^{o}C) are found to be increasing.
10. In scenario-C, for Palam area, daytime values of sensible heat flux (491.20 to 376 Wm^{-2}), net all wave radiation (622 to 475.60Wm^{-2}), storage heat flux values (159 to 118.30Wm^{-2}), surface temperature (47.10 to 46.90 ^{o}C) and latent heat flux values (175 to 73.5Wm^{-2}) are decreasing. For Safdarjung area, the daytime values of sensible heat flux (510.10 to 376 Wm^{-2}), net all wave radiation (638.30 to 485.40Wm^{-2}), storage heat flux values (168.70 to 125.80Wm^{-2}), surface temperature (46.90 to 45^{o}C) and latent heat flux (141.30 to 78.5Wm^{-2}) are decreasing.
11. Extreme values of day time & night time fluxes and surface temperature have been determined for three scenarios. Scenario-B significant changes have been found in in net all-wave radiation, turbulent heat fluxes and surface temperature extreme values as compared to other two scenarios. In Scenario-B, for Palam station, extreme values of day time latent heat flux values (924.24 to 486.32Wm^{-2}) are decreasing whereas as sensible heat flux values (555.91 to 555.95 Wm^{-2}), storage heat flux (204.32 to 268.27Wm^{-2}), net all-wave radiation (728.88 to 734.74Wm^{-2})

and surface temperature (52.85 to 53.12ºC) are found to be increasing over the years. For Safdarjung station, extreme values of daytime latent heat flux (961.27 to 592.48Wm^{-2}) and sensible heat flux (583.83 to 572.72Wm^{-2}) are decreasing whereas as storage heat flux (214.79 to 278.16Wm^{-2}), net all-wave radiation (741.61 to 744.52Wm^{-2}) and surface temperature (52.55 to 52.76℃) are increasing over the study period.

12. Comparing the results of three scenarios, Scenario-B results are indicating relative contribution of urbanization in changing micro-climate in term of adverse change in SEB fluxes and surface temperature. Due to urbanization over the years, high albedo LULC areas like irrigated/unirrigated have been converted in low albedo LULC classes like settlement and built-up surfaces. Also, high emissivity areas like trees and forest areas are converted into low emissivity areas like buildings and paved areas. This conversion is responsible in reducing reflected radiations resulting in increase in net all-wave radiations. The Scenario-B is establishing that LULC changes is affecting micro-climate adversely.
13. To establish quantitative relationship between LULC and surface energy fluxes, different forms of linear and non-linear regression techniques have been used.
14. For both stations, strong significant relationship has been found between annual night time values of net all-wave radiation (min_annual (Q*)) and built-up (B) and vegetation (V) respectively. Two other significant relationships have been found between annual minimum value of storage heat flux i.e., min_ annual (ΔQS) with built-up fractions and annual maximum value of storage heat flux i.e., max_ annual (ΔQS) with vegetation fractions for both areas i.e., Palam and Safdarjung.
15. Developed quantitative relationships are found to be useful in determining the relative changes in SEB fluxes corresponding to changes in LULC of any area. These equations further found to be useful in determining the possible effective adaptation measures in urban areas to contain adverse impacts of climate change
16. Potential of selected adaptation measures involving purposeful alterations in land cover and surfaces in different % in favorably altering the net all-wave radiation, turbulent heat fluxes and surface temperature have been explored through simulating the SEB fluxes corresponding to LULC information of respective adaptations.

17. A quantitative study of reactive adaptation to climate change can help in assessment of whether reactive adaptation is successful in offsetting adverse impacts of climate change. Possible adaptation by partial conversion of hard surfaces like paved areas with vegetation/grass and covering of roof tops with vegetation/grass have been found to be effective adaptation measures in limiting the adverse changes in surface energy balance and surface temperature.
18. Peak value of annual maximum net all-wave radiation can be reduced by 11.0 Wm^{-2} (occurred in the month of March) through 50% covering of built-up areas with vegetation/grass.
19. Reduction in peak value of annual minimum hourly storage heat flux has been reduced by -13.84Wm^{-2} considering all proposed adaptation measures (barren to vegetation, Built-up to grass, paved areas to grass etc.) at (occurred in the month of March) 50% conversion rate. Peak value of annual maximum hourly storage heat flux has been reduced by 17.26 Wm^{-2} considering all proposed adaptation measures (barren to vegetation, Built-up to grass, paved areas to grass etc.) at (occurred in the month of March) March 50% conversion rate.
20. Sensible and latent heat fluxes are also changing favorable in different adaptation measures. Latent heat flux is found to be increasing and sensible heat flux found to be decreasing in optimum adaptations which indicates the effectiveness of the adaptation measures in favorably altering the SEB fluxes.
21. A reduction of 0.21 ^{o}C in annual average maximum hourly surface temperature has been found from the optimum case of adaptation.
22. Partial covering of built-up areas with grass or vegetation has been found as the most effective adaptation measure. Further, loss of green areas and vegetation as a result of urbanization may further contribute to increase in day and night time temperature. Study results are successful in demonstrating quantitatively that suitable adaptation measures related to LULC are effective in limiting the adverse effects of climate change due to urbanization.

9.2 LIMITATIONS AND FUTURE SCOPE OF THE STUDY

The present work is successful in determining the impact of LULC on micro-climate using SEB modelling. However, this study has some limitations which are as follows:

1. In this study, limited data were available for validation of the model. It would have improved the calibration of model if more data were available.

2. SEB modelling has been performed using SUEWS model, therefore the study results have impact of all assumptions and uncertainties of the model.
3. Model is using number of sub-models to calculate different parameters required for the computation of SEB components. Therefore, the model results may also have computational uncertainties of these sub-models.
4. Model results are representing spatially averaged surface energy balance and behavior of an area whereas referenced data used for the calibration and validation was point data, that's why patterns of modelled and referenced data are matching quite satisfactorily but the values are not identical.
5. LULC information are extracted from medium resolution satellite images because high resolution images for all the years were not available. Therefore, errors of LULC classification may have affected the model results.
6. The data of surface characteristics have been taken from literature, whatever the uncertainties which were available in the data may have affected the model results.
7. Limited number of adaptation measures have been investigated to demonstrate the potential of LULC transformations. However, other adaptation measures may also be beneficial.
8. Model results should have been validated from detailed field observation, which has not been done due to non-availability of data.

Recommendation of future research work includes:

- Such modelling work can be improved by using high resolution LULC information.
- In the present study, modelling has been done at coarse resolution. In future, study can be performed at finer resolutions.
- Modelling results should be supported with detailed experimental observations.
- Potential of other adaptation measures may also be explored like conversion of blacktop bituminous road surfaces with more reflective road surfaces like cement, concrete and shading of walls using different types of material and use of more reflective surface for paving etc.

REFERENCES

Ab. Ghani, A., Ali, R., Zakaria, N.A., Hasan, Z.A., Chang, C.K., Ahamad, M.S.S., 2010. A temporal change study of the Muda River system over 22 years. International Journal of River Basin Management 8, 25–37.

Abeysingha, N.S., Singh, M., Sehgal, V.K., Khanna, M., Pathak, H., 2016. Analysis of trends in streamflow and its linkages with rainfall and anthropogenic factors in Gomti River basin of North India. Theoretical and Applied Climatology 123, 785–799.

Ackerman, B., 1985. Temporal March of the Chicago Heat Island. Journal of Applied Meteorology 24, 547.

Ahmed, B., Kamruzzaman, M., Zhu, X., Rahman, M., Choi, K., 2013. Simulating land cover changes and their impacts on land surface temperature in Dhaka, Bangladesh. Remote Sensing 5, 5969–5998.

Akbari, H., Cartalis, C., Kolokotsa, D., Muscio, A., Pisello, A.L., Rossi, F., Santamouris, M., Synnefa, A., Wong, N.H., Zinzi, M., 2016. Local climate change and urban heat island mitigation techniques – the state of the art Journal of Civil Engineering and Management, 22,1-16.

Ali-Toudert, F., Djenane, M., Bensalem, R., Mayer, H., 2005. Outdoor thermal comfort in the old desert city of Beni-Isguen, Algeria. Climate Research 28, 243–256.

Ali-Toudert, F., Mayer, H., 2007. Effects of asymmetry galler is overhanging facades and vegetation on thermal comfort in urban street canyons. Solar Energy.

Alpert, P., Krichak, S.O., Shafir, H., Haim, D., Osetinsky, I., 2008. Climatic trends to extremes employing regional modeling and statistical interpretation over the E. Mediterranean. Global and Planetary Change 63, 163–170.

Araya, Y.H., Cabral, P., 2010. Analysis and modeling of urban land cover change in Setubal and Sesimbra, Portugal. Remote Sensing 2, 1549–1563.

Argüeso, D., Evans, J.P., Fita, L., Bormann, K.J., 2014. Temperature response to future urbanization and climate change. Climate Dynamics 42, 2183–2199.

Arnfield, A. J., Grimmond, C.S.B., 1998. An urban canyon energy budget model and its application to urban storage heat flux modeling. Energy and Buildings 27, 61–68.

Arnfield, A.J., 2000. A simple model of urban canyon energy budget and its validation. Physical Geography.

Arnfield, A.J., 2003. Two decades of urban climate research: A review of turbulence, exchanges of energy and water, and the urban heat island. International Journal of Climatology 23, 1–26.

Arora, M., Goel, N.K., Singh, P., 2005. Evaluation of temperature trends over India. Hydrological Sciences Journal 50, 37–41.

Arora, V.K., Boer, G.J., 2010. Uncertainties in the 20th century carbon budget associated with land use change. Global Change Biology 16, 3327–3348.

Arrowsmith, C., Mandla, V.R., 2017. Institutional approaches for building intercultural understanding into the curriculum: an Australian perspective. Journal of Geography in Higher Education.

Avila, F.B., Pitman, a. J., Donat, M.G., Alexander, L. V., Abramowitz, G., 2012. Climate model simulated changes in temperature extremes due to land cover change. Journal of Geophysical Research 117, 1–19.

Baede, M., Report, I., Use, L., Change, L., Earth, T., 2000. Appendix I : Glossary Notes.

Baidya Roy, S., Avissar, R., 2002. Impact of land use/land cover change on regional hydrometeorology in Amazonia. Journal of Geophysical Research Atmospheres 107, LBA 4-1-LBA 4-12.

Baidya Roy, S., Hurtt, G.C., Weaver, C.P., Pacala, S.W., 2003. Impact of historical land cover change on the July climate of the United States. Journal of Geophysical Research: Atmospheres 108.

Baklanov, A., Mestayer, P.G., Clappier, A., 2008. Towards improving the simulation of meteorological fields in urban areas through updated/advanced surface fluxes description. Atmospheric Chemistry and Physics 8.

Baltas, E.A., 2009. Climate change and associated implications for the water policy framework in the basin of Venetikos. International Journal of Water Resources Development, 25(3), pp.491-506.

Barradas, V.L., Tejeda-Martínez, A. and Jáuregui, E., 1999. Energy balance measurements in a suburban vegetated area in Mexico City. Atmospheric Environment 33, 4109–4113.

Basistha, A., Arya, D.S., Goel, N.K., 2008. Spatial distribution of rainfall in Indian Himalayas - A case study of Uttarakhand Region. Water Resources Management 22, 1325–1346.

Basistha, A., Arya, D.S., Goel, N.K., 2009. Analysis of historical changes in rainfall in the Indian Himalayas. International Journal of Climatology 29, 555–572.

Basistha, A., Goel, N.K., Arya, D.S., Gangwar, S.K., 2007. Spatial pattern of trends in Indian sub-divisional rainfall. Technology 22, 47–57.

Bekele, H.M., 2009. Evaluation of Climate Change impact on Upper Blue Nile Basin Reservoirs. Arba Minch University.

Bera, S., 2017. Trend analysis of rainfall in Ganga Basin, India during 1901-2000. American Journal of Climate Change, 6, 116–131.

Best, M.J., 1998. A model to predict surface temperatures. Boundary-Layer Meteorology.

Best, M.J., 2005. Representing urban areas within operational numerical weather prediction models. Boundary-Layer Meteorology.

Best, M.J., 2006. Progress towards better weather forecasts for city dwellers: from short range to climate change. Theoretical and Applied Climatology.

Betts, R.A., 2001. Biogeophysical impacts of land use on present-day climate: near-surface temperature change and radiative forcing. Atmospheric Science Letters 2, 39–51.

Betts, R.A., Boucher, O., Collins, M., Cox, P.M., Falloon, P.D., Gedney, N., Hemming, D.L., Huntingford, C., Jones, C.D., Sexton, D.M.H., Webb, M.J., 2007. Projected increase in continental runoff due to plant responses to increasing carbon dioxide. Nature 448, 1037–1041.

Boberski, M., Allen, B., 2014. OWASP Application Security Verification Standard (ASVS). Owasp.

Bonan, G.B., 1997. Effects of land use on the climate of the United States. Climatic Change 37, 449–486.

Bonan, G.B., 1999. Frost followed the plow: Impacts of deforestation on the climate of the United States. Ecological Applications 9, 1305–1315.

Bookhagen, B., Burbank, D.W., 2006. Topography, relief, and TRMM-derived rainfall variations along the Himalaya. Geophysical Research Letters 33.

Bottyán, Z., Kircsi, A., Szegedi, S., Unger, J., 2005. The relationship between built-up areas and the spatial development of the mean maximum urban heat island in Debrecen, Hungary. International Journal of Climatology 25, 405–418.

Bounoua, L., DeFries, R.S., Imhoff, M.L., Steininger, M.K., 2004. Land use and local climate: A case study near Santa Cruz, Bolivia. Meteorology and Atmospheric Physics 86, 73–85.

Bourbia, F., Awbi, H.B., 2004. Building cluster and shading in urban canyon for hot dry climate Part 1: Air and surface temperature measurements. Renewable Energy 29, 249–262.

Brekke, L., Thrasher, B.L., Maurer, E.P., Pruitt, T., 2013. Downscaled CMIP3 and CMIP5 climate projections: Release of downscaled CMIP5 climate projections, comparison with preceding information, and summary of user needs. US Department of the Interior, Bureau of Reclamation 104.

Brovkin, V., Arora, V., Kato, E., Boysen, L., Gayler, V., 2012. Effect of land use changes on climate in CMIP5 Projections. Climate Research 14, 14356.

Bruse, M., Fleer, H., 1998. Simulating surface–plant–air interactions inside urban environments with a three dimensional numerical model. Environmental Modelling {&} Software.

Budyko, M.I., 1972. The future climate. Eos, Transactions American Geophysical Union.

Buraihi, F.H., Shariff, A.R.M., 2015. Selection of rainwater harvesting sites by using remote sensing and GIS techniques: A case study of Kirkuk, Iraq. Jurnal Teknologi 76, 75–81.

Calzadilla, A., Rehdanz, K., Betts, R., Falloon, P., Wiltshire, A., Tol, R.S.J., 2013. Climate change impacts on global agriculture. Climate Change 120, 357–374.

Carlson, T.N., Arthur, S.T., 2000. The impact of land use - land cover changes due to urbanization on surface microclimate and hydrology: a satellite perspective. Global and Planetary Change 25, 49–65.

Cavan, G., Handley, J.F., Aylen, J., Albertson, K., McMorrow, J., Lindley, S., McEvoy, D., 2006. Climate change and the visitor economy in the uplands. International Journal of Biodiversity Science & Management 2, 170–173.

Cayan, D.R., Douglas, A. V, 1984. Urban influences on surface temperatures in the Southwestern United-States during recent decades. Journal of Climate and Applied Meteorology 23, 1520–1530.

Chakraborty, S., Pandey, R.P., Chaube, U.C., Mishra, S.K., 2013. Trend and variability analysis of rainfall series at Seonath River Basin, Chhattisgarh (India). International Journal of Applied Sciences and Engineering Research 2, 425–434.

Chakraborty, S.D., Kant, Y., Mitra, D., 2015. Assessment of land surface temperature and heat fluxes over Delhi using remote sensing data. Journal of Environmental Management 148, 143–152.

Chang, H.H., Zhou, J., Fuentes, M., 2010. Impact of climate change on ambient ozone level and mortality in Southeastern United States. International Journal of Environmental Research and Public Health 7, 2866–2880.

Change, S., 2008. The phanerozoic record of global sea-level change. Science 1293, 1293–1298.

Charalampopoulos, I., Tsiros, I., Chronopoulou-Sereli, A., Matzarakis, A., 2013. Analysis of thermal bioclimate in various urban configurations in Athens, Greece. Urban Ecosystems 16, 217–233.

Chase, T.N., Pielke Sr., R. a., Kittel, T.G.F., Nemani, R.R., Running, S.W., 2000. Simulated impacts of historical land cover changes on global climate in northern winter. Climate Dynamics 16, 93–105.

Chen, F., 2007. The Noah land surface model in WRF: a short tutorial. NCAR, LSM Group Meeting, Apr.

Chen, X.-L., Zhao, H.-M., Li, P.-X., Yin, Z.-Y., 2006. Remote sensing image-based analysis of the relationship between urban heat island and land use/cover changes. Remote Sensing of Environment Thermal Remote Sensing of Urban Areas 104, 133–146.

Chen, Y., Wong, N.H., Yu, C., Hien, W.N., 2006. Thermal benefits of city parks. Energy and Buildings 38, 105–120.

Cheng, C.S., Auld, H., Li, Q., 2012. Possible impacts of climate change on extreme weather events at local scale in south – central Canada 963–979.

Chibbar, R.K., 1985. Soils of Delhi and their management. Soils of India and Their Management, pp.72-86.

Christen, A., Vogt, R., 2004. Energy and radiation balance of a central European city. International Journal of Climatology 24, 1395–1421.

Christidis, L., Rheindt, F.E., Boles, W.E., Norman, J.A., 2010. Plumage patterns are good indicators of taxonomic diversity, but not of phylogenetic affinities, in Australian grasswrens Amytornis (Aves: Maluridae). Molecular Phylogenetics and Evolution 57, 868–877.

Christidis, N., Stott, P.A., Brown, S.J., 2011. The role of human activity in the recent warming of extremely warm daytime temperatures. Journal of Climate 24, 1922–1930.

Christy, J.R., Norris, W.B., Redmond, K., Gallo, K.P., 2006. Methodology and results of calculating central California surface temperature trends: Evidence of human-induced climate change.Journal of Climate 19, 548–563.

Chung, U., Choi, J., Yun, J.I., 2004. Urbanization effect on the observed change in mean monthly temperatures between 1951-1980 and 1971-2000 in Korea. Climatic Change 66, 127–136.

Cinar, İ., 2015. Assessing the Correlation between Land Cover Conversion and Temporal Climate Change—A Pilot Study in Coastal Mediterranean City, Fethiye, Turkey. Atmosphere 6, 1102–1118.

Cleugh, H.A. and Grimmond, C.S.B., 2001. Modelling Regional Scale Surface Energy Exchanges and Growth in a Hetrogeneous, Urban-Rural Landscape. Boundary-Layer Meteorology 98, 1–31.

Cohen, J.L., Furtado, J.C., Barlow, M., Alexeev, V.A., Cherry, J.E., 2012. Asymmetric seasonal temperature trends. Geophysical Research Letters 39, 1–7.

Comber, A. J., Fisher, P. F., and Wadsworth, R.A., 2005. What is land cover. Planning and Design 32, 199–209.

Congalton, R.G.G., Green, K., 1999. Assessing the accuracy of remotely sensed data: principles and applications. Lewis Pub—lishers, Boca Raton, Fla.

Contribution to the Fifth Assessment Report of the Intergovernmental Panel on Climate Change, 2014. Climate Change 2013 - The Physical Science Basis, Climate Change 2013 - The Physical Science Basis.

Copeland, J.H., Pielke, R. A., Kittel, T.G.F., 1996. Potential climatic impacts of vegetation change: A regional modeling study. Journal of Geophysical Research 101, 7409.

Coseo, P., Larsen, L., 2014. How factors of land use/land cover, building configuration, and adjacent heat sources and sinks explain Urban Heat Islands in Chicago. Landscape and Urban Planning 125, 117–129.

Coulibaly, P., Dibike, Y.B., Anctil, F., 2005. Downscaling precipitation and temperature with Temporal Neural Networks. Journal of Hydrometeorology 6, 483–496.

Cox, P.M., Huntingford, C., Harding, R.J., 1998. A canopy conductance and photosynthesis model for use in a GCM land surface scheme. Journal of Hydrology 212–213, 79–94.

Crawford, T.M., Bluestein, H.B., 2000. An operational, diagnostic surface energy budget model. Journal of Applied Meteorology.

CSB, G., Blackett, M., Best, M., J Barlow, JJ Baik, S Belcher, SI Bohnenstengel, I Calmet, F Chen, A Dandou, K Fortuniak, M.L.G., R Hamdi, M Hendry, T Kawai, Y Kawamoto, H Kondo, ES Krayenhoff, SH Lee, T Loridan, A Martilli, V Masson, S Miao, K.O., 2010. The international urban energy balance models comparison project: first results from phase 1. Journal of Applied Meteorology and Climatology.

Cui, L., Shi, J., 2012. Urbanization and its environmental effects in Shanghai, China. Urban Climate 2, 1–15.

Cui, X., Graf, H.F., Langmann, B., Chen, W., Huang, R., 2006. Climate impacts of anthropogenic land use changes on the Tibetan Plateau. Global and Planetary Change 54, 33–56.

Cunderlik, J.M., Burn, D.H., 2004. Linkages between regional trends in monthly maximum flows and selected climatic variables. Journal of Hydrologic Engineering 9, 246–256.

Dandou, A., Tombrou, M., Akylas, E., 2005. Development and evaluation of an urban parameterization scheme in the Penn State/NCAR Mesoscale Model (MM5). Journal of Geophysical Research: Atmospheres.

Das, Y., 2015. Water balance and climatic classification of a tropical city Delhi -India. American Journal of Water Resources 3, 124–146.

Das, Y., Padmanabhamurty, B., 2008. Energy balance of a suburban vegetated area in a tropical city - Delhi (India). Journal of Environmental Science and Engineering 50, 103–110.

Das, Y., Padmanabhamurty, B., 2009. Energy and water balance studies in the boundary layer over Delhi (India). Contributions to Geophysics 39, 163–185.

Das, Y., Padmanabhamurty, B., 2009a. Spatial and temporal distributions of radiation balance components over Delhi. Contributions to Geophysics and Geodesy 39, 355–377.

Das, Y., Padmanabhamurty, B., Murty, A.S.N., 2014. Some parameterizations of Radiative Fluxes at Atmospheric Boundary Layer (ABL). Journal of Atmospheric 2, 1–5.

Dash, S.K., Hunt, J.C.R., 2007. Variability of climate change in India. Current Science 93, 782–788.

Davis, R.E., Knappenberger, P.C., Micheaels, P.J., Novicoff, W.M., 2004. Seasonality of climate-human mortality relationships in US cties and impacts of climate change. Climate Research 26, 61–76.

De Noblet-Ducoudré, N., Boisier, J.P., Pitman, A., Bonan, G.B., Brovkin, V., Cruz, F., Delire, C., Gayler, V., Van den Hurk, B.J.J.M., Lawrence, P.J. and Van Der Molen, M.K., 2012. Determining robust impacts of land-use-induced land cover changes on surface climate over North America and Eurasia: Results from the first set of LUCID experiments. Journal of Climate 25, 3261–3281.

De, U.S., Rao, G.S.P., 2004. Urban climate trends--the Indian scenario. Indian Geophysical Union. 8, 199–203.

Deng, M., MacE, G.G., Wang, Z., Okamoto, H., 2010. Tropical composition, cloud and climate coupling experiment validation for cirrus cloud profiling retrieval using Cloudsat Radar and CALIPSO Lidar. Journal of Geophysical Research Atmospheres 115.

Deng, X., Güneralp, B., Su, H., 2014. Systematic modeling of land use impacts on surface climate. Land Use Impacts on Climate.

Deng, X., Zhao, C., Yan, H., 2013. Systematic modeling of impacts of land use and land cover changes on regional climate: A review. Advances in Meteorology 2013.

Deng, X.Z., Shi, Q.L., Zhang, Q., Shi, C.C., Yin, F., 2015. Impacts of land use and land cover changes on surface energy and water balance in the Heihe River Basin of China, 2000-2010. Physics and Chemistry of the Earth 79–82, 2–10.

Dhakal, S., K. Hanaki, 2002. Improvement of urban warming by managing heat discharges and surface modifications in Tokyo. Energy and Buildings 34, 13–23.

Dhorde, A., Gadgil, A., 2009. Long-term temperature trends at four largest cities of India during the twentieth Century. Indian Geophysical Union 13, 85–97.

Diffenbaugh, N.S., 2009. Influence of modern land cover on the climate of the United States. Climate Dynamics 33, 945–958.

Dimri, A.P., Yasunari, T., Wiltshire, A., Kumar, P., Mathison, C., Ridley, J., Jacob, D., 2013. Application of regional climate models to the Indian winter monsoon over the western Himalayas. Science of the Total Environment 468–469, S36–S47.

Dong, J., Xiao, X., Chen, B., Torbick, N., Jin, C., Zhang, G., Biradar, C., 2013. Mapping deciduous rubber plantations through integration of PALSAR and multi-temporal Landsat imagery. Remote Sensing of Environment 134, 392–402.

Dong, S., Yan, X., Xiong, Z., 2013. Varying responses in mean surface air temperature from land use/cover change in different seasons over northern China. Acta Ecologica Sinica 33, 167–171.

Duhan, D., Pandey, A., Gahalaut, K.P.S., Pandey, R.P., 2013. Spatial and temporal variability in maximum, minimum and mean air temperatures at Madhya Pradesh in central India. Comptes Rendus - Geoscience 345, 3–21.

Duncan, J.M.A., Dash, J., Atkinson, P.M., 2012. Analysing temporal trends in the Indian summer monsoon and its variability at a fine spatial resolution.

Dupont, S., Mestayer, P.G., 2006. Parameterization of the urban energy budget with the submesoscale soil model. Journal of Applied Meteorology and.

Dutta, S., Geoinformatics for urban planning and management. Department of Civil Engineering, IIT Guwahati, Lecture.

Easterling, D. R., Horton B., Jones Ph. D., Peterson Th. C., Karl Th. R., Parker D. E., Salinger M. J., Razuvayev V., Plummer N., J.P.& F.C.K., 1997. Maximum and minimum temperature trends for the Globe. Science 277, 364–367.

Easterling, D.R., Evans, J.L., Groisman, P.Y., Karl, T.R., Kunkel, K.E., Ambenje, P., 2000. Observed variability and trends in extreme climate events: A Brief Review. Bulletin American Meteorological Society 417–425.

Eastman, J.L., Coughenour, M.B., Pielke, R.A., 2001. The regional effects of {CO2} and landscape change using a coupled plant and meteorological model. Glob. Change Biol. 7, 797–815.

Eliasson, I., 2000. The use of climate knowledge in urban planning. Landscape and urban planning 48, 31–44.

Erell, E., Williamson, T., 2006. Simulating air temperature in an urban street canyon in all weather conditions using measured data at a reference meteorological station. International Journal of Climatology.

Essery, R.L.H., Best, M.J., Betts, R.A., 2003. Explicit representation of subgrid heterogeneity in a GCM land surface scheme. Journal of Hydrometeorology.

Ezber, Y., Sen, O.L., Kindap, T., Karaca, M., 2007. Climatic effects of urbanization in Istanbul: a statistical and modeling analysis. International Journal of Climatology 27, 667–679.

Fall, S., Niyogi, D., Gluhovsky, A., Pielke, R.A., Kalnay, E., Rochon, G., 2010. Impacts of land use land cover on temperature trends over the continental United States: Assessment using the North American Regional Reanalysis. International Journal of Climatology 30, 1980–1993.

Fan, X., Ma, Z., Yang, Q., Han, Y., Mahmood, R., Zheng, Z., 2015. Land use/land cover changes and regional climate over the Loess Plateau during 2001-2009. Part I: observational evidence. Climatic Change 129, 427–440.

Fealy, R., Sweeney, J., 2008. Statistical downscaling of temperature, radiation and potential evapotranspiration to produce a multiple GCM ensemble mean for a selection of sites in Ireland. Irish Geography 41, 1–27.

Feddema, J.J., 2005. The Importance of Land-cover change in simulating future climates. Science 310, 1674–1678.

Feng, M., Wang, Q., Hao, Q., Yin, Y., Song, Z., Wang, H., Liu, H., 2016. Determinants of soil erosion during the last 1600 years in the forest-steppe ecotone in Northern China reconstructed from lacustrine sediments. Palaeogeography, Palaeoclimatology, Palaeoecology 449, 79–84.

Ferraro, F.R., Sills, A., Rood, R.T., Paltrinieri, B., Buonanno, R., 2003. Blue Straggler Stars: A direct comparison of star counts and population ratios in six Galactic Globular Clusters. ApJ 588, 464–477.

Feyisa, G.L., Dons, K., Meilby, H., 2014. Efficiency of parks in mitigating urban heat island effect: An example from Addis Ababa. Landscape and Urban Planning 123, 87–95.

Findell, K.L., Pitman, A.J., England, M.H., Pegion, P.J., 2009. Regional and global impacts of land cover change and sea surface temperature anomalies. Journal of Climate 22, 3248–3269.

Fischer, E. ~M., Schär, C., 2009. Future changes in daily summer temperature variability: driving processes and role for temperature extremes. Climate Dynamics 33, 917–935.

Foody, G.M., 2002. Status of land cover classification accuracy assessment. Remote Sensing of Environment 80, 185–201.

Forest Survey of India, 2013. India state of the forest report. Ministry of Environment and Forests, Dehra Dun, India 252.

Fortuniak, K., Offerle, B., 2004. Application of a slab surface energy balance model to determine surface parameters for urban areas. Lund Electronic Reports in.

Fortuniak, K., Offerle, B., Grimmond, C.S.B., 2009. Slab surface energy balance scheme and its application to parameterisation of the energy fluxes on urban areas, NATO ASI, Kiev, Ukraine, 4-15.05 2004,. Springer Berlin Heidelberg.

Frauenfeld, O.W., Zhang, T., Sereeze, M., 2005. Climate change and variability using European Centre for Medium-Range Weather Forcasts reanalysis (ERA-40) temperatures on the Tibetan Plateau. Journal of Geophysical Research 110.

Fu, C., 2003. Potential impacts of human-induced land cover change on East Asia monsoon. Global and Planetary Change.

Fujibe, F., 1995. Temperature rising trends at Japanese cities during the last hundred years and their relationships with population, population increasing rates and daily temperature ranges. Papers in Meteorology and Geophysics 46, 35–55.

Gadgil, A., Dhorde, A., 2005. Temperature trends in twentieth century at Pune, India. Atmospheric Environment 39, 6550–6556.

Gallo, K., Owen, T., 1999. Satellite-based adjustments for the urban heat island temperature bias. Journal of Applied Meteorology 38, 806–813.

Gallo, K.P., Owen, T.W., Easterling, D.R., Jamason, P.F., 1999. Temperature trends of the U.S. historical climatology network based on satellite-designated land use/land cover. Journal of Climate 12, 1344–1348.

Gao, Q., Yu, M., 1998. A model of regional vegetation dynamics and its application to the study of Northeast China Transect (NECT) responses to global change. Global Biogeochemical Cycles 12, 329–344.

Gao, X.J., Luo, Y., Lin, W.T., Zhao, Z.C., Giorgi, F., 2003. Simulation of effects of land use change on climate in China by a regional climate model. Advances in Atmospheric Sciences 20, 583–592.

Gao, Y., Fu, J.S., Drake, J.B., Lamarque, J.F., Liu, Y., 2013. The impact of emission and climate change on ozone in the United States under representative concentration pathways (RCPs). Atmospheric Chemistry and Physics 13, 9607–9621.

Georg a, G., Dudhia, J., Stauffer, D.R., 1994. A description of the fifth-generation Penn State/NCAR Mesoscale Model (MM5). NCAR Technical Note NCAR/TN-398+STR 121.

Georgi, J.N., Dimitriou, D., 2010. The contribution of urban green spaces to the improvement of environment in cities: Case study of Chania, Greece. Building and Environment 45, 1401–1414.

Gibbs, M.T., 2015. Guiding principles for infrastructure climate change risk and adaptation studies. Civil Engineering and Environmental Systems 0, 1–10.

Gill, S.E., Handley, J.F., Ennos, A. R., Pauleit, S., Pauliet, S., 2007. Adapting cities for climate change: The role of the Green Infrastructure. Built Environment 33, 115–133.

Gillner, S., Vogt, J., Tharang, A., Dettmann, S., Roloff, A., 2015. Role of street trees in mitigating effects of heat and drought at highly sealed urban sites. Landscape and Urban Planning 143, 33–42.

Giorgi, F., Lionello, P., 2008. Climate change projections for the Mediterranean region. Mediterranean climate: trends, variability and change 63, 90–104.

Giorgi, F., Mearns, L.O., 1999. Introduction to special section: Regional climate modeling revisited. Journal of Geophysical Research: Atmospheres (1984-2012) 104, 6335–6352.

Gocic, M., Trajkovic, S., 2013. Analysis of changes in meteorological variables using Mann-Kendall and Sen's slope estimator statistical tests in Serbia. Global and Planetary Change 100, 172–182.

Goenster, S., Wiehle, M., Gebauer, J., Mohamed Ali, A., Stern, R.D., Buerkert, A., 2015. Daily rainfall data to identify trends in rainfall amount and rainfall-induced agricultural events in the Nuba Mountains of Sudan. Journal of Arid Environments 122, 16–26.

Good, P.I., Hardin, J.W., 2006. Common errors in Statistics (and How to Avoid Them) Second Edition.

Goodhead, D.T., 1988. Spatial and temporal distribution of energy. Health Physcis 55, 231–240.

Goodridge, J.D., 1992. Urban bias influences on long-term California air temperature trends. Atmospheric Environment. Part B, Urban Atmosphere 26, 1–7.

Gordon, L.J., Steffen, W., Jainsson, B.F., Folke, C., Falkenmark, M., Johannessen, A., 2005. Human modification of global water vapor flows from the land surface. Proceedings of the National Academy of Sciences of the United States of America 102, 7612–7617.

Gorr, W.L., Kurland, K.S., 2008. ArcGIS 9: ArcMap Tutorial. ESRI, Inc.

Gowda, K., Manjuantha, K., 2008. Study of climatic changes at Davangere region by using climatological data. Water and Energy.

Grawe, D., Cai, X.M., Harrison, R.M., 2007. Large eddy simulation of shading effects on NO2 and O3 concentrations within an idealised street canyon. Atmospheric Environment 41, 7304–7314.

Gregory, J.M., Mitchell, J.F.B., 1995. Simulation of daily variability of surface temperature and precipitation over Europe in the current and 2xCO2 climates using the UKMO climate model. Quarterly Journal of the Royal Meteorological Society 121, 474–476.

Grimmond, C.S.B., Best, M., Barlow, J., Arnfield, A.J., Baik, J.-J., Baklanov, A., Belcher, S., Bruse, M., Calmet, I., Chen, F., Clark, P., Dandou, A., Erell, E., Fortuniak, K., Hamdi, R., Kanda, M., Kawai, T., Kondo, H., Krayenhoff, S., Lee, S.H., Limor, S.-B., Martilli, A., Masson, V., Miao, S., Mills, G., Moriwaki, R., Oleson, K., Porson, A., Sievers, U., Tombrou, M., Voogt, J., Williamson, T., 2009. Urban Surface Energy Balance Models: Model Characteristics and Methodology for a Comparison Study. Meteorological and Air Quality Models for Urban Areas 97–123.

Grimmond, C.S.B., Blackett, M., Best, M.J., Baik, J.J., Belcher, S.E., Beringer, J., Bohnenstengel, S.I., Calmet, I., Chen, F., Coutts, A., Dandou, A., Fortuniak, K., Gouvea, M.L., Hamdi, R., Hendry, M., Kanda, M., Kawai, T., Kawamoto, Y., Kondo, H., Krayenhoff, E.S., Lee, S.H., Loridan, T., Martilli, A., Masson, V., Miao, S., Oleson, K., Ooka, R., Pigeon, G., Porson, A., Ryu, Y.H., Salamanca, F., Steeneveld, G.J., Tombrou, M., Voogt, J.A., Young, D.T., Zhang, N., 2011. Initial results from phase 2 of the international urban energy balance model comparison. International Journal of Climatology 31, 244–272.

Grimmond, C.S.B., Blackett, M., Best, M.J., Barlow, J., Baik, J.J., Belcher, S.E., Bohnenstengel, S.I., Calmet, I., Chen, F., Dandou, A. and Fortuniak, K., 2010. The international urban energy balance models comparison project: first results from phase 1. Journal of Applied Meteorology and Climatology.

Grimmond, C.S.B., Cleugh, H.A., Oke, T.R., 1991. An objective urban heat storage model and its comparison with other schemes. Atmospheric Environment. Part B, Urban Atmosphere 25, 311–326.

Grimmond, C.S.B., Oke, T.R., 1991. An evapotranspiration-interception model for urban areas. Water Resources Research.

Grimmond, C.S.B., Oke, T.R., 1995. Comparison of Heat Fluxes from summertime Observations in the Suburbs of Four North American Cities. Journal of Applied Meteorology 34, 873–889.

Grimmond, C.S.B., Oke, T.R., 1999. Heat storage in urban areas: local-scale observations and evaluation of a simple model. Journal of Applied Meteorology 38, 922–940.

Grimmond, C.S.B., Oke, T.R., 2002. Turbulent Heat Fluxes in Urban Areas: observations and a Local-Scale Urban Meteorological Parameterization Scheme (LUMPS). Journal of Applied Meteorology 41, 792–810.

Grimmond, C.S.B., Oke, T.R., Steyn, D.G., 1986. Urban Water Balance: 1. A Model for daily totals. Water Resources Research 22, 1397–1403.

Grimmond, C.S.B., Best, M., Barlow, J., Arnfield, A.J., Baik, J.J., Baklanov, A., Belcher, S., Bruse, M., Calmet, I., Chen, F. and Clark, P., 2009. Urban surface energy balance models: model characteristics and methodology for a comparison study. In Meteorological and Air Quality Models for Urban Areas (pp. 97-123). Springer Berlin Heidelberg.

Grimmond, S., 2007. Urbanization and global environmental change: local effects of urban warming. The Geographical Journal 173, 83–88.

Grotch, S.L., MacCracken, M.C., 1991. The use of General Circulation Models to Predict Regional Climatic Change. Journal of Climate 4, 286–303.

Grundström, M., Pleijel, H., 2014. Limited effect of urban tree vegetation on NO2 and O3 concentrations near a traffic route. Environmental Pollution.

Ha, K.-J., Yun, K.-S., 2011. Climate change effects on tropical night days in Seoul, Korea. Theoretical and Applied Climatology 109, 191–203.

Hageback, J., Sundberg, J., Ostwald, M., Chen, D., Yun, X., Knutsson, P., 2005. Climate variability and land-use change in Danangou watershed, China - Examples of small-scale farmers' adaptation. Climatic Change 72, 189–212.

Halder, S., Saha, S.K., Dirmeyer, P.A., Chase, T.N., Goswami, B.N., 2016. Investigating the impact of land-use land-cover change on Indian summer monsoon daily rainfall and temperature during 1951-2005 using a regional climate model. Hydrology and Earth System Sciences 20, 1765–1784.

Halder, S., Saha, S.K., Dirmeyer, P.A., Chase, T.N., Goswami, B.N., 2015. Investigating the impact of land-use land-cover change on Indian summer monsoon daily rainfall and temperature during 1951 – 2005 using a regional climate model.Hydrology and Earth System Sciences.

Hale, R.C., Gallo, K.P., Loveland, T.R., 2008. Influences of specific land use/land cover conversions on climatological normals of near-surface temperature. Journal of Geophysical Research Atmospheres 113.

Hale, R.C., Gallo, K.P., Owen, T.W., Loveland, T.R., 2006. Land use/land cover change effects on temperature trends at U.S. Climate Normals stations. Geophysical Research Letters 33.

Hamdi, R., 2005. Numerical study of the atmospheric boundary layer over urban areas: validations for the cities of Basel and Marseilles. 34 /2005 Catholic university of Louvain, Belgium.

Hamed, K.H., Ramachandra Rao, A., 1998. A modified Mann-Kendall trend test for autocorrelated data. Journal of Hydrology 204, 182–196.

Hanasaki, N., Kanae, S., Oki, T., Masuda, K., Motoya, K., Shirakawa, N., Shen, Y., Tanaka, K., 2008. An integrated model for the assessment of global water resources. Part 1: Model description and input meteorological forcing. Hydrology and Earth System Sciences 12, 1007–1025.

Hanasaki, N., Kanae, S., Oki, T., Masuda, K., Motoya, K., Shirakawa, N., Shen, Y., Tanaka, K., 2008. An integrated model for the assessment of global water resources – Part 2: Applications and assessments. Hydrology and Earth System Sciences 12, 1027–1037.

Handmer, J., Honda, Y., Vicuna, S., Suarez, A., Honda, Y., Kundzewicz, Z., Arnell, N., Benito, G., Hatfield, J., Mohamed, I., Peduzzi, P., Wu, S., Sherstyukov, B., Takahashi, K.,

Yan, Z., Stocker, F., Qin, D., Dokken, D., Ebi, K., Mach, K., Plattner, G., Allen, S., Tignor, M., Midgley, P., 2012. Coordinating Lead Authors: Changes in impacts of climate extremes: Human systems and ecosystems changes in impacts of climate extremes: Human Systems and Ecosystems 232. Apurva Sanghi 231–290.

Hansen, J., Russel, G., Rind, D., Stone, P.H., Lacis, A., Lebedeff, S., Ruedy, R., Travis, L., 1983. Efficient three-dimensional global models for climate studies: models I and II. Monthly Weather 111, 609–662.

Hansen, J.E., 2005. A slippery slope: How much global warming constitutes "dangerous anthropogenic interference"? Climatic Change.

Hansen, M.C., Potapov, P. V, Moore, R., Hancher, M., Turubanova, S.A., Tyukavina, A., Thau, D., Stehman, S. V, Goetz, S.J., Loveland, T.R., Kommareddy, A., Egorov, A., Chini, L., Justice, C.O., Townshend, J.R.G., 2013. High-Resolution Global Maps of 21st-Century Forest Cover Change. Science 342, 850–853.

Harman, I.N., 2003. The Energy Balance of Urban Areas. The University of Reading, Department of Meteorology T 1–169.

Harman, I.N., Barlow, J.F., Belcher, S.E., 2004. Scalar fluxes from urban street canyons part II: model. Boundary-Layer Meteorology.

Harpham, C., Wilby, R.L., 2005. Multi-site downscaling of heavy daily precipitation occurrence and amounts. Journal of Hydrology 312, 235–255.

Hart, M., Sailor, D., 2009. Quantifying the influence of land-use and surface characteristics on spatial variability in the urban heat island. Theoretical and Applied Climatology 95, 397–406.

Hays, J.D., Lozano, J.A., Shackleton, N.J., Irving, G., 1976. Reconstruction of the Atlantic and western Indian Ocean sectors of the 18,000 BP Antarctic Ocean. Investigation of Late Quaternary Paleoceanography and Paleoclimatology 337–372.

Heaney, J.P., Pitt, R., Field, R., 1999. Innovative Urban Wet-Weather flow management systems 568.

Heisler, G.M., Grimmond, S., Grant, R.H., Souch, C., McPherson, E.G., Nowak, D.J., Rowntree, R.A., 1994. Investigation of the influence of Chicago's urban forests on wind and air temperature. Chicago's Urban Forest Ecosystem: Results of the Chicago Urban Forest Climate Project 19–40.

Helsel, D.R., Hirsch, R.M., 2002. Statistical methods in water resources: U.S. Geological Survey Techniques of Water Resources Investigations, Book 4, Chapter A3.

Heo, J., Yu, J., Giardino, J.R., Cho, H., 2015. Impacts of climate and land-cover changes on water resources in a humid subtropical watershed: A case study from East Texas, USA. Water and Environment Journal 29, 51–60.

Hertig, E., Jacobeit, J., 2008. Downscaling future climate change: Temperature scenarios for the Mediterranean area. Global and Planetary Change 63, 127–131.

Hessami, M., Gachon, P., Ouarda, T.T.B.M.J., St-Hilaire, A., 2008. Automated regression-based statistical downscaling tool. Environmental Modelling and Software 23, 813–834.

Högstrom, U., 1988. Nondimensional wind and temperature profiles in the atmospheric surface layer. Boundary-Layer Meteorology 42, 55–78.

Holtslag, A.A.M., Van Ulden, A.P., 1983. A simple scheme for daytime estimates of the Surface Fluxes from routine weather data. Journal of Climate and Applied Meteorology 22, 517–529.

Howe, P.D., Leiserowitz, A., 2013. Who remembers a hot summer or a cold winter? The asymmetric effect of beliefs about global warming on perceptions of local climate conditions in the U.S. Global Environmental Change 23, 1488–1500.

Huang, C., Zhang, M., Zou, J., Zhu, A., Chen, X., Mi, Y., Wang, Y., Yang, H., Li, Y., 2015a. Changes in land use, climate and the environment during a period of rapid economic development in Jiangsu Province, China. The Science of the Total Environment 536, 173–81.

Huang, C.L., Huang, C.C., Mai, F.D., Yen, C.L., Tzing, S.H., Hsieh, H.T., Ling, Y.C. and Chang, J.Y., 2015. Application of paramagnetic graphene quantum dots as a platform for simultaneous dual-modality bioimaging and tumor-targeted drug delivery. Journal of Materials Chemistry B 3, 651–664.

Huang, F., Xia, Z., Guo, L., Yang, F., 2013. Climate change detection and annual extreme temperature analysis of the Irtysh Basin. Theoretical and Applied Climatology 111, 465–470.

Huang, S.P., Taniguchi, M., Yamano, M., Wang, C.H., 2009. Detecting urbanization effects on surface and subsurface thermal environment - A case study of Osaka. Science of the Total Environment 407, 3142–3152.

Huang, Y., Dickinson, R.E., 2006. Impact of aerosol indirect effect on surface temperature over East Asia. Proceedings of the.

Iizumi, T., Yokozawa, M., Nishimori, M., 2009. Parameter estimation and uncertainty analysis of a large-scale crop model for paddy rice: Application of a Bayesian approach. Agricultural and Forest Meteorology 149, 333–348.

IMD, 2005. Annual Climate Summary 2005. IMD,Delhi.

International Peatland Society, 2008. Peatlands and Climate Change. International Peat Society 227.

IPCC, 2001. IPCC Third Assessment Report (TAR).Working group I: the scientific basis. IPCC 995.

IPCC, 2007.Climate Change 2007: Impacts, Adaptation and Vulnerability. Contribution of Working Group II to the Fourth Assessment Report of the Intergovernmental Panel on Climate Change, Cambridge University Press, Cambridge, UK, 982pp.

IPCC 2012. Managing the risks of extreme events and disasters to advance climate change adaptation. A special report of the intergovernmental panel on climate change. Cambridge University Press.

IPCC, 2013. Summary for Policymakers. Climate Change 2013: The physical science basis. contribution of working group I to the Fifth Assessment Report of the Intergovernmental Panel on Climate Change 33.

IPCC, Climate change 2014: mitigation of climate change. Cambridge University Press; 2015 Jan 26.

Jacob, D., Avissar, R., Bond, G., Gaffin, S., 2005. Radiative forcing of climate change: Expanding the concept and addressing uncertainties, National Research Council.

Jain, S.K., Kumar, V., Saharia, M., 2013. Analysis of rainfall and temperature trends in northeast India. International Journal of Climatology 33, 968–978.

Jain, S.K.., Kumar, V., 2012. Trend analysis of rainfall and temperature data for India. Current Science 102, 37–49.

Järvi, L., Grimmond, C.S.B., Christen, A., 2011. The Surface Urban Energy and Water Balance Scheme (SUEWS): Evaluation in Los Angeles and Vancouver. Journal of Hydrology 411, 219–237.

Järvi, L., Grimmond, C.S.B., Onomura, S., Lindberg, F., 2014. SUEWS Manual: Version 2014a.

Järvi, L., Grimmond, C.S.B., Taka, M., Nordbo, A., Setälä, H., Strachan, I.B., 2014. Development of the Surface Urban Energy and Water Balance Scheme (SUEWS) for cold climate cities. Geoscientific Model Development 7, 1691–1711.

Javed Mallick, Y.K., B.D.Bharath, 2008. Estimation of land surface temperature over Delhi using Landsat-7 ETM+. Indian Geophysical Union 12, 131–140.

Jhajharia, D., Dinpashoh, Y., Kahya, E., Singh, V.P., Fakheri-Fard, A., 2012. Trends in reference evapotranspiration in the humid region of northeast India. Hydrological Processes 26, 421–435.

Jiang, L., Ma, E., Deng, X., 2014. Impacts of irrigation on the heat fluxes and near-surface temperature in an inland irrigation area of Northern China. Energies 7, 1300–1317.

Jonsson, P., 2004. Vegetation as an urban climate control in the subtropical city of Gaborone, Botswana. International Journal of Climatology 24, 1307–1322.

Kalnay, E., Cai, M., 2003. Impact of urbanization and land-use change on climate. Nature 423, 528–531.

Kalnay, E., Cai, M., Li, H., Tobin, J., 2006. Estimation of the impact of land-surface forcings on temperature trends in eastern United States. Journal of Geophysical Research Atmospheres 111, D06106.

Kalyanapu, A.J., Burian, S.J., McPherson, T.N., 2009. Effect of land use-based surface roughness on hydrologic model output. Journal of Spatial Hydrology 9, 51–71.

Kampata, J.M., Parida, B.P., Moalafhi, D.B., 2008. Trend analysis of rainfall in the headstreams of the Zambesi River Basin in Zambia. Physics and Chemistry of the Earth 33, 621–625.

Kanda, M., 2006. Progress in the scale modeling of urban climate: Review. Theoretical and Applied Climatology 84, 23–33.

Kanda, M., Kawai, T., Kanega, M., Moriwaki, R., 2005. A simple energy balance model for regular building arrays. Boundary-Layer.

Kant, Y., Bharath, B.D., Mallick, J., Atzberger, C., Kerle, N., 2009. Satellite-based analysis of the role of land use/land cover and vegetation density on surface temperature regime of Delhi, india. Journal of the Indian Society of Remote Sensing 37, 201–214.

Karl, T.R., Diaz, H.F., Kukla, G., 1988. Urbanization: Its Detection and Effect in the United States Climate Record. Journal of Climate 1, 1099–1123.

Karpouzos, D.K.D.K., Kavalieratou, S., Babajimopoulos, C., 2010. Trend analysis of precipitation data in Pieria Region (Greece). European Water 30, 31–40.

Kendall, M.G., 1975. Rank correlation methods, 4th ed. Charles Griffith: London. San Francisco, CA.

Kerschgens, M.J., Hacker, J.M., 1985. On the energy budget of the convective boundary layer over an urban and rural environment. Beitrage zur Physik der Atmosph{ä}re.

Khadka, D., Pathak, D., 2016. Climate change projection for the marsyangdi river basin , Nepal using statistical downscaling of GCM and its implications in geodisasters. Geoenvironmental Disasters 2007.

Khan, M.S., Coulibaly, P., Dibike, Y., 2006. Uncertainty analysis of statistical downscaling methods. Journal of Hydrology 319.

Kharol, S.K., Kaskaoutis, D.G., Badarinath, K.V.S., Sharma, A.R., Singh, R.P., 2013. Influence of land use/land cover (LULC) changes on atmospheric dynamics over the arid region of Rajasthan state, India. Journal of Arid Environments 88, 90–101.

Kiely, G., Albertson, J.D., Parlange, M.B., 1998. Recent trends in diurnal variation of precipitation at Valentia on the west coast of Ireland. Journal of Hydrology 207, 270–279.

Kleczek, M.A., Steeneveld, G.J., Holtslag, A.A.M., 2014. Evaluation of the Weather Research and Forecasting Mesoscale Model for GABLS3: Impact of Boundary-Layer Schemes, Boundary Conditions and Spin-Up. Boundary-Layer Meteorology 152, 213–243.

Klemm, W., Heusinkveld, B.G., Lenzholzer, S., 2015. Psychological and physical impact of urban green spaces on outdoor thermal comfort during summertime in The Netherlands. Building and environment, 83, pp.120-128.

Klysik, K., 1996. Spatial and seasonal distribution of anthropogenic heat emissions in Lodz, Poland. Atmospheric Environment 30, 3397–3404.

Kondo, H., Genchi, Y., Kikegawa, Y., Ohashi, Y., 2005. Development of a multi-layer urban canopy model for the analysis of energy consumption in a big city: Structure of the urban canopy model and its basic performance. Boundary-Layer.

Kondo, H., Liu, F.H., 1998. A study on the urban thermal environment obtained through one-dimensional urban canopy model. Journal of Japan Society for Atmospheric.

Kothawale, D.R., Revadekar, J. V, Kumar, K.R., 2010. Recent trends in pre-monsoon daily temperature extremes over India. Journal of Earth System Science 119, 51–65.

Krayenhoff, E.S., Voogt, J.A., 2007. A microscale three-dimensional urban energy balance model for studying surface temperatures. Boundary-Layer Meteorology.

Krishnakumar, K.N., Prasada Rao, G.S.L.H. V, Gopakumar, C.S., 2009. Rainfall trends in twentieth century over Kerala, India. Atmospheric Environment 43, 1940–1944.

Krpo, A., Clappier, A., Muller, C., 2006. Numerical simulation of the interaction between buildings and atmosphere over large urban areas. Colloque numérique suisse (Schweizer Numerik Kolloquium) Lausanne, Switzerland

Kuckla, G., Gabin, J., T. R. Karl, 1986. Urban warming. Journal of Climate and Applied Meteorology 25, 1265–1270.

Kueppers, L.M., Snyder, M.A., 2012. Influence of irrigated agriculture on diurnal surface energy and water fluxes, surface climate, and atmospheric circulation in California. Climate Dynamics 38, 1017–1029.

Kumar, D., Mishra, V., Ganguly, A.R., 2014. Evaluating wind extremes in CMIP5 climate models. Climate Dynamics.

Kumar, V., Jain, S.K., 2010. Trends in seasonal and annual rainfall and rainy days in Kashmir Valley in the last century. Quaternary International 212, 64–69.

Kumar, V., Jain, S.K., Singh, Y., 2010. Analysis of long-term rainfall trends in India. Hydrological Sciences Journal 55, 484–496.

Kurn, D.M., Bretz, S.E., Huang, B., Akbari, H., 1994. The Potential for reducing air temperature and energy consumption through vegetative cooling. Energy and Environment.

Kusaka, H., Kondo, H., Kikegawa, Y., Kimura, F., 2001. A simple single-layer urban canopy model for atmospheric models: comparison with multi-layer and slab models. Boundary-Layer Meteorology.

Lamptey, B.L., Barron, E.J., Pollard, D., 2005. Impacts of agriculture and urbanization on the climate of the Northeastern United States. Global and Planetary Change 49, 203–221.

Landsberg, H.E., 1981. The Urban Climate.

Lankao, P., Nychka, D., Tribbia, L., 2008. Development and greenhouse gas emissions deviate from the ‘modernization’theory and ‘convergence’hypothesis. Climate Research.

Larsen, K., 2015. History of Norway.

Lazar, R., Podesser, A., 1999. An urban climate analysis of Graz and its significance for urban planning in the tributary valleys east of Graz (Austria). Atmospheric Environment 33, 4195–4209.

Lejeune, Q., Davin, E.L., Guillod, B.P., Seneviratne, S.I., 2015. Influence of Amazonian deforestation on the future evolution of regional surface fluxes, circulation, surface temperature and precipitation. Climate Dynamics 44, 2769–2786.

Lemonsu, A., Grimmond, C.S.B., Masson, V., 2004. Modeling the Surface Energy Balance of the Core of an Old Mediterranean City: Marseille. Journal of Applied Meteorology 43, 312–327.

Li, Y., Zhu, L.J., Zhao, X.Y., Li, S.C., Yan, Y., 2013. Urbanization impact on temperature change in China with emphasis on land cover change and human activity. Journal of Climate 26, 8765–8780.

Li, Z. and Mölders, N., 2008. Interaction of impacts of doubling CO2 and changing regional land-cover on evaporation, precipitation, and runoff at global and regional scales. International Journal of Climatology 28, 1653–1679.

Li, Z., Deng, X., Shi, Q., Ke, X., Liu, Y., 2013. Modeling the impacts of boreal deforestation on the near-surface temperature in european Russia. Advances in Meteorology 2013.

Li, Z., Liu, C., Dong, Y., Chang, X., Nie, X., Liu, L., Xiao, H., Lu, Y., Zeng, G., 2017. Response of soil organic carbon and nitrogen stocks to soil erosion and land use types in the Loess hilly–gully region of China. Soil and Tillage Research 166, 1–9.

Li, Z., Liu, W.Z., Zhang, X.C., Zheng, F.L., 2011. Assessing the site-specific impacts of climate change on hydrology, soil erosion and crop yields in the Loess Plateau of China. Climatic Change 105, 223–242.

Li, Zhao, N.M., 2008. Interaction of impacts of doubling CO2 and changing regional land-cover on evaporation, precipitation, and runoff at global and regional scales. International Journal of Climatology 28, 1653–1679.

Lim, Y.K., Cai, M., Kalnay, E., Zhou, L., 2005. Observational evidence of sensitivity of surface climate changes to land types and urbanization. Geophysical Research Letters 32, 1–4.

Lim, Y.W., 2008. Triple endobuttton technique in acromioclavicular joint reduction and reconstruction. Annals of the Academy of Medicine Singapore 37, 294–299.

Lin, J., Cromley, R.G., Civco, D.L., Hanink, D.M., 2013. GIScience & Remote Sensing Evaluating the use of publicly available remotely sensed land cover data for areal interpolation. GIScience and Remote Sensing 37–41.

Lin, T.P., Matzarakis, A., 2008. Tourism climate and thermal comfort in Sun Moon Lake, Taiwan. International Journal of Biometeorology 52, 281–290.

Lin, W., Zhang, L., Du, D., Yang, L., Lin, H., Zhang, Y., Li, J., 2009. Quantification of land use/land cover changes in Pearl River Delta and its impact on regional climate in summer using numerical modeling. Regional Environmental Change 9, 75–82.

Liu, J., Kuang, W., Zhang, Z., Xu, X., Qin, Y., Ning, J., Zhou, W., Zhang, S., Li, R., Yan, C. and Wu, S., 2014. Spatiotemporal characteristics, patterns, and causes of land-use changes in China since the late 1980s. Journal of Geographical Sciences, 24(2), pp.195-210.

Liu, F., Tao, F., Liu, J., Zhang, S., Xiao, D., Wang, M., Zhang, H., Bai, H., 2016. Effects of land use/cover change on land surface energy partitioning and climate in Northeast China. Theoretical and Applied Climatology.

Liu, J., Zhang, Z.X., Xu, X.L., Kuang, W.H., Zhou, W.C., Zhang, S.W., Li, R.D., Yan, C.Z., Yu, D.S., Wu, S.X., Nan, J., 2010. Spatial patterns and driving forces of land use change in China during the early 21st century. Journal of Geographical Sciences 20, 483–494.

Liu, J.M., Deng, X.Z., 2011. Influence of different land use on urban microenvironment in Beijing City, China. Journal of Food Agriculture and Environment 9, 1005–1011.

Liu, J.Y., Deng, X.Z., 2011. Impacts and mitigation of climate change on Chinese cities. Current Opinion in Environmental Sustainability 3, 188–192.

Liu, L., Liu, Z., Ren, X., Fischer, T., Xu, Y., 2011. Hydrological impacts of climate change in the Yellow River Basin for the 21st century using hydrological model and statistical downscaling model. Quaternary International 244, 211–220.

Liu, Y., Zhang, X., Xia, D., You, J., Rong, Y., Bakir, M., 2013. Impacts of Land-Use and Climate Changes on Hydrologic Processes in the Qingyi River Watershed, China. Journal of Hydrologic Engineering 18, 1495–1512.

Lo, C.P., Quattrochi, D.A., 2003. Land-Use and Land-Cover Change, Urban Heat Island Phenomenon, and Health Implications. Photogrammetric Engineering and Remote Sensing 69, 1053–1063.

Lu, D., Mausel, P., Brondízios, E. e, Moran, E., 2003. Change detection techniques. International Journal of Remote Sensing 25, 2365–2407.

Luo, Y., Liu, S., Fu, S., Liu, J., Wang, G., Zhou, G., 2008. Trends of pricipitation in Beijiang River Basin, Guangdong Province,China TT - Trends of pricipitation in Beijiang River Basin, Guangdong Province, China. Hydrological Processes.

Mahmood, R., Babel, M.S., 2014. Future changes in extreme temperature events using the statistical downscaling model (SDSM) in the trans-boundary region of the Jhelum river basin. Weather and Climate Extremes 5–6, 56–66.

Mahmood, R., Quintanar, A.I., Conner, G., Leeper, R., Dobler, S., Pielke, R. a., Beltran-Przekurat, A., Hubbard, K.G., Niyogi, D., Bonan, G., Lawrence, P., Chase, T., McNider, R., Wu, Y., McAlpine, C., Deo, R., Etter, A., Gameda, S., Qian, B., Carleton, A., Adegoke, J.O., Vezhapparambu, S., Asefi, S., Nair, U.S., Sertel, E., Legates, D.R., Hale, R., Frauenfeld, O.W., Watts, A., Shepherd, M., Mitra, C., Anantharaj, V.G., Fall, S., Chang,

H.-I., Lund, R., Treviño, A., Blanken, P., Du, J., Syktus, J., 2010. Impacts of Land Use/Land Cover change on climate and future research priorities. Bulletin of the American Meteorological Society 91, 37–46.

Mahura, A., Baklanov, A., Petersen, C., Sattler, K., Amstrup, B., Nielsen, N.W., 2006. ISBA scheme performance in high resolution modelling for low winds conditions. HIRLAM Newsletter.

Mann, H.B., 1945. Nonparametric tests against trend. Mann Source: Econometrica 13, 245–259.

Manwell, J.F., McGowan, J.G., Rogers, A.L., 2002. Wind energy explained, Wind Eng.

Martilli, A., Clappier, A., Rotach, M., 2002. An urban surface exchange parameterisation for mesoscale models. Boundary-Layer Meteorology.

Masson, V., 2000. A physically based scheme for the urban energy budget in atmospheric models. Boundary Layer Meteorology 94, 357–397.

Masson, V., Grimmond, C.S.B., Oke, T.R., 2002. Evaluation of the Town Energy Balance (TEB) Scheme with direct measurements from Dry Districts in Two Cities. American Meteorological Society 1011–1026.

McBean, E., Motiee, H., 2006. Assessment of impacts of climate change on water resources – a case study of the Great Lakes of North America. Hydrology and Earth System Sciences Discussions 3, 3183–3209.

McCarthy, M.P., Best, M.J., Betts, R.A., 2010. Climate change in cities due to global warming and urban effects. Geophysical Research Letters, 37,9.

McPherson Simpson, J., Xiao, Q., Wu, C., E., 2011. Million trees Los Angeles canopy cover and benefit assessment.pdf. Landscape and Urban Planning 99, 40–50.

McVEIGH, J.C., 1983. Sun Power: an introduction to the applications of solar energy.

Met Office unified model global atmosphere 6.0/6.1 and JULES global land 6.0/6.1 configurations. Geoscientific Model Development, 10(4), p.1487., 2017.

Middel, A., Brazel, A.J., Gober, P., Myint, S.W., Chang, H., Duh, J. Der, 2012. Land cover, climate, and the summer surface energy balance in Phoenix, AZ, and Portland, OR. International Journal of Climatology 32, 2020–2032.

Mills, G., 1997. An urban canopy-layer climate model. Theoretical and applied climatology.

Mimura, N., Pulwarty, R.S., Duc, D.M., Elshinnawy, I., Redsteer, M.H., Huang, H.Q., Nkem, J.N., Rodriguez, R. a. S., 2014. 15. Adaptation Planning and Implementation. Assessment Report 5- Climate Change 2014: Impacts, Adaptation, and Vulnerability. Part A: Global and Sectoral Aspects 869–898.

Modarres, R., da Silva, V.P.R., 2007. Rainfall trends in arid and semi-arid regions of Iran (Reza modarres) – Academia educational Journal of Arid Environments.

Mohan, M., Kandya, A., 2015. Impact of urbanization and land-use/land-cover change on diurnal temperature range: a case study of tropical urban airshed of India using remote sensing data. The Science of the total environment 506–507, 453–465.

Mohan, M., Kikegawa, Y., Gurjar, B., Bhati, S., 2013. Assessment of urban heat island effect for different land use–land cover from micrometeorological measurements and remote sensing data for megacity Delhi. Theoretical and applied.

Mohsin, T., Gough, W.A., 2010. Trend analysis of long-term temperature time series in the Greater Toronto Area (GTA). Theoretical and Applied Climatology 101, 311–327.

Mölders, N., Olson, M.A., 2004. Impact of urban effects on precipitation in high latitudes. J. Hydrometeor 5, 409–429.

Montavez, J.P., Jimenez, J.I., Sarsa, A., 2000. A Monte Carlo model of the nocturnal surface temperatures in urban canyons. Boundary-Layer Meteorology 96, 433–452.

Monteith, J.L., 1965. Evaporation and environment. Symposia of the Society for Experimental Biology 19, 205–234.

Morabito, M., Crisci, A., Messeri, A., Orlandini, S., Raschi, A., Maracchi, G., Munafò, M., 2016. The impact of built-up surfaces on land surface temperatures in Italian urban areas. Science of the Total Environment 551–552, 317–326.

Morris, K.I., Aekbal Salleh, S., Chan, A., Ooi, M.C.G., Abakr, Y.A., Oozeer, M.Y., Duda, M., 2015. Computational study of urban heat island of Putrajaya, Malaysia. Sustainable Cities and Society 19, 359–372.

Morris, R.L., Deavin, G., Hemelryk Donald, S., Coleman, R.A., 2016. Eco-engineering in urbanised coastal systems: Consideration of social values. Ecological Management and Restoration 17, 33–39.

Moss, R., Edmonds, J.A., Hibbard, K.A., Manning, M.R., Rose, S.K., van Vuuren, D., Carter, T.R., Emori, S., Kainuma, M., Kram, T., Meehl, G.A., Mitchell, J.F.B., Nakicenovic, N., Riahi, K., Smith, S.J., Stouffer, R.J., Thomson, A.M., Weyant, J.P., Wilbanks, T.J., 2010. The next generation of scenarios for climate change research and assessment. Nature 463, 747–756.

Motiee, H., McBean, E., 2009. An assessment of long-term trends in hydrologic components and implications for water levels in Lake Superior. Hydrology Research 40, 564.

Murphy, J.M., Booth, B.B.B., Collins, M., Harris, G.R., Sexton, D.M.H., Webb, M.J., 2007. A methodology for probabilistic predictions of regional climate change from perturbed physics ensembles. Philosophical transactions. Series A, Mathematical, physical, and engineering sciences 365, 1993–2028.

Musakwa, W., Van Niekerk, A., 2013. Implications of land use change for the sustainability of urban areas: A case study of Stellenbosch, South Africa. Cities 32, 143–156.

Nagar, S.G., Seetaramayya, P., Tyagi, A., Singh, S.S., 2002. Estimation of daytime surface fluxes of radiation and heat at Anand during 13-17 May 1997. Current Science 83, 39–46.

Naidu, C. V., Krishna, K.M., Rao, S.R., Bhanu Kumar, O.S.R.U., Durgalakshmi, K., Ramakrishna, S.S.V.S., 2011. Variations of Indian summer monsoon rainfall induce the weakening of easterly jet stream in the warming environment? Global and Planetary Change 75, 21–30.

Nalley, D., Adamowski, J., Khalil, B., Ozga-Zielinski, B., 2013. Trend detection in surface air temperature in Ontario and Quebec, Canada during 1967-2006 using the discrete wavelet transform. Atmospheric Research 132–133, 375–398.

Nayak, S., Mandal, M., 2012. Impact of land-use and land-cover changes on temperature trends over Western India. Current Science 102.

Nunez, M.N., Ciapessoni, H.H., Rolla, A., Kalnay, E., Cai, M., 2008. Impact of land use and precipitation changes on surface temperature trends in Argentina. Journal of Geophysical Research-Atmospheres 113.

Offerle, B., Grimmond, C.S.B., Fortuniak, K., Kłysik, K., Oke, T.R., 2006. Temporal variations in heat fluxes over a central European city centre. Theor Appl Climatol 84, 103–115.

Offerle, B., Grimmond, S., Oke, T.R., 2003. Parameterization of Net All-Wave Radiation for Urban Areas. Journal of Applied Meteorology 42, 1157–1173.

Oke, T.R., Cleugh, H.A., 1987. Urban heat storage derived as energy budget residuals. Boundary-Layer Meteorology 39, 233–245.

Oke, T.R., Spronken-Smith, R.A., Jaurequi, E., Grimmond, C.S.B., 1999. The energy balance of central Mexico City during the dry season. Atmospheric Environment 33, 3919–3930.

Oke, T.R.R., 1988. The urban energy balance. Progress in Physical Geography 12, 471–508.

Oleson, K.W., Bonan, G.B., Feddema, J., Vertenstein, M., Grimmond, C.S.B., 2008. An urban parameterization for a global climate model. Part I: Formulation and evaluation for two cities. Journal of Applied Meteorology and Climatology 47, 1038–1060.

Oliphant, A.J., Grimmond, C.S.B., Zutter, H.N., 2004. Heat storage and energy balance fluxes for a temperate deciduous forest. Agricultural and Forest.

Oliveira, S., Andrade, H., and Vaz, T., 2011. The cooling effect of green spaces as a contribution to the mitigation of urban heat: a case study in Lisbon. 46: 2186-2194. Building and Environment. 2186–2194.

Oron, G., DeMalach, Y., Gillerman, L., David, I., Lurie, S., 2002. SW—Soil and Water. Biosystems Engineering 81, 237–247.

Otukei, J.R., Blaschke, T., 2010. Land cover change assessment using decision trees, support vector machines and maximum likelihood classification algorithms. International Journal of Applied Earth Observation and Geoinformation 12.

Pachauri, R.K., Allen, M.R., Barros, V.R., Broome, J., Cramer, W., Christ, R., Church, J.A., Clarke, L., Dahe, Q., Dasgupta, P. and Dubash, N.K., 2014. Climate change 2014:

synthesis report. Contribution of Working Groups I, II and III to the fifth assessment report of the Intergovernmental Panel on Climate Change (p. 151). IPCC.

Pal, I., Al-Tabbaa, A., 2009. Trends in seasonal precipitation extremes–An indicator of 'climate change'in Kerala, India. Journal of Hydrology 367, 62–69.

Pal, I., Al-Tabbaa, A., 2011. Assessing seasonal precipitation trends in India using parametric and non-parametric statistical techniques. Theoretical and Applied Climatology 103, 1–11.

Pal, I., Al-Tabbaa, A., 2011. Monsoon rainfall extreme indices and tendencies from 1954-2003 in Kerala, India. Climatic Change 106, 407–419.

Pall, P., Aina, T., Stone, D. a, Stott, P. a, Nozawa, T., Hilberts, A.G.J., Lohmann, D., Allen, M.R., 2011. Anthropogenic greenhouse gas contribution to flood risk in England and Wales in autumn 2000. Nature 470, 382–385.

Paper, O., 2016. Impact of land use / land cover change on changes in surface solar radiation in eastern China since the reform and opening up. Theoretical and Applied Climatology 131–139.

Park, S.Y., Lee, K.W., Park, I.H., Ha, S.R., 2008. Effect of the aggregation level of surface runoff fields and sewer network for a SWMM simulation. Desalination 226, 328–337.

Parry Martin L., Group, V.W., 2007. Climate Change 2007 - Impacts, Adaptation and Vulnerability: Working Group II Contribution to the Fourth Assessment Report of the IPCC.

Parthasarathy, B., Dhar, O.N., 1974. Secular variations of regional rainfall over India. Quarterly Journal of the Royal Meteorological Society 100, 245–257.

Patra, J.P., Mishra, A., Singh, R., Raghuwanshi, N.S., 2012. Detecting rainfall trends in twentieth century (1871-2006) over Orissa State, India. Climatic Change 111, 801–817.

Pauleit, S., Ennos, R., Golding, Y., 2005. Modeling the environmental impacts of urban land use and land cover change - A study in Merseyside, UK. Landscape and Urban Planning 71, 295–310.

Pearlmutter, D., Bitan, A., Berliner, P., 1999. Microclimatic analysis of 'compact' urban canyons in an arid zone. Atmospheric Environment 33, 4143–4150.

Peng, J., Hu, M., Guo, S., Du, Z., Zheng, J., Shang, D., Levy Zamora, M., Zeng, L., Shao, M., Wu, Y.-S., Zheng, J., Wang, Y., Glen, C.R., Collins, D.R., Molina, M.J., Zhang, R., 2016. Markedly enhanced absorption and direct radiative forcing of black carbon under polluted urban environments. Proceedings of the National Academy of Sciences of the United States of America.

Penman, H.L., 1948. Natural Evaporation from Open Water, Bare Soil and Grass. Proceedings of the Royal Society of London. Series A, Mathematical and Physical Sciences 193, 120–145.

Perkins, S.E., Alexander, L. V, Nairn, J.R., 2012. Increasing frequency, intensity and duration of observed global heatwaves and warm spells. Geophysical Research Letters 39.

Pessacg, N.L., Solman, S., 2012. Effects of land-use changes on climate in southern South America. Climate Research 55.

Peterson, T.C., Gallo, K.P., Lawrimore, J., Owen, T.W., Huang, A., McKittrick, D. a., 1999. Global rural temperature trends. Geophysical Research Letters 26, 329–332.

Peterson, W.T., Schwing, F.B., 2003. A new climate regime in northeast pacific ecosystems. Geophysical Research Letters 30, 1–4.

Petralli, M., Massetti, L., Brandani, G., 2014. Urban planning indicators: useful tools to measure the effect of urbanization and vegetation on summer air temperatures. International Journal of Climatology, 34,4, 1236-1244.

Pettitt, A.N.N., 1979. A Non-Parametric Approach to the Change-Point Problem. Applied Statistics 28, 126.

Pielke, R.A., Marland, G., Betts, R.A., Chase, T.N., Eastman, J.L., Niles, J.O., Niyogi, D.D.N., Running, S.W., 2002. The influence of land-use change and landscape dynamics on the climate: relevance to climate - change policy beyond the radiative effect of greenhouse gases. Philosophical Transactions of the Royal Society A: Mathematical, Physical and Engineering Sciences 360, 1705–1719.

Pielke, R.A.S., 2005. Land Use and Climate Change. Eos, Transactions American Geophysical Union 310, 1625–1626.

Pielke, S.R.A., Adegoke, J.O., Chase, T.N., Marshall, C.H., Matsui, T., Niyogi, D., 2007. A new paradigm for assessing the role of agriculture in the climate system and in climate change. Agricultural and Forest Meteorology 142, 234–254.

Ping, Z., Anbang, W., Xinbao, Z., Xiubin, H., 2012. Soil conservation and sustainable eco-environment in the Loess Plateau of China. Environmental Earth Sciences 68, 633–639.

Pingale, S., Adamowski, J., Jat, M., Khare, D., 2015. Implications of spatial scale on climate change assessments. Journal of Water and Land Development 26, 37–56.

Pingale, S.M., Chandra, H., Sharma, H.C., Singh, R., 2013. Fuzzy logic rule-based modelling of natural spring flow in a hilly catchment of Tehri-Garhwal district, Uttarakhand, India. International Journal of Hydrology Science and Technology 3, 289–307.

Pingale, S.M., Khare, D., Jat, M.K., Adamowski, J., 2014. Spatial and temporal trends of mean and extreme rainfall and temperature for the 33 urban centers of the arid and semi-arid state of Rajasthan, India. Atmospheric Research 138, 73–90.

Pingale, S.M., Khare, D., Jat, M.K., Adamowski, J., 2016. Trend analysis of climatic variables in an arid and semi-arid region of the Ajmer District, Rajasthan, India. Journal of Water and Land Development 28, 3–18.

Pitman, A.J., De Noblet-Ducoudré, N., Cruz, F.T., Davin, E.L., Bonan, G.B., Brovkin, V., Claussen, M., Delire, C., Ganzeveld, L., Gayler, V., Van Den Hurk, B.J.J.M., Lawrence, P.J., Van Der Molen, M.K., Müller, C., Reick, C.H., Seneviratne, S.I., Strengen, B.J.,

Voldoire, A., 2009. Uncertainties in climate responses to past land cover change: First results from the LUCID intercomparison study. Geophysical Research Letters 36.

Polydoros, A., Cartalis, C., 2015. Assessing the impact of urban expansion to the state of thermal environment of peri-urban areas using indices. Urban Climate 14, 166–175.

Pongratz, J., Reick, C.H., Raddatz, T., 2010. Biogeophysical versus biogeochemical climate response to historical anthropogenic land cover change. Geophysical Research.

Potchter, O., Cohen, P., Bitan, A., 2006. Climatic behavior of various urban parks during hot and humid summer in the Mediterranean city of Tel Aviv, Israel. International Journal of Climatology 26, 1695–1711.

Prentice, I.C., Heimann, M., Sitch, S., 2001. Contribution of Working Group I to the Third Assessment Report of the Intergovernmental Panel on Climate Change, Climate Change 2001: The Scientific Basis.

Qian, C., 2014. Impact of land use/land cover change on changes in surface solar radiation in eastern China since the reform and opening up. Theoretical and Applied Climatology 1–9.

Qian, C., Zhou, W., Fong, S.K., Leong, K.C., 2015. Two approaches for statistical prediction of non-gaussian climate extremes: A case study of macao hot extremes during 1912-2012. Journal of Climate 28, 623–636.

Radiative forcing of climate change: Expanding the concept and addressing uncertainties, 2005.

Rahman, A., Kumar, Y., 2011. Urbanization and quality of urban environment using Remote Sensing and GIS techniques in East Delhi-India. Journal of Geographic Information System 3, 62–84.

Rai, R.K., Upadhyay, A., Ojha, C.S.P., 2010. Temporal variability of climatic parameters of Yamuna River Basin : Spatial Analysis of Persistence, Trend and Periodicity. The Open Hydrology Journal 4, 184–210.

Raj, K.B.G. and Fleming, K., 2008. Surface temperature estimation from Landsat ETM+ Data for a part of the Baspa Basin, NW Himalaya, India. Bulletin of Glaciological Research, 19–26.

Rao, R.R., Sivakumar, R., 2003. Seasonal variability of sea surface salinity and salt budget of the mixed layer of the north Indian Ocean. Journal of Geophysical Research 108.

Ren, G., Zhou, Y., 2014. Urbanization effect on trends of extreme temperature indices of national stations over mainland China, 1961-2008. Journal of Climate 27, 2340–2360.

Richter, M., 2016. Urban climate change-related effects on extreme heat events in Rostock, Germany. Urban Ecosystems 19, 849–866.

Rindfuss, R.R., Entwisle, B., Walsh, S.J., An, L., Badenoch, N., Brown, D.G., Deadman, P., Evans, T.P., Fox, J., Geoghegan, J., Gutmann, M., Kelly, M., Linderman, M., Liu, J., Malanson, G.P., Mena, C.F., Messina, J.P., Moran, E.F., Parker, D.C., Parton, W.,

Prasartkul, P., Robinson, D.T., Sawangdee, Y., Vanwey, L.K., Verburg, P.H., 2008. Land use change: complexity and comparisons. Journal of Land Use Science 3, 1–10.

Rogan, J., Ziemer, M., Martin, D., Ratick, S., Cuba, N., DeLauer, V., 2013. The impact of tree cover loss on land surface temperature: a case study of central Massachusetts using Landsat Thematic Mapper thermal data. Applied Geography 45, 49–57.

Rogers, D.J., Randolph, S.E., Snow, D.W., Hay, S.I., 2002. Satellite imagery in the study and forecast af malaria. Nature 415, 710–715.

Roy, D.B., Sparks, T.H., 2000. Phenology of British butterflies and climate change. Global change biology.

Roy, M., Rahaman, S., Paul, J., 1987. Regional variations in the trends and periodicities of annual rainfall over Bangladesh. International Journal of Scientific and Research Publications.

Roy, S. Sen, Balling, R.C., 2004. Trends in extreme daily precipitation indices in India. International Journal of Climatology 24, 457–466.

Rutter, A.J., Kershaw, A., Robins, P.C., Morton, A.J., 1972. A predictive model of rainfall interception in forests, 1. Derivation of the model from observation in a plantation of Corsian pine. Agric. Meteorology. 9, 367–384.

Saaroni, H., 2003. Long-term variations in summer temperatures over the Eastern Mediterranean. Geophysical Research Letters 30, 1946.

Sahoo, D., Smith, P.K., 2009. Hydroclimatic trend detection in a rapidly urbanizing semi-arid and coastal river basin. Journal of Hydrology 367, 217–227.

Sailor, D.J., Lu, L., 2004. A top-down methodology for developing diurnal and seasonal anthropogenic heating profiles for urban areas. Atmospheric Environment 38, 2737–2748.

Sailor, D.J.D.J., Vasireddy, C., 2006. Correcting aggregate energy consumption data to account for variability in local weather. Environmental Modelling and Software 21, 733–738.

Saito, K., Ishida, J.-I., Aranami, K., Hara, T., Segawa, T., Narita, M., Honda, Y., 2007. Nonhydrostatic Atmospheric Models and Operational Development at JMA. Journal of the Meteorological Society of Japan 85, 271–304.

Saitoh, T.S., Yamada, N., 2004. Experimental and numerical investigation of thermal plume in urban surface layer. Experimental Thermal and Fluid Science 28, 585–595.

Sajjad, S.H., Hussain, B., Ahmed Khan, M., Raza, A., Zaman, B., Ahmed, I., 2009. On rising temperature trends of Karachi in Pakistan. Climatic Change 96, 539–547.

Sanchez-Lorenzo, A., Wild, M., Brunetti, M., Guijarro, J.A., Hakuba, M.Z., Calbõ, J., Mystakidis, S., Bartok, B., 2015. Reassessment and update of long-term trends in downward surface shortwave radiation over Europe (1939-2012). Journal of Geophysical Research: Atmospheres 120, 9555–9569.

Sarkar, S., Chiu, L., Kafatos, M., Singh, R., 2007. Sensitivity of rainfall on land cover change over South East Asia: some observational results. Advances in Space Research.

Sarma, V.V.L.N., Krishna, G.M., Malini, B.H., Rao, K.N., 2001. Landuse/Landcover change detection through remote sensing and its climatic implications in the godavari delta region. Journal of the Indian Society of Remote Sensing 29, 85–91.

Schaefer, D., 2007. Recent climate change in Japan - spatial and temporal characteristics of trends of mean- , minimum- , and. Climate of the Past.

Scheiter, S., Langan, L., Higgins, S.I., 2013. Next-generation dynamic global vegetation models: Learning from community ecology. New Phytologist 198, 957–969.

Scherer, D., Fehrenbach, U., Beha, H.D., Parlow, E., 1999. Improved concepts and methods in analysis and evaluation of the urban climate for optimizing urban planning processes. Atmospheric Environment 33, 4185–4193.

Schubert, S., 1998. Downscaling local extreme temperature changes in south-eastern Australia from the CSIRO Mark2 GCM. International Journal of Climatology 18, 1419–1438.

Sen, P.K., 1968. Estimates of the regression coefficient based on Kendall's Tau. Journal of the American Statistical Association 63, 1379–1389.

Shamir, E., Megdal, S.B., Carrillo, C., Castro, C.L., Chang, H.I., Chief, K., Corkhill, F.E., Eden, S., Georgakakos, K.P., Nelson, K.M., Prietto, J., 2015. Climate change and water resources management in the Upper Santa Cruz River, Arizona. Journal of Hydrology 521, 18–33.

Sharma, D., Tomar, S., 2010. Mainstreaming climate change adaptation in Indian cities. Environment and Urbanization 22, 451–465.

Sharma, M., Dikshit, O., 2016. Comprehensive Study on Air Pollution and Green House Gases (GHGs) in Delhi. Indian Institute of Technology Kanpur 334.

Shashua-Bar, L., Hoffman, M.E., 2002. The Green CTTC model for predicting the air temperature in small urban wooded sites. Building and Environment.

Shashua-Bar, L., Hoffman, M.E., 2003. Geometry and orientation aspects in passive cooling of canyon streets with trees. Energy and Buildings 35, 61–68.

Shashua-Bar, L., Hoffman, M.E.M.E., 2004. Quantitative evaluation of passive cooling of the UCL microclimate in hot regions in summer, case study: Urban streets and courtyards with trees. Building and Environment 39, 1087–1099.

Shashua-Bar, L., Pearlmutter, D., Erell, E., 2009. The cooling efficiency of urban landscape stratergies in a hot dry climate. Landscape & Urban Planning 92, 179–186.

Shashua-Bar, L., Tsiros, I.X., Hoffman, M., 2012. Passive cooling design options to ameliorate thermal comfort in urban streets of a Mediterranean climate (Athens) under hot summer conditions. Building and Environment 57, 110–119.

Shepherd, J.M., Jin, M., 2004. Linkages between the built urban environment and Earth's Climate System. Eos, Transactions American Geophysical Union 85, 227.

Shuttleworth, W.J., 1978. A simplified one-dimensional theoretical description of the vegetation-atmosphere interaction. Boundary-Layer Meteorology.

Shuttleworth, W.J., 1983. Evaporation models in the global water budget. Variations in the global water budget.

Sidek, L., Ghani, A., Zakaria, N., Desa, M., Othman, N., 2006. An assessment of stormwater management practises in Malaysia.

Sievers, U., 1995. Verallgemeinerung der Stromfunktionsmethode auf drei Dimensionen. Meteorologische Zeitschrift.

Singh, D., Gupta, R.D., Jain, S.K., 2015. Study of daily extreme temperature indices over Sutlej basin, N-W Himalayan Region, India. Global Nest Journal 17, 301–311.

Singh, R., Kumar, A., 2015. Climate variability and water resource scarcity in drylands of Rajasthan, India. Geoenvironmental Disasters 2, 7.

Skelhorn, C., Lindley, S., Levermore, G., 2014. The impact of vegetation types on air and surface temperatures in a temperate city : A fine scale assessment in Manchester , UK. Landscape and Urban Planning 121, 129–140.

Solecki, W., Seto, K.C., Balk, D., Bigio, A., Boone, C.G., Creutzig, F., Fragkias, M., Lwasa, S., Marcotullio, P., Romero-Lankao, P., Zwickel, T., 2015. A conceptual framework for an urban areas typology to integrate climate change mitigation and adaptation. Urban Climate 14, 116–137.

Solomon, S., IPCC, I.P.O.C.C., 2007. Climate Change 2007 - The Physical Science Basis: Working Group I Contribution to the Fourth Assessment Report of the IPCC, Science.

Sonali, P., Kumar, D.N., 2013. Review of trend detection methods and their application to detect temperature changes in India. Journal of Hydrology 476, 212–227.

Souch, C., Grimmond, S., 2006. Applied climatology: urban climate. Progress in physical geography.

Spronken-Smith, R.A., Oke, T.R., 1998. The thermal regime of urban parks in two cities with different summer climates. International Journal of Remote Sensing 19, 2085–2104.

Spronken-Smith, R.A., Oke, T.R., 1999. Scale modelling of nocturnal cooling in urban parks. Boundary-Layer Meteorology 93, 287–312.

Sr, R.A.P., Marland, G., Betts, R.A., 2003. The influence of land-use change and landscape dynamics on the climate system: relevance to climate-change policy beyond the radiative effect of greenhouse gases. Philosophical transactions. Series A, Mathematical, physical, and engineering sciences Royal Society (Great Britain).

Srivastava, A., Naresh Kumar, S., Aggarwal, P.K., 2010. Assessment on vulnerability of sorghum to climate change in India. Agriculture, Ecosystems and Environment 138, 160–169.

Stathopoulou, M., Cartalis, C., 2007. Daytime urban heat islands from Landsat ETM+ and Corine land cover data: An application to major cities in Greece. Solar Energy 81, 358–368.

Steinschneider, S., Polebitski, A., Brown, C., Letcher, B.H., 2012. Toward a statistical framework to quantify the uncertainties of hydrologic response under climate change. Water Resources Research 48.

Stine, A.R., Huybers, P., Fung, I.Y., 2009. Changes in the phase of the annual cycle of surface temperature. Nature 457, 435–440.

Stone, B., Norman, J.M., 2006. Land use planning and surface heat island formation: A parcel-based radiation flux approach. Atmospheric Environment 40, 3561–3573.

Stone, D.A., Hansen, G., 2016. Rapid systematic assessment of the detection and attribution of regional anthropogenic climate change. Climate Dynamics 47, 1399–1415.

Streiling, S., Matzarakis, A., 2003. Influence of single and small clusters of trees on the bioclimatic of a city: A case study. Journal of Arboriculture 29, 309–316.

Su, Z., Su, Z., 2002. The Surface Energy Balance System (SEBS) for estimation of turbulent heat fluxes To cite this version : The Surface Energy Balance System (SEBS) for estimation of turbulent heat fluxes. Hydrology and Earth System Sciences 6, 85–99.

Subash, N., Sikka, A.K., Mohan, H.S.R., 2011. An investigation into observational characteristics of rainfall and temperature in Central Northeast India-a historical perspective 1889-2008. Theoretical and Applied Climatology 103, 305–319.

Subash, N., Singh, S.S., Priya, N., 2011. Extreme rainfall indices and its impact on rice productivity-A case study over sub-humid climatic environment. Agricultural Water Management 98, 1373–1387.

Sun, R.H., Chen, L.D., 2012. How can urban water bodies be designed for climate adaptation? Landscape and Urban Planning 105, 27–33.

Suribabu, C.R., Bhaskar, J., Neelakantan, T.R., 2012. Land use/cover change detection of Tiruchirapalli City, India, using integrated remote sensing and GIS tools. Journal of the Indian Society of Remote Sensing 40, no. 4 (2012): 699-708.

Tabari, H., Somee, B.S., Zadeh, M.R., 2011. Testing for long-term trends in climatic variables in Iran. Atmospheric Research 100, 132–140.

Taxak, A.K., Murumkar, A.R., Arya, D.S., 2014. Long term spatial and temporal rainfall trends and homogeneity analysis in Wainganga basin, Central India. Weather and Climate Extremes 4, 50–61.

Taylor, K.E., Stouffer, R.J., Meehl, G.A., 2012. An overview of CMIP5 and the experiment design. Bulletin of the American Meteorological Society 93, 485–498.

Thapliyal, V., Kulshrestha, S.M., 1991. Climate changes and trends over India. Mausam.

Theil, H., 1950. A Rank-Invariant method of linear and polynomial regression analysis. Proceedings of the Koninklijke Nederlandse Akademie Van Wetenschappen A 53, 345–381.

Thorsson, S., Lindberg, F., Björklund, J., Holmer, B., Rayner, D., 2011. Potential changes in outdoor thermal comfort conditions in Gothenburg, Sweden due to climate change: The influence of urban geometry. International Journal of Climatology 31, 324–335.

Thuiller, W., Lavorel, S., Araujo, M.B., Sykes, M.T., Prentice, I.C., 2005. Climate change threats to plant diversity in Europe. Proceedings of the National Academy of Sciences 102, 8245–8250.

Tian, B., Fetzer, E.J., Kahn, B.H., Teixeira, J., Manning, E., Hearty, T., 2013. Evaluating CMIP5 models using AIRS tropospheric air temperature and specific humidity climatology. Journal of Geophysical Research Atmospheres 118, 114–134.

Tigga, A., Hema Malini, B., 2011. Temperature Trends in Ranchi City, Jharkhand. Punjab Geographer 7.

Timbal, B., McAveney, B.J., 2001. An analogue-based method to downscale surface air temperature: Application for Australia. Climate Dynamics 17, 947–963.

Toggweiler, J., Key, R., 2001. Ocean circulation: Thermohaline circulation. Encyclopedia of Atmospheric Sciences 4, 1549--1555.

Tomozeiu, R., Cacciamani, C., Pavan, V., Morgillo, A., Busuioc, A., 2007. Climate change scenarios for surface temperature in Emilia-Romagna (Italy) obtained using statistical downscaling models. Theoretical and Applied Climatology 90, 25–47.

Trenberth, K.E., 2007. Coauthors, 2007: Observations: Surface and atmospheric climate change. Climate Change 2007: The Physical Science Basis, S. Solomon et al., Eds. Cambridge University Press.

Trusilova, K., Jung, M., Churkina, G., Karsten, U., Heimann, M., Claussen, M., 2008. Urbanization impacts on the climate in Europe: Numerical experiments by the PSU-NCAR mesoscale model (MM5). Journal of Applied Meteorology and Climatology 47, 1442–1455.

Tubiello, F.N., Rosenzweig, C., 2008. Agriculture: Aid. Africa Research Bulletin: Economic, Financial and Technical Series 45, 17716A--17716A.

U.S. Environmental Protection Agency (USEPA), 1999. Storm water technology fact sheet 7.

Upmanis, H., Eliasson, I., Lindqvist, S., 1998. The Influence of green areas on nocturnal temperatures in a high latitude city (Goeteborg, Sweden). International Journal of Climatology 18, 681–700.

V. G. Mitchell, H. A. Cleugh,C. S. B. Grimmond, J.X., 2008. Linking urban water balance and energy balance models to analyse urban design options. Hydrological Processes 22, 2891–2900.

Van Vuuren, D.P., Edmonds, J., Kainuma, M., Riahi, K., Thomson, A., Hibbard, K., Hurtt, G.C., Kram, T., Krey, V., Lamarque, J.F., Masui, T., 2011. The representative concentration pathways: an overview. Climatic Change 109, 5–31.

Vancutsem, C., Ceccato, P., Dinku, T. and Connor, S.J., 2010. Evaluation of MODIS Land Surface Temperature Data to Estimate Air Temperature in Different Ecosystems over Africa. Remote Sensing of Environment 114, 449.

Viegas, C. V, Luderitz, D., Bond, A., Luis, J., Ribeiro, D., Selig, P.M., 2013. Urban land planning : The role of a Master Plan in influencing local temperatures 35, 1–13.

Voldoire, A., Royer, J.F., 2004. Tropical deforestation and climate variability. Climate Dynamics. 22, 857–874.

Vose, R.S., Easterling, D.R., 2005. Maximum and minimum temperature trends for the globe: An update through 2004. Geophysical Research.

Wang, H., He, Q., Liu, X., Zhuang, Y., Hong, S., 2012. Global urbanization research from 1991 to 2009: A systematic research review. Landscape and Urban Planning 104, 299–309.

Wang, Q., Riemann, D., Vogt, S., Glaser, R., 2014. Impacts of land cover changes on climate trends in Jiangxi province China. International Journal of Biometeorology 58, 645–660.

Wang, R., Kalin, L., Kuang, W., Tian, H., 2014. Individual and combined effects of land use/cover and climate change on Wolf Bay watershed streamflow in southern Alabama. Hydrological Processes 28, 5530–5546.

Wang, Y., McBean, E., 2014. Uncertainty characterization of rainfall inputs used in the design of storm sewer infrastructure. Journal of Water Management Modeling.

Wang, Y., Sen, O.L., Wang, B., 2003. A highly resolved regional climate model (IPRC-RegCM) and its simulation of the 1998 severe precipitation event over China. Part I: Model description and verification of simulation. Journal of Climate 16, 1721–1738.

Wang, Z., Xi, M., Xiao, J., 2015. Risk assessment system of spatial city Gas Pipeline. Journal of Hydrology 123, 1118–1126.

Ward, H.C., Kotthaus, S., Järvi, L., Grimmond, C.S.B., 2016. Urban Climate Surface Urban Energy and Water Balance Scheme (SUEWS): Development and evaluation at two UK sites. UCLIM 18, 1–32.

Weng, Q., 2014. A remote sensing – GIS evaluation of urban expansion and its impact on surface temperature in the Zhujiang Delta , China. International Journal of Remote Sensing 22, 1999–2014.

Weng, Q.H., 2009. Thermal infrared remote sensing for urban climate and environmental studies: Methods, applications, and trends. Isprs Journal of Photogrammetry and Remote Sensing 64, 335–344.

Weng, Q.H., Yang, S.H., 2004. Managing the adverse thermal effects of urban development in a densely populated Chinese city. Journal of Environmental Management 70, 145–156.

Weyant, J., Azar, C., Kainuma, M., Kejun, J., 2009. Report of 2.6 versus 2.9 Watts/m2 RCPP evaluation panel. IPCC.

Wichansky, P.S., Weaver, C.P., Steyaert, L.T., Walko, R.L., 2006. Evaluating the effects of historical land cover change on summertime weather and climate in New Jersey. New Jersey's Environments: Past, Present, and Future, 128–163.

Wilby, R.L., Dawson, C.W., 2007. SDSM 4.2-A decision support tool for the assessment of regional climate change impacts User Manual. User Manual. London, UK 1–94.

Wilby, R.L., Dawson, C.W., 2013. The statistical downscaling model: Insights from one decade of application. International Journal of Climatology 33, 1707–1719.

Wilby, R.L., Dawson, C.W., Barrow, E.M., 2002. SDSM—a decision support tool for the assessment of regional climate change impacts. Environmental Modelling and Software 17, 147–159.

Wilby, R.L., Wigley, T.M.L., Conway, D., 1998. Statistical downscaling of general circulation model output: a comparison of methods. Water resources.

Woodward, F.I., Smith, T.M., Emanuel, W.R., 1995. A global primary productivity and phytogeography model. Global Biogeochemical Cycles 9, 471–490.

Xiao, H., Weng, Q., 2007. The impact of land use and land cover changes on land surface temperature in a karst area of China. Journal of Environmental Management 85, 245–257.

Xiao, Z., Liu, B., Liu, H., Zhang, D., 2012. Progress in climate prediction and weather forecast operations in China. Advances in Atmospheric Sciences 29, 943–957.

Xu, Z., Mahmood, R., Yang, Z.L., Fu, C., Su, H., 2015. Investigating diurnal and seasonal climatic response to land use and land cover change over monsoon Asia with the Community Earth System Model. Journal of Geophysical Research Atmospheres 120, 1137–1152.

Yadav, R., Tripathi, S.K., Pranuthi, G., Dubey, S.K., 2014. Trend analysis by Mann-Kendall test for precipitation and temperature for thirteen districts of Uttarakhand. Journal of Agrometeorology 16, 164–171.

Yan, Z.W., Li, Z., Xia, J.J., 2014. Homogenization of climate series: The basis for assessing climate changes. Science China Earth Sciences 57, 2891–2900.

Yang, X., Hou, Y., Chen, B., 2011. Observed surface warming induced by urbanization in east China. Journal of Geophysical Research Atmospheres 116.

Yang, Y.J., Wu, B.W., Shi, C. e., Zhang, J.H., Li, Y. Bin, Tang, W.A., Wen, H.Y., Zhang, H.Q., Shi, T., 2013. Impacts of Urbanization and Station-relocation on Surface Air Temperature Series in Anhui Province, China. Pure and Applied Geophysics 170, 1969–1983.

Yevjevich, V., 1971. The structure of inputs and outputs of hydrologic systems. In: systems approach to hydrology.

Yilmaz, G.R., Buzgan, T., Irmak, H., Safran, A., Uzun, R., 2009. The epidemiology of Crimean-Congo hemorrhagic fever in Turkey, 2002–2007. International Journal of Infectious Diseases.

Yin, L., Liebscher, J., 2006. Carbon – Carbon Coupling Reactions Catalyzed by Heterogeneous Palladium Catalysts. American Chemical Society.

Yoshida, H., Kuwauchi, Y., Jinschek, J.R., Sun, K., Tanaka, S., Kohyama, M., Shimada, S., Haruta, M., Takeda, S., 2012. Visualizing gas molecules interacting with supported Nanoparticulate Catalysts at reaction conditions. Science 335, 317–319.

Yoshida, H., Mønster, J., Scheutz, C., 2014. Plant-integrated measurement of greenhouse gas emissions from a municipal wastewater treatment plant. Water Research 61, 108–118.

Yoshida, R., Iizumi, T., Nishimori, M., 2014. Impact functions for land-use-induced surface warming, and their applications in uncertainty analysis. Climate Research 59, 77–87.

Yoshida, R., Iizumi, T., Nishimori, M., Yokozawa, M., 2012. Impacts of land-use changes on surface warming rates and rice yield in Shikoku, western Japan. Geophysical Research Letters 39.

Yue, S., Hashino, M., 2003. Long Term Trends of Annual and Monthly Precipitation in Japan1. JAWRA Journal of the American Water Resources Association 39, 587–596.

Zarenistanak, M., Dhorde, A.G., Kripalani, R.H., 2014. Trend analysis and change point detection of annual and seasonal precipitation and temperature series over southwest Iran. Journal of Earth System Science. 123, 281–295.

Zarenistanak, M., Dhorde, A.G.A.A., Kripalani, R.H., Dhorde, A.G.A.A., 2015. Trends and projections of temperature, precipitation, and snow cover during snow cover-observed period over southwestern Iran. Theoretical and Applied Climatology 122, 421–440.

Zeng, Y., 1991. Impacts of urbanization on population development in China. Ren Kou Xue Kan (Changchun Shi, China) 114, 1–5.

Zhang, N., Gao, Z., Wang, X., Chen, Y., 2010. Modeling the impact of urbanization on the local and regional climate in Yangtze River Delta, China. Theoretical and Applied Climatology 102, 331–342.

Zhang, R.H., 2015. Natural and human-induced changes in summer climate over the East Asian monsoon region in the last half century: A review. Advances in Climate Change Research 6, 131–140.

Zhang, S., Fan, W., Li, Y., Yi, Y., 2017. The influence of changes in land use and landscape patterns on soil erosion in a watershed. Science of the Total Environment 574, 34–45.

Zhang, S., Liu, Y., Wang, T., 2014. How land use change contributes to reducing soil erosion in the Jialing River Basin, China. Agricultural Water Management 133, 65–73.

Zhang, X., Srinivasan, R., Hao, F., 2007. Predicting hydrologic response to climate change in the Luohe River basin using the SWAT model. Transactions of the ASABE.

Zhou, L., Dickinson, R.E., Tian, Y., Fang, J., Li, Q., Kaufmann, R.K., Tucker, C.J., Myneni, R.B., 2004. Evidence for a significant urbanization effect on climate in China. Proceedings of the National Academy of Sciences of the United States of America 101, 9540–4.

Zilitinkevich, S.S., Baklanov, A.A., Mammarella, I., Joffre, S.M., 2006. The effect of stratification on the surface resistance for very rough vegetated and urban surfaces. Sixth International Conference on Urban Climate.

Annexure A

A1 : Projection results of mean rainfall in different RCP scenarios for different temporal scales at Safdarjung Station

Temporal	Observed	NCEP	RCP	RCP	RCP	NCEP	RCP	RCP	RCP
January	0.68	0.61	0.62	0.77	0.59	-10.23	-8.89	11.79	-14.17
February	0.63	0.51	0.53	0.65	0.60	-19.51	-16.05	1.77	-6.08
March	0.43	0.42	0.32	0.16	0.37	-3.19	-25.83	-63.14	-13.22
April	0.74	0.67	0.51	0.25	0.69	-9.55	-30.81	-66.95	-7.28
May	1.47	1.34	1.31	1.80	1.31	-8.60	-10.75	22.67	-10.59
June	3.14	2.83	3.01	2.86	2.63	-10.06	-4.22	-8.90	-16.32
July	5.35	5.04	5.59	4.16	4.72	-5.78	4.61	-22.26	-11.64
August	5.42	5.09	5.14	6.47	5.45	-6.11	-5.15	19.35	0.48
September	2.66	2.61	2.72	2.76	2.73	-1.58	2.46	4.03	2.76
October	0.77	0.83	0.92	0.23	0.79	8.06	19.66	-70.06	2.42
November	0.21	0.18	0.19	0.02	0.22	-17.21	-9.67	-90.80	3.14
December	0.46	0.49	0.85	0.31	0.45	4.55	83.09	-32.44	-3.68
Winter	0.59	0.54	0.67	0.57	0.54	-9.36	13.45	-3.45	-8.64
Spring	0.88	0.81	0.72	0.74	0.79	-7.96	-18.75	-16.11	-10.12
Summer	4.65	4.33	4.60	4.51	4.28	-6.85	-1.17	-2.98	-7.91
Autumn	1.21	1.20	1.27	1.00	1.24	-0.39	5.49	-17.53	2.71
Annual	1.84	1.73	1.82	1.71	1.72	-6.13	-1.04	-6.98	-6.51

A2: Projection results of maximum rainfall in different RCP scenarios for different temporal scales at Safdarjung Station

Temporal	Observed	NCEP	RCP	RCP	RCP	NCEP	RCP	RCP	RCP
January	78.00	43.27	47.05	50.88	50.10	-44.52	-39.68	-34.77	-35.77
February	40.00	35.73	37.99	43.31	45.28	-10.67	-5.02	8.29	13.20
March	27.00	37.84	33.69	29.55	32.92	40.15	24.76	9.43	21.94
April	108.00	44.41	46.73	40.36	56.01	-58.88	-56.73	-62.63	-48.14
May	112.00	76.74	73.31	65.59	77.54	-31.48	-34.54	-41.44	-30.77
June	134.00	98.98	112.08	106.25	90.73	-26.14	-16.36	-20.71	-32.29
July	181.00	111.86	124.31	104.96	105.72	-38.20	-31.32	-42.01	-41.59
August	150.00	152.61	165.07	150.16	157.05	1.74	10.05	0.11	4.70
September	108.00	118.63	121.44	110.33	119.77	9.84	12.44	2.16	10.90
October	93.00	81.58	132.09	84.25	80.71	-12.28	42.03	-9.41	-13.22
November	42.00	29.00	30.66	12.84	36.41	-30.94	-26.99	-69.44	-13.31
December	100.00	46.91	527.87	39.13	47.03	-53.09	427.87	-60.87	-52.97
Winter	100.00	54.23	527.87	56.72	56.55	-45.77	427.87	-43.28	-43.45
Spring	112.00	76.80	73.31	68.19	81.56	-31.43	-34.54	-39.12	-27.18
Summer	181.00	157.76	172.96	150.85	158.01	-12.84	-4.44	-16.66	-12.70
Autumn	108.00	118.88	148.99	117.96	125.50	10.08	37.95	9.22	16.21
Annual	181.00	160.85	568.18	152.27	165.92	-11.13	213.91	-15.88	-8.33

A3 : Projection results of wet days precipitation (%) in different RCP scenarios for different temporal scales at Safdarjung Station

Temporal	Observed	NCEP	RCP	RCP	RCP	NCEP	RCP	RCP	RCP
January	0.10	0.07	0.07	0.07	0.07	-33.91	-30.63	-35.83	-36.68
February	0.14	0.07	0.07	0.08	0.07	-52.69	-50.63	-43.42	-51.59
March	0.10	0.05	0.04	0.02	0.05	-51.35	-60.83	-82.59	-52.72
April	0.12	0.07	0.06	0.02	0.07	-38.73	-46.32	-81.46	-42.38
May	0.16	0.12	0.10	0.18	0.11	-27.71	-34.52	11.06	-30.61
June	0.26	0.20	0.20	0.17	0.20	-22.48	-22.39	-35.44	-23.56
July	0.40	0.32	0.32	0.31	0.32	-19.67	-18.54	-22.15	-20.48
August	0.34	0.28	0.29	0.37	0.30	-16.43	-14.49	9.21	-11.87
September	0.18	0.14	0.14	0.17	0.15	-23.22	-20.69	-3.67	-19.39
October	0.08	0.05	0.04	0.01	0.05	-30.60	-48.84	-90.84	-28.93
November	0.04	0.03	0.03	0.00	0.02	-40.00	-39.83	-92.96	-41.39
December	0.06	0.05	0.04	0.03	0.04	-19.94	-29.03	-45.21	-24.55
Winter	0.10	0.06	0.06	0.06	0.06	-39.28	-39.04	-41.05	-40.73
Spring	0.13	0.08	0.07	0.07	0.08	-37.38	-45.14	-42.08	-40.10
Summer	0.33	0.27	0.27	0.28	0.27	-19.28	-18.14	-14.83	-18.32
Autumn	0.10	0.07	0.07	0.06	0.08	-27.51	-30.76	-39.05	-24.98
Annual	0.16	0.12	0.12	0.12	0.12	-27.00	-28.37	-27.67	-26.88

A4: Projection results of mean dry spell precipitation in different RCP scenarios for different temporal scales at Safdarjung Station

Temporal	Observed	NCEP	RCP	RCP	RCP	NCEP	RCP	RCP	RCP
January	10.19	10.22	9.86	10.45	10.39	0.26	-3.27	2.55	1.93
February	8.32	10.13	10.17	9.10	10.12	21.74	22.19	9.33	21.61
March	8.89	12.77	15.37	20.59	12.94	43.55	72.82	131.52	45.49
April	9.09	9.98	11.83	18.87	10.39	9.83	30.25	107.69	14.34
May	7.33	7.08	8.59	5.00	7.52	-3.33	17.23	-31.70	2.56
June	4.77	4.86	4.54	5.40	4.76	1.85	-4.80	13.16	-0.10
July	3.32	3.08	3.32	3.22	3.33	-7.07	0.14	-3.00	0.47
August	3.81	3.62	3.48	2.79	3.65	-4.96	-8.44	-26.66	-4.14
September	7.49	6.34	6.05	5.13	5.88	-15.41	-19.19	-31.53	-21.54
October	12.26	12.35	17.12	25.88	11.87	0.73	39.62	111.04	-3.23
November	17.53	17.51	17.28	27.74	17.56	-0.08	-1.41	58.30	0.21
December	13.82	12.77	13.78	15.87	13.43	-7.58	-0.25	14.85	-2.82
Winter	13.11	14.13	14.26	14.66	14.55	7.79	8.82	11.85	10.99
Spring	10.16	11.65	14.75	13.46	12.30	14.62	45.10	32.43	20.98
Summer	4.17	3.97	3.93	3.80	4.05	-4.67	-5.64	-8.81	-2.82
Autumn	14.89	13.30	14.47	16.28	12.50	-10.70	-2.83	9.35	-16.06
Annual	9.46	9.39	9.96	9.87	9.52	-0.73	5.28	4.27	0.58

A5 : Projection results of mean wet spell precipitation in different RCP scenarios for different temporal scales at Safdarjung Station

Temporal	Observed	NCEP	RCP	RCP	RCP	NCEP	RCP	RCP	RCP
January	1.58	1.09	1.08	1.08	1.08	-31.34	-31.46	-31.38	-31.38
February	1.73	1.07	1.15	1.10	1.08	-37.93	-33.72	-36.63	-37.62
March	1.39	1.07	1.21	1.03	1.05	-22.86	-12.98	-25.79	-24.30
April	1.59	1.10	1.21	1.04	1.10	-31.29	-24.06	-34.73	-31.13
May	1.70	1.15	1.30	1.25	1.17	-31.91	-23.44	-26.56	-30.91
June	1.89	1.38	1.29	1.25	1.33	-26.90	-31.75	-33.92	-29.40
July	2.30	1.53	1.68	1.53	1.62	-33.19	-26.75	-33.16	-29.33
August	2.08	1.52	1.49	1.67	1.64	-26.74	-28.44	-19.57	-21.24
September	2.06	1.25	1.22	1.25	1.21	-39.51	-40.99	-39.43	-41.54
October	1.59	1.11	1.50	1.04	1.07	-30.13	-6.04	-34.97	-32.90
November	1.92	1.04	1.02	0.95	1.02	-45.68	-46.69	-50.43	-46.53
December	1.50	1.06	1.05	1.04	1.05	-29.41	-29.81	-30.35	-29.67
Winter	1.66	1.08	1.10	1.08	1.08	-35.06	-33.71	-34.72	-35.00
Spring	1.60	1.12	1.26	1.20	1.12	-29.80	-21.01	-24.55	-29.63
Summer	2.15	1.51	1.52	1.54	1.57	-30.01	-29.57	-28.60	-27.17
Autumn	1.92	1.19	1.24	1.24	1.15	-38.14	-35.46	-35.55	-40.15
Annual	1.92	1.32	1.37	1.37	1.34	-31.31	-28.62	-28.46	-30.22

A6 : Projection results of maximum wet spell length precipitation in different RCP scenarios for different temporal scales at Safdarjung Station

Temporal	Observed	NCEP	RCP	RCP	RCP	NCEP	RCP	RCP	RCP
January	5.00	2.55	2.50	2.55	2.55	-49.00	-50.00	-49.00	-49.00
February	4.00	2.40	2.85	2.60	2.50	-40.00	-28.75	-35.00	-37.50
March	4.00	2.15	2.75	1.45	2.20	-46.25	-31.25	-63.75	-45.00
April	6.00	2.50	3.40	1.90	2.60	-58.33	-43.33	-68.33	-56.67
May	14.00	3.35	4.60	4.25	3.85	-76.07	-67.14	-69.64	-72.50
June	25.00	5.40	4.60	3.95	5.50	-78.40	-81.60	-84.20	-78.00
July	30.00	6.80	9.10	6.95	7.50	-77.33	-69.67	-76.83	-75.00
August	9.00	6.25	6.55	7.60	8.15	-30.56	-27.22	-15.56	-9.44
September	8.00	4.20	4.10	4.50	3.90	-47.50	-48.75	-43.75	-51.25
October	6.00	2.70	3.95	1.25	2.20	-55.00	-34.17	-79.17	-63.33
November	10.00	1.80	1.50	0.95	1.50	-82.00	-85.00	-90.50	-85.00
December	7.00	2.15	2.10	2.05	2.10	-69.29	-70.00	-70.71	-70.00
Winter	7.00	2.90	3.10	2.95	2.90	-58.57	-55.71	-57.86	-58.57
Spring	14.00	3.35	4.75	4.25	3.90	-76.07	-66.07	-69.64	-72.14
Summer	30.00	7.75	9.35	8.25	8.75	-74.17	-68.83	-72.50	-70.83
Autumn	10.00	4.30	4.50	4.50	3.90	-57.00	-55.00	-55.00	-61.00
Annual	30.00	7.90	9.35	8.25	8.75	-73.67	-68.83	-72.50	-70.83

A7 : Projection results of maximum dry spell length precipitation in different RCP scenarios for different temporal scales at Safdarjung Station

Temporal	Observed	NCEP	RCP	RCP	RCP	NCEP%	RCP	RCP	RCP
January	31.00	31.00	31.00	31.00	31.00	0.00	0.00	0.00	0.00
February	29.00	28.80	28.80	28.45	28.75	-0.69	-0.69	-1.90	-0.86
March	31.00	31.00	31.00	31.00	31.00	0.00	0.00	0.00	0.00
April	30.00	29.90	30.00	30.00	30.00	-0.33	0.00	0.00	0.00
May	31.00	30.35	30.85	26.25	30.60	-2.10	-0.48	-15.32	-1.29
June	21.00	25.90	23.60	28.75	27.10	23.33	12.38	36.90	29.05
July	18.00	19.10	22.25	22.20	22.20	6.11	23.61	23.33	23.33
August	24.00	21.90	21.30	16.15	23.25	-8.75	-11.25	-32.71	-3.13
September	30.00	28.60	27.25	26.35	27.20	-4.67	-9.17	-12.17	-9.33
October	31.00	31.00	31.00	31.00	31.00	0.00	0.00	0.00	0.00
November	30.00	30.00	30.00	30.00	30.00	0.00	0.00	0.00	0.00
December	31.00	31.00	31.00	31.00	31.00	0.00	0.00	0.00	0.00
Winter	61.00	77.55	72.80	77.45	81.85	27.13	19.34	26.97	34.18
Spring	67.00	70.50	85.55	79.65	77.80	5.22	27.69	18.88	16.12
Summer	25.00	31.80	27.70	31.55	29.85	27.20	10.80	26.20	19.40
Autumn	91.00	79.30	83.00	85.30	77.80	-12.86	-8.79	-6.26	-14.51
Annual	129.00	101.2	112.8	117.80	108.75	-21.55	-12.56	-8.68	-15.70

A8 : Projection results of maximum N_tol precipitation in different RCP scenarios for different temporal scales at Safdarjung Station

Temporal	Observed	NCEP	RCP	RCP	RCP	NCEP	RCP	RCP	RCP
January	145.0	52.56	56.6	61.92	55.33	-63.76	-60.98	-57.30	-61.84
February	54.0	43.75	42.6	54.15	52.93	-18.98	-21.17	0.27	-1.98
March	42.0	47.92	42.4	30.48	37.17	14.09	0.91	-27.42	-11.50
April	189.0	53.26	58.1	42.79	66.67	-71.82	-69.23	-77.36	-64.72
May	135.0	99.27	99.5	87.42	94.38	-26.46	-26.30	-35.25	-30.09
June	282.0	146.99	164.3	145.83	116.81	-47.88	-41.74	-48.29	-58.58
July	227.0	176.69	209.1	145.17	157.07	-22.16	-7.90	-36.05	-30.81
August	256.0	214.38	252.8	222.61	242.65	-16.26	-1.23	-13.04	-5.21
September	209.0	157.36	170.0	149.31	150.14	-24.71	-18.66	-28.56	-28.16
October	134.0	99.55	202.3	92.01	95.96	-25.71	50.96	-31.33	-28.39
November	48.0	30.64	33.4	12.84	40.29	-36.17	-30.47	-73.26	-16.06
December	100.0	55.07	531.8	44.08	53.39	-44.93	431.81	-55.92	-46.61
Winter	145.0	64.44	533.2	69.36	66.28	-55.56	267.72	-52.17	-54.29
Spring	189.0	99.93	100.7	88.27	97.84	-47.13	-46.71	-53.29	-48.23
Summer	282.0	226.26	302.0	225.08	243.45	-19.77	7.11	-20.18	-13.67
Autumn	209.0	161.62	222.3	155.01	156.54	-22.67	6.37	-25.83	-25.10
Annual	282.0	226.28	649.4	228.34	244.55	-19.76	130.29	-19.03	-13.28

A9 : Projection results of mean maximum temperature in different RCP scenarios for different temporal scales at Safdarjung Station

Temporal	Observe	NCE	RCP2.	RCP4.	RCP8.	NCEP	RCP2.6	RCP4.5	RCP8.5
January	20.09	20.08	20.12	20.09	20.08	-0.09	0.13	-0.02	-0.08
February	22.86	22.96	22.73	22.84	22.74	0.46	-0.54	-0.07	-0.51
March	28.71	28.76	28.66	28.66	28.63	0.18	-0.16	-0.15	-0.25
April	35.28	35.31	35.07	35.24	35.13	0.10	-0.58	-0.13	-0.42
May	38.51	38.43	38.41	38.55	38.57	-0.23	-0.27	0.10	0.14
June	37.99	38.05	38.07	38.14	38.11	0.16	0.20	0.39	0.31
July	34.63	34.75	34.72	34.71	34.51	0.35	0.27	0.22	-0.35
August	33.31	33.31	33.18	33.19	33.16	0.01	-0.38	-0.34	-0.43
September	33.30	33.26	33.26	33.25	33.22	-0.11	-0.11	-0.14	-0.23
October	32.03	32.08	32.17	32.00	31.96	0.15	0.45	-0.08	-0.21
November	27.68	27.72	27.65	27.56	27.69	0.14	-0.11	-0.41	0.03
December	22.27	22.15	22.30	22.23	22.23	-0.53	0.11	-0.19	-0.17
Winter	21.71	21.69	21.69	21.69	21.65	-0.06	-0.10	-0.10	-0.25
Spring	34.16	34.15	34.04	34.14	34.10	0.00	-0.34	-0.05	-0.16
Summer	35.28	35.34	35.29	35.32	35.23	0.18	0.04	0.10	-0.14
Autumn	31.01	31.03	31.04	30.95	30.97	0.06	0.09	-0.20	-0.15
Annual	30.58	30.60	30.56	30.56	30.53	0.05	-0.08	-0.05	-0.17

A10 : Projection results of extreme maximum temperature (^{o}C) in diffrenet RCP scenarios at Safdarjung Station

Temporal	Observe	NCE	RCP2.	RCP4.	RCP8.	NCEP	RCP2.6	RCP4.5	RCP8.5
January	29.40	29.31	29.24	28.91	29.27	-0.30	-0.53	-1.68	-0.44
February	33.30	33.40	33.92	33.91	33.72	0.29	1.85	1.82	1.27
March	38.50	40.74	40.91	40.73	40.81	5.81	6.27	5.78	6.01
April	44.60	46.93	46.51	46.80	46.42	5.22	4.28	4.94	4.09
May	45.60	49.04	48.69	49.07	48.81	7.55	6.79	7.60	7.04
June	45.70	49.00	49.25	49.32	49.54	7.22	7.77	7.91	8.41
July	45.10	45.45	44.94	45.64	45.34	0.77	-0.36	1.20	0.54
August	43.00	41.64	41.72	41.54	41.44	-3.16	-2.97	-3.40	-3.62
September	38.50	41.11	41.08	41.36	40.87	6.78	6.70	7.42	6.15
October	38.30	39.87	40.35	40.13	39.89	4.11	5.34	4.79	4.15
November	37.20	37.38	37.43	37.17	37.64	0.49	0.61	-0.09	1.19
December	32.50	32.40	32.73	32.82	32.53	-0.30	0.70	1.00	0.09
Winter	33.30	33.56	34.23	34.18	33.89	0.77	2.81	2.64	1.77
Spring	45.60	49.09	48.69	49.07	48.81	7.65	6.79	7.60	7.04
Summer	45.70	49.00	49.25	49.32	49.54	7.22	7.77	7.91	8.41
Autumn	38.50	41.14	41.28	41.38	40.91	6.84	7.22	7.48	6.26
Annual	45.70	49.65	49.43	49.68	49.72	8.65	8.16	8.72	8.80

A11: Projection results of extreme minimum of maximum temperature in different RCP scenarios in different temporal scales at Safdarjung Station

Temporal	Observe	NCE	RCP2.	RCP4.	RCP8.	NCEP	RCP2.6	RCP4.5	RCP8.5
January	11.10	11.23	11.05	10.93	10.86	1.20	-0.49	-1.55	-2.13
February	9.50	11.80	11.94	11.87	11.44	24.23	25.71	24.90	20.38
March	15.90	15.99	16.79	16.75	16.73	0.54	5.59	5.34	5.22
April	19.90	22.51	23.43	24.05	23.35	13.10	17.75	20.85	17.32
May	25.70	28.14	27.94	28.34	28.50	9.49	8.71	10.29	10.88
June	26.50	26.68	26.38	26.99	27.03	0.67	-0.45	1.86	2.01
July	26.20	24.82	24.22	24.08	23.87	-5.27	-7.57	-8.07	-8.88
August	24.80	25.26	25.02	24.70	24.99	1.84	0.90	-0.41	0.75
September	23.30	25.51	25.50	25.53	25.48	9.46	9.43	9.59	9.38
October	21.30	23.92	23.95	23.97	24.00	12.32	12.46	12.52	12.68
November	15.80	17.54	17.88	17.96	18.11	11.03	13.16	13.65	14.61
December	10.10	11.81	11.80	11.51	11.60	16.93	16.79	13.99	14.88
Winter	9.50	10.68	10.69	10.45	10.47	12.37	12.56	9.95	10.17
Spring	15.90	15.99	16.79	16.75	16.73	0.54	5.59	5.34	5.22
Summer	24.80	24.47	24.09	23.85	23.70	-1.35	-2.87	-3.85	-4.42
Autumn	15.80	17.54	17.88	17.96	18.11	11.03	13.16	13.65	14.61
Annual	9.50	10.68	10.69	10.45	10.47	12.37	12.56	9.95	10.17

A12 : Projection results of maximum range of maximum temperature (^{o}C) in different RCP scenarios for different temporal scales at Safdarjung Station

Temporal	Observe	NCE	RCP2.	RCP4.	RCP8.	NCEP	RCP2.6	RCP4.5	RCP8.5
January	16.00	15.65	15.94	15.43	15.91	-2.21	-0.39	-3.57	-0.55
February	19.20	18.08	18.89	19.61	19.26	-5.85	-1.62	2.13	0.32
March	17.60	20.55	20.79	20.65	20.91	16.75	18.15	17.36	18.79
April	19.00	21.44	19.98	19.52	20.36	12.85	5.15	2.72	7.15
May	16.40	17.67	18.30	18.29	17.92	7.74	11.61	11.51	9.27
June	16.70	19.24	19.53	19.66	19.53	15.24	16.96	17.71	16.97
July	14.80	18.09	18.43	18.99	18.57	22.26	24.51	28.29	25.46
August	14.80	13.94	14.87	14.31	14.73	-5.80	0.50	-3.28	-0.46
September	14.10	13.51	13.82	13.71	13.82	-4.15	-1.99	-2.73	-1.96
October	14.70	13.93	14.43	14.07	14.09	-5.22	-1.87	-4.25	-4.15
November	14.30	16.60	16.89	16.89	17.10	16.11	18.13	18.09	19.59
December	15.80	17.80	18.75	18.44	18.59	12.64	18.66	16.72	17.68
Winter	21.10	20.17	20.88	21.67	21.38	-4.42	-1.02	2.71	1.35
Spring	27.00	30.71	29.13	30.43	29.66	13.74	7.88	12.72	9.85
Summer	19.20	22.14	22.64	23.09	22.98	15.30	17.94	20.28	19.68
Autumn	21.20	21.09	21.39	21.17	20.77	-0.54	0.88	-0.15	-2.02
Annual	34.60	36.45	36.37	37.26	37.06	5.36	5.13	7.68	7.12

A13 : Projection results of minimum range of maximum temperature (^{o}C) in different RCP scenarios for different temporal scales at Safdarjung Station

Temporal	Observe	NCE	RCP2.	RCP4.	RCP8.	NCEP	RCP2.6	RCP4.5	RCP8.5
January	2.20	8.02	7.63	7.77	7.57	264.52	246.94	252.99	244.09
February	5.30	8.30	9.11	8.85	10.08	56.66	71.96	67.06	90.27
March	7.10	9.45	10.00	10.32	12.03	33.03	40.79	45.38	69.47
April	5.60	9.31	10.08	9.98	10.77	66.32	80.03	78.14	92.35
May	2.30	8.60	8.87	9.05	8.80	274.06	285.57	293.49	282.82
June	4.00	9.63	9.58	9.67	9.69	140.80	139.61	141.78	142.34
July	3.20	8.53	8.94	8.77	8.86	166.70	179.28	174.08	176.88
August	1.20	6.87	7.06	7.27	7.42	472.38	488.36	506.14	518.23
September	1.50	6.88	6.72	6.64	6.69	358.66	347.69	342.57	346.08
October	3.30	6.66	7.01	6.75	7.45	101.97	112.50	104.55	125.78
November	3.80	7.61	8.15	8.06	9.25	100.19	114.56	112.14	143.50
December	3.80	8.66	8.89	9.42	9.92	127.81	133.98	147.86	160.97
Winter	6.50	11.47	11.82	12.34	13.10	76.44	81.88	89.87	101.51
Spring	14.00	17.52	19.50	19.79	19.39	25.16	39.30	41.33	38.47
Summer	7.30	13.32	13.91	14.08	13.55	82.52	90.51	92.87	85.64
Autumn	9.10	12.66	13.37	13.21	14.21	39.07	46.90	45.14	56.19
Annual	21.00	28.01	28.54	28.65	28.98	33.40	35.92	36.43	38.01

A14 : Projection results of mean minimum temperature in different RCP scenarios for different temporal scales at Safdarjung Station

Temporal	Observe	NCE	RCP2.	RCP4.	RCP8.	NCEP	RCP2.6	RCP4.5	RCP8.5
January	8.49	8.49	8.48	8.46	8.49	0.02	-0.05	-0.33	0.03
February	10.93	11.06	10.89	10.88	10.98	1.20	-0.37	-0.46	0.41
March	15.95	16.00	15.84	15.93	15.67	0.32	-0.65	-0.14	-1.72
April	21.66	21.69	21.52	21.58	21.49	0.15	-0.64	-0.33	-0.75
May	26.01	25.92	25.94	26.07	26.04	-0.33	-0.28	0.23	0.11
June	28.04	28.01	27.95	28.03	28.08	-0.11	-0.32	-0.04	0.13
July	27.68	27.71	27.63	27.66	27.60	0.11	-0.18	-0.08	-0.29
August	27.01	27.02	26.89	27.00	26.75	0.02	-0.46	-0.05	-0.96
September	25.33	25.30	25.38	25.31	25.34	-0.11	0.19	-0.06	0.06
October	20.18	20.37	20.24	20.20	20.24	0.96	0.30	0.09	0.29
November	14.05	14.13	14.03	14.04	13.95	0.54	-0.19	-0.12	-0.73
December	9.59	9.57	9.61	9.59	9.57	-0.22	0.16	0.03	-0.22
Winter	9.63	9.67	9.62	9.61	9.64	0.36	-0.09	-0.25	0.08
Spring	21.20	21.20	21.09	21.19	21.06	0.00	-0.49	-0.05	-0.64
Summer	27.57	27.57	27.48	27.56	27.47	0.01	-0.32	-0.06	-0.37
Autumn	19.86	19.94	19.88	19.85	19.85	0.41	0.14	-0.02	-0.05
Annual	19.61	19.64	19.57	19.60	19.55	0.15	-0.22	-0.07	-0.31

A15 : Projection results of extreme maximum of minimum temperature in different RCP scenarios for different temporal scales at Safdarjung Station

Temporal	Observe	NCE	RCP2.	RCP4.	RCP8.	NCEP	RCP2.6	RCP4.5	RCP8.5
January	16.40	17.20	16.28	16.40	16.45	4.89	-0.76	-0.01	0.29
February	19.20	20.14	20.12	19.72	20.44	4.91	4.77	2.69	6.46
March	23.60	26.28	26.28	26.21	25.79	11.36	11.35	11.05	9.29
April	30.60	32.05	32.07	32.08	31.89	4.72	4.81	4.84	4.21
May	35.00	35.83	36.34	36.21	36.25	2.37	3.84	3.45	3.57
June	35.90	36.70	37.20	37.28	36.98	2.24	3.62	3.85	3.00
July	35.30	34.88	34.28	34.08	34.47	-1.18	-2.89	-3.45	-2.34
August	33.40	32.12	31.74	32.19	31.71	-3.84	-4.98	-3.63	-5.07
September	30.20	30.83	31.24	31.16	31.13	2.08	3.43	3.18	3.08
October	28.50	29.61	30.17	30.10	30.22	3.88	5.86	5.63	6.05
November	26.20	24.72	24.55	24.40	24.13	-5.65	-6.28	-6.86	-7.89
December	19.20	17.86	17.81	17.55	17.77	-7.01	-7.23	-8.58	-7.46
Winter	19.20	20.21	20.12	19.72	20.44	5.24	4.77	2.69	6.46
Spring	35.00	35.84	36.34	36.21	36.25	2.41	3.84	3.45	3.57
Summer	35.90	36.72	37.20	37.28	36.98	2.27	3.62	3.85	3.00
Autumn	30.20	30.83	31.28	31.29	31.31	2.08	3.56	3.60	3.66
Annual	35.90	36.81	37.43	37.37	37.18	2.53	4.27	4.11	3.56

A16 : Projection results of extreme minimum of minimum temperature (^{o}C) in different RCP scenarios for different temporal scales at Safdarjung Station

Temporal	Observe	NCE	RCP2.	RCP4.	RCP8.	NCEP	RCP2.6	RCP4.5	RCP8.5
January	2.00	0.61	0.50	0.82	0.59	-69.71	-74.87	-59.03	-70.35
February	3.70	1.54	1.87	1.56	1.68	-58.38	-49.54	-57.91	-54.68
March	4.20	5.27	5.51	5.96	5.82	25.45	31.14	41.81	38.47
April	11.00	10.74	10.93	11.55	10.87	-2.33	-0.60	5.00	-1.20
May	15.80	15.38	16.16	16.19	16.02	-2.68	2.29	2.46	1.41
June	12.80	18.90	19.08	19.13	19.32	47.62	49.07	49.44	50.95
July	20.50	21.38	21.00	20.70	20.60	4.31	2.44	0.99	0.50
August	21.20	22.05	21.89	21.83	21.70	4.00	3.27	2.99	2.36
September	19.40	19.36	19.25	19.44	19.37	-0.21	-0.80	0.20	-0.14
October	12.60	11.41	10.63	10.57	10.48	-9.47	-15.65	-16.08	-16.79
November	5.60	4.45	3.46	3.70	3.45	-20.45	-38.20	-34.00	-38.44
December	2.70	1.53	1.58	1.90	1.56	-43.35	-41.44	-29.63	-42.06
Winter	2.00	0.46	0.38	0.57	0.30	-76.89	-81.14	-71.61	-85.08
Spring	4.20	5.27	5.51	5.96	5.82	25.45	31.14	41.81	38.47
Summer	12.80	18.90	19.08	19.13	19.32	47.62	49.07	49.44	50.95
Autumn	5.60	4.45	3.46	3.70	3.45	-20.45	-38.20	-34.00	-38.44
Annual	2.00	0.46	0.38	0.57	0.30	-76.89	-81.14	-71.61	-85.08

A17: Projection results of maximum range of minimum temperature in RCP scenarios for different temporal scales at Safdarjung Station

Temporal	Observe	NCE	RCP2.	RCP4.	RCP8.	NCEP	RCP2.6	RCP4.5	RCP8.5
January	12.50	14.06	13.93	13.45	13.77	12.45	11.47	7.63	10.17
February	12.10	15.33	15.96	15.93	16.27	26.73	31.88	31.67	34.46
March	14.70	18.23	18.26	17.42	17.42	23.98	24.21	18.51	18.48
April	15.00	18.68	18.05	18.16	18.28	24.54	20.32	21.08	21.85
May	15.90	18.00	18.11	17.58	18.01	13.19	13.92	10.54	13.26
June	20.10	15.42	16.12	15.85	15.44	-23.26	-19.79	-21.16	-23.18
July	11.10	11.83	11.53	11.75	12.03	6.54	3.84	5.83	8.40
August	11.60	8.58	8.58	9.09	8.48	-26.04	-26.05	-21.65	-26.86
September	8.60	10.00	10.61	10.10	10.30	16.31	23.41	17.49	19.73
October	12.20	15.81	17.18	16.88	16.83	29.57	40.81	38.40	37.91
November	16.60	17.31	18.48	18.17	18.58	4.30	11.32	9.45	11.90
December	11.60	14.07	14.44	13.95	14.44	21.27	24.49	20.27	24.52
Winter	14.40	17.83	17.63	17.30	18.05	23.83	22.45	20.12	25.36
Spring	26.80	28.32	28.19	27.82	28.22	5.67	5.20	3.82	5.28
Summer	20.10	15.73	16.18	16.01	15.60	-21.77	-19.51	-20.35	-22.39
Autumn	24.10	25.00	26.23	25.66	26.18	3.73	8.85	6.47	8.63
Annual	32.10	34.60	34.94	34.82	34.76	7.80	8.86	8.49	8.27

A18: Projection results of minimum range of minimum temperature in different RCP scenarios for different temporal scales at Safdarjung Station

Temporal	Observe	NCE	RCP2.	RCP4.	RCP8.	NCEP	RCP2.6	RCP4.5	RCP8.5
January	1.97	6.80	6.73	6.86	6.91	245.25	241.48	248.08	250.56
February	3.93	7.45	7.65	7.27	7.72	89.59	94.77	84.88	96.50
March	6.25	8.55	8.60	8.77	8.31	36.78	37.61	40.36	32.96
April	5.98	8.73	8.80	9.11	8.54	46.03	47.09	52.40	42.81
May	2.72	8.44	8.57	8.80	8.59	210.26	215.15	223.53	215.79
June	1.27	7.65	7.52	7.50	7.46	502.29	492.09	490.80	487.50
July	1.62	5.69	5.68	5.65	5.53	251.39	250.39	248.49	241.38
August	1.00	4.01	4.02	4.26	4.21	301.31	301.74	326.17	321.28
September	3.04	4.67	5.10	4.98	4.93	53.67	67.82	63.94	62.18
October	5.00	7.06	8.21	8.28	8.12	41.14	64.21	65.65	62.46
November	4.20	8.07	8.82	8.44	8.87	92.11	109.95	101.04	111.23
December	2.96	6.79	6.92	6.76	6.84	129.47	133.69	128.34	131.07
Winter	5.51	9.65	9.62	9.61	9.47	75.07	74.57	74.48	71.89
Spring	14.42	17.50	18.36	18.91	18.68	21.33	27.31	31.17	29.51
Summer	2.18	8.57	8.65	8.71	8.42	293.31	296.89	299.73	286.09
Autumn	14.20	16.91	18.25	17.89	18.52	19.07	28.49	25.96	30.43
Annual	20.87	27.74	27.67	28.12	27.90	32.91	32.59	34.76	33.68

LIST OF RESEARCH PUBLICATIONS

International Journal

1. Surendra P. Singh, and Mahesh K. Jat (2017) "Impact of Land use/Land Cover Change on Climatic Trends in an Urban Fringe" Meteorology and Atmospheric Physics, Springer (Communicated).
2. Surendra Singh, and Mahesh K. Jat (2017), "Assessment of Temperature Anomalies Trend at Local Scale for Delhi, India" International Journal of Earth Sciences and Engineering, ISSN 0974-5904, Volume 10, No. 01, February 2017, pp 62-74. (Scopus Listed)

International Conferences

1. S. P. Singh and M K. Jat. "Assessment of Climate Change Using Spatial and Temporal Trend Analysis of Climatic Data: A Case study of Delhi, India" HYDRO 2015, 20th International Conference on Hydraulics, Water Resources and River Engineering 17-19 December 2015 organized by department of Civil Engineering IITR. Page 125.
2. Surendra Pratap Singh and Mahesh Kumar Jat. "Down Scaled Climate Change Projections with Uncertainty Assessment Over India Capital Region Delhi Using A Statistical Downscaling Model Approach" International conference on climate change & sustainability 35th Session of Academy of Environmental Biology, Lucknow from 21st and 23rd DEC-2015 organized by Thakur College of Science & Commerce, Kandivali, Mumbai. Page 138.
3. Singh Surendra P. and Jat Mahesh K. Influence of land use/land cover (LULC) changes on atmospheric dynamics over the national capital region, Delhi India. Eighth India International Geographical Union (IGU) conference on Land use, water, Climate and Urban health in changing urban environments Nov 4-6, 2015 organized by SNDT women's University, Department of Geography, Pune, India. Page 56.

National Conference

Singh P. Surendra and Jat, M .K. "Impact of Anthropogenic Effects on Climate Change by using Advance Technology Method". National on Geo-Informatics in Rural, Urban & Climate Studies, Geomatrix-14 conducted by REA,CSRE, IIT Bombay on 6th -7th June , 2014. Page -49.